The Carbonylation of Organic Compounds by Visible Light Photoredox-Catalysis

Nenad Micic

ORCID: 0000-0001-8669-0820

Submitted in total fulfilment of the requirements for the degree of

Doctor of Philosophy

June 2020

School of Chemistry

The University of Melbourne

For

Marcus

&

Julian

Abstract

Palladium-catalysed alkoxy- and aminocarbonylation of aryl (pseudo)halides provides efficient access to aromatic esters and amides. The broad application of this approach has been restricted by functional group tolerance, high reaction temperatures and moderate catalyst efficiency. Free-radical carbonylation is a complementary approach not confined by the same inherent limitations of palladium-catalysed carbonylative cross-coupling methodology. The development of free-radical carbonylation has been hindered by the ability to selectively generate the carbon-centred radical species and the high pressures of carbon monoxide required to drive the carbonylation step.

This thesis describes the development of visible light photoredox-catalysed alkoxy- and aminocarbonylation of aryl (pseudo)halides. Visible light photoredox-catalysis is a potent method to generate carbon-centred radicals selectively under mild reaction conditions. Aryl radicals can be trapped by carbon monoxide to afford carbonyl compounds. Continuous flow chemistry is utilised throughout, employing tube-in-tube semipermeable membrane reactor technology, to enable precise control over reactions conditions and safe use of carbon monoxide.

Chapter 1 introduces carbonylation and elaborates on carbonylative cross-coupling of aryl (pseudo)halides. It further introduces continuous flow processing in synthetic chemistry (flow chemistry) and details the application of flow chemistry to carbonylative cross-coupling and photochemical reactions.

Chapter 2 established a continuous flow platform for high pressure gas-liquid photochemistry. The flow system consisted of a pumping module, a reagent delivery module, a Teflon AF-2400 tube-in-tube reactor for saturation of the reaction stream with carbon monoxide, a photoreactor and pressure regulation devices. The photoredox-catalysed alkoxycarbonylation of aryl diazonium salts was selected to evaluate the performance of the flow system. It was determined that excellent yields of the benzoate ester could be achieved at significantly lower partial pressures of carbon monoxide and processing time than in batch.

Chapter 3 details the development of a free-radical annulative addition/alkoxycarbonylation cascade reaction. The developed methodology was applied to the synthesis of a diverse library of novel 3-acetate functionalized 2,3-

dihydrobenzofurans from widely accessible allyl aryl diazonium ethers. Application of the previously established continuous flow system enabled dilute reaction conditions to effectively control the propagation of competitive intermolecular radical addition side reactions without compromising on reaction throughput or space-time yield.

Chapter 4 describes the development of photoredox-catalysed aminocarbonylation of aryl halides. The developed methodology was applied to the synthesis of both electron rich and electron deficient benzamides at room temperature. Spectroscopic and theoretical computational studies were conducted to elucidate the reaction mechanism. A novel tandem photoredox catalytic manifold was proposed that features the transformation of $Ir(dtbbpy)(ppy)_2]PF_6$ in the presence of DIPEA to generate a distinct highly reducing Ir-complex capable of engaging energy demanding aryl halides.

Chapter 5 provides a summary of the work described in this thesis. Supplementary data is included in the appendix.

Declaration

This is to certify that:

i. The thesis comprises only my original work toward the degree of Doctor of Philosophy except where indicated in the preface
ii. Due acknowledgement has been made in the text to all other material used
iii. The thesis is less than the maximum word limit in length (100,000), exclusive of tables, bibliographies and appendix.

_____

Nenad Micic

1st of June 2020

Preface

All work herein has been conducted by the candidate, Nenad Micic, except the density functional theory calculations. Work towards the thesis that was carried out in collaboration with others is detailed below.

Chapter 4:

- The density functional theory calculations were conducted by Dr Geethi Weragoda (The University of Melbourne)
- Photoluminescence studies and cyclic voltammetry were conducted under the guidance of Dr Timothy U. Connell (Royal Melbourne Institute of Technology)

I acknowledge Dr Anastasios Polyzos for his guidance and contribution in the drafting of the peer-reviewed publications and the review of this thesis. I acknowledge Dr Daniel E. Gómez for his technical assistance towards the photoluminescence studies.

I am grateful to the University of Melbourne for the Melbourne Research Scholarship, G. I. Feutrill Award and Faculty of Science Travelling Scholarship. I would further like to, on behalf of my supervisor, thank the University of Melbourne and CSIRO for the Joint Establishment Grant.

Acknowledgments

First and foremost, I would like to thank my supervisor, Dr Anastasios Polyzos, for inspiring and encouraging me to pursue research in flow chemistry as well as synthetic-organic chemistry. I am truly grateful and appreciative for all the support, guidance and understanding he has provided. I don't believe I would have commenced, let alone completed, this journey without him. I would like to extend this thank-you to the University of Melbourne and Commonwealth Scientific and Industrial Research Organisation (CSIRO) for not only their financial support but also as world-class research institutions that nurture the inner curiosity that drives all passionate research. It was my pleasure.

I would like to thank the entire Polyzos Group members, past and present, for being genuine and considerate. I appreciate all the conversation, laughter and comradery, even at the n^{th} +1 hour of a Friday 'afternoon' group meeting. To the post-docs that have graced the group: Dr Martin Brzozowski, Dr Milena Czyz, Dr Geethika Weragoda and Dr Timothy Connell, I am sincerely grateful for all the mentorship and productive discussions freely offered. I would like to thank fellow Polyzos Group PhD candidate Dean Van As, for sharing an office with me from the beginning until the end and for being a true peer in every aspect.

I acknowledge all the faculty members that have provided their assistance over the years. I would like to thank Sioe See Volaric and Catlin Hennessy for their help navigating the instrumentation. I thank my advisory committee, Prof. Frances Separovic, Prof. Mark Rizzacasa and Dr. Wallace Wong for their guidance and advice. I thank CSIRO's Dr. Christian Hornung, Tom Kohl and Ivan Martinez-Botella for their assistance on flow chemistry technical matters over the years and I apologise for all the fittings I've never returned. Thank you to Melbourne University Chemical Society – it was a pleasure helping co-ordinate events. Thank you to the Chemistry Postgraduate Society for the Friday Night Frothies.

I must thank my family for supporting me throughout. I thank my parents, Snezana and Predrag, for their generous support over the years. I extend my loving gratitude to my wife Ann for putting up with a broke uni student for 4 years. It hadn't been easy, particularly whilst writing the thesis and working full-time, but all good things

command effort and sacrifice. I thank Jelly-Bean for keeping my lap warm as I wrote. And finally, to my sons, Marcus and Julian, who opened my eyes and heart to a whole new wondrous world.

To synthetic-process chemistry,

Whilst life's obligations have dictated that we must part, I know our time together has far from ended.

Table of Contents

Contents

List of Abbreviations

^{1}H	proton
^{13}C	carbon-13
2,3-DHB	2,3-dihydrobenzofuran
9-alkyl-9-BBN	9-alkyl-9-borabicyclo[3.3.1]nonane
A	adsorption of light
Ac	acetyl
AIBN	2,2’azobis(isobutyronitrile)
Ar	aryl
ATC	atom transfer carbonylation
AUD	Australian dollar
Bn	benzyl
BNAH	1-benzyl-l,4-dihydronicotinamide
BPR	back-pressure regulator
b.p.	boiling point
bpy	2,2′-bipyridine
Bu	butyl
c	concentration
Cat.	catalyst
DABCO	1,4-diazabicyclo[2.2.2]octane
DBU	1,8-Diazabicyclo[5.4.0]undec-7-ene
DFT	density functional theory
DIPEA	*N*,*N*-diisopropylethylamine
DMAP	dimethylaminopyridine
DMF	*N*,*N*-dimethylformamide
DMSO	dimethyl sulfoxide
E_p^{red}	reductive peak potential
E^{ox}	oxidation potential
E^{red}	reduction potential
Et	ethyl
d^{c}ppe	1,2-bis(dicyclopentylphosphino)ethane
d^{i}ppp	1,3-bis(diisopropylphosphino)propane
dtbpy	4,4′-di-*tert*-butyl-2,2′-dipyridyl

equiv.	equivalents
FEP	fluorinated ethylene propylene
GAM	gas-addition module
h	hour(s)
HPLC	high-performance liquid chromatography
HRMS	High resolution mass spectrometry
iPr	isopropyl
ISC	intersystem crossing
IR	infrared
k_q	quenching rate constant
l	cell path length
LED	light emitting diode
Me	methyl
Mol	mole(s)
NMR	nuclear magnetic resonance
m.p.	melting point
Nu	nucleophile
OAc	acetate
PC	photocatalyst
PDI	*N,N*-bis(2,6-diisopropylphenyl)perylene3,4,9,10-bis(dicarboximide)
PEEK	polyether ether ketone
PFA	perfluoroalkoxy alkane
ppm	parts per million
ppy	2-phenylpyridine
PTFE	polytetrafluoroethylene
PTH	10-phenylphenothiazine
Py	pyridine
Q	quencher
Rh6G	rhodamine 6G
rt	room temperature
s	second(s)
SCE	saturated calomel electrode
SET	single electron transfer

TBT	tributyltin hydride
TEA	triethylamine
TOF	turnover frequency
t_r	residence time
TTMSS	tris(trimethylsilyl)silane
UV	ultraviolet
ε	molar extinction coefficient
τ_0	excited state lifetime

List of Tables

List of Figures

List of Publications.

- **Micic, N**.; Polyzos, A. "Radical Carbonylation Mediated by Continuous-Flow Visible-Light Photocatalysis: Access to 2,3-Dihydrobenzofurans". *Organic Letters*, **2018**, *20*, 4663.
- Forni, J. A.; **Micic, N**; Connell, T.; Weragoda, G.; Polyzos, A. "Tandem Photoredox Catalysis: Enabling Carbonylative Amidation of Aryl and Alkylhalides". *Angewandte Chemie International Edition*, **2020**, *59*, 18646.

List of Conference Presentations

Oral Presentation

- 42nd Annual Synthesis Symposium, Bio21 Institute, Parkville, Australia, December 2017.

Poster Presentations

- 43rd Annual Synthesis Symposium, Bio21 Institute, Parkville, Australia, December 2018.
- Organic18: RACI Organic Division National Conference, University of Western Australia, Perth, Australia, December 2018.
- RACI Centenary National Conference, Melbourne Convention and Exhibition Centre, Melbourne, Australia, July 2017.
- 25th International Symposium: Synthesis in Organic Chemistry, Oxford, United Kingdom, July 2017
- 41st Annual Synthesis Symposium, Bio21 Institute, Parkville, Australia, December 2016.

Chapter 1. Introduction

Carbonylative Cross-Coupling of Organo(pseudo)halides: Origins, Applications and Future Directions

1.1. The Importance of Carbonyl Compounds and Historical Account

The formation of carbon-carbon bonds is at the foundation of organic synthesis. The carbonyl functional group is a versatile synthetic handle that is integral to a plethora of both classical and modern carbon-carbon bond forming reactions (Scheme 1.1.1).[1–10] Its value derives from its own inherent reactivity, subject to nucleophilic attack at carbon and conversely electrophilic attack at oxygen, but also the polarizing effect on neighbouring atoms and functional groups. Moreover, carbonyl containing organic molecules are ubiquitous in nature (e.g. nucleotides, proteins, lipids),[11–14] within pharmaceuticals (e.g. active pharmaceutical ingredients, additives, delivery systems)[15–18] and the material sciences (e.g. polymers, photovoltaics, liquid crystals).[19–22] As such, synthetic methods to access carbonyl derivatives of organic molecules are of fundamental importance to the chemical sciences.

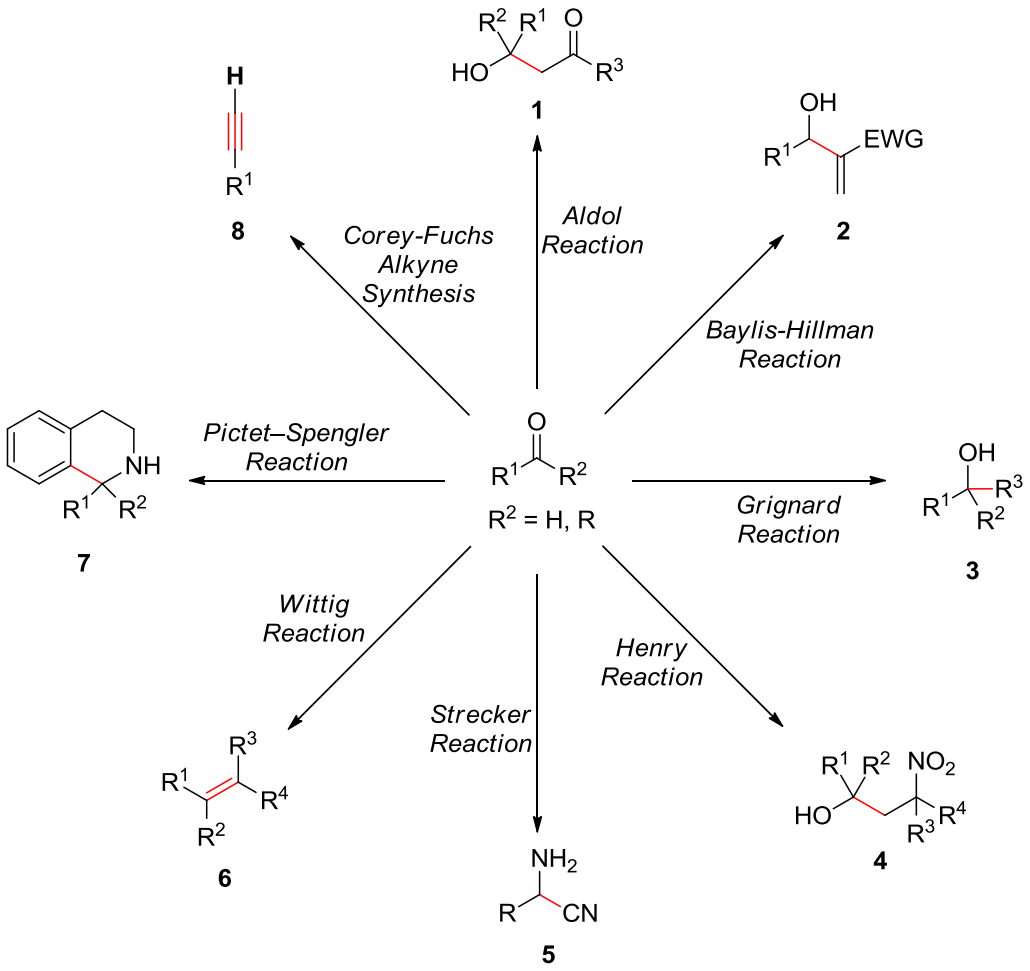

Scheme 1.1.1 Participation of the carbonyl functional group in classical C-C bond forming reactions. The newly formed C-C bond is highlighted in red.

The availability of direct synthetic routes to carbonyl compounds, such as aldehydes, ketones and carboxylic acid derivatives (esters, amides and acyl halides), from non-carbonyl-containing precursors, is not significantly featured in classical literature, despite the vast value of the carbonyl functional group. For example, esters are traditionally accessed by esterification of the corresponding carboxylic acid, anteriorly synthesized through oxidation procedures of relatively poor efficiency and chemoselectivity.[23–28]

The utilisation of carbon monoxide (CO) as a reagent to install a carbonyl group, herein defined as a carbonylation reaction, was established in the early 19th century. Carbonylation is considered an attractive approach to directly access carbonyl derivatives. In this approach, a new C-C bond is formed with introduction of the carbonyl functional group and the carbon number is increased by 1 as molecular complexity is increased. Furthermore, carbon monoxide is considered as an ideal C_1 building-block as it is inexpensive, readily available, derived from biomass and has absolute atom economy; features that was compatible with green chemistry principles and industrialization.[29–32] In 1856, Berthelot described the reaction of carbon monoxide and potassium hydroxide to afford potassium formate.[33] Although this marked substantial progress towards the first practical synthetic procedure for the preparation of formic acid, the use of carbon monoxide as a reagent in organic synthesis received very little attention for the following eight decades. The lack of interest may be attributed to its molecular properties,[31] imparting poor reactivity, thereby providing no practical or economic advantage to carbonyl containing organic compounds derived from natural products.

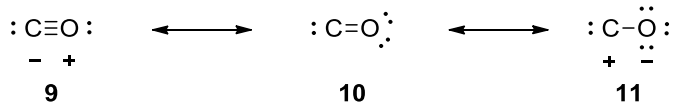

Scheme 1.1.2 Resonance structures of carbon monoxide.

Carbon monoxide is a diatomic molecule that has thee contributing resonance structures (Scheme 1.1.2). It has a large resonance energy of 234 kJ/mol, small electron affinity of -170 kJ/mol and a small dipole moment of 0.122 D with a net partial negative charge on carbon. A short C-O bond length of 112.8 pm and strong bond-dissociation energy of 1072 kJ/mol are consistent with triple bond character. Early approaches addressing

the poor inherent reactivity of carbon monoxide necessitated forcing reaction conditions or the use of stoichiometric energetic reagents and often resulted in the formation of multiple undesired products (Scheme 1.1.3).

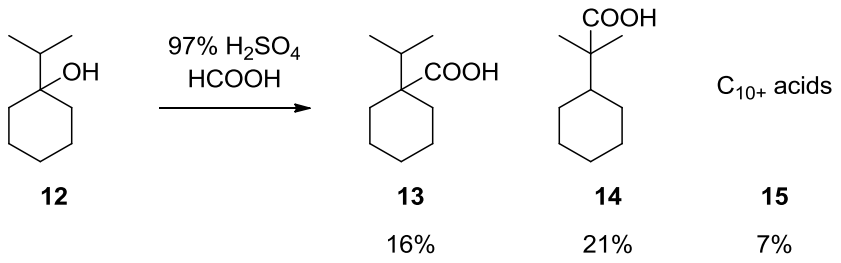

Scheme 1.1.3 Koch-Haaf carbonylation requires the use of a mixture of concentrated sulfuric acid and formic acid to generate CO and the highly reactive carbocation intermediate. Carbocation rearrangement leads to multiple product distribution.[34,35]

The advent of transition metal catalysis effected a paradigm shift in industrial chemistry. Accessible, simple, low-energy chemical feedstocks could be converted into value-added products efficiently and economically. This facilitated new opportunities for feedstocks that previously presented little potential for industrialisation. Spurred by the widespread availability of Producer gas in the early 20th century,[36] a mixture of carbon monoxide, nitrogen gas (N_2) and hydrogen gas (H_2) derived from the incomplete combustion of carbonaceous material, interest in utilising carbon monoxide for chemical synthesis was reinvigorated.[37] In 1938, O. Roelen discovered that a mixture of ethene, CO and H_2 in the presence of cobalt tetracarbonyl hydride $HCo(CO)_4$ gave propanal in high yield.[38] Shortly after, in 1939, Reppe demonstrated that homogeneous nickel carbonyl complexes can catalyse the reaction of olefins with carbon monoxide and a protic nucleophile to yield carboxylic acids and its derivatives.[39] Hydroformylation and hydroxy/alkoxy-carbonylation reactions have subsequently formed the basis of several large-scale industrial processes, most notably the Monsanto process for the manufacture of acetic acid from the reaction of carbon monoxide with methanol catalysed by a Rhodium complex (Scheme 1.1.4).[40] Despite large-scale application in industry since the early 20th century, carbonylation methods were seldom used in academic or complex organic syntheses, where there exists a general reluctance to use to use toxic and flammable gaseous reagents at high pressures and temperatures. CO is particularly hazardous due to its odourless and colourless nature.

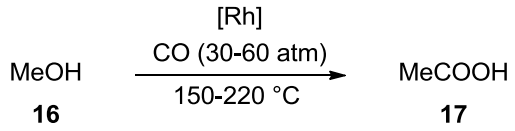

Scheme 1.1.4 The Monstanto Rh-catalysted hydroxycarbonylation of methanol proceeds at high temperature and high CO partial pressure.

The unequivocal importance of palladium-catalysed cross coupling reactions in organic synthesis was signified by awarding the 2010 Nobel Price to Richard F. Heck, Ei-ichi Negishi and Akira Suzuki for their pioneering contributions to the field.[41] A central feature of palladium-catalysed cross couplings reactions is the use of organohalides as widely accessible, bench stable and functionally diverse substrates that are amenable to multistep reaction design. In 1974, Heck and co-workers reported the Pd-catalysed alkoxy- and aminocarbonylation of aryl, benzyl and vinyl halides (Scheme 1.1.5).[42] Carbonylation reactions with palladium organophosphine complexes allowed for greater chemoselectivity. Furthermore, reactions could be performed under practical reaction conditions; temperatures below 180 °C, at atmospheric partial pressures of carbon monoxide, and using easily accessible, bench-stable catalyst precursors which are converted to the active catalytic species *in situ*. The efficiency and robust nature of Pd-catalysed carbonylative cross-coupling methodology as well as chemists' familiarity with cross-coupling protocols, greatly facilitated the uptake of carbonylation as a capability in the synthetic chemists' toolbox. Since the pioneering work by Heck, the Suzuki,[43,45] Hiyama,[44] Stille,[46] Negishi,[47] carbonylative Heck,[48] and Sonogahira[49] cross-coupling transformations of aryl halides have been reported (Scheme 1.1.6).

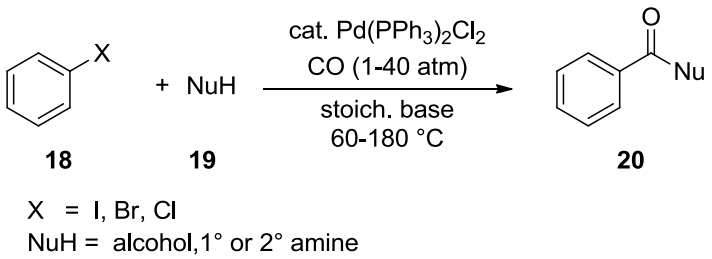

Scheme 1.1.5 Generalised palladium catalysed oxidative carbonylation of aryl halides.

The emergence of Pd-catalysed carbonylative cross-coupling methods enabled synthetic access to a broad range of organic carbonyl-containing products with complex molecular architectures from non-carbonyl-containing precursors. However, limitations, particularly relating to the poor reactivity of alkyl halides, isomerisation,

chemoselectivity, high reaction temperatures, and catalyst efficiency/turnover, needed to be addressed.

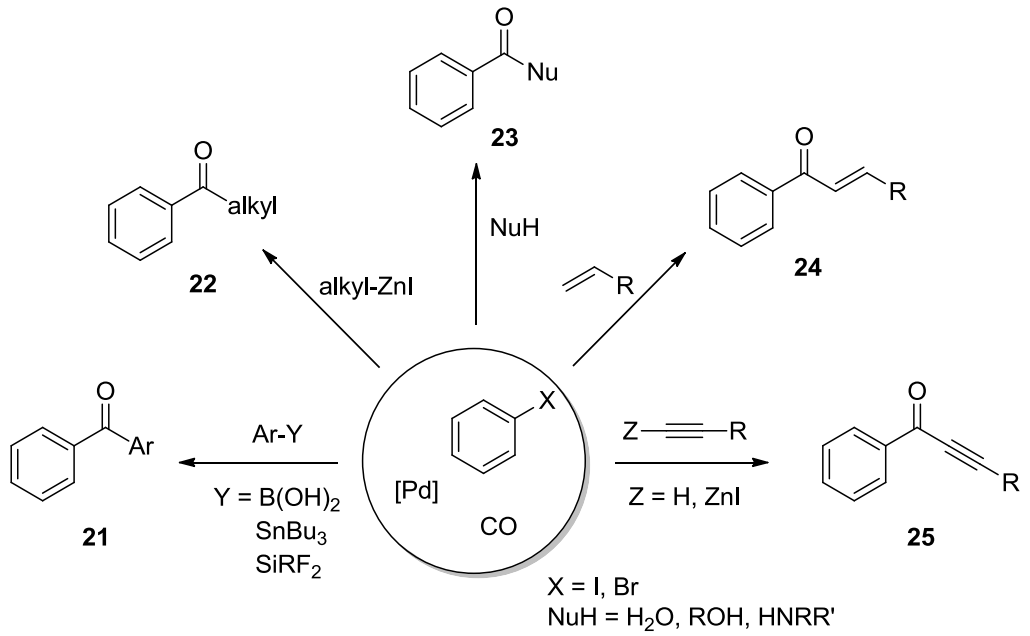

Scheme 1.1.6 The conversion of aryl halides to amides, esters, α,β-unsaturated ketones, alkynols and unsymmetrical ketones from can be realized via Pd-catalysed carbonylative cross-coupling.

1.2. Inherent Limitations in Pd-Catalysed Carbonylative Cross-Coupling

The limitations of Pd-catalysed carbonylation are best exemplified when the mechanism for a generalised oxidative carbonylation catalytic cycle is considered (Scheme 1.2.1). The oxidative carbonylation mechanism can be simplified to six elementary steps: (i) catalyst formation, (ii) oxidative addition, (iii) carbon monoxide coordination, (iv) carbonyl insertion, (v) nucleophilic substitution and (vi) reductive elimination. Thus, Pd-catalysed carbonylative coupling reactions begin with the generation of the active catalytic species. The active species capable of engaging in oxidative addition, is a 14-electron coordinatively unsaturated Pd(0) complex (**27**).[50] This species is generated *in situ* from coordinatively saturated 18-electron Pd-complex **26**. These precatalysts may be Pd(0)-complexes of the type PdL_4 (e.g. $Pd(PPh_3)_4$, PPh_3=triphenylphosphine) where the active catalytic species is generated by spontaneous endergonic deligation.[51] More commonly, the precatalyst is a bench-stable Pd(II)-complex of the type PdL_nX_2 ($Pd(OAc)_2$, $Pd(PPh_3)_2Cl_2$, n=0-2) which are

reduced *in situ* with excess phosphine ligand and base.[52] The active catalytic species is in equilibrium with a number of carbonyl species.[53] Carbonyl ligands deactivate the metal species towards oxidative addition by reducing the electron density of the metal through π back-donation.

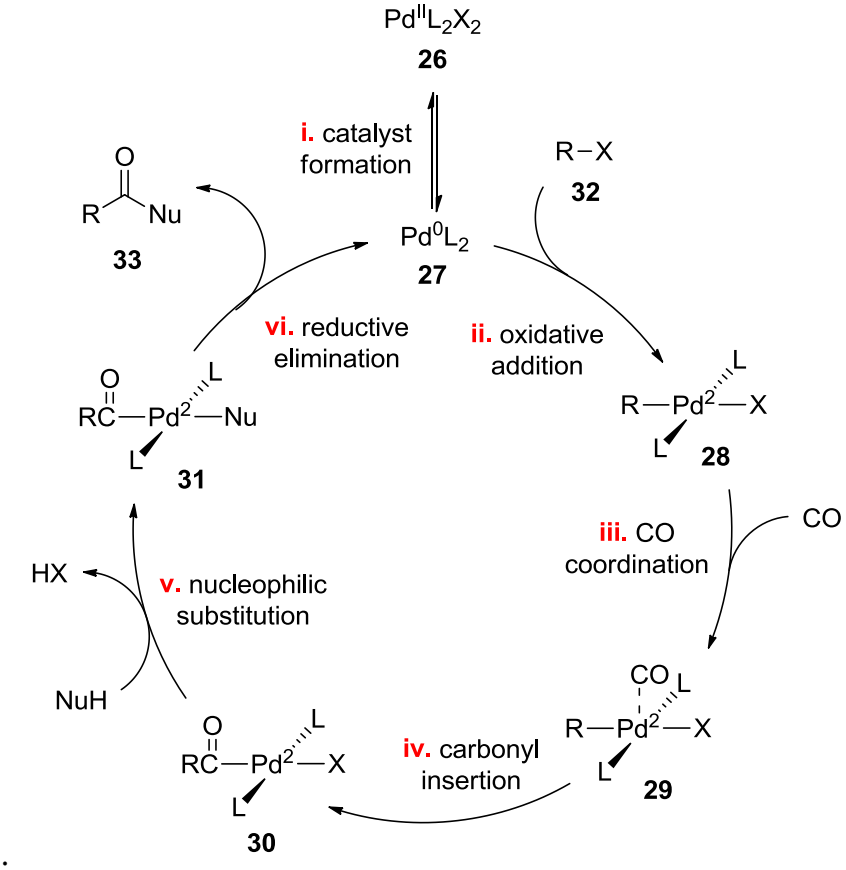

Scheme 1.2.1 Generalised oxidative carbonylation reaction mechanism.

Further, carbon monoxide acts to destabilize the active Pd(0) species, promoting aggregation of Pd(0) and formation of palladium black (an unactivated elemental palladium precipitate).[54] The rate of reaction can be reduced by the diminished availability of the active palladium species by these equilibria and deactivation pathways.

Castanet and co-workers reported that the partial pressure of carbon monoxide was the critical variable reaction parameter for the Pd-catalysed methoxycarbonylation of benzyl chloride (Scheme 1.2.2).[55] The partial pressure of carbon monoxide required precise monitoring to achieve acceptable catalyst turnover frequency (TOF). Pre-treatment of the catalyst precursor, formation of the active catalytic species

$PhCH_2Pd(PPh_3)_2Cl$ in the absence of carbon monoxide, was necessary to prevent catalyst decomposition. In the absence of catalyst pre-treatment, low pressures of carbon monoxide (1 atm) led to the complete inhibition of the carbonylation reaction, formation of precipitated palladium carbonyl species $Pd_3(CO)_3(PPh_3)_4$ and palladium black was observed.

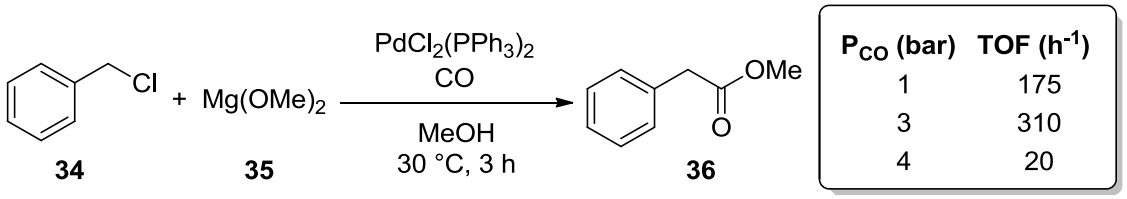

P_{CO} (bar)	TOF (h^{-1})
1	175
3	310
4	20

Scheme 1.2.2 Pd-catalysed methoxycarbonylation of benzyl chloride. Reaction conditions: $Mg(OCH_3)_2$ 18.5 mmol; $PhCH_2Cl$ 52.1 mmol; $PdCl_2(PPh_3)_2$ 0.14 mmol; methanol 25 mL; temperature 30 °C; reaction time 3 h. The reaction mixture was heated at 40 °C for 1 h before introducing CO.

The oxidative addition of organohalides to the Pd(0) under carbonylation reaction conditions species carries many similarities related Pd-catalysed cross-coupling reactions and inherent limitations. The rate oxidative addition of C-X bonds to Pd(0) complex decreases in order of C-I > C-Br >> C-Cl >> C-F.[55] This correlates directly with increasing C-X bond energies and increasing activation energy for the formation of the Pd(II) organometallic intermediate.[56] To facilitate this endergonic reaction step, long reaction times (4-48 h) and reaction temperatures exceeding 100 °C are typically required. Triaryl phosphines are suitable ligands for the carbonylation of aryl iodides and of aryl bromides under forcing conditions.[42,57–59] The large activation energy required for oxidative addition of organobromides, organochlorides and alkyl halides to the Pd(0)-triaryl phosphine complex renders it the rate determining step.[60]

To promote the rate of reaction, increases in election density on palladium centre are necessary to lower the transition energy barrier.[61] Buckwald and co-workers developed a protocol for the aminocarbonylation of aryl bromides using the electron-rich aryl substituted bisphosphane Xantphos as the ligand (Scheme 1.2.3).[62] Excellent reaction yields were obtained at reaction temperatures of 80-120 °C and prolonged reaction times (5-22 h). Further increasing the reaction temperature was not a viable approach to promote the rate of reaction as catalyst stability deteriorated at the elevated temperatures.

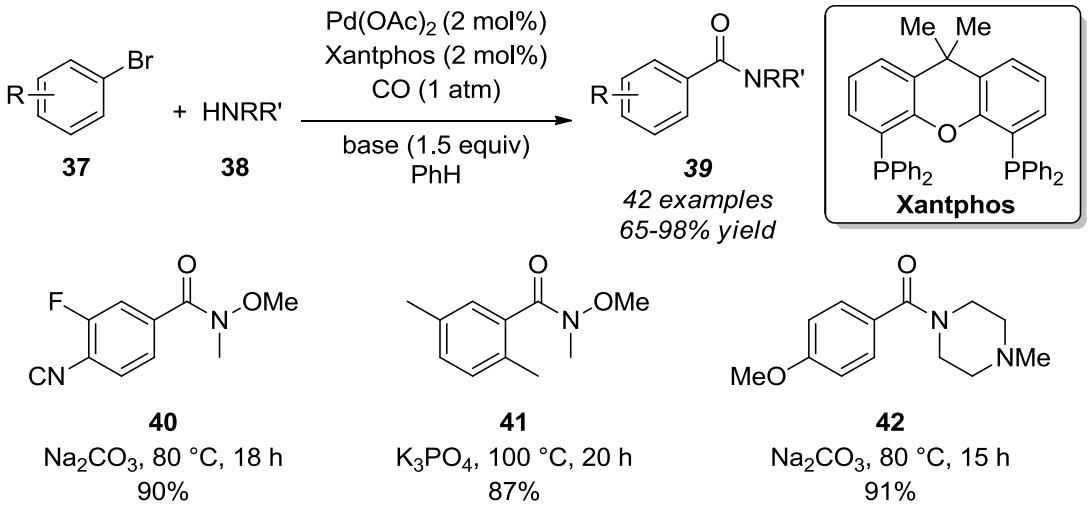

Scheme 1.2.3 Synthesis of benzamides via Pd-catalysed aminocarbonylation.

Milstein and co-worked employed the use of bulky and electron-rich alkyl-substituted bisphosphanes to convert aryl chlorides to carboxylic acid derivatives in high yields (Scheme 1.2.4).[63] Whilst bisphosphane **45**, bis(diisopropylphosphino)propane (d^{i}ppp), enabled facile oxidative addition of aryl chlorides to palladium, high reaction temperatures (150 °C) and long reaction times (20 h) were still required as the subsequent carbonylation elementary reactions are favoured by less electron density on palladium.[64] The C-F bond energy is sufficiently large that the Pd-catalysed carbonylation of organofluorides has not been realized.

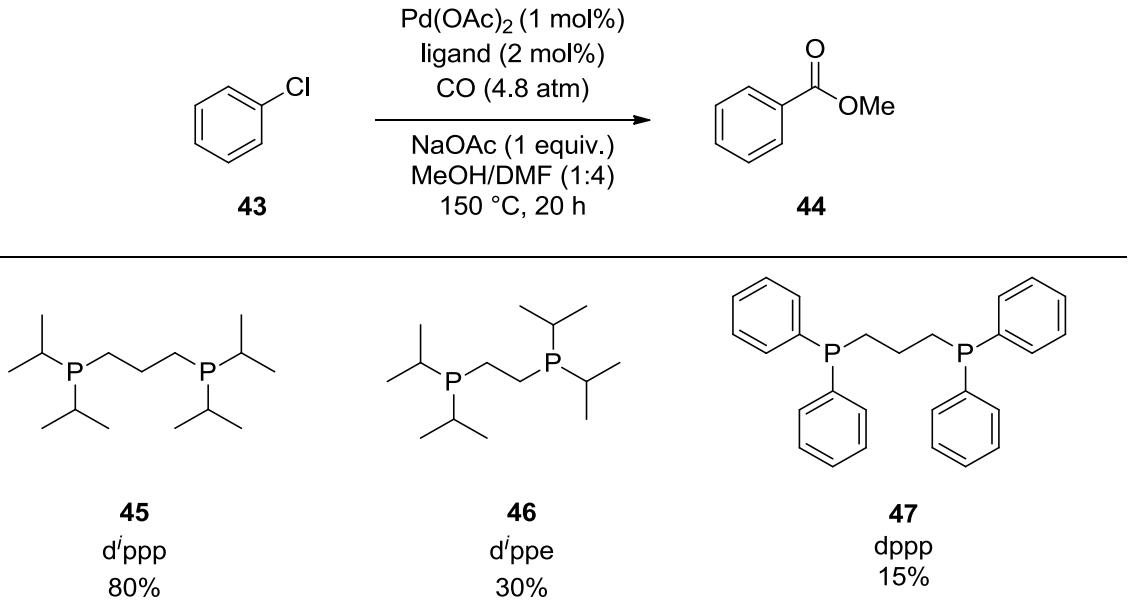

Scheme 1.2.4 Influence of ligand selection on the reactivity of chlorobenzene towards methoxycarbonylation.

Prior to carbonyl insertion, carbon monoxide must be introduced to the coordination sphere of the Pd-complex is a *cis* arrangement relative to the acyl precursor. The regioselctivity of carbon monoxide coordination, appropriate for cross-coupling is highly depended on the steric environment surrounding the palladium centre. For sterically unhindered Pd-complexes, carbon monoxide ligation is rapid.[65] Bernard investigated the reductive carbonylation of sterically hindered aryl halides with Et_3SiH as the hydrogen donor (Scheme 1.2.5).[66] In the presence of catalytic [1,2-bis(dicyclopentylphosphino)ethane]dichloropalladium(II) (d^cppe), quantitative conversion of 2-iodo-*m*-xylene (**48**) was observed yielding xylene (**50**) as the major product. Similar results were obtained with 2-bromo-*m*-xylene, indicating that oxidative addition was not the rate limiting step. This illustrates the potential for substrates to hinder the rate of carbonyl coordination and insertion by blocking access to coordination sites thereby providing the potential for unwanted reaction pathways.

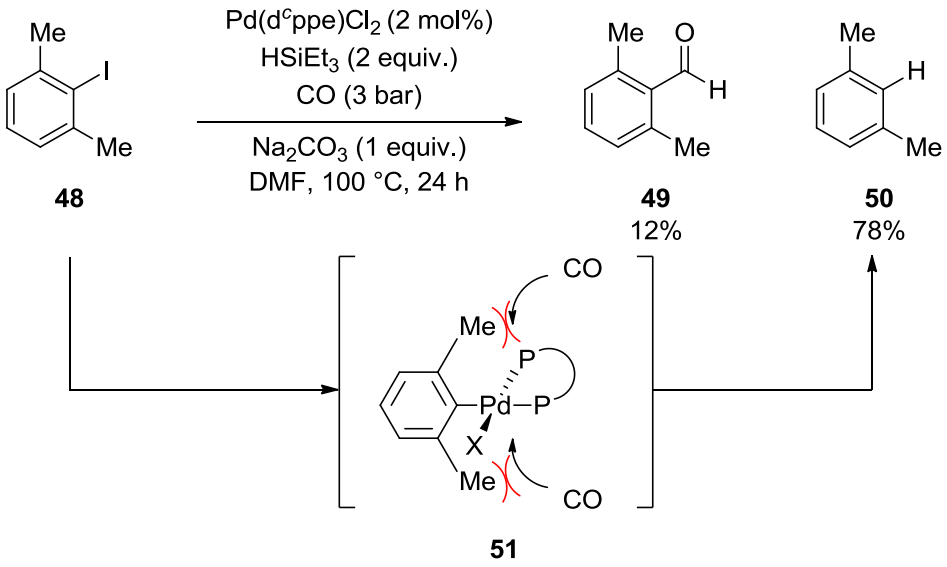

Scheme 1.2.5 Steric influence on reductive carbonylation of *ortho*-disubstitued aryl halides.

Where carbon monoxide binding was the rate limiting step and oxidative addition of the aryl halide to Pd(0) complex is facile, Yamamoto and co-workers demonstrated higher pressures can be utilised to promote carbon monoxide coordination (Scheme 1.2.6).[67] At high pressures, selectivity for the doubly carbonylated α-keto amide product **54** was achieved.

Following coordination of carbon monoxide to palladium, migratory insertion of the *cis* coordinated carbon monoxide to the Pd-aryl bond affords the phenylacylpalladium complex. Migratory insertion is reversible.[68,69] The rate of decarbonylation is greater for substrates bearing electron-withdrawing substituents than electron-donating substituents.[65] Thus, in instances where migratory insertion is the rate determining step, electron-poor organohalides will react slower then electron-rich substrates. In contrast, the rate of oxidative addition increases as the Hammett substituent constant increases.[51,70]

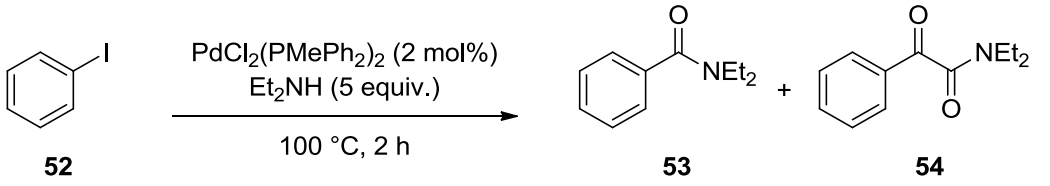

52 **53** **54**

P_{co} (atm)	total yield	product ratio (mono:bis)
5	33%	52:48
10	43%	39:61
47	100%	17:83

Scheme 1.2.6 Influence of CO pressure on the double carbonylation of iodobenzene.

The use of non-activated alkyl halides as electrophilic coupling partners for C(sp^3)-C bond forming reactions remains a major challenge. The propensity of the alkylpalladium species to undergo β-hydride elimination results in undesired isomerisation, hydrodehalogenation and elimination products.[71] The alkyl halide C(sp^3)-X bond is more electron-rich than the C(sp^2)-X bond in aryl and vinyl halides. This results in slow oxidative addition of alkyl halides relative to their analogous aryl and vinyl counterparts (rate of oxidative addition of organohalides to $Pd(PPh_3)_4$: vinyl-X > aryl-X > benzyl-X >> alkyl-X).[72] Bulky and electron rich ligands can be employed to promote oxidative addition at the expense of selectivity since decarbonylation and β-hydride elimination are promoted. Examples of Pd-catalysed $2e^-$ carbonylative cross-coupling reactions with unactivated alkyl halides are sparse and limited to examples where selectivity for CO insertion over β-hydride elimination is biased through the use of high pressures of carbon monoxide.[73]

Product formation may occur by direct nucleophilic attack at the acyl carbon or by initial bonding of the nucleophile to palladium followed by reductive elimination. Recent density functional theory (DFT) computational mechanistic studies support the

latter.[42,74] The nucleophile competes with the ligand and carbon monoxide for a coordination site *cis* to the acyl group. Carbon monoxide can deactivate the complex towards reductive elimination through formation of polynuclear carbonyl species.[53] Owing to steric factors, carbonylation with bulky nucleophiles, such as amines containing *tert*-butyl functionality, is inhibited. This is even more challenging for deactivated substrates where bulky, bidentate ligands are required. Arndtsen and co-workers utilised dimethylaminopyridine (DMAP) as the nucleophilic coupling partner to first generate a electrophilic aroyl-DMAP salt (Scheme 1.2.7).[75,76] Subsequent reaction with a sterically hindered proctic amine afforded the amide product. This approach necessitates multiple steps and the use of super-stoichiometric aryl chloride, thereby eroding atom economy.

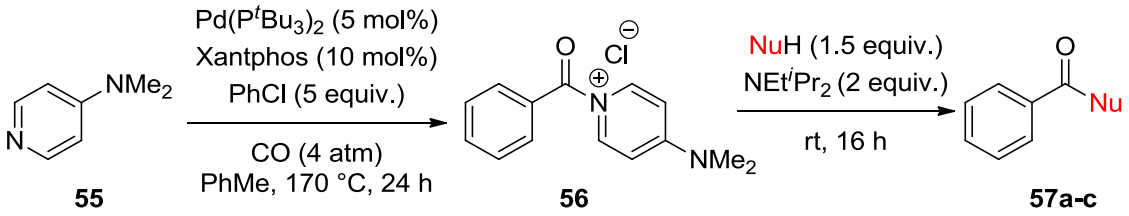

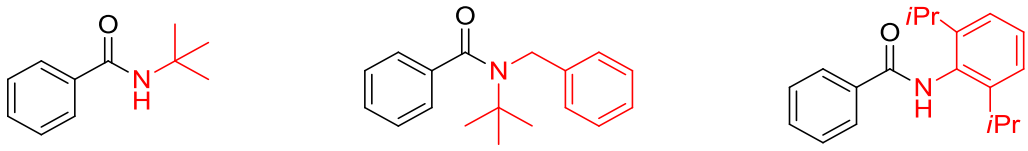

57a 77%

57b 54%

57c 75%

Scheme 1.2.7 Aminocarbonylation of bulky amines via aroyl-DMAP salts.

The versatility of Pd-catalysed cross-coupling methodology is enabled by the facile coordination of Pd(II) complexes to a diverse range of functional groups (alkenyl, alkynyl, boronate, silyl, amino, alkoxy). This inherent reactivity, however, often gives rise to poor chemoselectivity when multiple reactive functionality is present. Trzeciak demonstrated that achieving selective alkoxycarbonylation of aryl halides in the presence of an organoborane is challenging; selectivity favours the carbonylative Suzuki reaction (Scheme 1.2.8).[77]

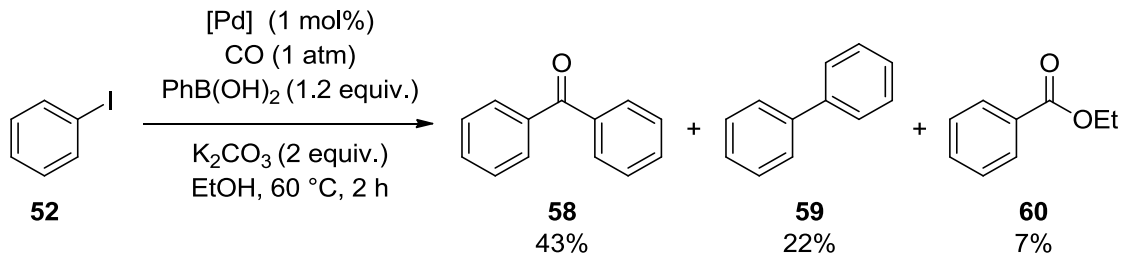

Scheme 1.2.8 Carbonylative Suzuki synthesis of unsymmetrical ketones in ethanol.

Base promoted reductive elimination is the final step in the catalytic cycle, affording the carbonylated product and regeneration of the active catalytic species. The requirement of stoichiometric base in conjunction with high reaction temperatures and long reaction times impairs functional group tolerance.

Since the pioneering work of Heck and co-workers, carbonylative cross-coupling methodology has been widely incorporated in industrial process and natural product synthesis.[78–80] Limitations relating to the chemoselectivity, functional group tolerance, β-hydride elimination, high reaction temperatures, and catalyst efficiency/turnover needed to be addressed. The limitations discussed (*vide supra*) are inherent to Pd-catalysed carbonylative cross coupling, resultant from an organopalladium species as the key intermediate in each step of the catalytic cycle. Future progress towards addressing these challenges rests with ligand design, however, the complex interplay of carbon monoxide and the uncontrolled formation of metal-carbonyl species, many of which are transient, preclude establishment of structure-activity relationships.

It is therefore imperative to move in an alternate, yet parallel, direction which is not confined by the inherent limitations present in $2e^-$ Pd-catalysed carbonylation chemistry. To streamline reaction design through deconvolution of the relationship between carbon monoxide pressure, ligand concentration and reaction kinetics is desirable.

1.3. Free-Radical Carbonylation

Free-radical carbonylation is an alternative and complementary organohalide carbonylation strategy to Heck carbonylation. Free-radical carbonylation proceeds via

single electron transfer (SET) processes; mechanistically unrelated to Pd-catalysed carbonylation and therefore does not share common inherent limitations.[81,82] The key intermediates of free-radical carbonylation are the carbon-centred radical **61** and acyl radical **62** (Scheme 1.3.1).[83–85] Reaction products and selectivity can be predicted from a wealth of knowledge on free-radical reactions and kinetics.

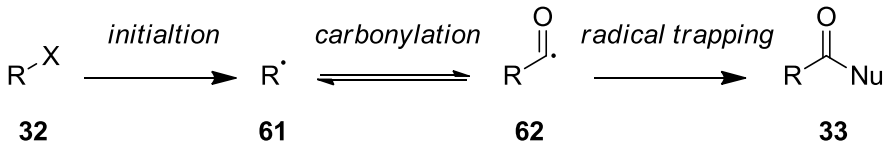

Scheme 1.3.1 Simplified free-radical carbonylation reaction mechanism.

In 1939, Faltings reported the reaction of carbon-centred radicals with carbon monoxide.[86] The formation of acetone was observed when a mixture of ethane and carbon monoxide was irradiated with ultraviolet (UV) light. In 1952, researchers at DuPoint, described the formation of polyketones by peroxide-initiated copolymerization of ethene and carbon monoxide and proposed the acyl radical as a key intermediate.[87] Early free-radical carbonylations were of limited synthetic utility and failed to attract the attention of synthetic chemists which is attributed to the low yields and extreme pressures employed, often in excess of 1000 atm.[88–91] The development of free-radical chemistry in the 1980s, saw a resurgence in free-radical carbonylation and, of particular importance, the development of free-radical carbonylation of organohalides.

Ryu and co-workers described the first efficient trapping of carbon-centred radicals by carbon monoxide (Scheme 1.3.2).[92] Alkyl, vinyl and aryl halides could be formylated employing tributyltin hydride (TBT) as the hydride donor and catalytic quantities of 2,2'-azobis(isobutyronitrile) (AIBN) as a thermal radical initiator. Notably, alkyl aldehydes could be synthesised without competitive isomerisation or elimination products. High carbon monoxide pressures (65-80 atm) were required to prevent the premature reduction of the alkyl halide by tin hydride and to supress decarbonylation. The use of tris(trimethylsilyl)silane (TTMSS), which is less reactive towards primary alkyl radicals compared to tributyltin hydride, allowed for carbon monoxide pressures below 20 atm.[93] Higher pressures were required to transform secondary and tertiary alkyl radicals into ketones in acceptable yields.

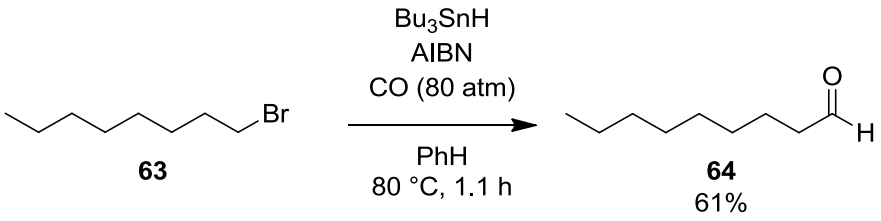

Scheme 1.3.2 Free-radical carbonylation of *n*-bromooctane.

Ryu and co-workers extended the above protocol to the three component coupling of alkyl and vinyl halides, carbon monoxide and activated alkenes to afford unsymmetrical ketones.[93] Vinyl radicals, which are more prone to hydrogen abstraction from tributyltin hydride than alkyl radicals,[94] were readily carbonylated to afford α,β-unsaturated ketones using TTMSS (Scheme 1.3.3) whereas attempts mediated by tributyltin tin were unsuccessful.

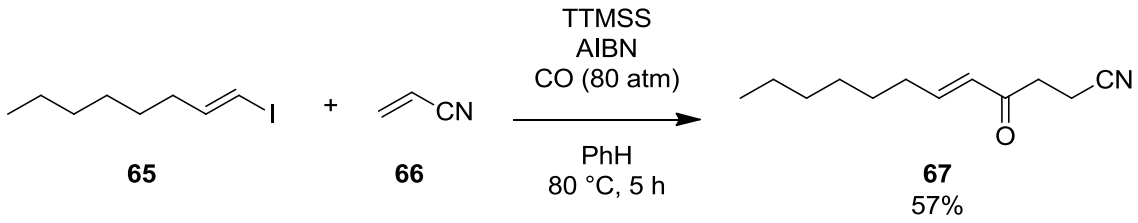

Scheme 1.3.3 Free-radical carbonylative ketone synthesis.

An alternate approach was taken to generate the carbon-centred radical avoiding thermal initiators and toxic radical mediators that could act as hydrogen donors. Ryu and co-workers reported the photolytic homolysis of alkyl iodides using a 500 W xenon lamp and stoichiometric base to afford esters and amides from alcohols, and amines, respectively (Scheme 1.3.4).[95,96] This reaction proceeded at room temperature and CO pressures below 50 atm. The reactions of primary alkyl iodides were slow and low yielding. Ryu has since coined this class of reactions as Atom Transfer Carbonylation (ATC) (Scheme 1.3.5).[97] In this approach, acyl iodides are generated *in situ* from acyl radicals and carbonyl derivatives can be accessed via ionic nucleophilic substitution reactions. This was applied to realize the photochemical aminocarbonylation of aryl iodides with carbon monoxide and amines. High pressures (70 atm) of CO were required to prevent hydrogen abstraction and quenching of the aryl radical. Due to the increased stability of C-Br bond, ATC methodology could not be extended to organobromides.

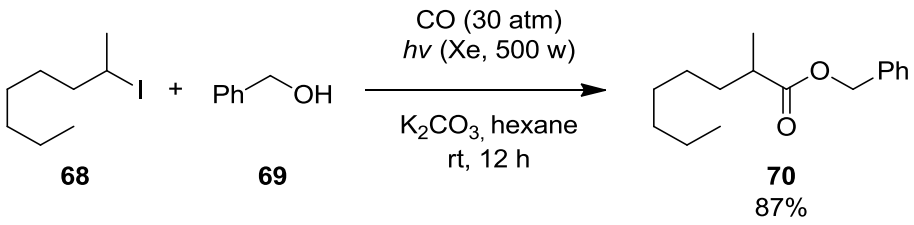

Scheme 1.3.4 Photochemical free-radical alkoxycarbonylation.

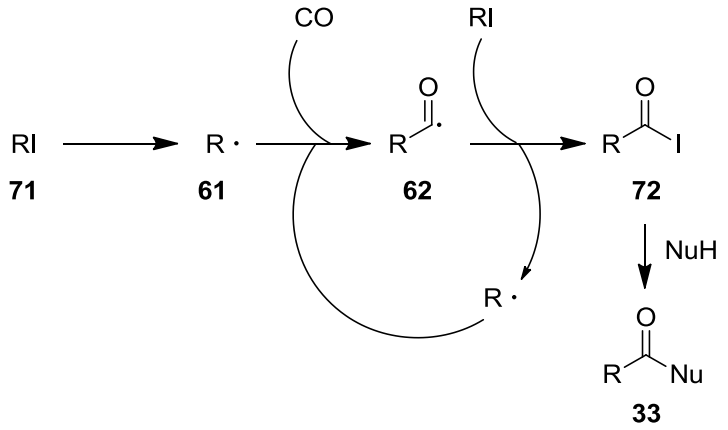

Scheme 1.3.5 Atom Transfer Carbonylation reaction mechanism.

Suzuki and co-workers reported on the palladium-catalysed carbonylative cross-coupling reaction of alkyl iodides with 9-alkyl-9-borabicyclo[3.3.1]nonane (9-alkyl-9-BBN) derivatives was accelerated by irradiation with 100 W unsmoked tungsten light (Scheme 1.3.6).[98] They proposed the reaction proceeded via a radical mechanism where a coordinatively unsaturated palladium complex facilitated the electron transfer to an alkyl halide to generate a radical pair ($Pd^{I}X$ + R·) with subsequent collapse to form the oxidative adduct (RPdX).

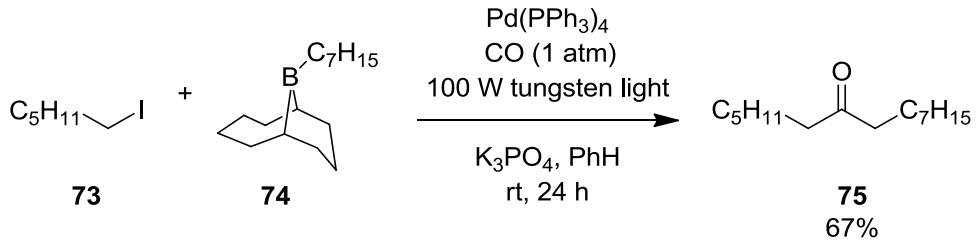

Scheme 1.3.6 Palladium-catalysed carbonylative cross-coupling accelerated by visible light.

Ryu, inspired by the work of Suzuki, reported that catalytic palladium accelerated Atom Transfer Carbonylation. The alkoxycarbonylation of primary alkyl iodides proceeded within 16 hours to afford alkyl benzoates in excellent yields (Scheme 1.3.7).[99] The

scope of palladium accelerated ATC methodology has been broadened to analogous variants of the carbonylative Heck, Sonogahira and Suzuki cross-coupling transformations (Scheme 1.3.8). [100–102]

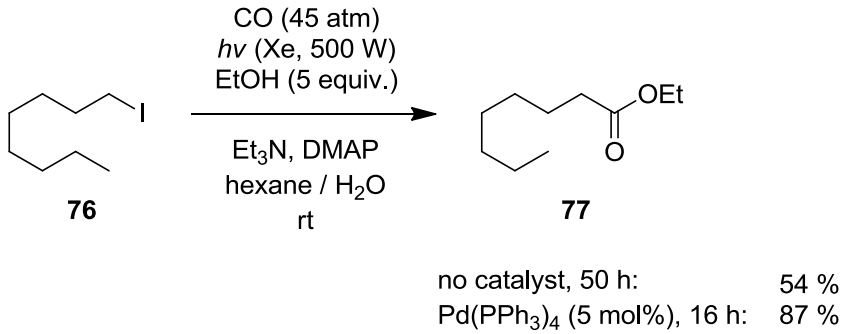

Scheme 1.3.7 Acceleration of photo-induced ATC reaction by palladium-catalysis.

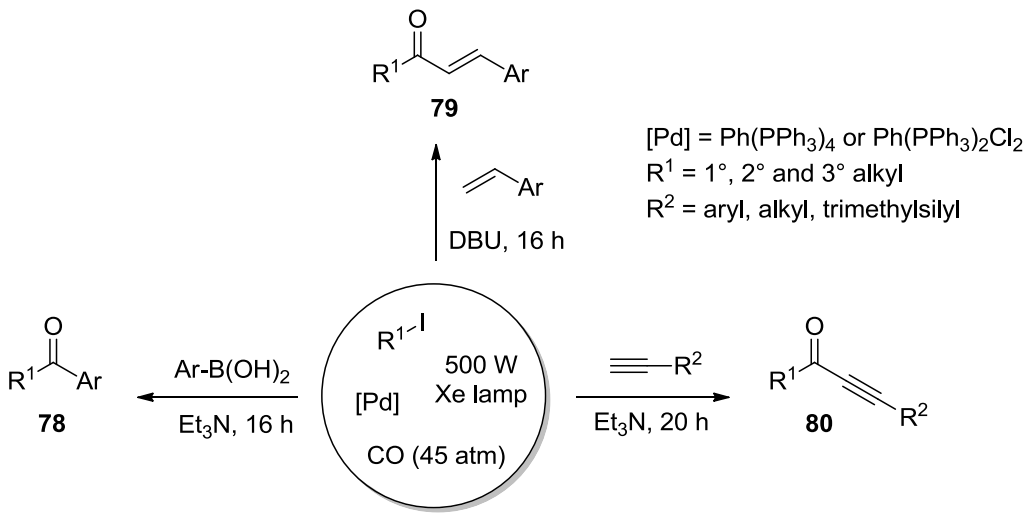

Scheme 1.3.8 Scope of the Pd/light accelerated ATC of alkyl iodides.

In 2012, Lei and co-workers reported the first transition metal free alkoxycarbonylation of aryl halides.[103] The use of 40 mol% of 1,10-phenanthroline as the initiator and potassium *tert*-butoxide was critical to this approach. *Tert*-butoxide acted as both the reducing agent and the nucleophile. A redox mechanism was proposed, initiated by a single electron reduction of the aryl halide to generate the aryl radical. Although this work was a significant milestone in transition metal free-radical carbonylation of aryl halides, the reaction scope was narrow and restricted to superstoichiometric potassium *tert*-butoxide as the nucleophilic coupling partner. To-date, the development of free-radical carbonylation had been limited by the selective generation of radical species.

Functional group compatibility was of concern as only robust functionality was compatible with the developed organostannane and high energy photolytic reaction conditions.

The emergence of visible light photoredox catalysis has provided an exciting new avenue for the selective and efficient generation of carbon-centred radicals under mild reaction conditions.[104–107] Visible light photoredox catalysis employs catalytic quantities of a light-sensitive photocatalyst (PC), typically a transition metal complex or organic dye. Upon excitation with visible light, these catalysts can mediate the transfer of electrons between chemical compounds through SET processes.

Photoactive transition metal complexes and organic dye materials have found numerous applications in materials and inorganic chemistry.[108–110] The potential of these materials as single electron photoredox catalysts in organic synthesis has only recently been recognised. The most commonly employed visible light photoredox catalysts are polypyridyl complexes of ruthenium or iridium, or xanthene derived organic dyes. Absorption of a photon in the visible region by the photocatalyst in its ground state generates a high-energy singlet state that undergoes rapid intersystem crossing (ISC) to the lowest energy triplet state (Figure 1.3.1).[111] The triplet state is long lived as unimolecular deactivation to the singlet ground state by phosphorescence is spin-forbidden.

This triplet state is the photoexcited species that engages in biomolecular outer sphere electron transfer. The photoexcited species is both more reducing and more oxidising than the ground state species. Due to its duplicity, the photoexcited species may proceed by oxidative or by reductive quenching (Scheme 1.3.9).

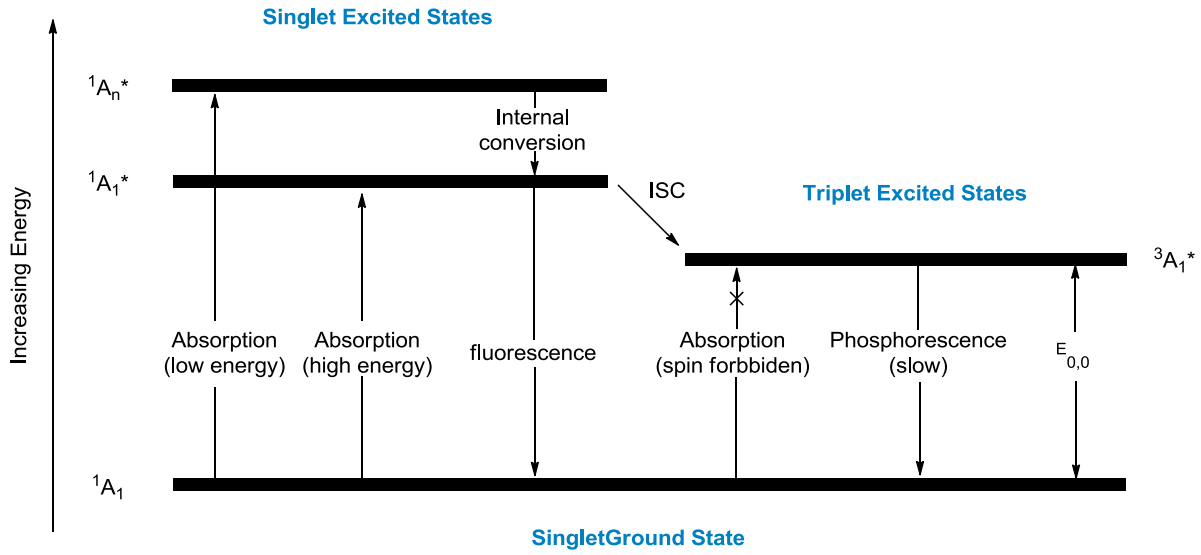

Figure 1.3.1 Generalised Jablonski diagram for a photoredox catalyst.

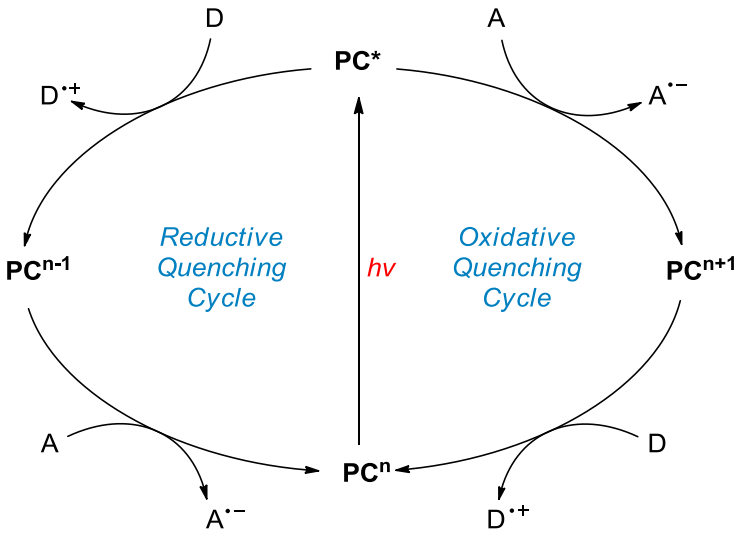

Scheme 1.3.9 Generalised oxidative and reductive quenching cycles of a photocatalyst. Photocatalyst (PC), electron acceptor (A), electron donor (B), oxidation state (n).

In the oxidative quenching cycle, the excited photocatalyst, **PC***, functions as reductant to produce the oxidised form of the photocatalyst $\mathbf{PC^{n+1}}$. This oxidised photocatalyst is a potent oxidant and may be reduced to return it to the ground state **PC**. The compound that quenches the excited photocatalyst through catalyst oxidation is said to be an oxidative quencher. Alternatively, the excited photocatalyst may proceed via a reductive quenching cycle. In the reductive quenching cycle, the photocatalyst is reduced at the first SET event then oxidised at the second SET to return it to its ground state.

The success of visible light photoredox catalysis can be attributed to the ability to tune the redox potentials of the catalyst.[111] Judicious pairing of catalyst and substrate can be used to control which quenching cycle follows excitation of the photocatalyst. To quantify the relative reductive and oxidative potentials of compounds it is convenient to describe the potential associated with an electrochemical half reaction ($E_{1/2}$), referenced to the saturated calomel electrode (SCE).

In 2015, the groups of Jacobi von Wagelin and Xiao simultaneously reported the first application of visible light photoredox catalysis to carbonylative cross-coupling.[112,113] Concerned about the possibly of deactivation of transition metal based catalysts via coordination of carbon monoxide, the xanthene based organic dyes eosin Y (Figure 1.3.10 a) and fluorescein (Figure 1.3.10 b) were employed as the catalytic photosensitizer. Owing to the relatively lower oxidation potentials compared to transition metal complexes, aryl diazonium salts were employed as the aryl radical precursor. Benzoate esters could be generated via coupling of the aryl diazonium salts with a variety of primary, secondary and tertiary alcohols at room temperature using low energy light-emitting diodes (LEDs) and high carbon monoxide pressure. The mild reaction conditions enabled compatibility with a diverse range of functional groups.

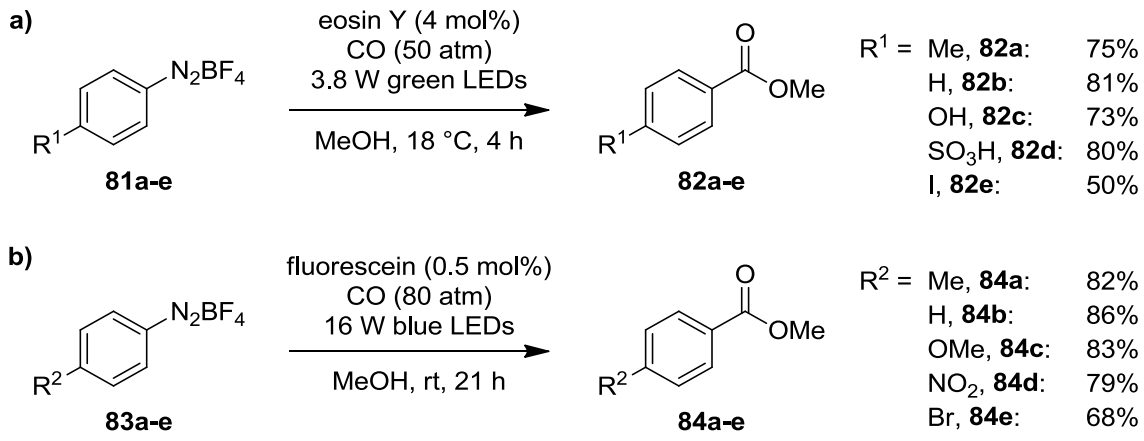

Scheme 1.3.10 Visible light photoredox carbonylation catalysed by a) eosin Y b) fluorescein.

The proposed reaction mechanism (Figure 1.3.11) involved the single election reduction of the aryl diazonium salt **85** by the photoexcited dye **PC***, to generate the aryl radical **86** and the oxidised dye radical cation $\mathbf{PC}^{+\bullet}$**.** The aryl radical is then trapped by CO to generate the benzoyl radical intermediate **87**. Single electron oxidation of the benzoyl

radical by the oxidised dye radical cation results in the regeneration of the photocatalyst **PC** and the formation of the acylium ion **88**. Reaction of the acylium ion with the alcohol affords the benzoate ester **89**. The developed methodology provided significant improvements over previous free-radical carbonylations, avoiding the use of high-pressure mercury or xenon lamps and toxic AIBN/TBT protocols. Notably, base was not required to promote the reaction.

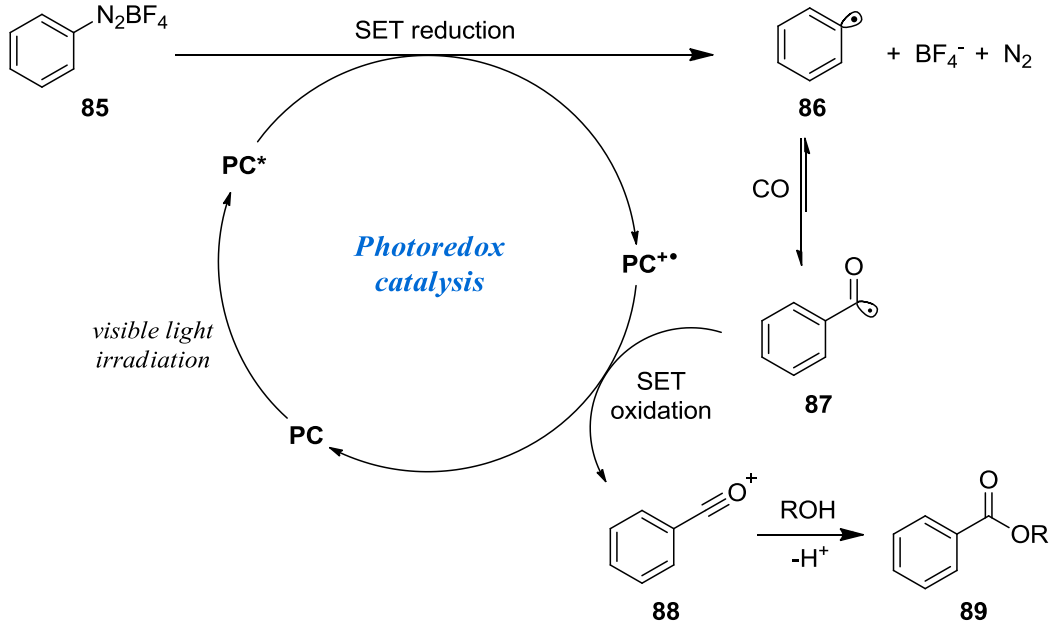

Scheme 1.3.11 Mechanism of visible light photoredox-catalysed carbonylation of aryldiazonium salts. PC denotes photocatalyst.

Gu and co-workers utilized the visible light photoredox carbonylation manifold for the synthesis of unsymmetrical biaryl ketones (**92**).[114,115] They proposed the acylium ion generated under photocatalytic condition could be reacted with a suitable π-nucleophile (Scheme 1.3.12). With catalytic eosin Y, under anhydrous reaction conditions and promoted by green LEDs, aryl diazonium tetrafluoroborates (**90**) carbonylatively cross-coupled with electron rich aromatics (**91**) in moderate to excellent yields. As no pre-functionalization of the π-nucleophile coupling partner is required; this represents an attractive alternative to the carbonylative Suzuki reaction.

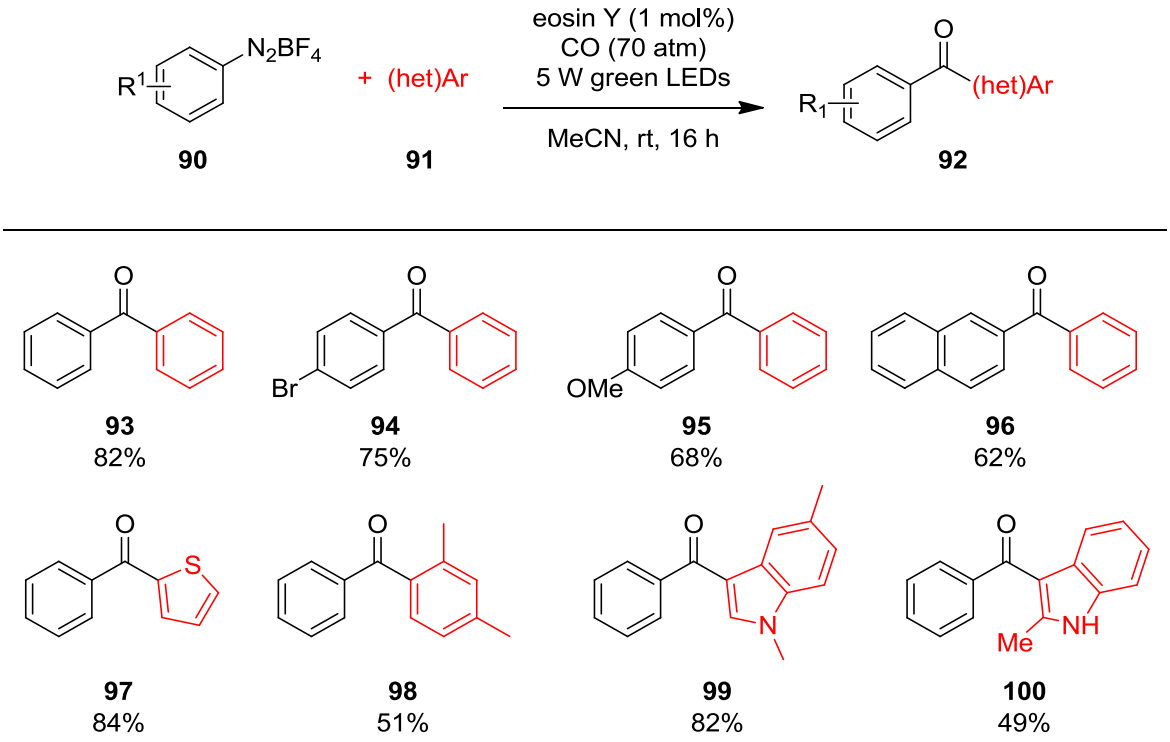

Scheme 1.3.10 Access to unsymmetrical ketones and functionalized indoles via visible light photoredox carbonylation.

Of particular interest to the development of visible light photoredox-catalysed carbonylations of organohalides are photoredox catalysed reductive dehalogenations. These reactions generate a carbon-centred radical from an organohalide by the single electron reduction induced homolysis of the carbon-halide bond. Early works in this field employed $Ru(bpy)_3Cl_2$ as the photoredox catalyst. Due to the limited ability of $Ru(bpy)_3(Cl)_2$ to act as a single electron reducing agent, the substrate scope was limited to activated iodides and bromides.[116–118]

Stephenson and co-workers made a considerable contribution to the field when they employed catalytic amounts of *fac*-tris[2-phenylpyridinato-C2,N]iridium(III) (*fac*-$Ir(ppy)_3$) for the reductive dehalogenation of unactivated alkyl, alkenyl and aryl iodides (Scheme 1.3.11).[119] The use of tributylamine in combination with Hantzsch ester or formic acid was necessary as the stoichiometric reductant. Excellent functional group tolerance was observed towards benzyl ethers, silyl ether, free alcohols, acetals, lactones, esters, aryl bromides, aryl chlorides, distal olefins, sulphonamides, tosylates and carbamates.

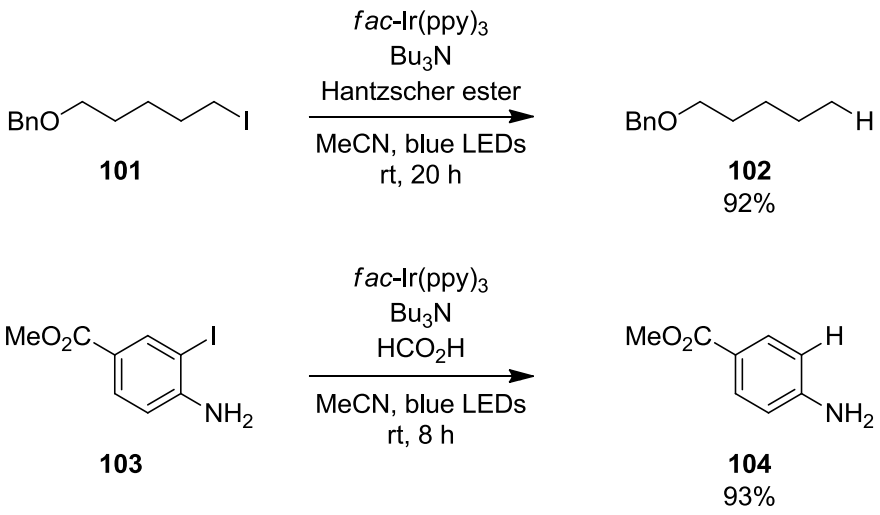

Scheme 1.3.11 Visible light photoredox-catalysed reductions of unactivated alkyl iodides and aryl iodides.

In 2016, Odell and co-workers reported the *fac*-Ir(ppy)$_3$-catalysed free-radical aminocarbonylation of unactivated alkyl iodides (Scheme 1.3.12).[120] The reaction proceeded at low pressure and with broad amine scope. Secondary alkyl iodides reacted efficiently whereas primary and tertiary alkyl iodides gave poor yields. Significantly, this represented the first merger of photoredox catalysis and organohalide carbonylation.

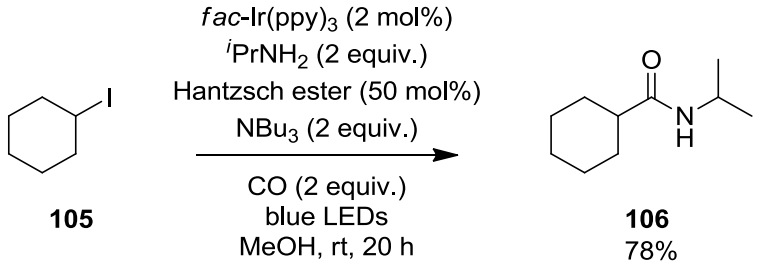

Scheme 1.3.12 Visible light photoredox-catalysed aminocarbonylation of cyclohexyliodide.

Since the pioneering work by Ryu, significant progress towards addressing the limitations of traditional Pd-catalysed carbonylative cross-coupling has been made. Most notably, alkyl halides can be employed as the electrophilic coupling partner without β-hydride elimination. The development of photochemical activation of organohalides enables these reactions to proceed efficiently at ambient temperature. Photocatalyst activity appears to be independent of carbon monoxide concentration. The ability of carbon monoxide to drive reaction kinetics is straightforward, more

pressure is better, and has clear advantages for reaction design. The application of visible light photoredox catalysis has broadened the scope of free-radical carbonylative reactions by facilitating single electron transfer processes under benign reaction conditions, however, there is still significant progress to be made. The use of energy demanding substrates, such as aryl halides, remains underdeveloped. Reaction times are quite long, on the hour scale, comparable to those of Pd-catalysed carbonylation. The high carbon monoxide pressures required necessitates the use of an expensive specialized autoclave apparatus. These capabilities are beyond those of a typical synthesis laboratory. Further, there exists a general reluctance to use toxic flammable reactive gases under pressure, the hazards of which are intensified by scale.

1.4. Flow Chemistry – Enabling Photochemical and Gas-Liquid Transformations

Photochemical transformations of reactive gases, where the photon can be considered as a reagent, encounter several challenges in conventional batch reactors. One limitation is the uneven distribution of photons throughout the reaction mixture. The attenuation effect of photon transport (Lambert-Beer law) can result in photons not penetrating past the first few millimetres of reaction mixture. Photochemical transformations in batch reactors, where the surface area to volume ratio is low, are often reaction rate limited by irradiation efficiency and performance upon scale-up is significantly impeded.[121]

In the batch regime, the chemical reactor is a batch reactor. The reagents are charged into the reactor, well mixed, and undergo reaction for a certain period (defined as the reaction time), then discharged. The use of continuous flow processing to perform chemical reactions is known as ‘flow chemistry’ (also known as ‘continuous flow’). Flow chemistry is an alternative approach to the batch regime for chemical synthesis. In flow chemistry, a chemical reaction is run in a continuously flowing stream. A defining feature of flow chemistry is the chemical composition is a function of its longitudinal position in the reactor. This is directly opposite to an idealized batch reactor, where composition is a function of time and does not feature macroscopic transfer of fluid.[122]

In flow chemistry, pumps are used to continuously deliver reagents from a reservoir (Figure 1.4.1). This could be single pump, or there could be several where the streams meet and mix in a mixing zone. The reagents are then delivered to the reactor. These reactors can be of tubular design constructed of inert fluoropolymer or be can chip based with very sophisticated fluidic pathways and geometry. The reactor may be subjected to manipulation like the batch regime, including heating, microwave irradiation, light irradiation, cooling and ultrasound. Flow chemistry enables the precise control of process conditions which is facilitated by high reactor surface area to volume ratio allowing rapid heat and mass transfer to occur. Following reaction additional manipulations may be performed such as quenching, prior to collection.

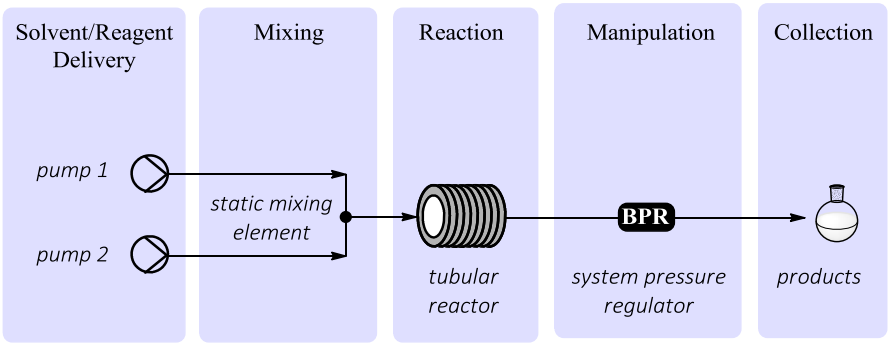

Figure 1.4.1 Schematic of a continuous flow microreactor system.

There are numerous examples demonstrating the ability of flow chemistry to assist in photochemical transformations.[123,124] The high surface area to volume ratio of continuous flow microreactors allow for the entire reaction solution to be homogenously irradiated. Typically, greater selectivity and shorter reaction (residence time, t_r) times, in the range of an order of magnitude, are observed when compared to the corresponding batch system and facile scaling can be achieved through conventional flow chemistry scaling strategies.

Another limitation of conventional batch reactors arises due to inefficient interfacial contact area between the liquid and gas phase, leading to poor mass transfer and reduced performance. High pressures are often required to drive the transfer of gaseous reagents into the liquid reaction phase. Owing to the difficulty of handling gases under high pressure, such reactions are often avoided in research laboratories.

Buchwald and Jensen demonstrated that the mass transfer limitations associated with performing biphasic carbonylation reactions using conventional techniques could be addressed by employing flow microreactors (Scheme 1.4.1).[125] In contrast to conventional benchtop reactions at atmospheric pressure,[42] where the amide product is exclusively obtained, aminocarbonylation performed in the microreactor produced the double carbonylated α-ketoamide **110** along with the amide **109**. High selectivity for the α-ketoamide could be obtained control by further increasing CO pressure. The formation of the double carbonylated product was attributed to superior gas-liquid contact area.

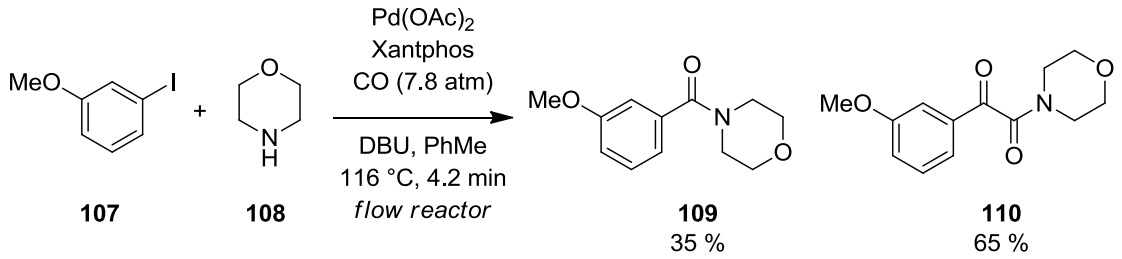

Scheme 1.4.1 Aminocarbonylation of 3-iodoanisole in a continuous flow microreactor.

Csajági and co-workers reported the development of a continuous flow method for the aminocarbonylation of halogenated carboxylic acids at high temperatures and pressures (Scheme 1.4.2).[126] They observed a remarkable improvement in performance compared to a pressurized autoclave and a conventional flask under CO-balloon pressure, indicating that intimate contact between the liquid and gas phases is critical to the success of the reaction.

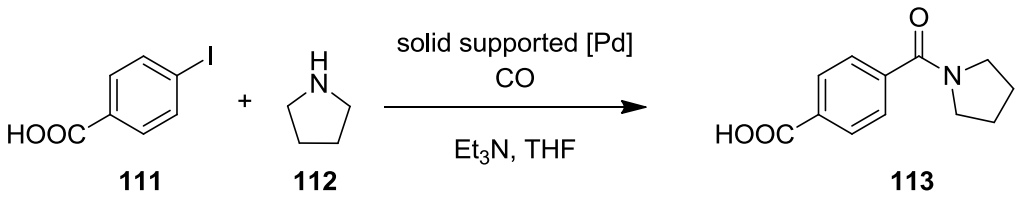

Flow (100 °C, 1.5 min. 30 atm): 83 %
Autoclave (100 °C, 60 min, 30 atm): 12 %
Ballon (68 °C, 60 min, 1 atm): 52 %

Scheme 1.4.2 Comparison of yields of flow and batch palladium-catalysed aminocarbonylation.

Initial work employing carbon monoxide in continuous flow reactors were performed under gas-liquid biphasic conditions and involved segmented flow (Figure 1.4.2). In

segmented flow, gas bubbles are separated by small plugs of liquid. Takebayashi and co-workers reported the efficiency of flow carbonylation of nitrobenzene to phenylisocyanate was significantly influenced by the size and distribution of CO gas bubbles in the reactor.[127] Challenges are encountered when performing flow chemistry in the segmented flow regime. These challenges include: control of the gas morphology, the accurate determination of residence time and poor reproducibility of results.

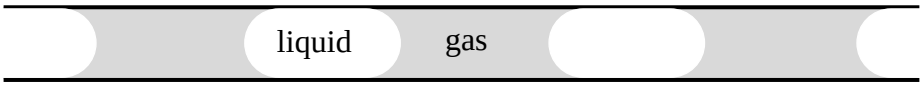

Figure 1.4.2 Schematic of gas-liquid segmented flow within a tube.

To address the limitations encountered in the segmented flow regime, Ley and co-workers pioneered the use of gas-permeable polymer membranes as a means of achieving well defined gas-liquid contact (Figure 1.4.3).[128] The reactor design consisted of two concentric tubes, with the inner tube comprising of a highly gas-permeable but liquid-impermeable amorphous fluoropolymer, Teflon AF-2400,[129] to load gas into a liquid stream prior to entering the reactor. The solvent or reagent stream flows within the inner membrane while gas fills the outer tubing and diffuses across the membrane and into the liquid stream. With this approach, the reaction stream remains homogenous. This technology has since been extended to reactions involving ammonia,[129] hydrogen[130] and carbon monoxide.[131]

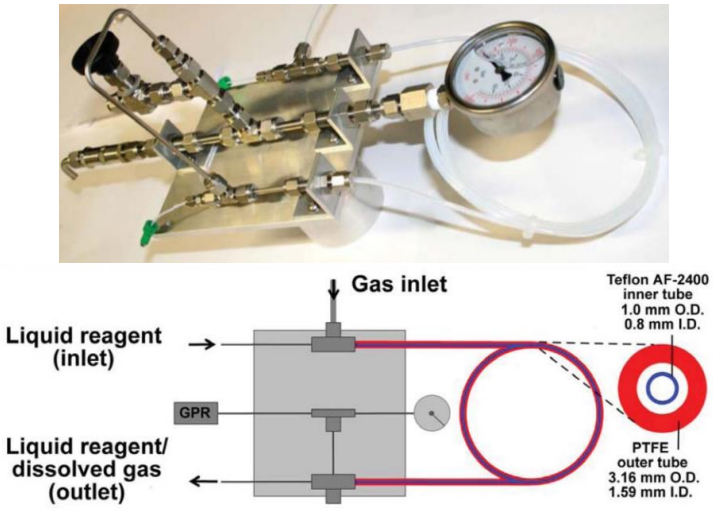

Figure 1.4.3 Tube-in-tube reactor designed by Ley *et al*. Reprinted with permission.

Leadbeater and co-workers reported continuous flow palladium-catalysed alkoxcarbonylation of aryl iodides using a proprietary tube-in-tube reactor where it was possible to load gas and heat simultaneously (Scheme 1.4.4).[132] They observed increased yields when compared to operating in segmented flow mode under similar conditions.[133]

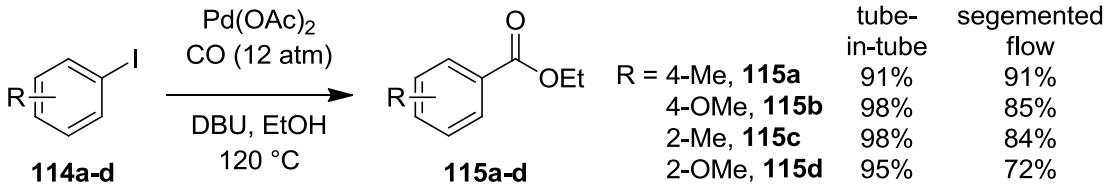

Scheme 1.4.4 Tube-in-tube and segmented flow alkoxycarbonylation of aryl iodide. DBU = 1,8-Diazabicyclo[5.4.0]undec-7-ene.

In order to eliminate the hazards associated with pressurized carbon monoxide gas cylinders, Ryu developed Heck carbonylation methods were carbon monoxide gas was generated *ex situ* through the sulfuric acid promoted dehydration of formic acid (Figure 1.4.4).[134] The high chemical compatibility of Teflon AF-2400 within the tube-in-tube reactor promoted intimate gas-liquid contact between two otherwise incompatible streams.

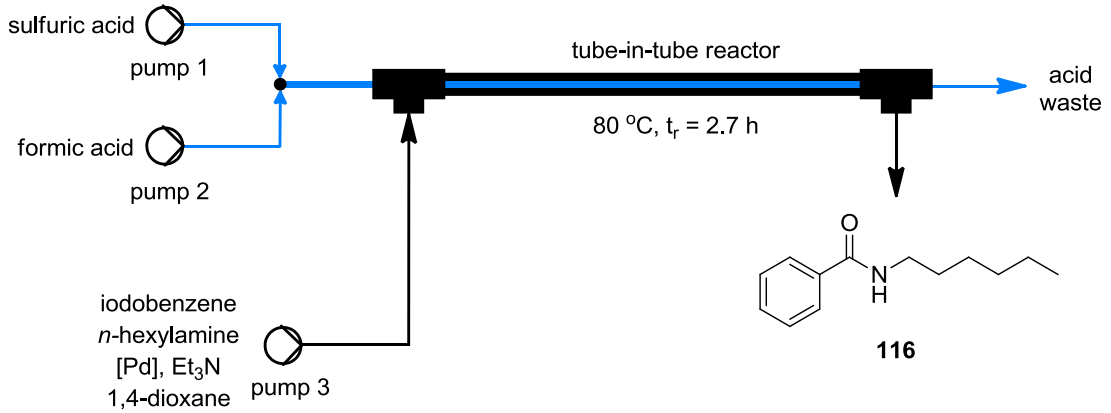

Figure 1.4.4 Microflow tube-in-tube system for *ex situ* generation of CO.

1.5. Summary

The development of new environmentally benign and efficient methods of obtaining carbonyl compounds from organohalides remains a frontier challenge in modern synthetic-organic chemistry. Free-radical carbonylation is a complementary approach not confined by the same inherent limitations of palladium-catalysed carbonylative cross coupling methodology. Free-radical carbonylation is dependent on the selective generation of the carbon-centred and acyl radical species. Visible light photoredox catalysis has been used to generate carbon-centred radicals under mild reaction conditions with broad functional group tolerance. The application of visible light photoredox catalysis is largely limited to the carbonylation of high-energy substrates; there are no examples of visible light photoredox carbonylation of aryl halides. *The development of novel visible light photoredox catalysed carbonylation methodology will provide access to carbonyl derivatives from non-carbonyl precursors with greater selectivity and efficiency than current methodology.*

In order to realise the potential of visible light photoredox carbonylation, methodology must move away from employing classical batch laboratory techniques. Photochemical and heterogeneous gas-liquid transformations are often hampered by the effects of low surface area to volume ratios and inadequate control of reaction conditions. Flow chemistry enables precise control over reactions conditions and safe use of reactive gases. An advantage of flow chemistry is the ability to access reaction conditions not possible with conventional batch chemistry. Recent advancements detail the use of semi-permeable membrane technology in flow chemistry to facilitate reactions of gaseous reagents beyond that possible in batch reactors.[33] *The application of flow chemistry to photocatalysed carbonylations, employing the use of tube-in-tube reactors, will provide greater control of reaction conditions and access to broader range of reaction conditions than batch methodology, facilitating the development and accessibility of efficient photochemical carbonylation methodology.*

1.6. Research Aims

Photocatalytic free-radical carbonylative coupling of electrophilic aryl coupling partners, such as aryl (pseudo)halides, remains underdeveloped relative to electrophilic alkyl coupling partners. The primary objective of the research in this thesis is to expand the scope and efficiency of visible light photoredox catalysed carbonylative cross-coupling of aryl (pseudo)halides. These aims are realized through the development of novel photocatalytic manifolds and protocol for high pressure gas-liquid transformations in continuous flow. The specific aims of the project are as follows:

- To establish a flow chemistry protocol for high pressure homogeneous photochemical transformations of carbon monoxide with a tube-in-tube reactor.
- To develop continuous flow methodology for the visible light photoredox-catalysed alkoxycarbonylation of aryl diazonium salts.
- To apply the developed continuous flow methodology to address a standing synthetic challenge in palladium-catalysed carbonylation.
- To develop methodology for the visible light photoredox-catalysed carbonylation of aryl halides.

Chapter 2. The Development of Continuous Flow Photoredox Carbonylation

Enabling Efficient, Safe and Scalable High Pressure Gas-Liquid Photochemistry

2.1. Introduction

Methods for photoredox-catalysed carbonylation have been exclusively developed in batch mode.[113,115,120,135–137] Gas-liquid reactions utilising batch reactors are limited to heterogeneous reactions where the reagents are charged into the reactor, pressurised with CO, sealed and irradiated. The standard reactor configuration is that of a cylindrical stainless-steel vessel with two flanged end fittings (Figure 2.1.1). One flange contains the connections required to deliver reagents and monitor pressure. The other flanged end houses a quartz window, providing the means to irradiate the contents of the vessel. Owing to the corrosive nature of the reaction mixture, reagents are not directly delivered to the reactor but rather placed in a quartz cuvette housed inside the pressure vessel, necessitating partial disassembly of the reactor between reactions.

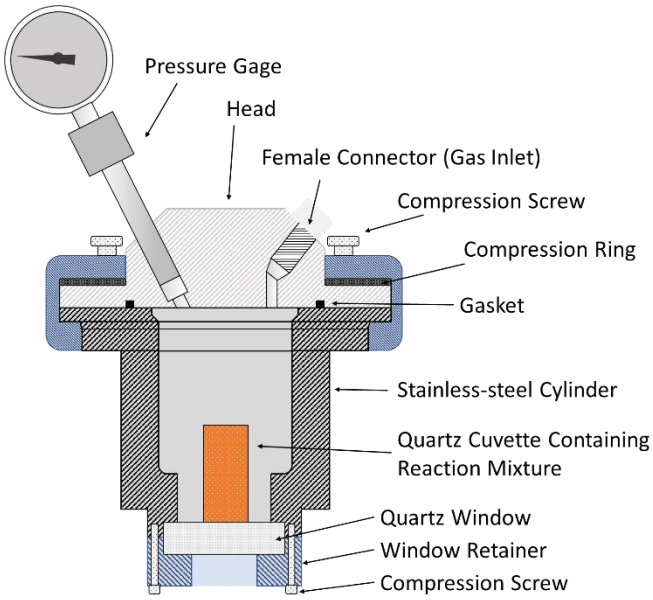

Figure 2.1.1 Schematic of a photochemical gas-liquid batch reactor.

Several limitations are associated with this mode of operation. Reaction scale-up is challenging as the traditional scale-up strategy, increasing the reactor size through proportional scaling of dimensions, is inhibited by the attenuation effect of photon transport. The Bouguer-Lamber-Beer equation (eq. 2.1) defines this effect, expressing the adsorption of light (A) as directly proportional to the path length (l), molar extinction coefficient (ε) of the chromophore and its concentration (c).[138] The impact this phenomenon has on batch photochemistry is exemplified by considering a hypothetical chemical reaction catalysed by eosin Y where the photon flux through the

reactor is greatly diminished following the first 0.5 mm of the reaction medium (Figure 2.1.2).

$$A = log_{10}\frac{I_0}{I} = \varepsilon cl \qquad \text{(eq. 2.1)}$$

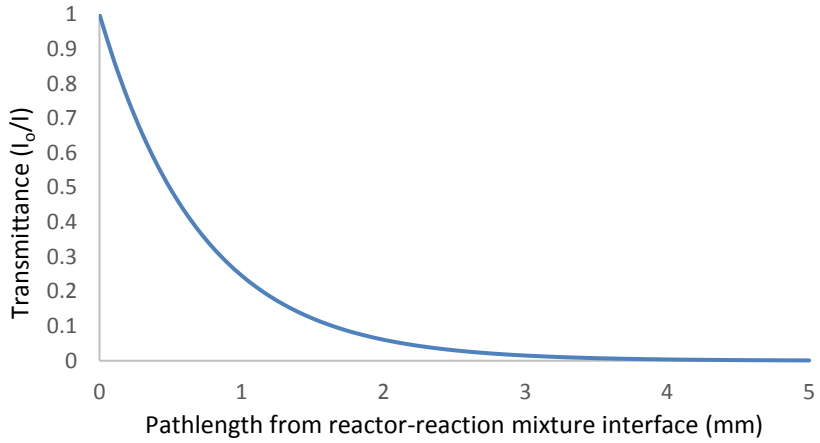

Figure 2.1.2. Relationship of between the absorption of light (539 nm) and path length of a cuvette containing a solution of eosin Y (1 mM, ε= 60,803$M^{-1}cm^{-1}$)[139] in acetonitrile.

Increasing the volume of the batch photoreactor through proportional scaling of the reactor's dimensions is an inefficient scale-up strategy as mass transfer limitations result in prolonged reaction times exposing the reaction medium to over-irradiation. This is demonstrated in the work by Booker-Milburn in which the scaling of an intra-molecular [5+2] photocycloaddition was one of the main impediments to achieve the total synthesis of the natural product Stemona alkaloid (+/-)-neostenine (Scheme 2.2.1).[140] This key reaction could be performed on a 50 mg scale in a 100 mL immersion-well batch photoreactor. Upon scaling the reaction poor yields were observed despite the complete consumption of the starting material. It was shown that the [5+2] product was susceptible to further reactions including [2+2] dimerization and photo-degradation. To overcome these limitations, a continuous flow reactor was developed and fashioned from fluorinated ethylene propylene (FEP) tubular photoreactor (2.7 mm inner diameter). This approach paved the way for efficient scaling of the reaction to gram scale with short residence times (Figure 2.1.3).

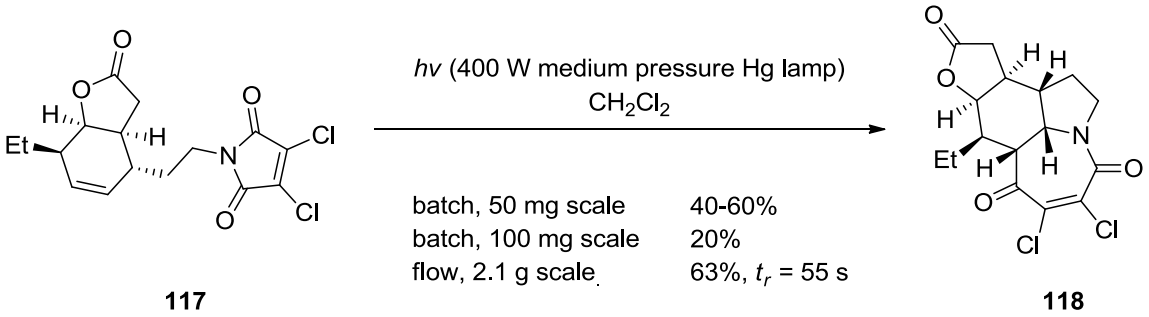

Scheme 2.1.1. [5 + 2] Maleimide photocycloaddition in batch and in continuous flow reported by Booker-Milburn.[140]

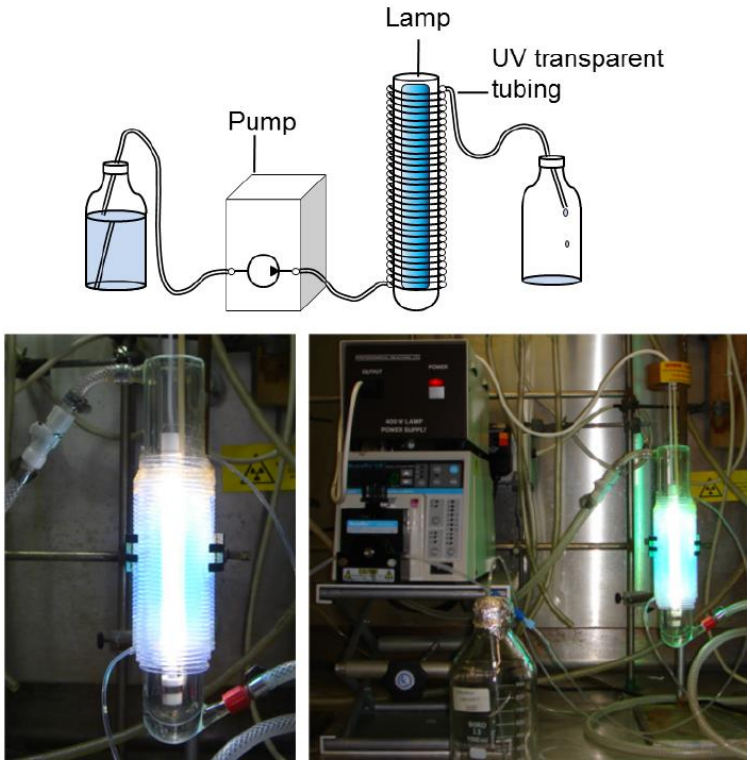

Figure 2.1.3. A schematic of the photochemical reactor (above) and images of the FEP photochemical flow reactor developed by Booker-Milburn (reprinted with permission from ref 141).[141]

Utilisation of reactive toxic gaseous reagents at high pressure poses a considerable safety risk due to the potential for explosive decompression and exposure to the gas. The risk is greater when operating in the batch regime compared to flow, as the reactor requires a large reservoir of gas, often a third of the total reactor volume, to facilitate mass transfer. Further, increasing the scale of the reaction increases the risk as the working volume of gas in batch is proportional to the reactor volume.

In flow, the inventory of gas is moderated as reagents are continuously fed to and consumed in the reactor. Reaction scale-up can be achieved in flow without an increase in reactor volume. Implementing controls to manage the risk is particularly challenging for photochemically driven processes where the material of construction required for the reactor must be suitably transmissive to the desired wavelength. For visible light driven reactions, such materials (e.g. pyrex, quartz, sapphire) have greatly reduced mechanical strength compared to steel alloys. Laboratory-scale batch solutions are expensive, in excess of AUD $30,000 for a basic configuration (100 mL Parr reactor with quartz window),[142] limiting the accessibility of the chemistry to the wider chemical community. The required window thickness is proportional to the system pressure and exponentially proportional to the window's characteristic length (diameter for round windows).[143] For high pressure gas-liquid batch photoreactors capable of delivering multi-kilogram quantities, the required window thickness is prohibitively large.

Gas-liquid reactions in flow using a variety of reactor technologies including bubble column, packed bed, spray columns, falling-film, impinging jet absorber, tubular reactor have been developed to facilitate gas-liquid reactions and transfer processes.[144–151] From these designs, falling-film and tubular reactors are compatible with high pressure photochemical applications; the others suffer from similar deficits as the corresponding batch reactor. By combining continuous flow methodology with microreactor technology, the narrow channels, often less than 1000 µm, provide uniform irradiation of the reaction mixture and enhancement of the gas-liquid interfacial area to 9,000 m^2/m^3 – an order of magnitude larger than conventional reactors.[152]

Falling-film reactors use gravity to direct the liquid phase over a plate, forming thin liquid films. These films are very thin (0.1-3 mm) and are contacted with the gas phase facilitating rapid mass and heat transfer through very high interfacial areas of up to 50,000 m^2/m^3.[153] Hessel and co-workers utilised a falling-film microreactor developed by Mainz Institute of Microtechnology for the hydrogenation of nitrobenzene.[154] Nitrobenzene conversion was highly dependent on film thickness and rheology. As the film characteristics are a function of the volumetric flow rate, the residence time in the reactor is fixed, impairing reaction optimization. Further, as flow is gravimetrically driven, residence times are limited to the second scale and require modification of the reactor dimensions to alter the residence time.

Tubular microreactors conventionally involve pumping fluid through a single channel formed from a tube. As the gas phase and liquid phase meet at the inlet to the reactor Taylor-flow is formed as depicted in chapter 1 Figure 1.4.2. Alternatively, as discussed in chapter 1.4, membrane tube-in-tube reactors can circumvent mass transfer limitations associated with heterogeneous catalysis by preloading the gas into the reaction mixture whilst maintaining homogeneity. Tubular microreactors are robust, modular and accessible platforms for performing gas-liquid photochemistry. Numerous flow chemistry technology vendors have commercial pumps, photoreactors and tube-in-tube reactors available. Significantly, the use of bespoke tubular microreactors systems in the literature is prevalent and individual components are derived from high-performance liquid chromatography systems (HPLC). Idle HPLC pumps can be readily commandeered for reagent delivery in flow chemistry applications. Photoreactors are formed by coiling of the fluoropolymer tube around a support scaffold and irradiated with common LEDs arrays or a compact fluorescent lamp (Figure 2.1.4). Fluoropolymer tubing is affordable, abundantly available and highly transmissive to visible-light irradiation (>98%). The high tensile strength of fluoropolymer, in conjunction with its tubular design, accommodates for a broad range of pressures, up to 172 bar.[155] Residence time control is achieved by adjusting the volumetric flow rate. System pressure is mechanically set via implementation of back-pressure regulators (BPR) in series at the reactor outlet. Scale-up can be achieved in a straightforward manner by allowing more time for elution and/or increasing reaction through-put by increasing the volumetric flow rate (increasing pump speed) and increasing the reactor volume (longer reactor tubing length and/or tubing internal diameter).[156]

Figure 2.1.4. Simple yet highly effective flow tubular photoreactor developed by Noël and co-workers. Photoreactor is comprised of a flexible LED strip and PFA microtubing coiled around two deconstructed syringes. Cooling is provided by compressed air. Reprinted with permission from ref 156.

Despite the advantages of performing gas-liquid photochemical reactions with tubular microreactors, methodology for the continuous flow photocatalytic carbonylation of organic compounds remains underdeveloped. The primary aim of this chapter was to establish a continuous flow platform capable of efficiently promoting visible light driven free-radical carbonylation chemistry in a safe, scalable and predictable manner. Furthermore, it was desirable to facilitate the uptake of the developed chemistry herein by the wider chemical community by employing technology that is unintimidating, that being technology that presents low financial, technical and safety risk. In order to evaluate the performance of the developed continuous flow carbonylation platform against the autoclave batch photoreactor, the photoredox catalysed alkoxycarbonylation of aryldiazonium salts was translated to flow.

2.2. Apparatuses and Methods

Solvent Delivery

Positive displacement pumps were required to deliver solvents under high pressure. The developed flow systems accommodated a host of pumps (Table 2.2.1). The critical criterion for pump selection was its maxing working pressure.

The pumps were selected on the basis of technical specification, commercial availability and cost. They provided flowrates between 0.1 mL/min to 50 mL/min and up to 650 bar. Reciprocating pumps are robust and affordable. Reciprocating pumps were fitted with stainless steel pump heads with inbuilt pressure sensors. In contrast to the batch reactor, the pump can be constructed of stainless steel as harsh reactive radical intermediates are not generated inside the pump. Syringe pumps offer superior chemical compatibility but have a lower maximum working pressure rating.

Table 2.2.1. Commercially available flow chemistry pumping modules

	
Vapourtec R2 Module	**Uniqsis Flowsyn Pump Module**
Reciprocating pump	Reciprocating pump
min-max flow rate: 0.05 - 10 mL/min	min-max flow rate: 0.05 - 10 mL/min
42 bar maximum working pressure	100 bar maximum working pressure
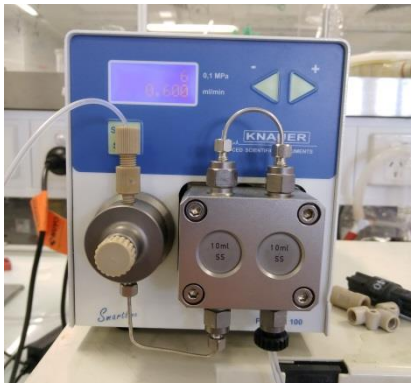	
Knauer Smartline Pump 100	**Syrris Asia Series Syringe Pump**
Reciprocating pump	Syringe pump
min-max flow rate: 0.01-10 mL/min	min-max flow rate: 0.01-20 mL/min
400 bar maximum working pressure	20 bar maximum working pressure

Reagent Delivery

The reagent delivery module is comprised of a 6-port injection valve fitted with a 2-5 mL sample loop (Figure 2.1.1). The sample loop houses the reaction mixture. Carrier solvent pumping is continuous and initially bypasses the reaction mixture. When the

valve is actuated, the carrier solvent stream is directed through the sample loop where it forces the reaction mixture downstream through the flow system as a plug.

The selection criteria for injection valves was the maximum operating pressure. Commercial continuous flow systems featuring motorized injection valves as well as manual injection valves were utilised (Figure 2.2.2). Stainless steel manual injection valves are inexpensive and robust. The Vapourtec R2 Module and Uniqsis Pump Module have a stainless-steel injection valve integrated on the unit. Stainless steel valves have maximum working pressures exceeding 100 atm. The Syrris Asia Series Reagent Injector is a standalone unit with PTFE wetted parts and a maximum working pressure of 20 atm.

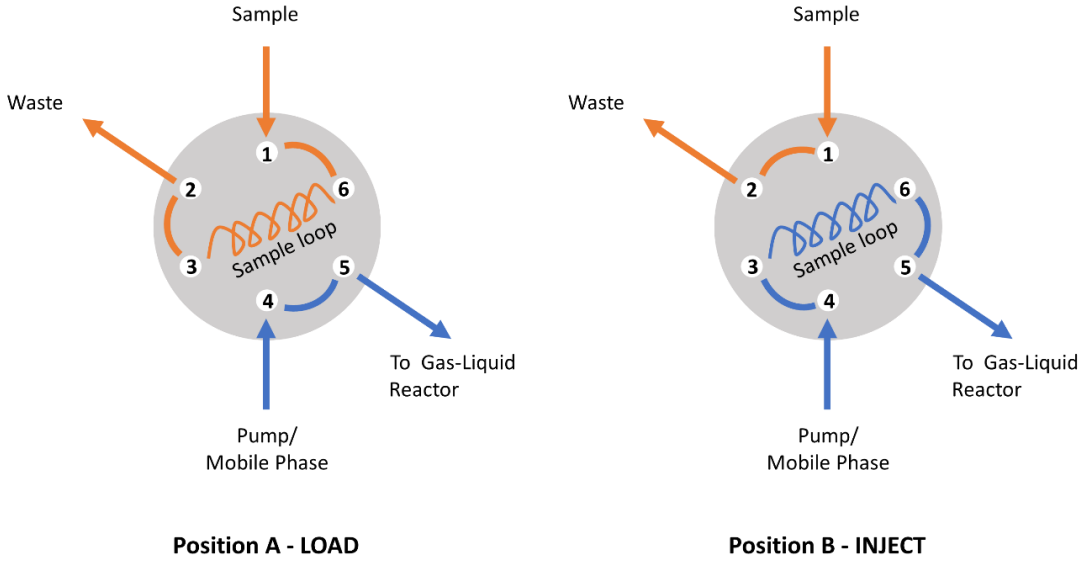

Figure 2.2.1. Schematic and flow paths of the load and inject positions of a 6-port injection valve fitted with a sample loop.

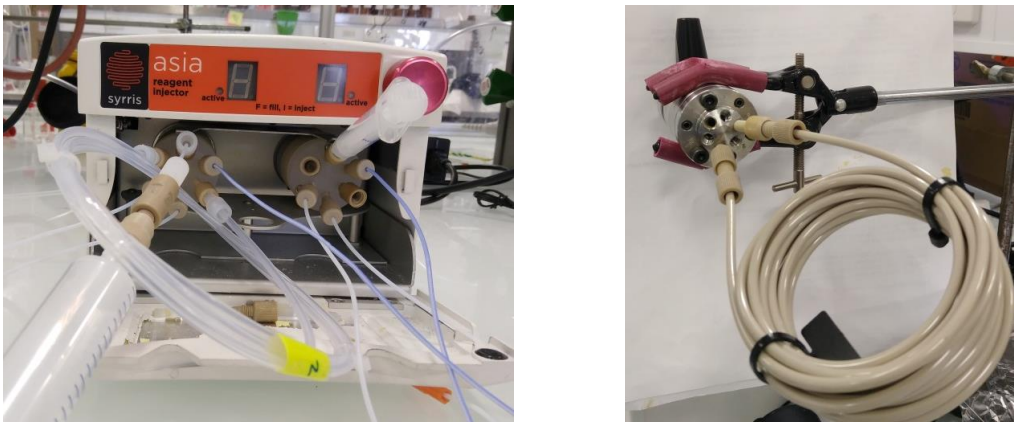

Figure 2.2.2. Syrris Asia Series Reagent Injector (left) and Rheodyne model 7725 manual sample injector valve fitted with 5 mL sample loop (right).

CO Loading

CO was introduced into the reaction stream via tube-in-tube membrane reactor technology.[157] For reactions up to 24 atm of CO, a Uniqsis Gas Addition Module was utilized. Where CO pressure in excess of 24 atm were required, the module was modified: the pressure release valve was removed and capped, the pressure gage replaced with needle gauge rated to 70 bar and 1/16", 1.0 mm i.d., polytetrafluoroethylene (PTFE) tubing (maximum working pressure 25 atm) substituted for 1/16", 1.0 mm i.d., polyether ether ketone (PEEK) tubing (maximum working pressure 340 atm).

A bespoke tube-in-tube gas-liquid reactor was also developed. This tube-in-tube reactor was designed to be compact so that it be irradiated within the bespoke photochemical reactors available in the laboratory (Figure 2.2.3). A schematic of the reactor, coiled around a support scaffold, is shown in Figure 2.2.4. Tube-in-tube reactors reported in literature utilise a semi-permeable membrane within a stainless steel or PTFE tube. Stainless-steel is opaque and ridged, and therefore unsuitable for use in photochemical reactors. Perfluoroalkoxy alkane (PFA) tubing (1/8" o.d., 1.59 mm i.d.) was used as the outer tube due to its high visible light transmissivity. Teflon AF-2400 was selected at the gas permeable membrane for its high permeability to gases and chemical resistance. The tube-in-tube reactor had an annular channel volume of 0.53 mL, and inner channel volume of 0.27 mL. Stainless steel Swagelok 1/8" T-pieces were used to form the junctions between the inner membrane and outer tube. These junctions were susceptible to failure and the use of a 0.8 mm o.d. stainless steel capillary was found necessary to support the Teflon AF-2400 membrane at the junctions. Where CO was generated *ex situ*, dehydration of formic acid proceeded in the inner channel, as concentrated sulfuric acid (>60%) is incompatible with the stainless-steel T-pieces. Degradation of the stainless-steel capillaries was observed, however, they appeared integral and there was no fouling of the reactor.

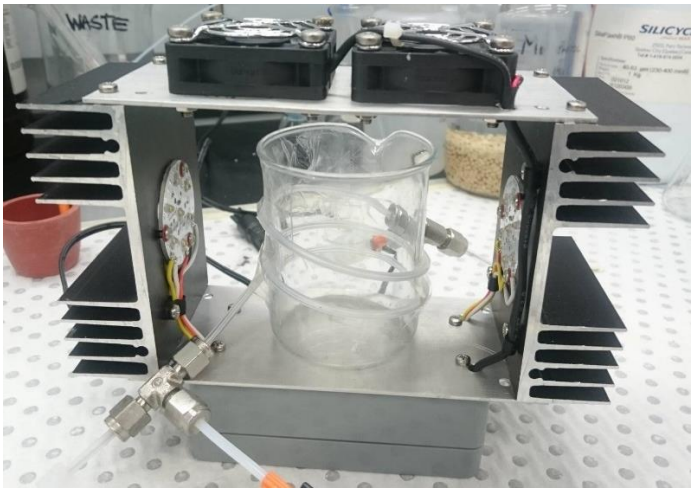

Figure 2.2.3 The tube-in-tube gas-liquid photoreactor coiled around a Pyrex® beaker and flanked by two LED (530 nm, 7 W) arrays.

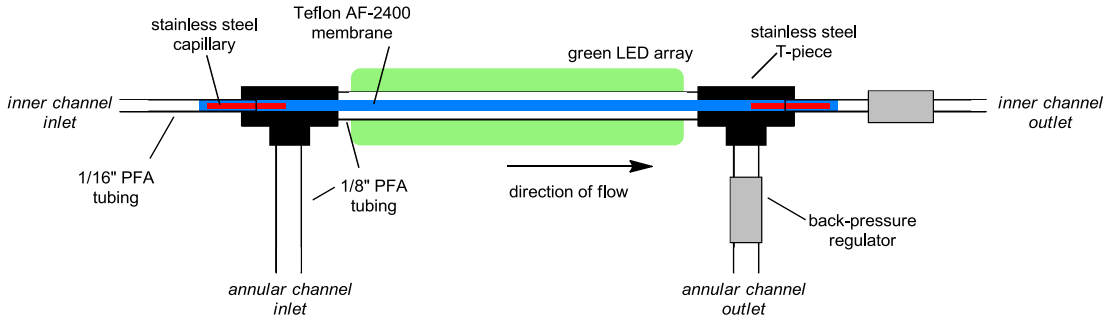

Figure 2.2.4 Schematic of the tube-in-tube photoreactor.

Tubular Photoreactor

The flow photoreactor comprised of PFA tubbing (1/16” o.d., 0.75 mm i.d, reactor volume was 0.5 mL) coiled around solid supports housed within a bespoke LED assembly (Figure 2.2.5). Each assembly contained two replicate 7W LEDs (Figure 2.2.6). LEDs were purchased from Luxeonstar (blue light: 450±15 nm, green light: 530±15 nm). The assembly was air cooled to maintain the reactor at room temperature.

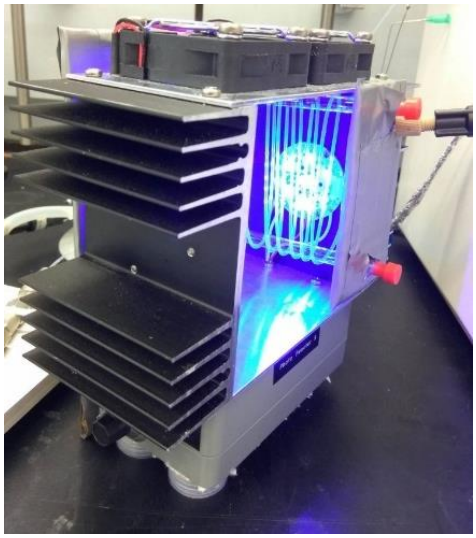

Figure 2.2.5. Flow Photoreactor.

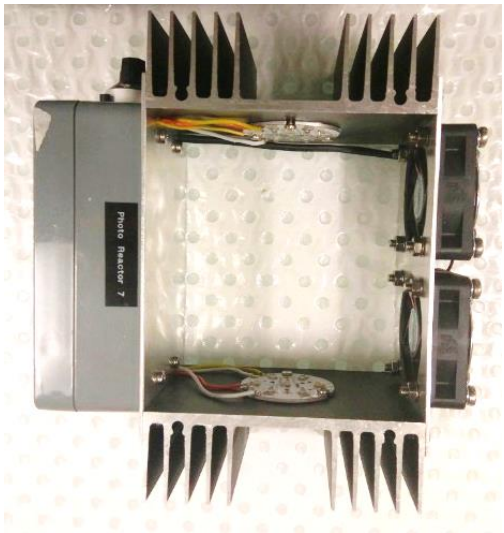

Figure 2.2.6. LED Housing Assembly. The twin 60 mm fans maintain the reactor at room temperature. The LEDs are mounted on stainless steel heatsinks to prevent the LEDs from overheating.

Pressure Regulation

The desired system pressure was achieved with the Upchurch Scientific back-pressure regulators. The small devices were installed at the end of the flow path, prior to elution into the collection vial (Figure 2.2.7). The back-pressure regulators are valves that maintain upstream pressure by only opening when upstream pressure exceeds their pressure rating. System pressure could be gradually altered through the

addition/subtraction of back pressure regulators in series. Gas pressure was independently controlled by the regulator attached to the CO cylinder.

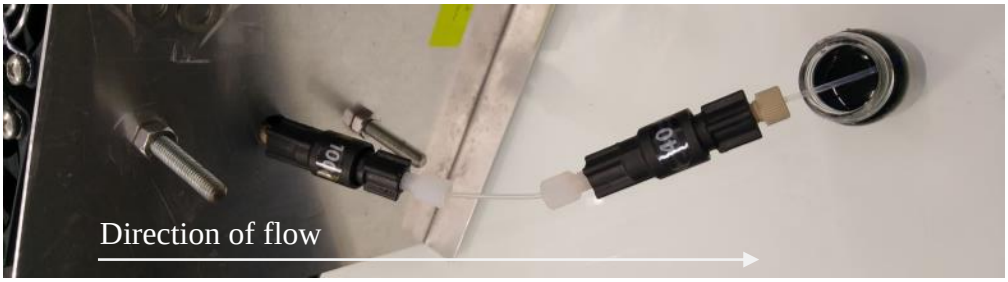

Figure 2.2.7. Two back-pressure regulators rated at 100 psi and 40 psi bar respectively, are installed in series to afford 9.5 atm upstream system pressure.

Generalized Alkoxycarbonylation Procedure

A solution of aryldiazonium tetrafluoroborate and photocatalyst dissolved in methanol was sonicated to facilitate dissolution prior to sparging with N_2 for 10 minutes. Concurrently, the flow system was primed by flushing with the deoxygenated carrier solvent (composition of carrier solvent and reaction solvent were the same) for 10 minutes at a flow rate of 200 μL.min^{-1} or greater. For reactions where CO was generated *ex situ*, the formic acid and sulfuric acid flow rates were set to 10.4 μL/min and 43.4 μL/min respectively. For reactions were CO gas was supplied from a cylinder, the tube-in-tube reactor was charged with the desired CO pressure. With the volumetric flow rate of the carrier solvent pump adjusted to deliver the desired residence time, the reaction mixture was injected into the sample loop, the LED arrays were turned on and the reagent injector module switched to the 'inject' position. The product stream was collected, concentrated *in vacuo* and the yield of benzoate determined by ^{1}H NMR analysis with maleic acid as the internal standard. Refer to tables and discussion for the flow system configuration, concentration of reactants and catalyst, LED intensity, system pressure and flow rates.

2.3. High Pressure Homogenous Gas-Liquid Photochemical Continuous Flow Platform – Design and Development

Free radical photoredox carbonylation requires high CO pressure to drive the aryl radical to the acyl radical. Xiao and co-workers demonstrated that the yield of

alkoxycarbonylated product was strongly dependent on the CO pressure (Figure 2.3.1).[113] High CO pressure (80 atm) was required in batch autoclaves to overcome limitations in mass-transfer. The rate of CO depletion is greatest at the reactor-window junction where catalyst activity is localised. Mass-transfer limitations from the reactor headspace, the CO gas reservoir, to the reactor-window junction results in inadequate CO solution concentrations as the reactions proceed.

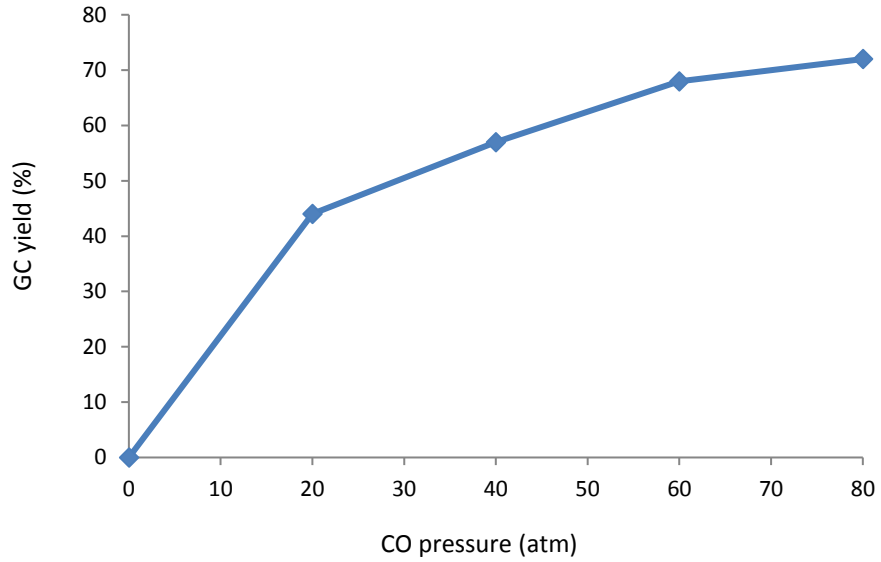

Figure 2.3.1 The influence of initial CO pressure on the methoxycarbonylation of 4-(ethoxycarbonyl)benzenediazonium catalysed by fluorescein (0.5 mol%) in batch (10 h).[113]

It was postulated that a tube-in-tube gas-liquid photoreactor with a small reactor cross sectional area (0.4 mm^2) would enable continuous saturation of the liquid phase with CO and low photon impedance thereby act to increase the effective CO available for interaction with the aryl radical intermediate. Initial efforts were directed towards investigating the mild pressure (<20 atm CO) free radical alkoxycarbonylation of benzenediazonium tetrafluoroborate in continuous flow.

The development of the gas-liquid photochemical continuous flow platform began with a process flow diagram (Figure 2.3.2). The process flow diagram indicates the separate steps (unit operations) of the process, with input and outputs, in sequential order. It was necessary to divide the process into numerous unit operations. Each unit operation corresponds to a single piece or set of related pieces of equipment. It was important to construct the flow platform in this modular nature as it allows for flexibility of process conditions (flow rates, pressures, product through-put, irradiation conditions etc.) which

facilitates reaction discovery and lowers operational complexity. By decoupling solvent delivery and reagent delivery, rapid screening can be achieved by loading sequential reaction mixtures with only a short pause, approximately 30 min, between valve actuations. Disassembly of the flow system, reactor or release of CO pressure is not required between experiments

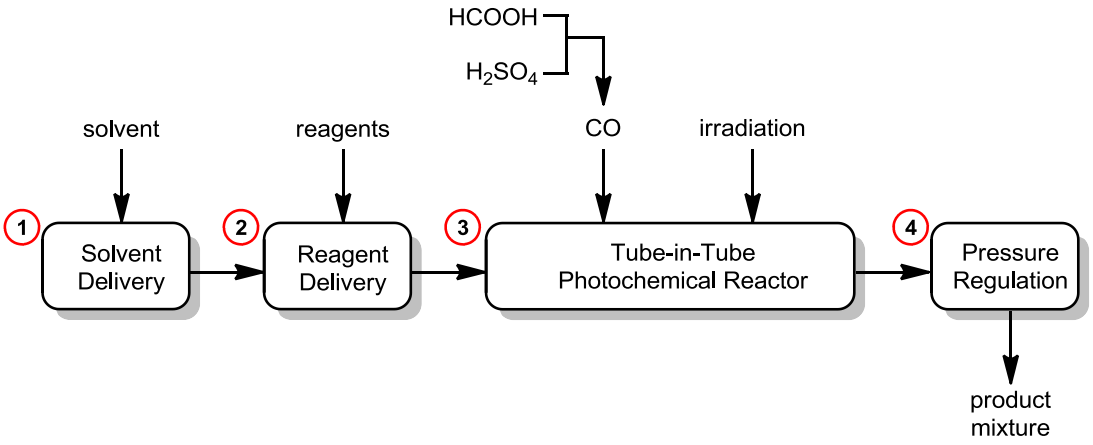

Figure 2.3.2 Process flow diagram for the carbonylation of organic compounds.

To negate the necessity for external CO pressure (CO cylinder), CO was generated *ex situ* by the dehydration of formic acid with sulfuric acid. The Syrris Asia Series pumping module and reagent delivery module were utilized due to compatibility with concentrated acids. The dehydration of formic acid proceeded in the inner channel of the tube-in-tube photoreactor, as concentrated (>60%) sulfuric acid is incompatible with the stainless-steel T-pieces. A 4:1 volumetric flow rate ratio of sulfuric acid to formic acid resulted in larges plugs of CO forming in the inner channel which did not diminish significantly in magnitude over the course of the tubular reactor. This indicated that excess CO was generated by the dehydration reaction. The system pressure and CO pressure were controlled by back-pressure regulators. It was found that the channel pressure, determined by a pressure sensor at the pump outlet, was approximately 2 atm below the manufacturers specification and the system pressure fluctuated between ±1 atm. To prevent CO out-gassing in the reaction stream, which could lead to unwanted segmented flow, the differential pressure between the inner and annular channel was maintained within 5 atm. The process flow diagram was developed into the flow platform in Figure 2.3.3.

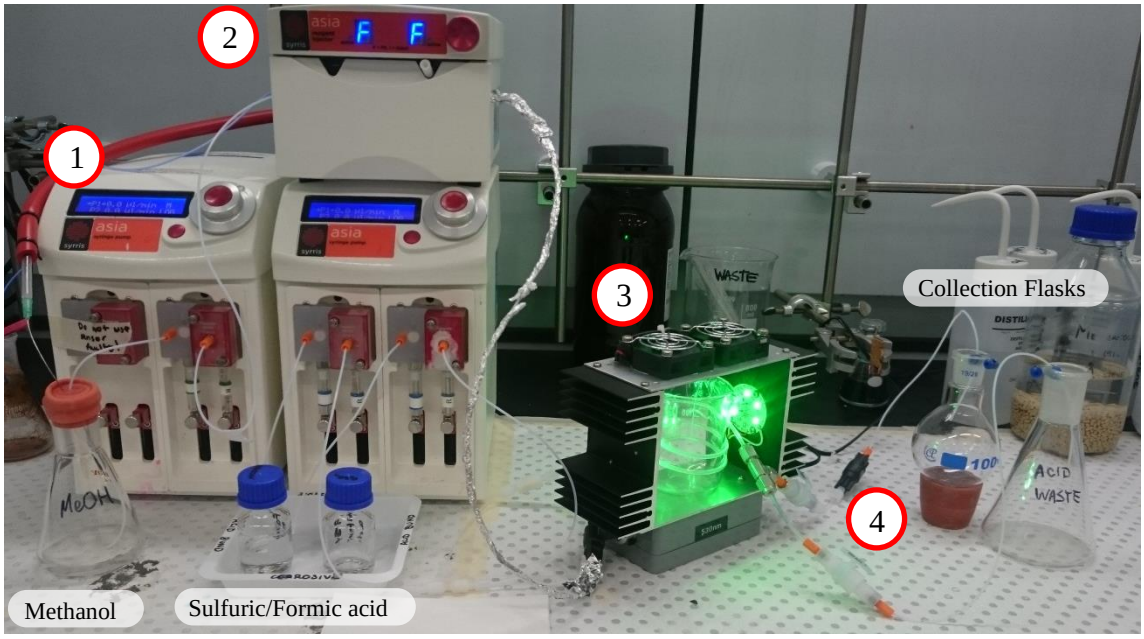

Figure 2.3.3. Continuous flow alkoxycarbonylation platform equipped with a gas-liquid photoreactor and *ex situ* generation of CO.

With the assembly of the prototype flow system, the alkoxycarbonylation of aryl diazonium tetrafluoroborates was investigated. Initial studies were carried out under reaction conditions analogous to the corresponding batch synthesis reported by Jacobi von Wangelin (Scheme 2.3.1).[112] Under irradiation with green light, solutions of 4-methoxybenzenediazonium tetrafluoroborate (**119**) and eosin Y were passed through the gas-liquid photoreactor and enriched with *ex situ* generated CO. With methanol as solvent, under 8 atm of CO pressure, the reaction afforded methyl 4-methoxybenzoate (**120**) in 12% yield (Entry 1, Table 2.3.1), determined by ^{1}H-NMR analysis with malic acid as the internal standard. The initial concentration of the diazonium salt was 0.025 M. Dilute reaction conditions were required to ensure complete solution of eosin Y. Complete conversion of the diazonium salt was observed. Increasing CO pressure to 16 atm resulted in a small increase in the yield of methoxycarbonylated product (Entry 2, Table 2.3.1). This outcome was unexpected owing to the strong dependence of alkoxycarbonylation on CO pressure. The activity of eosin Y had been shown to be retarded in the presence of acetonitrile.[157] With acetonitrile as the co-solvent (Entry 3 and 4, Table 2.3.1), a reduction in the conversion of the diazonium salt was observed accompanied by an increase in reaction selectivity. The response to increasing CO pressure in the presence of acetonitrile was aligned with that reported in literature. The

results suggested that the flow system was limited by mass-transfer of CO across the AF-2400 membrane.

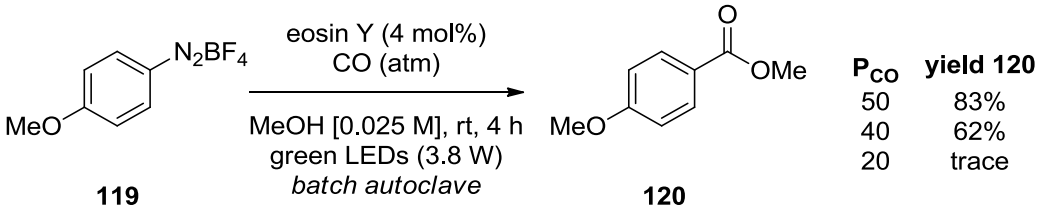

Scheme 2.3.1 Visible light photoredox methoxycarbonylation of aryl diazonium salts in batch develop by Jacobi von Wangelin and co-workers.

Table 2.3.1. Photoredox mediated alkoxycarbonylation in a tube-in-tube flow photoreactor.

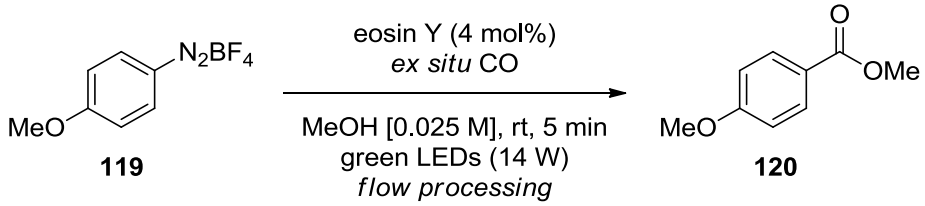

entry	solvent	CO pressure (atm)	conv. (%)[a]	yield 120 (%)[a]
1	MeOH	8	>99	12
2	MeOH	16	>99	14
3	MeOH/MeCN (1:1)	8	47	12
4	MeOH/MeCN (1:1)	16	52	27

[a] ^{1}H NMR yields with maleic acid as the internal standard.

Attempts were made to recover the starting material to determine the mass balance of the reaction. Despite repeated attempts, complete mass balance could not be obtained. It was reasoned the reduced product, anisole (b.p. 153 °C at 1 atm),[158] may have been favoured under the reaction conditions, which was removed during evaporative workup. Anisole may be formed through α-hydrogen abstraction from methanol by the aryl radical.[159] To ensure that the corresponding reduction product could be observed and quantified, subsequent optimisation studies were conducted with the higher molecular weight substrate, using 4-phenoxybenzenediazonium tetrafluoroborate (**121**). The corresponding reduced product, diphenylether (**123**) (b.p of 257 °C at 1 atm)[160] was unlikely to be removed *in vacuo*.

The mass-transfer limitation was addressed by pre-saturation of the reaction stream with CO prior to irradiation in the tube-in-tube photoreactor (Table 2.3.2). The CO

concentration prior to irradiation had that greatest influence on alkoxycarbonylation yield. Although the reported yields may appear low, Jacobi von Wangelin reported less than 5% alkoxycarbonylated product yield at 20 atm of CO pressure under batch conditions, highlighting the process intensification ability of the developed flow platform.

Table 2.3.2. Comparison of flow reactor system configurations

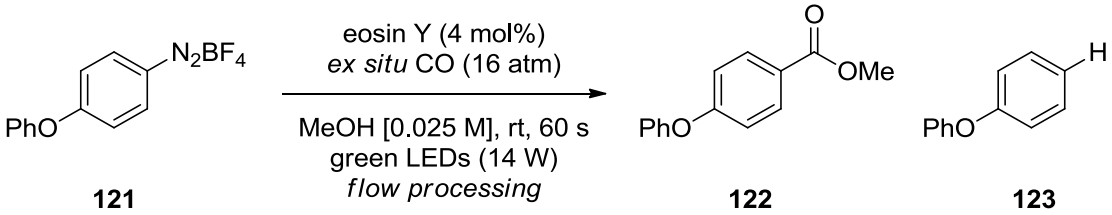

121 **122** **123**

entry	system configuration	conv. (%)[a]	yield 122 (%)[a]	yield 123 (%)[a]
1	tube-in-tube flow photoreactor	>99	11	4
2	pre-saturation prior to tube-in-tube flow photoreactor	>99	23	44
3	pre-saturation prior to tubular photoreactor	>99	21	26

[a] ^{1}H NMR yields with maleic acid as the internal standard.

A limitation of *ex situ* generation of CO is use of back pressure regulators to control gas pressure. Cartridge-type back pressure regulators afford poor control over the gas phase and significant pressure fluctuations were observed resulting in outgassing of CO in the reaction stream. Pressure fluctuations increased as system pressure increased making *ex situ* CO generation unfeasible at pressures exceeding 20 atm. To enable precise control over gas pressure and to reduce system complexity, CO gas from a cylinder was utilized as the pressure of CO can be easily regulated. A new configuration was developed where commercially available Uniqsis Gas-Liquid Module to introduce CO gas into the reaction stream prior to entering the flow photoreactor (Figure 2.3.4). The Uniqsis FlowSyn system was utilized for solvent and reagent delivery up to 65 atm.

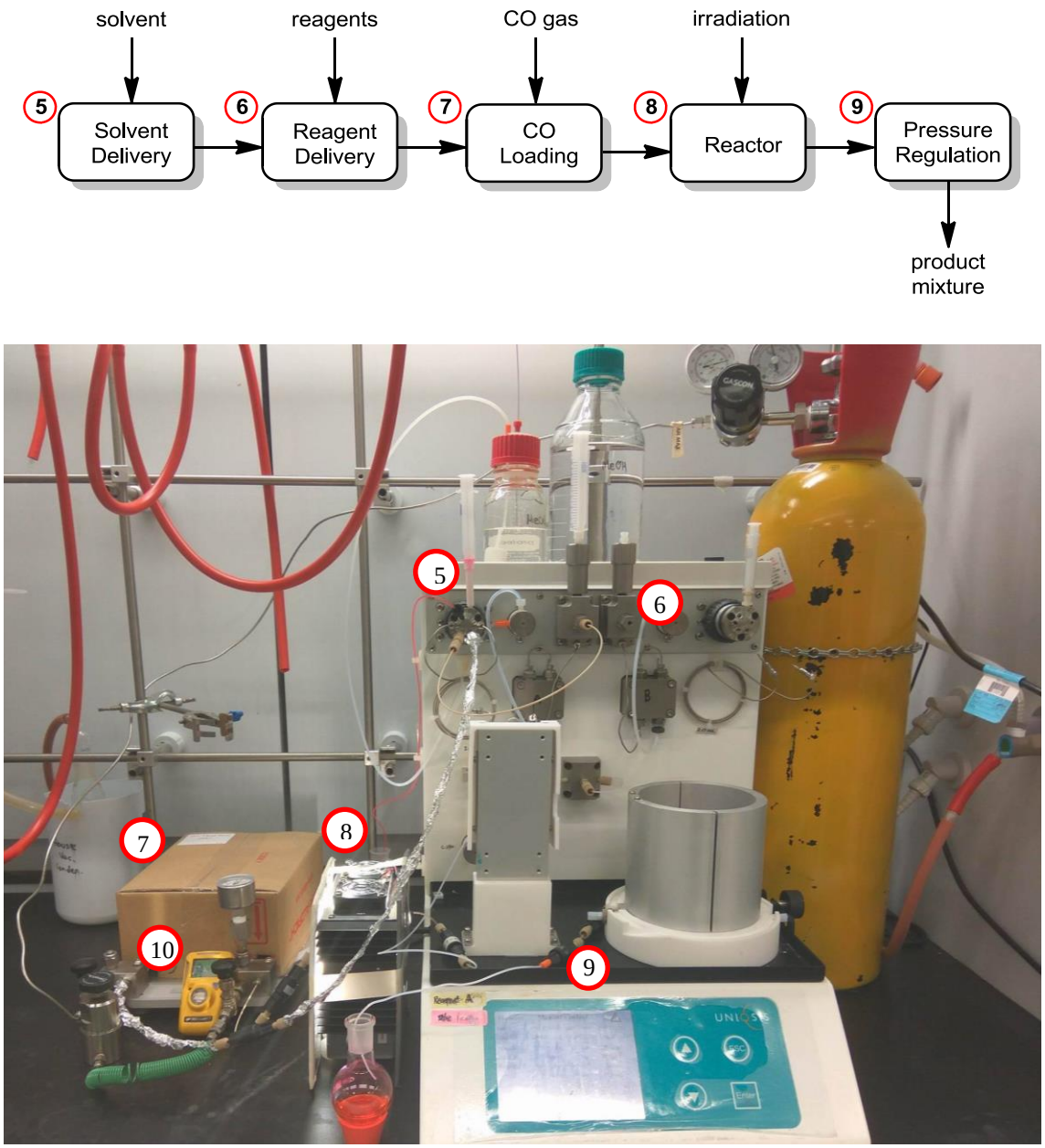

Figure 2.3.4. The developed flow system process flow diagram and configuration. FlowSyn system pumps (5) the reaction mixture from the sample loop (6) to the gas-liquid module (7). The gas-liquid module is shielded from light to prevent premature reaction. The CO charged reaction mixture is then delivered to the photoreactor (8). Back pressure regulators maintain the desired system pressure (9). CO detector/alarm (10).

2.4. Continuous Flow Methoxycarbonylation of Aryldiazonium Salts - Results and Discussion

Initial investigation towards the mild pressure methoxycarbonylation of benzenediazonium tetrafluoroborate with eosin Y as the photoredox catalyst yielded the competitive hydrodediazoniation product, diphenyl ether, as the major product. The transition to CO supplied from a compressed gas cylinder afforded comparable yields to *ex situ* generated CO of alkoxycarbonylated product and reduced product (Figure 2.4.1).

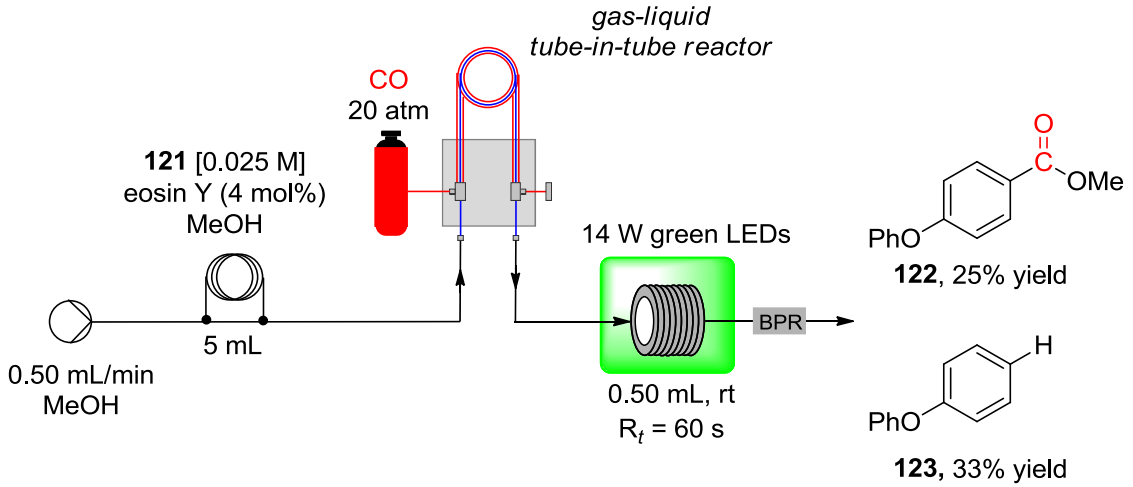

Figure 2.4.1. Eosin Y catalysed methoxycarbonylation with preloading of CO via the tube-in-tube gas-liquid reactor.

It was postulated that a co-solvent with C-H bond dissociation energy greater than methanol (**124**) could be utilized to decrease the thermodynamic drive towards hydrogen abstraction by the photogenerated aryl radical (Figure 2.4.2).

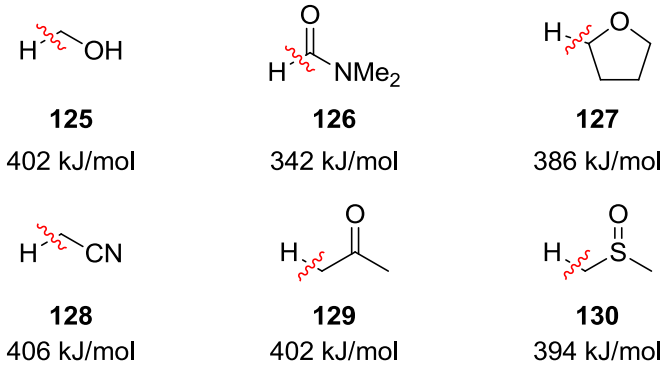

Figure 2.4.2. C-H bond dissociation energy of polar organic solvents.[161]

A solvent screen was performed but was limited by the poor solubility of diazonium salt in non-polar solvent. Acetonitrile (**127**) afforded greater selectivity for the methoxycarbonylated product, however, the rate of reaction was substantially reduced (Figure 2.4.3. – green trend lines). Acetone (**128**), in a 1:1 ratio with methanol, resulted in 36% consumption of the diazonium salt and yielded 16% of **122** along with 16% of **123**. Prolonged reaction times (50 min) did not furnish full conversion of the diazonium salt. Utilisation of the fluorescein in lieu of eosin Y demonstrated a strong positive correlation between acetonitrile concentration and selectivity (Figure 2.4.3 – blue trend lines). With the solvent comprised of 95% v/v acetonitrile, with the reminder methanol, the developed methoxycarbonylation reaction afford methyl 4-phenoxybenzoate in 61% yield at 20 atm CO pressure Figure (2.4.4). Despite the dilute reaction conditions employed, the developed flow methoxycarbonylation reaction provided a reaction throughput of 0.0915 mmol·h^{-1} and a space-time yield of 0.183 mmol·h^{-1}·mL^{-1}, an order of magnitude larger than the corresponding batch methoxycarbonylation reaction at 80 atm CO pressure (0.0077 mmol·h^{-1} and 0.0138 mmol·h^{-1}·mL^{-1} respectively).[113]

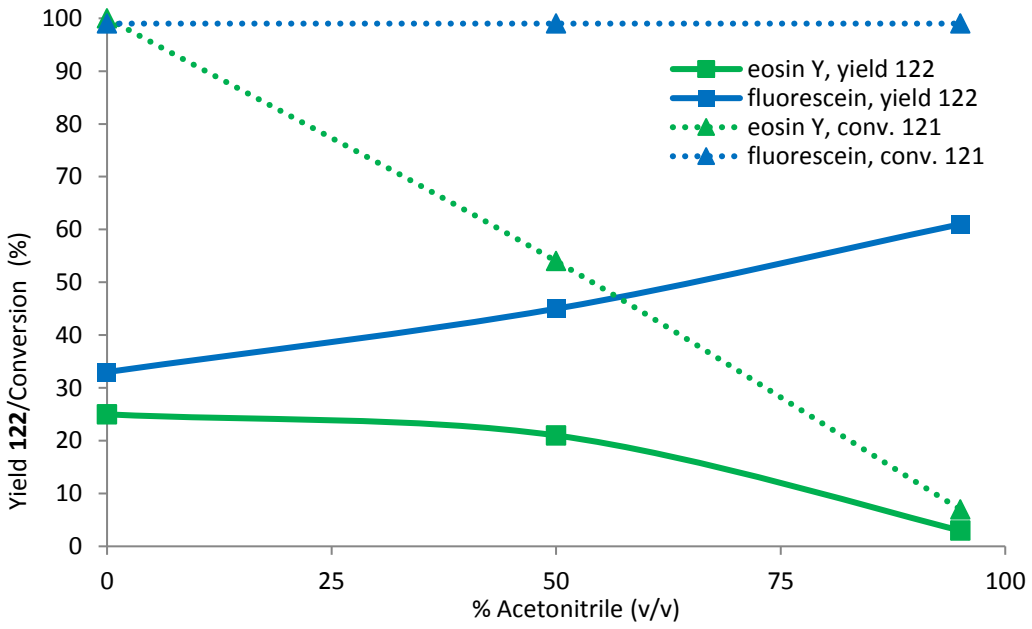

Figure 2.4.3. Comparison of eosin Y and fluorescein catalysed methoxycarbonylation. Unless otherwise stated, reactions were carried out with 4-phenoxybenzenediazonium tetrafluoroborate (0.125 mmol), photocatalyst (4 mol%), MeOH/MeCN (95:5, 5 mL), CO (20 atm), irradiation (14 W, green for eosin Y, blue for fluorescein), room temperature, 1 minute (5 min for fluorescein).

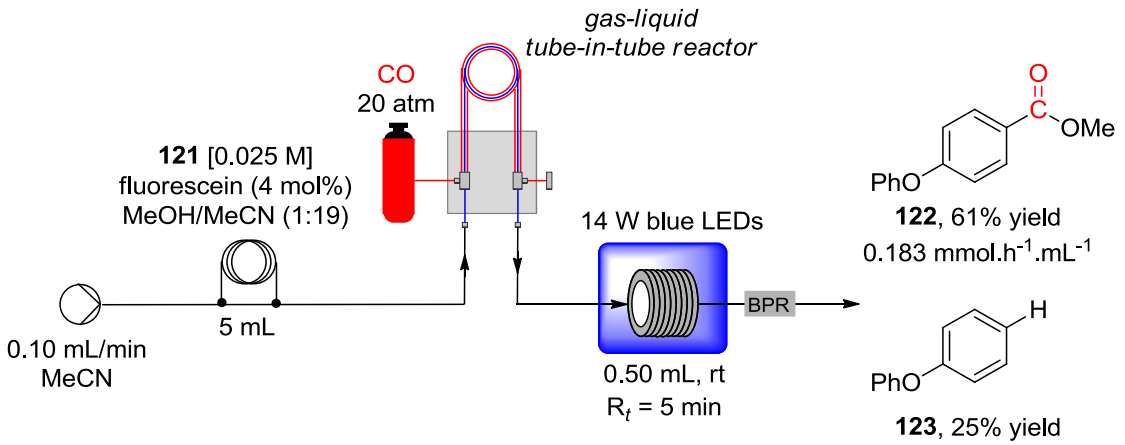

Figure 2.4.4. Fluorescein catalysed methoxycarbonylation with MeCN as the solvent.

Complexes of Ruthenium and Iridium are known to form stable complexes with CO resulting in catalyst deactivation.[162–164]It was anticipated that the mild CO pressures, ambient reaction temperature and short residence times enabled by microreactor technology could potentially relieve unwanted catalyst deactivation. When the archetypical ruthenium photocatalyst, $Ru(bpy)_3Cl_2$ was utilised, the desired esterified product **122** was obtained in good yield with complete consumption of the diazonium salt **121** (Table 2.4.1, entry 1). The catalyst loading could be reduced to 1 mol%, yielding **122** in good yields (Table 2.4.2, entry 2-4), without loss in activity. This suggested that transition metal photocatalysts are not significantly deactivated under the developed reaction conditions. Control reactions indicated that both catalyst and blue-light irradiation are essential for reactivity.

Table 2.4.1. Flow photo-methoxycarbonylation catalyst screen.

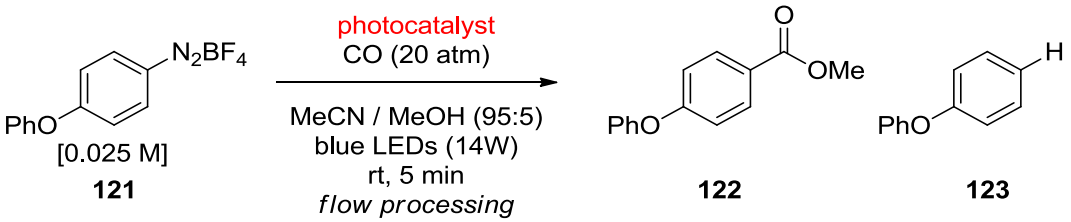

entry	photocatalyst (mol%)	yield 122 (%)[a]	yield 123 (%)[a]
1	$Ru(bpy)_3Cl_2 \cdot 6H_2O$ (4 mol%)	58	21
2	$Ru(bpy)_3Cl_2 \cdot 6H_2O$ (1 mol%)	63	15
3	$[Ir(dtbbpy)(ppy)_2]PF_6$ (1 mol%)	45	6
4	$(Ir[dF(CF_3)ppy]_2(dtbpy))PF_6$ (1 mol%)	62	15

[a] ^{1}H-NMR yields with maleic acid as the internal standard.

Photoredox catalysts that are transition metal complexes of Ruthenium and Iridium typically exhibit longer exited state lifetimes, reduced photo- bleaching and tuneable redox potentials than their organic dye counterparts.[157,165,166] Significantly, $Ru(bpy)_3Cl_2 \cdot 6H_2O$ has improved solubility in acetonitrile compared to fluorescein. In conjunction with the lower catalyst loading, this enabled $Ru(bpy)_3Cl_2 \cdot 6H_2O$ to promote methoxycarbonylation in flow at elevated concentration compare to fluorescein facilitating greater reaction throughput. A CO pressure screen was conducted at 0.1 M relative to the diazonium salt and determined 45 bar CO pressure to be optimum (Figure 2.4.5).

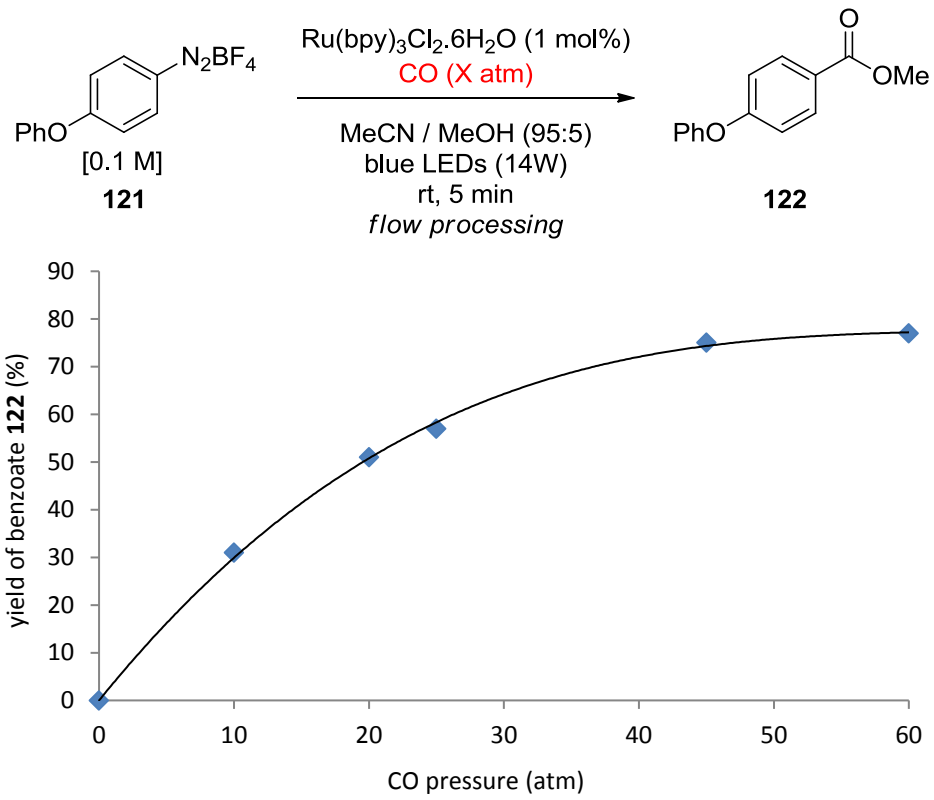

Figure 2.4.5. Effect of carbon monoxide pressure on reaction yield.

To demonstrate the facile scalability of the developed procedure, the reaction was conducted on the gram scale without modification of the flow platform. Operating in the continuous flow regime, 5 mmol of phenoxybenzene diazonium tetrafluoroborate was processed to afford 952 mg of methyl 4-phenoxybenzoate in 83% isolated yield (Figure 2.4.6).

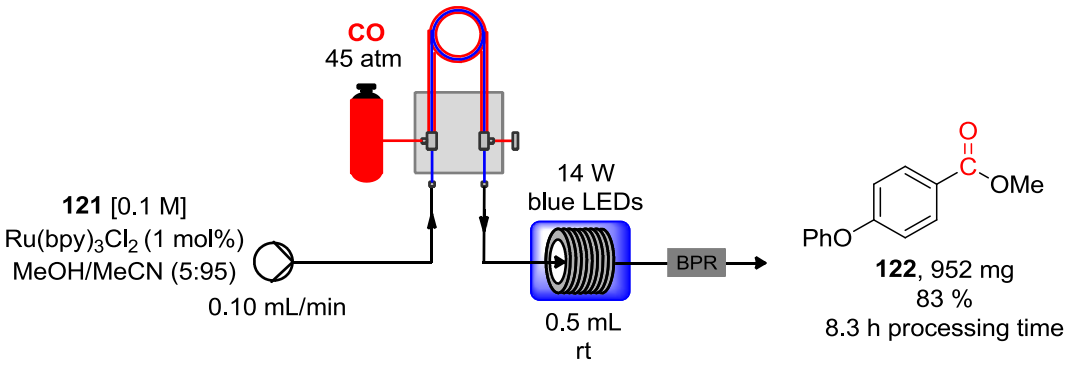

Figure 2.4.6. Continuous flow photoredox-catalysed methoxycarbonylation reaction scale-up.

2.5. Enhancing the Accessibility of the Flow Photo-Carbonylation Platform

The sluggish proliferation of high-pressure batch photochemical carbonylation in the synthesis community is, in part, attributed to the significant cost of the apparatuses – the photo-autoclave reactor – required to perform the chemistry. These assets have limited applicability outside of high-pressure photochemistry. The developed continuous flow system is intrinsically modular in nature. This lowers the financial cost and improves accessibility by allowing individual components to be interchangeable regardless of make or model. Research institutions with existing flow chemistry capability can rapidly access the developed flow system at little financial cost. Further, the modular nature of the flow system enables the platform to be further delineated to be applicable to a plethora of chemistries including electrochemistry, flash, solid supported, multistep, phase transfer catalysis, living polymerizations and reaction scale-up.[167] Research institutions without existing flow chemistry capability can make a strong business case to acquire the flow chemistry assets necessary to implement the developed continuous flow photoredox mediated carbonylation.

To demonstrate the enhanced accessibility of the developed chemistry, a flow platform was developed comprising of prevalent economical components (Figure 2.5.1). This economical flow platform features a Knauer Smartline Pump 100, standalone manual inject valve fitted with a 2 mL sample loop, bespoke tube-in-tube reactor (constructed as shown in Figure 2.2.4) coupled with a 1.5 mL tubular photoreactor irradiated by a 40 W Kessel LED lamp. When subjected to the optimized methoxycarbonylation reaction

conditions, the increased photon flux provided by the Kessel lamp allows for full consumption of **121** with a photoreactor residence time of 3 minutes, affording the aromatic ester **122** in 79% isolated yield (Figure 2.5.2). The higher volumetric flowrates accessed by scaling-out the photoreactor results in a significant throughput increase to 2.37 mmol·h^{-1} with a space-time yield of 1.58 mmol·h^{-1}·mL^{-1}. Reaction screening can be performed efficiently with a total run time of less than 5 minutes and no requirement to depressurise the system between runs. A cost analysis highlights the economy of this approach with the total flow system a fraction of the cost of the Parr photoreactor (Table 2.5.1).

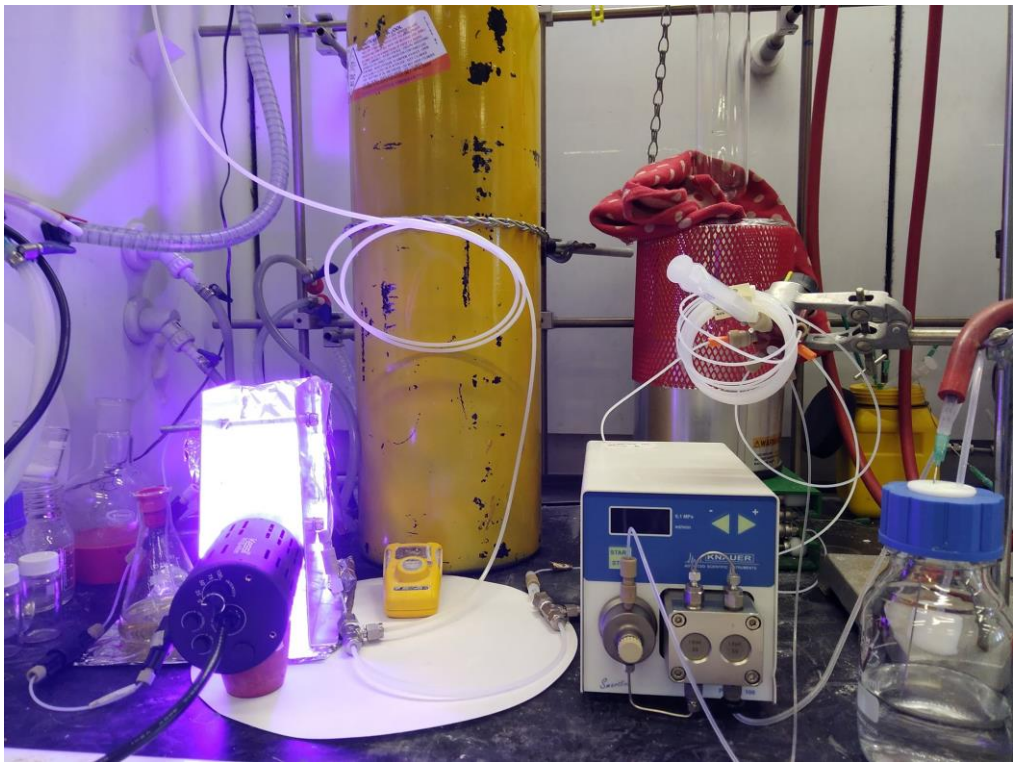

Figure 2.5.1. An economical flow platform derived from bespoke and non-specialized commercial units capable of performing high-pressure continuous flow photo-carbonylations.

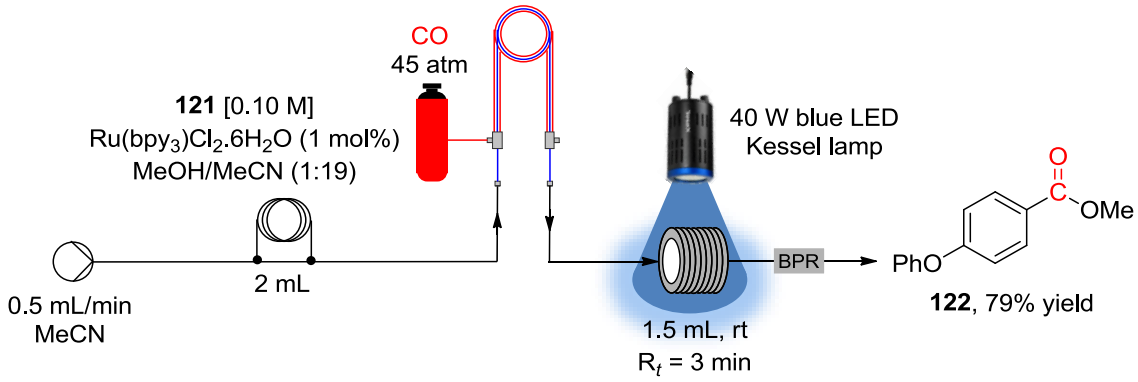

Figure 2.5.2. Cost analysis of an economical flow platform capable of performing rapid high-pressure continuous flow photo-carbonylations.

Table 2.5.1. High-pressure photochemical flow system cost analysis.

Component		Price (AUD $)	
Knauer P 2.1S Pump with 10ml stainless-steel pump head[a]		6,165	
Knauer A1358V1 Manual injection valve,[a] 6-port/3-channel PEEK, 1/16", 200 bar PPS rotor-seal		977	
	Subtotal		7142
2 mL sample loop			
1/16″ PFA tubing (452.7 cm)		63	
Super Flangeless™ Fittings		8	
	Subtotal		71
Tube-in-tube gas-liquid reactor[b]			
Teflon® AF-2400 tubing (20 cm)		60	
Swagelok T-pieces		70	
1/8″ PTFE tubing (20 cm)		6	
1/16″ PFA tubing (20 cm)		5	
Super Flangeless™ Fittings		16	
	Subtotal		157
1.5 mL Photochemical flow-reactor[b]			
1/16″ PFA tubing (339.5 cm)76		49	
Kessel 440 nm LED lamp		239	
Support Scaffold		10	
Desk fan		10	
	Subtotal		308
Back Pressure Regulators (3 units)		450	
	Total		**8,128**

[a] Representative replacement as the models used are discontinued.
[b] Bespoke component.

2.6. Conclusion

Methods for the continuous flow visible light photoredox-catalysed methoxycarbonylation of aryl diazonium salts were established. The developed methodology utilized the organic dye fluorescein or the transition metal complex $Ru(bpy)_3Cl_2.6H_2O$ to achieve the three-component coupling of an arenediazonium salt, carbon monoxide and an alcohol in excellent yields. Three gas-liquid photochemical continuous flow platforms, incorporating Teflon™ AF2400 tube-in-tube reactor technology, were developed to enable the reaction to proceed efficiently and safely.

The first platform was designed to have a maximum working pressure of 20 atm (Figure 2.3.3). This design constraint was introduced as many chemically resistant commercial flow platforms are limited to this maximum working pressure. Selectivity for the desired methoxycarbonylated product over the undesired competitive hydrodediazoniation product could be achieved at reduced CO pressure of 20 atm by employing dilute reaction conditions, acetonitrile as co-solvent and fluorescein and the photoredox catalyst. It was demonstrated that dilution is an effective strategy in flow as the throughput and space-time yield of the developed flow process was an order of magnitude greater than the comparative batch process.

The second flow system developed is capable to operating at high pressure – up to 75 atm (Figure 2.3.4). Polypyridyl transition-metal complexes of ruthenium and iridium were employed at 1 mol% catalyst loading and a photoreactor residence time of 5 minutes, to yield rapid and complete consumption of the diazonium salt reactant. This indicated that significant deactivation of CO sensitive transition metal complexes was not observed under the developed flow conditions. The enhanced solubility and reactivity of $Ru(bpy)_3Cl_2.6H_2O$ in acetonitrile compared to the organic dye photocatalysts facilitated higher reaction through put as the reaction concentration could be increased to 0.1 M, relative to the diazonium salt, with no catalyst precipitation observed. With $Ru(bpy)_3Cl_2.6H_2O$ as the photocatalyst, excellent isolated yields of the methoxycarbonylated product could be obtained by driving selectivity for the ester product through elevated CO pressure of 45 atm. The continuous flow photo-methoxycarbonylation reaction was scaled-up by a factor of 10 to yield 952 mg of methyl 4-phenoxybenzoate with no further process development required.

The third flow platform was constructed from readily available and affordable components, avoiding the use of commercial flow chemistry modules (Figure 2.4.7). Taking advantage of the modular design, components were readily tailored to enhance reaction throughput, providing the ability to rapidly screen reactions without compromising on performance and safety profile. This work signifies the ability of flow chemistry to alleviate the practical and financial challenges associated with high-pressure photochemistry of reactive gases, which is often the prohibitive factor when considering entering this reaction space.

2.7. Chapter 2 Experimental

Synthesis of Diazonium Salts

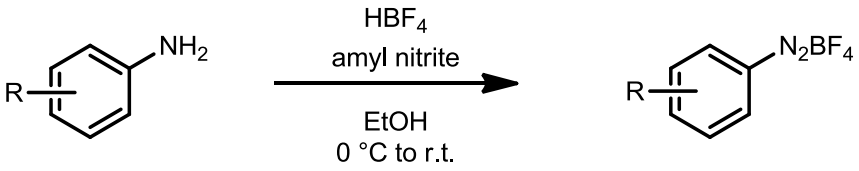

Prepared according to the method of Blanchet.[168] To a solution of parent aniline (1 equiv.) in ethanol, HBF_4 (48% in water, 1.1 equiv.) was added at room temperature. The mixture was cooled to 0 °C and amyl nitrite (2.0 equiv.) was added dropwise. After addition, the mixture was stirred at 0 °C for 15 min then allowed to reach room temperature. Diethyl ether (20 mL) was added to the reaction mixture. The mixture was cooled to -20 °C to induce crystallisation. The resulting solids were filtered, washed with copious amounts of diethyl ether and dried under high vacuum to afford the arenediazonium tetrafluoroborate.

Warning!!

CO is an odourless, colourless, flammable, reactive and toxic gas. A comprehensive risk assessment was performed, with reference to the material's safety data sheet, prior to any reactions with CO. Controls implemented were the installation of two CO gas detectors fitted with audible alarm and an emergency shut off valve. One CO detector was set inside the fume hood and the secondary detector was carried on the lapel.

The aryl diazonium tetrafluoroborates utilized were stable at room temperature for prolonged periods (weeks). The use of aryl diazonium chlorides – and other small

anionic counterions – was avoid as these compounds are known to degrade rapidly and may explode therefore are a significant hazard.

4-Methoxybenzenediazonium tetrafluoroborate (119)

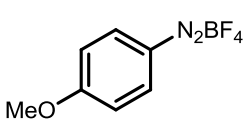

Compound **119** was prepared according to the general procedure with p-anisidine (9.0 mmol, 1.11 g). Isolated as a white solid (1.55 g, 75%). **^{1}H NMR** (400 MHz, DMSO-d_6): δ [ppm] = 8.61 (dd, *J* = 9.4 Hz, 2H), 7.48 (dd, *J* = 9.42 Hz, 2H), 4.04 (s, 3H); **HRMS** (ESI): calculated for $[C_7H_7N_2O]^+$: m/z = 135.0558, found: m/z = 135.0541. Analytical data is in agreement with previously reported literature data.[168]

4-Phenoxybenzenediazonium tetrafluoroborate (121)

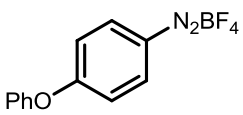

Compound **121** was prepared according to the general procedure with 4-phenoxyaniline (4.5 mmol, 833 mg). Isolated as an off-white solid (1.22 g, 92%). **^{1}H NMR** (400 MHz, DMSO-d_6): δ [ppm] = 8.66-8.62 (m, 2H), 7.61-7.55 (m, 2H), 7.43-7.37 (m, 3H), 7.32-7.27 (m, 2H); **HRMS** (ESI): calculated for $[C_{12}H_9N_2O]^+$: m/z = 197.0715, found: m/z = 197.0708. Analytical data is in agreement with previously reported literature data.[169]

Gram-Scale Continuous Flow Photoredox-Catalysed Methoxycarbonylation of Arenediazonium Salts Procedure

The flow system was primed with deoxygenated MeCN. A solution of 4-phenoxybenzene tetrafluoroborate (5.0 mmol, 1.42 g, 1.0 equiv.), MeOH (1 mL) and $Ru(bpy)_3Cl_2.6H_2O$ (37.5 mg, 1 mol %) in MeCN (49 mL) was sparged with N_2 (15 min). This mixture, maintained under positive pressure with N_2 and shielded from light, was pumped (flow rate 0.10 mL/min) through the GAM and enriched with CO (45 atm) then irradiated in the photoreactor (5 min residence time) prior to collection. To allow the reaction mixture to elute completely, 5 mL of deoxygenated MeCN was added to the reaction mixture reservoir just prior to it running dry. Back pressure regulators were installed at the reactor outlet to maintain the reaction stream at 45±5 atm. The product stream was collected (over 8.33 hours), concentrated *in vacuo* and the crude residue

purified by flash chromatography (0→10% EtOAc in hexane) to afford methyl 4-phenoxybenzoate as a pale-yellow solid (952 mg, 82%).

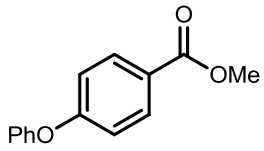

Methyl 4-phenoxybenzoate (120)

^{1}H NMR (400 MHz, $CDCl_3$): δ [ppm] = 8.01 (d, *J* = 8.66 Hz, 2H), 7.39 (t, *J* = 7.79 Hz, 2H), 7.19 (t, *J* = 7.34 Hz, 1H), 7.03 (dd, *J* = 32.34, 8.29 Hz, 4H), 3.89 (s, 3H); **^{13}C NMR** (100 MHz, $CDCl_3$): δ [ppm] = 166.62, 161.86, 155.67, 131.74, 130.09, 124.56, 124.52, 120.16, 117.33, 52.05; **HRMS** (ESI): calculated for $[C_{14}H_{13}O_3]^+$: m/z = 229.0864, found: m/z = 229.0866; Analytical data is in agreement with previously reported literature data.[113]

Chapter 3. Photocatalytic Annulative Meerwein Addition/Alkoxycarbonylation

Access to 3-Acetate Functionalized 2,3-Dihydrobenzofurnas

Components of this chapter have been published as:

Micic, N.; Polyzos, A. "Radical Carbonylation Mediated by Continuous-Flow Visible-Light Photocatalysis: Access to 2,3-Dihydrobenzofurans". *Organic Letters*, **2018**, *20*, 4663.

3.1. Introduction

The 2,3-dihydrobenzofuran (2,3-DHB) skeleton is a structural motif prevalent in a vast array of bioactive molecules including natural products and synthetic compounds with diverse biological activity (Scheme 3.1).[170–175] Recently, 3-acetate functionalised 2,3-DHBs, derivatives of 2,3-dihydro-benzofuranyl-3-acetic acid, have surfaced as novel oral therapeutics for type 2 diabetes mellitus.[176,177] The most promising candidate from the 3-acetate functionalised 2,3-DHB series is fasiglifam (**137**), a first-in-class GPR40 receptor agonist.[178] Whilst clinical trials were terminated following phase III due to liver toxicity, investigations towards 3-acetate functionalised 2,3-DHBs as GPR40 receptor agonists remain ongoing.[179–181]

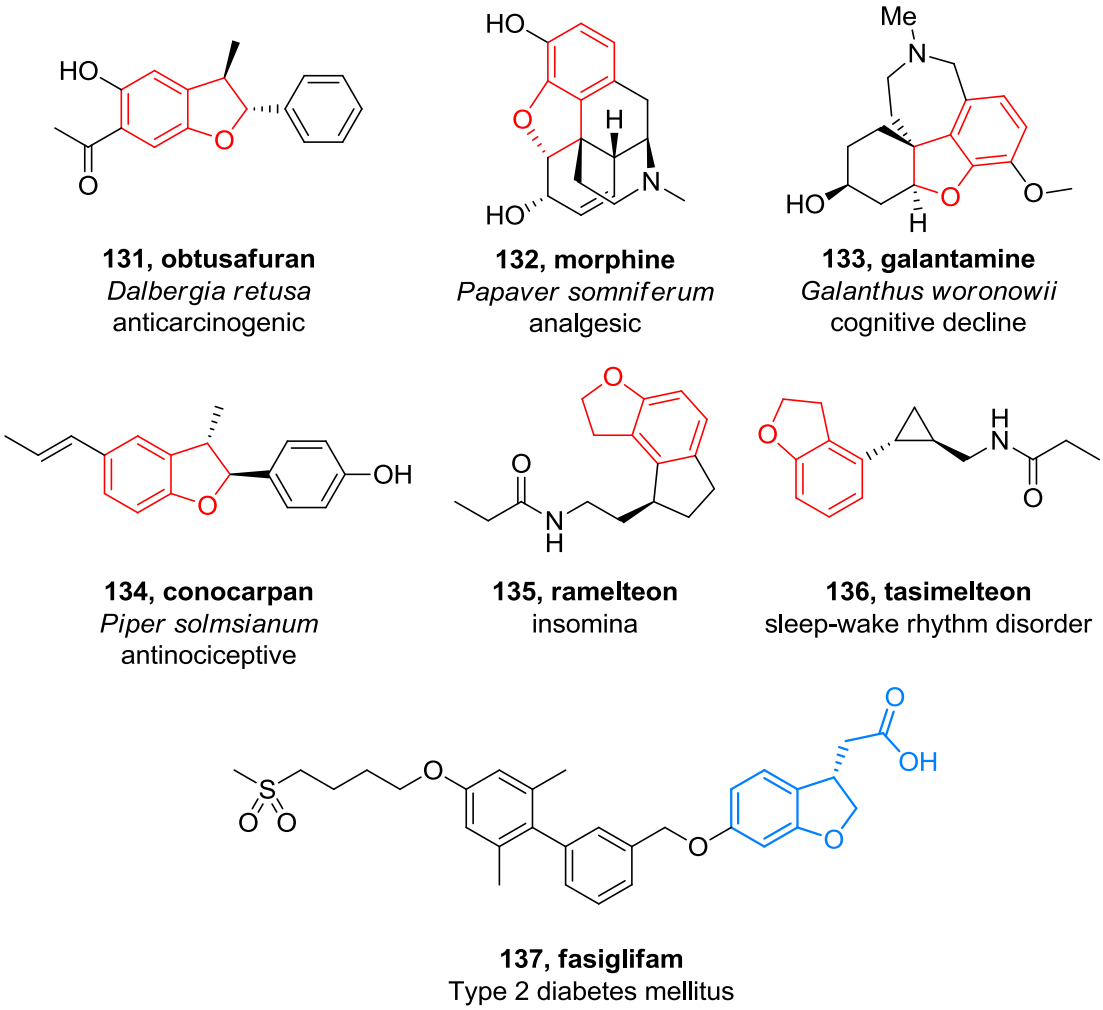

Scheme 3.1.1. Natural products and therapeutics incorporating the 2,3-DHB motif. The 2,3-DHB structural motif is highlighted in red. The 3-acetate 2,3-DHB structural motif is highlighted in blue.

There are several synthetic approaches for the formation of 2,3-DHB derivatives (Scheme 3.1.2). These approaches may be classified according to the final step in the synthesis. In class 1, the Favorskii rearrangement of 4-chromanones is employed.[182,183] In class 2, transition metal-catalysed intramolecular C-O bond formation of 2-halophenethyl alcohols is the final step.[184,185] Class 3 exploits a [2+2+2] cycloaddition reaction to generate both ring systems in a single step.[186] Class 4 involves the intramolecular cyclization of a aryl allyl ether.[187–189] In class 5, the hydrogenation of benzofurans gives rise to the analogous 2,3-DHBs.[190] Finally, class 6 comprises the intramolecular C−H insertion reaction of aryldiazoacetates.[191,192]

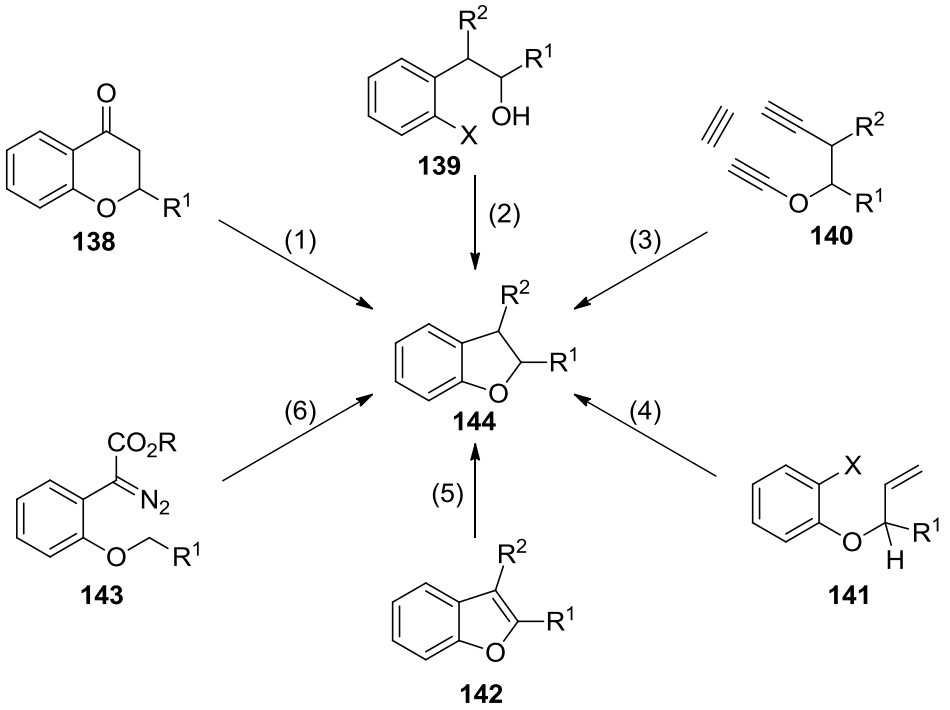

Scheme 3.1.2. Synthetic avenues to the 2,3-dihydroxybenzofuran structural motif.

Despite the availability of traditional and modern methodology to access the 2,3-DHB motif, methodology for the direct construction of esterified derivatives of 3-acetate functionalized 2,3-DHB remains underdeveloped. Access to 3-acetate functionalized 2,3-DHBs is most notably achieved via a 4 step sequence (Scheme 3.1.3): (**a**) Pechmann condensation of a phenol (**145**) with 4-bromoethylacetoacetate with concentrated sulfuric acid as the condensation agent, (**b**) Perkin reaction of the resultant 3-bromocourmarin (**146**) to afford the benzofuran-2-carboxylic acid (**147**), (**c**) hydrogenation of the C_2-C_3 double bond followed by (**d**) esterification of carboxylic acid **148** with thionyl chloride.[190] The requirement of concentrated acids, a

hydrogenation step and carboxylic acid activation for esterification restricts functional group tolerance and restricts atom economy.

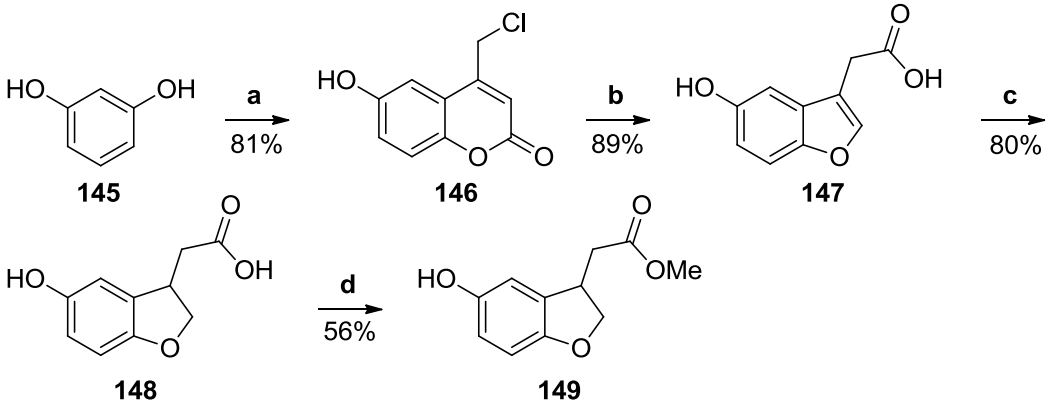

Scheme 3.1.3. Traditional synthesis of 2,3-dihydro-benzofuranyl-3-acetic acids.[11] (a) ethyl 4-chloroacetoacetate, H_2SO_4, 0 °C to rt; (b) KOH, reflux; (c) Pd/C, H_2 (30 psi), MeOH, rt; (d); $SOCl_2$, MeOH, 0 °C.

In 2010, Correia and co-workers reported the development of a carbonylative Heck-Matsuda reaction of allyloxy-tethered aryl diazonium salts (**150**) that afforded 2,3-dihydrobenzofuran acetic acid derivatives (scheme 3.1.4).[193] This tandem cyclisation/carbonylation approach is an attractive synthetic strategy due to its mild reaction conditions and atom economy. Furthermore, a diverse series of 2-allyloxy aryl diazonium salt substrates can be efficiently generated via diazotization from a wealth of commercially available 2-aminophenols.

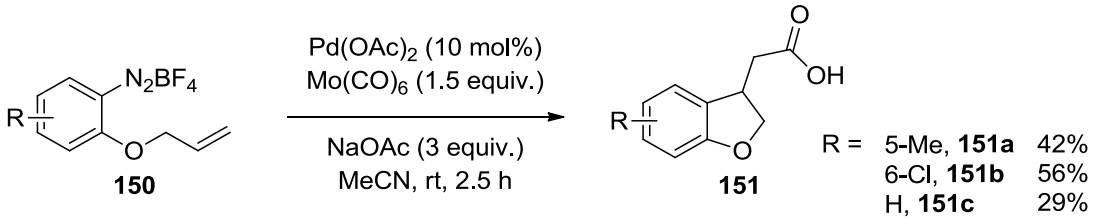

Scheme 3.1.4. Carbonylative Heck-Matsuda reaction of allyloxy-tethered aryl diazonium salts.

The synthesis of heterocycles with Pd-catalysed cascade Heck-reaction/carbonylation reaction, where the carbonyl group is installed pendant to the ring system (*exo*-carbonylation), is particularly challenging owing to multiple product distribution derived from competitive side reactions (Scheme 3.1.5).[194] Premature CO insertion, biscarbonylation, and β-hydride elimination pathways following oxidative addition of the palladium complex to aryl (pseudo)halides are the major competing reaction

pathways. Specifically, the synthesis of 2,3-DHBs by this strategy is plagued by β-hydride elimination arising from the transition of an aryl-palladium species **153** to the alkyl-palladium species **161**.[195] With two β-hydrogens *cis* to the alkyl group, the alkyl-palladium species **161** is positioned well towards β-hydride elimination.

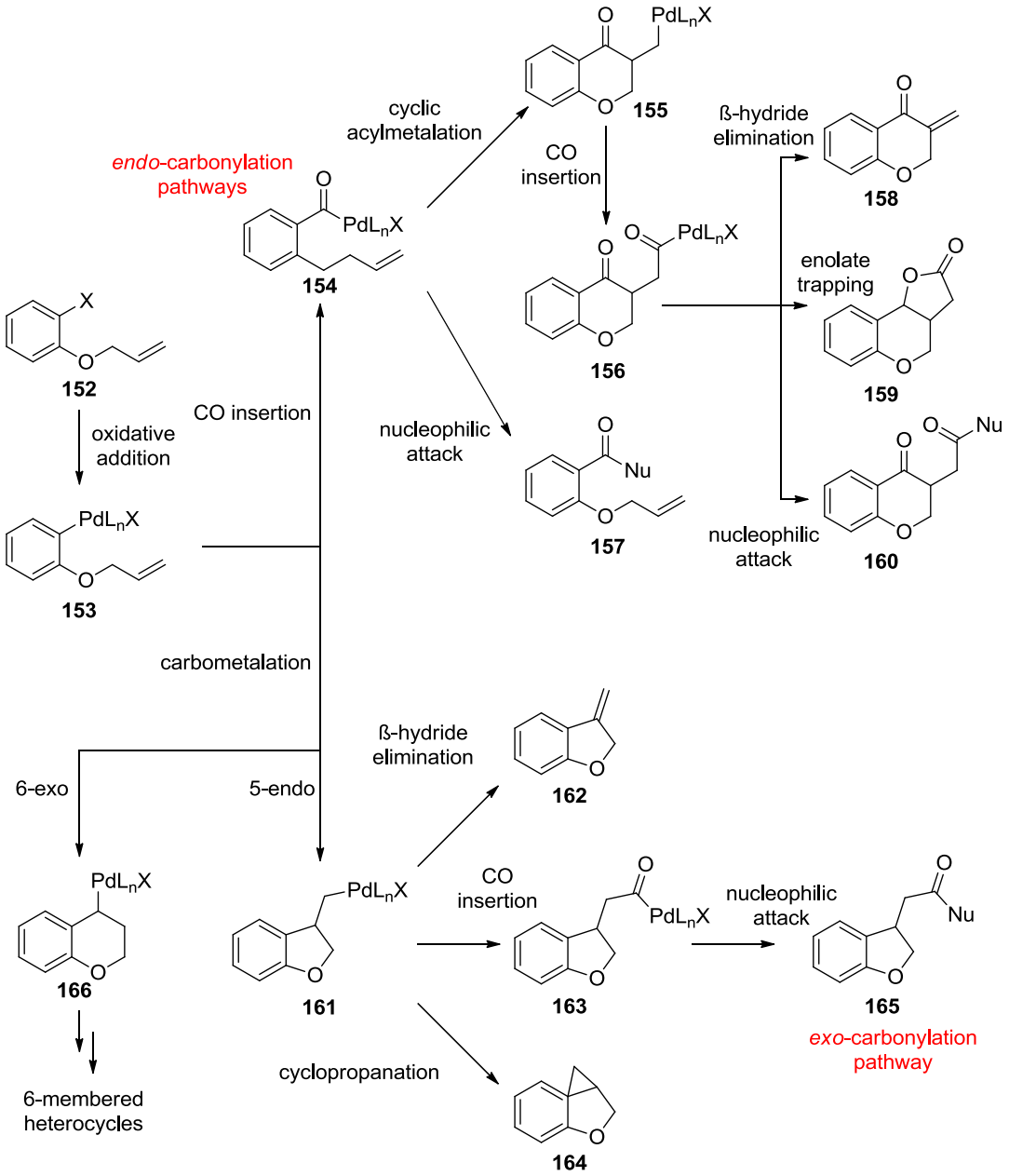

Scheme 3.1.5. Reaction pathways of the palladium-catalysed carbonylative Heck reaction with an alkenyl tether.

In contrast to Pd-catalysed carbonylation of alkynyl-tethered aryl (pseudo)halides, a free-radical approach is not afflicted by competitive premature CO insertion, biscarbonylation, and β-hydride elimination reactions. Radical trapping experiments performed by Beckwith and co-workers with Bu_3SnH,[196] coupled with the slow

addition of aryl radicals to CO,[84] indicate that the rate of 5-exo cyclization of 2-allyloxy tethered aryl radicals outcompetes CO trapping by the tethered aryl radical. Free-radical carbonylation of allyl-tethered aryl halides has been applied to afford acetaldehyde-functionalized O-heterocycles with organostannane reagents (Scheme 3.1.6 a).[197] The limitations of organostannane mediated free-radical methodology relates to poor functional group tolerance, the use of stoichiometric toxic reagents, the requirement for high-pressure CO (85 atm), and a coupling partner that is an effective radical acceptor.

In 2015, Xiao reported a single example of annulative Meerwein addition/alkoxycarbonylation of 2-allyloxybenzenediazonium salt **168** catalysed by the organo-photoredox catalyst fluorescein (Scheme 3.1.6 b).[113] Remarkably novel reactivity was achieved as a simple nucleophile was engaged as the coupling partner under catalytic reaction conditions. Despite this milestone, the photoredox-catalysed carbonylative cyclisation of alkenyl-tethered aryl(pseudo)halides had not been developed.

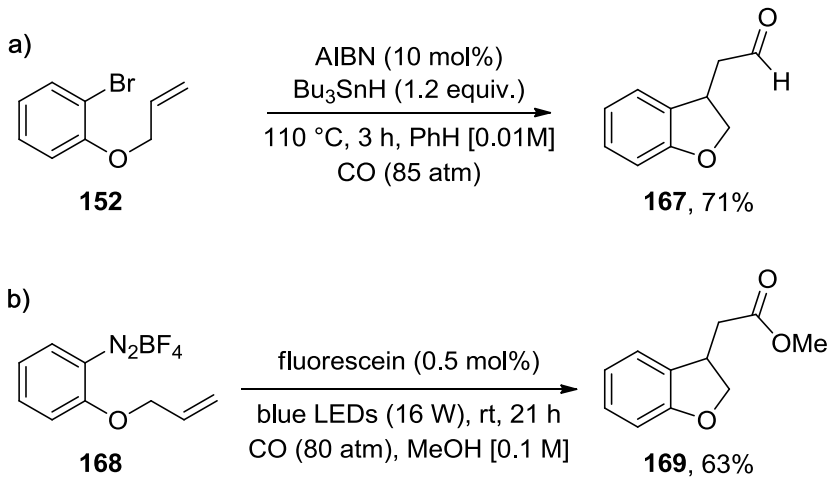

Scheme 3.1.6. Tandem radical addition/cyclisation/carbonylation yielding functionalised 2,3-DHBs.

This chapter describes the exploration of synthetic strategies enabling the annulative Meerwein addition/alkoxycarbonylation of alkenyl-tethered arenediazonium salts mediated by visible-light photocatalysis and continuous flow processing. The developed methodology provides access to esterified derivatives of 2,3-dihydrobenzofurans with significant regio- and chemoselectivity under mild reaction conditions. Continuous flow

processing was applied, enabling short residence times, low partial pressure of gaseous CO and straightforward scale-up to be realized.

3.2 Reaction Design and Development

The synthetic strategy to generate 3-acetate-functionalized 2,3-dihydrobenzofurans from allyloxy-tethered benzenediazonium tetrafluoroborate (**168**) via a photoredox-catalysis is depicted on Scheme 3.2.1. The reaction is initiated via photoexcitation of the ground state photocatalyst (PC). SET from the excited state photocatalyst (PC*) to the tethered aryldiazonium salt **168** induces homolytic cleavage of the C−N bond, yielding the aryl radical **170** and oxidatively quenched photocatalyst ($PC^{\bullet+}$). Intramolecular radical alkene addition produces the primary alkyl radical intermediate **171**. Reaction of **171** with CO furnishes the acyl radical **172**. Regeneration of the photocatalyst (PC) is achieved by SET from the acyl radical to the oxidized photocatalyst ($PC^{\bullet+}$) yielding the acylium ion **173**. Concurrently, radical chain propagation may occur by means of oxidation of intermediate **172** by the substrate **168**. Reaction of the acylium ion with an alcohol affords the 2,3-dihydro-benzofuranyl-3-acetate ester **169**.

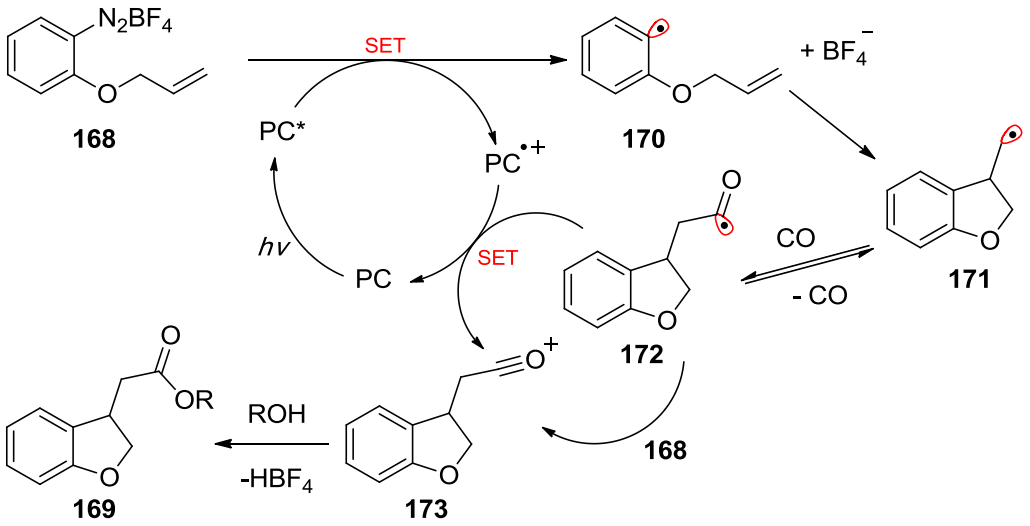

Scheme 3.2.1. Mechanistic proposal for the photoredox catalysed Meerwein addition/alkoxycarbonylation of 2-allyloxybenzene tetrafluoroborates.

It was hypothesised that intermolecular radical addition of intermediates **171** and **172** into the alkene bond would give rise to dimeric and polymeric products. Dilute reaction conditions were employed to supress this undesired reaction pathway. Continuous flow processing was implemented to facilitate the carbonylation reaction under dilute

reaction conditions. The flow configuration, adopted from Chapter 2, was comprised of a Uniqsis FlowSyn system equipped with a Uniqsis Gas Addition Module 1 (GAM) for CO delivery (Figure 3.2.1). The commercial system was connected to a bespoke built tubular flow photoreactor (total internal volume of 0.5 mL). Two 250 psi back pressure regulators were connected in series at the outlet to maintain the system under pressure and to prevent outgassing of CO.

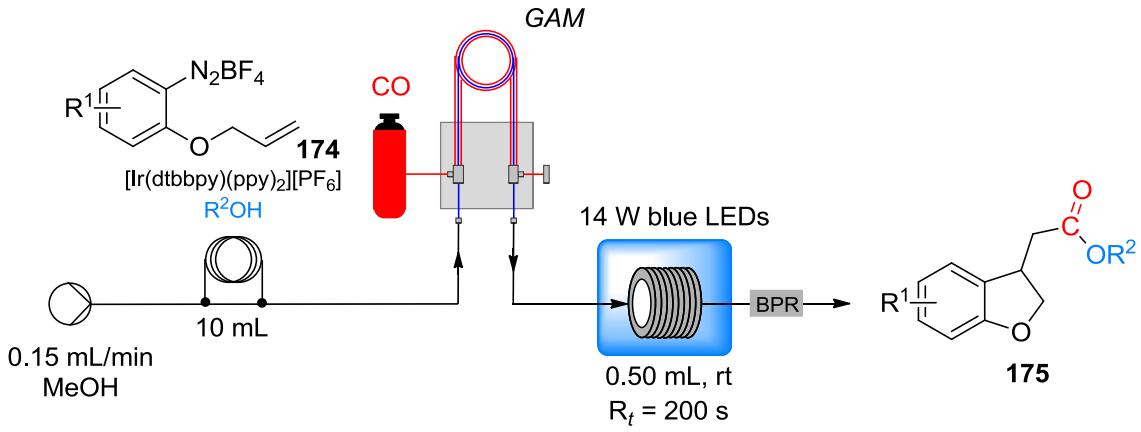

Figure 3.2.1. A schematic of the optimized gas-liquid photoreactor configuration employed.

Investigations began by examining a series of photocatalysts (Table 3.2.1.). Dilute (0.02 M relative to **168**) homogenous methanolic solutions of 2-allyloxybenzenediazonium tetrafluoroborate (**168**) and photocatalyst were pumped through the GAM (0.15mL/min), enriched with CO at 25 atm, then irradiated with blue light at room temperature to give methyl 2-(2,3-dihydrobenzofuran-3-yl)acetate (**169**). The photoreactor residence time was 200 seconds. With $[Ir(dtbbpy)(ppy)_2][PF_6]$ as the photocatalyst, the reaction afforded the desired methoxycarbonylated product **2a** in good yield (Table 3.2.1, entry 1). Interestingly, complexes of iridium or ruthenium were not deactivated under the reaction conditions by the strong coordinating character of CO and outperformed the organic photocatalysts screened. Full conversion of **168** was observed for complexes of Iridium and Ruthenium, and fluorescein catalysed reactions.

Table 3.2.1. Reaction development: catalyst screen.

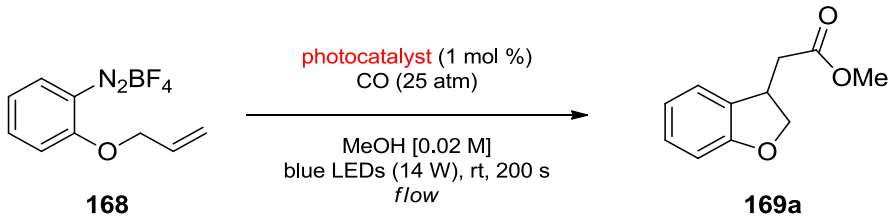

168 **169a**

entry	photocatalyst	yield 169a (%)[a]
1	$[Ir(dtbbpy)(ppy)_2]PF_6$	74
2	fluorescein	57
3	eosin Y (green LEDs)	40
4	methylene blue (green LEDs)	3
5	rhodamine B (green LEDs)	52
6	rhodamine 6G (green LEDs)	55
7	$[Ir(dF(CF_3)ppy)_2(dtbbpy)]PF_6$	66
8	$[Ru(bpy)_3]Cl_2.6H_2O$	67
9	$[Ru(bpz)_3][PF_6]_2$	66

[a] ^{1}H-NMR yields with maleic acid as the internal standard.

Increasing the concentration of substrate **168** resulted in polymerised by-products (Table 3.2.2, entry 1). A minor reduction in yield was observed upon lowering the concentration of methanol to 5% v/v (Table 3.2.2, entry 2-3). Stoichiometric quantities of alcohol resulted in diminished yields (Table 3.2.2, entry 4). The solvent screen was limited by the solubility of the diazonium salt in solvents of varying polarity. Substitution of acetonitrile for acetone, *N*,*N*-dimethylformamide (DMF) or dimethyl sulfoxide (DMSO) resulted in poor yields (Table 3.2.2, entry 5-7). At photoreactor residence times below 200 seconds, complete conversion of the arenediazonium salt was observed with a reduction in alkoxycarbonylated product, indicating the higher volumetric flow rate (0.45 mL/min) through the GAM did not result in CO saturation of the reaction phase (Table 3.2.2, entry 8). Longer residence times had no impact on observable yield. Reducing the catalyst loading to 0.5 mol% proved beneficial affording the desired ester **169a** in 73% isolated yield (Table 3.2.2, entry 9). A further reduction of catalyst loading was counterproductive (Table 3.2.2, entry 10). Control reactions revealed that irradiation and photocatalyst were essential to the transformation (Table 3.2.2, entry 11-12). Crude reaction mixtures were analysed by ^{1}H NMR and identified trace amounts 3-methyl-2,3-dihydrobenzofuran, suggesting the competitive reduction of **168** may be occurring under the reaction conditions.

Table 3.2.2. Reaction development: reaction parameters and controls.

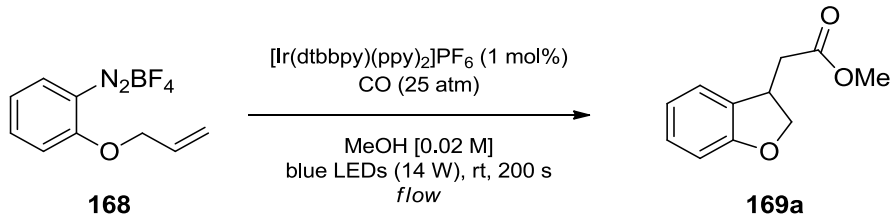

168 **169a**

entry	variation from scheme conditions	yield 169a (%)[a]
1	0.04 M concentration	53
2	MeCN/MeOH (1:1)	69
3	MeCN/MeOH (95:5)	64
4	10 equiv. of MeOH in MeCN	47
5	Me_2CO/MeOH (1:1)	42
6	DMF/MeOH (1:1)	17
7	DMSO/MeOH (1:1)	30
8	100 s photoreactor residence time	69
9	0.5 mol % [Ir]	85 (73)
10	0.2 mol % [Ir]	81
11	no catalyst	trace
12	no light	n.d.

[a] ^{1}H-NMR yields with maleic acid as the internal standard.

The pressure of CO was modulated to determine if the concentration of dissolved CO was limiting the reaction yield. Increasing the pressure of CO gas beyond 25 atm did not result in an increase in carbonylated products, suggesting intermolecular alkene addition was no longer a significant competing reaction pathway (Figure 3.2.2).

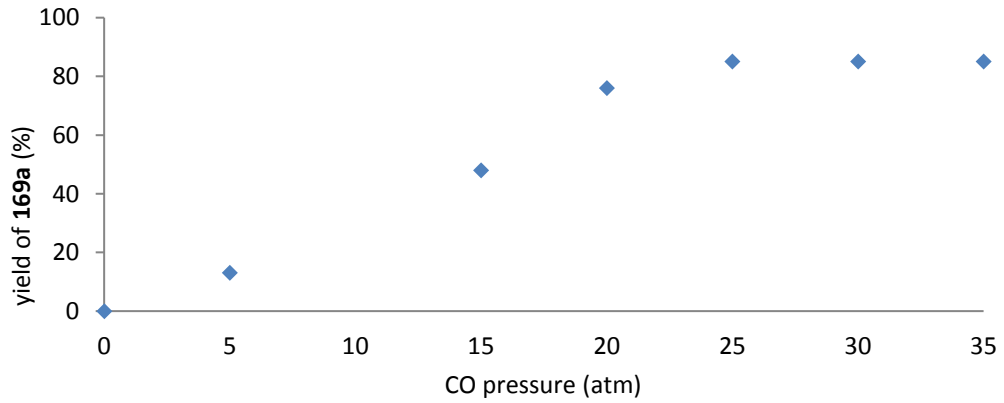

Figure 3.2.2. Effect of carbon monoxide pressure on reaction yield.

3.3. Annulative Meerwein Addition/Alkoxycarbonylation Reaction Scope

With the optimal reaction conditions established, the scope of the developed methodology was investigated (Figure 3.2.1). In all cases, excluding methanol and ethanol, acetonitrile was required as co-solvent to facilitate dissolution of the diazonium salt. Where the volatility of the coupling partner was low, acetonitrile was used in 95% v/v. Alkyl alcohols, including sterically hindered *tert*-butyl alcohol and cyclohexyl alcohol, were excellent coupling partners (**168a-f**). Phenol, capable of forming azo compounds with addition to arenediazonium salts,[198] afforded phenoxy esterified product **168h** in a modest yield. Alcohols with hydrogens prone to radical abstraction, participated without quenching of the alkyl radical (**168h-k**).[199] *Cis*-3-hexen-1-ol, with an internal alkene prone to palladium-catalysed olefin isomerisation, furnished the unsaturated ester **168k** with retention of double bond configuration. 2-Chloroethanol was compatible with the transformation, yielding **168l** which is well suited for further functionalization. Alcohols with unprotected carbonyl or terminal alkene/alkyne functionality were tolerated albeit in diminished yield (**169m-o**).

The generality of the optimised conditions was examined against a series of allyl arenediazonium ethers (Figure 3.3.2). Generally, weakly donating and electron withdrawing substituents afforded the desired radical annulation/carbonylation product in good to excellent yields. The arene's methyl substitution pattern did not have an appreciable influence on reaction yield (**176a-c**). Bromo, chloro and fluoro45-substituents participated smoothly without observable biscarbonylation products. This is in contrast to Pd-catalysed carbonylation where careful selection of reaction conditions are required to prevent undesired oxidative addition into the aryl-halide bond. Iodo substitution (**176h**) resulted in competitive biscarbonylation and dehalohydrogenated products as detected by ^{1}H NMR. The reaction yield was acceptable with methoxy substitution at the C6 position (**176j**). Methoxy, acetamide and phenoxy substitution at the C5 position did not furnish the carbocyclized product in appreciable quantities, instead yielding the hydrodediazotized allyl arene ether, suggesting that strongly donating substitution impairs the radical addition step. The presence of a nitro group (**176l**) resulted in poor conversion of diazonium salt with the reaction mixture quickly

turning dark red in colour, which was attributed to the redox activity of nitrobenzenes derivatives.[200]

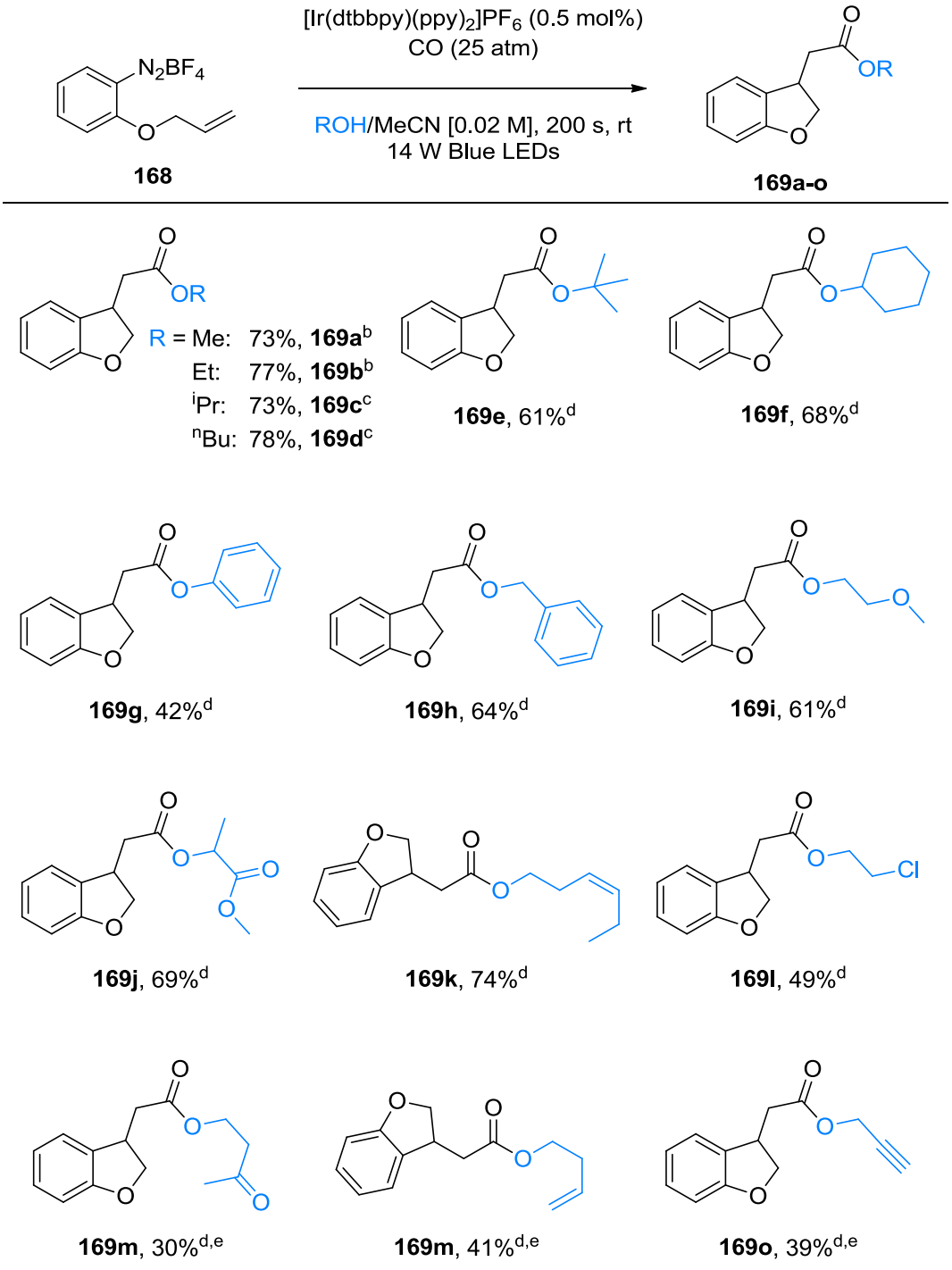

Figure 3.3.1. [a]Reaction conditions: **168** (0.2 mmol), $[Ir(dtbbpy)(bpy)_2]PF_6$ (0.5 mol%), ROH/MeCN (10 mL), CO (25 atm), irradiation (450 nm LED, 14 W), room temperature, 200 s, isolated yields. [b]No MeCN v/v as co-solvent. [c]50% v/v MeCN used as co-solvent. [d]95% v/v MeCN used as co-solvent. [e] ^1H NMR yield given.

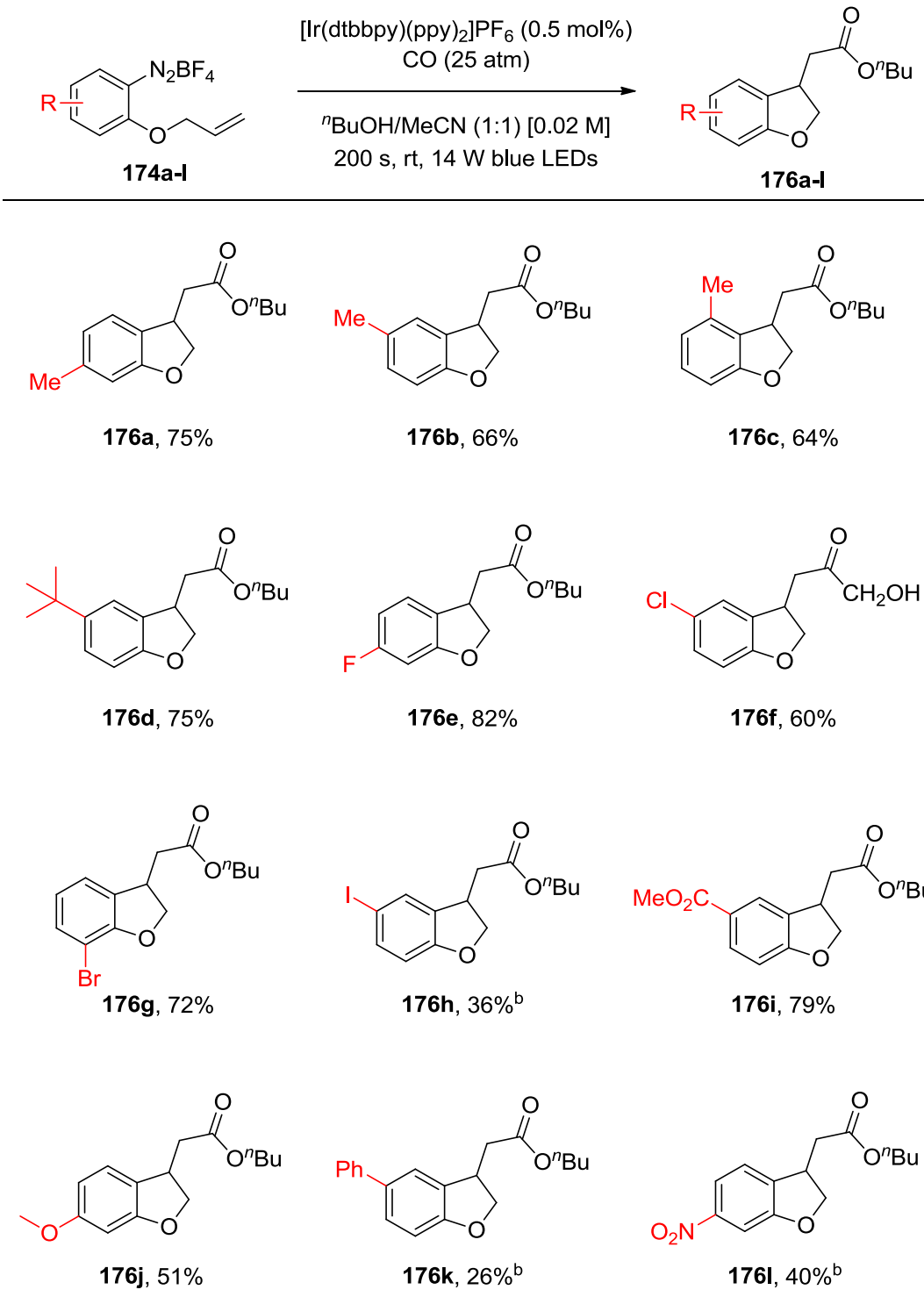

Figure 3.3.2. [a]Reaction conditions: **174** (0.2 mmol), $[Ir(dtbbpy)(bpy)_2]PF_6$ (0.5 mol%), *n*BuOH/MeCN 1:1 v/v (10 mL), CO (25 atm), irradiation (450 nm LED, 14 W), room temperature, 200 s, isolated yields. [b] ^1H NMR yield given.

The scope of unsaturated ortho-tethered arenediazonium salts compatible with the standard reaction conditions was examined (Figure 3.3.3). Methallyloxy derivative **177a** yielded the functionalized 2,3-DHB **177b**, with an all carbon quaternary center at the C3 position, in good yield. The reaction scope was extended the synthesis of functionalized benzofuran **178b** and chromane **178c** through the use of a propargyloxy and 1-butenyloxy tether, respectively.

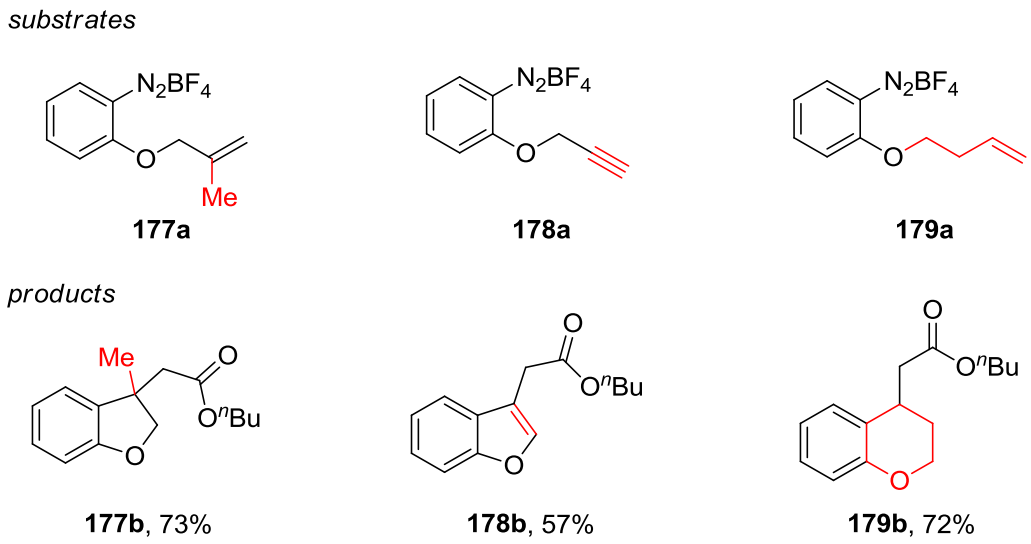

Figure 3.3.3. [a]Reaction conditions: **174** (0.2 mmol), $[Ir(dtbbpy)(bpy)_2]PF_6$ (0.5 mol%), *n*BuOH/MeCN 1:1 v/v (10 mL), CO (25 atm), irradiation (450 nm LED, 14 W), room temperature, 200 s, isolated yields. [b] ^1H NMR yield given.

As described in chapter 2, the scale up of high-pressure dilute photochemical reactions in batch is not trivial. The innate scalability of the developed flow protocol was demonstrated by performing the transformation at gram scale (Figure 3.3.4). This represents a scale factor of 20. To expedite a preparative scale reaction the reaction throughput was increased by a factor of 3. This was achieved by scaling-out the GAM and photoreactor volumes and increasing the volumetric flow rate threefold; the internal geometries of the reactors were not altered, instead the flow path within the reactors was increased. In continuous flow mode, 4.0 mmol of **168** was processed within 9 hours to afford the ethoxy ester **169b** in 72% isolated yield.

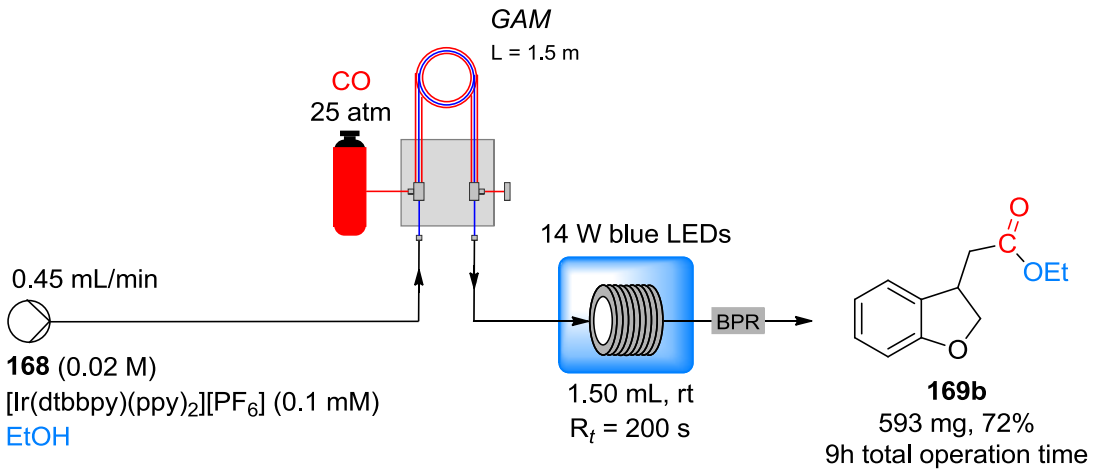

Figure 3.3.4. Photoredox mediated radical annulation/ethoxycarbonylation scale-up.

3.4. Conclusion

A continuous-flow visible-light photoredox catalytic approach for the tandem annulative Meerwein addition/alkoxycarbonylation of alkenyl-tethered arenediazonium salts was developed. Continuous flow processing enabled dilute reaction conditions to effectively be employed to control the propagation of competitive intermolecular radical addition side reactions. This enabled significantly reduced CO pressures to be employed compared to batch and allowed for facile scale-up. The developed methodology was applied to the synthesis of a diverse library of novel 3-acetate functionalized 2,3-dihydrobenzofurans from widely accessible allyloxy benzenediazonium ethers. This work exemplifies a strategy to overcome the chemo- and regio-selective challenges associated with Pd-catalysed annulative Heck-reaction/carbonylation through a free-radical approach whilst affording broad functional group tolerance and high atom economy.

3.5. Chapter 3 Experimental

General Procedure

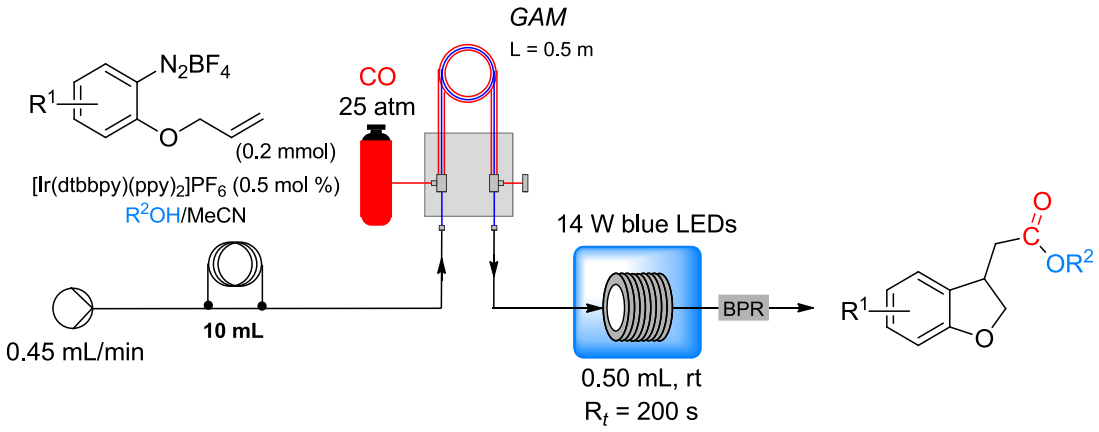

Figure 3.5.1. Annulative Meerwien addition/alkoxyarbonylation reaction scheme.

A solution of the arene diazonium salt (0.20 mmol, 1.0 equiv.) and $[Ir(dtbbpy)(ppy)_2]PF_6$ (0.5 mol %) in 10 mL of alcohol (with MeCN as co-solvent, as required) was sparged with N_2 (5 min) and loaded into a 10 mL sample loop. This mixture was pumped (flow rate 0.15 mL/min) through the GAM and enriched with CO (25 atm) then irradiated in the photoreactor (200 s residence time). The product stream was collected, concentrated *in vacuo* and the crude residue purified by preparative TLC (EtOAc/hexanes, 1:9) to afford the pure product. Back pressure regulators were installed at the reactor outlet to maintain the reaction stream at 25 atm.

Procedure for Continuous-Flow Radical Ethoxycarbonylation

A solution of 2-allyloxybenzene diazonium tetrafluoroborate (5.0 mmol, 1.0 equiv.) and $[Ir(dtbbpy)(ppy)_2]PF_6$ (0.5 mol %) in ethanol (250 mL) was sparged with N_2 (15 min). This mixture, maintained under positive pressure with N_2 and shielded from light, was pumped (flow rate 0.45 mL/min) through the GAM and enriched with CO (25 atm) then irradiated in the photoreactor (200 s residence time) prior to collection. To allow the system to reach steady state operation, the first 20 mL of the product stream was discarded. The following 200 mL of product stream was collected (over 7.44 hours), concentrated *in vacuo* and the crude residue purified by flash chromatography (EtOAc/hexanes, 1:19) to afford pure ethyl 2-(2,3-dihydrobenzofuran-3-yl)acetate as a

yellow oil (593 mg, 72%). Back pressure regulators were installed at the reactor outlet to maintain the reaction stream at 25 atm.

Product Characterization

Methyl 2-(2,3-dihydrobenzofuran-3-yl)acetate (169a)

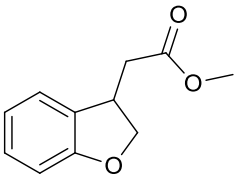

Compound **169a** was prepared according to the general procedure with **168** (0.2 mmol, 49.6 mg). No co-solvent was required. Isolated as a yellow oil (28.1 mg, 73%). **^{1}H NMR** (400 MHz, $CDCl_3$): δ [ppm] = 7.18-7.12 (m, 2H), 6.87 (t, *J* = 7.0 Hz, 1H), 6.80 (d, *J* = 7.6 Hz, 1H), 4.75 (dd, *J* = 9.1, 9.1 Hz, 1H), 4.25 (dd, *J* = 9.2, 6.3 Hz, 1H), 3.93 – 3.83 (m, 1H), 3.73 (s, 3H), 2.80 (dd, *J* = 16.5, 5.3 Hz, 1H), 2.59 (dd, *J* = 16.5, 9.5 Hz, 1H). **^{13}C NMR** (100 MHz, $CDCl_3$); δ [ppm] = 172.45, 159.93, 129.21, 128.85, 124.35, 120.72, 109.91, 76.86, 52.00, 39.39, 38.43; **HRMS** (ESI): calculated for $[C_{11}H_{13}O_3]^+$: m/z = 193.0859, found: m/z = 193.0860. Analytical data is in agreement with previously reported literature data.[201]

Ethyl 2-(2,3-dihydrobenzofuran-3-yl)acetate (169b)

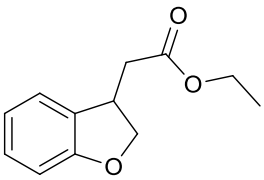

Compound **169b** was prepared according to the general procedure with **168** (0.2 mmol, 49.6 mg). No co-solvent was required. Isolated as an yellow oil (31.8 mg, 77%). **^{1}H NMR** (400 MHz, $CDCl_3$): δ [ppm] = 7.18-7.12 (m, 2H), 6.86 (t, *J* = 7.4 Hz, 1H), 6.80 (d, *J* = 8.0 Hz, 1H), 4.76 (dd, *J* = 9.1, 9.1 Hz, 1H), 4.26 (dd, *J* = 9.2, 6.4 Hz, 1H), 4.18 (td, *J* = 7.1 Hz, *J* = 7.1 Hz 2H), 3.92 – 3.84 (m, 1H), 3.73 (s, 3H), 2.79 (dd, *J* = 16.4, 5.3 Hz, 1H), 2.58 (dd, *J* = 16.4, 9.5 Hz, 1H), 1.28 (dd, *J* = 7.15 Hz, *J* = 7.15 Hz, 3H). **^{13}C NMR** (100 MHz, $CDCl_3$); δ [ppm] = 171.96, 159.94, 129.27, 128.79, 124.35, 120.68, 108.86, 76.59, 60.89, 39.63, 38.44, 14.35; **HRMS** (ESI): calculated for $[C_{12}H_{15}O_3]^+$: m/z = 207.1016, found: m/z = 207.1012; **IR** (ν/cm^{-1}, neat): 2953, 2891, 1732, 1611, 1597, 1482, 1461, 1436, 1361, 1317, 1287, 1233, 1195, 1162, 1106, 1016, 963, 887, 848, 835, 797, 749.

***iso*-Propyl 2-(2,3-dihydrobenzofuran-3-yl)acetate (169c)**

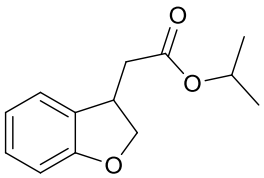

Compound **169c** was prepared according to the general procedure with **168** (0.2 mmol, 49.6 mg). 50% v/v MeCN was used as co-solvent. Isolated as a yellow oil (32.2 mg, 73%). **^{1}H NMR** (400 MHz, CDCl3): δ [ppm] = 7.17-7.12 (m, 2H), 6.86 (t, *J* = 7.4 Hz, 1H), 6.80 (d, *J* = 8.0 Hz, 1H), 5.05 (sep, *J* = 6.27 Hz, 1H), 4.75 (dd, *J* = 9.1, 9.1 Hz, 1H), 4.26 (dd, *J* = 9.2, 6.5 Hz, 1H), 3.92 – 3.83 (m, 1H), 2.76 (dd, *J* = 16.3, 5.3 Hz, 1H), 2.55 (dd, *J* = 16.3, 9.4 Hz, 1H), 1.25 (d, *J* = 6.3 Hz, 6H); **^{13}C NMR** (100 MHz, $CDCl_3$): δ [ppm] = 171.46, 159.94, 129.32, 128.75, 124.36, 120.66, 109.84, 76.83, 68.36, 39.93, 38.49, 21.96; **HRMS** (ESI): calculated for $[C_{13}H_{17}O_3]^+$: m/z = 221.1172, found: m/z = 221.1171; **IR** (ν/cm^{-1}, neat): 2981, 1724, 1612, 1597, 1483, 1462, 1415, 1374, 1314, 1286, 1233, 1176, 1105, 1017, 969, 948, 902, 862, 823, 749.

***n*-Butyl 2-(2,3-dihydrobenzofuran-3-yl)acetate (169d)**

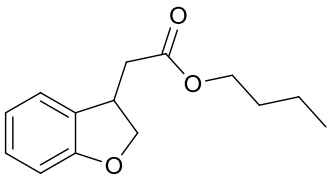

Compound **169d** was prepared according to the general procedure with **168** (0.2 mmol, 49.6 mg). 50% v/v MeCN was used as co-solvent. Isolated as an yellow oil (36.6 mg, 78%). **^{1}H NMR** (400 MHz, $CDCl_3$): δ [ppm] = 7.17-7.12 (m, 2H), 6.86 (t, *J* = 7.4 Hz, 1H), 6.80 (d, *J* = 7.9 Hz, 1H), 4.75 (dd, *J* = 9.1, 9.1 Hz, 1H), 4.26 (dd, *J* = 9.2, 6.4 Hz, 1H), 4.13 (dd, *J* = 6.7 Hz, *J* = 6.7 Hz, 2H), 3.93 – 3.83 (m, 1H), 2.80 (dd, *J* = 16.4, 5.3 Hz, 1H), 2.58 (dd, *J* = 16.3, 9.5 Hz, 1H), 1.67-1.57 (m, 2H), 1.44-1.32 (m, 2H), 0.94 (dd, *J* = 7.4 Hz, *J* = 7.4 Hz, 3H); **^{13}C NMR** (100 MHz, $CDCl_3$): δ [ppm] =172.06, 159.93, 129.26, 128.79, 124.34, 120.69, 109.86, 76.87, 64.82, 39.63, 38.46, 30.75, 19.27, 13.84; **HRMS** (ESI): calculated for $[C_{14}H_{19}O_3]^+$: m/z = 235.1329, found: m/z = 235.1325; **IR** (ν/cm^{-1}, neat): 2960, 1729, 1612, 1597, 1482, 1461, 1414, 1393, 1356, 1315, 1286, 1233, 1163, 1062, 1017, 966, 835, 749.

***t*-Butyl 2-(2,3-dihydrobenzofuran-3-yl)acetate (169e)**

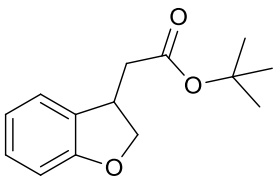

Compound **169e** was prepared according to the general procedure with **168** (0.2 mmol, 49.6 mg). 95% v/v MeCN was used as co-solvent. Isolated as a yellow oil (28.6 mg, 61%). **^{1}H NMR** (400 MHz, $CDCl_3$): δ [ppm] = 7.17-7.11 (m, 2H), 6.86 (t,

J = 7.4 Hz, 1H), 6.79 (d, *J* = 8.0 Hz, 1H), 4.74 (dd, *J* = 9.1, 9.1 Hz, 1H), 4.26 (dd, *J* = 9.1, 6.6 Hz, 1H), 3.89 – 3.79 (m, 1H), 2.71 (dd, *J* = 16.2, 5.3, 1H), 2.51 (dd, *J* = 16.2, 9.3 Hz, 1H), 1.46 (s, 9H); **^{13}C NMR** (100 MHz, $CDCl_3$): δ [ppm] = 171.07, 159.82, 129.30, 128.50, 124.21, 120.45, 109.63, 81.00, 76.68, 40.67, 38.43, 28.06; **HRMS** (ESI): calculated for $[C_{14}H_{19}O_3]^+$: m/z = 235.1329, found: m/z = 235.1301; **IR** (ν/cm^{-1}, neat): 2978, 1724, 1612, 1597, 1482, 1461, 1393, 1367, 1287, 1232, 1146, 1017, 967, 869, 838, 748.

Cyclohexyl 2-(2,3-dihydrobenzofuran-3-yl)acetate (169f)

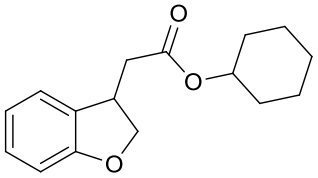

Compound **169f** was prepared according to the general procedure with **168** (0.2 mmol, 49.6 mg). 95% v/v MeCN was used as co-solvent. Isolated as a yellow oil (35.4 mg, 68%). **^{1}H NMR** (400 MHz, $CDCl_3$): δ [ppm] = 7.17-7.12 (m, 2H), 6.86 (t, *J* = 7.4 Hz, 1H), 6.80 (d, *J* = 8.0 Hz, 1H), 4.86-4.79 (m, 1H), 4.75 (dd, *J* = 9.1, 9.1 Hz, 1H), 4.27 (dd, *J* = 9.2, 6.5 Hz, 1H), 3.93 – 3.83 (m, 1H), 2.78 (dd, *J* = 16.3, 5.3, 1H), 2.57 (dd, *J* = 16.3, 9.4, 1H), 1.93-1.18 (m, 11H); **^{13}C NMR** (100 MHz, $CDCl_3$): δ [ppm] = 171.35, 159.94, 129.33, 128.72, 124.34, 120.64, 109.82, 76.82, 73.23, 39.95, 38.54, 31.74, 25.44, 23.85; **HRMS** (ESI): calculated for $[C_{16}H_{21}O_3]^+$: m/z = 261.1485, found: m/z = 261.1422; **IR** (ν/cm^{-1}, neat): 2936, 2853, 1719, 1611, 1597, 1482, 1445, 1415, 1385, 1361, 1318, 1290, 1236, 1223, 1178, 1154, 1113, 1038, 1014, 978, 945, 801, 749, 728.

Phenyl 2-(2,3-dihydrobenzofuran-3-yl)acetate (169g)

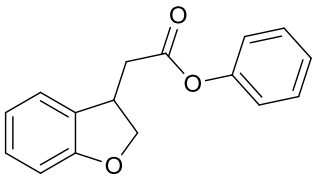

Compound **169g** was prepared according to the general procedure with **168** (0.2 mmol, 49.6 mg). 95% v/v MeCN was used as co-solvent. Isolated as an orange amorphous solid (21.4 mg, 42%). **^{1}H NMR** (400 MHz, $CDCl_3$): δ [ppm] = 7.43-7.37 (m, 2H), 7.29-7.22 (m, 2H), 7.21-7.16 (m, 1H), 7.10-7.07 (m, 2H), 6.90 (t, *J* = 7.4 Hz, 1H), 6.84 (d, *J* = 8.0 Hz, 1H), 4.80 (dd, *J* = 9.1, 9.1 Hz, 1H), 4.37 (dd, *J* = 9.3, 6.2 Hz, 1H), 3.95 – 4.04 (m, 1H), 3.05 (dd, *J* = 16.7, 5.5 Hz, 1H), 2.86 (dd, *J* = 16.7, 9.2 Hz, 1H); **^{13}C NMR** (100 MHz, $CDCl_3$): δ [ppm] = 170.54, 159.99, 150.56, 129.65, 129.02,128.94, 126.18, 124.50, 121.57, 120.83, 110.02, 76.71, 39.68, 38.46; **HRMS** (ESI): calculated for $[C_{16}H_{15}O_3]^+$: m/z = 255.1016, found: m/z = 255.1021; **IR** (ν/cm^{-1},

neat): 3044, 2923, 2852, 1747, 1596m 1482, 1456, 1408, 1378, 1368, 1317, 1287, 1244, 1191, 1164, 1145, 1072, 1016, 950, 926, 891, 866, 804, 757, 746, 705, 688.

Benzyl 2-(2,3-dihydrobenzofuran-3-yl)acetate (169h)

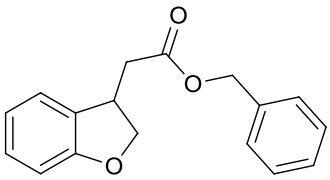

Compound **169h** was prepared according to the general procedure with **168d** (0.2 mmol, 49.6 mg). 95% v/v MeCN was used as co-solvent. Isolated as a yellow oil (34.3 mg, 64%). **^{1}H NMR** (400 MHz, $CDCl_3$): δ [ppm] = 7.42-7.32 (m, 5H), 7.15-7.12 (m, 2H), 6.85 (t, *J* = 7.4 Hz, 1H), 6.80 (d, *J* = 7.9 Hz, 1H), 5.22-5.11 (m, *J* = 2.55 Hz, 2H), 4.74 (dd, *J* = 9.1, 9.1 Hz, 1H), 4.26 (dd, *J* = 9.2, 6.4 Hz, 1H), 3.94 – 3.85 (m, 1H), 2.85 (dd, *J* = 16.5, 5.3 Hz, 1H), 2.64 (dd, *J* = 16.3, 9.2 Hz, 1H); **^{13}C NMR** (100 MHz, $CDCl_3$): δ [ppm] = 171.78, 159.92, 135.74, 129.13, 128.83, 128.77, 128.55, 128.48, 124.36, 120.72, 109.89, 76.80, 66.76, 39.60, 38.45; **HRMS** (ESI): calculated for $[C_{17}H_{16}O_3]^+$: m/z = 269.1172, found: m/z = 269.1180; **IR** (ν/cm^{-1}, neat): 3035, 2892, 1730, 1611, 1597, 1482, 1460, 1412, 1383, 1355, 1314, 1286, 1233, 1153, 1017, 955, 835, 748, 696.

2-Methoxyethyl 2-(2,3-dihydrobenzofuran-3-yl)acetate (169i)

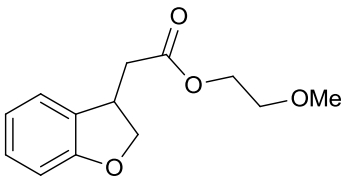

Compound **169i** was prepared according to the general procedure with **168** (0.2 mmol, 49.6 mg). 50% v/v MeCN was used as co-solvent. Isolated as a yellow oil (28.8 mg, 61%). **^{1}H NMR** (400 MHz, $CDCl_3$): δ [ppm] = 7.17-7.12 (m, 2H), 6.87 (t, *J* = 7.4 Hz, 1H), 6.80 (d, *J* = 8.0 Hz, 1H), 4.75 (dd, *J* = 9.1, 9.1 Hz, 1H), 4.30-4.23 (m, 3H), 3.93-3.84 (m, 1H), 3.60 (dd, *J* = 4.7 Hz, *J* = 4.7 Hz, 2H), 3.39 (s, 3H), 2.85 (dd, *J* = 16.6, 5.3 Hz, 1H), 2.63 (dd, *J* = 16.6, 9.5 Hz, 1H); **^{13}C NMR** (100 MHz, $CDCl_3$): δ [ppm] = 171.98, 159.94, 129.18, 128.82, 124.37, 120.70, 109.87, 76.80, 70.48, 63.88, 59.15, 39.45, 38.42; **HRMS** (ESI): calculated for $[C_{13}H_{17}O_4]^+$: m/z = 237.1121, found: m/z = 237.1119; **IR** (ν/cm^{-1}, neat): 2891, 1730, 1611, 1597, 1482, 1461, 1412, 1378, 1352, 1315, 1286, 1234, 1199, 1171, 1127, 1102, 1033, 1017, 964, 878, 835, 800, 750.

Methyl 2-(2-(2,3-dihydrobenzofuran-3-yl)acetoxy)propanoate (169j)

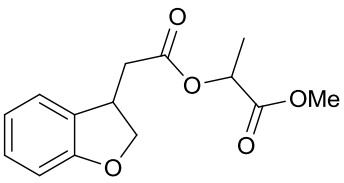

Compound **169j** was prepared according to the general procedure with **168d** (0.2 mmol, 49.6 mg, 1:1 dr). 50% v/v MeCN was used as co-solvent. Isolated as an inseparable mixture of diastereoisomers, yellow oil (36.5 mg, 59%). **^{1}H NMR** (400 MHz, $CDCl_3$): δ [ppm] = 7.19-7.12 (m, 2H), 6.87 (t, *J* = 7.4 Hz, 1H), 6.80 (d, *J* = 8.0 Hz, 1H), 5.17-5.10 (m, 1H), 4.79-4.71 (m, 1H), 4.34-4.25 (m, 1H), 3.97-3.85 (m, 1H), 3.77 (d, 3H), 2.95-2.81 (m, 1H), 2.73-2.66 (m, 1H), 1.51 (dd, *J* = 7.1, 1.6 Hz, 3H); **^{13}C NMR** (100 MHz, $CDCl_3$): δ [ppm] = 171.40, 171.35, 171.20, 171.16, 159.95, 159.94, 129.12, 129.03, 128.87, 128.86, 124.41, 124.37, 120.74, 120.71, 109.91, 109.89, 76.71, 76.66, 68.96, 52.57, 39.35, 39.21, 38.45, 38.36, 17.05; **HRMS** (ESI): calculated for $[C_{14}H_{17}O_5]^+$: m/z = 265.1071, found: m/z = 265.1076; **IR** (ν/cm^{-1}, neat): 3050, 2954, 1736, 1611, 1597, 1483, 1461, 1365, 1308, 1285, 1246, 1161, 1133, 1097, 1047, 1017, 966, 848, 835, 805, 750, 668.

(Z)-Pent-2-en-1-yl 2-(2,3-dihydrobenzofuran-3-yl)acetate (169k)

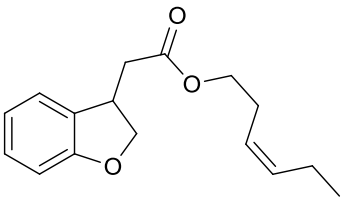

Compound **169k** was prepared according to the general procedure with **168d** (0.2 mmol, 49.6 mg). 95% v/v MeCN was used as co-solvent. Isolated as a yellow oil (38.5 mg, 74%). **^{1}H NMR** (400 MHz, $CDCl_3$): δ [ppm] = 7.19-7.11 (m, 2H), 6.86 (t, *J* = 7.4 Hz, 1H), 6.80 (d, *J* = 7.9 Hz, 1H), 5.56-5.49 (m, 1H), 5.34-5.28 (m, 1H), 4.75 (dd, *J* = 9.1, 9.1 Hz, 1H), 4.26 (dd, *J* = 9.2, 6.4 Hz, 1H), 4.13 (dd, *J* = 6.9 Hz, *J* = 6.9 Hz, 2H), 3.91-3.84 (m, 1H) , 2.79 (dd, *J* = 16.5, 5.2 Hz, 1H), 2.58 (dd, *J* = 16.5, 9.5 Hz, 1H), 2.39 dt, *J* = 7.0 Hz, *J* = 7.0 Hz, 2H), 2.06 (dq, *J* = 7.5 Hz, *J* = 7.5 Hz, 2H), 0.98 (dd, *J* = 7.5 Hz, *J* = 7.5 Hz, 3H); **^{13}C NMR** (100 MHz, $CDCl_3$): δ [ppm] = 171.80, 159.78, 134.71, 129.08, 128.64, 124.19, 123.51, 120.53, 109.71, 76.71, 64.27, 39.44, 38.29, 26.67, 20.60, 14.20; **HRMS** (ESI): calculated for $[C_{16}H_{21}O_3]^+$: m/z = 261.1485, found: m/z = 261.1486; **IR** (ν/cm^{-1}, neat): 3011, 2963, 1731, 1612, 1597, 1482, 1461, 1414, 1388, 1355, 1315, 1286, 1234, 1162, 1105, 1070, 1017, 965, 867, 835, 797, 749.

2-Chloroethyl 2-(2,3-dihydrobenzofuran-3-yl)acetate (169l)

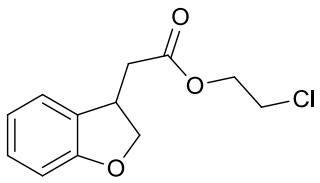

Compound **169l** was prepared according to the general procedure with **168** (0.2 mmol, 49.6 mg). 95% v/v MeCN was used as co-solvent. Isolated as a yellow amorphous solid (23.6 mg, 49%). **^{1}H NMR** (400 MHz, $CDCl_3$): δ [ppm] = 7.20-7.10 (m, 2H), 6.87 (t, *J* = 7.4 Hz, 1H), 6.81 (d, *J* = 8.0 Hz, 1H), 4.76 (dd, *J* = 9.1 Hz, *J* = 9.1 Hz, 1H), 4.38 (dd, *J* = 5.6 Hz, *J* = 5.6 Hz, 2H), 4.28 (dd, *J* = 9.2, 6.4 Hz, 1H), 3.95-3.83 (m, 1H), 3.70 (dd, *J* = 5.6 Hz, *J* = 5.6 Hz, 2H), 2.86 (dd, *J* = 16.5, 5.2 Hz, 1H), 2.65 (dd, *J* = 16.6, 9.5 Hz, 1H); **^{13}C NMR** (100 MHz, $CDCl_3$): δ [ppm] = 171.57, 159.92, 128.99, 128.91, 124.35, 120.75, 109.93, 76.73, 64.37, 41.65, 39.35, 38.38; **HRMS** (ESI): calculated for $[C_{12}H_{14}ClO_3]^+$: m/z = 241.0626, found: m/z = 241.0622; **IR** (ν/cm^{-1}, neat): 2979, 2952, 2891, 1726, 1595, 1478, 1456, 1438, 1412, 1396, 1360, 1321, 1299, 1287, 1235, 1217, 1179, 1153, 1151, 1109, 1087, 1057, 1015, 962, 924, 887, 865, 833, 793, 756, 712, 656, 604.

***n*-Butyl 2-(6-methyl-2,3-dihydrobenzofuran-3-yl)acetate (176a)**

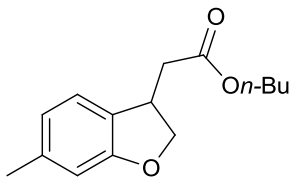

Compound **176a** was prepared according to the general procedure with **174a** (0.2 mmol, 52.4 mg). 50% v/v MeCN was used as co-solvent. Isolated as a yellow oil (37.2 mg, 75%). **^{1}H NMR** (400 MHz, $CDCl_3$): δ [ppm] = 7.03 (d, *J* = 7.5 Hz, 1H), 6.68 (t, *J* = 7.54 Hz, 1H), 6.63 (s, 1H), 4.74 (dd, *J* = 9.0 Hz, *J* = 9.0 Hz 1H), 4.25 (dd, *J* = 9.2, 6.4 Hz, 1H), 4.12 (dd, *J* = 6.6 Hz, *J* = 6.6 Hz, 2H), 3.87 – 3.79 (m, 1H), 2.77 (dd, *J* = 16.4, 5.3 Hz, 1H), 2.56 (dd, *J* = 16.4, 9.5 Hz, 1H), 2.30 (s, 3H), 1.66-1.59 (m, 2H), 1.43-1.34 (m, 2H), 0.95 (dd, *J* = 7.4 Hz, *J* = 7.4 Hz, 3H); **^{13}C NMR** (100 MHz, $CDCl_3$); δ [ppm] = 172.10, 160.17, 139.01, 126.31, 123.88, 121.38, 110.54, 77.09, 64.75, 39.72, 38.21, 30.75, 21.61, 19.26, 13.82; **HRMS** (ESI): calculated for $[C_{15}H_{21}O_3]^+$: m/z = 249.1485, found: m/z = 249.1488; **IR** (ν/cm^{-1}, neat): 2958, 2929, 2868, 1730, 1622, 1593, 1498, 1459, 1428, 1365, 1306, 1251, 1168, 1134, 1112, 1090, 1062, 1005, 966, 914, 855, 804, 748, 674.

***n*-Butyl 2-(5-methyl-2,3-dihydrobenzofuran-3-yl)acetate (176b)**

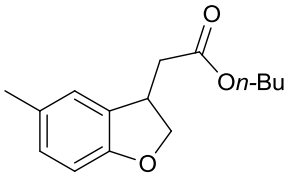

Compound **176b** was prepared according to the general procedure with **174b** (0.2 mmol, 52.4 mg). 50% v/v MeCN was used as co-solvent. Isolated as a yellow oil (32.8 mg, 66%). **^{1}H NMR** (400 MHz, $CDCl_3$): δ [ppm] = 6.98-6.92 (m, 2H), 6.69 (d, *J* = 8.0 Hz, 1H), 4.73 (t, *J* = 9.0 Hz, 1H), 4.23 (dd, *J* = 9.2, 6.4 Hz, 1H), 4.13 (dd, *J* = 6.6 Hz, *J* = 6.6 Hz, 2H), 3.87 – 3.80 (m, 1H), 2.78 (dd, *J* = 16.4, 5.3 Hz, 1H), 2.56 (dd, *J* = 16.4, 9.5 Hz, 1H), 2.28 (s, 3H), 1.66-1.59 (m, 2H), 1.43-1.34 (m, 2H), 0.95 (dd, *J* = 7.4 Hz, *J* = 7.4 Hz, 3H); **^{13}C NMR** (100 MHz, $CDCl_3$); δ [ppm] =172.12, 157.82, 129.97, 129.28, 129.13, 214.88, 109.36, 76.96, 64.78, 39.59, 38.56, 30.77, 20.93, 19.27, 13.84; **HRMS** (ESI): calculated for $[C_{15}H_{21}O_3]^+$: m/z = 249.1485, found: m/z = 249.1489; **IR** (ν/cm^{-1}, neat): 2960, 2897, 2871, 1719, 1611, 1494, 1468, 1419, 1398, 1366, 1321, 1291, 1244, 1224, 1179, 1126, 1091, 1063, 1032, 965, 951, 892, 811, 771, 739, 729, 707, 684, 608.

***n*-Butyl 2-(7-methyl-2,3-dihydrobenzofuran-3-yl)acetate (176c)**

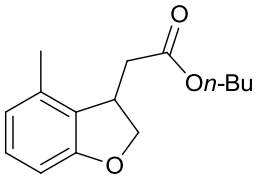

Compound **176c** was prepared according to the general procedure with **176c** (0.2 mmol, 52.4 mg). 50% v/v MeCN was used as co-solvent. Isolated as a yellow oil (31.8 mg, 64%). **^{1}H NMR** (400 MHz, $CDCl_3$): δ [ppm] = 7.05 (t, *J* = 7.8 Hz, 1H), 6.70-6.61 (m, 2H), 4.60 (t, *J* = 8.8 Hz, 1H), 4.40 (dd, *J* = 9.4, 3.2 Hz, 1H), 4.12 (dd, *J* = 6.8 Hz, *J* = 6.8 Hz, 2H), 3.83 – 3.75 (m, 1H), 2.74 (dd, *J* = 16.5, 3.1 Hz, 1H), 2.51 (dd, *J* = 16.5, 11.2 Hz, 1H), 2.30 (s, 3H), 1.67-1.57 (m, 2H), 1.44-1.32 (m, 2H), 0.95 (t, *J* = 7.4, 3H); **^{13}C NMR** (100 MHz, $CDCl_3$); δ [ppm] = 172.26, 159.78, 134.72, 128.76, 127.64, 122.23, 107.39, 76.52, 64.81, 38.07, 37.99, 30.75, 19.28, 18.57, 13.85; **HRMS** (ESI): calculated for $[C_{15}H_{21}O_3]^+$: m/z = 249.1485, found: m/z = 249.1488; **IR** (ν/cm^{-1}, neat): 2956, 2931, 2873, 1729, 1598, 1459, 1357, 1313, 1243, 1212, 1165, 1064, 1023, 961, 946, 917, 774, 757, 736, 647.

***n*-Butyl 2-(5-(*tert*-butyl)-2,3-dihydrobenzofuran-3-yl)acetate (176d)**

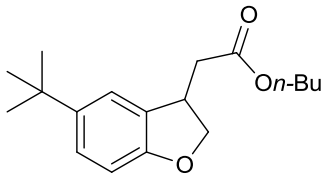

Compound **176dp** was prepared according to the general procedure with **174d** (0.2 mmol, 60.8 mg). 50% v/v MeCN was used as co-solvent. Isolated as an orange oil (58.1 mg, 75%). **^{1}H NMR** (400 MHz, $CDCl_3$): δ [ppm] = 7.17-7.14 (m, 2H), 6.72 (d, *J* = 8.2 Hz, 1H), 4.73 (t, *J* = 9.0 Hz, 1H), 4.24 (dd, *J* = 9.1, 6.4 Hz, 1H), 4.12 (dd, *J* = 6.6 Hz, *J* = 6.6 Hz, 2H), 3.89 – 3.79 (m, 1H), 2.80 (dd, *J* = 16.3, 5.2 Hz, 1H), 2.58 (dd, *J* = 16.4, 9.6 Hz, 1H), 1.65-1.58 (m, 2H), 1.42-1.31 (m, 2H), 1.28 (s, 9H), 0.93 (dd, *J* = 7.4 Hz, *J* = 7.4 Hz, 3H); **^{13}C NMR** (100 MHz, $CDCl_3$); δ [ppm] = 172.15, 157.70, 143.74, 128.87, 125.59, 121.17, 109.01, 77.09, 64.77, 39.68, 38.71, 34.45, 31.83, 30.78, 19.28, 13.83; **HRMS** (ESI): calculated for $[C_{18}H_{27}O_3]$+: m/z = 291.1955, found: m/z = 291.1958; **IR** (ν/cm^{-1}, neat): 2956, 2873, 1732, 1612, 1492, 1466, 1392, 1362, 1310, 1287, 1242, 1168, 1120, 1070, 966, 886, 817, 741, 661.

***n*-Butyl 2-(6-fluoro-2,3-dihydrobenzofuran-3-yl)acetate (176e)**

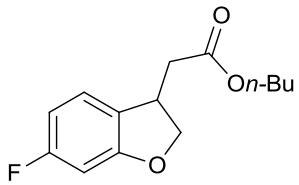

Compound **176e** was prepared according to the general procedure with **174e** (0.2 mmol, 53.2 mg). 50% v/v MeCN was used as co-solvent. Isolated as a yellow oil (41.4 mg, 82%). **^{1}H NMR** (400 MHz, $CDCl_3$): δ [ppm] = 7.06 (t, *J* = 6.7 Hz, 1H), 6.62-6.46 (m, 2H), 4.79 (dd, *J* = 9.1 Hz, *J* = 9.1 Hz, 1H), 4.31 (dd, *J* = 7.6 Hz, 1H *J* = 7.6 Hz, 1H), 4.12 (dd, *J* = 6.5 Hz, *J* = 6.5 Hz, 2H), 3.88 – 3.76 (m, 1H), 2.75 (dd, *J* = 16.4, 5.3 Hz, 1H), 2.57 (dd, *J* = 16.5, 9.2 Hz, 1H), 1.67-1.55 (m, 2H), 1.44-1.30 (m, 2H), 0.94 (dd, *J* = 7.3 Hz, *J* = 7.3 Hz, 3H); **^{13}C NMR** (100 MHz, $CDCl_3$); δ [ppm] = 171.72, 163.42 (d, *J* = 243.7 Hz), 161.0 (d, *J* = 13.1 Hz), 124.77 (d, *J* = 2.6 Hz), 124.48 (d, *J* = 10.6 Hz), 107.11 (d, *J* = 22.9 Hz), 98.17 (d, *J* = 26.5 Hz), 77.91, 64.71, 39.54, 37.63, 30.59, 19.11, 13.67; **^{19}F NMR** (376 MHz, $CDCl_3$); δ [ppm] = -114.31; **HRMS** (ESI): calculated for $[C_{14}H_{18}FO_3]^+$: m/z = 253.1234, found: m/z = 253.1232; **IR** (ν/cm^{-1}, neat): 2961, 2934, 2873, 1730, 1611, 1492, 1439, 1392, 1357, 1329, 1306, 1260, 1171, 1130, 1089, 974, 839, 800, 755, 615.

***n*-Butyl 2-(5-chloro-2,3-dihydrobenzofuran-3-yl)acetate (176f)**

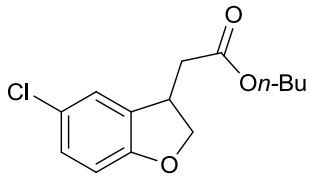

Compound **176f** was prepared according to the general procedure with **174f** (0.2 mmol, 56.5 mg). 50% v/v MeCN was used as co-solvent. Isolated as a yellow oil (32.3 mg, 60%). **^{1}H NMR** (400 MHz, $CDCl_3$): δ [ppm] = 7.10 (m, *2*H), 6.71 (d, *J* = 8.5 Hz, 1H), 4.77 (t, *J* = 9.0 Hz, 1H), 4.28 (t, *J* = 7.9 Hz, 1H), 4.13 (dd, *J* = 5.6 Hz, *J* = 5.6 Hz, 2H), 3.86 (m, 1H), 2.75 (d, *J* = 16.3 Hz, 1H), 2.59 (dd, *J* = 16.5, 9.3 Hz, 1H), 1.68-1.58 (m, 2H), 1.44-1.31 (m, 2H), 0.94 (dd, *J* = 7.4 Hz, *J* = 7.4 Hz, 3H); **^{13}C NMR** (100 MHz, $CDCl_3$); δ [ppm] = 171.72, 158.68, 131.26, 128.69, 125.35, 124.63, 110.80, 77.72, 64.97, 39.38, 38.49, 30.75, 19.28, 13.85; **HRMS** (ESI): calculated for $[C_{14}H_{18}ClO_3]^+$: m/z = 269.0939, found: m/z = 269.0942; **IR** (ν/cm^{-1}, neat):2961, 2935, 2868, 1729, 1603, 1480, 1465, 1416, 1391, 1358, 1311, 1270, 1237, 1167, 1114, 1092, 1065, 962, 879, 811, 742, 671.

***n*-Butyl 2-(7-bromo-2,3-dihydrobenzofuran-3-yl)acetate (176g)**

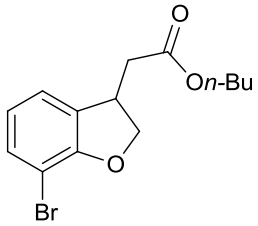

Compound **176g** was prepared according to the general procedure with **174g** (0.2 mmol, 65.4 mg). 50% v/v MeCN was used as co-solvent. Isolated as a yellow oil (45.1 mg, 72%). **^{1}H NMR** (400 MHz, $CDCl_3$): δ [ppm] = 7.29 (d, *J* = 8.0 Hz, 1H), 7.09 (d, *J* = 7.4 Hz, 1H), 6.74 (t, *J* = 7.7 Hz, 1H), 4.85 (dd, *J* = 9.2 Hz, *J* = 9.2 Hz, 1H), 4.36 (dd, *J* = 9.1, 6.7 Hz, 1H), 4.12 (dd, *J* = 6.6 Hz, *J* = 6.6 Hz, 2H), 4.00-3.90 (m, 1H), 2.79 (dd, *J* = 16.6, 5.4 Hz, 1H), 2.61 (dd, *J* = 16.6, 9.3 Hz, 1H), 1.67-1.55 (m, 2H), 1.43-1.30 (m, 2H), 0.93 (dd, *J* = 7.4 Hz, , *J* = 7.4 Hz, 3H); **^{13}C NMR** (100 MHz, $CDCl_3$); δ [ppm] = 171.68, 157.18, 131.86, 130.73, 123.39, 122.16, 103.01, 77.25, 64.93, 39.54, 39.36, 30.73, 19.26, 13.82; **HRMS** (ESI): calculated for $[C_{14}H_{18}BrO_3]^+$: m/z = 313.0434, found: m/z = 313.0434 ; **IR** (ν/cm^{-1}, neat): 2956, 2935, 2873, 1729, 1603, 1583, 1474, 1448, 1414, 1391, 1356, 1313, 1262, 1215, 1170, 1130, 1093, 1056, 957, 869, 831, 770, 733.

Methyl 3-(2-*n*-butoxy-2-oxoethyl)-2,3-dihydrobenzofuran-5-carboxylate (176i)

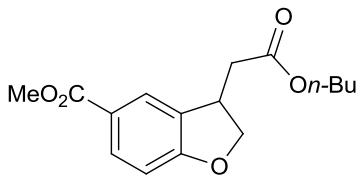

Compound **176i** was prepared according to the general procedure with **174i** (0.2 mmol, 61.2 mg). 50% v/v MeCN was used as co-solvent. Isolated as a colorless oil (46.2 mg, 79%). **^{1}H NMR** (400 MHz, $CDCl_3$): δ [ppm] = 7.57 (d, *J* = 7.8 Hz, 1H), 7.41 (s, 1H), 7.19 (d, *J* = 7.8 Hz, 1H), 4.79 (dd, *J* = 9.2 Hz, *J* = 9.2 Hz, 1H), 4.30 (dd, *J* = 9.2, 6.6 Hz, 1H), 4.11 (dd, *J* = 6.7 Hz, *J* = 6.7 Hz, 2H), 3.93-3.88 (m, 4H), 2.79 (dd, *J* = 16.5, 5.4 Hz, 1H), 2.59 (dd, *J* = 16.6, 9.3 Hz, 1H), 1.65-1.55 (m, 2H), 1.42-1.30 (m, 2H), 0.92 (dd, *J* = 7.4 Hz, *J* = 7.4 Hz, 3H); **^{13}C NMR** (100 MHz, $CDCl_3$); δ [ppm] = 171.70, 166.94, 160.15, 134.80, 131.10, 124.09, 122.70, 110.68, 77.25, 64.95, 52.29, 39.25, 38.38, 30.72, 19.25, 13.81; **HRMS** (ESI): calculated for $[C_{16}H_{21}O_5]^+$: m/z = 293.1384, found: m/z = 293.1387 ; **IR** (ν/cm^{-1}, neat): 2956, 2938, 2873, 1721, 1590, 1494, 1432, 1281, 1265, 1213, 1172, 1117, 1077, 980, 946, 886, 841, 798, 760, 735.

***n*-Butyl 2-(6-methoxy-2,3-dihydrobenzofuran-3-yl)acetate (176j)**

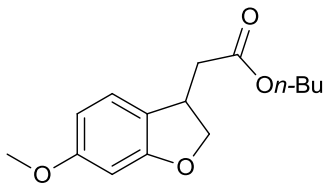

Compound **176j** was prepared according to the general procedure with **174j** (0.2 mmol, 55.6 mg). 50% v/v MeCN was used as co-solvent. Isolated as a yellow oil (27.0 mg, 51%). **^{1}H NMR** (400 MHz, $CDCl_3$): δ [ppm] = 7.03 (d, *J* = 8.1 Hz, 1H), 6.44-6.36 (m, 2H), 4.75 (dd, *J* = 9.0 Hz, *J* = 9.0 Hz, 1H), 4.27 (dd, *J* = 8.8, 6.5 Hz, 1H), 4.11 (dd, *J* = 6.6 Hz, *J* = 6.6 Hz, 2H), 3.84-3.72 (m, 4H), 2.74 (dd, *J* = 16.3, 5.2 Hz, 1H), 2.55 (dd, *J* = 16.3, 9.3 Hz, 1H), 1.67-1.56 (m, 2H), 1.43-1.33 (m, 2H), 0.94 (dd, *J* = 7.4 Hz, *J* = 7.4 Hz, 3H); **^{13}C NMR** (100 MHz, $CDCl_3$); δ [ppm] = 171.95, 161.11, 160.73, 124.24, 121.18, 106.13, 96.26, 77.57, 64.60, 55.47, 39.71, 37.75, 30.60, 19.11, 13.68; **HRMS** (ESI): calculated for $[C_{15}H_{21}O_4]^+$: m/z = 265.1434, found: m/z = 265.1434 ; **IR** (ν/cm^{-1}, neat): 2956, 2932, 2873, 2832, 1729, 1621, 1597, 1497, 1466, 1446, 1391, 1351, 1278, 1193, 1171, 1142, 1112, 1086, 1028, 973, 915, 829, 797, 744, 632.

***n*-Butyl 2-(3-methyl-2,3-dihydrobenzofuran-3-yl)acetate (177b)**

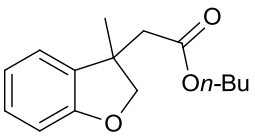

Compound **177b** was prepared according to the general procedure with **177a** (0.2 mmol, 52.4 mg). 50% v/v MeCN was used as co-solvent. Isolated as a yellow oil (36.3 mg, 73%). **^{1}H NMR** (400 MHz, $CDCl_3$): δ [ppm] = 7.18-7.07 (m, 2H), 6.88 (t, *J* = 7.4 Hz, 1H), 6.80 (d, *J* = 8.0 Hz, 1H), 4.64 (d, *J* = 9.1 Hz, 1H), 4.31 (d, *J* = 9.12 Hz, 1H), 4.06 (dd, *J* = 6.6 Hz, 2H), 2.67 (dt, *J* = 11 Hz, *J* = 11 Hz, 2H), 1.63-1.51 (m, 2H), 1.43 (s, 3H), 1.38-1.29 (m, 2H), 0.92 (dd, *J* = 7.34 Hz, *J* = 7.34 Hz, 3H); **^{13}C NMR** (100 MHz, $CDCl_3$); δ [ppm] = 171.37, 159.21, 134.36, 128.67, 122.85, 120.76, 110.01, 82.48, 64.60, 44.57, 43.97, 30.72, 25.39, 19.28, 13.83; **HRMS** (ESI): calculated for $[C_{15}H_{21}O_3]$+: m/z = 249.1485, found: m/z = 249.1490; **IR** (ν/cm^{-1}, neat): 2961, 2932, 2873, 1730, 1600, 1480, 1458, 1383, 1338, 1277, 1241, 1191, 1163, 1106, 1068, 1017, 978, 833, 747, 661.

***n*-Butyl 2-(benzofuran-3-yl)acetate (178b)**

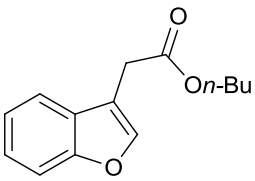

Compound **178b** was prepared according to the general procedure with **178a** (0.2 mmol, 49.2 mg). 50% v/v MeCN was used as co-solvent. Isolated as a yellow oil (26.5 mg, 57%). **^{1}H NMR** (400 MHz, $CDCl_3$): δ [ppm] = 7.63 (s, 1H), 7.57 (d, *J* = 7.4 Hz, 1H), 7.48 (d, *J* = 8.1 Hz, 1H), 7.34-7.23 (m, 2H), 4.14 (dd, *J* = 6.7 Hz, *J* = 6.7 Hz, 2H), 3.71 (s, 2H), 1.66-1.56 (m, 2H), 1.40-1.30 (m, 2H), 0.91 (dd, *J* = 7.4 Hz, *J* = 7.4 Hz, 3H); **^{13}C NMR** (100 MHz, $CDCl_3$); δ [ppm] = 170.92, 155.31, 142.95, 127.76, 124.57, 122.72, 119.82, 113.33, 111.64, 65.16, 30.73, 29.98, 19.23, 13.81; **HRMS** (ESI): calculated for $[C_{14}H_{17}O_3]^+$: m/z = 233.1172, found: m/z = 233.1176; **IR** (ν/cm^{-1}, neat): 2952, 2930, 2873, 1734, 1595, 1453, 1312, 1277, 1254, 1162, 1096, 1065, 1008, 970, 857, 743, 707.

***n*-Butyl 2-(chroman-4-yl)acetate (179b)**

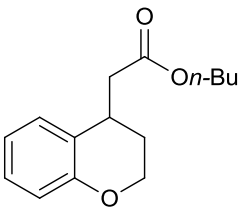

Compound **179b** was prepared according to the general procedure with **179a** (0.2 mmol, 52.4 mg). 50% v/v MeCN was used as co-solvent. Isolated as a yellow oil (35.8 mg, 72%). **^{1}H NMR** (400 MHz, $CDCl_3$): δ [ppm] = 7.14-7.08 (m, 2H), 6.88-6.80 (m, 2H), 4.22-4.09 (m, 4H), 3.40-3.32 (m, 1H), 2.80 (dd, *J* = 15.5, 4.7 Hz,

1H), 2.53 (dd, *J* = 15.5, 10.1 Hz, 1H), 2.20-2.12 (m, 1H), 1.88-1.81 (m, 1H), 1.66-1.59 (m, 3H (2H aliphatic + 1H from H_2O peek)), 1.44-1.33 (m, 2H) 0.94 (dd, *J* = 7.4 Hz, *J* = 7.4 Hz, 3H); **^{13}C NMR** (100 MHz, $CDCl_3$); δ [ppm] = 172.41, 154.67, 128.86, 127.96, 124.72, 120.53, 117.19, 64.68, 63.32, 42.52, 30.79, 30.65, 27.48, 19.30, 13.86; **HRMS** (ESI): calculated for $[C_{15}H_{21}O_3]^+$: m/z = 249.1485, found: m/z = 249.1486; **IR** (ν/cm^{-1}, neat): 2950, 2930, 2873, 1730, 1608, 1581, 1489, 1453, 1387, 1352, 1270, 1224, 1160, 1119, 1079, 1060, 1038, 1025, 964, 827, 750.

Preparation of Substrates

2-(Allyloxy)-arenediazonium tetrafluoroborates were prepared in 3-4 steps from their corresponding 2-nitrophenols or 2-aminophenols (Scheme 3.6.1).

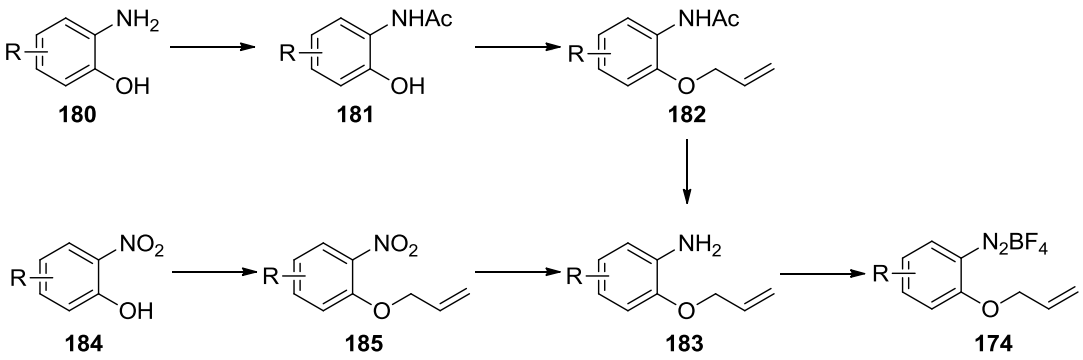

Figure 3.6.1. Synthetic route to 2-(allyloxy)-arenediazonium tetrafluoroborates.

2-(Allyloxy)aniline,[202] 2-(allyloxy)-4-methylaniline,[203] 2-(allyloxy)-5-methylaniline,[202] 2-(allyloxy)-6-methylaniline,[204] 2-(allyloxy)-4-fluoroaniline,[205] 2-(allyloxy)-5-chloroaniline,[202] 2-(allyloxy)-3-bromoaniline,[202] methyl 4-(allyloxy)-3-aminobenzoate,[205] 2-(but-3-en-2-yloxy)aniline,[202] 2-(prop-2-yn-1-yloxy)aniline,[202] 2-(but-3-en-1-yloxy)aniline[202] and *N*-(5-(*t*-butyl)-2-hydroxyphenyl)acetamide[201] were prepared according to literature procedures. The synthesis and characterisation of novel anilines and their novel precursor compounds is described below.

Diazotization of ortho-Allylated Anilines

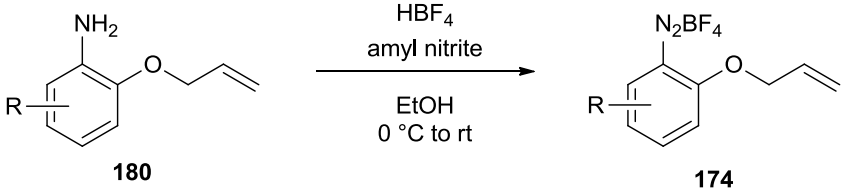

Figure 3.6.2. Synthesis of 2-(allyloxy)-arenediazonium tetrafluoroborates.

Prepared by an adapted method of Blanchet.[168] An aqueous HBF_4 solution (48% w/w, 2.0 equiv.) was added, at room temperature, to a solution of the parent aniline (0.1 M, 1 equiv.) in ethanol. The mixture was cooled to 0 °C and amyl nitrite (2.0 equiv.) was added dropwise. The mixture was stirred at 0 °C for 15 min then vigorously stirred for 1 hour at room temperature. Diethyl ether (30 mL) was added, and the resulting precipitate collected by vacuum filtration and washed with copious amounts of diethyl ether. Recrystallisation from $MeOH/Et_2O$ afforded the pure arenediazonium tetrafluoroborate salt.

2-(Allyloxy)benzenediazonium tetrafluoroborate (168)

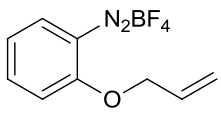

Compound **168** was prepared according to the general procedure with 2-(allyloxy)aniline (5.0 mmol, 746 mg). Isolated as a beige solid (686 mg, 92%). **^{1}H NMR** (400 MHz, DMSO-d_6): δ [ppm] = 8.53 (dd, *J* = 8.4, 1.7 Hz, 1H), 8.21 (ddd, *J* = 9.0, 7.4, 1.6 Hz, 1H), 7.67 (d, *J* = 8.8 Hz, 1H), 7.45 (t, *J* = 7.9 Hz, 1H), 6.15-6.04 (m, 1H), 5.56 (dq, *J* = 17.3, 1.5 Hz, 1H), 5.42 (dq, *J* = 10.6, 1.3 Hz, 1H), 5.06 (dt, *J* = 5.3, 1.5 Hz, 2H). **^{13}C NMR** (100 MHz, DMSO-d_6): δ [ppm] = 160.90, 143.56, 132.42, 131.10, 122.96, 119.76, 115.64, 102.61, 71.57; **HRMS** (ESI): calculated for $[C_9H_9N_2O]^+$: m/z = 161.0715, found: m/z = 161.0715. Analytical data is in agreement with previously reported literature data.[113]

2-(Allyloxy)-4-methylbenzenediazonium tetrafluoroborate (174a)

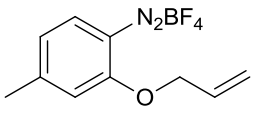

Compound **174a** was prepared according to the general procedure with 2-(allyloxy)-4-methylaniline (1.0 mmol, 163 mg). Isolated as a white solid (222 mg, 85%). **^{1}H NMR** (400 MHz, DMSO-d_6): δ [ppm] = 8.39 (d, *J* = 8.6, 1H), 7.56 (s, 1H), 7.29 (d, *J* = 8.6 Hz, 1H), 6.16-6.04 (m, 1H), 5.55 (dd, *J* = 17.3, 1.5 Hz, 1H), 5.41 (dd, *J* = 10.6, 1.4 Hz, 1H), 5.03 (d, *J* = 5.3 Hz, 2H), 2.55 (s, *J* = 8.4, 1.7 Hz, 3H); **^{13}C NMR** (100 MHz, DMSO-d_6): δ [ppm] = 160.95, 157.36, 131.91, 131.12, 124.23, 119.70, 115.73, 98.80, 71.40, 23.01; **HRMS** (ESI): calculated for $[C_{10}H_{11}N_2O]^+$: m/z = 175.0871, found: m/z = 175.0866; **IR** (ν/cm^{-1}, neat): 3109, 2253, 1592, 170, 1477, 1422, 1384, 1364, 1287, 1270, 1172, 1038, 989, 936, 918, 862, 809, 703; **m.p.**: 119.8 °C (decomp.).

2-(Allyloxy)-5-methylbenzenediazonium tetrafluoroborate (174b)

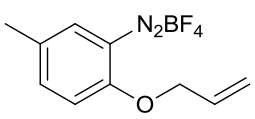

Compound **174b** was prepared according to the general procedure with 2-(allyloxy)-5-methylaniline (1.0 mmol, 163 mg). Isolated as a pale brown solid (216 mg, 82%). **^{1}H NMR** (400 MHz, DMSO-d_6): δ [ppm] = 8.31 (d, *J* = 1.3 Hz, 1H), 8.06 (dd, *J* = 9.1, 2.0 Hz, 1H), 7.59 (d, *J* = 9.0 Hz, 1H), 6.15-6.02 (m, 1H), 5.54 (dq, *J* = 17.3, 1.55 Hz, 1H), 5.40 (dq, *J* = 10.6, 1.4 Hz, 1H), 5.03 (dt, *J* = 5.3, 1.5 Hz, 2H), 2.38 (s, 3H); **^{13}C NMR** (100 MHz, DMSO-d_6): δ [ppm] = 159.51, 144.78, 132.84, 131.21, 130.54, 119.63, 115.53, 101.78, 71.45, 19.63; **HRMS** (ESI): calculated for $[C_{10}H_{11}N_2O]^+$: m/z = 175.0871, found: m/z = 175.0866; **IR** (ν/cm^{-1}, neat): 3094, 2261, 1611, 1559, 1508, 1448, 1422, 1296, 1267, 1218, 1163, 1037, 982, 933, 908, 883, 830, 706; **m.p.**: 109.8 °C (decomp.).

2-(Allyloxy)-6-methylbenzenediazonium tetrafluoroborate (174c)

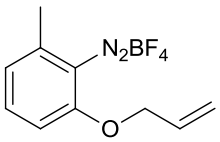

Compound **174c** was prepared according to the general procedure with 2-(allyloxy)-6-methylaniline (1.0 mmol, 163 mg). Isolated as a beige solid (255 mg, 97%). **^{1}H NMR** (400 MHz, DMSO-d_6): δ [ppm] = 8.10 (t, *J* = 8.3 Hz, 1H), 7.49 (d, *J* = 8.8 Hz, 1H), 7.33 (d, *J* = 7.7 Hz, 1H), 6.16-6.03 (m, 1H), 5.54 (d, *J* = 17.3 Hz, 1H), 5.42 (d, *J* = 10.6 Hz, 1H), 5.06 (d, *J* = 5.3 Hz, 2H), 2.67 (s, 3H); **^{13}C NMR** (100 MHz, DMSO-d_6): δ [ppm] = 161.06, 144.14, 143.00, 131.13, 124.04, 119.77, 112.80, 103.26, 71.61, 18.09; **HRMS** (ESI): calculated for $[C_{10}H_{11}N_2O]^+$: m/z = 175.0871, found: m/z = 175.0869; **IR** (ν/cm^{-1}, neat): 3087, 2968, 2258, 1611, 1563, 1507, 1447, 1422, 1298, 1268, 1218, 1164, 1034, 985, 934, 907, 831, 797, 705; **m.p.**: 130.1 °C (decomp.).

2-(Allyloxy)-5-(*tert*-butyl)benzenediazonium tetrafluoroborate (174d)

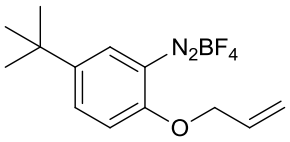

Compound **174d** was prepared according to the general procedure with **183a** (1.0 mmol, 205 mg). Isolated as a white solid (253 mg, 73%). **^{1}H NMR** (400 MHz, DMSO-d_6): δ [ppm] = 8.55 (d, *J* = 2.3 Hz, 1H), 8.53 (dd, *J* = 8.32, 2.4 Hz, 1H), 7.60 (d, *J* = 9.3 Hz, 1H), 6.15-6.02 (m, 1H), 5.54 (d, *J* = 17.3 Hz, 1H), 5.40 (d, *J* = 10.6 Hz, 1H), 5.06 (d, *J* = 5.2 Hz, 2H), 1.31 (2, 9H); **^{13}C NMR** (100 MHz, DMSO-d_6): δ [ppm] = 159.38, 145.75, 141.65, 131.25, 127.98, 119.64, 115.57, 101.84, 71.51, 34.87, 30.35; **HRMS** (ESI): calculated for $[C_{13}H_{17}N_2O]^+$: m/z = 217.1341, found: m/z = 217.1345; **IR** (ν/cm^{-1}, neat):

2958, 2258, 1606, 1555, 1503, 1426, 1370, 1300, 1271, 1178, 1037, 990, 925, 900, 842, 826, 795, 713; **m.p.**: 101.7-102.9 °C.

2-(Allyloxy)-4-fluorobenzenediazonium tetrafluoroborate (174e)

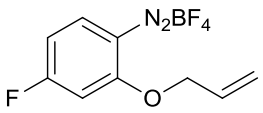

Compound **174e** was prepared according to the general procedure with 2-(allyloxy)-4-fluoroaniline (1.0 mmol, 167 mg). Isolated as a white solid (234 mg, 90%). **^{1}H NMR** (400 MHz, $CDCl_3$): δ [ppm] = 8.67 (dd, *J* = 9.4, 5.6 Hz, 1H), 7.73 (dd, *J* = 10.8, 2.3 Hz, 1H), 7.43-7.38 (m, 1H), 6.17-6.02 (m, 1H), 5.57 (dd, *J* = 17.3, 1.4 Hz, 1H), 5.43 (dd, *J* = 10.6, 1.2 Hz, 1H), 5.06 (d, *J* = 5.4 Hz, 2H); **^{13}C NMR** (100 MHz, $CDCl_3$): δ [ppm] = 171.00 (d, *J* = 267.5 Hz), 164.04 (d, *J* = 15.2 Hz), 136.26 (d, *J* = 14.1 Hz), 131.08, 120.58, 112.41 (d, *J* = 26.1 Hz), 104.73 (d, *J* = 28.7 Hz), 99.67 (d, *J* = 2.0 Hz), 72.88; **HRMS** (ESI): calculated for $[C_9H_{8F}N_2O]^+$: m/z = 179.0621, found: m/z = 179.0617; **IR** (ν/cm^{-1}, neat): 3119, 3092, 2271, 1602, 1575, 1478, 1455, 1418, 1382, 1297, 1190, 1150, 1038, 1003, 953, 941, 930, 866, 821, 766, 702; **m.p.**: 102.5-103.0 °C.

2-(Allyloxy)-5-chlorobenzenediazonium tetrafluoroborate (174f)

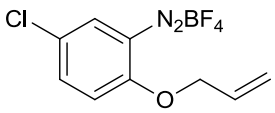

Compound **174f** was prepared according to the general procedure with 2-(allyloxy)-5-chloroaniline (1.0 mmol, 184 mg). Isolated as a pale yellow solid (140 mg, 50%). **^{1}H NMR** (400 MHz, DMSO-d_6): δ [ppm] = 8.72 (d, *J* = 2.7 Hz, 1H), 8.33 (dd, *J* = 9.4, 2.7 Hz, 1H), 7.72 (d, *J* = 9.4 Hz, 1H), 6.14-6.02 (m, 2H), 5.55 (dd, *J* = 17.3, 1.4 Hz, 1H), 5.42 (dd, *J* = 10.6, 1.1 Hz, 2H), 5.09 (d, *J* = 5.3 Hz, 2H); **^{13}C NMR** (100 MHz, DMSO-d_6): δ [ppm] = 160.10, 143.52, 130.86, 130.43, 125.25, 119.94, 117.60, 104.06, 72.18; **HRMS** (ESI): calculated for $[C_9H_8ClN_2O]^+$: m/z 195.0325, found: m/z = 195.0330.

2-(Allyloxy)-3-bromobenzenediazonium tetrafluoroborate (174g)

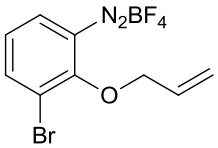

Compound **174g** was prepared according to the general procedure with 2-(allyloxy)-3-bromoaniline (2.0 mmol, 456 mg). Isolated as a white solid (580 mg, 89%). (decomposes in DMSO-d_6) **^{1}H NMR** (400 MHz, CD_3CN): δ [ppm] = 8.44-8.39 (m, 2H), 7.52 (t, *J* = 9.3 Hz, 1H), 6.25-6.15 (m, 1H), 5.56 (dd, *J* = 17.1, 1.3 Hz, 1H), 5.45 (dd, *J* = 10.3, 0.5 Hz, 1H), 5.07 (dd, *J* = 6.3, 0.8 Hz, 2H); **^{13}C NMR** (100 MHz, CD_3CN): δ [ppm] = 159.32, 149.11, 133.14, 132.22, 128.42, 122.80, 118.23, 111.65, 78.93; **HRMS** (ESI): calculated for

$[C_9H_8BrN_2O]^+$: m/z = 238.9820, found: m/z = 238.9820; **IR** (ν/cm^{-1}, neat): 3094, 2286, 1574, 1556, 1463, 1422, 1363, 1279, 1240, 1212, 1044, 961, 937, 909, 821, 783, 723; **m.p.**: 116.9 °C (decomp.).

2-(Allyloxy)-5-(methoxycarbonyl)benzenediazonium tetrafluoroborate (174i)

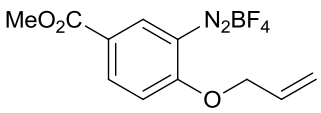

Compound **174i** was prepared according to the general procedure with methyl 4-(allyloxy)-3-aminobenzoate (1.0 mmol, 207 mg). Isolated as a white solid (296 mg, 97%). **^{1}H NMR** (400 MHz, DMSO-d$_6$): δ [ppm] = 8.69 (dd, *J* = 8.7 Hz, 1H), 8.00 (s, 1H), 7.91 (d, *J* = 8.7 Hz, 1H), 6.17-6.05 (m, 1H), 5.56 (d, *J* = 17.3 Hz, 1H), 5.43 (d, *J* = 10.6 Hz, 1H), 5.19 (d, *J* = 5.2 Hz, 2H), 3.96 (s, 1H); **^{13}C NMR** (100 MHz, DMSO-d$_6$): δ [ppm] = 163.75, 160.49, 141.65, 133.10, 131.02, 122.53, 119.66, 115.64, 107.09, 72.07, 53.59; **HRMS** (ESI): calculated for $[C_{11}H_{11}N_2O_3]^+$: m/z = 219.0777, found: m/z = 219.0780; **IR** (ν/cm^{-1}, neat): 3104, 2278, 1729, 1598, 1579, 1471, 1440, 1429, 1366, 1308, 1261, 1229, 1158, 1100, 1026, 990, 955, 884, 791, 757, 705; **m.p.**: 99.2-100.3 °C.

2-(Allyloxy)-4-methoxybenzenediazonium tetrafluoroborate (174j)

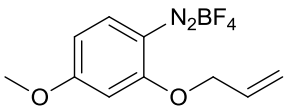

Compound **174j** was prepared according to the general procedure with **183b** (1.0 mmol, 179 mg). Isolated as a beige solid (256 mg, 92%). **^{1}H NMR** (400 MHz, DMSO-d$_6$): δ [ppm] = 8.43 (d, *J* = 9.4 Hz, 1H), 7.10 (d, *J* = 2.2 Hz, 1H), 7.04 (dd, *J* = 9.4, 2.2 Hz, 1H), 6.13-6.05 (m, 1H), 5.55 (dd, *J* = 17.3, 1.5 Hz, 1H), 5.42 (dd, *J* = 10.6, 1.3 Hz, 1H), 5.05 (d, *J* = 5.4 Hz, 2H), 4.06 (s, 3H); **^{13}C NMR** (100 MHz, DMSO-d$_6$): δ [ppm] = 171.46, 163.91, 134.34, 131.06, 119.85, 111.89, 100.43, 91.49, 71.73, 57.91; **HRMS** (ESI): calculated for $[C_{10}H_{11}N_2O_2]^+$: m/z = 191.0821, found: m/z = 191.0818; **IR** (ν/cm^{-1}, neat): 3101, 2195, 1585, 1564, 1488, 1454, 1401, 1366, 1312, 1268, 1223, 1177, 1086, 1040, 1012, 990, 948, 827, 711, 695; **m.p.**: 111.1 °C (decomp.).

2-((2-Methylallyl)oxy)benzenediazonium tetrafluoroborate (177a)

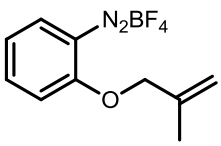

Compound **177a** was prepared according to the general procedure with 2-(but-3-en-2-yloxy)aniline (1.0 mmol, 163 mg). Isolated as a beige solid (162 mg, 62%). **^{1}H NMR** (400 MHz, DMSO-d$_6$): δ [ppm] = 8.54 (dd, *J* = 8.4, 1.7 Hz 1H), 8.21 (ddd, *J* = 8.9, 7.4, 1.6 Hz, 1H), 7.66 (d, *J* = 8.8 Hz, 1H), 7.45 (t, *J* = 7.9 Hz, 1H), 5.19 (s, 1H), 5.10 (s, 1H), 4.97 (s, 2H), 1.84 (s,

3H); **^{13}C NMR** (100 MHz, DMSO-d_6): δ [ppm] = 160.87, 143.52, 138.58, 132.34, 122.96, 115.55, 114.34, 102.64, 74.01, 18.95; **HRMS** (ESI): calculated for $[C_{10}H_{11}N_2O]^+$: m/z = 175.0871, found: m/z = 175.0867; **IR** (ν/cm^{-1}, neat): 3107, 2268, 1660, 1592, 1567, 1488, 1442, 1389, 1294, 1268, 1177, 1147, 1032, 997, 901, 831, 762, 741, 710; **m.p.**: 97.9 °C (decomp.).

2-(Prop-2-yn-1-yloxy)benzenediazonium tetrafluoroborate (178a)

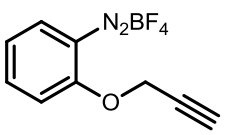

Compound **178a** was prepared according to the general procedure with 2-(prop-2-yn-1-yloxy)aniline (1.0 mmol, 147 mg). Isolated as a brown solid (139 mg, 57%). **^{1}H NMR** (400 MHz, DMSO-d_6): δ [ppm] = 8.57 (dd, *J* = 8.4, 1.7 Hz, 1H), 8.27 (ddd, *J* = 9.0, 7.4, 1.6 Hz, 1H), 7.71 (d, *J* = 8.4 Hz, 1H), 7.51 (ddd, *J* = 8.4, 7.5, 0.9 Hz, 1H), 5.34 (d, *J* = 2.4 Hz, 2H), 3.94 (t, *J* = 2.4 Hz, 1H); **^{13}C NMR** (100 MHz, DMSO-d_6): δ [ppm] = 159.52, 143.44, 132.71, 123.51, 115.61, 103.20, 81.24, 76.69, 59.07; **HRMS** (ESI): calculated for $[C_9H_7N_2O]^+$: m/z = 159.0559, found: m/z = 159.0557. Analytical data is in agreement with previously reported literature data.[168]

2-(But-3-en-1-yloxy)benzenediazonium tetrafluoroborate (179a)

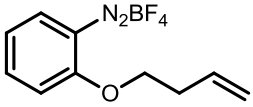

Compound **179a** was prepared according to the general procedure with 2-(but-3-en-1-yloxy)aniline (1.0 mmol, 163 mg). Isolated as a pale red solid (224 mg, 91%). **^{1}H NMR** (400 MHz, DMSO-d_6): δ [ppm] = 8.50 (dd, *J* = 8.4, 1.7 Hz, 1H), 8.22 (ddd, *J* = 8.9, 7.4, 1.7 Hz, 1H), 7.71 (d, *J* = 8.6 Hz, 1H), 7.44 (ddd, *J* = 8.4, 7.5, 09 Hz, 1H), 6.00-5.86 (m, 1H), 5.24 (dq, *J* = 17.2, 1.7 Hz, 1H), 5.17-5.17 (m, 1H), 4.51 (t, *J* = 6.4 Hz, 1H), 2.63-2.58 (m, 2H); **^{13}C NMR** (100 MHz, DMSO-d_6): δ [ppm] = 161.31, 143.71, 133.79, 132.36, 122.87, 117.91, 115.49, 102.42, 70.52, 32.16; **HRMS** (ESI): calculated for $[C_{10}H_{11}N_2O]^+$: m/z = 175.0871, found: m/z = 175.0870. Analytical data is in agreement with previously reported literature data.[206]

Preperation of Novel ortho-Allylated Anilines

2-(Allyloxy)-5-(*tert*-butyl)aniline (183a)

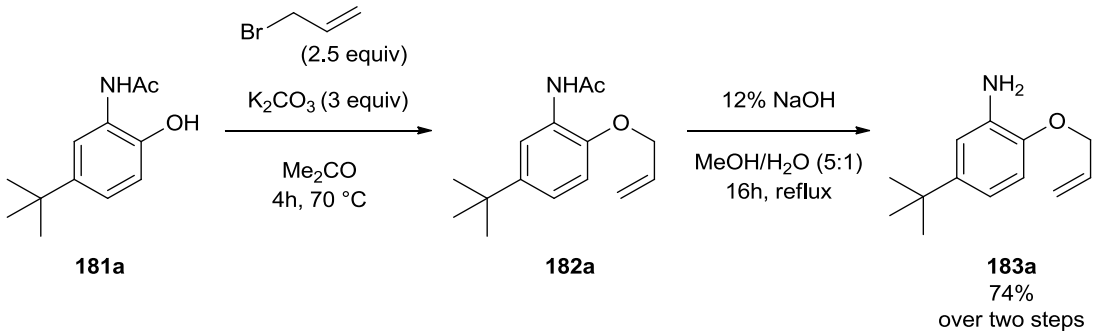

Figure 3.6.3. Synthesis of 2-(allyloxy)-5-(*tert*-butyl)aniline.

A suspension of *N*-(5-(*t*-butyl)-2-hydroxyphenyl)acetamide (4.0 mmol, 829 mg), potassium carbonate (12 mmol, 1.66 g), allyl bromide (10 mmol, 866 µL) in dry acetone (10 mL) was vigorously stirred at 70 °C for 4 hours in a sealed vial. After cooling to room temperature, the reaction mixture was filtered through a plug of Celite with acetone. The filtrate was concentrated *in vacuo* and the residue taken up in CH_2Cl_2 (20 mL) and washed with water (3x 20 mL). The organic layer was collected and the solvent removed *in vacuo.* The resultant yellow oil was dissolved in 12% w/w NaOH solution (2 mL, 5:1 MeOH/H_2O) and heated at reflux for 16 hours. The reaction mixture was quenched with ice-cold water (10 mL) and extracted with CH_2Cl_2 (5x 25 mL). The combined organic layers were dried over Mg_2SO_4, filtered and the solvent removed *in vacuo* to afford 2-(allyloxy)-5-(*t*-butyl)aniline (**183a**) as a yellow oil (608 mg, 74%). **^{1}H NMR** (400 MHz, $CDCl_3$): δ [ppm] = 6.79 (s, 1H), 6.74-6.71 (m, 2H), 6.14-603 (m, 1H), 5.41 (dd, *J* = 17.2, 1.4 Hz, 1H), 5.27 (dd, *J* = 10.5, 1.0 Hz, 1H), 4.55 (d, *J* = 5.3 Hz, 1H), 3.79 (bs, 2H), 1.28 (s, 9H); **^{13}C NMR** (100 MHz, $CDCl_3$): δ [ppm] = 144.46, 144.34, 135.83, 133.92, 117.39, 115.14, 113.07, 111.68, 69.47, 34.2, 31.64; **HRMS** (ESI): calculated for $[C_{13}H_{19}NO]^+$: m/z = 206.1539, found: m/z = 206.1543; **IR** (ν/cm^{-1}, neat): 3462, 3373, 2956, 2867, 1609, 1514, 1460, 1425, 1392, 1362, 1291, 1252, 1207, 1157, 1021, 994, 925, 862, 823, 796, 762.

2-(Allyloxy)-4-methoxyaniline (183b)

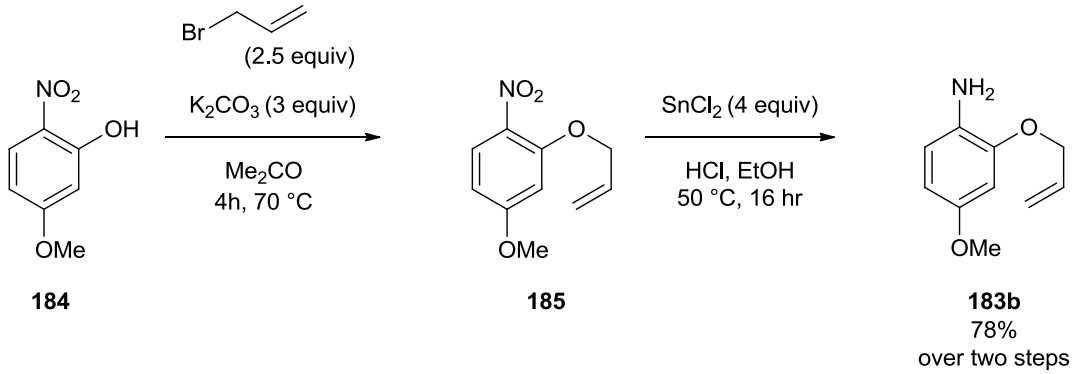

Figure 3.6.4. Synthesis of 2-(allyloxy)-4-methoxyaniline.

A suspension of 5-methoxy-2-nitrophenol (4.0 mmol, 872 mg), potassium carbonate (12 mmol, 1.66 g), allyl bromide (10 mmol, 866 µL) in dry acetone (10 mL) was vigorously stirred at 70 °C for 4 hours in a sealed vial. After cooling to room temperature, the reaction mixture was filtered through a plug of Celite with acetone. The filtrate was concentrated *in vacuo* and the residue taken up in CH_2Cl_2 (20 mL) and washed with water (3x 20 mL). The organic layer was collected and the solvent removed *in vacuo.* The resultant yellow oil was dissolved in ethanol, and treated with $SnCl_2$ (16 mmol, 3.04 g), followed by 32% aqueous HCl solution (0.1 mL). The reaction mixture was heated at 50 °C for 16 hours. After cooling to 0 °C, it was basified to pH 14 with 5 M aqueous NaOH solution and extracted with ethyl acetate (5x50 mL). The combined organic layers were washed with brine, dried over $MgSO_4$, filtered and the solvent removed *in vacuo*. The crude residue was purified by flash chromatography on silica (EtOAc/hexanes, 1:5) to afford 2-(allyloxy)-4-methoxyaniline (**183b**) as yellow oil (559 mg, 78%). **^{1}H NMR** (400 MHz, $CDCl_3$): δ [ppm] = 6.67 (d, *J* = 8.4 Hz, 1H), 6.45 (d, *J* = 2.5 Hz, 1H), 6.36 (dd, *J* = 8.4, 2.3 Hz, 1H), 6.13-6.00 (m, 1H), 5.41 (d, *J* = 17.3 Hz, 1H), 5.28 (d, *J* = 10.5 Hz, 1H), 4.54 (d, *J* = 5.3 Hz, 2H), 3.74 (s, 3H), 3.22 (bs, 2H); **^{13}C NMR** (100 MHz, $CDCl_3$): δ [ppm] = 153.18, 147.40, 133.43, 129.93, 117.73, 115.68, 104.79, 100.83, 69.40, 55.90; **HRMS** (ESI): calculated for $[C_{10}H_{13}NO]^+$: m/z = 180.1019, found: m/z = 180.1018; **IR** (ν/cm^{-1}, neat): 3388, 3297, 3086, 2957, 3002, 2957, 2926, 2866, 2836, 1602, 1504, 1443, 1433, 1422, 1361, 1285, 1268, 1232, 1197, 1149, 1092, 1042, 1018, 997, 934, 887, 828, 790, 721, 700, 662.

Chapter 4. Photocatalytic Aminocarbonylation of Unactivated Aryl Halides

Carbonylative amidation of energy demanding aryl & heteroaryl halides enabled by visible light tandem photoredox-catalysis in continuous flow

Components of this chapter have been accepted for publication as:

Forni, J. A.; **Micic, N**; Connell, T.; Weragoda, G.; Polyzos, A. 'Tandem Photoredox Catalysis: Enabling Carbonylative Amidation of Aryl and Alkylhalides". *Angewandte Chemie International Edition*, **2020**, *59*, 18646

4.1. Introduction

N-acylation reactions of nitrogen are the most frequently executed reaction, accounting for 16% of all reactions for the discovery and preparation of drug candidate molecules.[207] Of the examined compounds, 54% contained amide functionality, with aromatic amides comprising 31% of the total population. As such, synthetic methods to access aromatic amides are of vital importance due the prevalence of this structural motif in pharmaceuticals, natural products[208,209] and preparation thereof (Scheme 4.1.1).

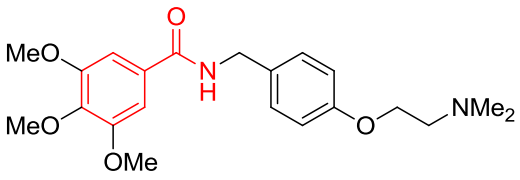

186, trimethobenzamide
antiemetic

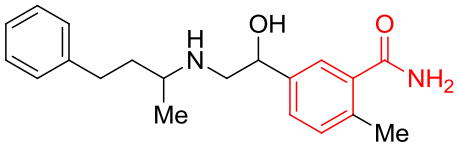

187, labetalol
antihypertensive

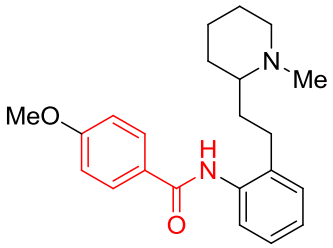

188, encainide
antiarrhythmic

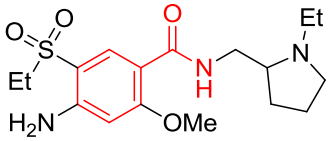

189, amisulpride
antipsychotic

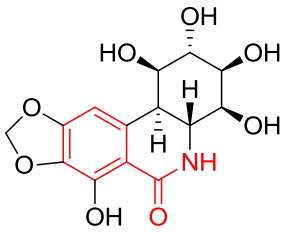

190, pancratistatin
Pancratium littorale

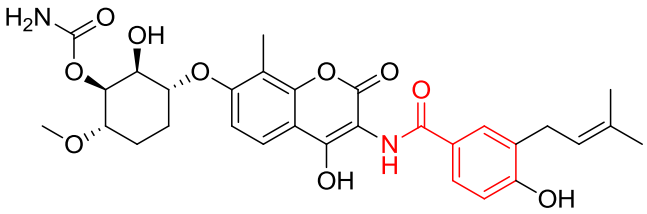

191, novobiocin
streptomyces niveus
antibiotic

Scheme 4.1.1. Active pharmaceutical ingredients and natural products containing benzamide functionality.

Within the pharmaceutical industry, current approaches to amide formation rely heavily on conventional methods that use of stoichiometric coupling reagents: acid chlorides, mixed anhydrides and carbodiimides.[210] While general and established technology, the

methodologies are expensive and do not comply with green chemistry principles. Significantly, a survey of the synthesis of 84 drug candidate molecules featuring an *N*-acylation step has highlighted that catalytic amide formation is not a synthetic strategy prioritised nor harnessed by the medicinal chemist.[210] The need for improved and industrially relevant methods for amide formation was indicated by the American Chemical Society Green Chemistry Institute and a consortium of global pharmaceutical companies (GlaxoSmithKline, Pfizer, Merck, Lilly, AstraZeneca) which concluded that 'amide formation avoiding poor atom economy reagents' was the top priority research focus.[211]

Palladium-catalysed cross-coupling methodologies are indispensable for organic synthesis. Its impact on organic synthesis was recognized by jointly the awarding the 2010 Nobel Prize to R. Heck, E. Negishi and A. Suzuki for palladium-catalysed cross-coupling in organic synthesis.[212] Access to aromatic amides by cross-coupling methodology can be accomplished by Heck-type aminocarbonylation; the three-component Pd-catalysed coupling of an aryl halide, CO and an amine (Scheme 4.1.2 a).[42] Through this catalytic approach, efficient atom economy can be realized as no pre-functionalisation of the amine or CO, the idealized C_1 building block, is required. Further, the advantage of this approach is attributed to accessibility of aryl halides as, chemically diverse and bench-stable reagents that are amenable to multi-step synthesis design. This methodology is not without limitations; coordination of CO to Pd reduces catalyst activity towards oxidative addition of the aryl halide. This necessitates the use of forcing conditions (high reaction temperatures, long reaction times) whilst favouring low partial pressures of CO that further reduce catalyst efficiency.[62]

The pursuit of carbonylation methodology that operates under benign reaction conditions has led to the development of visible light photoredox-catalysed carbonylation methods. In pioneering studies by Jacobi von Wangelin *et. al.* and Xiao *et. al.*, the carbonylation of arenediazonium salts was achieved with photoredox-catalysis (Scheme 4.1.2 b).[113,137] In the process, electron transfer from the excited photocatalyst readily reduces arenediazonium salts ($E_p^{red} \sim -0.05$ V vs SCE) generating an aryl radical. At high CO pressures (~80 atm) this intermediate is converted to an acyl radical and subsequently oxidized to a benzylidyneoxonium salt by the oxidized photocatalyst, in a net neutral catalytic cycle. Due to the electrophilicity of arenediazonium salts, this methodology is incompatible with moderate to strong

nucleophilic species; alcohols and π-nucleophiles are typical coupling partners, affording aromatic esters and ketones respectively. Furthermore, diazoniums salts are synthesized via diazotization of the corresponding arylamine, limiting the reaction scope to functionality compatible with the diazotization step.[213]

This chapter details the development of a method for the aminocarbonylation of unactivated aryl halides as radical precursors using photoredox-catalysis (Scheme 4.1.2 c). A novel tandem catalytic manifold is employed where the *in situ* generation of a highly reducing species via a second catalytic cycle addressed the limitations of traditional photoredox catalysis. By combining aryl halides and carbonylative photoredox-catalysis, the strengths of carbonylative cross-coupling and photoredox-catalysis are drawn, whilst minimizing their limitations. Continuous flow processing facilitated the safe and efficient use of CO; permitting short reaction times, straightforward scale-up, reduced working volume and pressure of CO compared to batch.

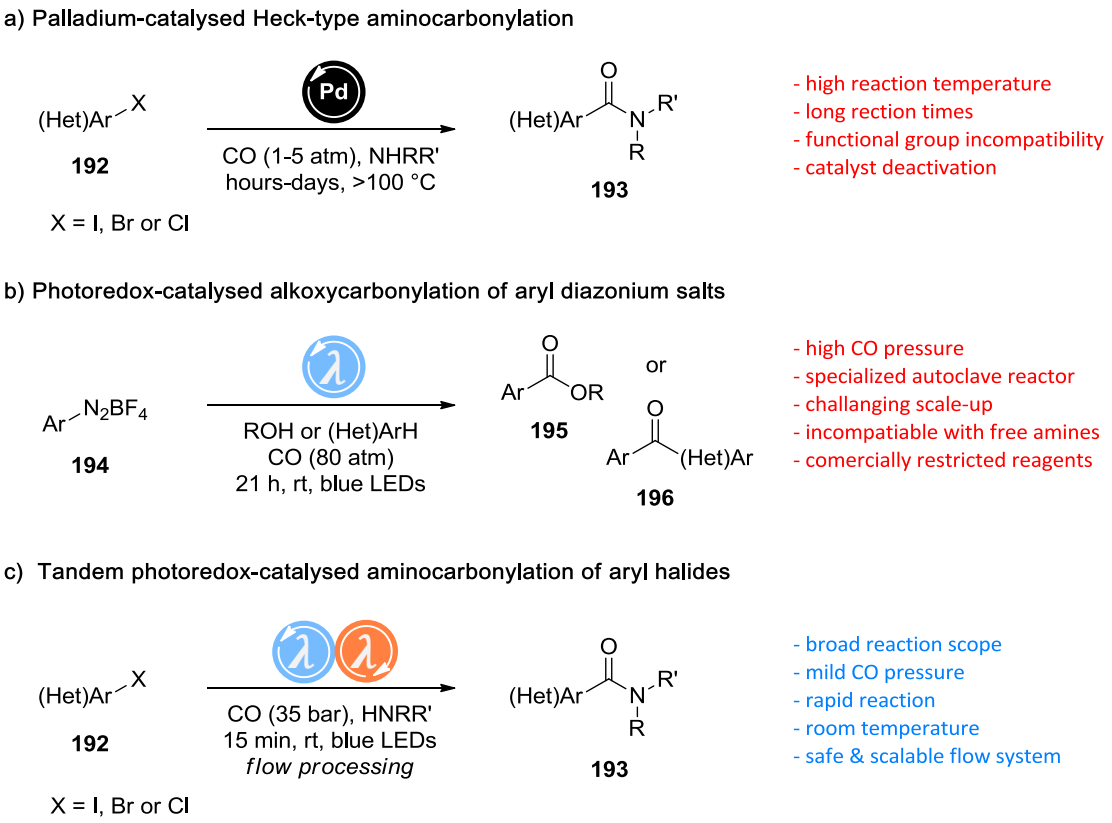

Scheme 4.1.2. Methods for the catalytic carbonylation of aryl (pseudo)halides.

4.2. Photoredox Aminocarbonylation Reaction Design

A generalised reaction mechanism for the proposed photoredox-catalysed carbonylation of aryl halides is shown in Scheme 4.2.1. The reaction is initiated by the single electron reduction of the aryl halide **197** by the photocatalyst to afford the aryl radical **199,** which is susceptible to trapping by CO, and the halide anion.

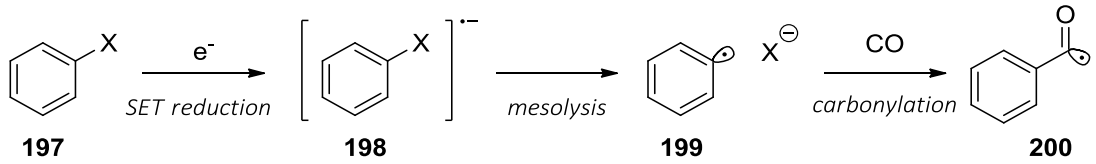

Scheme 4.2.1. Reaction pathway for the generation of acyl radicals from aryl halides.

Reaction design began with evaluating the photoredox catalysts that can engage in single election reduction of aryl halides. For SET from the catalyst to the aryl halide substrate be thermodynamically feasible, the catalyst, either in its photo-induced excited state or its single-electron reduced state, must have an oxidation potential matching the substrate reductive peak potential (E_p^{red}), that is, it must satisfy the condition in Equation 4.2.1.[106] This is illustrated in Scheme 4.2.2 where photo-excited $[Ru(bpy)_3]^{2+}$ ($E^{ox} = E_{1/2}(Ru^{II*}/Ru^{III})$ = –0.81 V vs SCE) is unable to engage benzyl bromide (E_p^{red} = –1.2 V vs SCE) whereas its single-electron-reduced analogue, $[Ru(bpy)_3]^{+}$ ($E_{1/2}(Ru^{II}/Ru^{I})$ = –1.33 V vs SCE), is a more powerful reductant and effectively able to reduce the substrate to afford the benzyl radical **208** (Scheme 4.2.2).[118]

Equation 4.2.1. $$E_p^{red} - E^{ox} \geq 0 \ V \ vs \ SCE$$

The reduction peak potential of a series of activated and unactivated aryl iodides, and bromide was determined experimentally by cyclic voltammetry (Figure 4.2.1). Cyclic voltammetry was performed using a Metrohm Autolab Model PGSTAT100 electrochemical workstation and GPES V4.9 software. Measurements were conducted using a glassy carbon working electrode, a platinum wire as the counter electrode, and a leakless Ag^+/Ag reference electrode. All measurements were performed in anhydrous acetonitrile with tetrabutylammonium hexafluorophosphate (NBu_4PF_6) as the supporting electrolyte. The working electrode was polished, rinsed with acetonitrile and dried under a stream of N_2 before each experiment. Measurements were performed

under an inert atmosphere and redox potentials were reported relative to a Fc^{+}/Fc internal standard (E^{red} = 0.40 V vs SCE).[214]

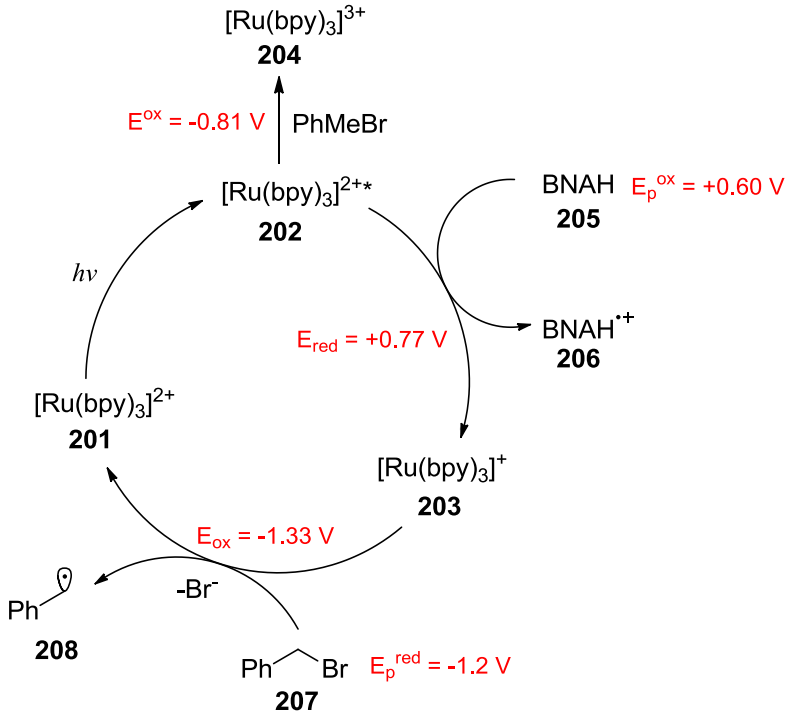

Scheme 4.2.2. Single electron reduction of benzyl bromide via $Ru(bpy)_3Cl_2$ photoredox catalysis. BNAH = 1 -benzyl-l,4-dihydronicotinamide.

The determined peak potentials, in conjunction with select peak potentials disclosed in the literature,[215] were plotted against photoredox catalysts reported to engage in the SET reduction of aryl halides (Figure 4.2.2).[216–219] Both the identity of the halide as well as the substitution pattern have considerable influence on the reductive peak potential of the aryl halides. Activated aryl halides and unactivated aryl iodides have mild reduction potentials (E_p^{red} > –2 V vs SCE). Unactivated aryl bromides and deactivated aryl halides have high reduction potentials (E_p^{red} ~2.2 V vs SCE). Stephenson first reported the generation of aryl radical from activated aryl bromides and unactivated aryl iodides via the oxidation quenching of *fac*-$Ir(ppy)_3$.[119] The SET reduction of unactivated (hetero)aryl bromides with the organophotocatalyts 10-phenylphenothiazine and rhodamine 6G has since been reported however long reaction times, up to 72 h, and high catalyst loadings were required to achieve complete conversion.[217,218] The single electron reduction of deactivated aryl halides, those baring electron donating substitution, remains a frontier challenge in photoredox catalysis owing to their negative reduction potentials (E_p^{red} < –2.5 vs SCE) that well exceed the redox potential of available photocatalysts.

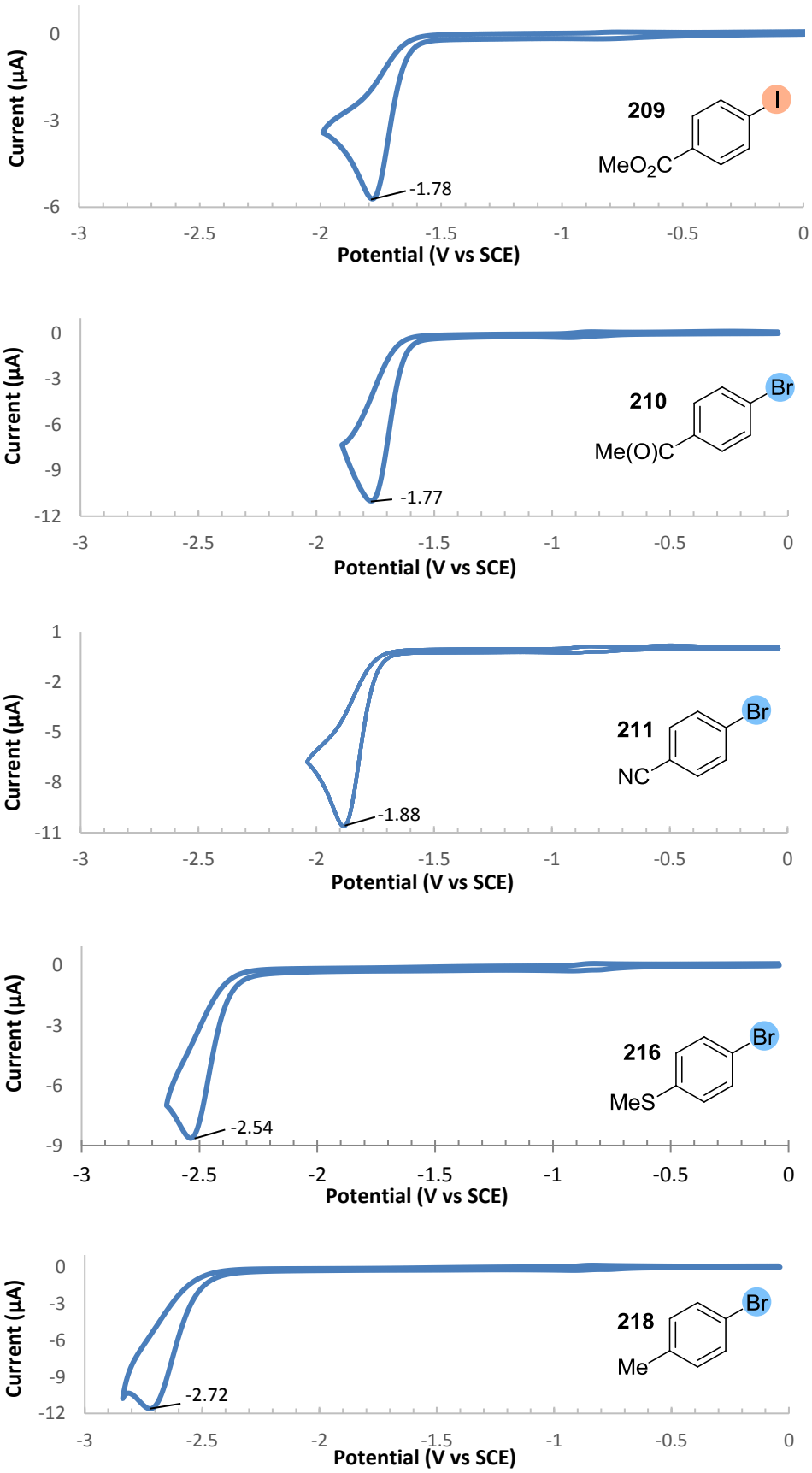

Figure 4.2.1. Experimentally determined cyclic voltammograms of aryl halides.

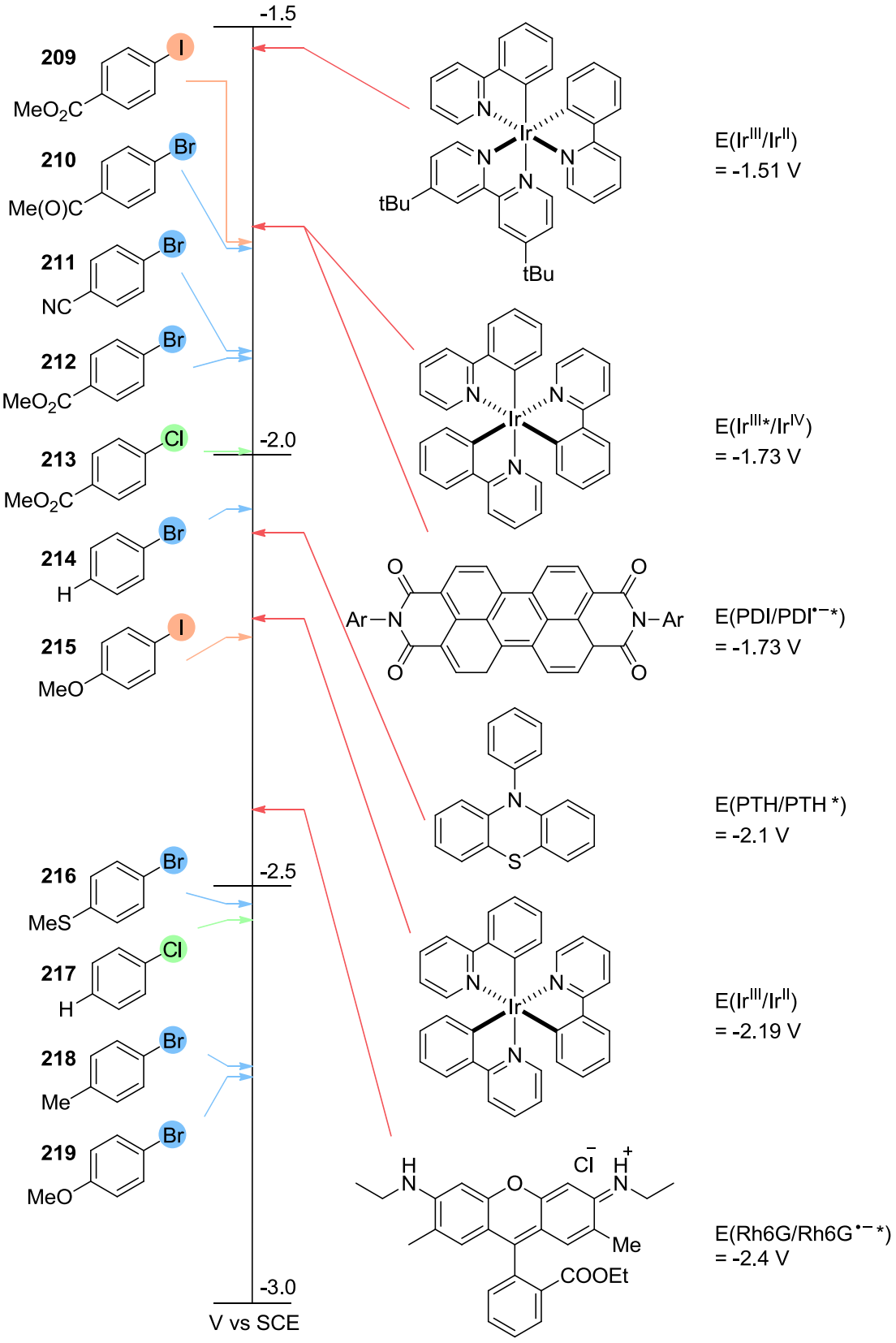

Figure 4.2.2. Redox potentials of strongly reducing photocatalysts and aryl halides.[107,166,215,220] PDI = *N*,*N*-bis(2,6-diisopropylphenyl)perylene3,4,9,10-bis(dicarboximide). PTH = 10-phenylphenothiazine. Rh6G = Rhodamine 6G.

The Polyzos group recently developed methodology for the reductive dehalogenation of unactivated aryl halides promoted by the common photocatalyst $[Ir(dttbpy)(ppy)_2]PF_6$ (**Ir1**) (Table 4.2.1).[215] Hydrodehalogenation was postulated to proceed via the formation of aryl radicals from the aryl halide precursors. Notably, complete conversion of deactivated aryl iodides, deactivated aryl bromides and activated chlorides was observed within 24 hrs.

Table 4.2.1. Photoredox mediated reductive dehalogenation of unactivated aryl halides.[a]

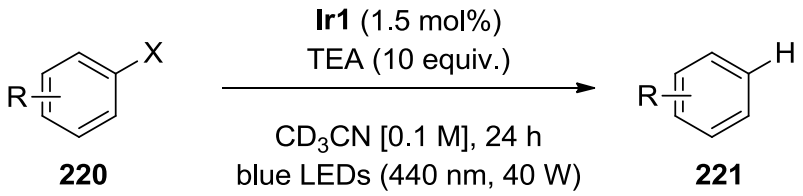

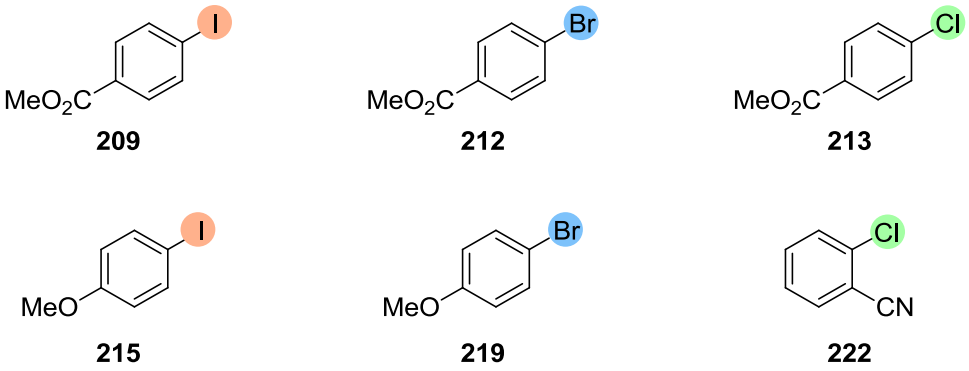

[a]Yields determined by integration of ^{1}H NMR peaks to an internal standard.

A novel tandem photoredox catalytic cycle was proposed (Scheme 4.2.3, a).[215] When irradiated in the presence of TEA, the **Ir1** is converted *in situ* into a distinct highly reducing iridium analogue **Ir2** via successive hydrogen transfers ([H]) from $TEA^{\bullet+}$ onto the $dtbbpy^{\bullet-}$ ligand of $\mathbf{Ir1}^-$ (Scheme 4.2.3, a (i)). Photoexcitation of **Ir2** forms a powerful reductant, **Ir2*** (E^{ox} = −1.70 V vs SCE), capable of engaging aryl halides (**223**) in photon-induced single electron transfer. Oxidative quenching of **Ir2*** by the aryl halide **223** furnishes the aryl radical anion pair **224** and $\mathbf{Ir2}^+$. **Ir2** turnover can be achieved upon reaction of $\mathbf{Ir2}^+$ with $\mathbf{Ir1}^-$ (Scheme 4.2.3, a (ii)) or completion of the tandem catalytic cycle via hydrogen abstraction (Scheme 4.2.3, a (iii)).[215] Spectroscopic and deuterium labelled studies showed the structure of **Ir2** to exhibit semi-saturation of the dtbbpy ligand (Scheme 4.2.3, b).[215] The complex is characterised by absorption maximum in the visible range of 460 nm and a change in luminescence of the solution from yellow to green. It was envisioned that aryl radicals

generated under this photocatalytic reaction manifold can be reacted with CO to form acyl radials (Scheme 4.2.3, c). Subsequent nucleophilic attack by an amine and single electron oxidation would furnish the desired carbonylative amidation product **225** (Scheme 4.2.3, c).

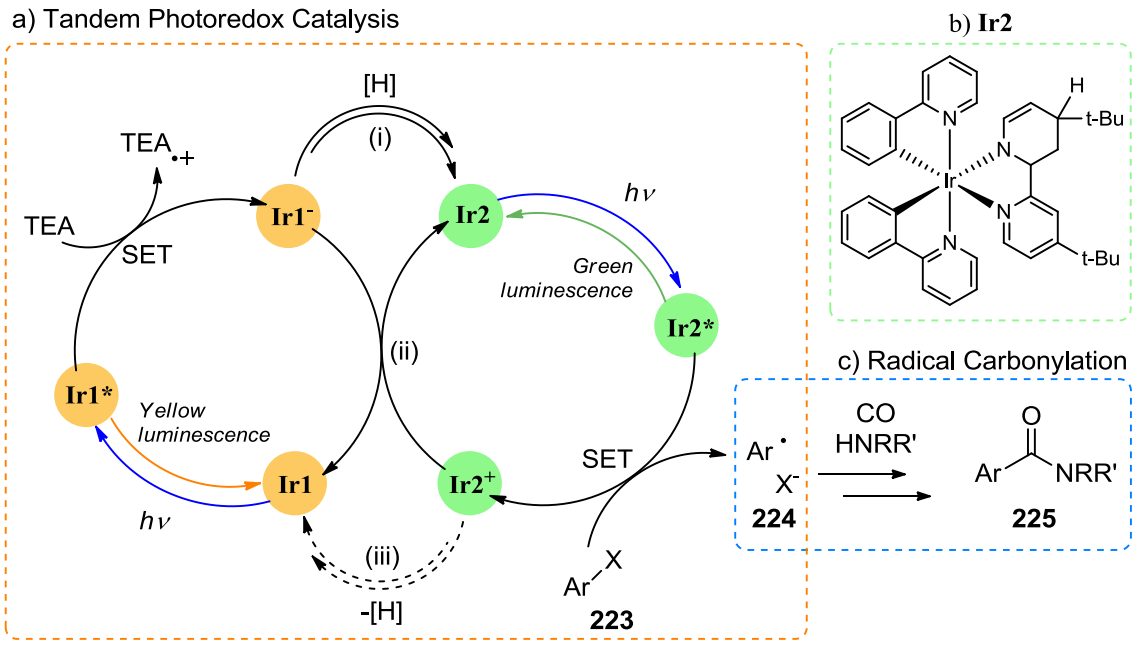

Figure 4.2.3. a) The tandem photoredox catalysis mechanism of $[Ir(dtbbpy)(ppy)_2]^+$ enabling access to energy demanding aryl halides. b) Structure of **Ir2**. c) Carbonylation of aryl halides via tandem photoredox catalysis reaction concept.

4.3. Photoredox Aminocarbonylation Reaction Development

Reaction development began with the establishment of a continuous flow platform (Figure 4.3.1). The platform consisted of a Uniqsis FlowSyn flow system for solvent pumping and reagent delivery. A modified Uniqsis Gas Addition Module was used for gaseous CO delivery. The module was rated to a maximum pressure 60 atm of CO gas. The total length of the gas-liquid reactor was reduced from the commercially supplied length of 1 m (1.89 mL total volume) to 30 cm (0.57 mL total volume), with an inner channel (liquid stream) volume of 0.15 mL and an annular channel (CO gas) volume 0.42 mL. A reduction in the length of the gas-liquid reactor was found to reduce the strain at the compression fitting were the Teflon™ 2400 tubing is interfaced with the PEEK tubing. Long gas-liquid reactor lengths resulted in intermittent failure at this

junction when system pressure exceeded 40 atm and the Rheodyne injection value is actuated due to pressure drop as the sample loop is pressurized. The magnitude of the pressure drop, typically 5-20 atm, was proportional to the size of the sample loop and inversely proportional to the flow rate. At all times, the gas-liquid reactor inner channel pressure was maintained within 5 atm of the annular channel to prevent failure of the gas-liquid membrane. Pressure was regulated by multiple back-pressure regulators in series.

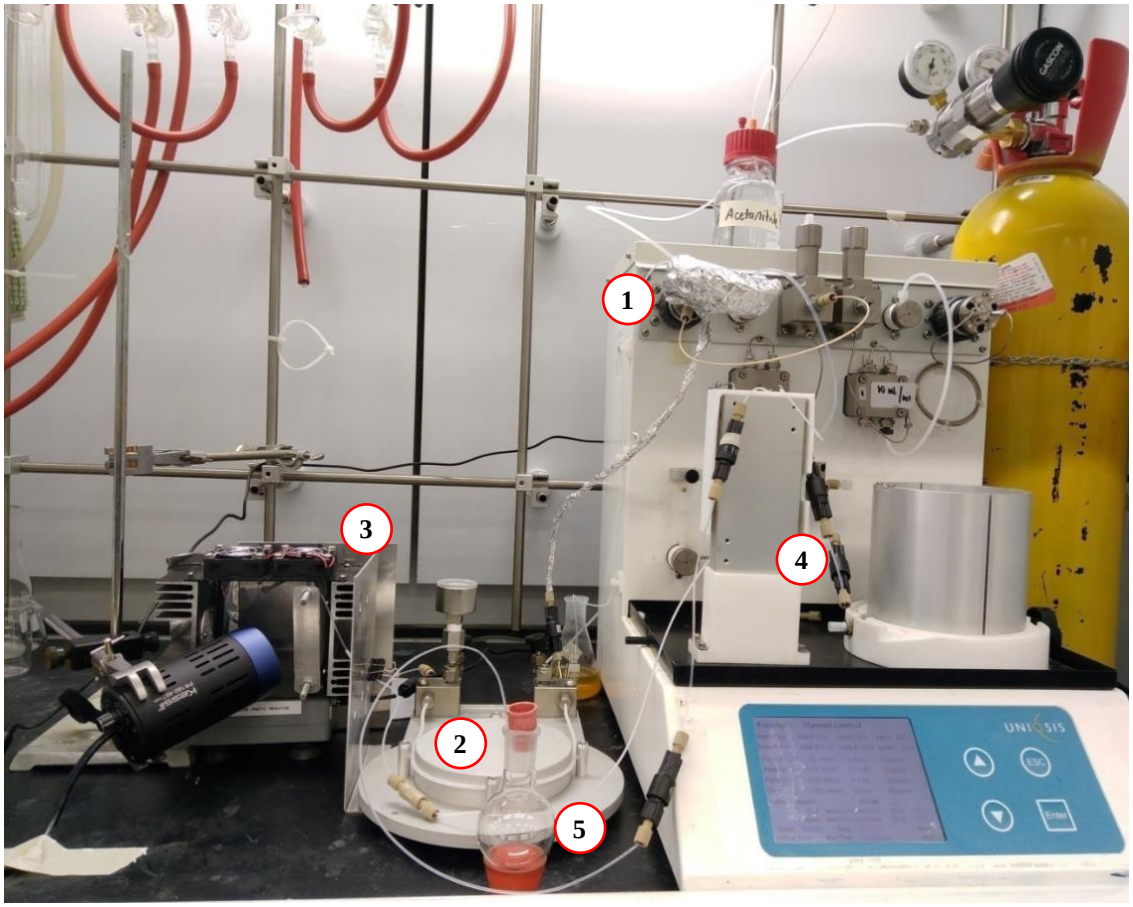

Figure 4.3.1. The photocatalytic aminocarbonylation continuous flow platform. (1) Uniqsis FlowSyn system. (2) Modified Uniqsis Gas Addition Module. (3) Tubular Photoreactor. (4) Back pressure regulators. (5) Collection flask.

The bespoke flow photoreactor, comprised of perfluoroalkoxy alkane (PFA) tubbing (0.75 mm i.d, reactor volume was 1.5 ml) coiled around solid supports, was housed within a LED assembly (Figure 4.3.2). Each assembly contained two internal 7 W LED arrays and an external 40 W LED lamp.

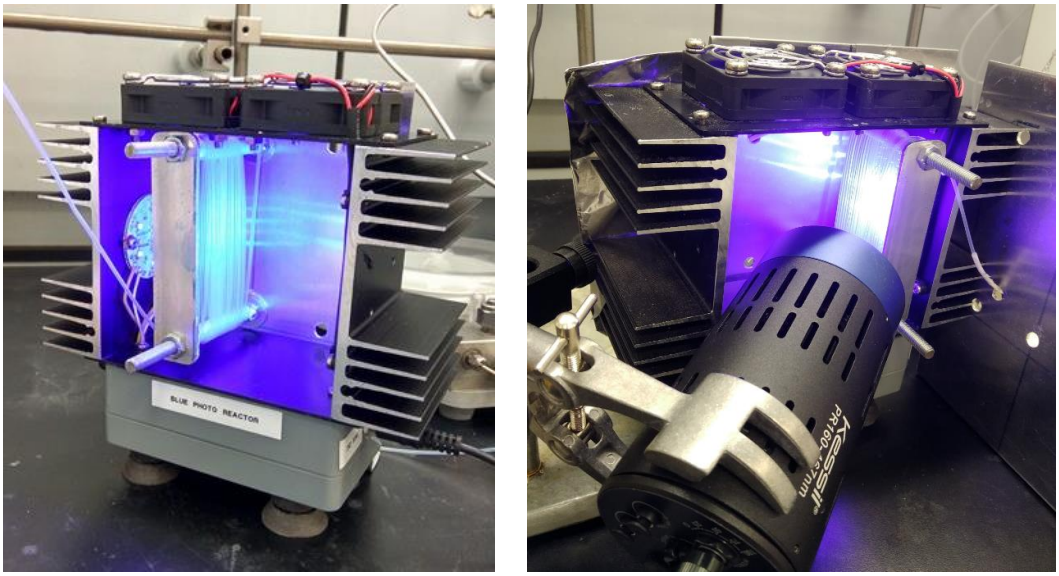

Figure 4.3.2. The flow photoreactor operating at 14 W (left) and at 54 W (right).

The photo-catalysed aminocarbonylation of methyl 4-iodobenzoate (**226**) was selected as the model transformation due to the reductive peak potential (E_p^{red} = −1.78 V vs SCE) of the substrate closely aligning with the excited state potential for **Ir2*** (E^{ox}= −1.70 V vs SCE).[215] On the basis of previously established conditions for the reduction of aryl halides by the tandem photoredox system,[215] screening of reaction conditions commenced with stoichiometric excess of DIPEA as the sacrificial reductant, the catalyst [Ir(dttbpy)(ppy)$_2$]PF_6 and 2 equivalents of morpholine as the amine coupling partner. An acetonitrilic solution of these reagents were pumped through the gas-liquid reactor, enriched with CO at 25 atm then irradiated inside the photoreactor with blue light. The volumetric flow rate was set to 0.3 mL/min, translating to a photoreactor residence time of 5 min. The reaction furnished the desired aminocarbonylated product, methyl 4-(morpholine-4-carbonyl)benzoate, **227** in 47% yield with complete consumption of the aryl iodide observed (Table 4.3.1, entry 1). *fac*-Ir(ppy)$_3$ has a similar excited state oxidation potential as **Ir2***.[119] Accordingly, *fac*-Ir(ppy)$_3$ resulted in complete conversion of the aryl halide and provided **227** in marginally lower yield (Table 4.3.1, entry 2). Conversely, the organo-photoredox catalysts screened were significantly less active (Table 4.3.1, entry 3 and 4).

Table 4.3.1. Reaction optimisation: catalyst screen.

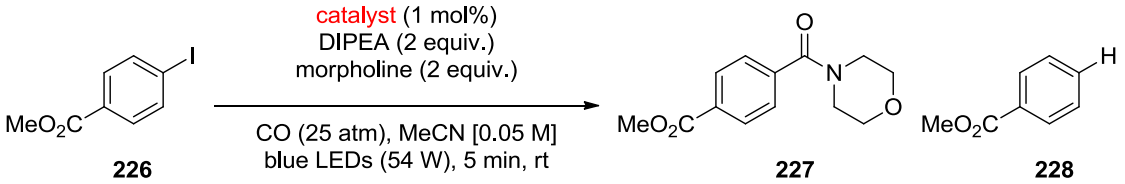

226 **227** **228**

entry	additive	conv. (%)[a]	yield 227 (%)[a]	yield 228 (%)[a]
1	$[Ir(dtbbpy)(ppy)_2]PF_6$	>99	47	49
2	*fac*-$Ir(ppy)_3$	>99	45	53
3	10-phenyl phenothiazine	2	trace	trace
4	rhodamine 6G	13	7	6

[a] ^{1}H-NMR yield calculated with 1,3,5-trimethylbenzene as the internal standard.

With **Ir1** as the photocatalyst, an increase of CO gas pressure to 35 atm in conjunction with a reduction in the equivalents of sacrificial reductant to 1.2 equivalents, the influence of sacrificial reductant on reactivity was examined. An increase in selectivity was observed indicating that DIPEA was strongly promoting the undesired hydrodehalogenation reaction (Table 4.3.2, entry 1). Similar selectivity for **227** was achieved when DIPEA was replaced with tributylamine or TEA, albeit with reduced conversion of **226** (Table 4.3.2, entry 2 and 3). Hydrodehalogenation was the principal competing reaction pathway, with methyl benzoate (**228**) accounting for the majority of the mass balance. The reaction of an aryl radical with an aliphatic acyclic amine, affording the α-amino radical and the quenched arene, is exergonic.[161] As a strategy to suppress this undesired reaction pathway, substitution of the reductive quencher with tertiary amines in absence of α-hydrogen(s) liable to hydrogen abstraction was explored. DABCO, with bridgehead nitrogens that yield reaction with an aryl radical endergonic, resulted in in unappreciable conversion (Table 4.3.2, entry 4). Aromatic amines bereft of α-hydrogens did not promote the reaction (Table 4.3.2, entry 5-7), supporting the implication of hydrogen abstraction or proton transfer from the tertiary amine in the catalytic cycle.

Table 4.3.2. Reaction optimisation: sacrificial reductant screen.

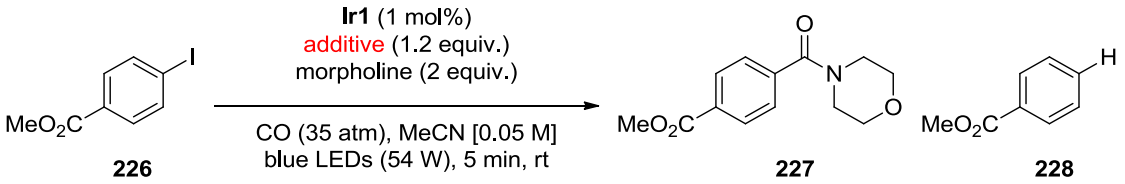

entry	additive	conv. (%)[a]	yield 227 (%)[a]	yield 228 (%)[a]
1	DIPEA	97	70	23
2	tributylamine	76	50	21
3	TEA	50	39	7
4	DABCO	7	5	2
5	9-phenylcarbazole	<5	trace	trace
6	triphenylamine	<5	trace	trace
7	4-methoxytriphenylamine	<5	trace	trace

[a] ^{1}H-NMR yield calculated with 1,3,5-trimethylbenzene as the internal standard. 1,4-diazabicyclo[2.2.2]octane (DABCO).

In extension of this strategy to supress undesired quenching of the aryl halide, the concentration of amines in solution was reduced. The reaction proved insensitive to the concentration of amine coupling partner (Table 4.3.3, entries 1-4). Significantly, morpholine could be lowered to 1.05 equivalents with no change in reactivity (Table 4.3.3, entry 4). Reducing DIPEA equivalents showed improved selectivity at the expense of lower conversion (Table 4.3.3, entries 4-6). With 1.05 equivalents of DIPEA, a 5:1 ratio of the desired aminocarbonylated product to the undesired hydrodehalogenated product could be achieved (Table 4.3.3, entry 7).

To accelerate the reaction, the catalyst loading was increased to 2 mol% (Table 4.3.4, entry 1). A slight increase in conversion was observed coupled with a decrease in selectivity. This can be accounted for by the photocatalyst acting as a hydrogen shuttle, proving a source of labile hydrogens for abstraction by the aryl radical.[221] Increasing the reaction concentration with respect to the aryl iodide resulted in diminished yield of the carbonylated product (Table 4.3.4, entry 3). Decreasing the concentration to 0.02 M afforded marginally improved selectivity, however, the decrease in reaction throughput outweighed the benefit (Table 4.3.4, entry 4). Screening a range of solvents indicated that acetonitrile was superior (Table 4.3.4, entries 5-10). Reducing the LED intensity to 14 W resulted in decrease conversion (Table 4.3.4, entry 11). An increase the LED

intensity to 80 W (2 × Kessel LED lamps) did not accelerate the reaction suggesting further optimization of the flow photoreactor was possible to achieve comparable results with reduced power consumption (Table 4.3.4, entry 12). Increasing the CO gas pressure to 50 atm did not improve selectivity nor increase the reaction rate (Table 4.3.4, entry 13). Reducing CO gas pressure to 25 atm resulted in diminished yield (Table 4.3.4, entry 14). Extending the photoreactor residence time to 15 min by reducing the volumetric flow rate to 0.1 mL/min provided complete conversion of the substrate **226** and afforded **227** in 74% isolated yield (Table 4.3.4, entry 15). Control reactions indicated that DIPEA, **Ir1**, and irradiation were essential for the transformation (Table 4.3.4, entries 16-18).

Table 4.3.3. Reaction optimisation: amine equivalence screen.

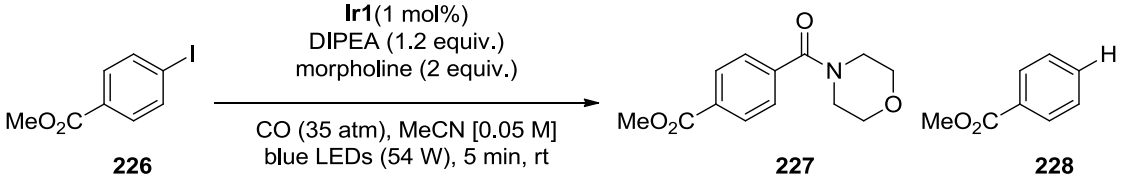

entry	deviation from scheme conditions	conv. (%)[a]	yield 227 (%)[a]	yield 228 (%)[a]
1	None	97	70	26
2	morpholine (1.5 equiv.)	95	71	23
3	morpholine (1.2 equiv.)	92	71	20
4	morpholine (1.05 equiv.)	92	71	20
5	morpholine (1.05 equiv.) DIPEA (1.5 equiv.)	>99	61	35
6	morpholine (1.05 equiv.) DIPEA (1.05 equiv.)	89	74	15

[a] ^{1}H-NMR yield calculated with 1,3,5-trimethylbenzene as the internal standard.

Table 4.3.4. Optimization and control experiments for the aminocarbonylation of methyl 4-iodobenzoate in flow.

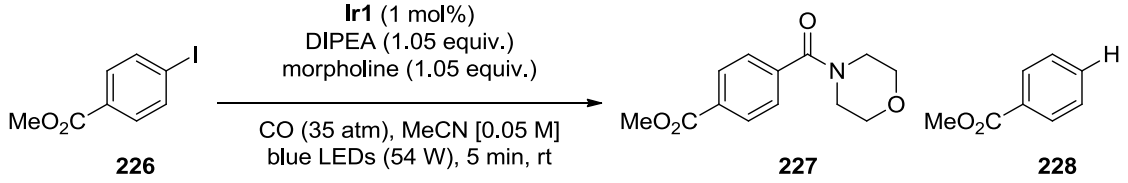

226 **227** **228**

entry	deviation from scheme conditions	conv. (%)[a]	yield 227 (%)[a]	yield 228 (%)[a]
1	none	89	74	15
2	2 mol% **Ir1**	92	71	20
3	**226** [0.1 M]	86	55	22
4	**226** [0.02 M]	87	76	11
5	solvent: propionitrile	33	16	9
6	solvent: dimethyl sulfoxide	37	3	6
7	solvent: dimethylformamide	48	17	2
8	solvent: acetone	46	34	18
9	solvent: dichloromethane	36	22	12
10	solvent: ethyl acetate	30	24	4
11	14 W blue LEDs	79	66	13
12	80 W blue LEDs	93	72	19
13	50 atm CO gas pressure	90	75	15
14	25 atm CO gas pressure	88	55	31
15	R_t = 15 min	>99	79 (74)	20
16	No DIPEA	<5	trace	n.d.
17	No catalyst	<5	trace	n.d.
18	No light	0	n.d.	n.d.

[a] ^{1}H-NMR yield calculated with 1,3,5-trimethylbenzene as the internal standard. Isolated yield in parenthesis. n.d. = none detected.

4.4. Photoredox Aminocarbonylation Reaction Scope

With the optimised reaction conditions established, the aryl iodides and aryl bromide reaction scope were evaluated (Table 4.4.1). Aryl iodides and bromides bearing electron withdrawing substitution yielded their respective benzamide products in good to excellent isolated yields (**229aa-229lb**). Electron rich aryl halides and unactivated aryl bromides necessitated a minor increase in DIPEA (1.2 or 1.5 equiv.), morpholine (1.2 equiv.) and residence time (30 min) in order to achieve full conversion. To suppress hydrodehalogenation at elevated DIPEA and morpholine concentration, CO pressure was increased to 45 atm. 4-bromoacetophenone (**229cb**) did not appreciably afford the desired amide functionalized acetophenone; the amide functionalized α-methylbenzylalcohol was recovered as the major product, indicating reduction of the carbonyl functional group.

Significantly, aryl bromides could be selectively carbonylated in the presence of boronate esters (**229ib**), demonstrating exceptional orthogonality relative to Pd-catalysed aminocarbonylation where Suzuki coupling products dominate.[222] Gratifyingly, aminocarbonylation of electron-rich substrates (**229ma-229tb**) proceeded efficiently. Full conversion of the screened aryl iodide and bromide substrates was observed with the developed reaction conditions. Notably, when **229tb** (4-bromothioanisole, E_p^{red} = –2.54 V vs SCE) was subjected to the same reaction conditions with *fac*-Ir(ppy)$_3$ in lieu of **Ir1**, quantitative recovery of the **229tb** was observed. This highlights the ability of tandem visible light photoredox-catalysis to engage energy demanding substrates outside the scope of a conventional photoredox cycle. The developed transformation proceeded well with halogenated pyridines (**229sa and 229sb**). Interestingly, 7-iodo-1H-indole (**229ta**) was tolerated while its *N-tert*-butyloxycarbonyl protected analogue afforded its respective aminocarbonyled product in 29% yield − determined by ^{1}H NMR integration against an internal standard.

The reaction was extended to the room-temperature aminocarbonylation of methyl 4-chlorobenzoate (**229ac**). Despite its sluggish reactivity, achieving 43% conversion with 3 equivalents of DIPEA and a prolonged residence time of 120 min, the result is notable as the carbonylation of aryl chlorides at room-temperature by traditional transition metal catalysis has not been accomplished.[223–225]

Table 4.4.1. Aryl iodide and aryl bromide scope.[a]

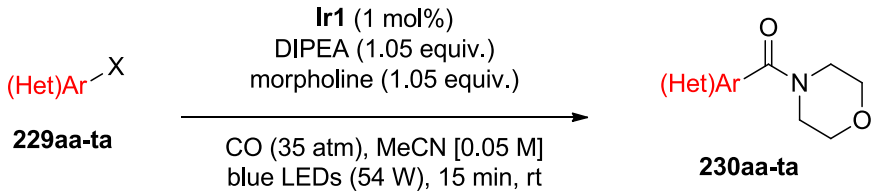

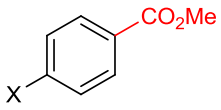

I: **229aa** 74%
Br: **229ab** 75%[b]
Cl: **229ac** 27%

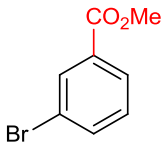

229bb 74%[b]

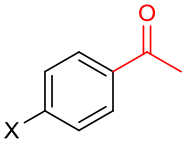

I: **229ca** 58%
Br: **229cb** 0%[b]

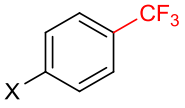

I: **229da** 67%
Br: **229db** 60%[b]

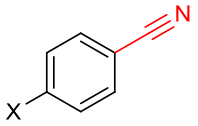

I: **229ea** 65%
Br: **229eb** 53%[b]

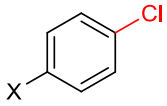

I: **229fa** 66%
Br: **229fb** 62%[b]

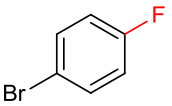

229gb 71%[b]

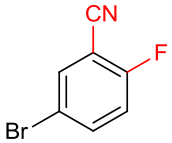

229hb 46%[b]

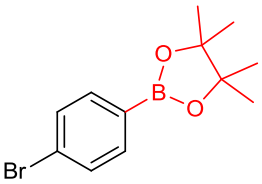

229ib 54%[b]

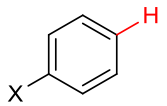

I: **229ja** 88%[b]
Br: **229jb** 79%[b]

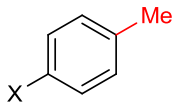

I: **229ka** 71%[b]
Br: **229kb** 70%[b]

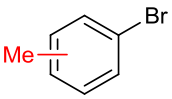

ortho: **229la** 53%[b]
meta: **229lb** 70%[b]

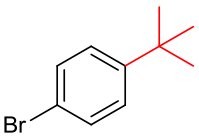

229mb 75%[b]

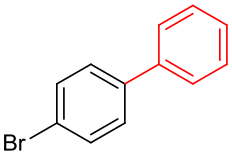

229nb 70%[b]

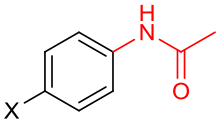

I: **229oa** 70%[c]
Br: **229ob** 72%[c]

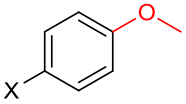

I: **229pa** 68%[c]
Br: **229pb** 54%[c]

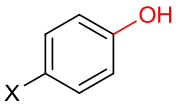

I: **229qa** 40%[c]
Br: **229qb** 47%[c]

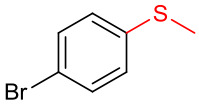

229rb 72%[c]

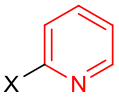

I: **229sa** 59%[b]
Br: **229sb** 63%[b]

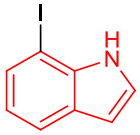

229ta 41%[b]

[a]Unless otherwise noted, reactions carried out with aryl halide (0.25 mmol), $[Ir(dtbbpy)(ppy)_2]PF_6$ (1 mol %), DIPEA (1.05 equiv.), morpholine (1.05 equiv.), MeCN (5 mL), CO (35 atm), 54 W blue LED irradiation, room temperature, 15 min photoreactor residence time. Isolated yields are given. [b]DIPEA (1.2 equiv.), morpholine (1.2 equiv.), CO (45 atm). [c]DIPEA (1.5 equiv.), morpholine (1.2 equiv.), 30 min, CO (45 atm). [d] 43% conversion.

The photoredox aminocarbonylation reaction was conducted on the gram-scale (Figure 4.4.1). To facilitate a preparative scale reaction, the gas-liquid reactor and photoreactor volumes were scaled-out by a factor of 4. Operating in the continuous-flow regime, 10 mmol of methyl 4-iodobenzoate (**229aa**) was processed to afford 1.8 g of methyl 4-(morpholine-4-carbonyl)benzoate (**230aa)** in 72% isolated yield. The reaction throughput was 216 mg/h (0.86 mmol/h).

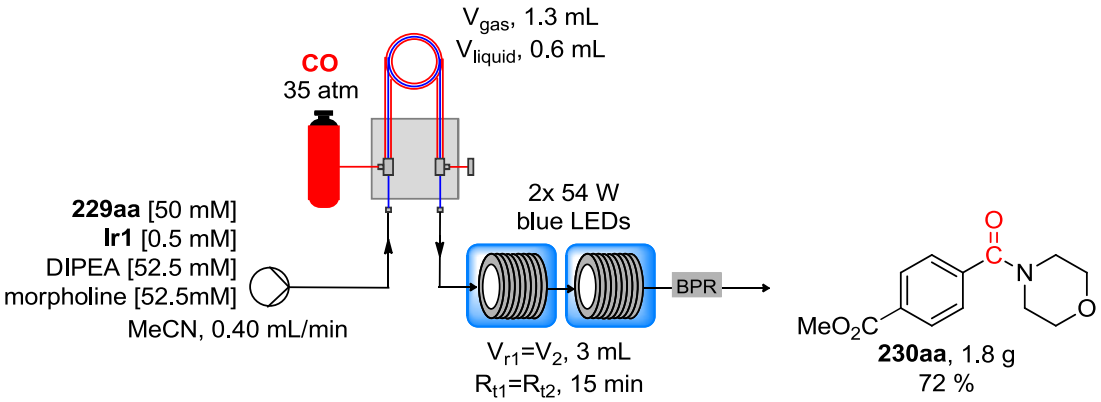

Figure 4.4.1 Reaction scheme for the gram-scale carbonylative cross-coupling of methyl 4-iodobenzoate and morpholine. Abbreviations as follows: reactor volume (V_r), residence time (R_t).

The generality of the developed reaction was investigated with respect to the amine coupling partner (Table 4.4.2). Bromobenzene was elected as the aryl halide. Aliphatic cyclic amines (**232a-232b**) were better tolerated than secondary acyclic amines (**232c**). Increasing the amine equivalents relative to bromobenzene was required for primary aliphatic amines to readily participate in the free-radical aminocarbonylation reaction (**232d-232g**), suggesting the nucleophilicity of the amine was important. Under the developed conditions, ethanolamine did not yield detectable quantities of the alkoxycarbonylated benzamide as determined by ^{1}H NMR analysis of the crude reaction mixture. The carbonylative coupling of *tert*-butylamine proceeded smoothly despite its steric bulk. Allyl amine, containing a terminal alkene that is susceptible to radical addition by the nucleophilic aryl radical intermediate species,[226] gave *N*-allyl benzamide **232i** in good yield. The reaction of propargyl amine yielded only trace amount of its corresponding benzamide **232j**. Anilines were not compatible (**232k-232l)**. The methodology appeared to be intolerant towards thioether functionality (**232m-232n**) but amenable to thiofuran functionality (**232o**).

Table 4.4.2. Amine coupling partner scope.[a]

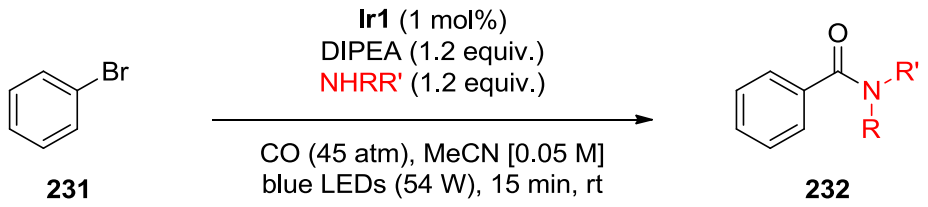

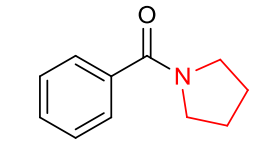

232a, 69%

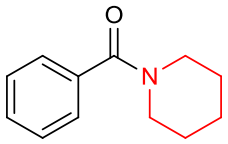

232b, 74%

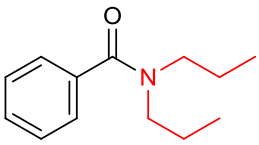

232c, 58%

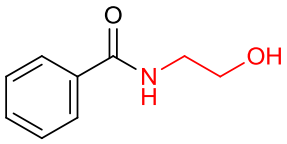

232d, 42%[b]

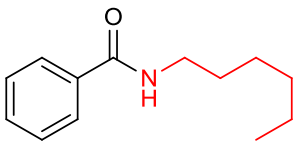

232e, 70%[b]

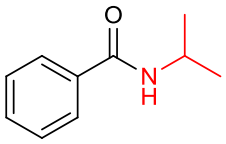

232f, 67%[b]

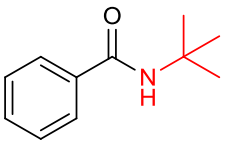

232g, 55%[b]

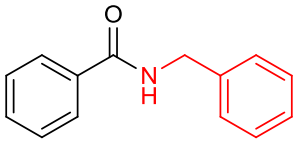

232h, 60%

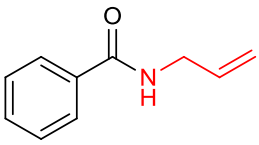

232i, 59%

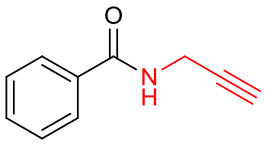

232j, (7%)[c]

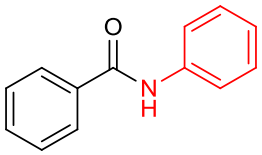

232k, (trace)[c]

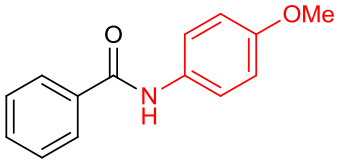

232l, (trace%)[c]

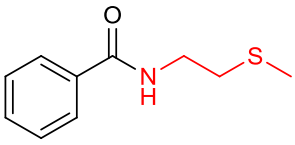

232m, (3%)[c]

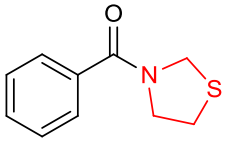

232n, (trace)[c]

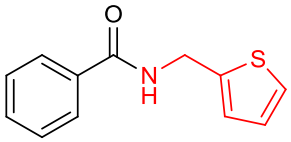

232o, (22%)[c]

aUnless otherwise noted, reactions carried out with bromobenzene (0.25 mmol), [Ir(dtbbpy)(ppy)2]PF6 (1 mol %), DIPEA (1.2 equiv.), morpholine (1.2 equiv.), MeCN (5 mL), CO (45 atm), 54 W blue LED irradiation, room temperature, 15 min photoreactor residence time. Isolated yields are given. b5 equiv. amine.c reaction yield determined by integration of 1H NMR against an internal standard.

The developed reaction was further applied to a free-radical addition/aminocarbonylation cascade reaction (Scheme 4.1.1). The doubly carbonylated α-keto amide **234** was the dominate reaction product. Synthetic access to this methylene α-keto amide functionalized 1,2-dihydrobenzofuran structural motif is remains unexplored as conventional amidation protocols are challenging, requiring pre-functionalization of the benzofuran, and Pd-catalysed carbonylative methodology results in a distribution of products.[227,228]

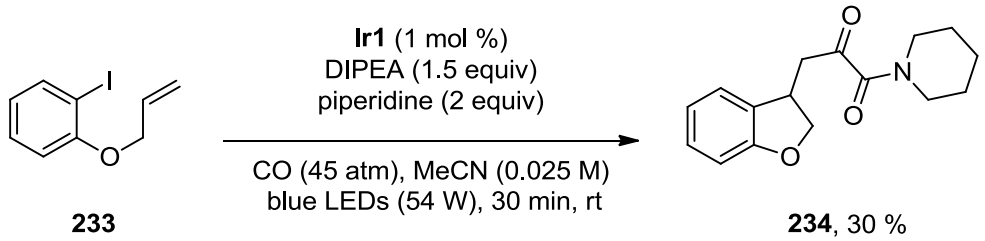

233 **234**, 30 %

Scheme 4.4.1 Free-radical addition/aminocarbonylation cascade reaction.

4.5. Mechanistic Investigations

Spectroscopic approaches were utilised to elucidate the mechanism of the catalytic cycle. Steady-state luminescence quenching studies were performed to confirm the *in situ* generation of **Ir2** under the reaction conditions. A 2 mL acetonitrile solution of DIPEA (75 mM) and **Ir1** (150 μM) sequentially sparged with nitrogen for 5 minutes then irradiated for 5 minutes (40 W, 440 nm). A 1 mL aliquot of a deoxygenated solution of 4-bromothioanisole in acetonitrile was added to afford the desired concentration. Samples were sparged for a further 5 min whilst shielded from ambient light. Steady-state emission spectra were collected using a Varian Cary Eclipse fluorescence spectrophotometer (λ_{ex} = 400 nm, 5 nm slits). The quenching experiments showed that luminescence of **Ir2** was quenched in the presence of 4-bromothioanisole. A Stern-Volmer plot was calculated using I_0/I; where I_0 and I are the integrated emission intensities in the absence and presence of quencher (*Q*) respectively (Figure 4.5.1). The linearity of the Stern−Volmer plot is indicative of dynamic quenching and suggests that the quenching involves only a reaction between the emitting state of the **Ir2** and the aryl bromide substrate. The calculated quenching rate constant ($k_q = 2.6\times10^6$

$M^{-1}s^{-1}$) indicates sluggish electron transfer, several orders of magnitude below diffusion limited processes. The quenching rate constant, k_q was calculated by fitting a linear regression to solve the equation: $\frac{I_0}{I} = 1 + k_q\tau_0.Q$, were the excited state lifetime (τ_0) of **Ir2** was previously determined to be 2.24 µs.[215]

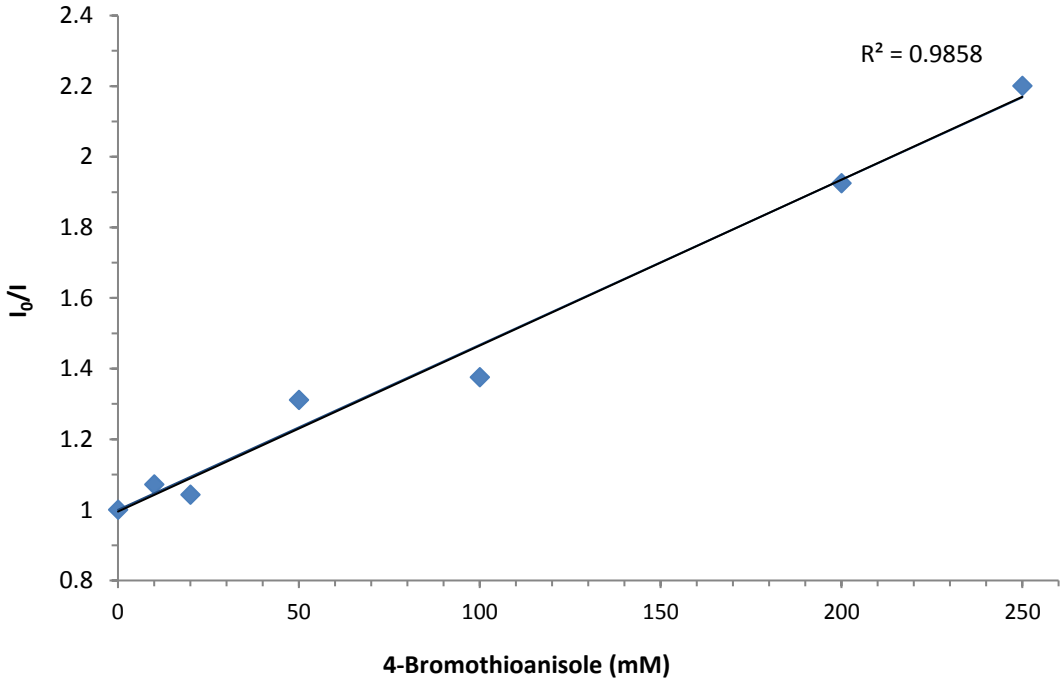

Figure 4.5.1. Stern-Volmer emission quenching plot of **Ir2** with 4-bromothioanisole.

Transient absorption spectroscopy was used to further illuminate the nature of this dynamic interaction. Irradiation (λ = 410 nm) of a solution containing 0.1 mM **Ir1** and 50 mM DIPEA resulted in the rapid formation of **Ir1**$^-$ (Figure 4.5.2) followed by exponential decay and the concomitant increase in emission intensity attributable to **Ir2*** (Figure 4.5.3).[215] When repeated including the addition of methyl 4-iodobenzoate, no appreciable absorption or emission attributable to either intermediate was observed, suggesting rapid oxidation of **Ir1**$^-$ back to **Ir1** via electron transfer to methyl 4-iodobenzoate. Substituting this substrate for 4-bromothioanisole, **Ir1**$^-$ formed along with emission assigned to **Ir2*** The emission profile of **Ir2*** is of much lower intensity suggesting that it is now quenched by the energy demanding aryl bromide substrate. The reduced absorbance intensity of **Ir1**$^-$ is attributed to quenching by **Ir2**$^+$.

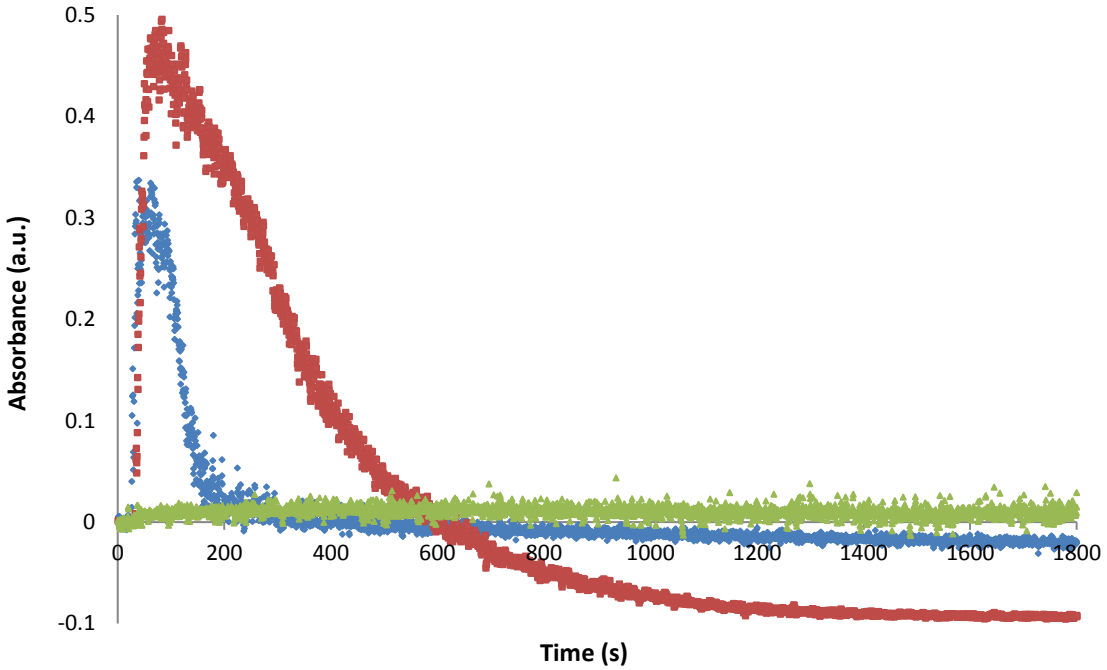

Figure 4.5.2. Absorbance of $[Ir(dtbbpy^{\bullet-})(ppy)_2]^0$ (monitored at λ_{abs} = 534 nm) formed from replicate reactions of $[Ir(dtbbpy)(ppy)_2]^+$ (0.1 mM) and DIPEA (50 mM) irradiated with blue light with the addition of no reductive quencher (red data points), 4-bromothioanisole (50 mM, blue) or of methyl 4-iodobenzoate (50 mM, green).

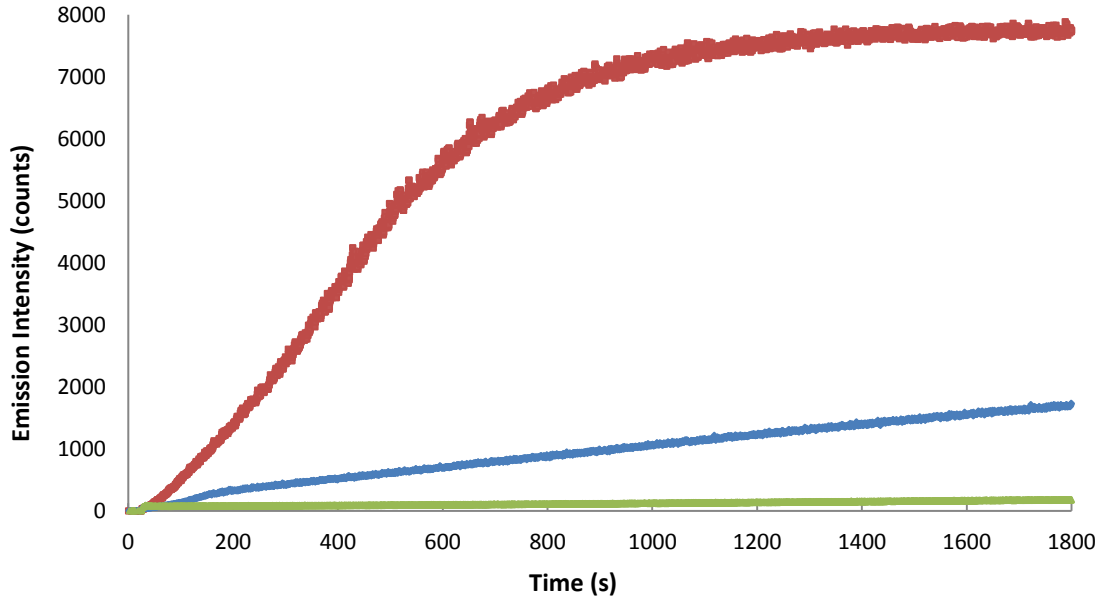

Figure 4.5.3. Emission of **Ir2** (monitored at λ_{em} = 515 nm) formed from replicate reactions of $[Ir(dtbbpy)(ppy)_2]^+$ (0.1 mM) and DIPEA (50 mM) irradiated with blue light with the addition of no reductive quencher (red data points), 4-bromothioanisole (50 mM, blue) or of methyl 4-iodobenzoate (50 mM, green).

With consideration of the spectroscopic evidence, a plausible mechanism comprising of two interconnected photoredox cycles was postulated for the generation of aryl radicals from aryl halides under the developed reaction conditions (Scheme 4.5.1).

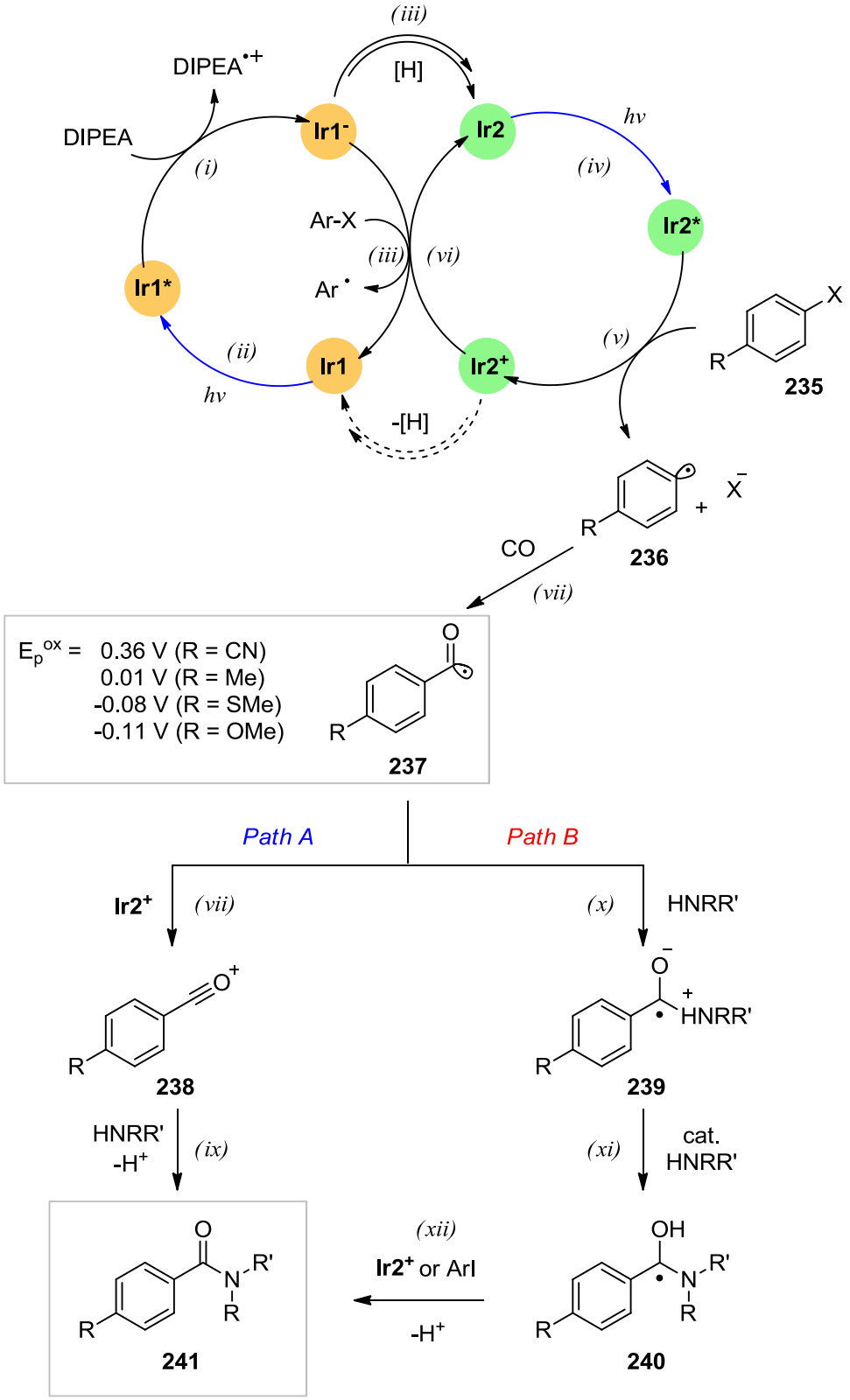

Scheme 4.5.1. Postulated reaction mechanism for the visible-light photoredox aminocarbonylation of aryl halides.

The tandem photoredox cycle facilitates the reductions of aryl halides over a large reduction potential range. Excitation of ground state **Ir1** with blue light generates the long lived excited-state **Ir1*** (Scheme 4.5.1, *i*). Reductive quenching with DIPEA generates **Ir1**$^{-}$ and DIPEA$^{\bullet+}$ (Scheme 4.5.1, *ii*). Depending on the energy demands of a given substrate, electron transfer may occur directly from **Ir1**$^{-}$ (E^{ox}(**Ir1***/**Ir1**$^{-}$) = −1.51 V vs SCE)[107] or **Ir2*** (E^{ox} (**Ir2***/**Ir2**+) = −1.70 V vs SCE)[215]. Kinetic measurements suggest that readily reducible aryl halides, such as methyl 4-iodobenzoate (E_p^{red} = −1.78 vs SCE), undergo electron transfer with the less reducing **Ir1**$^{-}$ (Scheme 4.5.1, *iii*). In the presence of energy demanding aryl halides, electron transfer from **Ir1**$^{-}$ is thermodynamically unfavourable and reduction of the dtbbpy$^{\bullet-}$ dominates, generating **Ir2** (Scheme 4.5.1, *iv*). Photoexcitation generates the more highly reducing excited state catalyst **Ir2*** which can engage in the SET reduction of energy demanding substrates such as 4-bromothioanisole (E_p^{red} = −2.54 V vs SCE) (Scheme 4.5.1, *v*). The mismatch in redox potentials may be accounted for by the inaccuracies of comparing irreversible reductive peak potentials of organic molecules to the reversible or quasi-reversible redox potentials of the metal photocatalyst.[229,230] For substrates that sit well below these reduction potentials (E_p^{red} > 2.5 V) we cannot rule out the occurrence of other pathways; the species **Ir2**$^{-}$ (E^{ox}(**Ir2**$^{-}$/ **Ir2**) = −2.2 V vs SCE)[215] may be formed following reductive quenching of **Ir2*** by **Ir1**$^{-}$. The catalytic cycle is closed by the reduction of **Ir2**$^{+}$ by **Ir1**$^{-}$ or by highly reducing species such as the of hydroxybenzyl radical intermediate **240** (Scheme 4.5.1, *vi*).

Trapping of the aryl radical **236** by CO affords the acyl radical **237** (Scheme 4.5.1, *vii*). The conversion of this intermediate to the product via two possible pathways. In path A, single electron oxidation of the acyl radical by the oxidized photocatalyst **Ir2**$^{+}$ (E^{red}(**Ir2**$^{+}$/ **Ir2**) = 0.88 V vs SCE)[215] results in the formation of the acylium ion **238** (Scheme 4.5.1, *vii*). Density functional theory (DFT) computations, performed on the M06-2X/6-311+G(d,p) level of theory, revealed this step to be thermodynamically feasible with the calculated oxidation potentials of the acyl radical intermediate **237** to be between −0.11 and 0.36 V vs SCE depending on substitution on the aromatic ring. Reaction of the acylium ion with the amine affords the aromatic amide **241** (Scheme 4.5.1, *ix*). Alternatively, the reaction may proceed via nucleophilic addition of the amine to the acyl radical gives the zwitterionic intermediate **239** (Scheme 4.5.1, *x*). Amine-assisted intermolecular proton transfer of **239** yields the reducing **240** (Scheme

4.5.1, *xi*).[231] Formation of the amide may follow oxidation of **240** by electron transfer to the catalyst or by radical chain propagation followed by deprotonation (Scheme 4.5.1, *xii*). The oxidation potential of a series of hydroxybenzyl radical species (**242**) were computed (Scheme 4.5.2). Hydroxybenzyl radical species (E_p^{red} = −0.75 to −1.29 vs SCE) have been reported to engage in radical chain propagation with the aryl iodides,[231] however aryl bromides, which have a lower reduction potential, are unlikely to proceed via the chain propagation pathway. This observation may account for the lower DIPEA loading required to achieve full conversion for aryl iodides compared to aryl bromides. Control experiments were performed to ascertain which pathway was the major contributor. When *n*-butyl alcohol was the nucleophilic coupling partner, only 14% of the desired product **247** could be detected by ^{1}H NMR despite full conversion of bromobenzene. Alcohols are not expected to efficiently participate in direct nucleophilic attack of the acyl radical,[232] but are expected to react with acyl radicals at near diffusion limited reaction,[233] thus suggesting path B as the predominate reaction pathway.

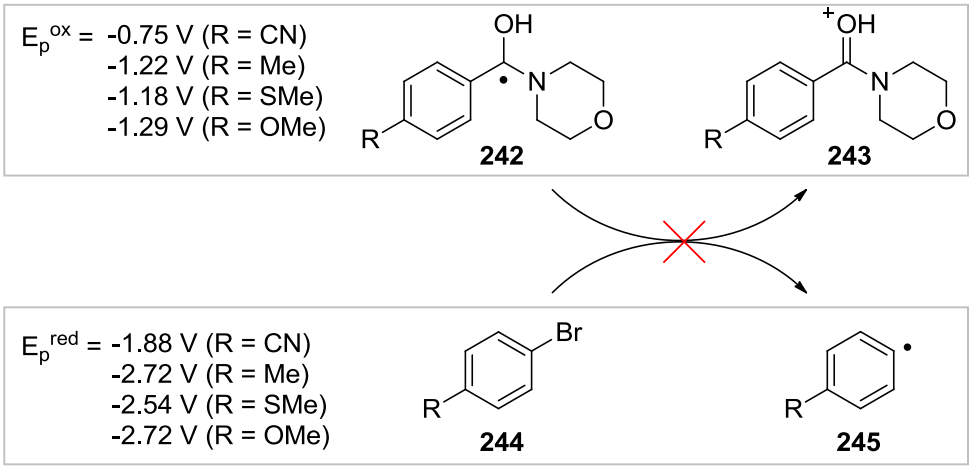

Scheme 4.5.2. Thermodynamically unfavoured radical chain propagation. Redox potentials recorded against SCE.

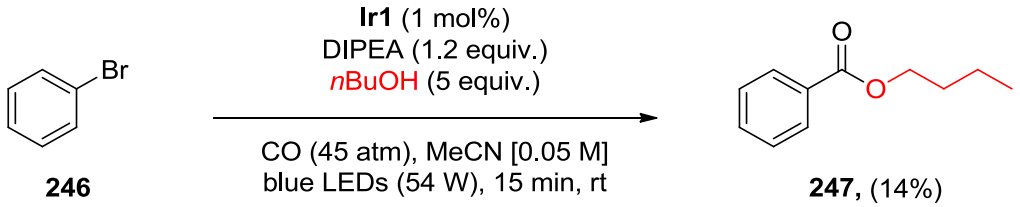

Scheme 4.5.3. Control experiment with *n*-butanol.

4.6. Conclusion

Benzamides are ubiquitous in the discovery and preparation of active pharmaceutical ingredients. Synthetic routes to benzamides employed in drug discovery and development are reliant on conventional acylation methodologies of inefficient atom economy and poor chemoselectivity. Heck aminocarbonylation enables the three-component coupling of an amine, aryl halides and CO thereby affording benzamides with excellent atom economy. This strategy is not without its limitations. The requirement of high temperatures in combination with stoichiometric base and palladium restricts functional group tolerance and catalytic efficiency.

Methodology for the visible light photoredox-catalysed carbonylation of aryl halides was developed. The reaction enabled the carbonylative coupling of aliphatic amines and aryl iodides/bromides with significant functional group tolerance. Atom economy is conserved as this catalytic approach required only a small stoichiometric excess (1.05-1.5 equiv.) of sacrificial reductant to promote the reaction. Aryl chlorides were amenable to the reaction conditions, but further optimisation and elaboration of scope is required. The application of tandem photoredox-catalysis in conjunction with continuous flow processing allowed for the energy demanding transformation to proceed under benign reaction conditions. Notably, the aminocarbonylation of aryl bromides and chlorides proceeded at room-temperature. The developed methodology was applied to the synthesis of both electron rich and electron deficient hetero-benzamides. Experimental and theoretical studies were conducted to elucidate the reaction mechanism. Spectroscopic investigations suggested that irradiation of $[Ir(dtbbpy)(ppy)_2]PF_6$ in the presence of DIPEA generates a distinct highly reducing Ir-complex capable of engaging energy demanding aryl halides. Theoretical studies probed the fate of the aryl radical following reaction with CO, indicating that nucleophilic attack of the amine onto the acyl radical is the predominate reaction pathway. Through utilization of the tandem photoredox manifold, it was demonstrated that photoredox-catalysed carbonylation of arenes is no longer restricted to high energy aryl radical precursors, aryl diazonium salts and aryl sulfonyl chlorides, that are incompatible with strong nucleophiles such as amines.

4.7. Chapter 4 Experimental

Reagents

Unless otherwise stated, aryl halides, reagents, catalysts and solvents were purchased from Merck, Sigma-Aldrich or TCI and were used without further purification. Acetonitrile was used as supplied (HPLC grade). $[Ir(dtbbpy)(ppy)_2]PF_6$,[202] 10-phenylphenothiazine,[217] 1-(allyloxy)-2-iodobenzene[234] and 2-(4-bromophenyl)-4,4,5,5-tetramethyl-1,3,2-dioxaborolane[235] was prepared according to literature procedures.

Steady-state and Transient Spectroscopy

Steady-state emission spectra were recorded using a Varian Cary Eclipse Fluorescence Spectrophotometer. Kinetic measurements were performed using a custom-made spectrometer (Figure 4.7.1). A quartz cuvette with a Teflon septum cap and stirrer bar comprising $[Ir(dtbbpy)(ppy)_2]PF_6$ (0.1 mM), DIPEA (50 mM) and aryl halide (50 mM) where appropriate was sparged with Ar for 10 min. The cuvette was placed in a 3D printed holder above a magnetic stirrer. Samples were irradiated using a Thorlabs SOLIS-445C LED operated using a DC20 LED driver, with a measured light intensity of 190 mW/cm^2. For absorption measurements a Thorlabs MCWHL5 Cold White LED was used for the broadband lightsource. Emission or absorbance was collected by a fibre optic mounted behind a Thorlabs FEL0500 long pass filter (500 nm) and detected using an Andor iDus 420 CCD camera. Spectra were collected and processed using Andor Solis software.

Electrochemistry

Cyclic voltammetry was performed using a Metrohm Autolab Model PGSTAT100 electrochemical workstation and GPES V4.9 software. Measurements were conducted using a glassy carbon working electrode, a platinum wire as the counter electrode, and a leakless Ag^+/Ag reference electrode. Electrodes were purchased from eDAQ. All measurements were carried out in anhydrous acetonitrile with NBu_4PF_6 as the supporting electrolyte. The working electrode was polished, rinsed with acetonitrile and dried under a stream of N_2 before each experiment. Measurements were performed

under an inert atmosphere and redox potentials were reported relative to a Fc^{+}/Fc internal standard ($E^{o\prime}$ = 0.40 V vs SCE).[214]

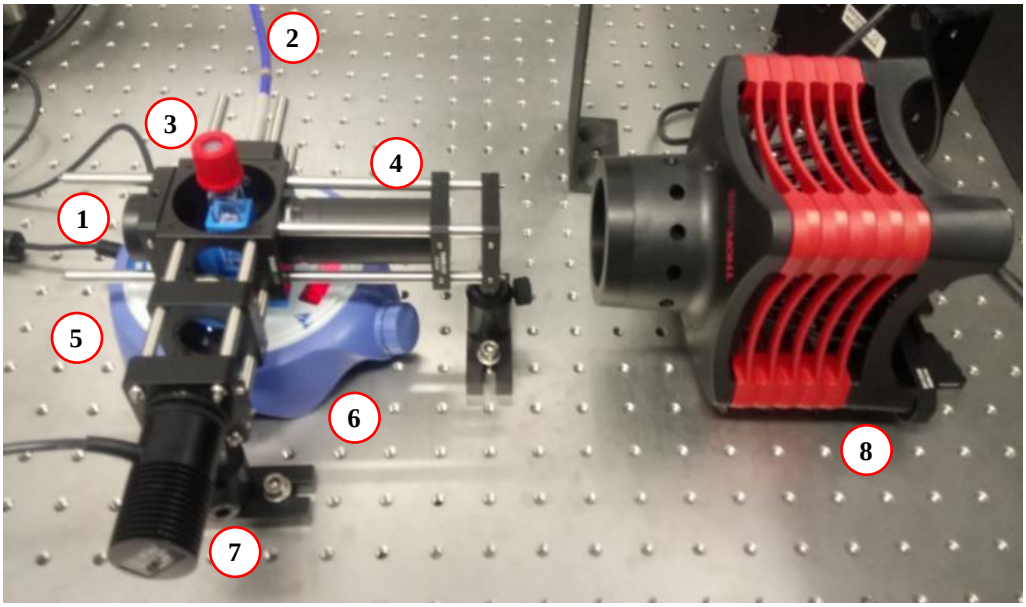

Figure 4.7.1. Spectrometer for Kinetic measurements. Custom made spectrometer setup for measuring reaction intermediates of photoredox reactions. Components: power meter (1), fibre optic to CCD (2), cuvette (3), aperture and lens (4), focusing lens (5), stirrer (6), broadband white LED (7), blue LED (8).

Aminocarbonylation General Procedure

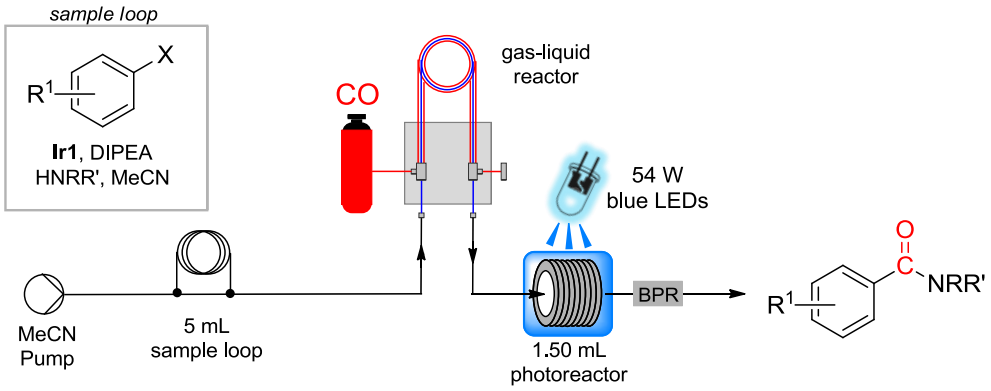

Figure 4.7.2 Generalised flow photoredox carbonylation reaction scheme.

METHOD A: A solution of the aryl halide (0.25 mmol, 1.0 equiv.), $[Ir(dtbbpy)(ppy)_2]PF_6$ (1 mol %, 2.28 mg), DIPEA (1.05 equiv, 45.8 µL) and corresponding coupling partner (1.05 equiv.) in 5 mL of MeCN was sparged with N_2 (5 min) then loaded into a 5 mL sample loop. This mixture was pumped (flow rate 0.10 mL/min) through the gas-liquid reactor and enriched with CO (35 atm CO gas pressure) then irradiated in the photoreactor (15 min residence time). The product stream was

collected, concentrated *in vacuo* and the crude residue purified by chromatography (SiO_2) to afford the pure product.

METHOD B: A solution of the aryl halide (0.25 mmol, 1.0 equiv.), $[Ir(dtbbpy)(ppy)_2]PF_6$ (1 mol %, 2.28 mg), DIPEA (1.2 equiv., 52.3 µL) and corresponding coupling partner (1.2 equiv. or 5 equi.v) in 5 mL of MeCN was sparged with N_2 (5 min) then into a 5 mL sample loop. This mixture was pumped (flow rate 0.10 mL/min) through the gas-liquid reactor and enriched with CO (45 atm CO gas pressure) then irradiated in the photoreactor (15 min residence time). The product stream was collected, concentrated *in vacuo* and the crude residue purified by chromatography (SiO_2) to afford the pure product.

METHOD C: A solution of the aryl halide (0.25 mmol, 1.0 equiv.), $[Ir(dtbbpy)(ppy)_2]PF_6$ (1 mol %, 2.28 mg), DIPEA (1.5 equiv., 65.4 µL) and corresponding coupling partner (1.2 equiv.) in 5 mL of MeCN was sparged with N_2 (5 min) then loaded into a 5 mL sample loop. This mixture was pumped (flow rate 0.05 mL/min) through the gas-liquid reactor and enriched with CO (45 atm CO gas pressure) then irradiated in the photoreactor (30 min residence time). The product stream was collected, concentrated *in vacuo* and the crude residue purified by chromatography (SiO_2) to afford the pure product.

Note: To prevent failure of the AF-2400 membrane, the pressure of the inner and annular channels of the gas-liquid reactor was maintained to within 5 atm. This was achieved by increasing the system back-pressure whilst simultaneously increasing the CO gas pressure after the sample loop injection valve had been actuated.

Gram-Scale Aminocarbonylation of Methyl 4-Iodobenzoate Procedure

A solution of methyl 4-iodobenzoate (10 mmol, 2.62 g, 1.0 equiv.), $[Ir(dtbbpy)(ppy)_2]PF_6$ (1 mol %, 2.28 mg), DIPEA (1.05 equiv., 45.8 µL) and morpholine (1.05 equiv.) in MeCN (300 mL) was sparged with N_2 (15 min) (Figure 4.4.1). This mixture, maintained under positive pressure with N_2 and shielded from light, was pumped (flow rate 0.60 mL/min) through the gas-liquid reactor and enriched with CO (35 atm CO gas pressure) then irradiated in the photoreactor (15 min residence time). To allow the system to reach steady state operation, the first 50 mL of the product stream was discarded. The following 200 mL of product stream was collected

(over 8.33 hours), concentrated in vacuo and the crude residue purified by flash chromatography (EtOAc/hexanes, 0:1 to 1:1) to afford pure methyl 4-(morpholine-4-carbonyl)benzoate as a yellow solid (1.80 mg, 72%).

Product Characterization of Isolated Compounds

methyl 4-(morpholine-4-carbonyl)benzoate (230aa)

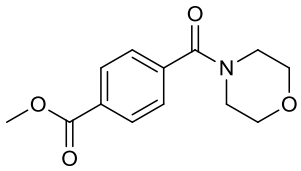

Compound **230aa** was prepared according to method A with methyl 4-iodobenzene (0.25 mmol, 49.6 mg) and morpholine (0.263 mmol, 22.9 µL). The crude product was purified by flash column chromatography on silica gel (1:1 EtOAc/hexanes) to provide the pure product as a white solid (45.7 mg, 74%). **^{1}H NMR** (400 MHz, $CDCl_3$): δ [ppm] = 8.07 (d, *J* = 8.2 Hz, 2H), 7.45 (d, *J* = 8.2 Hz, 2H), 3.91 (s, 3H), 3.31 - 3.83 (m, 8H). **^{13}C NMR** (100 MHz, $CDCl_3$); δ [ppm] = 169.4, 166.3, 139.6, 131.4, 130.0, 127.2, 66.9, 52.5, 48.2, 42.6. Analytical data is in agreement with previously reported literature data.[236]

methyl 4-(morpholine-4-carbonyl)benzoate (230ab)

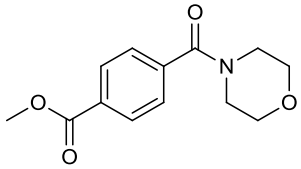

Compound **230ab** was prepared according to method B with methyl 4-bromobenzene (0.25 mmol, 53.8 mg) and morpholine (0.30 mmol, 26.2 µL). The crude product was purified by flash column chromatography on silica gel (1:1 EtOAc/hexanes) to provide the pure product as a pale yellow solid (46.2 mg, 75%). **^{1}H NMR** (400 MHz, $CDCl_3$): δ [ppm] = 8.08 (d, *J* = 8.1 Hz, 2H), 7.47 (d, *J* = 8.1 Hz, 2H), 3.93 (s, 3H), 3.31 - 3.85 (m, 8H). **^{13}C NMR** (100 MHz, $CDCl_3$); δ [ppm] = 169.4, 166.3, 139.6, 131.4, 129.9, 127.1, 66.9, 52.4, 48.1, 42.5. Analytical data is in agreement with previously reported literature data.[236]

methyl 3-(morpholine-4-carbonyl)benzoate (230bb)

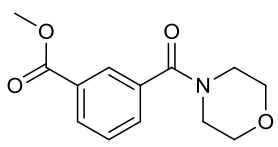

Compound **230bb** was prepared according to method B with methyl 3-bromobenzene (0.25 mmol, 53.8 mg) and morpholine (0.30 mmol, 26.2 µL). The crude product was purified by flash column chromatography on silica gel (1:1 EtOAc/hexanes) to provide the pure product

as a pale yellow solid (45.5 mg, 74%). **^{1}H NMR** (400 MHz, $CDCl_3$): δ [ppm] = 8.03 - 8.11 (m, 2H), 7.56 - 7.62 (m, 1H), 7.45 - 7.53 (m, 1H), 3.33 - 3.93 (m, 12). **^{13}C NMR** (100 MHz, $CDCl_3$); δ [ppm] = 169.4, 166.3, 135.7, 131.6, 131.0, 130.6, 129.0, 128.2, 66.9, 52.5, 48.3, 42.7. Analytical data is in agreement with previously reported literature data.[237]

1-(4-(morpholine-4-carbonyl)phenyl)ethan-1-one (230ca)

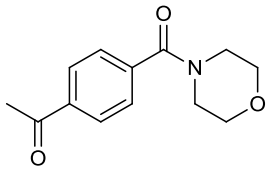

Compound **230ca** was prepared according to method A with 4′-iodoacetophenone (0.25 mmol, 61.5 mg) and morpholine (0.263 mmol, 22.9 µL). The crude product was purified by flash column chromatography on silica gel (1:1 EtOAc/hexanes) to provide the pure product as a yellow solid (33.8 mg, 58%). **^{1}H NMR** (400 MHz, $CDCl_3$): δ [ppm] = 8.00 (d, *J* = 8.1 Hz, 2H), 7.50 (d, *J* = 8.1 Hz, 2H), 3.34 - 3.84 (m, 8H), 2.62 (s, 3H). **^{13}C NMR** (100 MHz, $CDCl_3$); δ [ppm] = 197.3, 169.3, 139.7, 137.9, 128.6, 127.3, 66.8, 48.1, 42.5, 26.8. Analytical data is in agreement with previously reported literature data.[142]

morpholino(4-(trifluoromethyl)phenyl)methanone (230da)

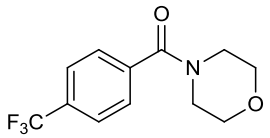

Compound **230da** was prepared according to method A with 4-iodobenzotrifluoride (0.25 mmol, 68.0 mg) and morpholine (0.263 mmol, 22.9 µL). The crude product was purified by flash column chromatography on silica gel (1:1 EtOAc/hexanes) to provide the pure product as a pale yellow solid (43.2 mg, 67%). **^{1}H NMR** (400 MHz, $CDCl_3$): δ [ppm] = 7.68 (d, *J* = 8.0 Hz, 2H), 7.52 (d, *J* = 8.0 Hz, 2H), 3.27 - 3.92x (m, 8H). **^{13}C NMR** (100 MHz, $CDCl_3$); δ [ppm] = 169.0, 139.0 (d, $J_{C\text{-}F}$ = 1.2 Hz, 2C), 132.0 (q, $J_{C\text{-}F}$ = 32.7 Hz, 1C), 127.6, 125.8 (q, $J_{C\text{-}F}$ = 3.8 Hz, 2C), 123.7 (q, $J_{C\text{-}F}$ = 271 Hz, 1C), 66.9, 48.2, 42.7. **^{19}F NMR** (376 MHz, CDCl3); δ [ppm] = -63.5. Analytical data is in agreement with previously reported literature data.[238]

morpholino(4-(trifluoromethyl)phenyl)methanone (230db)

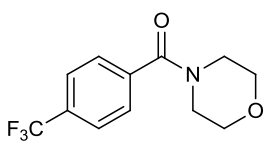

Compound **230db** was prepared according to method B with 4-bromobenzotrifluoride (0.25 mmol, 56.3 mg) and morpholine (0.30 mmol, 26.2 µL). The crude product was purified by flash column chromatography on silica gel (1:1 EtOAc/hexanes) to provide the pure product as a pale yellow solid (39.0 mg, 60%). **^{1}H NMR** (400 MHz, $CDCl_3$): δ [ppm] = 7.68 (d,

J = 8.1 Hz, 2H), 7.52 (d, *J* = 8.0 Hz, 2H), 3.30 - 3.86 (m, 8H). **^{13}C NMR** (100 MHz, $CDCl_3$); δ [ppm] = 169.0, 139.0 (d, J_{C-F} = 1.2 Hz, 2C), 131.9 (q, J_{C-F} = 32.6 Hz, 1C), 127.6, 125.8 (q, J_{C-F} = 3.8 Hz, 2C), 123.7 (q, J_{C-F} = 271 Hz, 1C), 66.9, 48.2, 42.7. **^{19}F NMR** (376 MHz, CDCl3); δ [ppm] = -63.4. Analytical data is in agreement with previously reported literature data.[238]

4-(morpholine-4-carbonyl)benzonitrile (230ea)

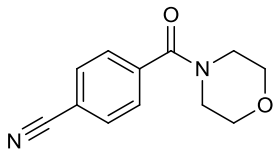

Compound **230ea** was prepared according to method A with 4-iodobenzonitrile (0.25 mmol, 57.3 mg) and morpholine (0.263 mmol, 22.9 µL). The crude product was purified by flash column chromatography on silica gel (1:1 EtOAc/hexanes) to provide the pure product as a yellow solid (35.0 mg, 65%). **^{1}H NMR** (400 MHz, $CDCl_3$): δ [ppm] = 7.71 (d, *J* = 8.1 Hz, 2H), 7.50 (d, *J* = 8.1 Hz, 2H), 3.28 - 3.86 (m, 8H). **^{13}C NMR** (100 MHz, $CDCl_3$); δ [ppm] = 168.4, 139.7, 132.6, 127.9, 188.1, 113.8, 66.8, 48.1, 42.6. Analytical data is in agreement with previously reported literature data.[237]

4-(morpholine-4-carbonyl)benzonitrile (230eb)

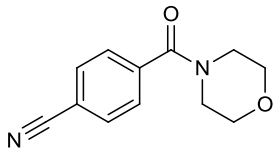

Compound **230eb** was prepared according to method B with 4-bromobenzonitrile (0.25 mmol, 45.5 mg) and morpholine (0.30 mmol, 26.2 µL). The crude product was purified by flash column chromatography on silica gel (1:1 EtOAc/hexanes) to provide the pure product as a pale yellow solid (28.6 mg, 53%). **^{1}H NMR** (400 MHz, $CDCl_3$): δ [ppm] = 7.72 (d, *J* = 8.2 Hz, 2H), 7.50 (d, *J* = 8.2 Hz, 2H), 3.25 - 3.85 (m, 8H). **^{13}C NMR** (100 MHz, $CDCl_3$); δ [ppm] = 168.4, 139.7, 132.6, 127.9, 118.1, 113.8, 66.8, 48.1, 42.6. Analytical data is in agreement with previously reported literature data.[237]

(4-chlorophenyl)(morpholino)methanone (230fa)

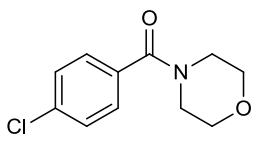

Compound **230fa** was prepared according to method A with 1-chloro-4-iodobenzene (0.25 mmol, 59.6 mg) and morpholine (0.263 mmol, 22.9 µL). The crude product was purified by flash column chromatography on silica gel (1:1 EtOAc/hexanes) to provide the pure product as a yellow solid (37.1 mg, 66%). **^{1}H NMR** (400 MHz, $CDCl_3$): δ [ppm] = 7.31 - 7.44 (m, 4H), 3.30 - 3.89 (m, 8H). **^{13}C NMR** (100 MHz, $CDCl_3$); δ [ppm] = 169.4, 136.0,

133.6, 128.9, 128.7, 66.9, 48.2, 42.6. Analytical data is in agreement with previously reported literature data.[237]

(4-chlorophenyl)(morpholino)methanone (230fb)

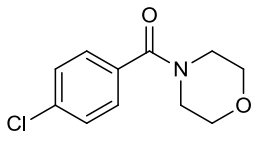

Compound **230fb** was prepared according to method B with 1-bromo-4-iodobenzene (0.25 mmol, 47.9 mg) and morpholine (0.30 mmol, 26.2µL). The crude product was purified by flash column chromatography on silica gel (1:1 EtOAc/hexanes) to provide the pure product as a yellow oil (34.9 mg, 62%). **^{1}H NMR** (400 MHz, $CDCl_3$): δ [ppm] = 7.31 - 7.44 (m, 4H), 3.29 - 3.90 (m, 8H). **^{13}C NMR** (100 MHz, $CDCl_3$); δ [ppm] = 169.4, 136.1, 133.7, 129.0, 128.8, 66.9, 48.3, 42.7. Analytical data is in agreement with previously reported literature data.[237]

(4-fluorophenyl)(morpholino)methanone (230gb)

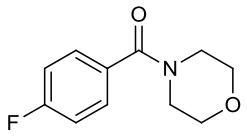

Compound **230gb** was prepared according to method B with 1-bromo-4-fluorobenzene (0.25 mmol, 43.8 mg) and morpholine (0.30 mmol, 26.2 µL). The crude product was purified by flash column chromatography on silica gel (1:1 EtOAc/hexanes) to provide the pure product as a pale yellow oil (37.1 mg, 71%). **^{1}H NMR** (400 MHz, $CDCl_3$): δ [ppm] = 7.35 - 7.45 (m, 2H), 7.04 - 7.14 (m, 2H), 3.27 - 3.87 (m, 8H). **^{13}C NMR** (100 MHz, $CDCl_3$); δ [ppm] = 169.6, 163.6 (d, $J_{C\text{-}F}$ = 249 Hz, 1C), 131.4 (d, $J_{C\text{-}F}$ = 3.5 Hz, 1C), 129.6 (d, $J_{C\text{-}F}$ = 8.5 Hz, 2C), 133.8 (d, $J_{C\text{-}F}$ = 21.8 Hz, 2C), 67.0, 48.2, 42.6. **^{19}F NMR** (376 MHz, CDCl3); δ [ppm] = -123.6. Analytical data is in agreement with previously reported literature data.[237]

2-fluoro-5-(morpholine-4-carbonyl)benzonitrile (230hb)

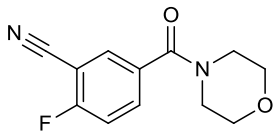

Compound **230hb** was prepared according to method B with 5-bromo-2-fluorobenzonitrile (0.25 mmol, 50.0 mg) and morpholine (0.30 mmol, 26.2 µL). The crude product was purified by flash column chromatography on silica gel (1:1 EtOAc/hexanes) to provide the pure product as a pale yellow oil (27.1 mg, 46%). **^{1}H NMR** (400 MHz, $CDCl_3$): δ [ppm] = 7.64 - 7.74 (m, 2H), 7.24 - 7.33 (m, 4H), 3.25 - 3.90 (m, 8H). **^{13}C NMR** (100 MHz, $CDCl_3$); δ [ppm] = 167.2, 165.2 (d, $J_{C\text{-}F}$ = 262 Hz, 1C), 134.3 (d, $J_{C\text{-}F}$ = 8.8 Hz, 1C), 132.8, 132.6 (d, $J_{C\text{-}F}$ = 4.1 Hz, 2C), 117.1 (d, $J_{C\text{-}F}$ = 20.0 Hz, 1C), 113.1, 102.2 (d,

$J_{C\text{-}F}$ = 15.9 Hz, 1C), 66.8, 48.5, 43.0. **^{19}F NMR** (376 MHz, CDCl3); δ [ppm] = -116.9. **HRMS** (ESI): calculated for $[C_{12}H_{12}FN_2O_2]^+$: m/z = 235.0877, found: m/z = 235.0875 ; **IR** (ν/cm^{-1}, neat): 3059, 2972, 2925, 2860, 2239, 1632, 1502, 1459, 1433, 1258, 1189, 1114, 1024, 828, 731.

morpholino(4-(4,4,5,5-tetramethyl-1,3,2-dioxaborolan-2-yl)phenyl)methanone (230ib)

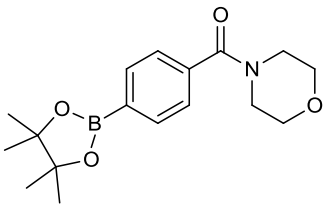

Compound **230ib** was prepared according to method B with 2-(4-bromophenyl)-4,4,5,5-tetramethyl-1,3,2-dioxaborolane (0.25 mmol, 70.7 mg) and morpholine (0.30 mmol, 26.2 µL). The crude product was purified by flash column chromatography on silica gel (1:1 EtOAc/hexanes) to provide the pure product as a white solid (42.8 mg, 54%). **^{1}H NMR** (400 MHz, $CDCl_3$): δ [ppm] = 7.83 (d, *J* = 8.0 Hz, 2H), 7.37 (d, *J* = 8.0 Hz, 2H), 3.33 - 3.81 (m, 8H), 1.33 (s, 12H). **^{13}C NMR** (100 MHz, $CDCl_3$); δ [ppm] = 170.4, 137.9, 135.0, 126.3, 84.2, 67.0, 48.2, 42.6, 25.0. Analytical data is in agreement with previously reported literature data.[239]

morpholino(phenyl)methanone (230ja)

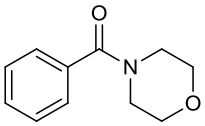

Compound **230ja** was prepared according to method B with iodobenzene (0.25 mmol, 51.0 mg) and morpholine (0.30 mmol, 26.2 µL). The crude product was purified by flash column chromatography on silica gel (1:1 EtOAc/hexanes) to provide the pure product as a pale yellow oil (42.0 mg, 88%). **^{1}H NMR** (400 MHz, $CDCl_3$): δ [ppm] = 7.35 - 7.43 (m, 5H), 3.35 - 3.85 (m, 8H). **^{13}C NMR** (100 MHz, $CDCl_3$); δ [ppm] = 170.4, 135.3, 129.9, 128.6, 127.1, 66.9, 48.3, 42.6. Analytical data is in agreement with previously reported literature data.[236]

morpholino(phenyl)methanone (230jb)

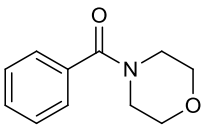

Compound **230jb** was prepared according to method B with bromobenzene (0.25 mmol, 39.3 mg) and morpholine (0.30 mmol, 26.2 µL). The crude product was purified by flash column chromatography on silica gel (1:1 EtOAc/hexanes) to provide the pure product as a pale yellow oil (37.7 mg, 79%). **^{1}H NMR** (400 MHz, $CDCl_3$): δ [ppm] = 7.35 - 7.43 (m, 5H), 3.35 - 3.86 (m, 8H). **^{13}C NMR** (100 MHz, $CDCl_3$); δ [ppm] = 170.5, 135.4, 130.0,

128.6, 127.2, 70.0, 48.4, 42.7. Analytical data is in agreement with previously reported literature data.[236]

morpholino(*p*-tolyl)methanone (230ka)

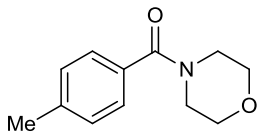

Compound **230ka** was prepared according to method B with 4-iodotoluene (0.25 mmol, 54.5 mg) and morpholine (0.30 mmol, 26.2 µL). The crude product was purified by flash column chromatography on silica gel (1:1 EtOAc/hexanes) to provide the pure product as a pale yellow oil (36.4 mg, 71%). **^{1}H NMR** (400 MHz, $CDCl_3$): δ [ppm] = 7.30 (d, *J* = 8.0 Hz, 2H), 7.20 (d, *J* = 8.0 Hz, 2H), 3.37 - 3.87 (m, 8H), 2.37 (s, 3H). **^{13}C NMR** (100 MHz, $CDCl_3$); δ [ppm] = 170.7, 140.2, 132.4, 129.3, 127.3, 67.0, 48.4, 42.8, 21.5. Analytical data is in agreement with previously reported literature data.[237]

morpholino(*p*-tolyl)methanone (230kb)

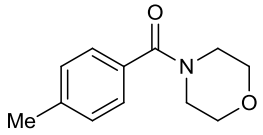

Compound **230kb** was prepared according to method B with 4-bromotoluene (0.25 mmol, 42.8 mg) and morpholine (0.30 mmol, 26.2 µL). The crude product was purified by flash column chromatography on silica gel (1:1 EtOAc/hexanes) to provide the pure product as a pale yellow oil (35.9 mg, 70%). **^{1}H NMR** (400 MHz, $CDCl_3$): δ [ppm] = 7.29 (d, *J* = 8.0 Hz, 2H), 7.20 (d, *J* = 8.0 Hz, 2H), 3.37 - 3.85 (m, 8H), 2.36 (s, 3H). **^{13}C NMR** (100 MHz, $CDCl_3$); δ [ppm] = 170.7, 140.2, 132.4, 129.2, 127.3, 67.0, 48.5, 42.7, 21.5. Analytical data is in agreement with previously reported literature data.[237]

morpholino(*o*-tolyl)methanone (230la)

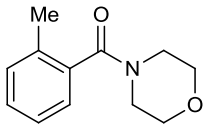

Compound **230la** was prepared according to method B with 2-bromotoluene (0.25 mmol, 42.8 mg) and morpholine (0.30 mmol, 26.2 µL). The crude product was purified by flash column chromatography on silica gel (1:1 EtOAc/hexanes) to provide the pure product as a yellow oil (27.2 mg, 53%). **^{1}H NMR** (400 MHz, $CDCl_3$): δ [ppm] = 7.12 - 7.31 (m, 4H), 7.20 (d, *J* = 8.0 Hz, 2H), 3.86 - 3.72 (m, 4H), 3.62 - 3.52 (m, 2H), 3.29 - 3.17 (m, 2H), 2.31 (s, 3H). **^{13}C NMR** (100 MHz, $CDCl_3$); δ [ppm] = 170.2, 135.7, 134.3, 130.6, 129.2, 126.1, 125.9, 67.1, 67.0, 47.4, 42.0, 19.2. Analytical data is in agreement with previously reported literature data.[237]

morpholino(*m*-tolyl)methanone (230lb)

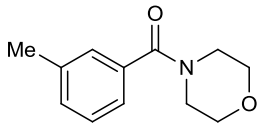

Compound **230lb** was prepared according to method B with 3-bromotoluene (0.25 mmol, 42.8 mg) and morpholine (0.30 mmol, 26.2 µL). The crude product was purified by flash column chromatography on silica gel (1:1 EtOAc/hexanes) to provide the pure product as a pale yellow oil (35.9 mg, 70%). **^{1}H NMR** (400 MHz, $CDCl_3$): δ [ppm] = 7.13 - 7.31 (m, 4H), 3.31 - 3.90 (m, 8H), 2.37 (s, 3H). **^{13}C NMR** (100 MHz, $CDCl_3$); δ [ppm] = 170.8, 138.6, 135.4, 130.7, 128.5, 127.8, 124.1, 67.0, 48.3, 42.7, 21.5. Analytical data is in agreement with previously reported literature data.[237]

(4-(*tert*-butyl)phenyl)(morpholino)methanone (230mb)

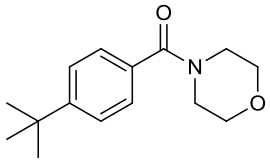

Compound **230mb** was prepared according to method B with 1-bromo-4-*tert*-butylbenzene (0.25 mmol, 53.3 mg) and morpholine (0.30 mmol, 26.2 µL). The crude product was purified by flash column chromatography on silica gel (2:3 EtOAc/hexanes) to provide the pure product as a pale yellow oil (46.4 mg, 75%). **^{1}H NMR** (400 MHz, $CDCl_3$): δ [ppm] = 7.41 (d, *J* = 8.3 Hz, 2H), 7.33 (d, *J* = 8.3 Hz, 2H), 3.37 - 3.83 (m, 8H), 1.31 (s, 9H). **^{13}C NMR** (100 MHz, $CDCl_3$); δ [ppm] = 170.7, 153.3, 132.4, 127.1, 125.5, 67.0, 48.3, 42.7, 34.9, 31.3. Analytical data is in agreement with previously reported literature data.[240]

[1,1'-biphenyl]-4-yl(morpholino)methanone (230nb)

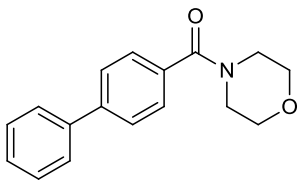

Compound **230nb** was prepared according to method B with 4-bromobiphenyl (0.25 mmol, 58.3 mg) and morpholine (0.30 mmol, 26.2 µL). The crude product was purified by flash column chromatography on silica gel (1:1 EtOAc/hexanes) to provide the pure product as a white solid (46.5 mg, 70%). **^{1}H NMR** (400 MHz, $CDCl_3$): δ [ppm] = 7.55 - 7.67 (m, 4H), 7.41 - 7.53 (m, 4H), 7.33 - 7.41 (m, 1H), 3.38 - 3.93 (m, 8H). **^{13}C NMR** (100 MHz, $CDCl_3$); δ [ppm] = 170.3, 142.9, 140.2, 134.0, 129.0, 127.9, 127.8, 127.3, 127.2, 67.0, 48.3, 42.6. Analytical data is in agreement with previously reported literature data.[241]

***N*-(4-(morpholine-4-carbonyl)phenyl)acetamide (230oa)**

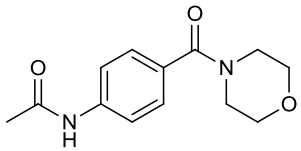

Compound **230oa** was prepared according to method C with 4′-iodoacetanilide (0.25 mmol, 65.3 mg) and morpholine (0.30 mmol, 26.2 µL). The crude product was purified by flash column chromatography on silica gel (1:1 to 1:0 EtOAc/hexanes) to provide the pure product as a pale yellow solid (43.3 mg, 70%). **^{1}H NMR** (400 MHz, $CDCl_3$): δ [ppm] = 8.80 (s, 1H), 7.46 (d, *J* = 8.4 Hz, 2H), 7.25 (d, *J* = 8.5 Hz, 2H), 3.33 - 3.84 (m, 8H), 2.08 (s, 3H). **^{13}C NMR** (100 MHz, $CDCl_3$); δ [ppm] = 170.5, 169.4, 140.2, 130.1, 128.0, 119.8, 66.9, 48.4, 42.9, 24.4. **HRMS** (ESI): calculated for $[C_{13}H_{17}N_2O_3]^+$: m/z = 249.1234, found: m/z = 249.1227; **IR** (ν/cm^{-1}, neat): 3266, 3185, 3108, 3057, 2989, 2919, 2867, 1694, 1598, 1529, 1433, 1360, 1253, 1114, 1013, 849, 766, 743, 662. **m.p.**: 185.5 - 186.6 °C.

***N*-(4-(morpholine-4-carbonyl)phenyl)acetamide (230ob)**

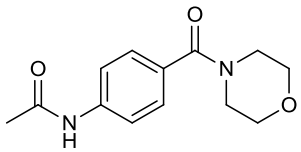

Compound **230ob** was prepared according to method C with 4′-bromoacetanilide (0.25 mmol, 53.5 mg) and morpholine (0.30 mmol, 26.2 µL). The crude product was purified by flash column chromatography on silica gel (1:1 to 1:0 EtOAc/hexanes) to provide the pure product as a white solid (44.9 mg, 72%). **^{1}H NMR** (400 MHz, $CDCl_3$): δ [ppm] = 8.77 (s, 1H), 7.45 (d, *J* = 8.4 Hz, 2H), 7.25 (d, *J* = 8.4 Hz, 2H), 3.33 - 3.86 (m, 8H), 2.08 (s, 3H). **^{13}C NMR** (100 MHz, $CDCl_3$); δ [ppm] = 170.5, 169.4, 140.1, 130.1, 128.0, 119.8, 66.9, 48.4, 42.8, 24.4.

(4-methoxyphenyl)(morpholino)methanone (230pa)

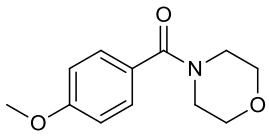

Compound **230pa** was prepared according to method C with 4-iodoanisole (0.25 mmol, 58.5 mg) and morpholine (0.30 mmol, 26.2 µL). The crude product was purified by flash column chromatography on silica gel (1:1 to 3:2 EtOAc/hexanes) to provide the pure product as a yellow oil (37.4 mg, 68%). **^{1}H NMR** (400 MHz, $CDCl_3$): δ [ppm] = 7.37 (d, *J* = 8.7 Hz, 2H), 6.90 (d, *J* = 8.7 Hz, 2H), 3.81 (s, 3H), 3.46 - 3.77 (m, 8H). **^{13}C NMR** (100 MHz, $CDCl_3$); δ [ppm] = 170.1, 161.0, 129.3, 127.4, 113.9, 67.0, 55.5, 48.1, 43.2. Analytical data is in agreement with previously reported literature data.[237]

(4-methoxyphenyl)(morpholino)methanone (230pb)

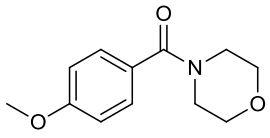

Compound **230pb** was prepared according to method C with 4-bromoanisole (0.25 mmol, 46.8 mg) and morpholine (0.30 mmol, 26.2 µL). The crude product was purified by flash column chromatography on silica gel (1:1 to 3:2 EtOAc/hexanes) to provide the pure product as a yellow oil (29.8 mg, 54%). **^{1}H NMR** (400 MHz, $CDCl_3$): δ [ppm] = 7.38 (d, *J* = 8.8 Hz, 2H), 6.91 (d, *J* = 8.8 Hz, 2H), 3.82 (s, 3H), 3.52 - 3.78 (m, 8H). **^{13}C NMR** (100 MHz, $CDCl_3$); δ [ppm] = 170.5, 161.0, 129.3, 127.4, 113.9, 67.0, 55.5, 48.4, 43.3. Analytical data is in agreement with previously reported literature data.[237]

(4-hydroxyphenyl)(morpholino)methanone (230qa)

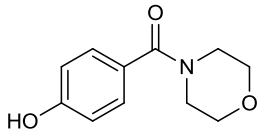

Compound **230qa** was prepared according to method C with 4-iodophenol (0.25 mmol, 55.0 mg) and morpholine (0.30 mmol, 26.2 µL). The crude product was purified by flash column chromatography on silica gel (1:1 to 1:0 EtOAc/hexanes) to provide the pure product as a white solid (20.6 mg, 40%). **^{1}H NMR** (400 MHz, $CDCl_3$): δ [ppm] = 8.51 (brs, 1H), 7.21 (d, *J* = 8.5 Hz, 2H), 6.70 (d, *J* = 8.5 Hz, 2H), 3.37 - 3.99 (m, 8H). **^{13}C NMR** (100 MHz, $CDCl_3$); δ [ppm] = 171.6, 158.9, 129.3, 125.5, 115.7, 67.0, 48.7, 43.3. Analytical data is in agreement with previously reported literature data.[242]

(4-hydroxyphenyl)(morpholino)methanone (230qb)

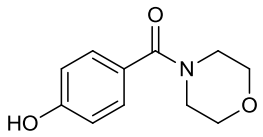

Compound **230qb** was prepared according to method C with 4-bromophenol (0.25 mmol, 43.3 mg) and morpholine (0.30 mmol, 26.2 µL). The crude product was purified by flash column chromatography on silica gel (1:1 to 1:0 EtOAc/hexanes) to provide the pure product as a white solid (24.5 mg, 47%). **^{1}H NMR** (400 MHz, $CDCl_3$): δ [ppm] = 8.51 (brs, 1H), 7.21 (d, *J* = 8.5 Hz, 2H), 6.70 (d, *J* = 8.5 Hz, 2H), 3.37 - 3.92 (m, 8H). **^{13}C NMR** (100 MHz, $CDCl_3$); δ [ppm] = 171.6, 158.9, 129.3, 125.5, 115.7, 67.0, 48.6, 43.2. Analytical data is in agreement with previously reported literature data.[242]

(4-(methylthio)phenyl)(morpholino)methanone (230rb)

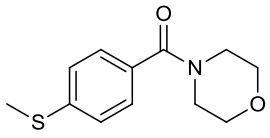

Compound **230rb** was prepared according to method C with 4-bromothiophenol (0.25 mmol, 50.8 mg) and morpholine (0.30 mmol, 26.2 µL). The crude product was purified by flash column chromatography on silica gel (2:3 to 1:0 EtOAc/hexanes) to provide the pure product as a white solid (42.9 mg, 72%). **^{1}H NMR** (400 MHz, $CDCl_3$): δ [ppm] = 7.31 (d, *J* = 8.2 Hz, 2H), 7.23 (d, *J* = 8.3 Hz, 2H), 3.37 - 3.80 (m, 8H), 2.46 (s, 3H). **^{13}C NMR** (100 MHz, $CDCl_3$); δ [ppm] = 170.1, 141.5, 131.4, 127.8, 125.8, 66.9, 48.3, 42.8, 15.3. Analytical data is in agreement with previously reported literature data.[243]

morpholino(pyridin-2-yl)methanone (230sa)

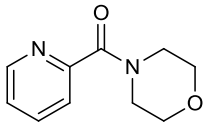

Compound **230sa** was prepared according to method B with 2-iodopyridine (0.25 mmol, 51.3 mg) and morpholine (0.30 mmol, 26.2 µL). The crude product was purified by preparative TLC (1:1 EtOAc/hexanes) to provide the pure product as a yellow solid (28.4 mg, 59%). **^{1}H NMR** (400 MHz, $CDCl_3$): δ [ppm] = 8.54 - 8.61 (m, 1H), 7.76 - 7.84 (m, 1H), 7.65 - 7.70 (m, 1H), 7.32 - 7.38 (m, 1H), 3.61 - 3.86 (m, 8H). **^{13}C NMR** (100 MHz, $CDCl_3$); δ [ppm] = 167.6, 153.8, 148.4, 137.3, 124.8, 124.3, 67.2, 67.0, 47.9, 42.9. Analytical data is in agreement with previously reported literature data.[243]

morpholino(pyridin-2-yl)methanone (230sb)

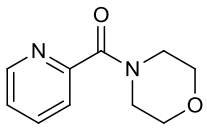

Compound **230sb** was prepared according to method B with 2-bromopyridine (0.25 mmol, 39.5 mg) and morpholine (0.30 mmol, 26.2 µL). The crude product was purified by preparative TLC (1:1 EtOAc/hexanes) to provide the pure product as a pale yellow solid (30.3 mg, 63%). **^{1}H NMR** (400 MHz, $CDCl_3$): δ [ppm] = 8.52 - 8.60 (m, 1H), 7.75 - 7.84 (m, 1H), 7.63 - 7.70 (m, 1H), 7.30 - 3.38 (m, 1H), 3.60 - 3.85 (m, 8H). **^{13}C NMR** (100 MHz, $CDCl_3$); δ [ppm] =167.6, 153.7, 148.3, 137.3, 124.8, 124.3, 67.1, 66.9, 47.8, 42.9. Analytical data is in agreement with previously reported literature data.[243]

(1H-indol-7-yl)(morpholino)methanone (230ta)

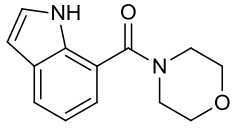

Compound **230ta** was prepared according to method B with 7-iodoindole (0.25 mmol, 60.8 mg) and morpholine (0.30 mmol, 26.2

µL). The crude product was purified by preparative TLC (1:1 EtOAc/hexanes) to provide the pure product as an grey-clear oil (23.5 mg, 41%). **^{1}H NMR** (400 MHz, $CDCl_3$): δ [ppm] = 9.18 (brs, 1H), 7.73 (d, *J* = 7.9 Hz, 1H), 7.24 - 7.29 (m, 1H), 7.18 - 7.22 (m, 1H), 7.06 - 7.13 (m, 1H), 6.55 - 6.60 (m, 1H), 3.70 - 3.82 (m, 8H). **^{13}C NMR** (100 MHz, $CDCl_3$); δ [ppm] =169.7, 135.2, 129.4, 125.5, 123.6, 121.4, 118.6, 116.4, 102.7, 67.2, 45.8. **HRMS** (ESI): calculated for $[C_{13}H_{15}N_2O_2]^+$: m/z = 231.1128, found: m/z = 231.1125; **IR** (ν/cm^{-1}, neat): 3280, 3058, 2966, 2921, 2856, 1615, 1583, 1430, 1335, 1277, 1260, 1202, 1112, 1057, 1042, 981, 794, 729.

phenyl(pyrrolidin-1-yl)methanone (232a)

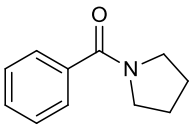

Compound **232a** was prepared according to method B with bromobenzene (0.25 mmol, 39.3 mg) and pyrrolidine (0.30 mmol, 25.0 µL). The crude product was purified by preparative TLC (1:3 EtOAc/hexanes) to provide the pure product as a pale yellow oil (30.2 mg, 69%). **^{1}H NMR** (400 MHz, $CDCl_3$): δ [ppm] = 7.45 - 7.53 (m, 2H), 7.42 - 7.33 (m, 3H), 3.63 (t, d, *J* = 7.0 Hz, 2H), 3.40 (t, *J* = 6.6 Hz, 2H), 1.81 - 1.98 (m, 4H). **^{13}C NMR** (100 MHz, $CDCl_3$); δ [ppm] = 169.8, 137.3, 129.8, 128.3, 127.1, 49.7, 46.2, 26.5, 24.6. Analytical data is in agreement with previously reported literature data.[244]

phenyl(piperidin-1-yl)methanone (232b)

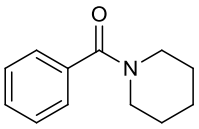

Compound **232b** was prepared according to method B with bromobenzene (0.25 mmol, 39.3 mg) and piperidine (0.30 mmol, 29.6 µL). The crude product was purified by preparative TLC (1:3 EtOAc/hexanes) to provide the pure product as a yellow oil (35.2 mg, 74%). **^{1}H NMR** (400 MHz, $CDCl_3$): δ [ppm] = 7.33 - 7.40 (m, 5H), 3.60 - 3.78 (m, 2H), 3.23 - 3.41 (m, 2H), 1.44 - 1.69 (m, 6H). **^{13}C NMR** (100 MHz, $CDCl_3$); δ [ppm] = 170.4, 136.6, 129.4, 128.5, 126.8, 48.8, 432.2, 26.6, 25.7, 24.7. Analytical data is in agreement with previously reported literature data.[243]

***N,N*-dipropylbenzamide (232c)**

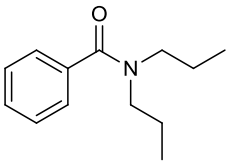

Compound **232c** was prepared according to method B with bromobenzene (0.25 mmol, 39.3 mg) and dipropylamine (0.30 mmol, 41.1 µL). The crude product was purified by preparative

TLC (1:3 EtOAc/hexanes) to provide the pure product as a yellow oil (29.6 mg, 58%). **^{1}H NMR** (400 MHz, $CDCl_3$): δ [ppm] = 7.29 - 7.42 (m, 5H), 3.52 - 3.35 (m, 2H), 3.06 - 3.21 (m, 2H), 1.43 - 1.74 (m, 4H), 0.65 - 1.02 (m, 6H). **^{13}C NMR** (100 MHz, $CDCl_3$); δ [ppm] = 171.9, 137.5, 129.1, 128.4, 126.5, 50.8, 46.3, 22.0, 20.8, 11.5, 11.1. Analytical data is in agreement with previously reported literature data.[242]

***N*-hexylbenzamide (232d)**

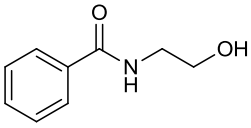

Compound **232d** was prepared according to method B with bromobenzene (0.25 mmol, 39.3 mg) and ethanolamine (1.25 mmol, 90.4 µL). The crude product was purified by preparative TLC (1:1 EtOAc/hexanes) to provide the pure product as a white solid (17.22 mg, 42%). **^{1}H NMR** (400 MHz, $CDCl_3$): δ [ppm] = 7.56 (d, *J* = 7.26 Hz 2H), 7.48 (t, *J* = 7.37 Hz, 1H), 7.38 (d, *J* = 7.54 Hz 2H), 6.92 (brs, 1H), 3.79 (t, *J* = 4.96 Hz, 2H), 3.59 (q, *J* = 5.15 Hz, 2H), 3.34 (brs, 1H). Analytical data is in agreement with previously reported literature data.[245]

***N*-hexylbenzamide (232e)**

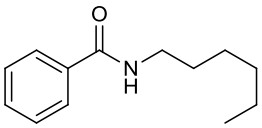

Compound **232e** was prepared according to method B with bromobenzene (0.25 mmol, 39.3 mg) and hexylamine (1.25 mmol, 165 µL). The crude product was purified by preparative TLC (1:3 EtOAc/hexanes) to provide the pure product as a yellow oil (35.9 mg, 70%). **^{1}H NMR** (400 MHz, $CDCl_3$): δ [ppm] = 7.69 - 7.83 (m, 2H), 7.34 - 7.50 (m, 3H), 6.41 (brs, 1H), 3.41 (q, *J* = 6.7 Hz, 2H), 1.51 - 1.63 (m, 2H), 1.21 - 1.38 (m, 6H), 0.80 - 0.83 (m, 3H). **^{13}C NMR** (100 MHz, $CDCl_3$); δ [ppm] = 167.6, 134.9, 131.3, 128.6, 127.0, 40.2, 31.6, 29.7, 26.8, 22.7, 14.1. Analytical data is in agreement with previously reported literature data.[245]

***N*-isopropylbenzamide (232f)**

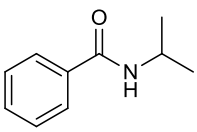

Compound **232f** was prepared according to method B with bromobenzene (0.25 mmol, 39.3 mg) and isopropylamine (0.25 mmol, 25.8 µL). Isopropylamine was added to the reaction mixture after the N_2 sparge. The crude product was purified by preparative TLC (1:3 EtOAc/hexanes) to provide the pure product as a white solid (27.4 mg, 67%). **^{1}H NMR** (400 MHz, $CDCl_3$): δ [ppm] = 7.75 (d, *J* = 7.3 Hz, 2H), 7.35 - 7.50 (m, 3H), 6.05 (brs, 1H), 4.18 - 4.37 (m,

1H), 1.25 (d, *J* = 6.6 Hz, 6H). **^{13}C NMR** (100 MHz, $CDCl_3$); δ [ppm] = 166.8, 135.1, 131.3, 128.6, 126.9, 42.0, 22.9. Analytical data is in agreement with previously reported literature data.[246]

***N*-(*tert*-butyl)benzamide (232g)**

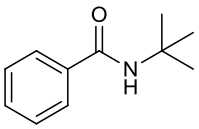

Compound **232g** was prepared according to method B with bromobenzene (0.25 mmol, 39.3 mg) and *tert*-butylamine (1.25 mmol, 132 µL). *Tert*-butylamine was added to the reaction mixture after the N_2 sparge. The crude product was purified by preparative TLC (1:3 EtOAc/hexanes) to provide the pure product as a white solid (24.3 mg, 55%). **^{1}H NMR** (400 MHz, $CDCl_3$): δ [ppm] = 7.69 - 7.74 (m, 2H), 7.36 - 7.49 (m, 3H), 5.97 (brs, 1H), 1.47 (s, 9H). **^{13}C NMR** (100 MHz, $CDCl_3$); δ [ppm] = 167.0, 136.0, 131.2, 128.6, 126.8, 51.7, 29.0. Analytical data is in agreement with previously reported literature data.[246]

***N*-benzylbenzamide (232h)**

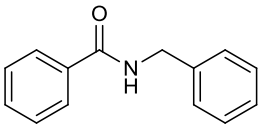

Compound **232h** was prepared according to method B with bromobenzene (0.25 mmol, 39.3 mg) and benzylamine (0.25 mmol, 32.8 µL). The crude product was purified by preparative TLC (1:3 EtOAc/hexanes) to provide the pure product as a white solid (31.8 mg, 60%). **^{1}H NMR** (400 MHz, $CDCl_3$): δ [ppm] = 7.74 - 7.85 (m, 2H), 7.27 - 7.53 (m, 8H), 6.62 (brs, 1H), 4.63 (d, *J* = 5.7 Hz, 2H). **^{13}C NMR** (100 MHz, $CDCl_3$); δ [ppm] = 167.5, 138.3, 134.5, 131.6, 128.6, 128.7, 128.0, 127.7, 127.1, 44.2. Analytical data is in agreement with previously reported literature data.[245]

***N*-allylbenzamide (232i)**

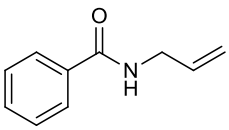

Compound **232i** was prepared according to method B with bromobenzene (0.25 mmol, 39.3 mg) and allylamine (0.25 mmol, 22.5 µL). The crude product was purified by preparative TLC (1:3 EtOAc/hexanes) to provide the pure product as a yellow oil (24.0 mg, 59%). **^{1}H NMR** (400 MHz, $CDCl_3$): δ [ppm] = 7.74 - 7.83 (m, 2H), 7.38 - 7.53 (m, 3H), 6.39 (brs, 1H), 5.93 (ddt, *J* = 16.8, 10.8, 5.7 Hz, 1H), 5.12 - 5.30 (m, 2H), 4.07 (t, *J* = 5.02 Hz, 2H). **^{13}C NMR** (100 MHz, $CDCl_3$); δ [ppm] = 167.5, 134.5, 134.3, 131.6, 128.7, 127.0, 116.7, 42.5. Analytical data is in agreement with previously reported literature data.[247]

3-(2,3-dihydrobenzofuran-3-yl)-1-(piperidin-1-yl)propane-1,2-dione (234)

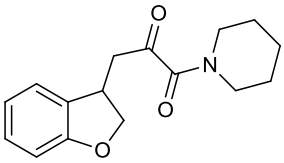

A solution of the 1-(allyloxy)-2-iodobenzene (0.125 mmol, 32.5 mg, 1.0 equiv.), $[Ir(dtbbpy)(ppy)_2]PF_6$ (1 mol %, 1.14 mg), DIPEA (1.5 equiv., 32.8 µL) and piperidine (2 equiv., 24.7 µL) in 5 mL of MeCN was sparged with N_2 (5 min) then loaded into a 5 mL sample loop. This mixture was pumped (flow rate 0.05 mL/min) through the GAM and enriched with CO (45 atm CO gas pressure) then irradiated in the photoreactor (30 min residence time). The product stream was collected, concentrated in vacuo and the crude residue purified by preperative TLC (1:4 EtOAc/hexanes) to afford 10.7 mg, 30 %, of **234** as a yellow oil. **^{1}H NMR** (400 MHz, $CDCl_3$): δ [ppm] = 7.10 - 7.18 (m, 2H), 6.78 - 6.88 (m, 2H), 4.81 (t, *J* = 9.1 Hz, 1H), 4.15 - 4.23 (m, 1H), 3.88 - 3.99 (m, 1H), 3.53 - 3.59 (m, 2H), 3.24 - 3.37 (m, 3H), 3.06 (dd, J = 18.6, 9.1 Hz, 1H), 1.56 - 1.71 (m, 6H). **^{13}C NMR** (100 MHz, $CDCl_3$); δ [ppm] = 199.8, 165.0, 159.8, 129.0, 128.8, 124.3, 120.7, 109.8, 76.7, 46.8, 45.6, 42.7, 36.8, 26.4, 25.4, 24.4. **HRMS** (ESI): calculated for $[C_{16}H_{20}NO_3]^+$: m/z = 274.1438, found: m/z = 274.1430; **IR** (ν/cm^{-1}, neat): 2940, 2860, 1709, 1634, 1481, 1460, 1231, 1092, 992, 966, 853, 750.

Determination of Yields by ^{1}H NMR Analysis

The spectra of compounds with yields determined by ^{1}H NMR integration against 1,3,5-trimethylbenzene (0.07289 mmol, 10 µL) are given below. Diagnostic protons marked by red asterisk.

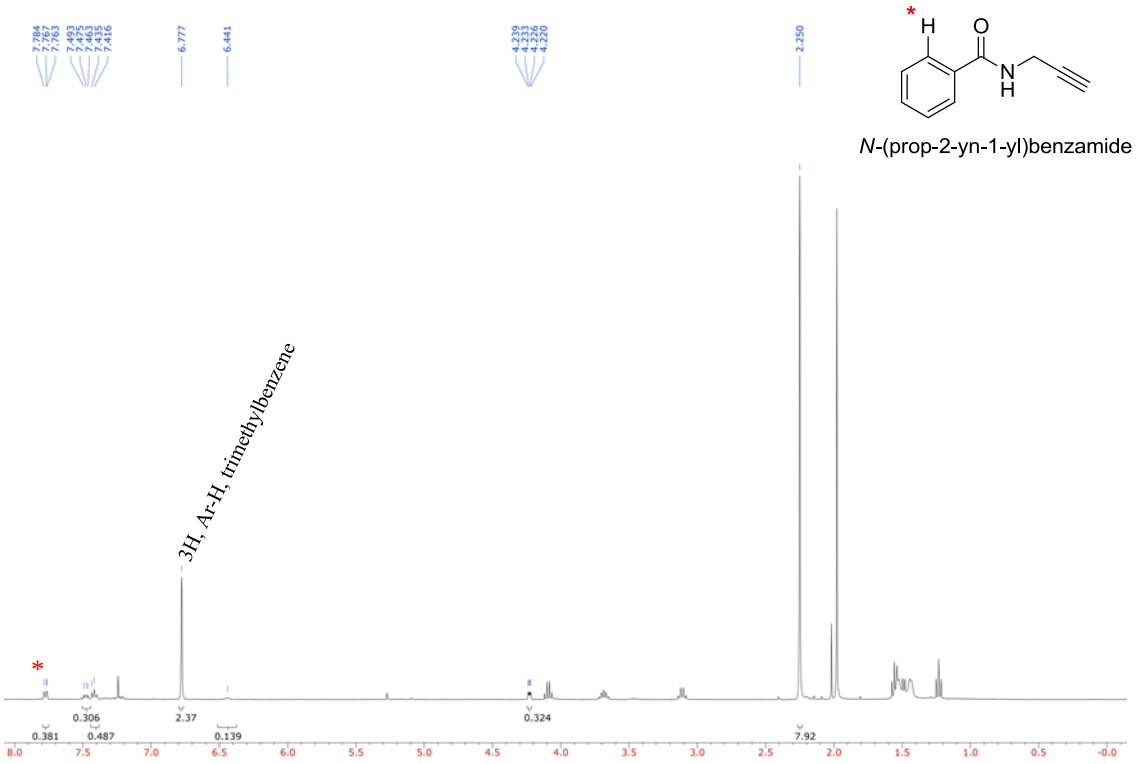

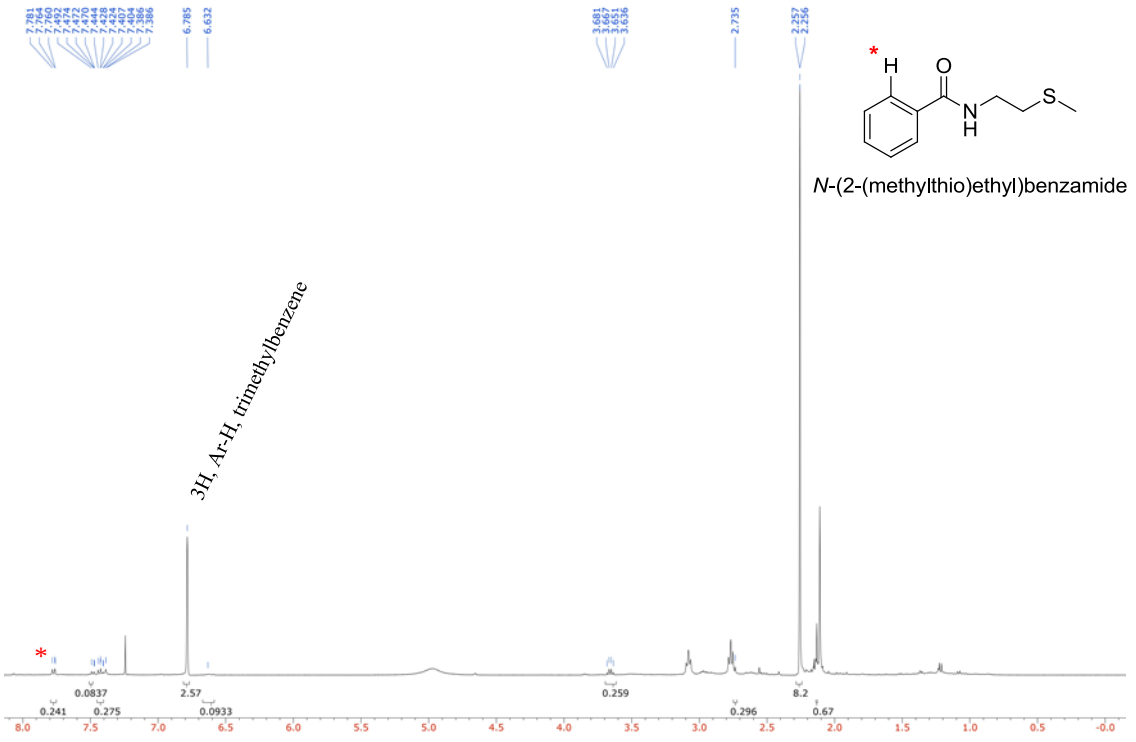

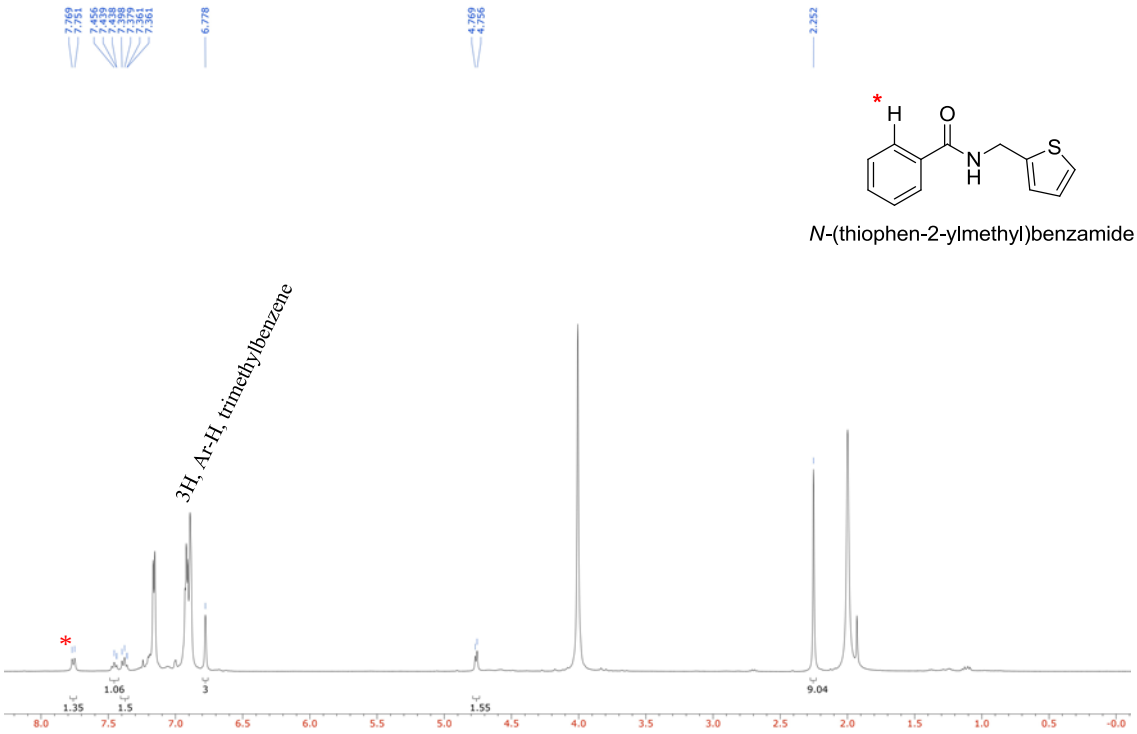

N-(thiophen-2-ylmethyl)benzamide

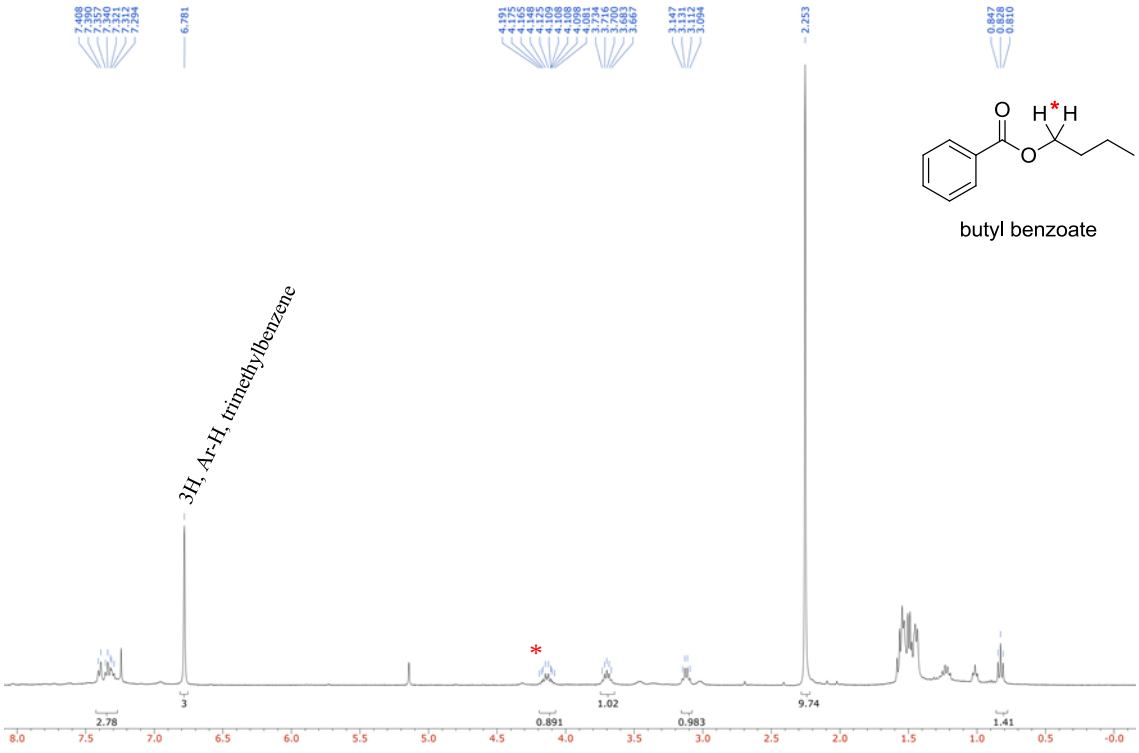

butyl benzoate

DFT Calculations of Redox Potentials in Acetonitrile

Density Functional Theory (DFT) calculations were performed by Dr. Geethika K. Weragoda and computed with the Gaussian 09 program. Geometry optimizations for the reduced and oxidized forms of each molecule were carried out using the M06-2X and B3LYP functionals with the 6-311+G(d,p) basis set which have been shown to give realisable results.[137] The CPCM formalism for the Self Consistent Reaction Field (SCRF) model of solvation was employed to account for solvation in acetonitrile. All optimized structures were confirmed to be located at local minima and have no imaginary frequencies. Redox potentials were calculated for those optimised structures and the Gibbs free energies acquired as the sum of electronic and thermal free energies. Redox properties of the anticipated intermediate cation/radical pairs were calculated according to the H. G. Roth et al, using the following equation and results are summarised in Table 4.7.2.[248]

$$E_{1/2}^{o,calc} = -\frac{(G_{298}[\text{reduced}] - G_{298}[\text{oxidized}])}{n_e \mathcal{F}} - E_{1/2}^{o,SHE} + E_{1/2}^{o,SCE}$$

Where n_e is the number of electrons transferred, F is the Faraday constant (23.061 kcal mol^{-1} V^{-1}), $E_{1/2}^{o,SHE}$ is the absolute value for the standard hydrogen electrode (4.281 V) and $E_{1/2}^{o,SCE}$ is the potential of the saturated calomel electrode (SCE) relative to SHE in acetonitrile (0.141 V) and G_{298}[reduced] and G_{298}[oxidized] are the DFT calculated Gibbs free energies in acetonitrile.[249] Cartesian coordinates and energies for all DFT calculated structures are located in the supplementary information.

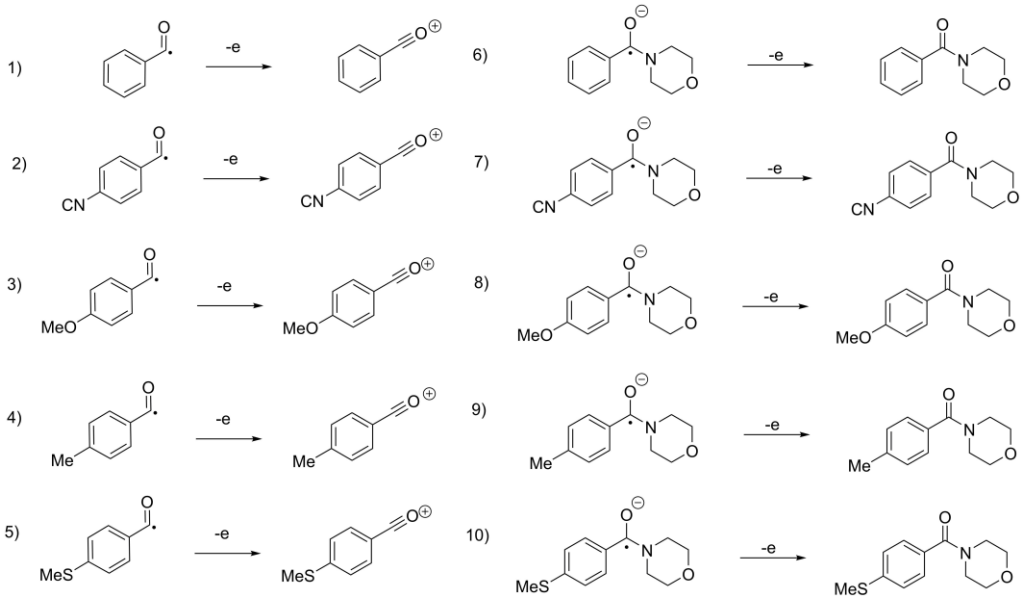

Figure 4.7.3. Computed single electron oxidation reaction schemes (1/2).

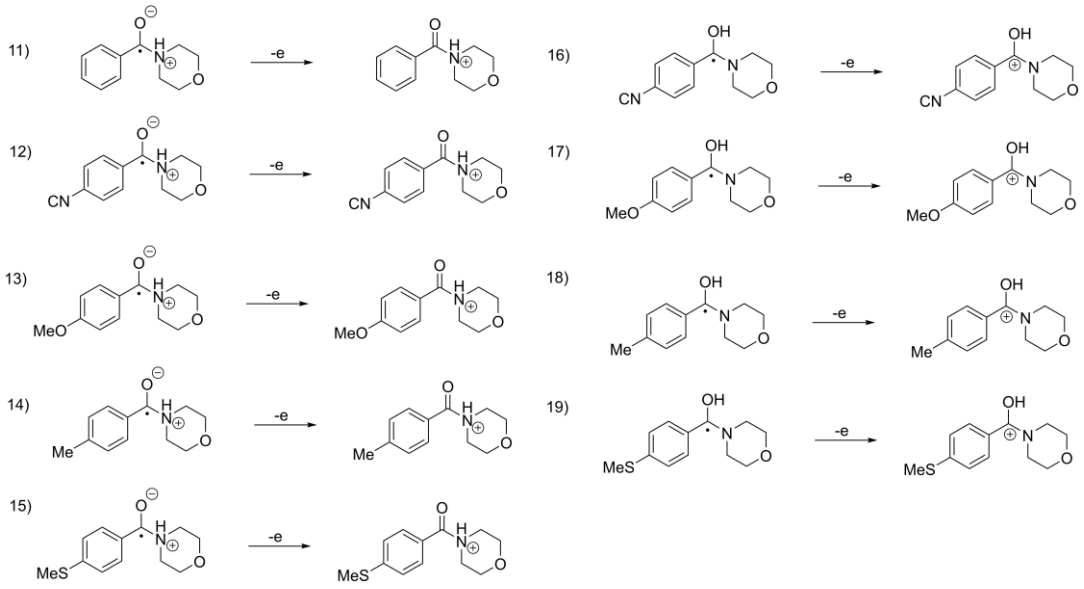

Figure 4.7.3. Computed single electron oxidation reaction schemes (2/2).

Table 4.7.2. Summarised calculated redox potentials.

Reaction	ΔE(eV) vs. SCE	
	B3LYP/6-311+G(d,p)	M06-2X/6-311+G(d,p)
1	0.10	0.09
2	0.36	0.35
3	-0.11	-0.11
4	0.01	0.06
5	-0.08	-0.05
6	-2.34	-2.36
7	-1.74	-1.73
8	-2.47	-2.52
9	-2.45	-2.44
10	-2.20	-2.22
11	-0.95	-0.93
12	-0.44	-0.47
13	-1.14	-1.12
14	-1.02	-1.03
15	-0.96	-0.95
16	-0.67	-0.69
17	-1.13	-1.14
18	-1.07	-1.11
9	-1.00	-1.02

Chapter 5. Conclusion

5.1 Conclusion

This thesis described the development of visible light photoredox-catalysed alkoxy- and aminocarbonylation of aryl (pseudo)halides. Through the development of novel photocatalytic manifolds and protocol for high pressure gas-liquid transformations in continuous flow, the scope, efficiency and accessibility of photoredox-catalysed carbonylation was elaborated.

To realise the potential of visible light photoredox carbonylation, methodology must evolve beyond high-pressure batch photoreactors. Photochemical and heterogeneous gas-liquid transformations are hampered by the effects of low surface area-to-volume ratios and inadequate control of reaction conditions in these autoclave-type reactors. Chapter 1 details the development of three continuous flow platforms for high-pressure photochemistry with reactive gases. Each system incorporates a Teflon AF2400 gas-liquid reactor module for the safe and efficient introduction of carbon monoxide into the reaction stream (Figure 5.1.1).

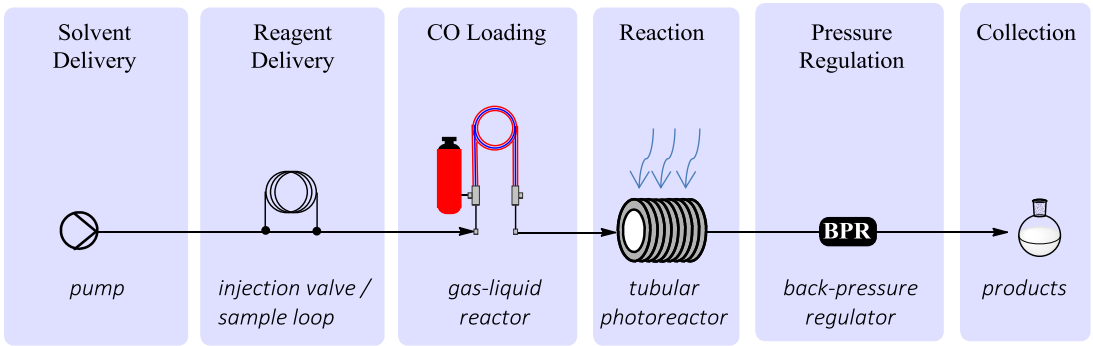

Figure 5.1.1 Schematic of the continuous flow microreactor systems employed.

The visible light photoredox-catalysed methoxycarbonylation of aryl diazonium salts was selected to evaluate the performance of the developed flow systems against the equivalent batch reaction reported in literature (Scheme 5.1.1).[113] The developed methodology utilised the organic dye fluorescein or the transition-metal complex $Ru(bpy)_3Cl_2.{}_6H_2O$ to achieve the three-component coupling of an arenediazonium salt (**248**), carbon monoxide and an alcohol in excellent yields. The methodology is characterised by significantly lower partial pressures of carbon monoxide and processing time relative to batch. The first flow platform developed had a maximum working pressure of 20 atm. Selectivity for the desired methoxycarbonylated product

(**249**) over the undesired competitive hydrodediazoniation product was achieved by employing dilute reaction conditions and catalysed by the organic dye fluorescein. Dilution was shown to be an effective strategy in flow as the throughput and space-time yield of the developed flow process was two orders of magnitude greater than the comparative batch process.

The second flow system had a maximum working pressure of 75 atm. It was determined that $Ru(bpy)_3Cl_2.6H_2O$ exhibited enhanced solubility and reactivity in acetonitrile compared to the organic dye photocatalysts thereby facilitating higher reaction throughput. With $Ru(bpy)_3Cl_2.6H_2O$ as the photocatalyst, excellent isolated yields of the methoxycarbonylated product were obtained by driving selectivity for the ester product through elevated CO pressure of 45 atm without employing dilute reaction conditions. The continuous flow photo-methoxycarbonylation reaction was scaled by a factor of 10 to yield 952 mg of methyl 4-phenoxybenzoate in absence of further process development.

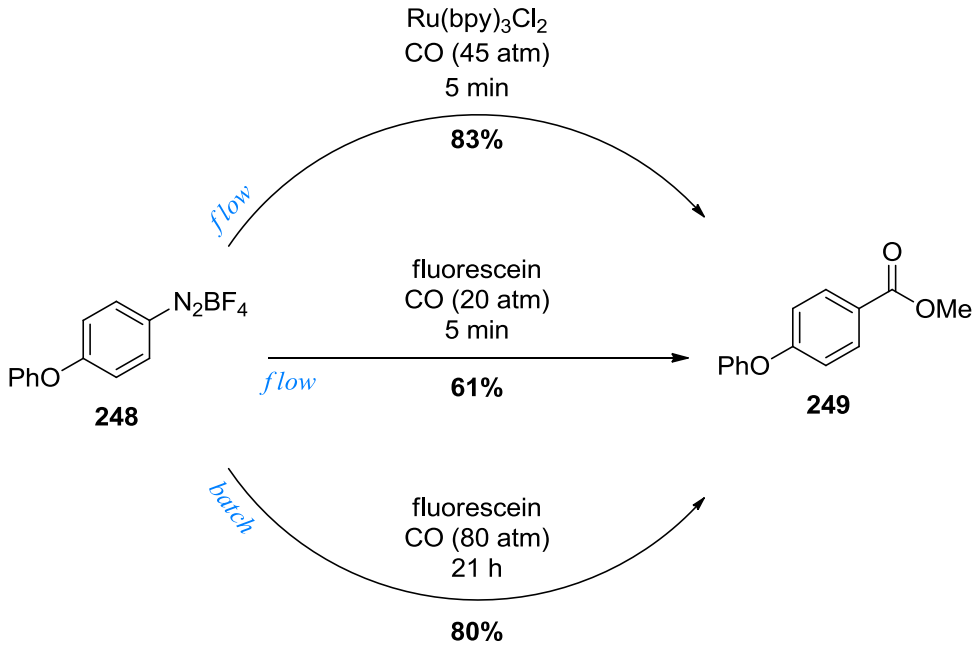

Scheme 5.1.1. Comparison of photoredox-catalysed alkoxycarbonylation in flow and in batch. Batch procedure develop by Xiao *et. al.*[113]

The third flow platform was developed to enhance reaction throughput and enable rapid reaction screening. It featured a reaction throughput of 2.37 $mmol \cdot h^{-1}$ and reaction screening could be performed at 5 minutes per run. This was enabled by scaling up the flow photoreactor volume to 1.5 mL and reducing the residence time to 3 minutes by

employing a 40 W blue LED lamp. The developed flow platform was constructed from readily available modules or bespoke components. It demonstrated that the financial burden associated with high-pressure photochemistry of reactive gases, in excess of AUD$30,000 for a batch autoclave photoreactor, can be alleviated through flow chemistry.

In chapter 2, the developed high-pressure flow photochemical technology was utilised to address a standing challenge in Pd-catalysed carbonylation. A free-radical annulative addition/alkoxycarbonylation cascade reaction was developed (Scheme 5.1.2). The methodology was applied to the synthesis of a series 3-acetate functionalized 2,3-dihydrobenzofurans (**251**). The reaction exhibited excellent regioselectivity with exclusive formation of the 5-exocylisation product and biscarbonylation was not observed. Significantly, it was found that 25 atm of CO was optimum indicating that the trapping of the alkyl radical by CO was not the yield limiting step. Application of the established continuous flow system developed in Chapter 1 enabled dilute reaction conditions to effectively control the propagation of competitive intermolecular radical addition side reactions without compromising on reaction throughput or space-time yield. The reaction was scaled-out to afford 593 mg of ethyl 2-(2,3-dihydrobenzofuran-3-yl)acetate in 9h total processing time. The space-time yield was determined to be 360 mmol.L^{-1}.h^{-1}, two orders of magnitude higher than the corresponding batch reaction. Due to the electrophilicity of arenediazonium salts, this methodology was incompatible with moderate to strong nucleophilic species such as amines, limiting the scope of the coupling partner to alcohols, affording aromatic esters.

Scheme 5.1.2. Photoredox-catalysed radical addition/alkoxycarbonlytation in flow.

To extend the scope of photoredox-carbonylation reactions to aminocarbonylation, Chapter 4 explored the use of aryl halides as aryl radical precursors (Scheme 5.1.3). The photoredox-catalysed aminocarbonylation of aryl halides had been limited by the ability to selectivity generate the aryl radical. A novel catalytic manifold was developed that

utilised Ir(dtbbpy)(ppy)$_2$]PF$_6$ in the presence of DIPEA to generate a distinct highly reducing Ir-complex (**Ir2**) capable of engaging energy demanding aryl halides. The developed methodology was applied to the synthesis of both electron rich and electron deficient benzamides at room temperature. Extending the scope to allyoxy-tethered aryl halides yielded the doubly carbonylated α-keto amide **232** via free-radical annulative addition/aminocarbonylation cascade. Fluorescence quenching and transient absorption spectroscopy studies indicated that the mechanism of aryl radical generation is highly dependent on the reduction potential of the aryl halide substrate and may proceed via **Ir1**$^{-}$, **Ir2*** or **Ir2**$^{-}$. Theoretical computational studies probed the fate of the aryl radical following reaction with CO, indicating that nucleophilic attack of the amine onto the acyl radical is the dominate reaction pathway. Significantly, this work represents a singular catalytic system for the carbonylation of both electron rich and electron deficient aryl iodides and bromides. The scope of photoredox-catalysed carbonylation of arenes is no longer restricted to aryl diazonium salts and aryl sulfonyl chlorides, which are incompatible amines.

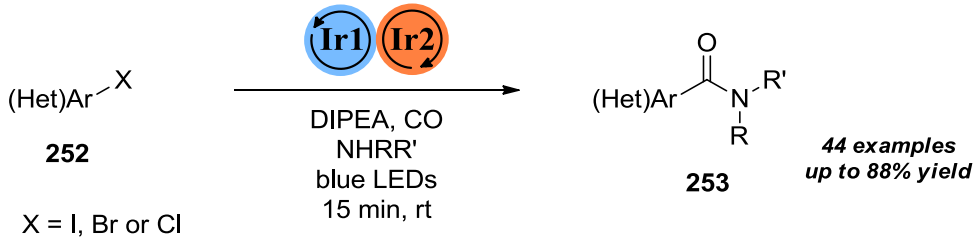

Scheme 5.1.3. Photoredox-catalysed aminocarbonylation of aryl halides in continuous flow.

References

[1] E. J. Corey, P. L. Fuchs, *Tetrahedron Lett.* **1972**, *13*, 3769–3772.
[2] A. Strecker, *Liebigs Ann. Chem.* **1854**, *91*, 349–351.
[3] V. Grignard, *CR Acad. Sci* **1900**, *130*, 1322–1324.
[4] A. Pictet, T. Spengler, *Chem. Ber.* **1911**, *44*, 2030–2036.
[5] G. Wittig, U. Schöllkopf, *Chem. Ber* **1954**, *97*, 1318–1330.
[6] A. B. Baylis, M. E. D. Hillman, *Celanese Corp. DE* **1972**, *2155113*.
[7] L. Henry, *Bull. Soc. Chim. Fr* **1895**, *13*, 999.
[8] R. Kane, *Ann. Phys. Chen.* **1838**, *44*, 475.
[9] J. J. Li, C. Limberakis, D. A. Pflum, *Modern Organic Synthesis in the Laboratory*, Oxford University Press, Oxford, **2007**.
[10] L. Kürti, B. Czakó, *Strategic Applications of Named Reactions in Organic Synthesis*, Elsevier Science, Burlington, **2005**.
[11] B. Lythgoe, A. R. Todd, *Symp. Soc. Exp. Biol.*, **1947**, p. 15.
[12] H. Musso, *Angew. Chem.* **1956**, *68*, 313–323.
[13] H. Nikaido, *Microbiol. Mol. Biol. Rev.* **1996**, *67*, 29–47.
[14] R. Mahadevan, S. T. Cole, R. Brosch, J. Parkhill, T. Garnier, C. Churcher, D. Harris, S. V Gordon, K. Eiglmeier, S. Gas, *Nature* **1998**, *393*, 537–544.
[15] E. K. Davison, M. A. Brimble, *Curr. Opin. Chem. Biol.* **2019**, *52*, 1–8.
[16] S. K. Khetan, T. J. Collins, *Chem. Rev.* **2007**, *107*, 2319–2364.
[17] M. Wacker, *Int. J. Pharm.* **2013**, *457*, 50–62.
[18] R. C. Rowe, P. J. Sheskey, P. J. Weller, *Handbook of Pharmaceutical Excipients*, Pharmaceutical Press, **2009**.
[19] T. J. White, D. J. Broer, *Nat. Mater.* **2015**, *14*, 1087–1098.
[20] C. Huang, S. Barlow, S. R. Marder, *J. Org. Chem.* **2011**, *76*, 2386–2407.
[21] S. Kitagawa, R. Kitaura, S. I. Noro, *Angew. Chem. Int. Ed.* **2004**, *43*, 2334–2375.
[22] D. Schmaljohann, *Adv. Drug Deliv. Rev.* **2006**, *58*, 1655–1670.
[23] J. Smidt, W. Hafner, R. Jira, J. Sedlmeier, R. Sieber, R. Rüttinger, H. Kojer, *Angew. Chem.* **1959**, *71*, 176–182.
[24] J. U. Nef, *Liebigs Ann.* **1894**, *280*, 263–291.
[25] K. Bowden, I. M. Heilbron, E. R. H. Jones, B. C. L. Weedon, *J. Chem. Soc.* **1946**, 39–45.
[26] R. Criegee, *Ber.* **1931**, *64*, 260–266.
[27] A. Pinner, F. Klein, *Ber.* **1877**, *10*, 1889–1897.
[28] C. Harries, *Liebigs Ann.* **1905**, *343*, 311–344.
[29] M. Patel, X. Zhang, A. Kumar, *Renew. Sustain. Energy Rev.* **2016**, *53*, 1486–1499.
[30] S. J. Jeon, S. H. Jeong, B. J. Kim, U. D. Lee, *Emerg. Areas Bioeng.* **2018**, *1*, 215
[31] J. Bierhals, *Ullmann's Encycl. Ind. Chem.* **2001**.
[32] P. Anastas, N. Eghbali, *Chem. Soc. Rev.* **2010**, *39*, 301–312.
[33] M. Berthelot, *Am. J. Pharm.* **1856**, 557.
[34] H. Koch, W. Haaf, *Liebigs Ann.* **1958**, *618*, 251–266.
[35] J. A. Peters, H. van Bekkum, *Recl. Trav. Chim. Pays-Bas* **1971**, *90*, 65–80.
[36] H. Hiller, R. Reimert, H.-M. Stönner, *Ullmann's Encycl. Ind. Chem.* **2011**.
[37] F. Franz, T. Hans, *Process for the. Production of Paraffin-Hydrocarbons with. More than One Carbon Atom*, **1930**, US1746464A.
[38] R. Otto, *Verfahren Zur Herstellung von Sauerstoffhaltigen Verbindungen*, **1938**, DE849548C.

[39] W. Reppe, *A Process for Producing Acrylic Acid, Its Esters and Substitute Products*, **1939**, DE854948C.
[40] G. J. Sunley, D. J. Watson, *Catal. Today* **2000**, *58*, 293–307.
[41] S. Forsén, *Trends Sci.* **2011**, *7*, 41–44.
[42] A. Schoenberg, R. F. Heck, *J. Org. Chem.* **1974**, *39*, 3327–3331.
[43] B. M. O'Keefe, N. Simmons, S. F. Martin, *Org. Lett.* **2008**, *10*, 5301–5304.
[44] Y. Hatanaka, T. Hiyama, *Chem. Lett.* **1989**, *18*, 2049–2052.
[45] T. Ishiyama, H. Kizaki, N. Miyaura, A. Suzuki, *Tetrahedron Lett.* **1993**, *34*, 7595–7598.
[46] J. Lindh, A. Fardost, M. Almeida, P. Nilsson, *Tetrahedron Lett.* **2010**, *51*, 2470–2472.
[47] Y. Tamaru, H. Ochiai, Y. Yamada, Z. Yoshida, *Tetrahedron Lett.* **1983**, *24*, 3869–3872.
[48] J. M. Tour, E. Negishi, *J. Am. Chem. Soc.* **1985**, *107*, 8289–8291.
[49] T. Kobayashi, M. Tanaka, *J. Chem. Soc. Chem. Commun.* **1981**, 333–334.
[50] C. Amatore, A. Jutand, A. Suarez, *J. Am. Chem. Soc.* **1993**, *115*, 9531–9541.
[51] J.-F. Fauvarque, F. Pflüger, M. Troupel, *J. Organomet. Chem.* **1981**, *208*, 419–427.
[52] C. Amatore, A. Jutand, A. Thuilliez, *Organometallics* **2001**, *20*, 3241–3249.
[53] M. Hidai, M. Kokura, Y. Uchida, *J. Organomet. Chem.* **1973**, *52*, 431–435.
[54] F. Bertoux, E. Monflier, Y. Castanet, A. Mortreux, *J. Mol. Catal. A Chem.* **1999**, *143*, 23–30.
[55] R. Gaviño, S. Pellegrini, Y. Castanet, A. Mortreux, O. Mentré, *Appl. Catal. A Gen.* **2001**, *217*, 91–99.
[56] T. Imamoto, *Compr. Org. Synth.* **2010**, 793–809.
[57] S. Fuse, S. Sugiyama, T. Takahashi, *Chem. Asian J.* **2010**, *5*, 2459–2462.
[58] S. Ho, G. Bondarenko, D. Rosa, B. Dragisic, A. Orellana, *J. Org. Chem.* **2012**, *77*, 2008–2012.
[59] L. Ran, Z. Ren, Y. Wang, Z. Guan, *Chem. Asian J.* **2014**, *9*, 577–583.
[60] P. Fitton, E. A. Rick, *J. Organomet. Chem.* **1971**, *28*, 287–291.
[61] M. Portnoy, D. Milstein, *Organometallics* **1993**, *12*, 1655–1664.
[62] J. R. Martinelli, D. A. Watson, D. M. M. Freckmann, T. E. Barder, S. L. Buchwald, *J. Org. Chem.* **2008**, *73*, 7102–7107.
[63] Y. Ben-David, M. Portnoy, D. Milstein, *J. Am. Chem. Soc.* **1989**, *111*, 8742–8744.
[64] C. F. J. Barnard, *Org. Process Res. Dev.* **2008**, *12*, 566–574.
[65] P. E. Garrou, R. F. Heck, *J. Am. Chem. Soc.* **1976**, *98*, 4115–4127.
[66] L. Ashfield, C. F. J. Barnard, *Org. Process Res. Dev.* **2007**, *11*, 39–43.
[67] M. Iizuka, Y. Kondo, *ChemComm.* **2006**, 1739–1741.
[68] M. B. Andrus, J. Liu, E. L. Meredith, E. Nartey, *Tetrahedron Lett.* **2003**, *44*, 4819–4822.
[69] Y. Obora, Y. Tsuji, T. Kawamura, *J. Am. Chem. Soc.* **1993**, *115*, 10414–10415.
[70] C. Amatore, E. Carre, A. Jutand, M. A. M'Barki, *Organometallics* **1995**, *14*, 1818–1826.
[71] M. E. O'Reilly, S. Dutta, A. S. Veige, *Chem. Rev.* **2016**, *116*, 8105–8145.
[72] A. Ariafard, Z. Lin, *Organometallics* **2006**, *25*, 4030–4033.
[73] K. S. Bloome, E. J. Alexanian, *J. Am. Chem. Soc.* **2010**, *132*, 12823–12825.
[74] F. Ozawa, N. Kawasaki, H. Okamoto, T. Yamamoto, A. Yamamoto, *Organometallics* **1987**, *6*, 1640–1651.
[75] J. S. Quesnel, A. Fabrikant, B. A. Arndtsen, *Chem. Sci.* **2016**, *7*, 295–300.

[76] P.-L. Lagueux-Tremblay, A. Fabrikant, B. A. Arndtsen, *ACS Catal.* **2018**, *8*, 5350–5354.
[77] P. Wójcik, M. Mart, S. Ulukanli, A. M. Trzeciak, *RSC Adv.* **2016**, *6*, 36491–36499.
[78] K. C. Nicolaou, P. G. Bulger, D. Sarlah, *Angew. Chem. Int. Ed.* **2005**, *44*, 4442–4489.
[79] C. Torborg, M. Beller, *Adv. Synth. Catal.* **2009**, *351*, 3027–3043.
[80] X.-F. Wu, H. Neumann, M. Beller, *Chem. Rev.* **2013**, *113*, 1–35.
[81] I. Ryu, N. Sonoda, *Angew. Chem. Int. Ed.* **1996**, *35*, 1050–1066.
[82] S. Sumino, A. Fusano, T. Fukuyama, I. Ryu, *Acc. Chem. Res.* **2014**, *47*, 1563–1574.
[83] W. B. Motherwell, D. Crich, *Free Radical Chain Reactions in Organic Synthesis*, Elsevier, **2013**.
[84] C. Chatgilialoglu, D. Crich, M. Komatsu, I. Ryu, *Chem. Rev.* **1999**, *99*, 1991–2070.
[85] C.-J. Li, *Chem. Rev.* **2005**, *105*, 3095–3166.
[86] K. Faltings, *Ber.* **1939**, *72*, 1207–1215.
[87] M. M. Brubaker, D. D. Coffman, H. H. Hoehn, *J. Am. Chem. Soc.* **1952**, *74*, 1509–1515.
[88] R. E. Foster, A. W. Larchar, R. D. Lipscomb, B. C. McKusick, *J. Am. Chem. Soc.* **1956**, *78*, 5606–5611.
[89] T. Susuki, J. Tsuji, *J. Org. Chem.* **1970**, *35*, 2982–2986.
[90] C. Walling, E. S. Savas, *J. Am. Chem. Soc.* **1960**, *82*, 1738–1744.
[91] D. D. Coffman, R. Cramer, W. E. Mochel, *J. Am. Chem. Soc.* **1958**, *80*, 2882–2887.
[92] I. Ryu, K. Kusano, A. Ogawa, N. Kambe, N. Sonoda, *J. Am. Chem. Soc.* **1990**, *112*, 1295–1297.
[93] I. Ryu, M. Hasegawa, A. Kurihara, A. Ogawa, S. Tsunoi, N. Sonoda, *Synlett* **1993**, *1993*, 143–145.
[94] M. Newcomb, *Tetrahedron* **1993**, *49*, 1151–1176.
[95] I. Ryu, K. Nagahara, N. Kambe, N. Sonoda, S. Kreimerman, M. Komatsu, *ChemComm* **1998**, 1953–1954.
[96] K. Nagahara, I. Ryu, M. Komatsu, N. Sonoda, *J. Am. Chem. Soc.* **1997**, *119*, 5465–5466.
[97] I. Ryu, *Chem. Soc. Rev.* **2001**, *30*, 16–25.
[98] T. Ishiyama, N. Miyaura, A. Suzuki, *Tetrahedron Lett.* **1991**, *32*, 6923–6926.
[99] T. Fukuyama, S. Nishitani, T. Inouye, K. Morimoto, I. Ryu, *Org. Lett.* **2006**, *8*, 1383–1386.
[100] S. Sumino, T. Ui, Y. Hamada, T. Fukuyama, I. Ryu, *Org. Lett.* **2015**, *17*, 4952–4955.
[101] S. Sumino, T. Ui, I. Ryu, *Org. Lett.* **2013**, *15*, 3142–3145.
[102] A. Fusano, T. Fukuyama, S. Nishitani, T. Inouye, I. Ryu, *Org. Lett.* **2010**, *12*, 2410–2413.
[103] H. Zhang, R. Shi, A. Ding, L. Lu, B. Chen, A. Lei, *Angew. Chem. Int. Ed.* **2012**, *51*, 12542–12545.
[104] J. K. Matsui, S. B. Lang, D. R. Heitz, G. A. Molander, *ACS Catal.* **2017**, *7*, 2563–2575.
[105] J. Xie, H. Jin, A. S. K. Hashmi, *Chem. Soc. Rev.* **2017**, *46*, 5193–5203.
[106] C. K. Prier, D. A. Rankic, D. W. C. MacMillan, *Chem. Rev.* **2013**, *113*, 5322–5363.

[107] J. M. R. Narayanam, C. R. J. Stephenson, *Chem. Soc. Rev.* **2011**, *40*, 102–113.
[108] T. J. Meyer, *Acc. Chem. Res.* **1989**, *22*, 163–170.
[109] H. Takeda, O. Ishitani, *Coord. Chem. Rev.* **2010**, *254*, 346–354.
[110] K. Kalyanasundaram, M. Grätzel, *Coord. Chem. Rev.* **1998**, *177*, 347–414.
[111] G. J. Kavarnos, *Fundamentals of Photoinduced Electron Transfer*, VCH New York Etc, **1993**.
[112] M. Majek, A. Jacobi von Wangelin, *Acc. Chem. Res.* **2016**, *49*, 2316–2327.
[113] W. Guo, L. Lu, Y. Wang, Y. Wang, J. Chen, W. Xiao, *Angew. Chem. Int. Ed.* **2015**, *54*, 2265–2269.
[114] L. Gu, C. Jin, J. Liu, *Green Chem.* **2015**, *17*, 3733–3736.
[115] H.-T. Zhang, L.-J. Gu, X.-Z. Huang, R. Wang, C. Jin, G.-P. Li, *Chinese Chem. Lett.* **2016**, *27*, 256–260.
[116] J. M. R. Narayanam, J. W. Tucker, C. R. J. Stephenson, *J. Am. Chem. Soc.* **2009**, *131*, 8756–8757.
[117] S. Fukuzumi, S. Koumitsu, K. Hironaka, T. Tanaka, *J. Am. Chem. Soc.* **1987**, *109*, 305–316.
[118] K. Hironaka, S. Fukuzumi, T. Tanaka, *Perkin Trans.* **1984**, 1705–1709.
[119] J. D. Nguyen, E. M. D'amato, J. M. R. Narayanam, C. R. J. Stephenson, *Nat. Chem.* **2012**, *4*, 854.
[120] S. Y. Chow, M. Y. Stevens, L. Åkerbladh, S. Bergman, L. R. Odell, *Chem. Eur. J.* **2016**, *22*, 9155–9161.
[121] A. M. Braun, L. Jakob, E. Oliveros, C. A. O. do Nascimento, *Adv. Photochem.* **1993**, *18*, 235–314.
[122] O. Levenspiel, *Chemical Reactor Omnibook*, Lulu. Com, **2013**.
[123] F. R. Bou-Hamdan, P. H. Seeberger, *Chem. Sci.* **2012**, *3*, 1612–1616.
[124] Y. Su, N. J. W. Straathof, V. Hessel, T. Noel, *Chem. Eur. J.* **2014**, *20*, 10562–10589.
[125] E. R. Murphy, J. R. Martinelli, N. Zaborenko, S. L. Buchwald, K. F. Jensen, *Angew. Chem. Int. Ed.* **2007**, *46*, 1734–1737.
[126] C. Csajági, B. Borcsek, K. Niesz, I. Kovács, Z. Szekelyhidi, Z. Bajko, L. Ürge, F. Darvas, *Org. Lett.* **2008**, *10*, 1589–1592.
[127] Y. Takebayashi, K. Sue, S. Yoda, T. Furuya, K. Mae, *Chem. Eng. J.* **2012**, *180*, 250–254.
[128] M. O'Brien, I. R. Baxendale, S. V Ley, *Org. Lett.* **2010**, *12*, 1596–1598.
[129] P. R. Resnick, W. H. Buck, in *Fluoropolymers 2*, Springer, **2002**, pp. 25–33.
[130] M. O'Brien, N. Taylor, A. Polyzos, I. R. Baxendale, S. V Ley, *Chem. Sci.* **2011**, *2*, 1250–1257.
[131] P. Koos, U. Gross, A. Polyzos, M. O'Brien, I. Baxendale, S. V Ley, *Org. Biomol. Chem.* **2011**, *9*, 6903–6908.
[132] M. A. Mercadante, N. E. Leadbeater, *Org. Biomol. Chem.* **2011**, *9*, 6575–6578.
[133] C. B. Kelly, C. Lee, M. A. Mercadante, N. E. Leadbeater, *Org. Process Res. Dev.* **2011**, *15*, 717–720.
[134] C. Brancour, T. Fukuyama, Y. Mukai, T. Skrydstrup, I. Ryu, *Org. Lett.* **2013**, *15*, 2794–2797.
[135] Q. Zhou, W. Guo, W. Ding, X. Wu, X. Chen, L. Lu, W. Xiao, *Angew. Chem. Int. Ed.* **2015**, *54*, 11196–11199.
[136] A. Cartier, E. Levernier, V. Corcé, T. Fukuyama, A. Dhimane, C. Ollivier, I. Ryu, L. Fensterbank, *Angew. Chem.* **2019**, *131*, 1803–1807.
[137] M. Majek, A. Jacobi von Wangelin, *Angew. Chem. Int. Ed.* **2015**, *54*, 2270–2274.
[138] J. D. J. Ingle. *Crouch*. SR Spectrochemical Analysis Prentice Hall, **1988**.

[139] V. Srivastava, P. P. Singh, *RSC Adv.* **2017**, *7*, 31377–31392.
[140] M. D. Lainchbury, M. I. Medley, P. M. Taylor, P. Hirst, W. Dohle, K. I. Booker-Milburn, *J. Org. Chem.* **2008**, *73*, 6497–6505.
[141] J. P. Knowles, L. D. Elliott, K. I. Booker-Milburn, *Beilstein J. Org. Chem.* **2012**, *8*, 2025–2052.
[142] Quote obtained from John Morris Inc. on the 9th Septemer 2019.
[143] R. J. Roark, W. C. Young. *Formulas for Stress and Strain*, McGraw-Hill, **1954**.
[144] W. J. A. Wammes, J. Middelkamp, W. J. Huisman, C. M. DeBass, K. R. Westerterp, *AIChE J.* **1991**, *37*, 1849–1862.
[145] W. Liu, *AIChE J.* **2002**, *48*, 1519–1532.
[146] A. L. Márquez, G. Wild, N. Midoux, *Chem. Eng. Process.* **1994**, *33*, 247–260.
[147] T. Noël, V. Hessel, *ChemSusChem* **2013**, *6*, 405–407.
[148] H. Zhang, G. Chen, J. Yue, Q. Yuan, *AIChE J.* **2009**, *55*, 1110–1120.
[149] K. F. Lam, E. Sorensen, A. Gavriilidis, *Chem. Eng. Res. Des.* **2013**, *91*, 1941–1953.
[150] A. Tamir, D. Herskowits, V. Herskowits, *Chem. Eng. Process.* **1990**, *28*, 165–172.
[151] A. M. Dehkordi, *AIChE J.* **2002**, *48*, 2230–2239.
[152] J. Yue, G. Chen, Q. Yuan, L. Luo, Y. Gonthier, *Chem. Eng. Sci.* **2007**, *62*, 2096–2108.
[153] K. Jähnisch, U. Dingerdissen, *Chem. Eng. Technol.* **2005**, *28*, 426–427.
[154] K. K. Yeong, A. Gavriilidis, R. Zapf, V. Hessel, *Chem. Eng. Sci.* **2004**, *59*, 3491–3494.
[155] IDEX Health & Science, in *Fluid. Opt. Prod. Inf.*, **2016**, pp. 37–55.
[156] N. J. W. Straathof, Y. Su, V. Hessel, T. Noël, *Nat. Protoc.* **2016**, *11*, 10.
[157] M. Brzozowski, M. O'Brien, S. V Ley, A. Polyzos, *Acc. Chem. Res.* **2015**, *48*, 349–362.
[158] H. Kirss, M. Kuus, E. Siimer, *J. Chem. Eng. Data* **2009**, *54*, 2128–2131.
[159] E. G. Janzen, D. E. Nutter Jr, C. A. Evans, *J. Phys. Chem.* **1975**, *79*, 1983–1984.
[160] K. M. Wiggins, T. W. Hudnall, Q. Shen, M. J. Kryger, J. S. Moore, C. W. Bielawski, *J. Am. Chem. Soc.* **2010**, *132*, 3256–3257.
[161] Y.-R. Luo, *Handbook of Bond Dissociation Energies in Organic Compounds*, CRC Press, **2002**.
[162] M. Haukka, J. Kiviaho, M. Ahlgren, T. A. Pakkanen, *Organometallics* **1995**, *14*, 825–833.
[163] G. B. Deacon, J. M. Patrick, B. W. Skelton, N. C. Thomas, A. H. White, *Aust. J. Chem.* **1984**, *37*, 929–945.
[164] M. Majek, F. Filace, A. J. von Wangelin, *Beilstein J. Org. Chem.* **2014**, *10*, 981–989.
[165] D. M. Arias-Rotondo, J. K. McCusker, *Chem. Soc. Rev.* **2016**, *45*, 5803–5820.
[166] N. A. Romero, D. A. Nicewicz, *Chem. Rev.* **2016**, *116*, 10075–10166.
[167] M. B. Plutschack, B. Pieber, K. Gilmore, P. H. Seeberger, *Chem. Rev.* **2017**, *117*, 11796–11893.
[168] W. Erb, A. Hellal, M. Albini, J. Rouden, J. Blanchet, *Chem. Eur. J.* **2014**, *20*, 6608–6612.
[169] B. Xing, L. Li, C. Ni, J. Hu, *Chinese J. Chem.* **2019**.
[170] S. Dhillon, M. Clarke, *Drugs* **2014**, *74*, 505–511.
[171] K. Kato, K. Hirai, K. Nishiyama, O. Uchikawa, K. Fukatsu, S. Ohkawa, Y. Kawamata, S. Hinuma, M. Miyamoto, *Neuropharmacology* **2005**, *48*, 301–310.
[172] R. Z. Da Silva, R. A. Yunes, M. M. de Souza, F. Delle Monache, V. Cechinel-

Filho, *J. Nat. Med.* **2010**, *64*, 402–408.
[173] J. Marco-Contelles, M. do Carmo Carreiras, C. Rodríguez, M. Villarroya, A. G. García, *Chem. Rev.* **2006**, *106*, 116–133.
[174] R. Schmitz, *Pharm. Hist.* **1985**, *27*, 61–74.
[175] L. Jurd, G. Manners, K. Stevens, *J. Chem. Soc. Chem. Commun.* **1972**, 992–993.
[176] N. Negoro, S. Sasaki, M. Ito, S. Kitamura, Y. Tsujihata, R. Ito, M. Suzuki, K. Takeuchi, N. Suzuki, J. Miyazaki, *J. Med. Chem.* **2012**, *55*, 1538–1552.
[177] E. Defossa, M. Wagner, *Bioorg. Med. Chem. Lett.* **2014**, *24*, 2991–3000.
[178] N. Negoro, S. Sasaki, S. Mikami, M. Ito, M. Suzuki, Y. Tsujihata, R. Ito, A. Harada, K. Takeuchi, N. Suzuki, *ACS Med. Chem. Lett.* **2010**, *1*, 290–294.
[179] C. Chen, H. Li, Y.-Q. Long, *Bioorg. Med. Chem. Lett.* **2016**, *26*, 5603–5612.
[180] Z. Sun, T. Zhou, X. Pan, Y. Yang, Y. Huan, Z. Xiao, Z. Shen, Z. Liu, *Bioorg. Med. Chem. Lett.* **2018**, *28*, 3050–3056.
[181] Z. Li, L. Hu, X. Wang, Z. Zhou, L. Deng, Y. Xu, L. Zhang, *Bioorg. Chem.* **2019**, *92*, 103254.
[182] V. K. Tandon, A. K. Awasthi, K. A. Singh, *Heterocycles* **2010**, *80*, 593–600.
[183] E. A. Boyle, F. R. Mangan, R. E. Markwell, S. A. Smith, M. J. Thomson, R. W. Ward, P. A. Wyman, *J. Med. Chem.* **1986**, *29*, 894–898.
[184] K. E. Torraca, S.-I. Kuwabe, S. L. Buchwald, *J. Am. Chem. Soc.* **2000**, *122*, 12907–12908.
[185] S. Kuwabe, K. E. Torraca, S. L. Buchwald, *J. Am. Chem. Soc.* **2001**, *123*, 12202–12206.
[186] Y. Komine, A. Kamisawa, K. Tanaka, *Org. Lett.* **2009**, *11*, 2361–2364.
[187] D. Lapotre, H. Deleuze, B. Maillard, K. Mulholland, *Synth. Commun.* **2001**, *31*, 3207–3218.
[188] Q. Liu, B. Han, W. Zhang, L. Yang, Z.-L. Liu, W. Yu, *Synlett* **2005**, *2005*, 2248–2250.
[189] Y. Yoshimi, H. Kanai, K. Nishikawa, Y. Ohta, Y. Okita, K. Maeda, T. Morita, *Tetrahedron Lett.* **2013**, *54*, 2419–2422.
[190] M. Basanagouda, Narayanachar, I. B. Majati, S. S. Mulimani, S. B. Sunnal, R. V Nadiger, A. S. Ghanti, S. F. Gudageri, R. Naik, A. Nayak, *Synth. Commun.* **2015**, *45*, 2195–2202.
[191] H. M. L. Davies, M. V. A. Grazini, E. Aouad, *Org. Lett.* **2001**, *3*, 1475–1477.
[192] H. Saito, H. Oishi, S. Kitagaki, S. Nakamura, M. Anada, S. Hashimoto, *Org. Lett.* **2002**, *4*, 3887–3890.
[193] F. A. Siqueira, J. G. Taylor, C. R. D. Correia, *Tetrahedron Lett.* **2010**, *51*, 2102–2105.
[194] E. Negishi, C. Copéret, S. Ma, T. Mita, T. Sugihara, J. M. Tour, *J. Am. Chem. Soc.* **1996**, *118*, 5904–5918.
[195] R. C. Carmona, O. D. Köster, C. R. D. Correia, *Angew. Chem. Int. Ed.* **2018**, *57*, 12067–12070.
[196] A. N. Abeywickrema, A. L. J. Beckwith, *J. Chem. Soc. Chem. Commun.* **1986**, 464–465.
[197] I. Ryu, T. Niguma, S. Minakata, M. Komatsu, S. Hadida, D. P. Curran, *Tetrahedron Lett.* **1997**, *38*, 7883–7886.
[198] K. Haghbeen, E. W. Tan, *J. Org. Chem.* **1998**, *63*, 4503–4505.
[199] Y.-R. Luo, *Comprehensive Handbook of Chemical Bond Energies*, CRC Press, **2007**.
[200] X.-J. Yang, B. Chen, L.-Q. Zheng, L.-Z. Wu, C.-H. Tung, *Green Chem.* **2014**, *16*, 1082–1086.

[201] M. M. G. Antonisse, B. H. M. Snellink-Ruël, I. Yigit, J. F. J. Engbersen, D. N. Reinhoudt, *J. Org. Chem.* **1997**, *62*, 9034–9038.
[202] D. Tordera, M. Delgado, E. Ort, H. J. Bolink, J. Frey, M. K. Nazeeruddin, E. Baranoff, *Chem. Mater.* **2012**, *24*, 1896–1903.
[203] E. Kumarasamy, R. Raghunathan, S. Jockusch, A. Ugrinov, J. Sivaguru, *J. Am. Chem. Soc.* **2014**, *136*, 8729–8737.
[204] M. Hartmann, A. Studer, *Angew. Chem. Int. Ed.* **2014**, *53*, 8180–8183.
[205] J. Ouyang, X. Su, Y. Chen, Y. Yuan, Y. Li, *Tetrahedron Lett.* **2016**, *57*, 1438–1441.
[206] A. L. J. Beckwith, G. F. Meijs, *J. Org. Chem.* **1987**, *52*, 1922–1930.
[207] S. D. Roughley, A. M. Jordan, *J. Med. Chem.* **2011**, *54*, 3451–3479.
[208] J. D. Mullins, T. J. Macek, *J. Am. Pharm. Assoc.* **1960**, *49*, 245–248.
[209] S. Danishefsky, J. Y. Lee, *J. Am. Chem. Soc.* **1989**, *111*, 4829–4837.
[210] J. S. Carey, D. Laffan, C. Thomson, M. T. Williams, *Org. Biomol. Chem.* **2006**, *4*, 2337–2347.
[211] D. J. C. Constable, P. J. Dunn, J. D. Hayler, G. R. Humphrey, J. L. Leazer Jr, R. J. Linderman, K. Lorenz, J. Manley, B. A. Pearlman, A. Wells, *Green Chem.* **2007**, *9*, 411–420.
[212] C. C. C. Johansson Seechurn, M. O. Kitching, T. J. Colacot, V. Snieckus, *Angew. Chem. Int. Ed.* **2012**, *51*, 5062–5085.
[213] F. Mo, G. Dong, Y. Zhang, J. Wang, *Org. Biomol. Chem.* **2013**, *11*, 1582–1593.
[214] N. G. Connelly, W. E. Geiger, *Chem. Rev.* **1996**, *96*, 877–910.
[215] T. U. Connell, C. L. Fraser, M. L. Czyz, Z. M. Smith, D. J. Hayne, E. H. Doeven, J. Agugiaro, D. J. D. Wilson, J. L. Adcock, A. D. Scully, *J. Am. Chem. Soc.* **2019**, *141*, 17646–17658.
[216] J. J. Devery III, J. D. Nguyen, C. Dai, C. R. J. Stephenson, *ACS Catal.* **2016**, *6*, 5962–5967.
[217] E. H. Discekici, N. J. Treat, S. O. Poelma, K. M. Mattson, Z. M. Hudson, Y. Luo, C. J. Hawker, J. R. de Alaniz, *Chem. Commun.* **2015**, *51*, 11705–11708.
[218] I. Ghosh, B. König, *Angew. Chem. Int. Ed.* **2016**, *55*, 7676–7679.
[219] I. Ghosh, T. Ghosh, J. I. Bardagi, B. König, *Science.* **2014**, *346*, 725–728.
[220] A. J. Fry, R. L. Krieger, *J. Org. Chem.* **1976**, *41*, 54–57.
[221] D. J. van As, T. U. Connell, M. Brzozowski, A. D. Scully, A. Polyzos, *Org. Lett.* **2018**, *20*, 905–908.
[222] Y. Yamamoto, *Adv. Synth. Catal.* **2010**, *352*, 478–492.
[223] A. M. Trzeciak, J. J. Ziolkowski, *Coord. Chem. Rev.* **2005**, *249*, 2308–2322.
[224] A. G. Sergeev, A. Spannenberg, M. Beller, *J. Am. Chem. Soc.* **2008**, *130*, 15549–15563.
[225] J. Y. Wang, A. E. Strom, J. F. Hartwig, *J. Am. Chem. Soc.* **2018**, *140*, 7979–7993.
[226] M. R. Heinrich, *Chem. Eur. J.* **2009**, *15*, 820–833.
[227] J. A. Nieman, M. D. Ennis, *J. Org. Chem.* **2001**, *66*, 2175–2177.
[228] M. Amézquita-Valencia, H. Alper, *J. Org. Chem.* **2016**, *81*, 3860–3867.
[229] S. F. Nelsen, P. J. Hintz, *J. Am. Chem. Soc.* **1972**, *94*, 7114–7117.
[230] R. Y. Lai, A. J. Bard, *J. Phys. Chem. A* **2003**, *107*, 3335–3340.
[231] T. Kawamoto, H. Matsubara, T. Fukuyama, I. Ryu, *Chem. Lett.* **2018**, *47*, 1169–1171.
[232] D. Koziakov, A. J. von Wangelin, *Org. Biomol. Chem.* **2017**, *15*, 6715–6719.
[233] H. Mayr, A. R. Ofial, *Acc. Chem. Res.* **2016**, *49*, 952–965.
[234] A. Dahlén, A. Petersson, G. Hilmersson, *Org. Biomol. Chem.* **2003**, *1*, 2423–

2426.
[235] I. Kalvet, T. Sperger, T. Scattolin, G. Magnin, F. Schoenebeck, *Angew. Chem. Int. Ed.* **2017**, *56*, 7078–7082.
[236] M. Sayes, A. B. Charette, *Green Chem.* **2017**, *19*, 5060–5064.
[237] T. T. Dang, Y. Zhu, J. S. Y. Ngiam, S. C. Ghosh, A. Chen, A. M. Seayad, *ACS Catal.* **2013**, *3*, 1406–1410.
[238] T. Kawamoto, A. Sato, I. Ryu, *Chem. Eur. J.* **2015**, *21*, 14764–14767.
[239] R. De Simone, I. Bruno, R. Riccio, K. Stadler, J. Bauer, A. M. Schaible, S. Laufer, O. Werz, *Bioorg. Med. Chem.* **2012**, *20*, 5012–5016.
[240] Y. Tu, L. Yuan, T. Wang, C. Wang, J. Ke, J. Zhao, *J. Org. Chem.* **2017**, *82*, 4970–4976.
[241] J. Li, S. He, H. Fu, X. Chen, M. Tang, D. Zhang, B. Wang, *Res. Chem. Intermed.* **2018**, *44*, 2289–2303.
[242] L. Wang, M. Yu, C. Wu, N. Deng, C. Wang, X. Yao, Adv. Synth. Catal., **2016**, *358*, 2631-2641
[243] S. W. Krabbe, V. S. Chan, T. S. Franczyk, S. Shekhar, J. G. Napolitano, C. A. Presto, J. A. Simanis, *J. Org. Chem.* **2016**, *81*, 10688–10697.
[244] L. Wang, M. Yu, C. Wu, N. Deng, C. Wang, X. Yao, *Adv. Synth. Catal.* **2016**, *358*, 2631–2641.
[245] T. T. Dang, Y. Zhu, J. S. Y. Ngiam, S. C. Ghosh, A. Chen, A. M. Seayad, *ACS Catal.* **2013**, *3*, 1406–1410.
[246] T. Kaicharla, M. Thangaraj, A. T. Biju, *Org. Lett.* **2014**, *16*, 1728–1731.
[247] J. Li, M. J. Lear, Y. Hayashi, *Angew. Chem. Int. Ed.* **2016**, *55*, 9060–9064.
[248] H. G. Roth, N. A. Romero, D. A. Nicewicz, *Synlett* **2016**, *27*, 714–723.
[249] A. A. Isse, A. Gennaro, *J. Phys. Chem. B* **2010**, *114*, 7894–7899.

Appendix

A.1. General Experimental

Materials

Unless otherwise stated, reagents, catalysts and solvents were purchased from Merck, Sigma-Aldrich, Thermo Fisher Scientific or TCI and were used without further purification. Acetonitrile and methanol were used as supplied (HPLC grade). Anhydrous solvents were prepared by storing stock solvent over 3 Å molecular sieves for 48 hours. Carbon monoxide (grade 2.9) was purchased from CoreGas. Solvents were deoxygenated by sparging with nitrogen gas for 15 minutes prior to use. Flash chromatography was performed on silica gel (Merck Kieselgel 60, 0.040-0.063 mm). Preparative TLC was conducted using Analtech silica gel matrix preparative TLC plates (1.00 mm). Teflon® AF-2400 was purchased from Cambridge Reactor Design. Tubing and fluidic connections were purchased from Upchurch Scientific (IDEX Health & Science).

Instrumentation

Nuclear Magnetic Resonance (NMR) spectra were recorded on a Varian MR400 system (400 MHz for ^{1}H; 100 MHz for ^{13}C; 376 MHz for ^{19}F). Spectra were calibrated relative to solvent residual peaks. ^{19}F NMR spectra were calibrated using trifluoroacetic acid as the reference standard. Data for ^{1}H are reported as follows: chemical shift, multiplicity (s = singlet, d = doublet, t = triplet, dt = doublet of triplets, dd = doublet of doublets, ddd = doublet of doublets, q = quartet, dq = doublet of quartets, m = multiplet, brs = broad singlet), coupling constants (Hz), and integration. High resolution mass spectrometry was conducted on an Agilent 1100 autosampler system coupled to an Agilent 6520 Quadrupole Time of Flight (Q-TOF) mass spectrometer. Infrared spectra were recorded on a Perkin Elmer Spectrum 100 FT-IR in attenuated total reflectance (ATR) mode. Melting points were measured on an Electrothermal 1A6304 melting point apparatus and are uncorrected.

A.2. Chapter 2 NMR spectra

4-Methoxybenzenediazonium tetrafluoroborate (119)

^{1}H-NMR (DMSO-d_6, 400 MHz)

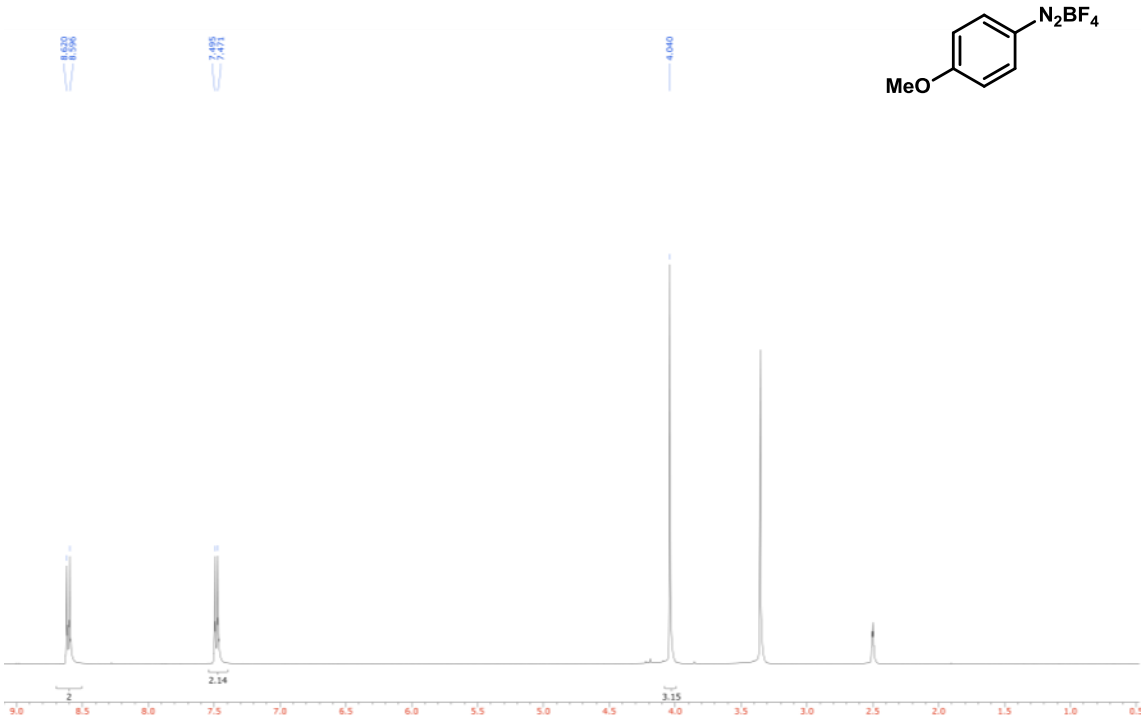

4-Phenoxybenzenediazonium tetrafluoroborate (121)

^{1}H-NMR (DMSO-d_6, 400 MHz)

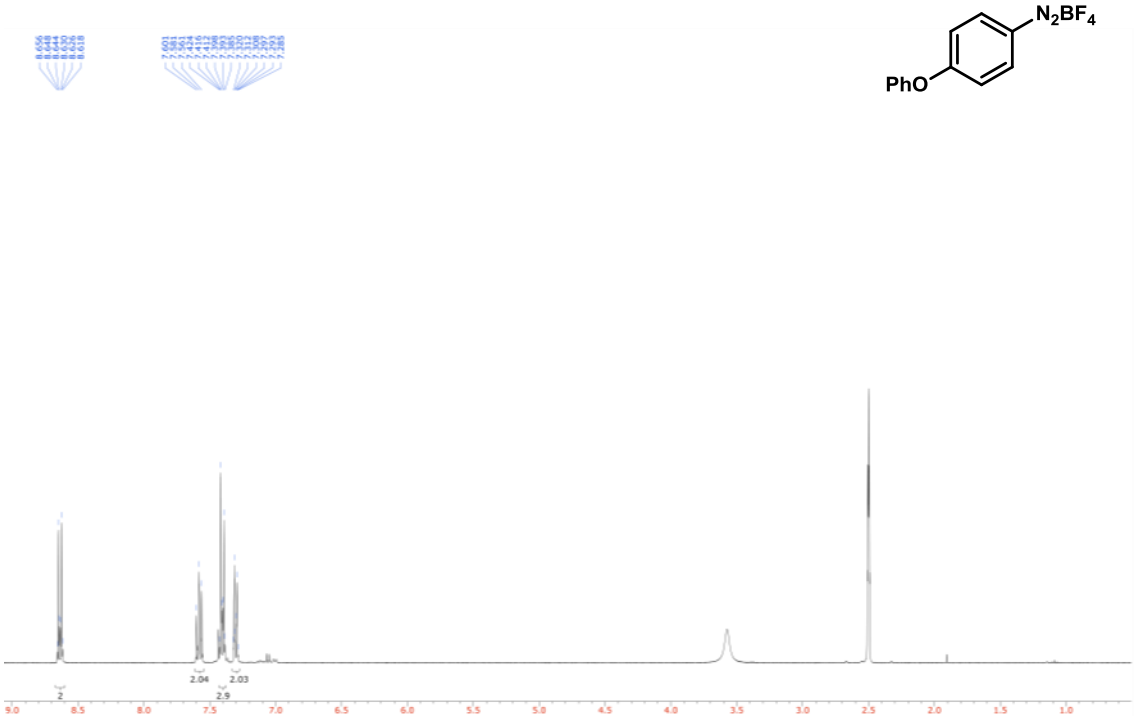

Methyl 4-Phenoxybenzoate (122)

^{1}H-NMR ($CDCl_3$, 400 MHz)

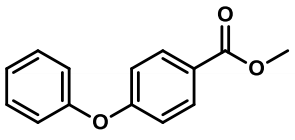

^{13}C-NMR ($CDCl_3$, 100 MHz)

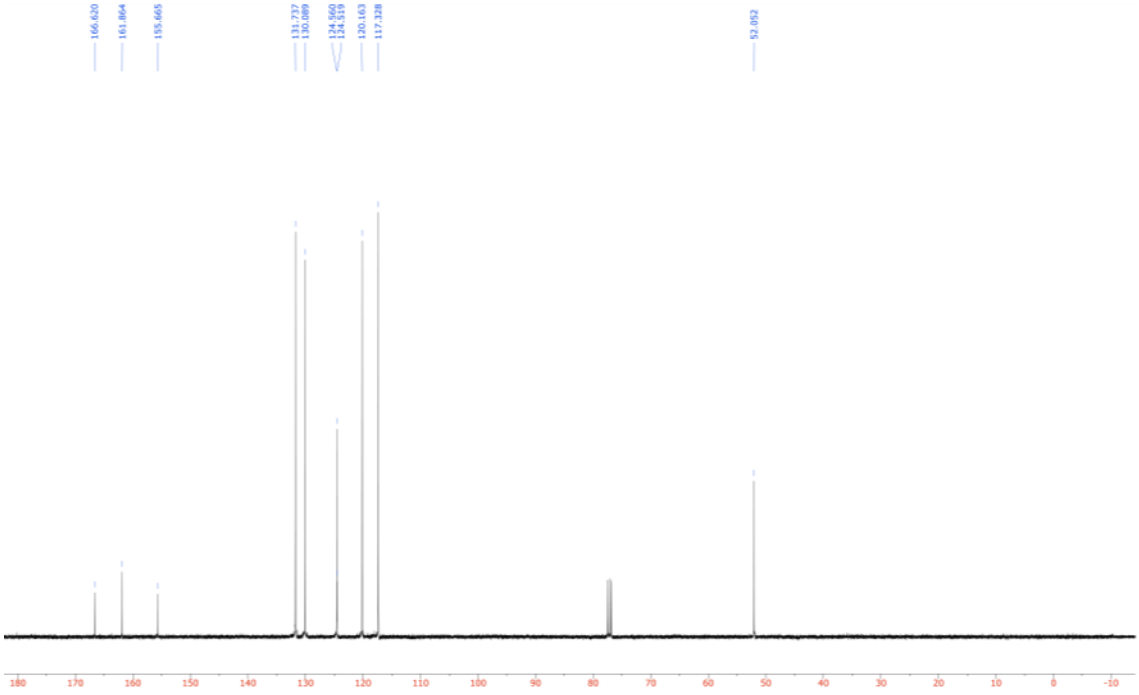

A.3. Chapter 3 NMR spectra

Methyl 2-(2,3-dihydrobenzofuran-3-yl)acetate (169a)

^{1}H-NMR ($CDCl_3$, 400 MHz)

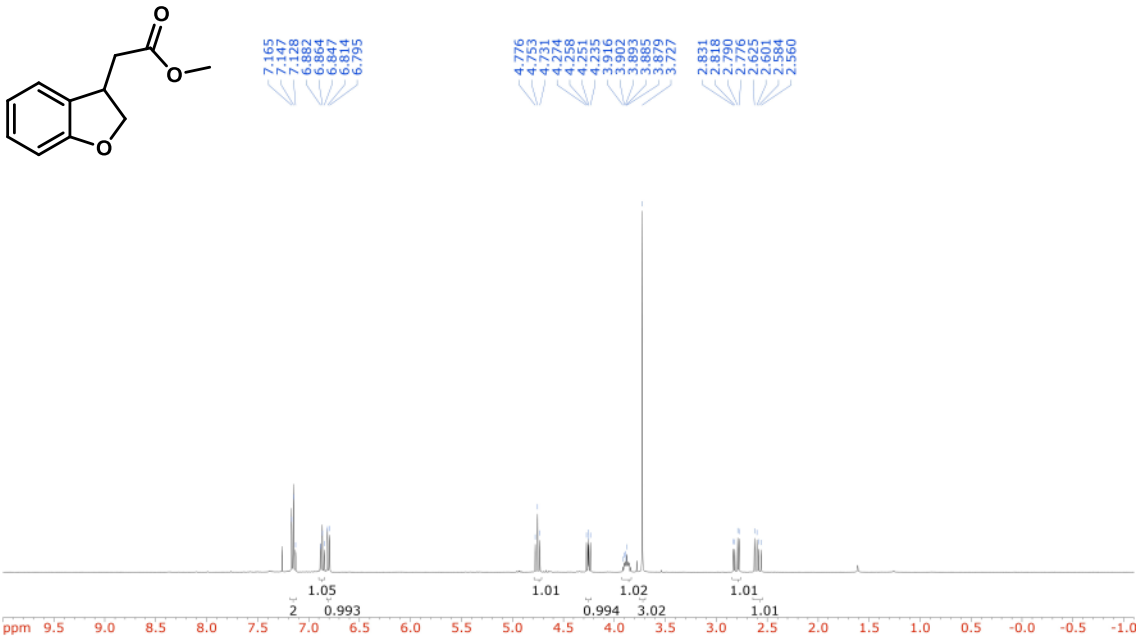

^{13}C-NMR ($CDCl_3$, 100 MHz)

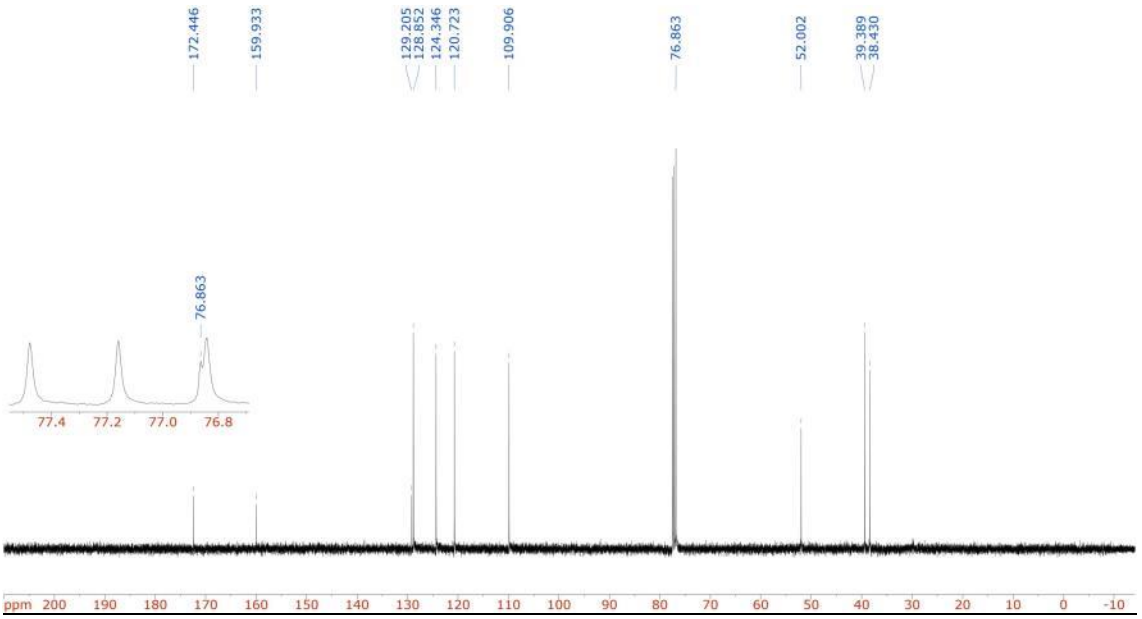

Ethyl 2-(2,3-dihydrobenzofuran-3-yl)acetate (169b)

^{1}H-NMR ($CDCl_3$, 400 MHz)

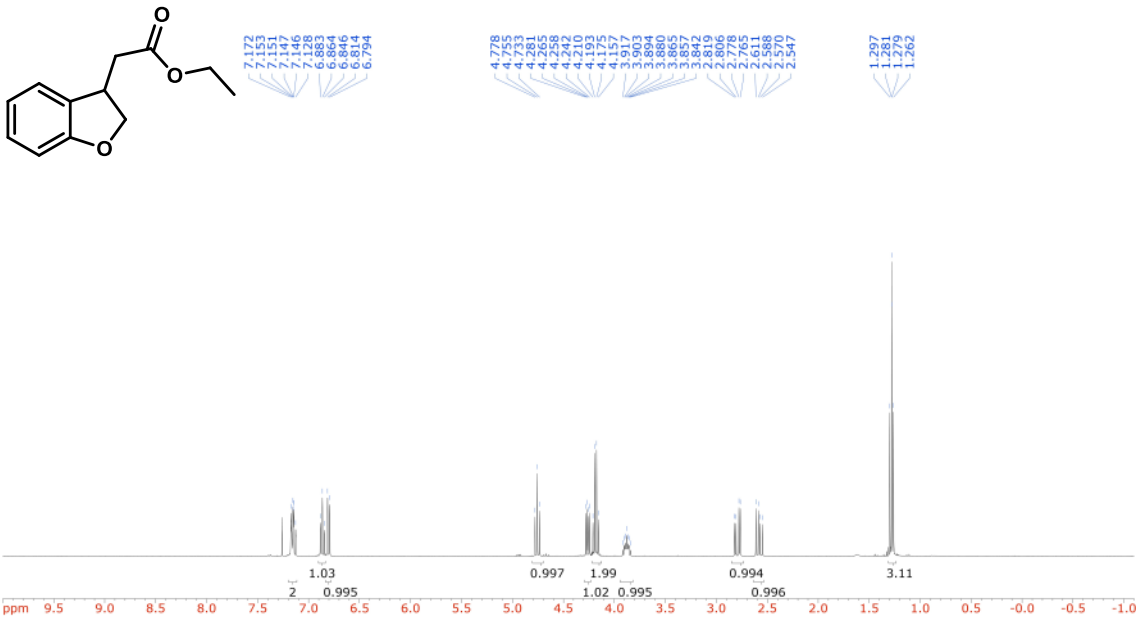

^{13}C-NMR ($CDCl_3$, 100 MHz)

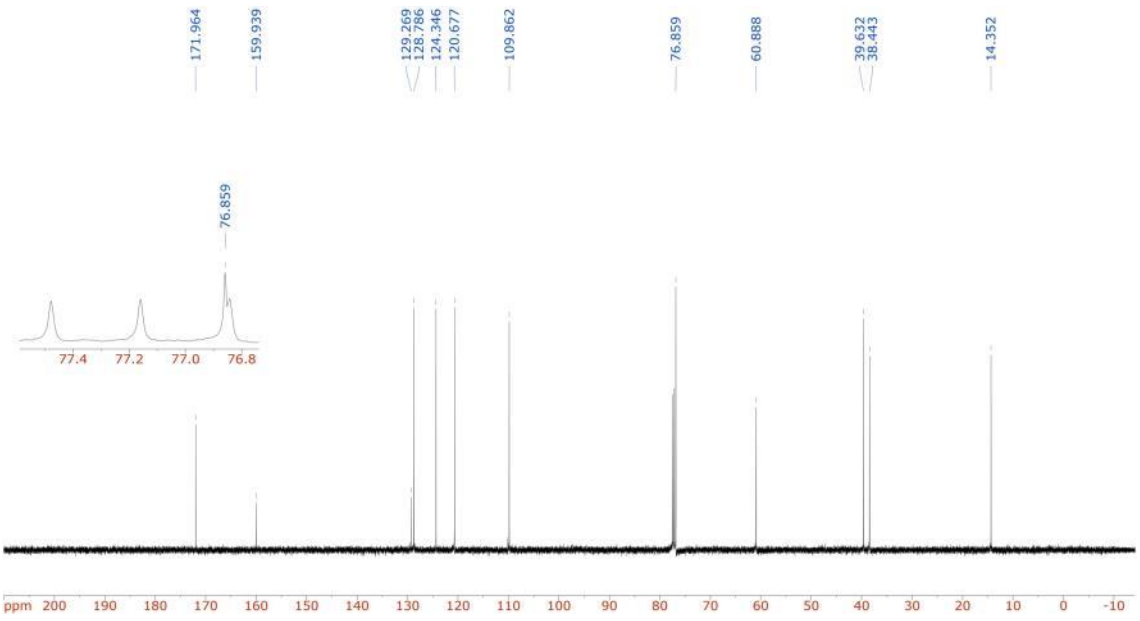

***iso*-Propyl 2-(2,3-dihydrobenzofuran-3-yl)acetate (169c)**

^{1}H-NMR ($CDCl_3$, 400 MHz)

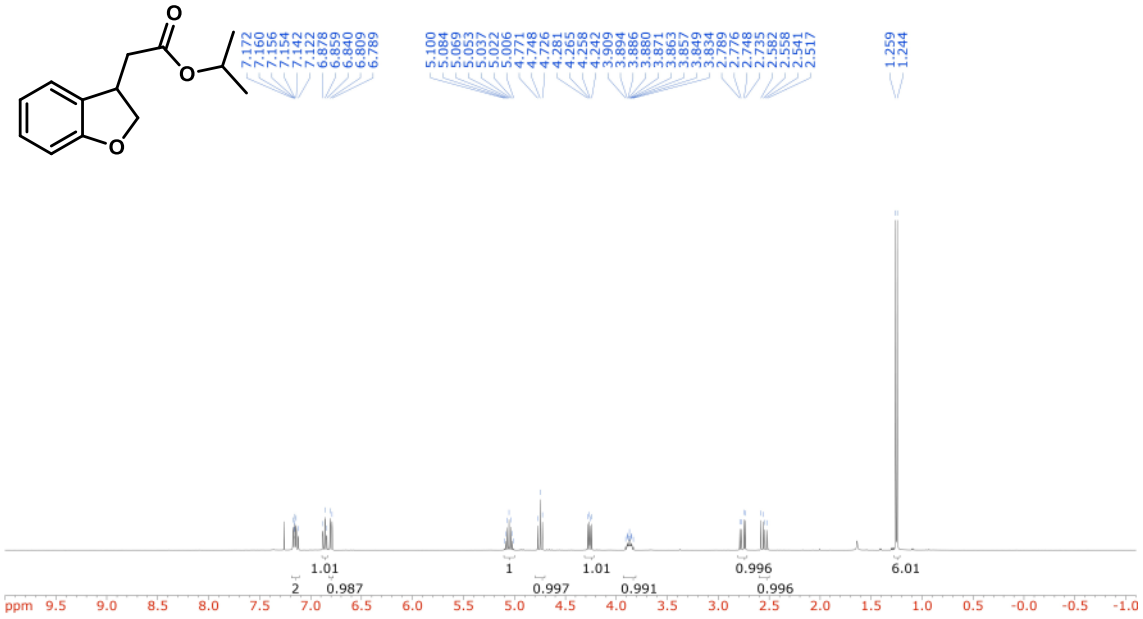

^{13}C-NMR ($CDCl_3$, 100 MHz)

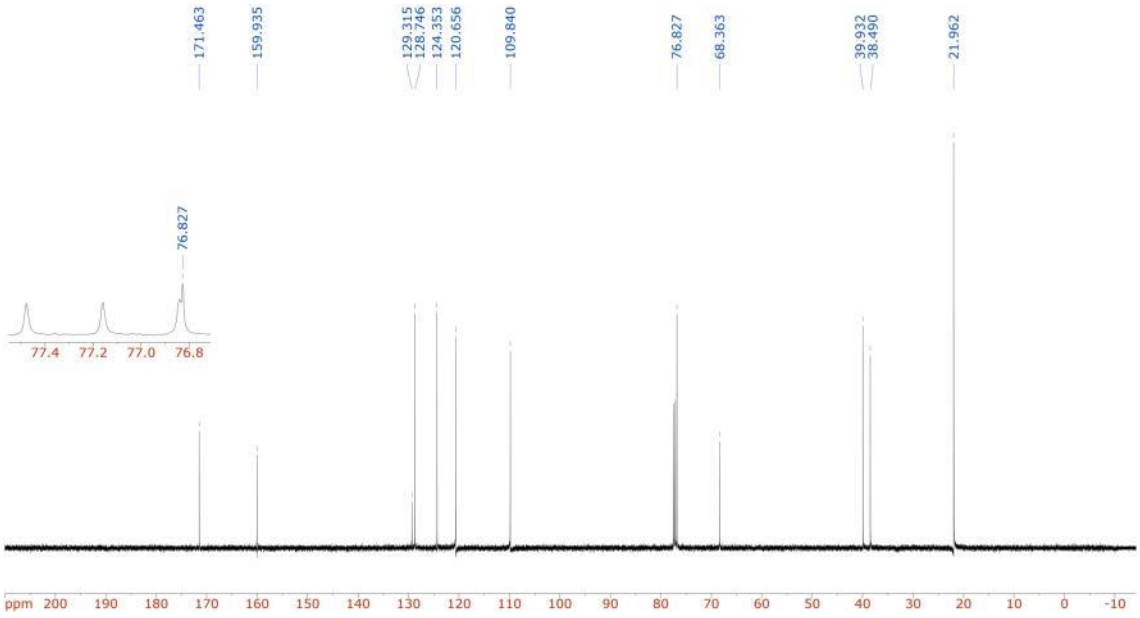

_n_-Butyl 2-(2,3-dihydrobenzofuran-3-yl)acetate (169d)

^{1}H-NMR ($CDCl_3$, 400 MHz)

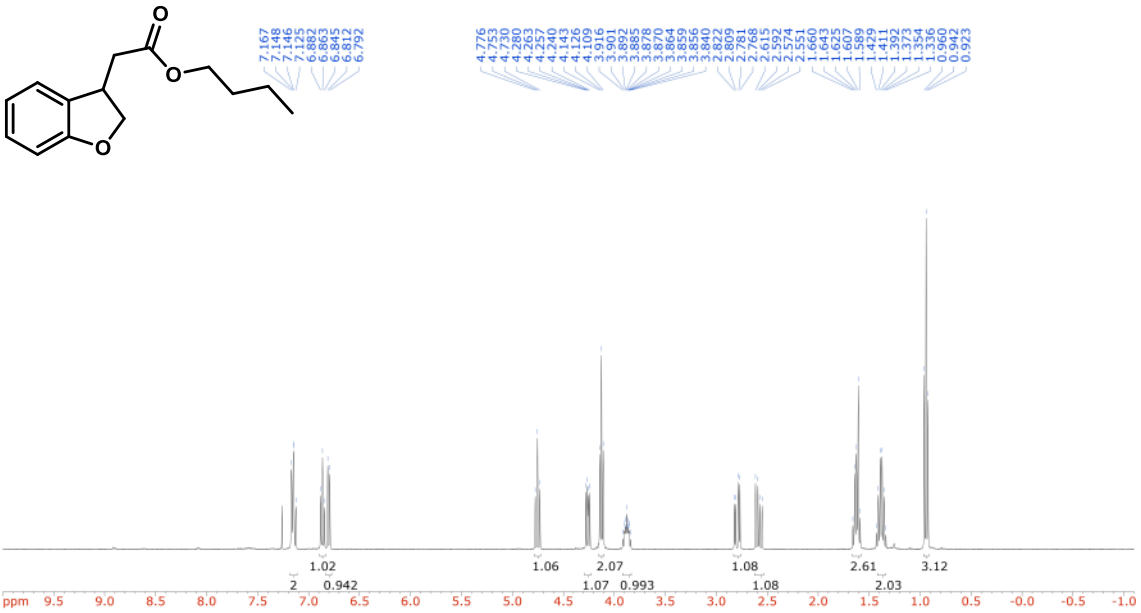

^{13}C-NMR ($CDCl_3$, 100 MHz)

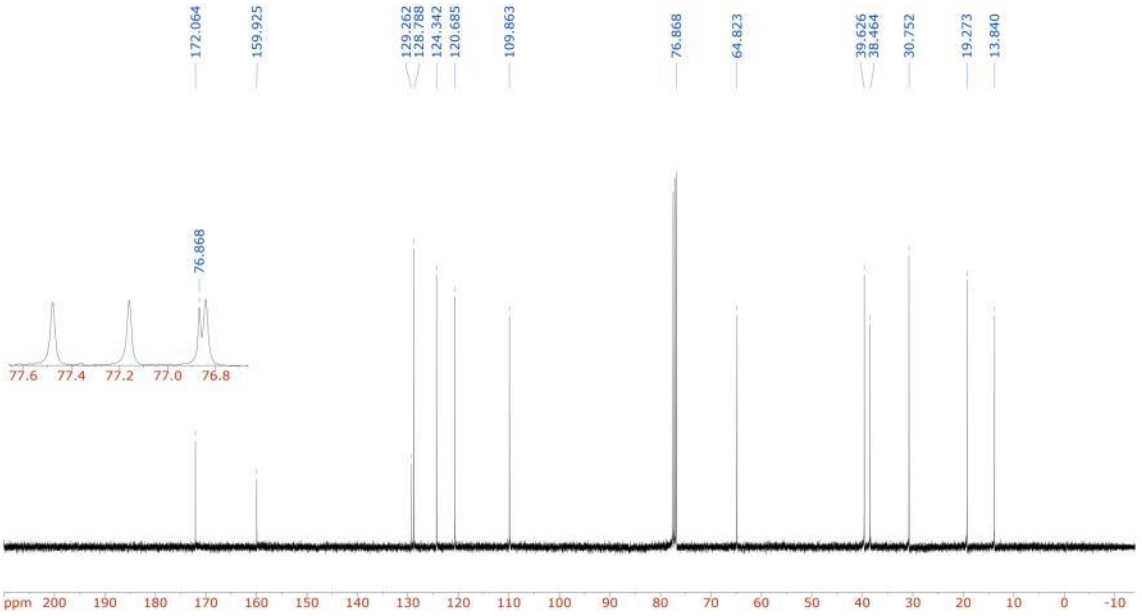

_t_-Butyl 2-(2,3-dihydrobenzofuran-3-yl)acetate (169e)

^{1}H-NMR ($CDCl_3$, 400 MHz)

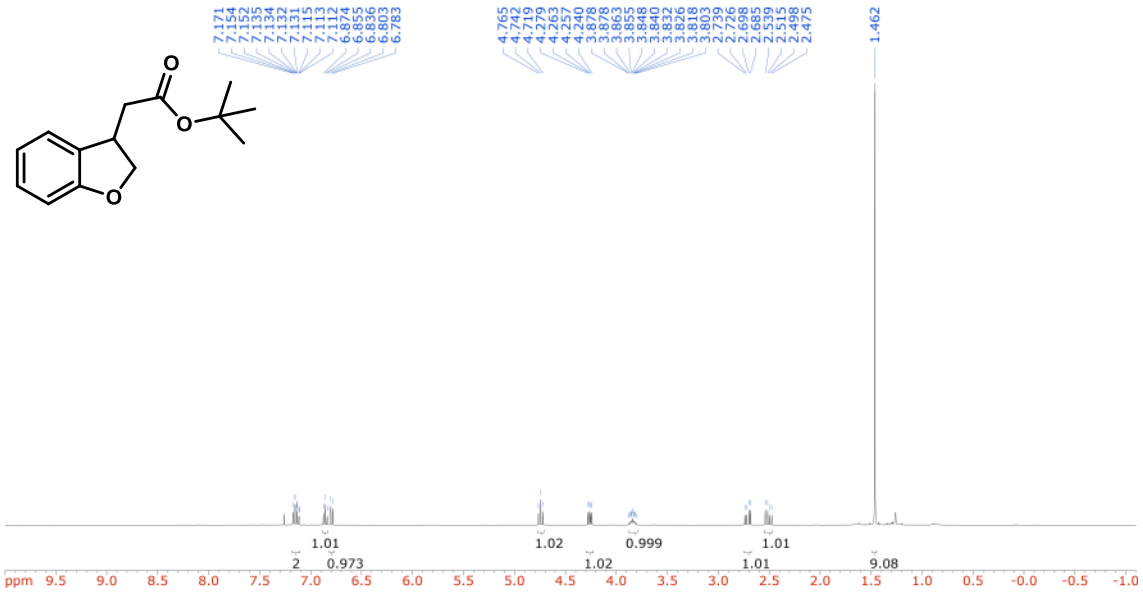

^{13}C-NMR ($CDCl_3$, 100 MHz)

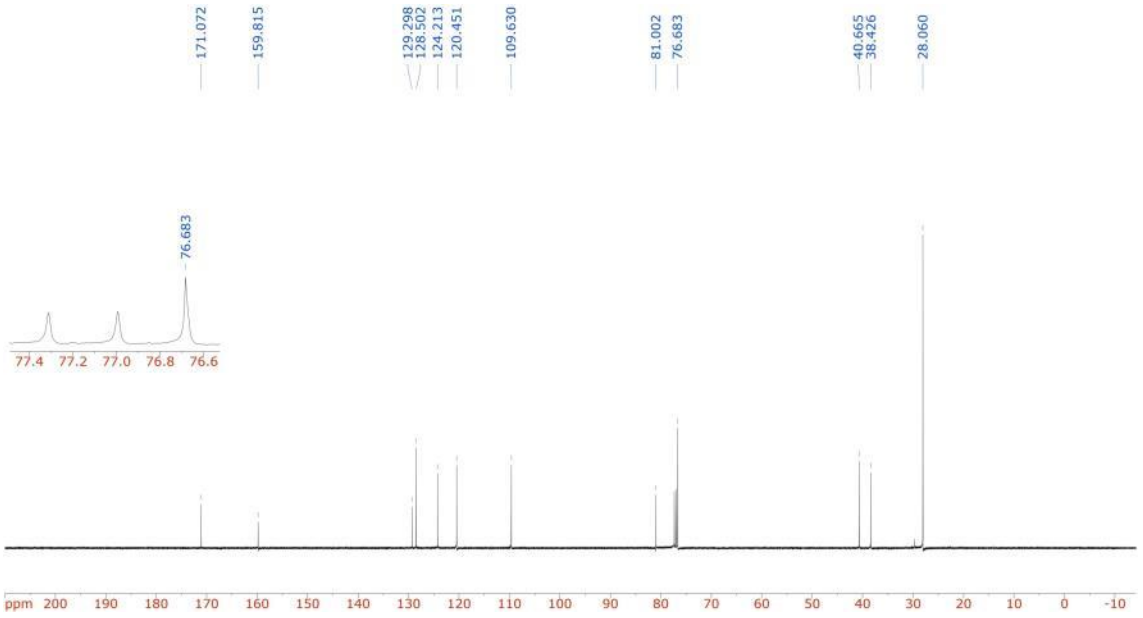

Cyclohexyl 2-(2,3-dihydrobenzofuran-3-yl)acetate (169f)

^{1}H-NMR ($CDCl_3$, 400 MHz)

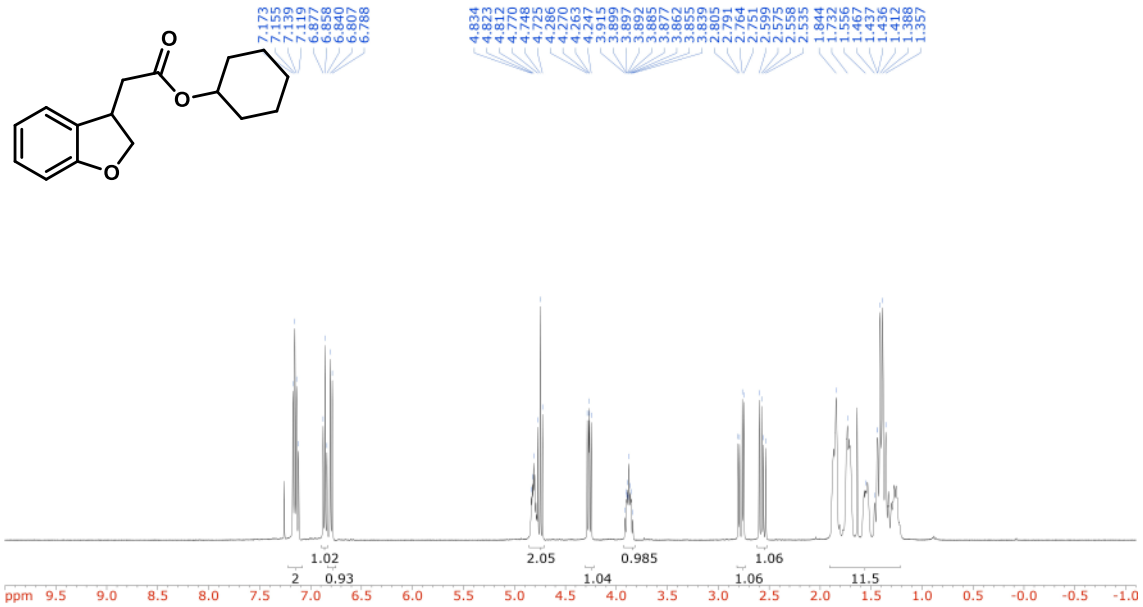

^{13}C-NMR ($CDCl_3$, 100 MHz)

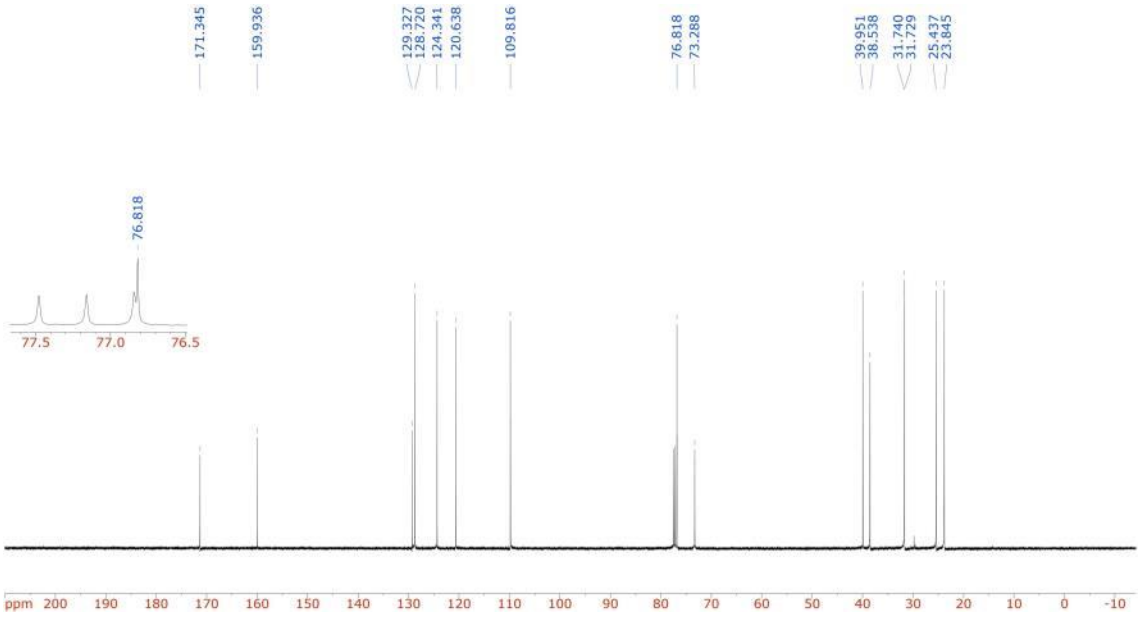

Phenyl 2-(2,3-dihydrobenzofuran-3-yl)acetate (169g)

^{1}H-NMR ($CDCl_3$, 400 MHz)

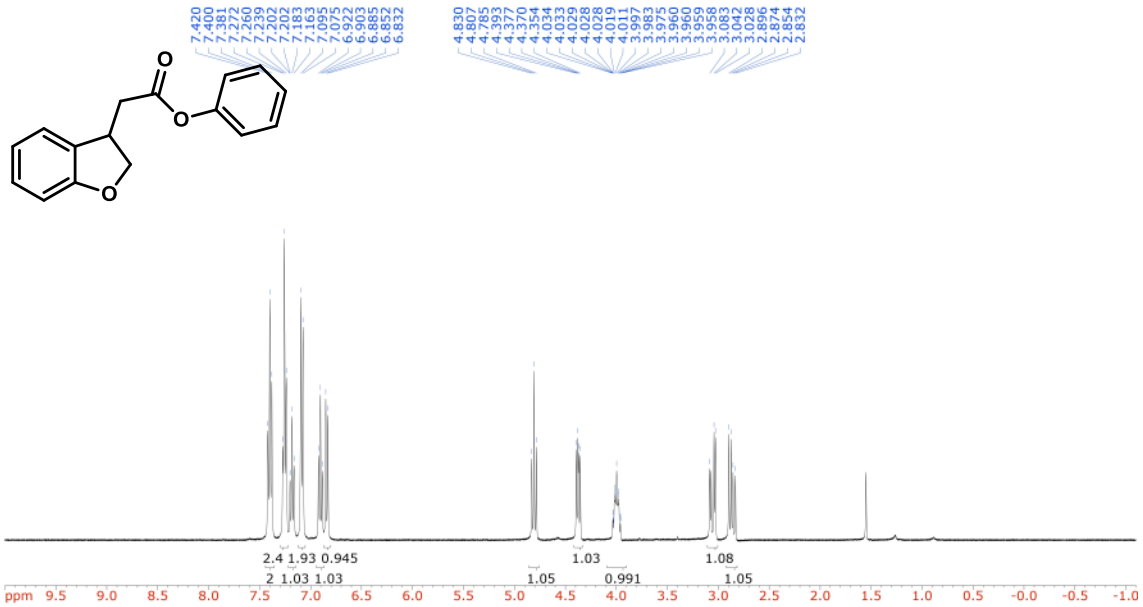

^{13}C-NMR ($CDCl_3$, 100 MHz)

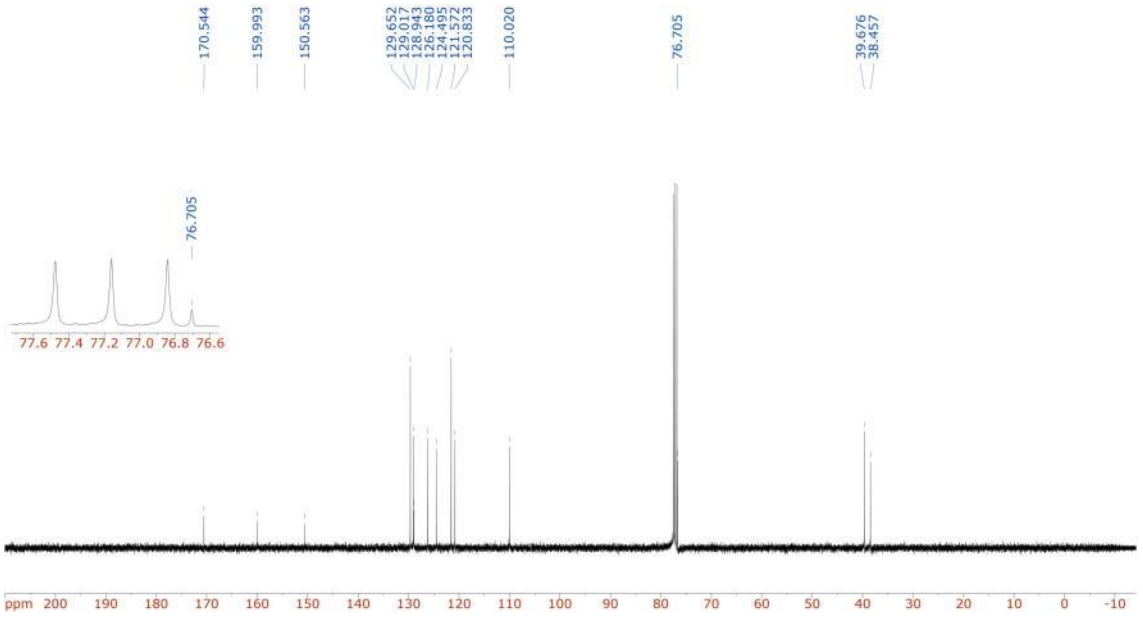

Benzyl 2-(2,3-dihydrobenzofuran-3-yl)acetate (169h)

^{1}H-NMR ($CDCl_3$, 400 MHz)

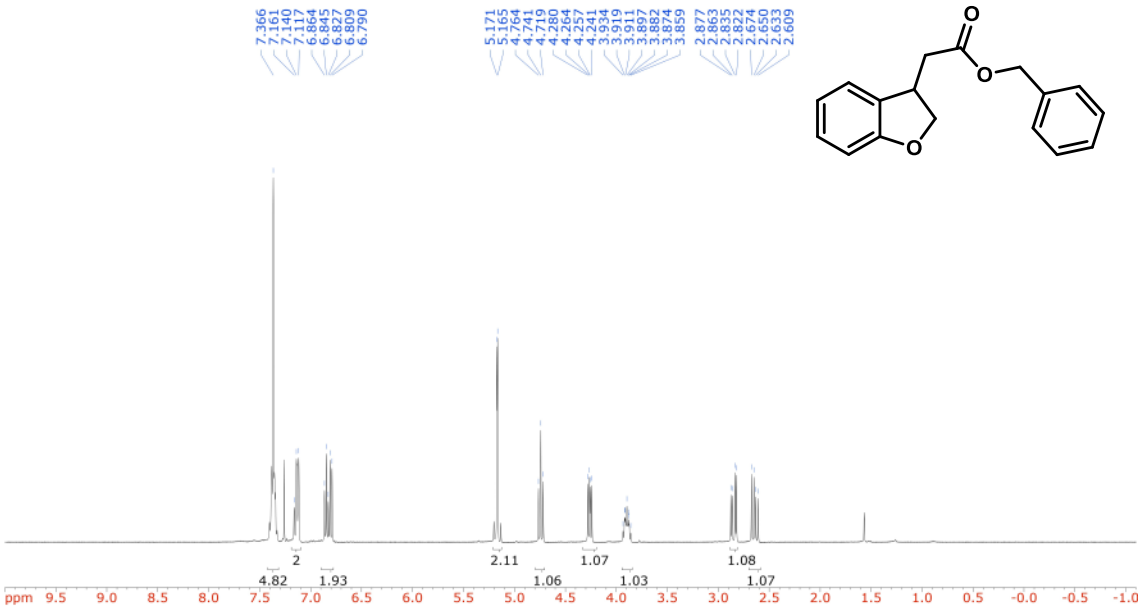

^{13}C-NMR ($CDCl_3$, 100 MHz)

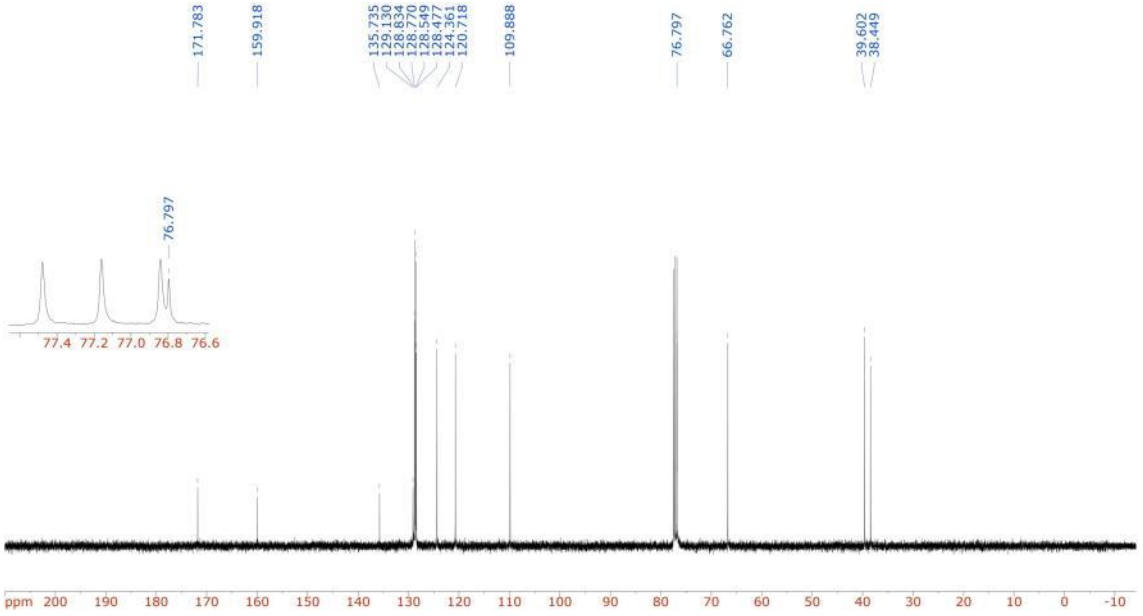

2-Methoxyethyl 2-(2,3-dihydrobenzofuran-3-yl)acetate (169i)

^{1}H-NMR ($CDCl_3$, 400 MHz)

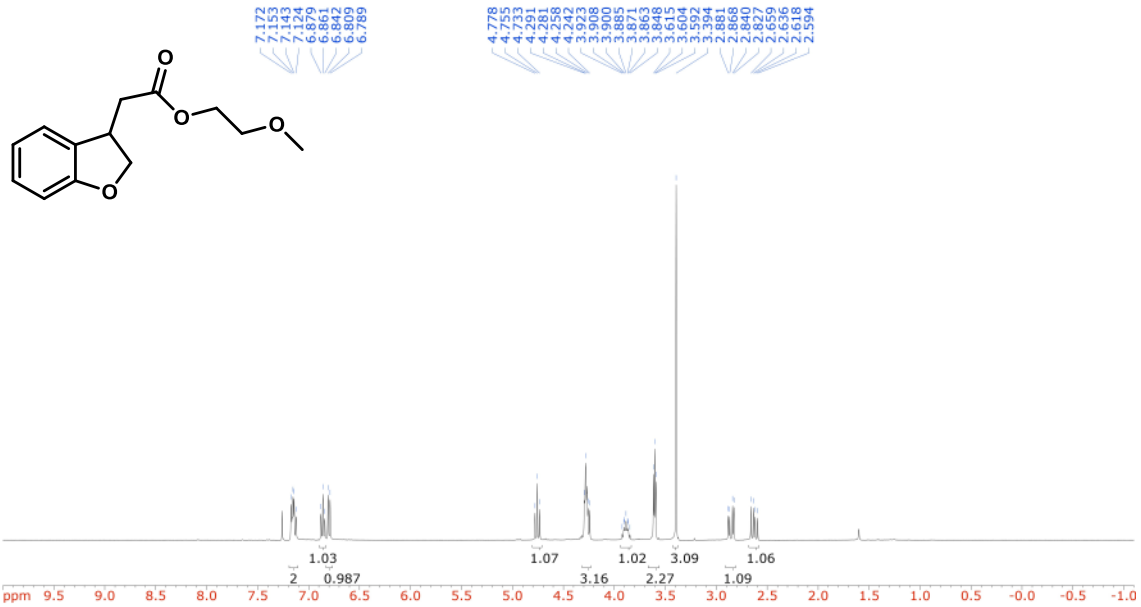

^{13}C-NMR ($CDCl_3$, 100 MHz)

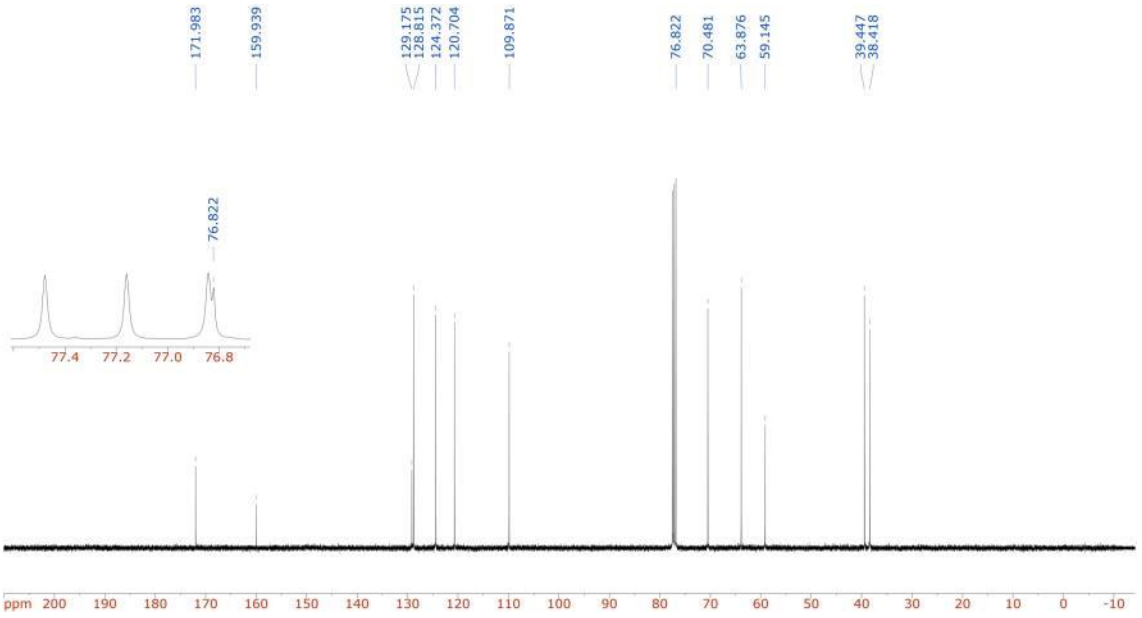

Methyl 2-(2-(2,3-dihydrobenzofuran-3-yl)acetoxy)propanoate (169j)

^{1}H-NMR ($CDCl_3$, 400 MHz)

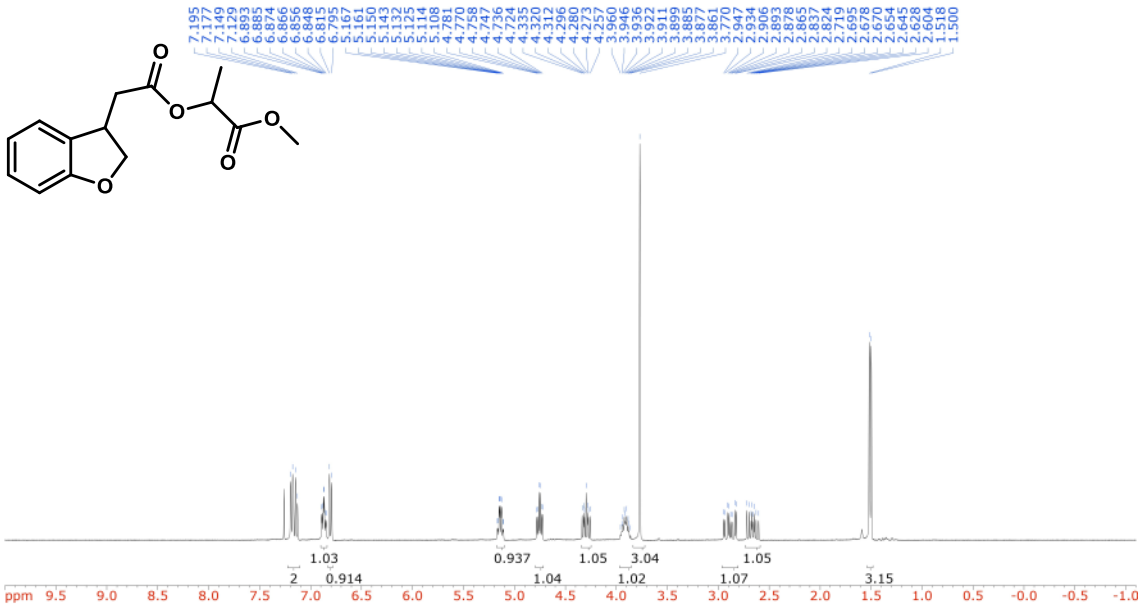

^{13}C-NMR ($CDCl_3$, 100 MHz)

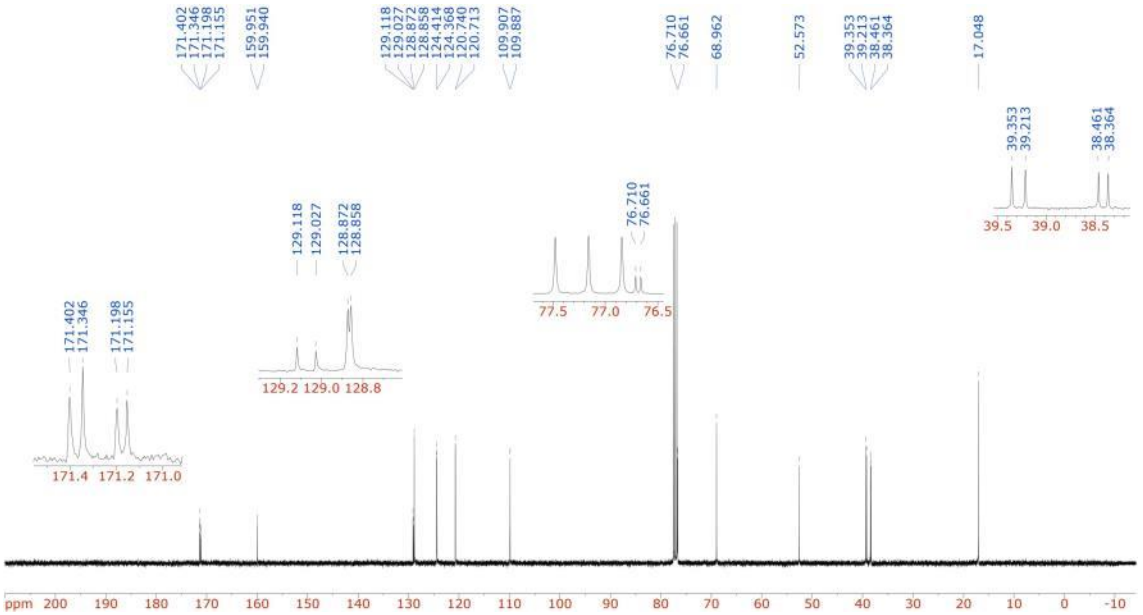

(Z)-Pent-2-en-1-yl 2-(2,3-dihydrobenzofuran-3-yl)acetate (169k)

^{1}H-NMR ($CDCl_3$, 400 MHz)

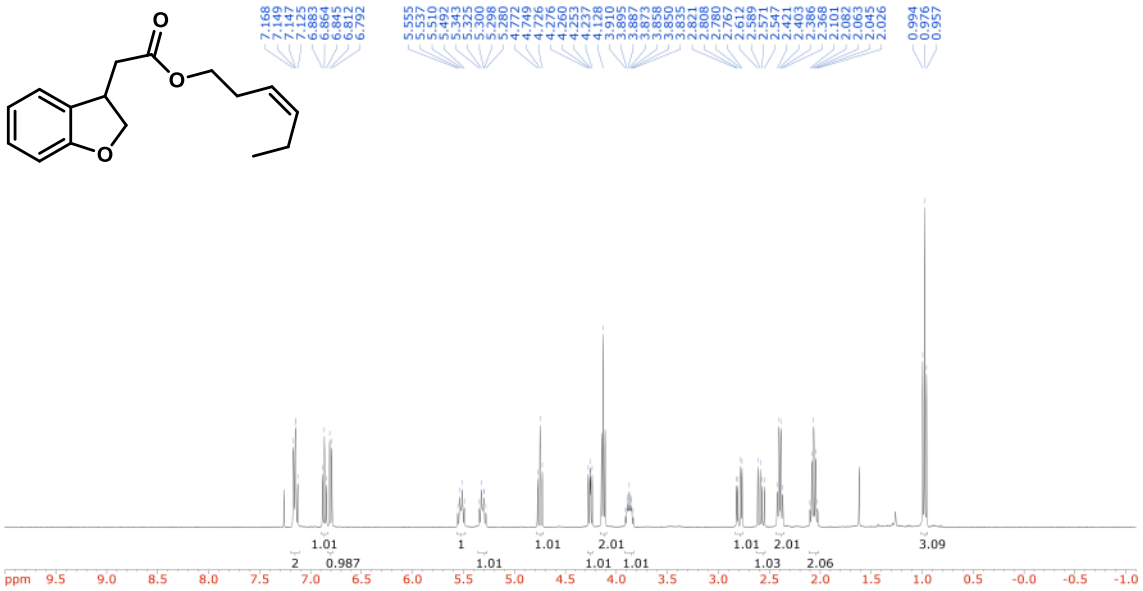

^{13}C-NMR ($CDCl_3$, 100 MHz)

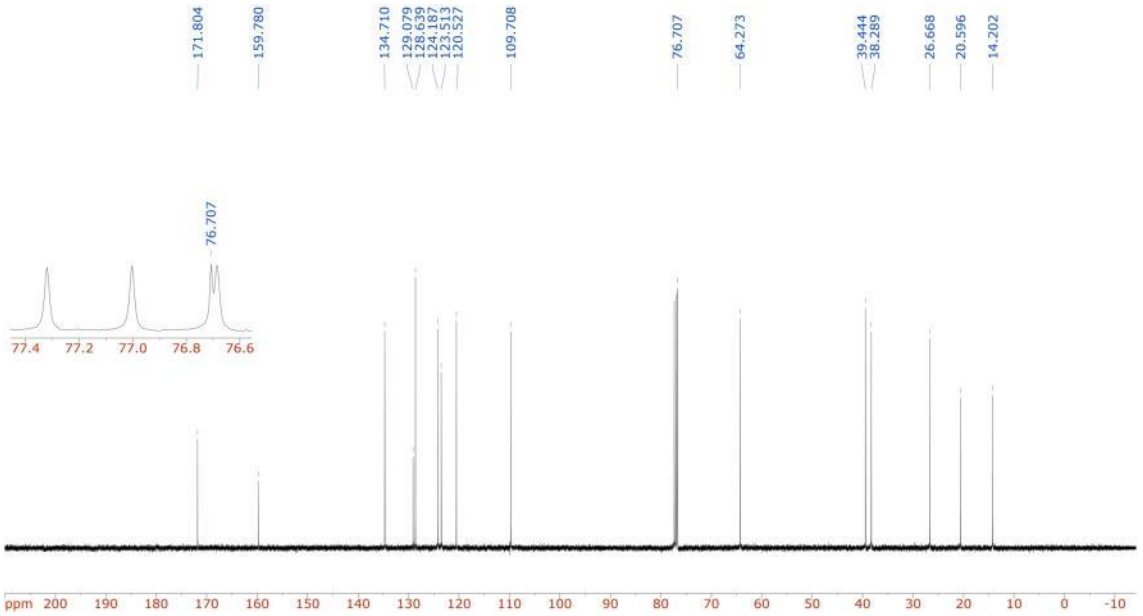

2-Chloroethyl 2-(2,3-dihydrobenzofuran-3-yl)acetate (169l)

^{1}H-NMR ($CDCl_3$, 400 MHz)

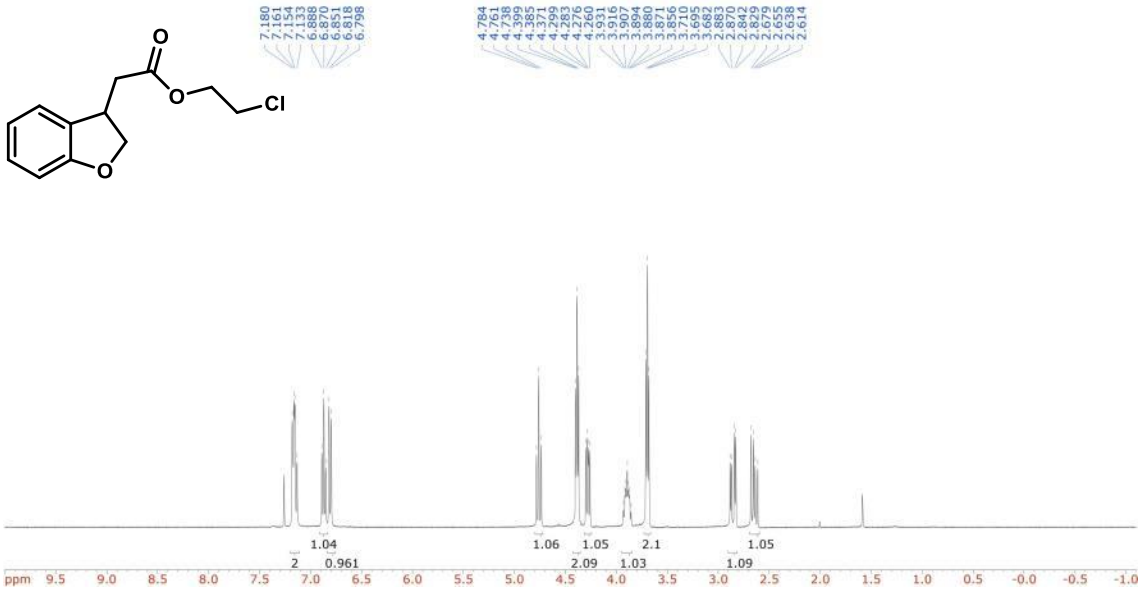

^{13}C-NMR ($CDCl_3$, 100 MHz)

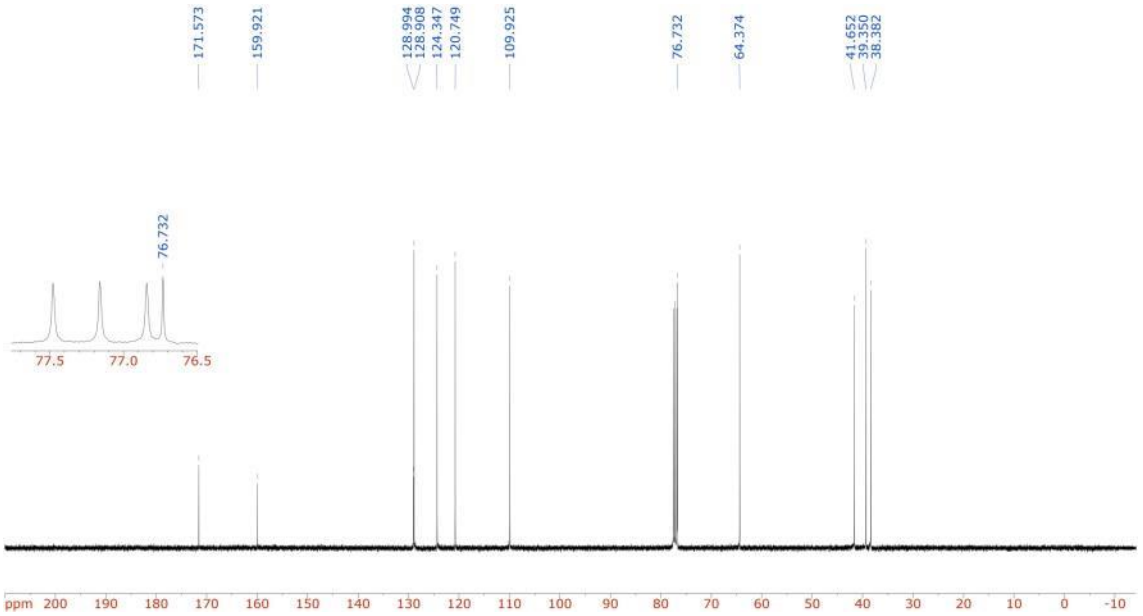

_n_-Butyl 2-(6-methyl-2,3-dihydrobenzofuran-3-yl)acetate (176a)

^{1}H-NMR ($CDCl_3$, 400 MHz)

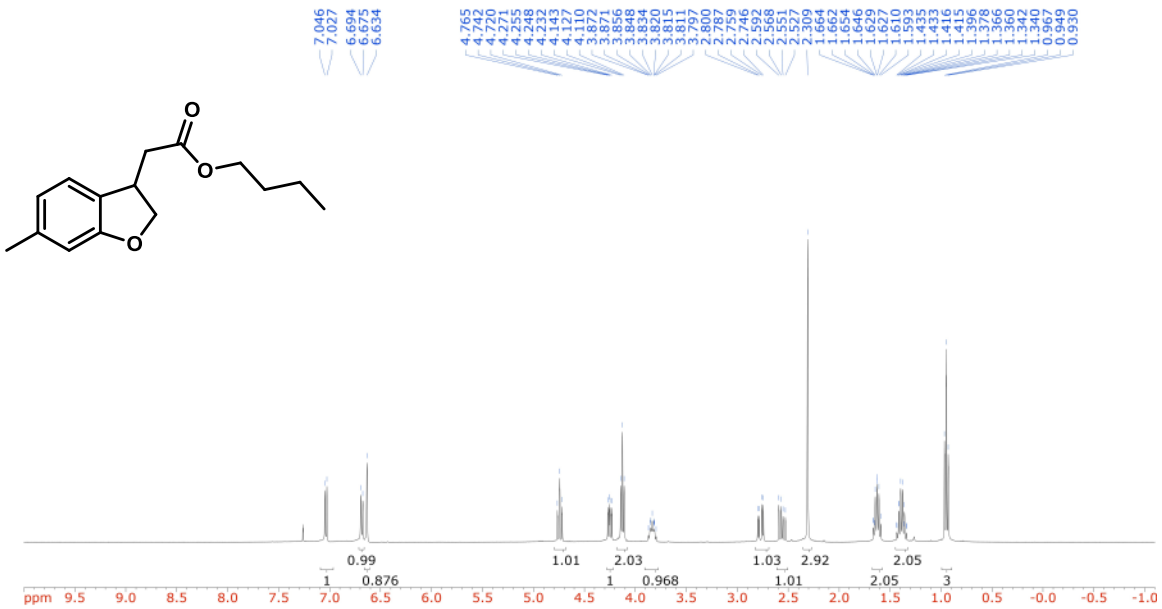

^{13}C-NMR ($CDCl_3$, 100 MHz)

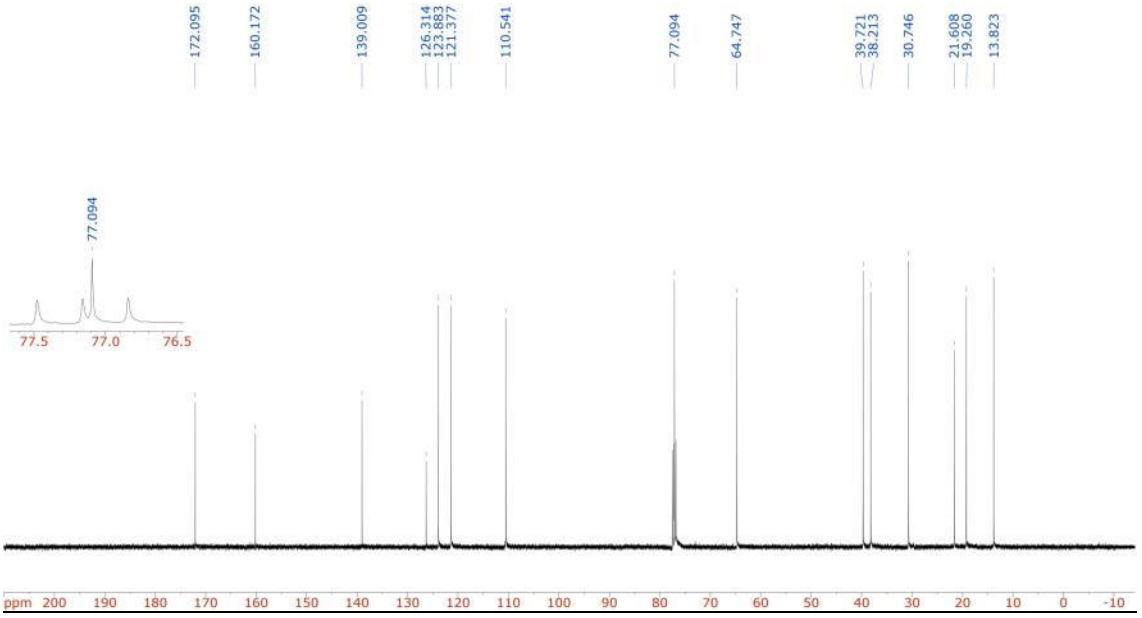

_n_-Butyl 2-(5-methyl-2,3-dihydrobenzofuran-3-yl)acetate (176b)

^{1}H-NMR ($CDCl_3$, 400 MHz)

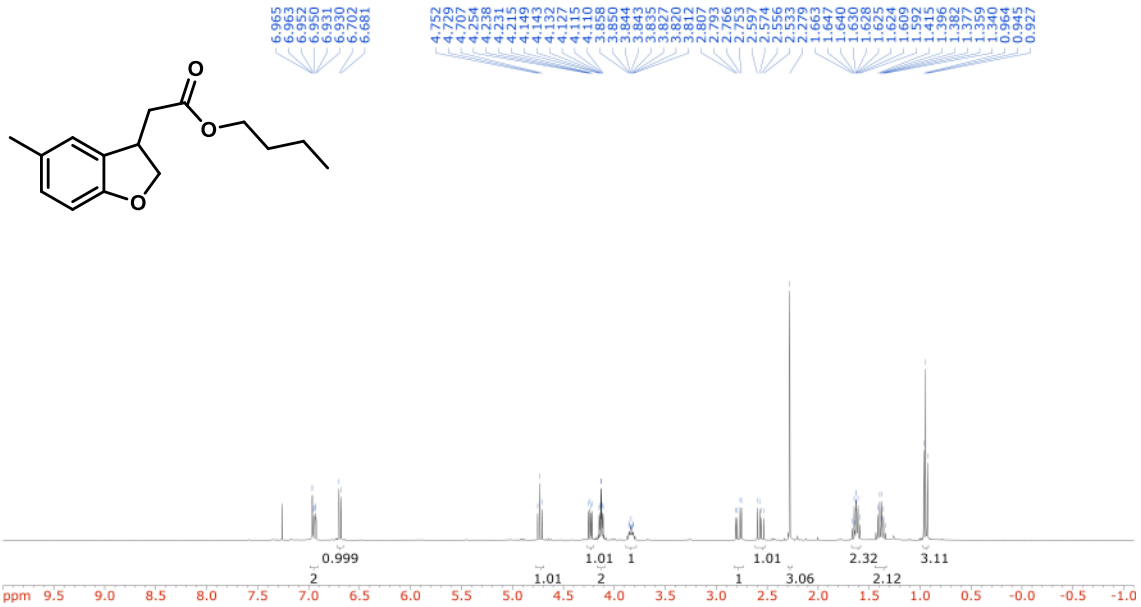

^{13}C-NMR ($CDCl_3$, 100 MHz)

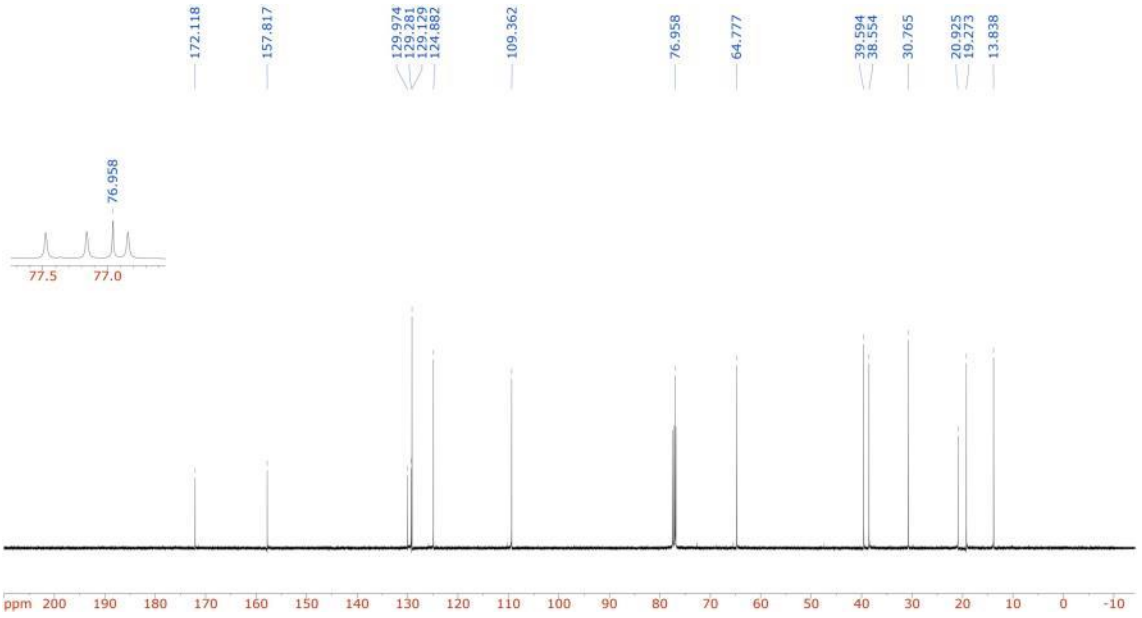

_n_-Butyl 2-(7-methyl-2,3-dihydrobenzofuran-3-yl)acetate (176c)

^{1}H-NMR ($CDCl_3$, 400 MHz)

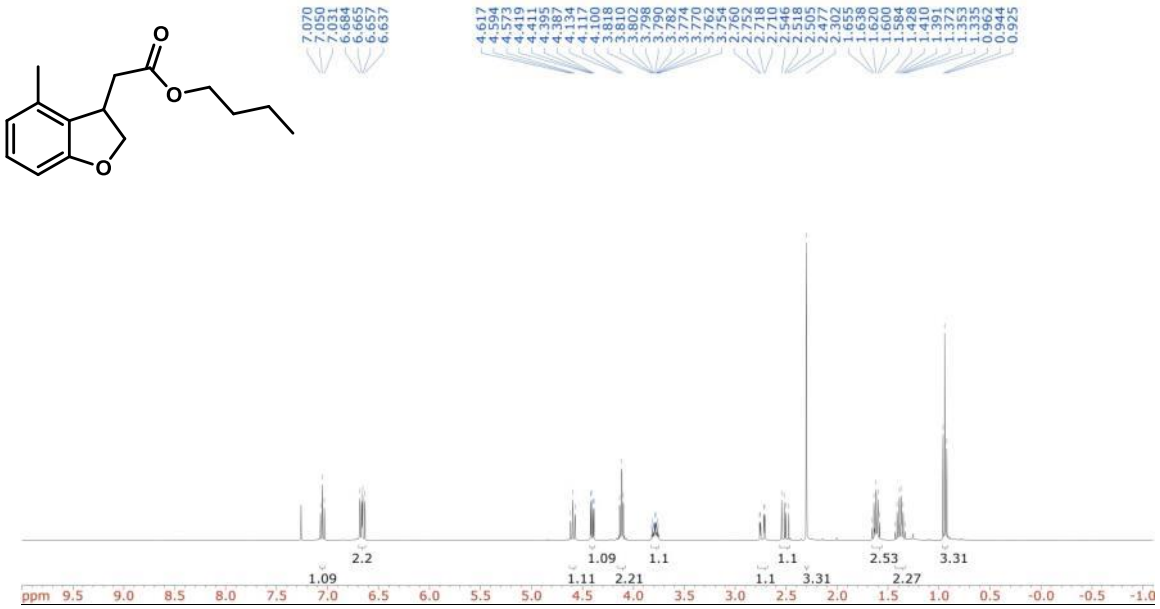

^{13}C-NMR ($CDCl_3$, 100 MHz)

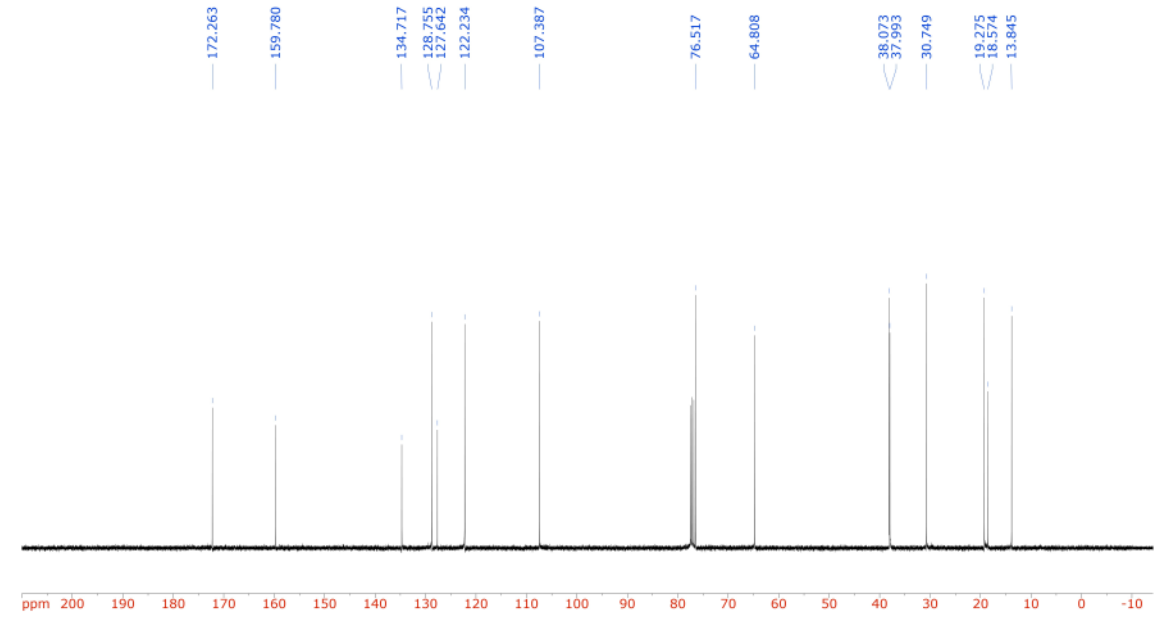

_n_-Butyl 2-(5-(_tert_-butyl)-2,3-dihydrobenzofuran-3-yl)acetate (176d)

^{1}H-NMR ($CDCl_3$, 400 MHz)

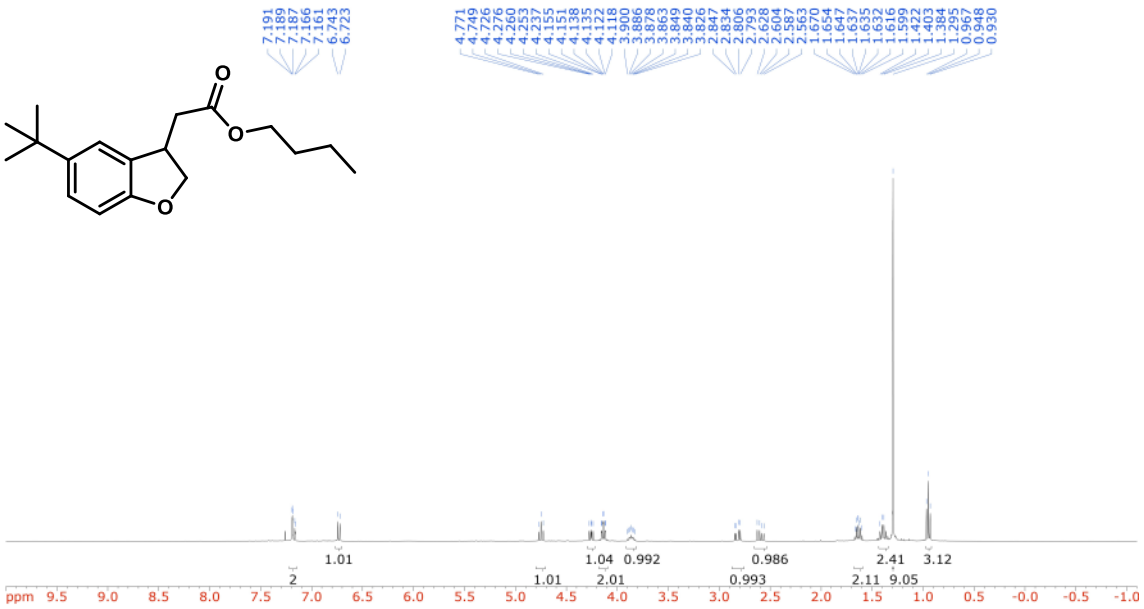

^{13}C-NMR ($CDCl_3$, 100 MHz)

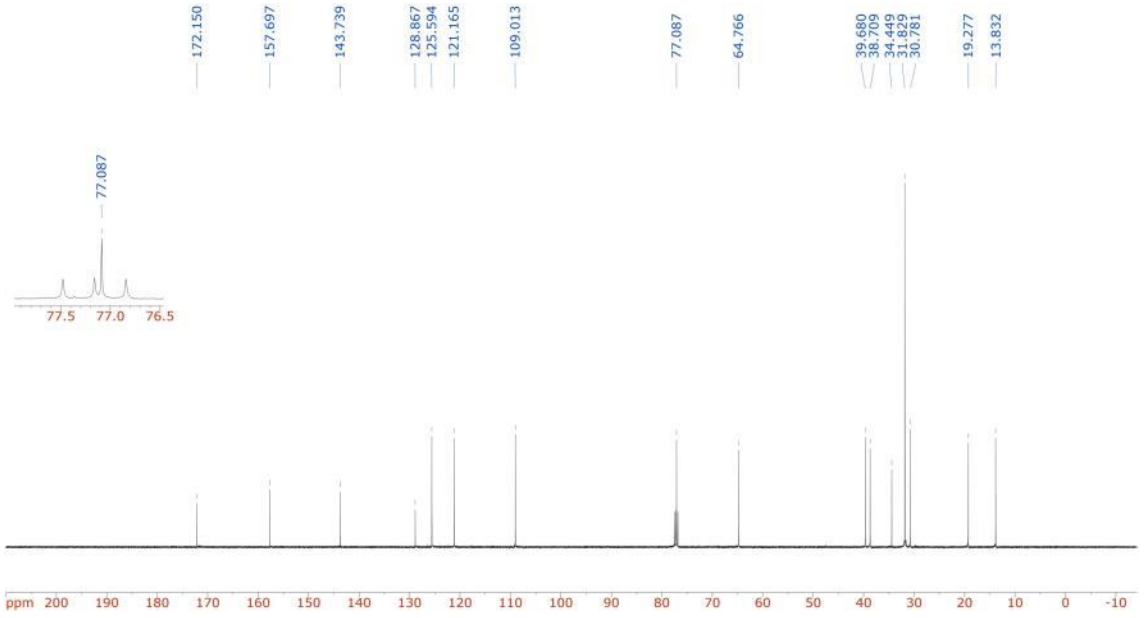

_n_-Butyl 2-(6-fluoro-2,3-dihydrobenzofuran-3-yl)acetate (176e)

^{1}H-NMR ($CDCl_3$, 400 MHz)

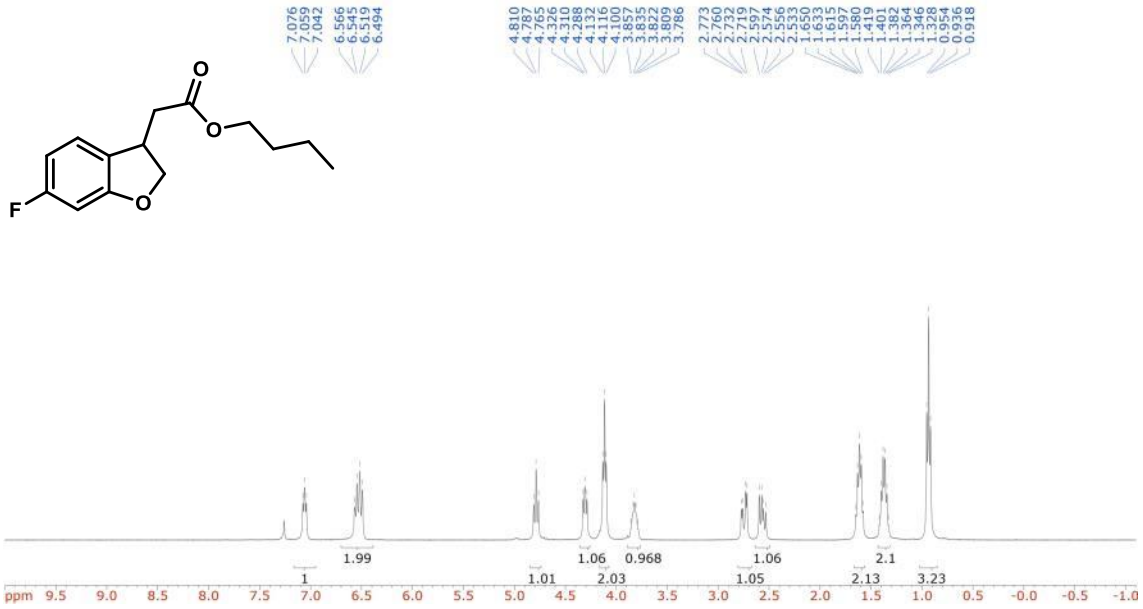

^{13}C-NMR ($CDCl_3$, 100 MHz)

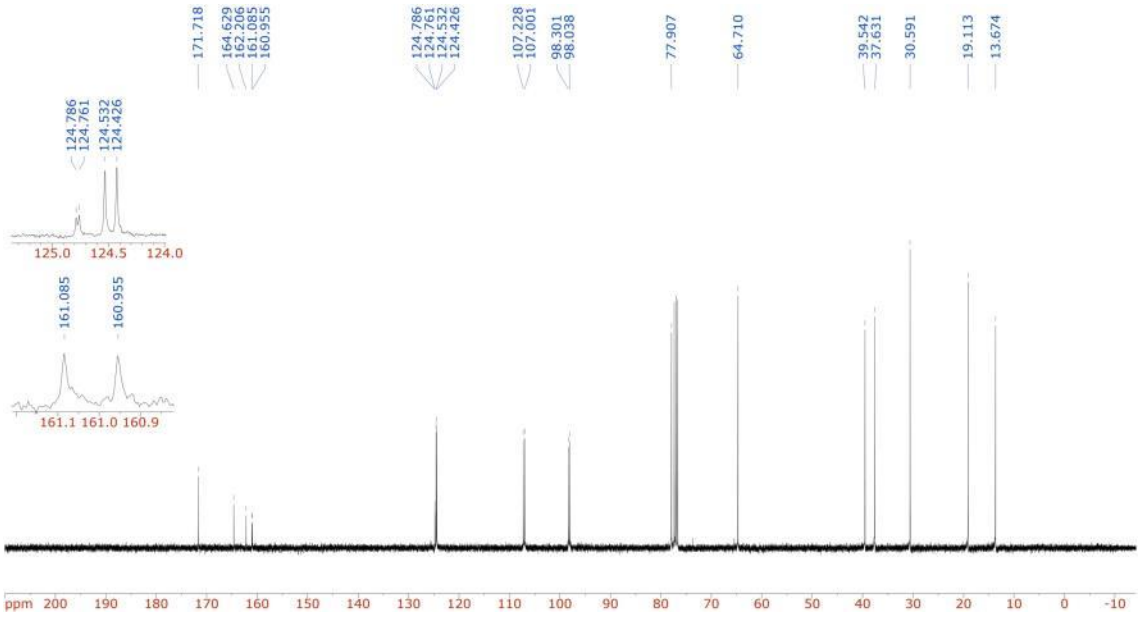

_n_-Butyl 2-(6-fluoro-2,3-dihydrobenzofuran-3-yl)acetate (176e)

^{19}F-NMR ($CDCl_3$, 376 MHz)

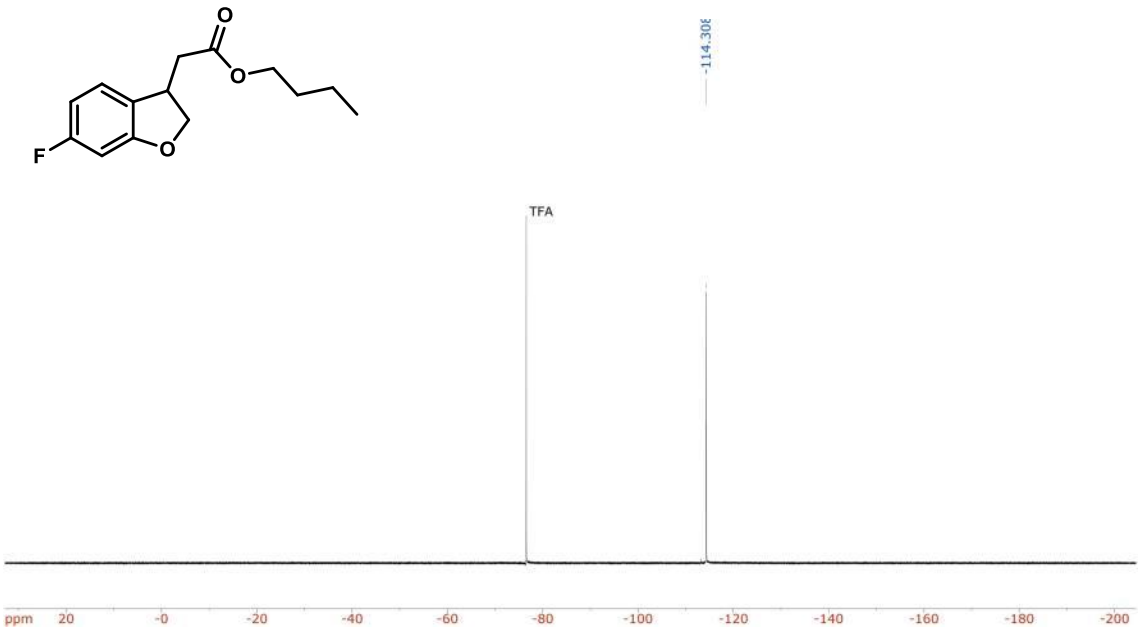

_n_-Butyl 2-(5-chloro-2,3-dihydrobenzofuran-3-yl)acetate (176f)

^{1}H-NMR ($CDCl_3$, 400 MHz)

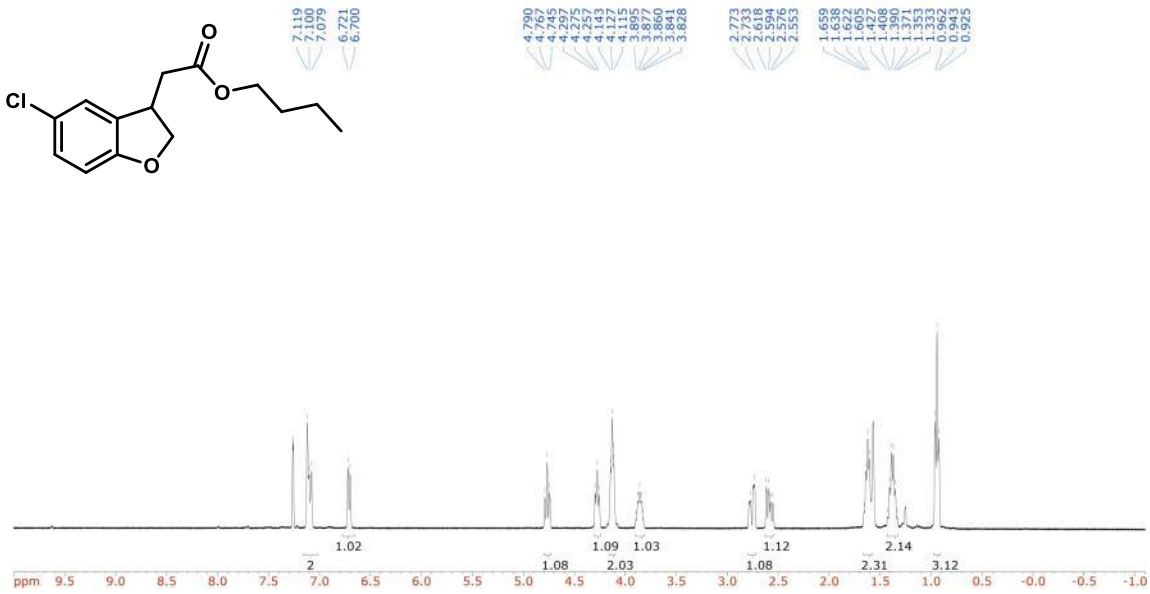

^{13}C-NMR ($CDCl_3$, 100 MHz)

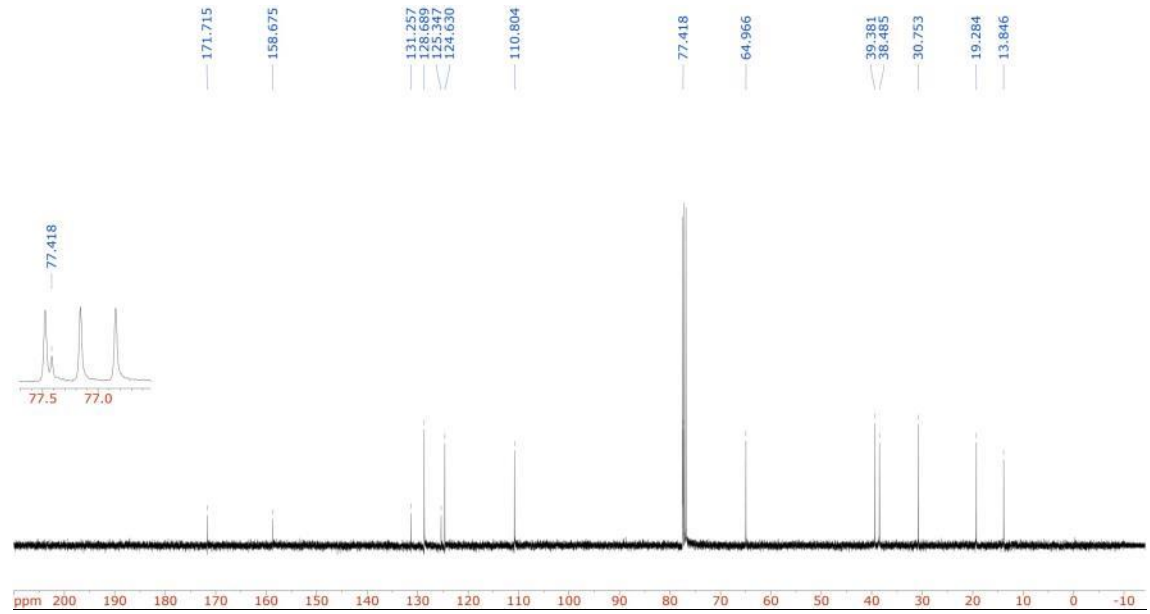

n-Butyl 2-(7-bromo-2,3-dihydrobenzofuran-3-yl)acetate (176g)

^{1}H-NMR ($CDCl_3$, 400 MHz)

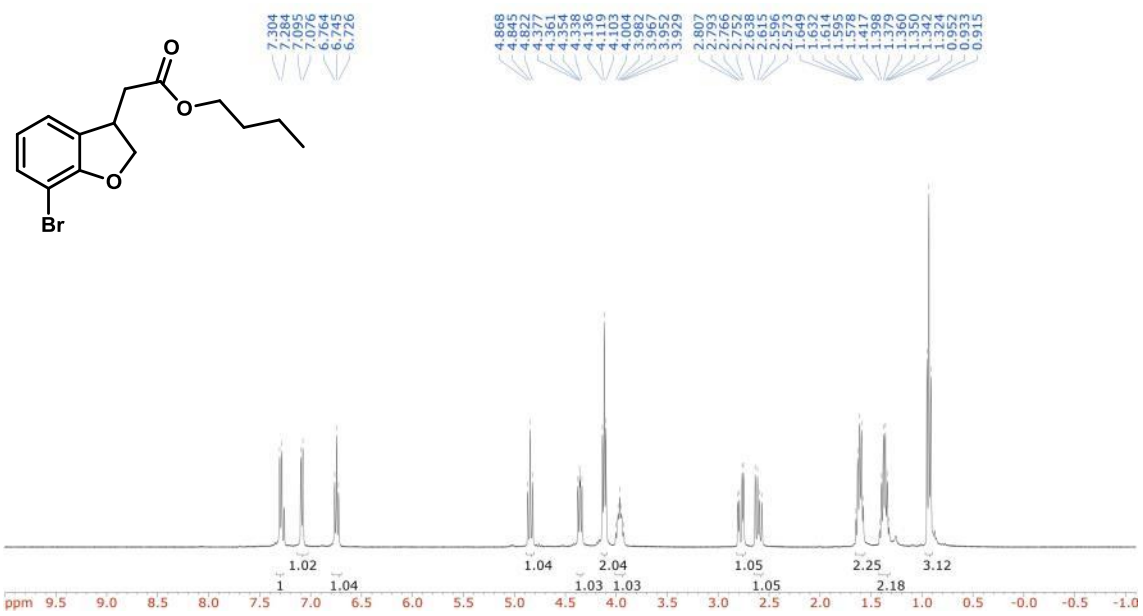

^{13}C-NMR ($CDCl_3$, 100 MHz)

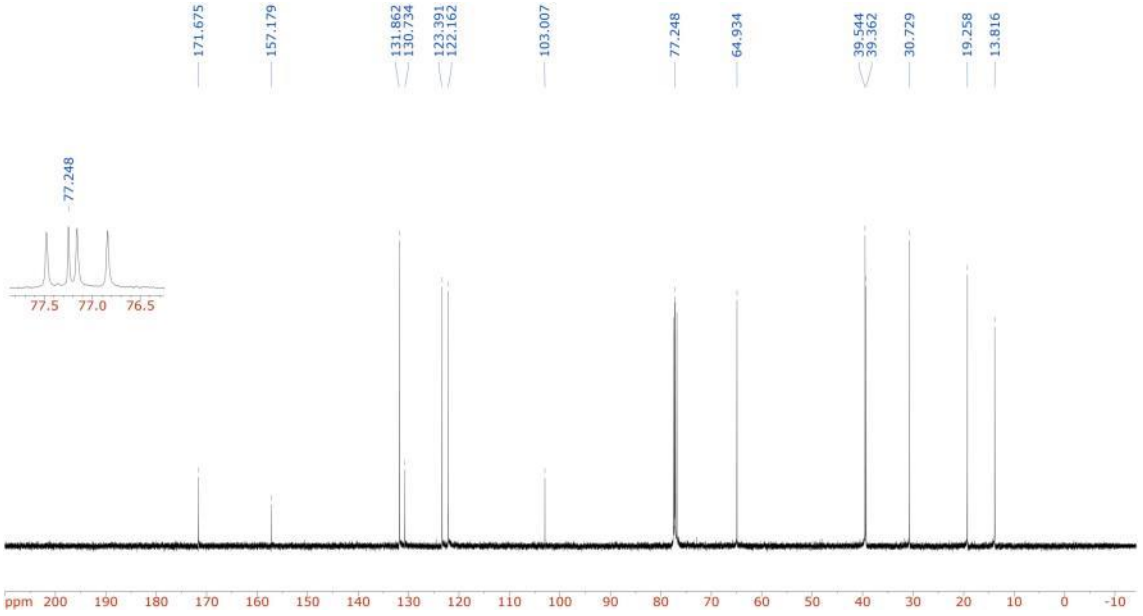

Methyl 3-(2-butoxy-2-oxoethyl)-2,3-dihydrobenzofuran-5-carboxylate (176i)

^{1}H-NMR ($CDCl_3$, 400 MHz)

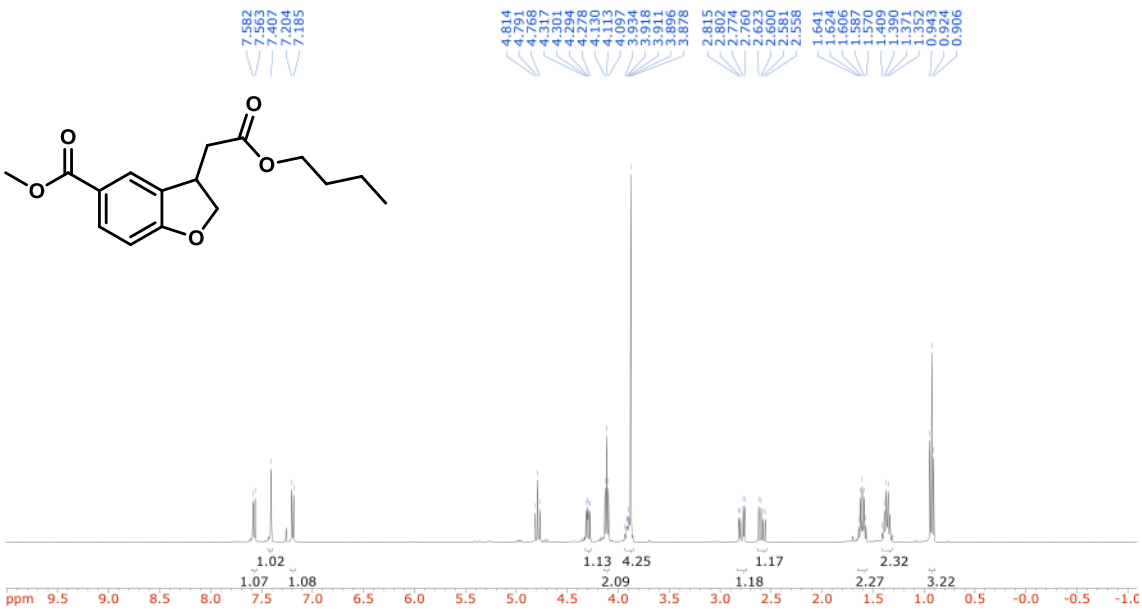

^{3}C-NMR ($CDCl_3$, 100 MHz)

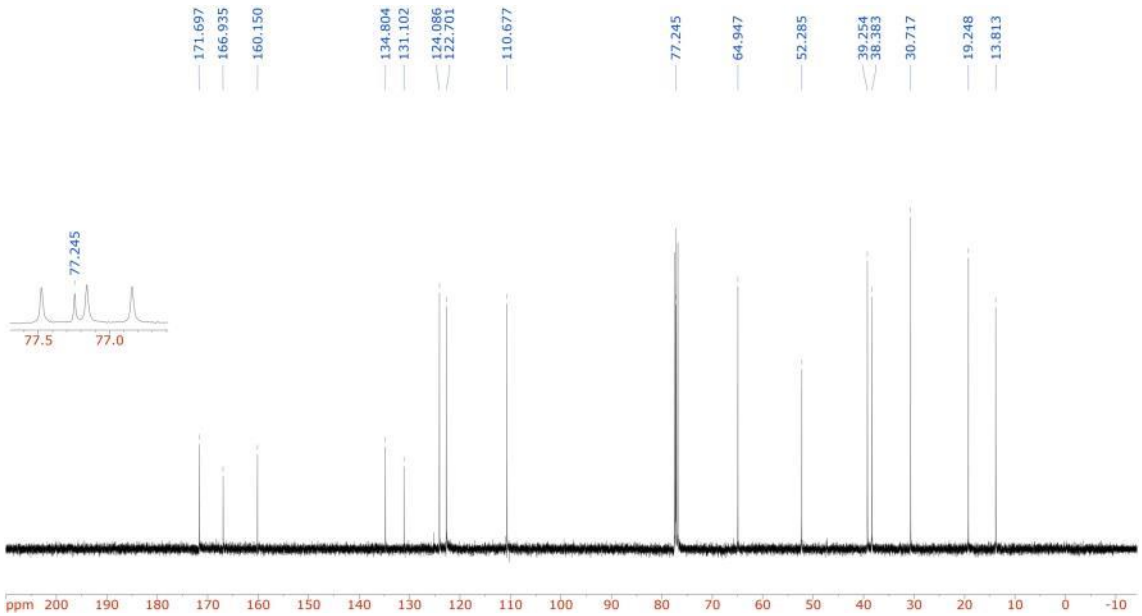

_n_-Butyl 2-(6-methoxy-2,3-dihydrobenzofuran-3-yl)acetate (176j)

^{1}H-NMR ($CDCl_3$, 400 MHz)

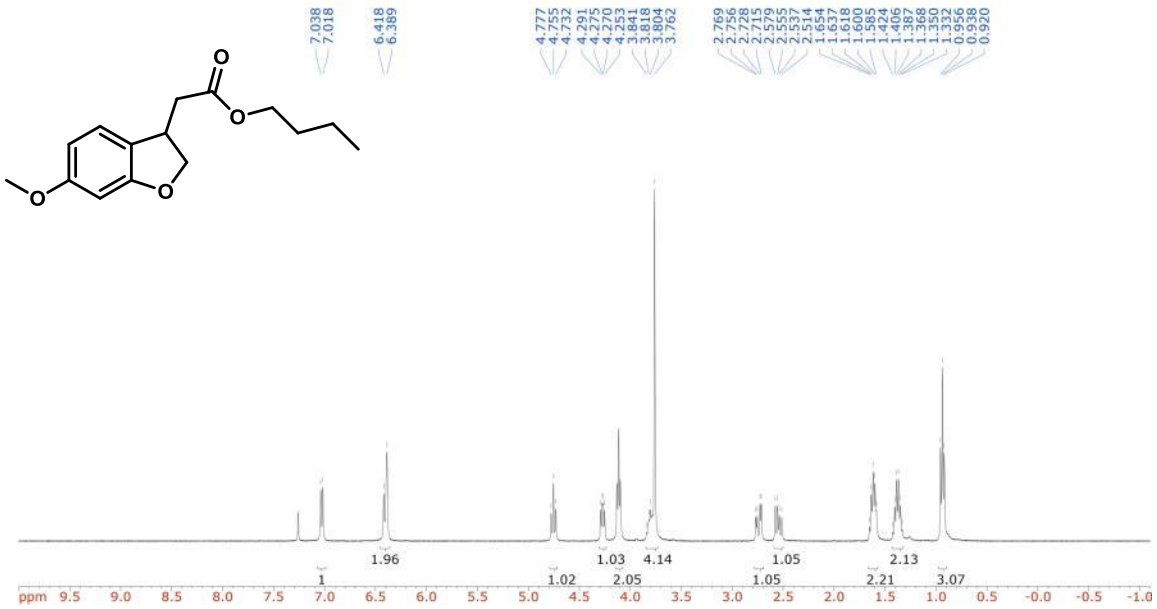

^{13}C-NMR ($CDCl_3$, 100 MHz)

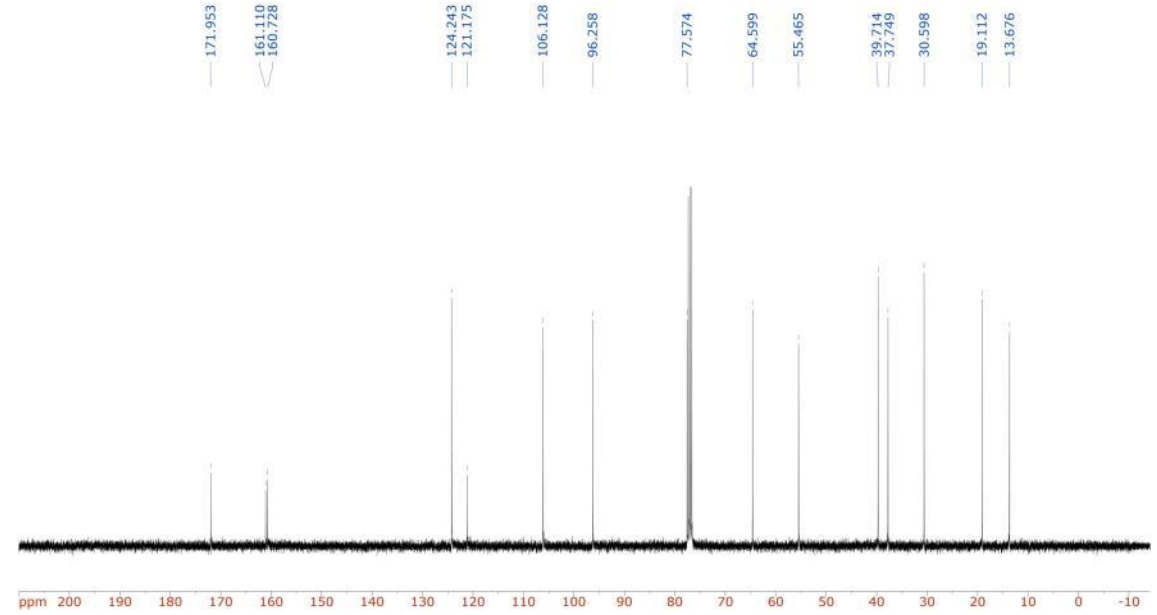

_n_-Butyl 2-(3-methyl-2,3-dihydrobenzofuran-3-yl)acetate (177b)

^{1}H-NMR ($CDCl_3$, 400 MHz)

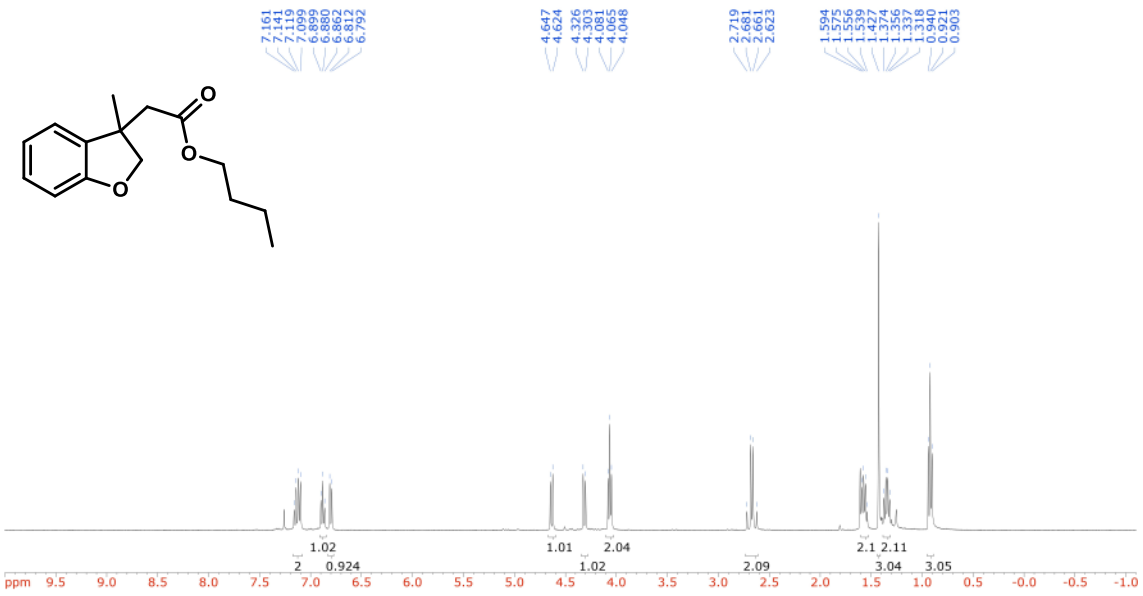

^{13}C-NMR ($CDCl_3$, 100 MHz)

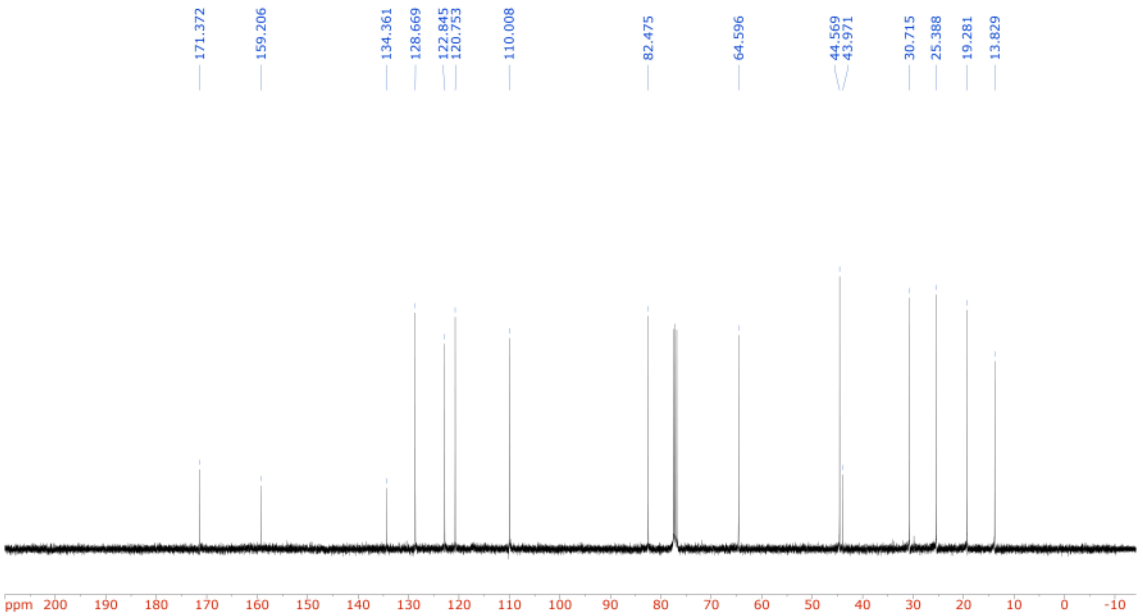

_n_-Butyl 2-(benzofuran-3-yl)acetate (178b)

^{1}H-NMR ($CDCl_3$, 400 MHz)

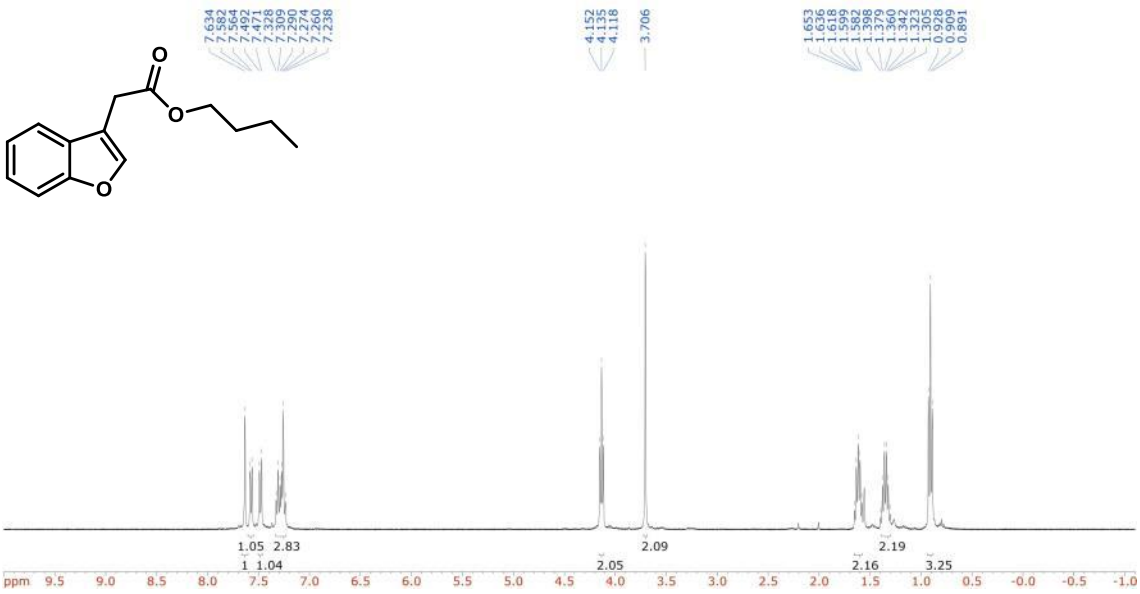

^{13}C-NMR ($CDCl_3$, 100 MHz)

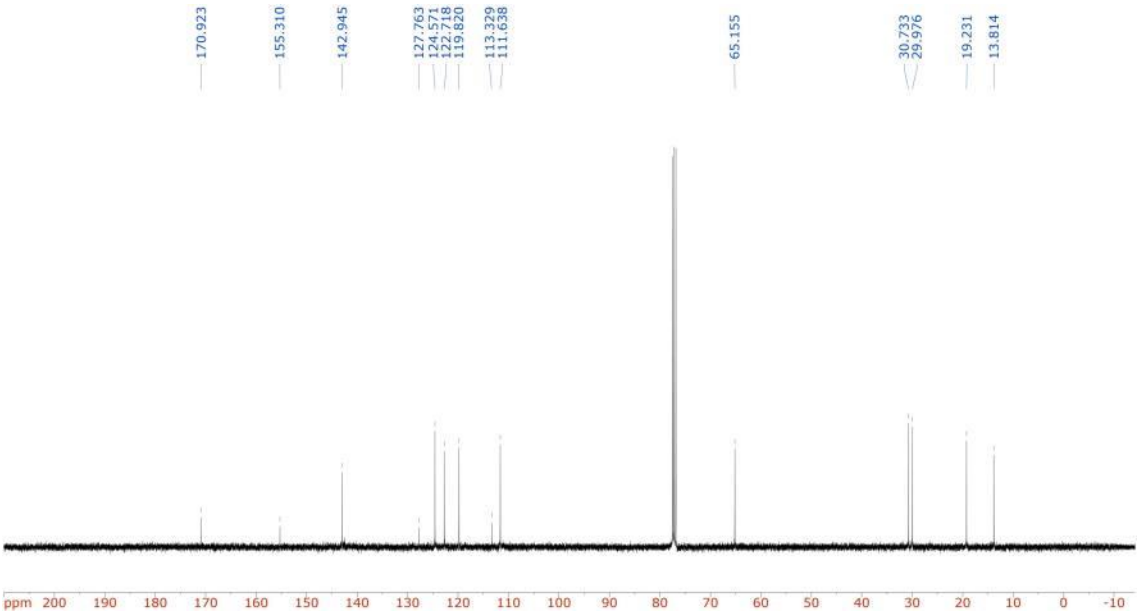

_n_-Butyl 2-(chroman-4-yl)acetate (179c)

^{1}H-NMR ($CDCl_3$, 400 MHz)

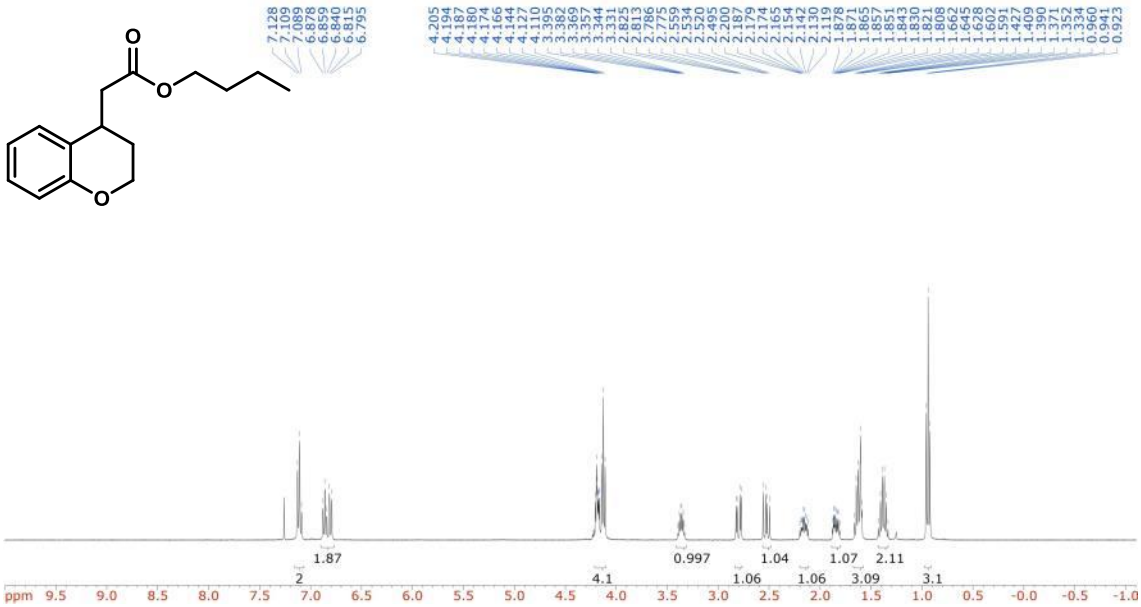

^{13}C-NMR ($CDCl_3$, 100 MHz)

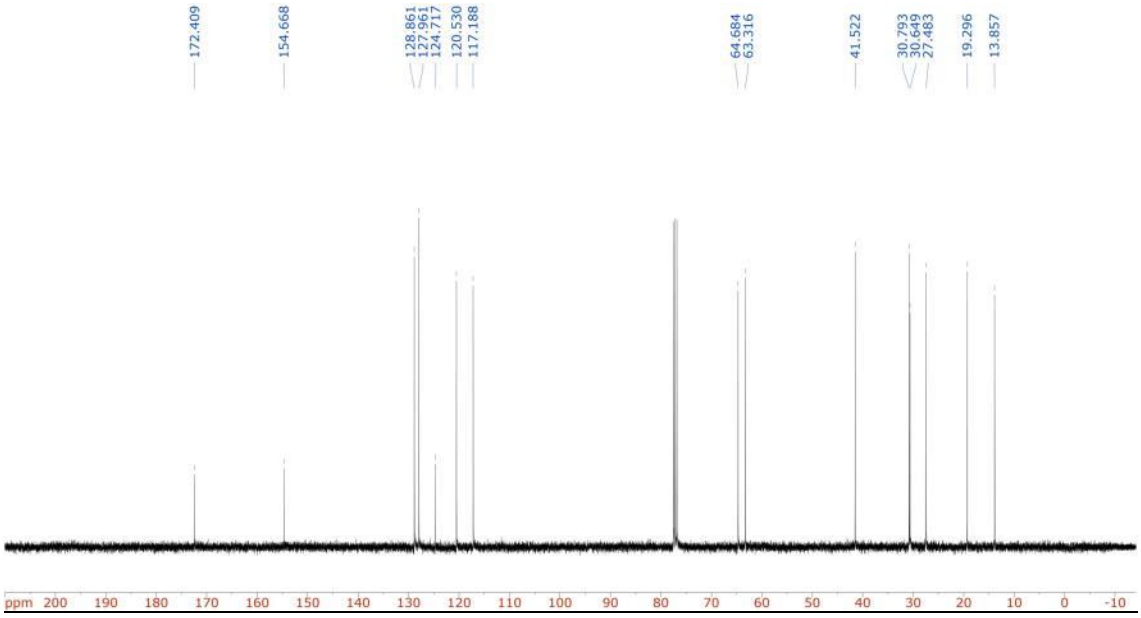

2-(allyloxy)benzenediazonium tetrafluoroborate (168)

^{1}H-NMR (DMSO-d_6, 400 MHz)

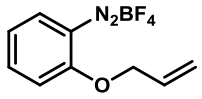

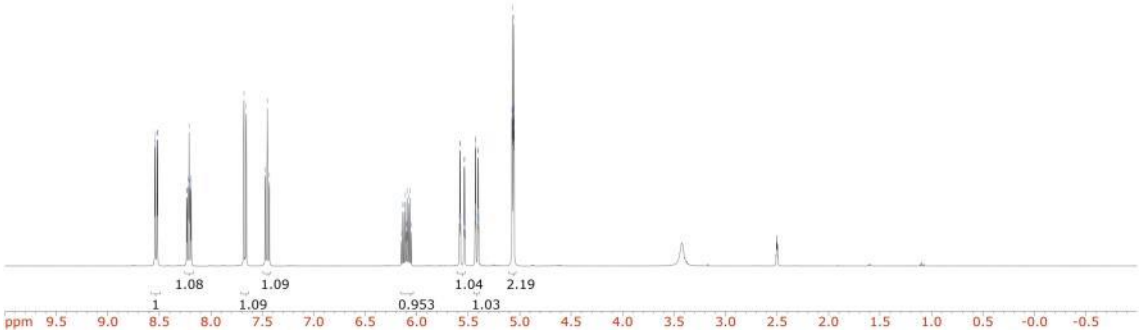

^{13}C-NMR (DMSO-d_6, 100 MHz)

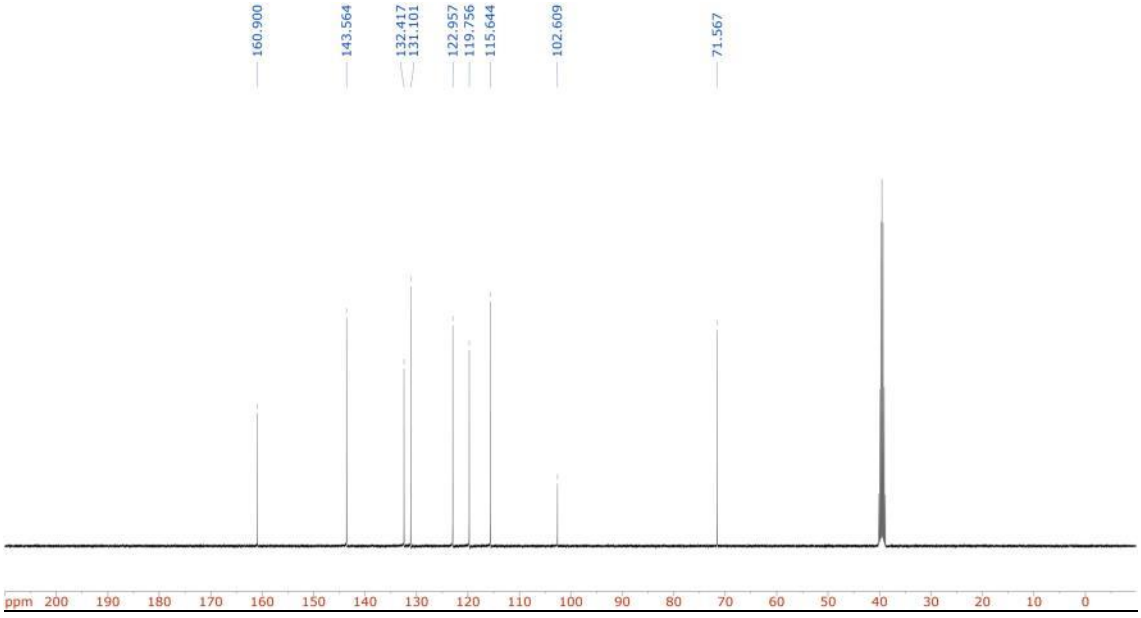

2-(allyloxy)-4-methylbenzenediazonium tetrafluoroborate (174a)

^{1}H-NMR (DMSO-d_6, 400 MHz)

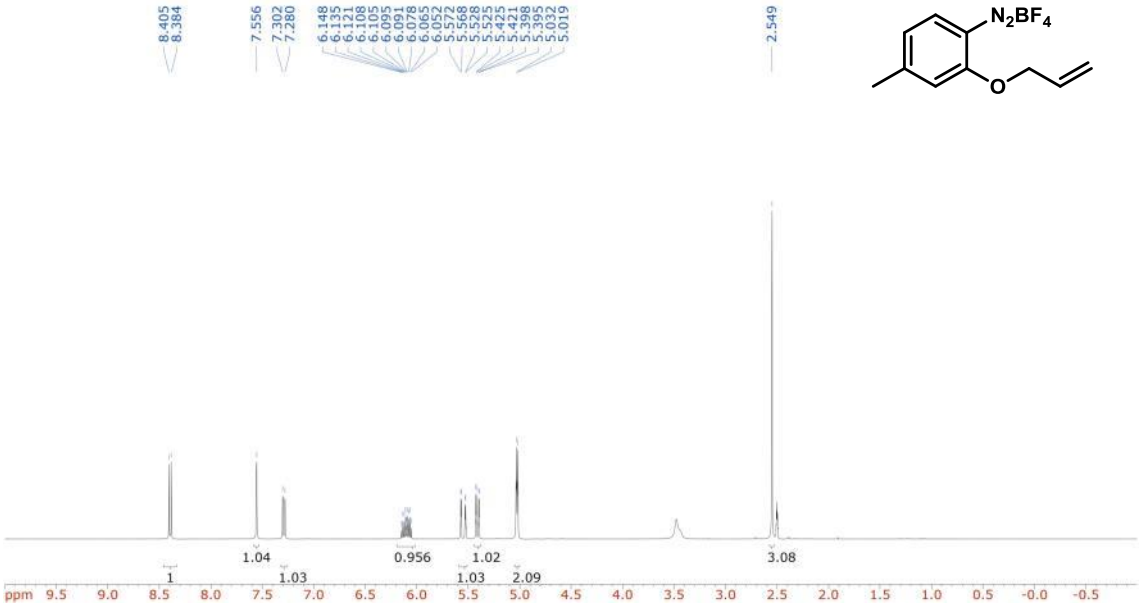

^{13}C-NMR (DMSO-d_6, 100 MHz)

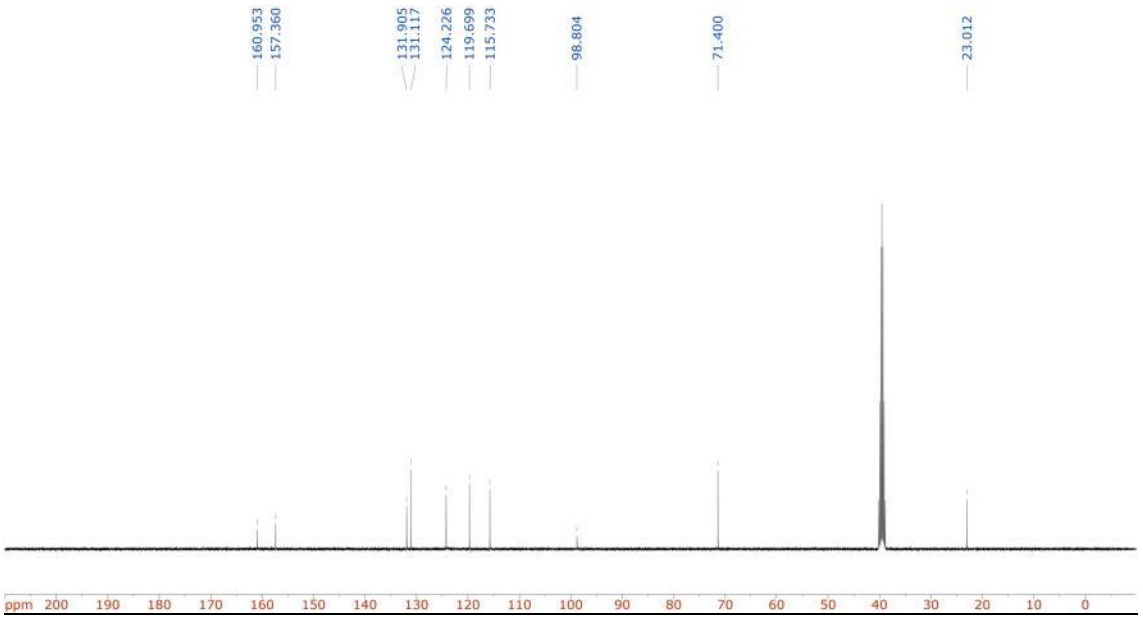

2-(allyloxy)-5-methylbenzenediazonium tetrafluoroborate (174b)

^{1}H-NMR (DMSO-d_6, 400 MHz)

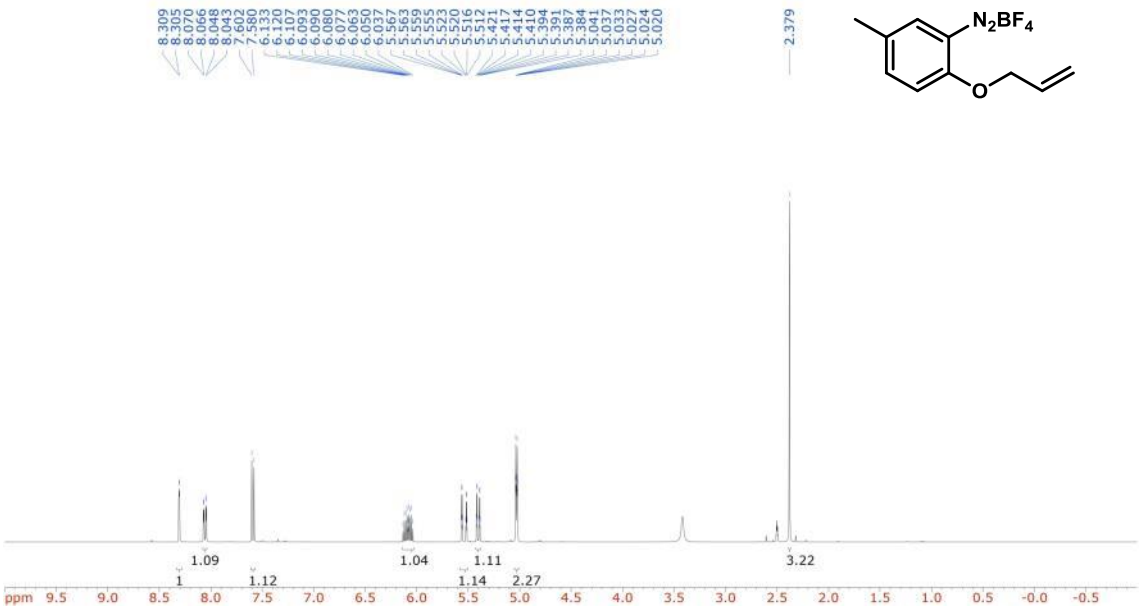

^{13}C-NMR (DMSO-d_6, 100 MHz)

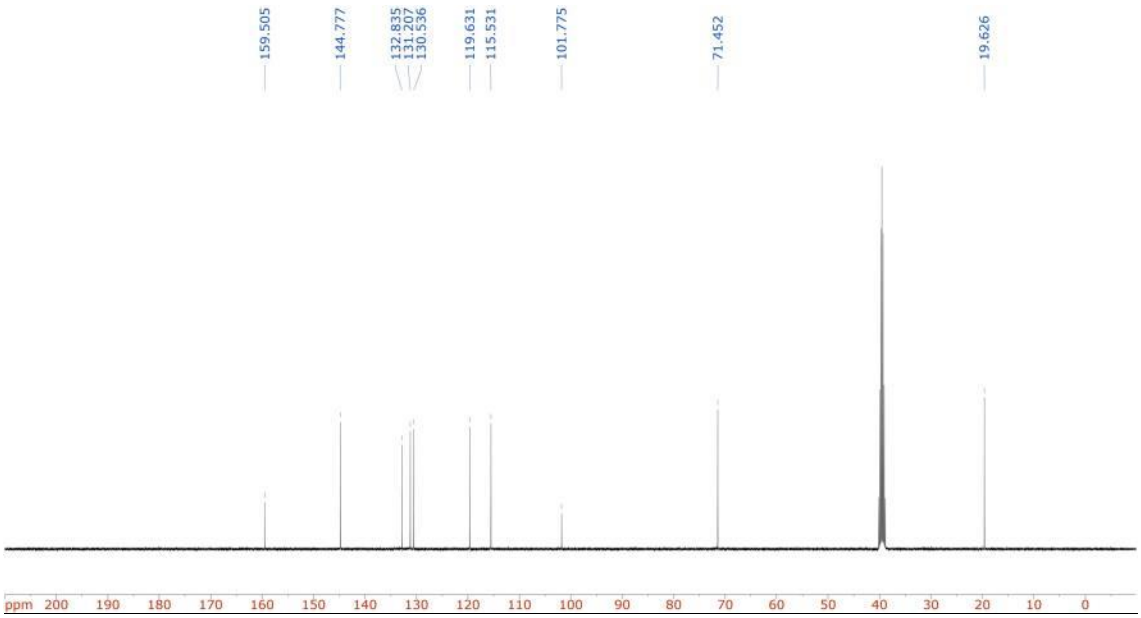

2-(allyloxy)-6-methylbenzenediazonium tetrafluoroborate (174c)

^{1}H-NMR (DMSO-d_6, 400 MHz)

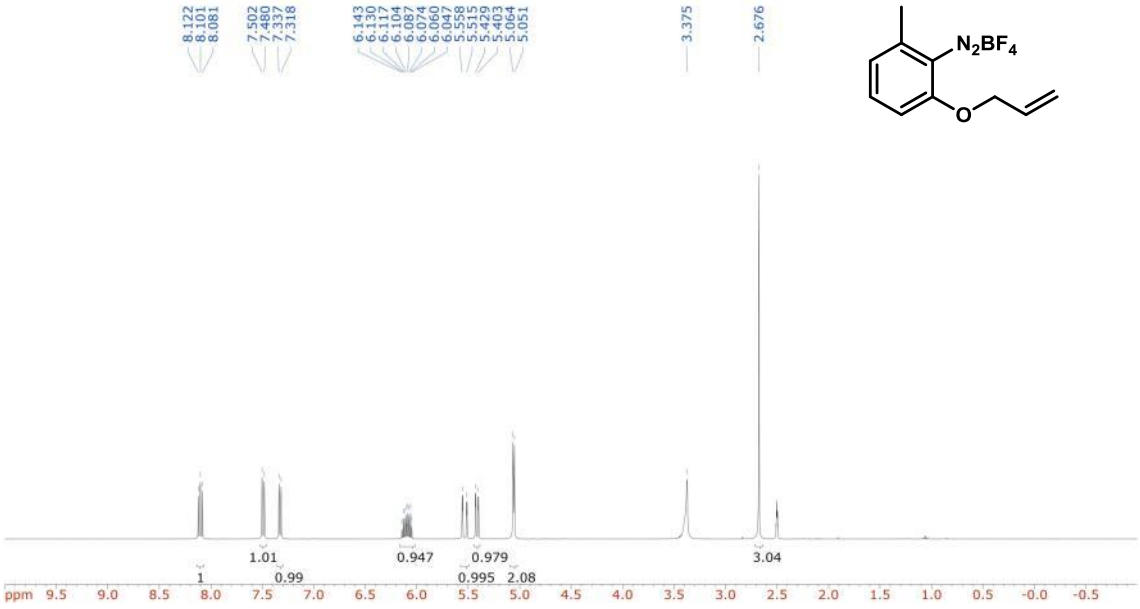

^{13}C-NMR (DMSO-d_6, 100 MHz)

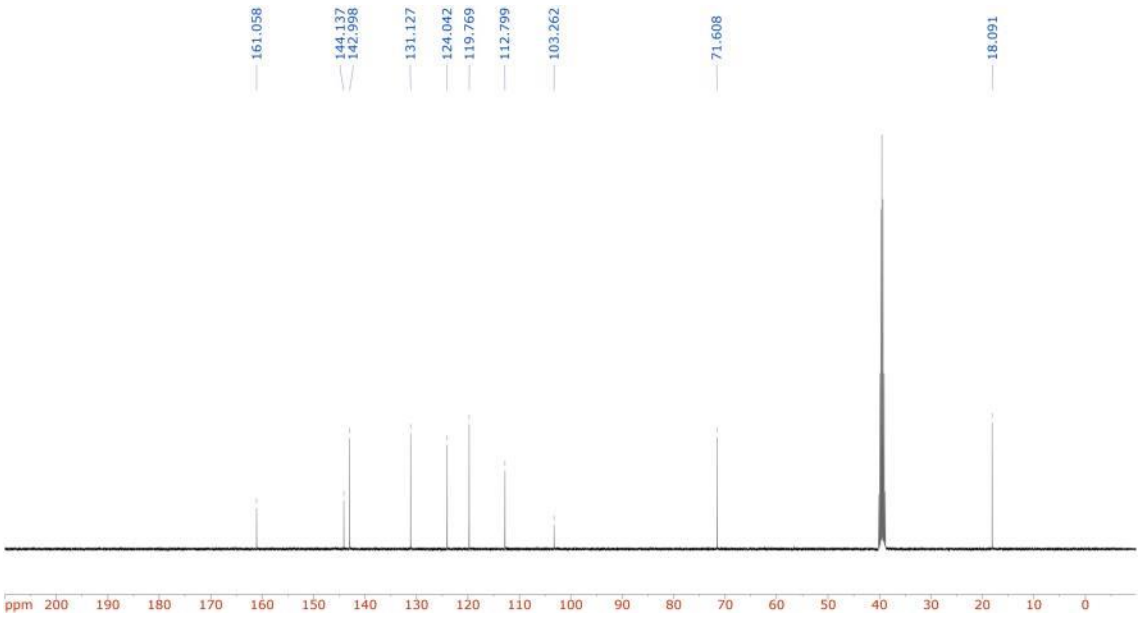

2-(allyloxy)-5-(*tert*-butyl)benzenediazonium tetrafluoroborate (174d)

^{1}H-NMR (DMSO-d_6, 400 MHz)

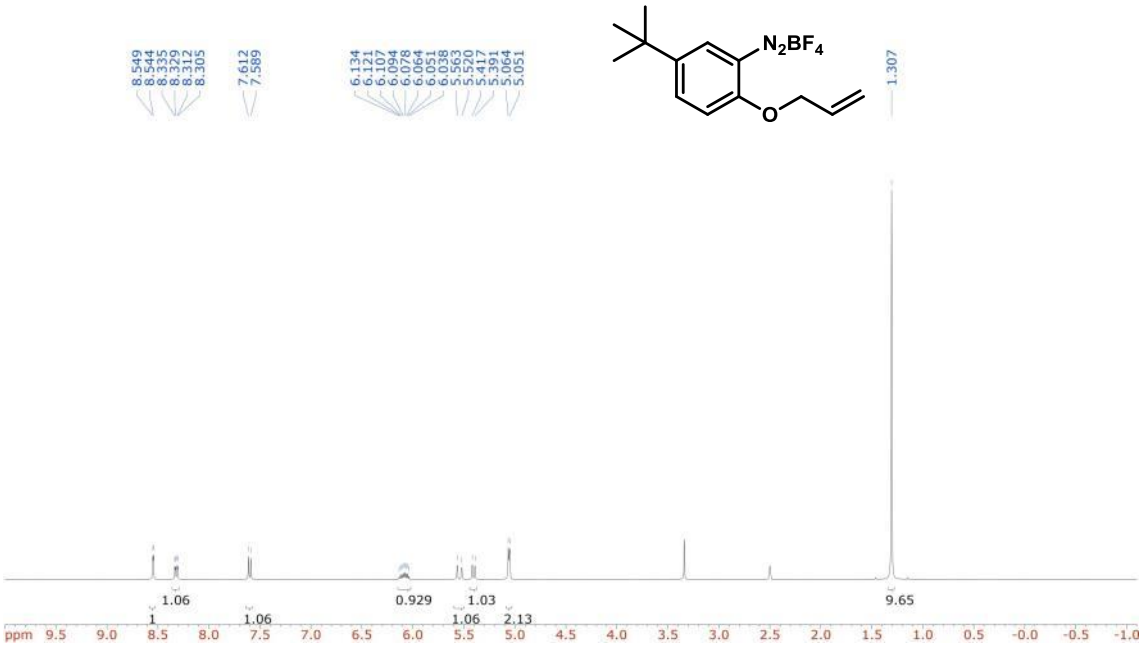

^{13}C-NMR (DMSO-d_6, 100 MHz)

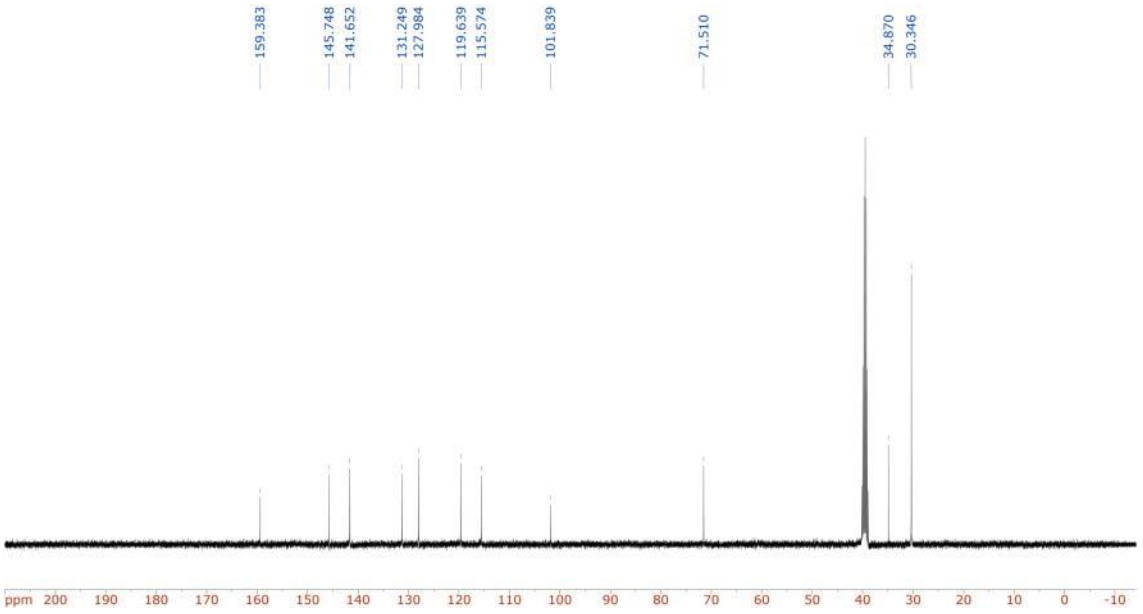

2-(allyloxy)-4-fluorobenzenediazonium tetrafluoroborate (174e)

^{1}H-NMR (DMSO-d_6, 400 MHz)

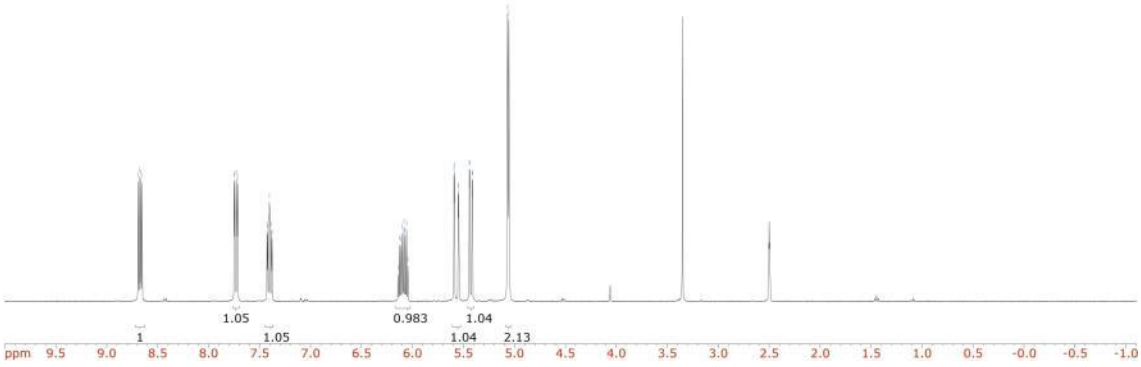

^{13}C-NMR (DMSO-d_6, 100 MHz)

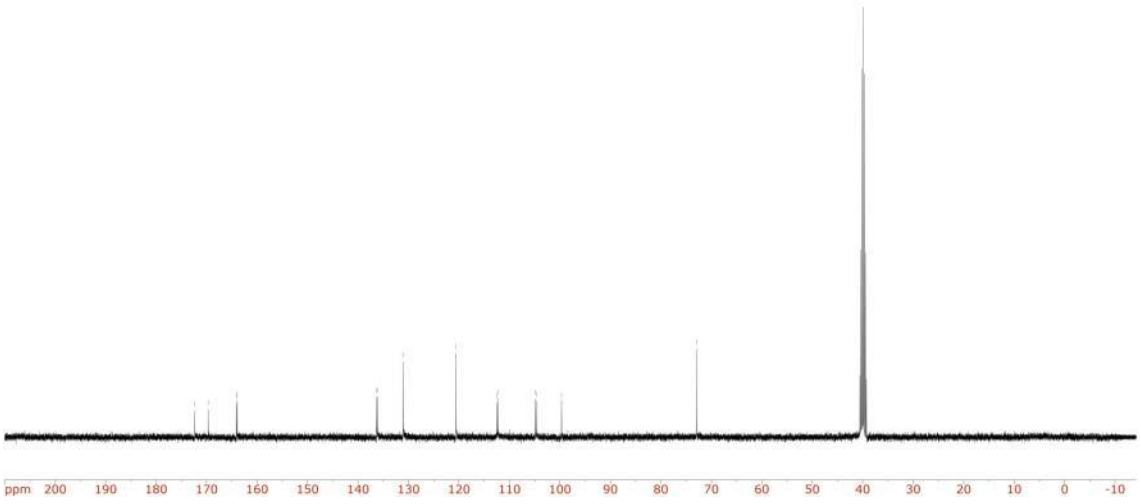

2-(allyloxy)-3-bromobenzenediazonium tetrafluoroborate (174g)

^{1}H-NMR (CD_3CN, 400 MHz)

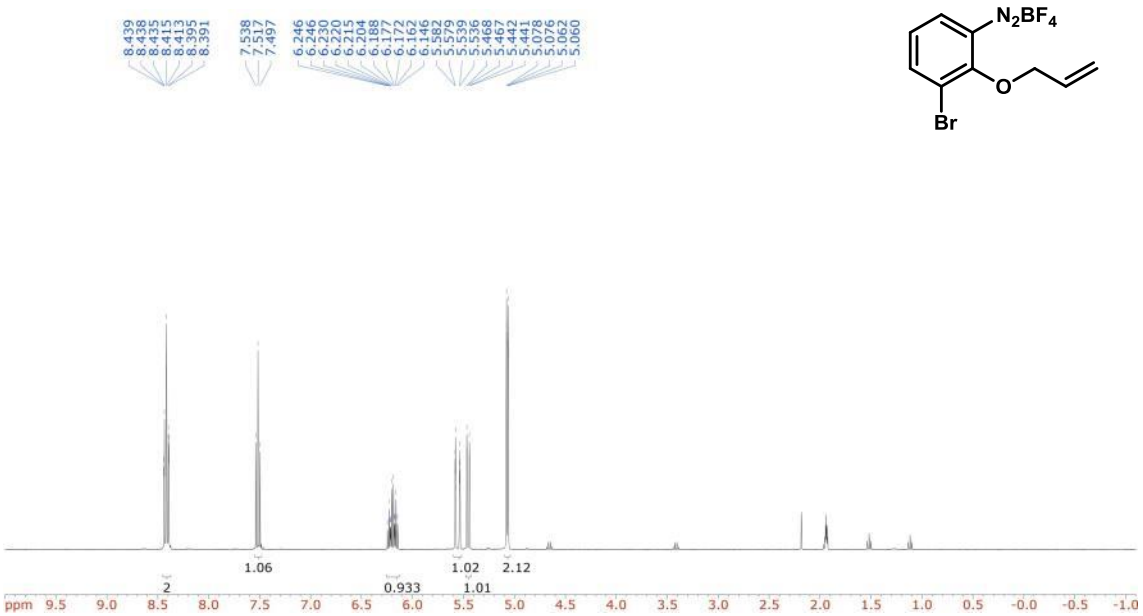

^{13}C-NMR (CD_3CN, 100 MHz)

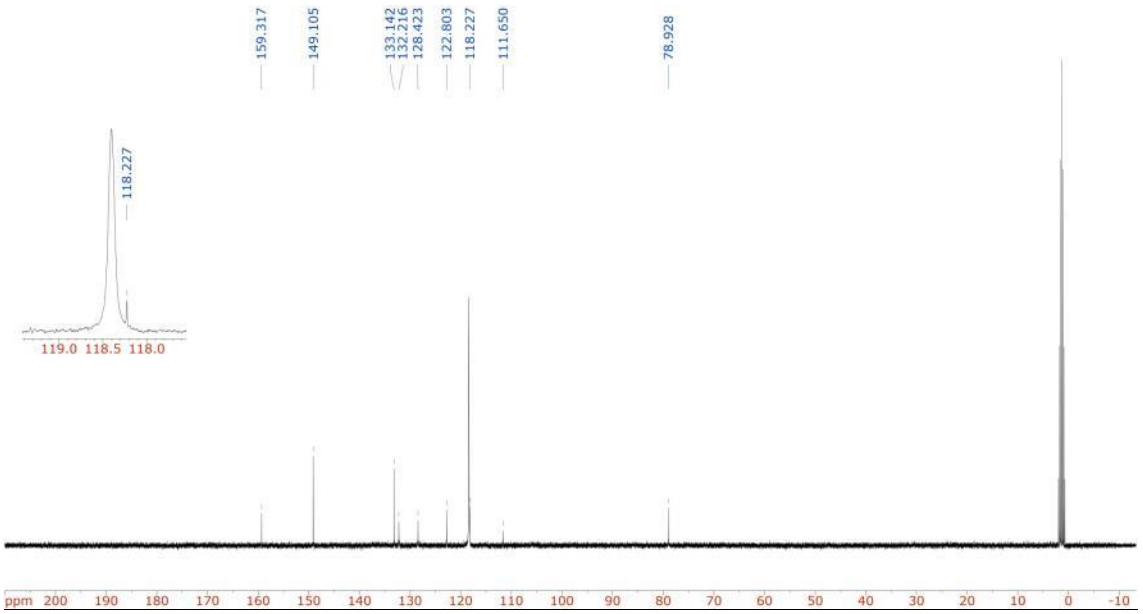

2-(allyloxy)-5-(methoxycarbonyl)benzenediazonium tetrafluoroborate (174i)

^{1}H-NMR (DMSO-d_6, 400 MHz)

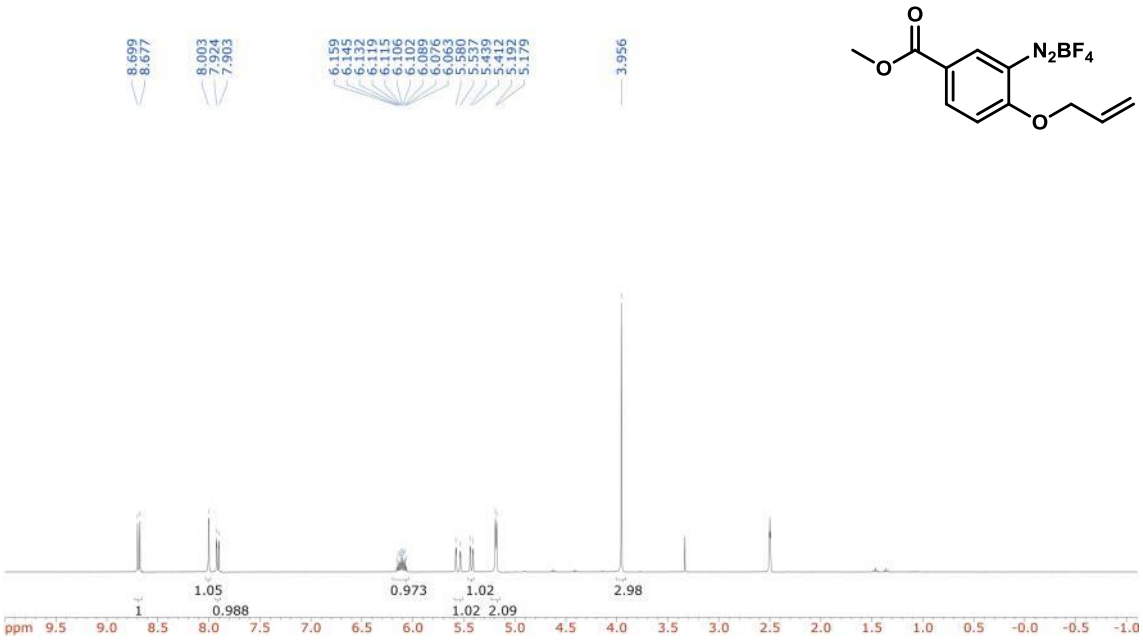

^{13}C-NMR (DMSO-d_6, 100 MHz)

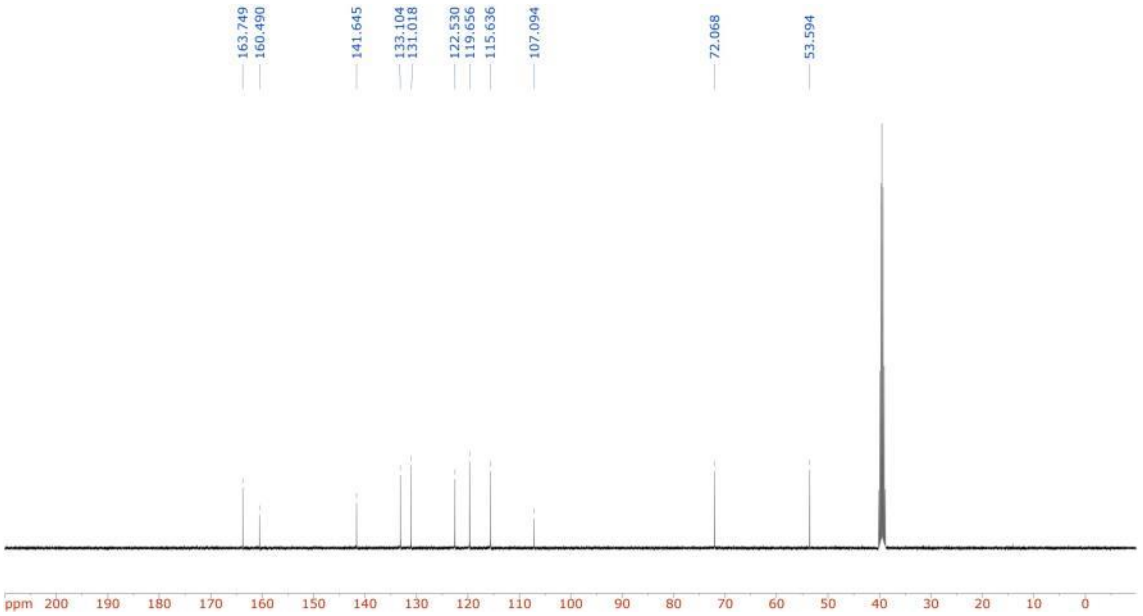

2-(allyloxy)-4-methoxybenzenediazonium tetrafluoroborate (174j)

^{1}H-NMR (DMSO-d_6, 400 MHz)

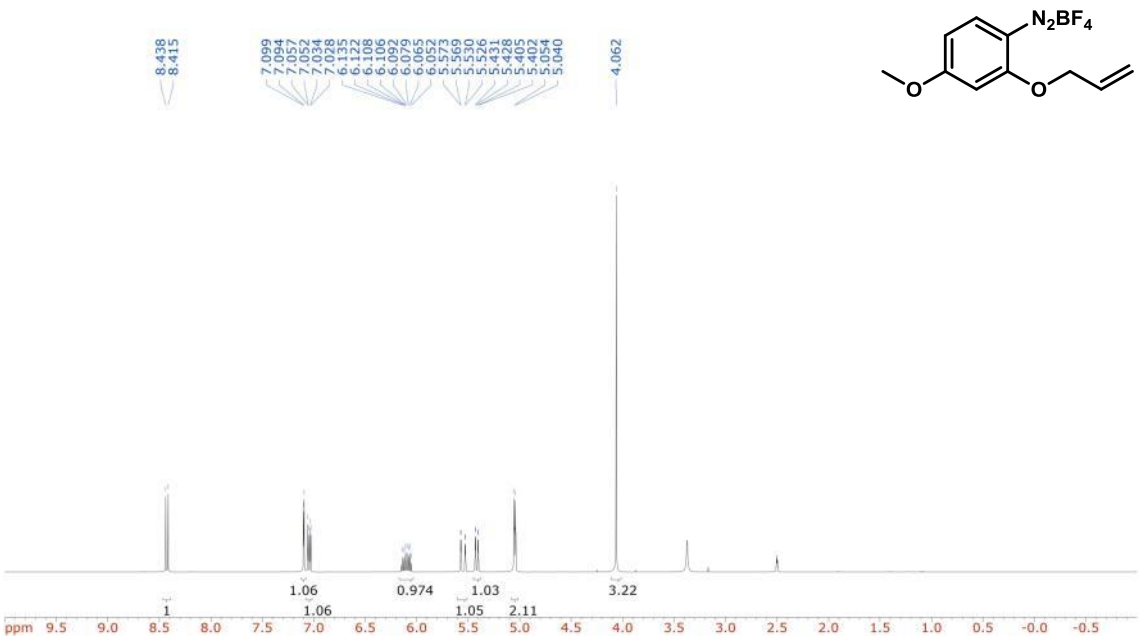

^{13}C-NMR (DMSO-d_6, 100 MHz)

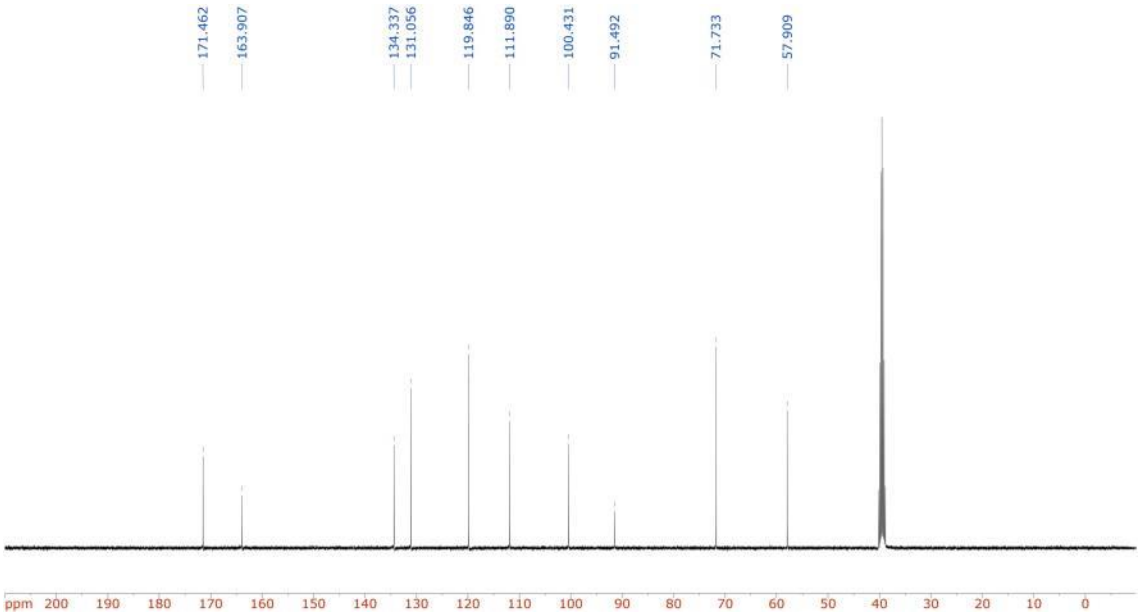

2-((2-methylallyl)oxy)benzenediazonium tetrafluoroborate (177a)

^{1}H-NMR (DMSO-d_6, 400 MHz)

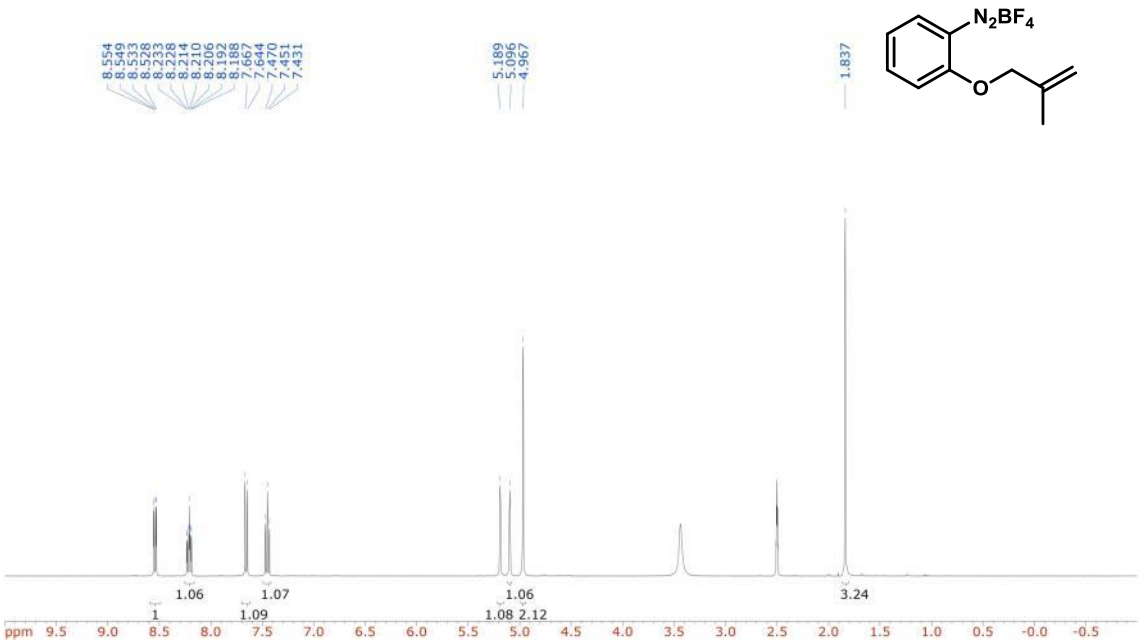

^{13}C-NMR (DMSO-d_6, 100 MHz)

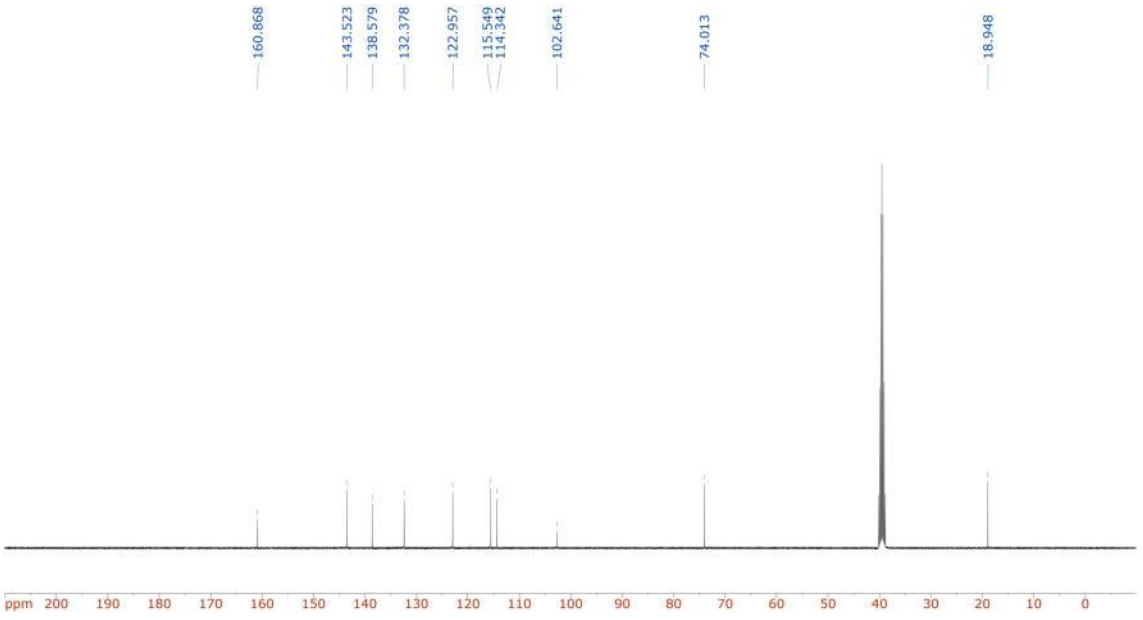

2-(prop-2-yn-1-yloxy)benzenediazonium tetrafluoroborate (178a)

^{1}H-NMR (DMSO-d_6, 400 MHz)

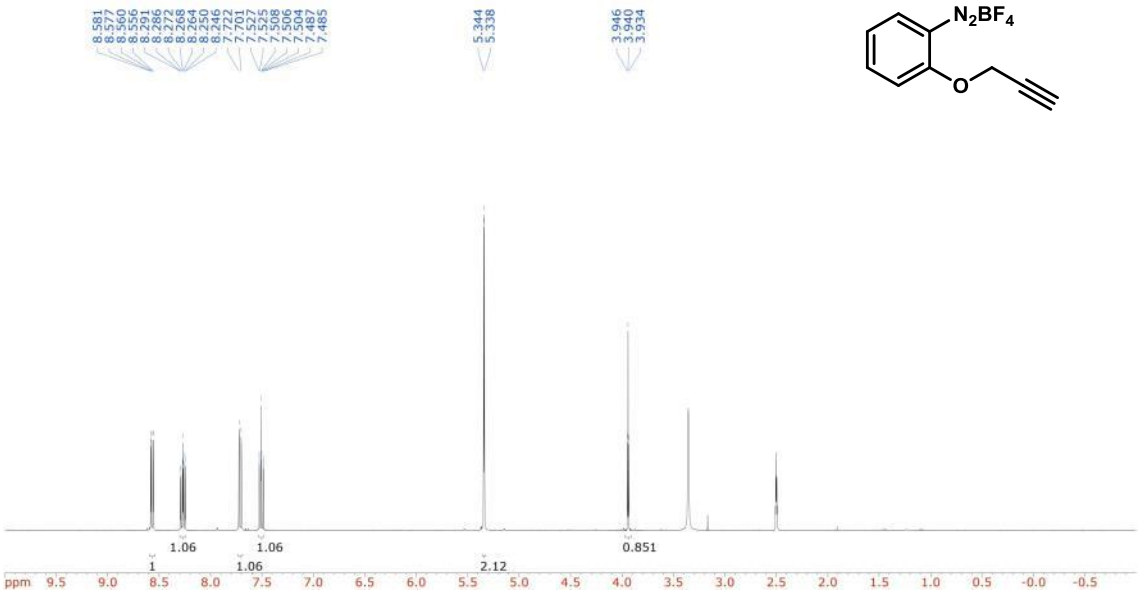

^{13}C-NMR (DMSO-d_6, 100 MHz)

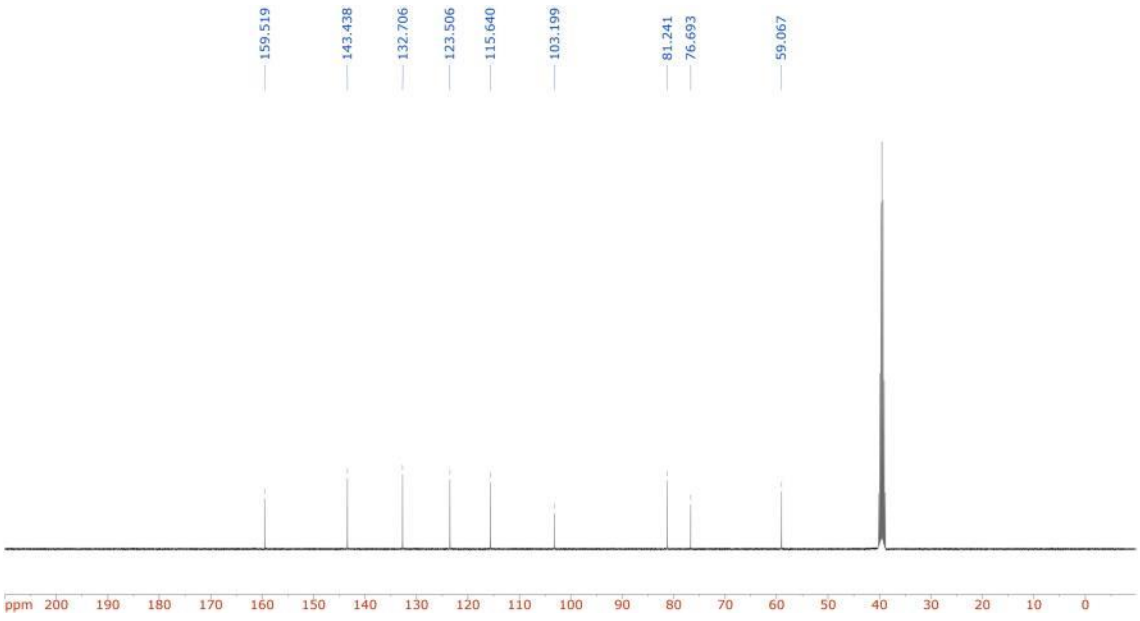

2-(but-3-en-1-yloxy)benzenediazonium tetrafluoroborate (179a)

^{1}H-NMR (DMSO-d_6, 400 MHz)

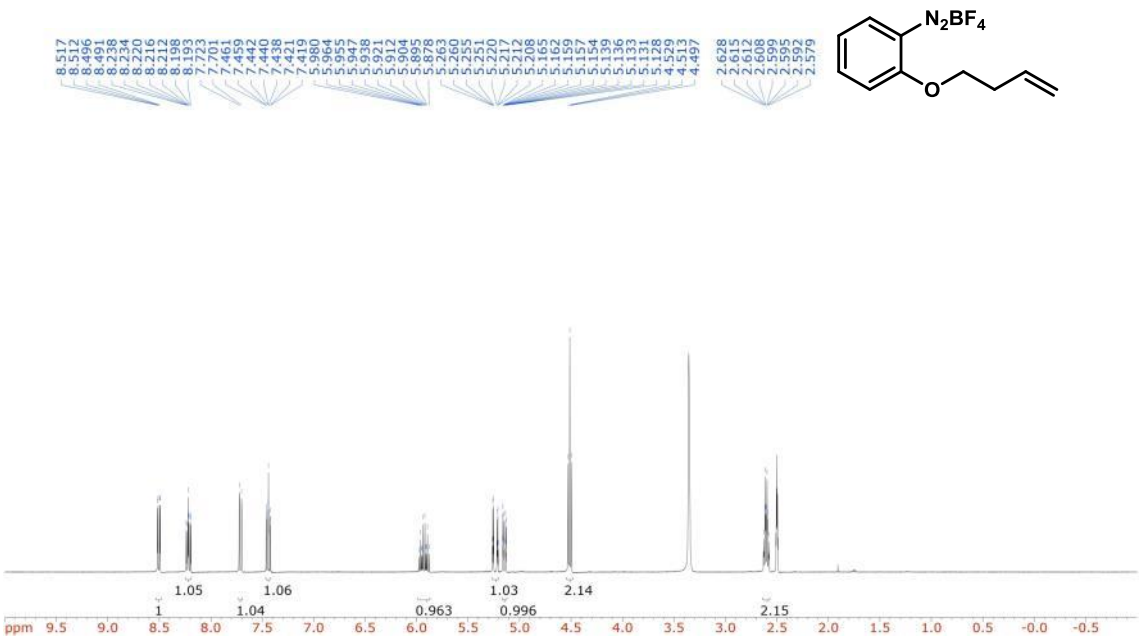

^{13}C-NMR (DMSO-d_6, 100 MHz)

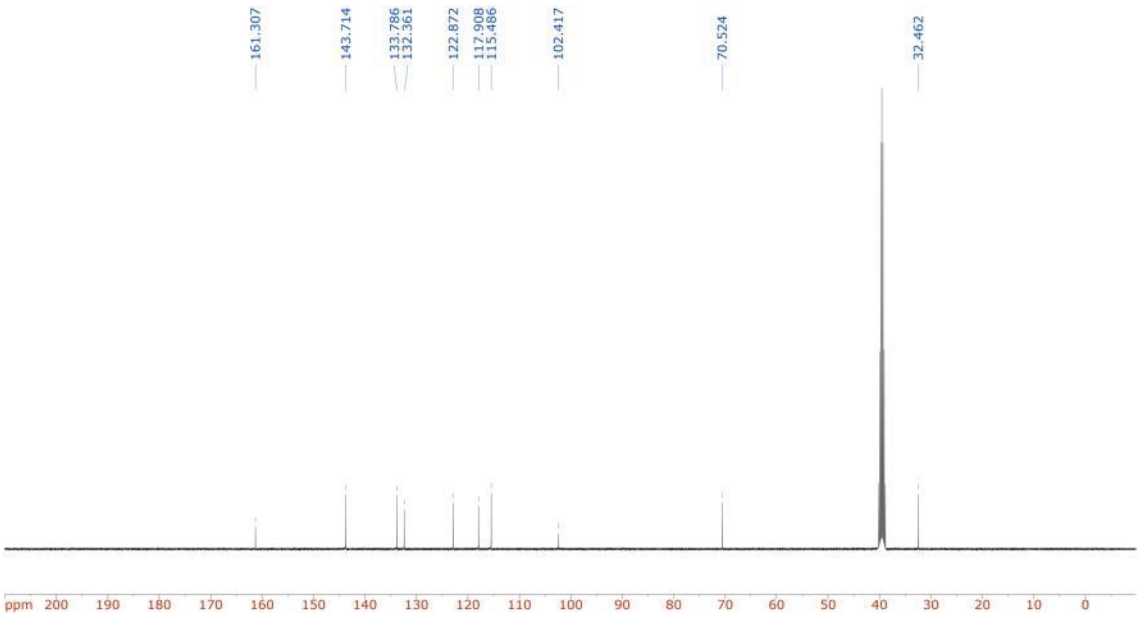

2-(allyloxy)-5-(*t*-butyl)aniline (183a)

^{1}H-NMR ($CDCl_3$, 400 MHz)

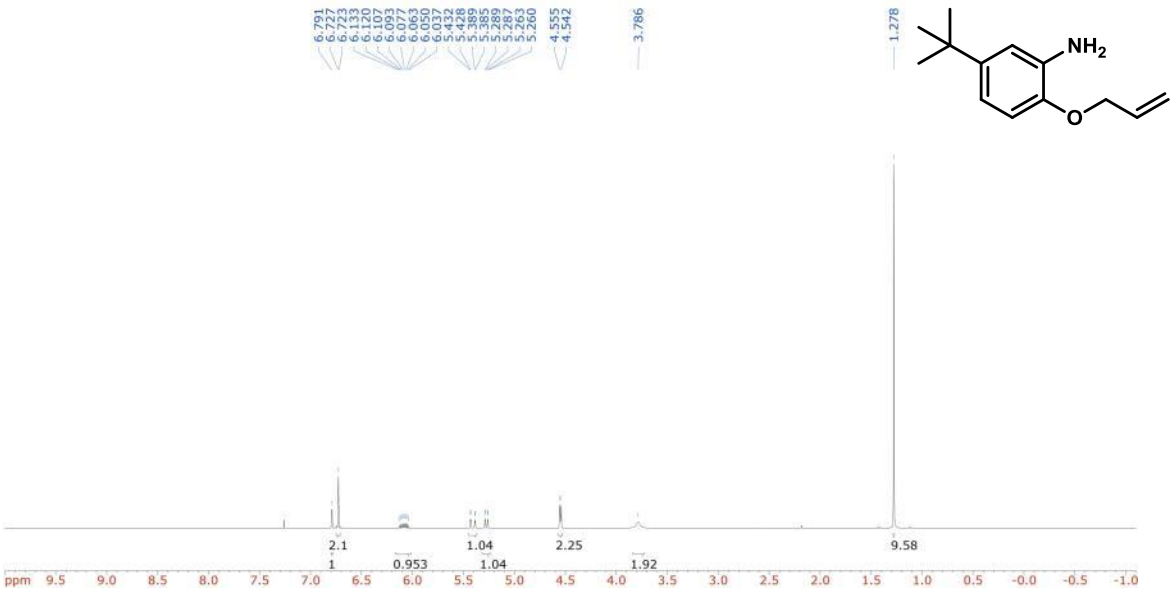

^{13}C-NMR ($CDCl_3$, 100 MHz)

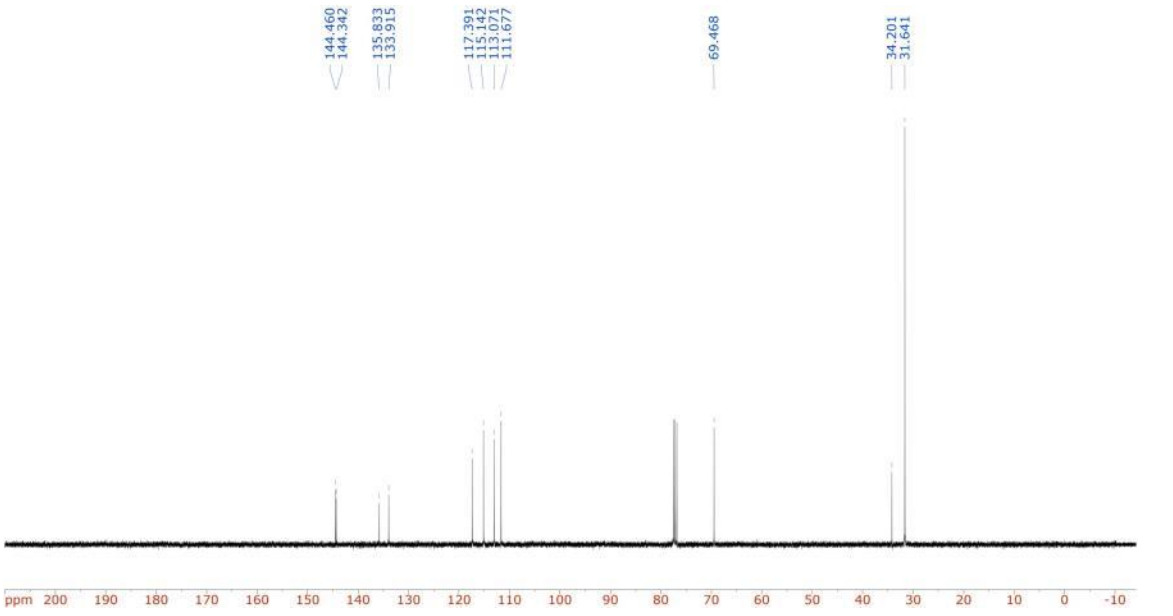

2-(allyloxy)-4-methoxyaniline (183b)

^{1}H-NMR ($CDCl_3$, 400 MHz)

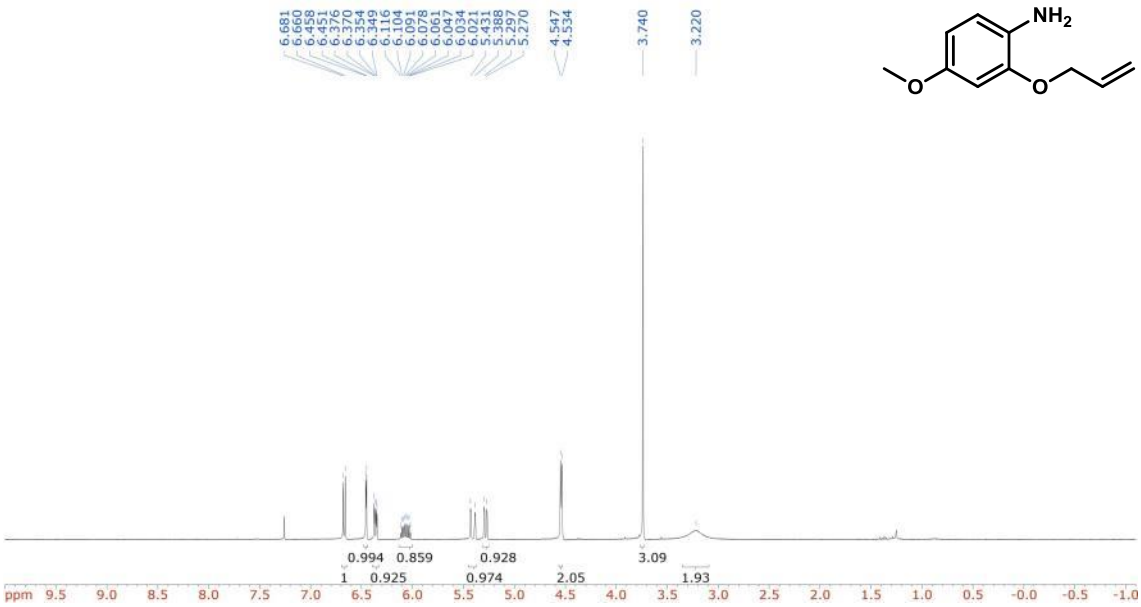

^{13}C-NMR ($CDCl_3$, 100 MHz)

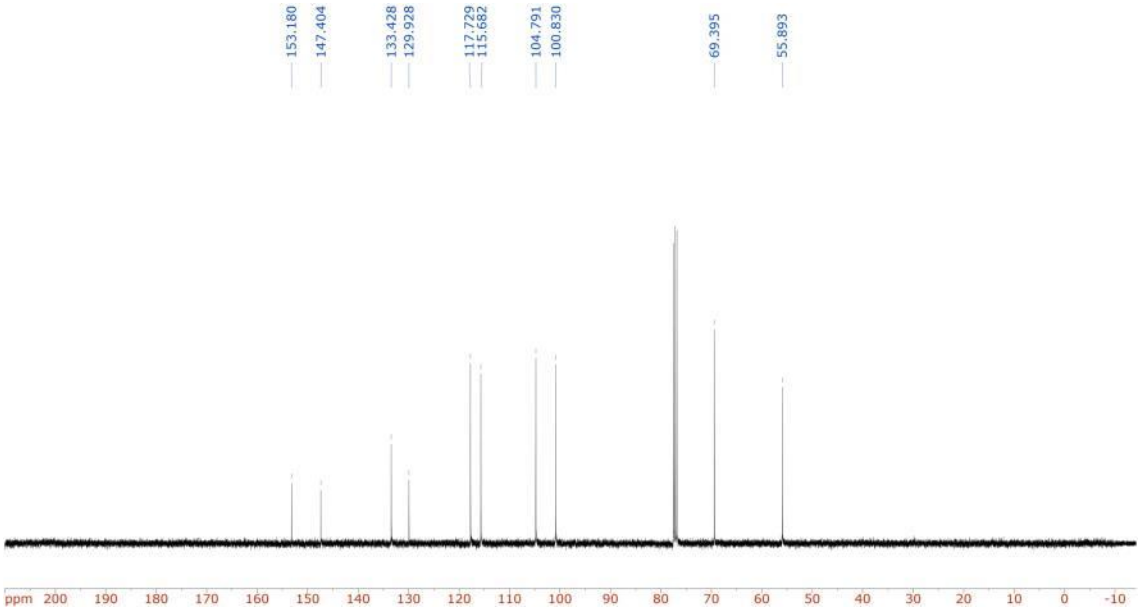

A.4. Chapter 4 NMR spectra

methyl 4-(morpholine-4-carbonyl)benzoate (230aa)

^{1}H-NMR ($CDCl_3$, 400 MHz)

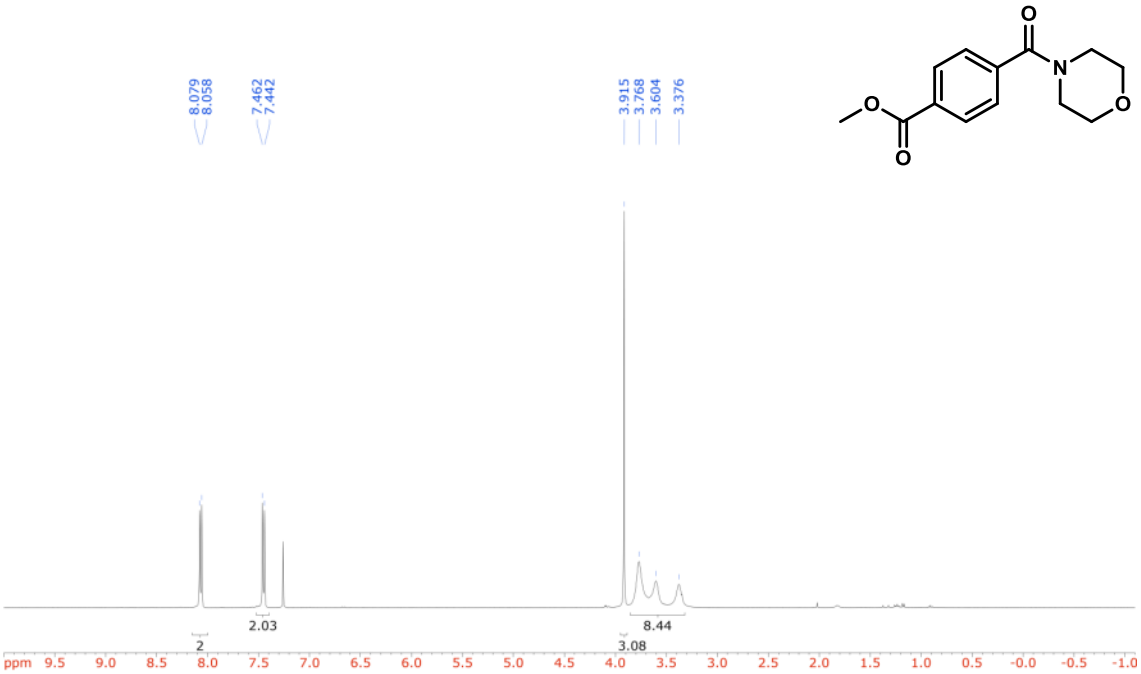

^{13}C-NMR ($CDCl_3$, 100 MHz)

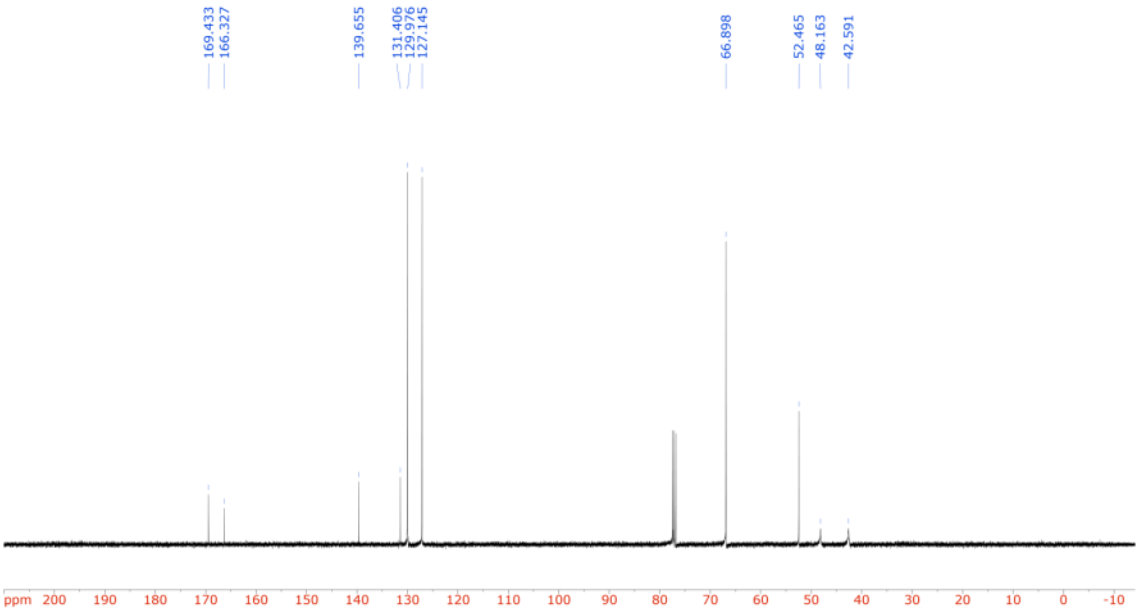

methyl 4-(morpholine-4-carbonyl)benzoate (230ab)

^{1}H-NMR ($CDCl_3$, 400 MHz)

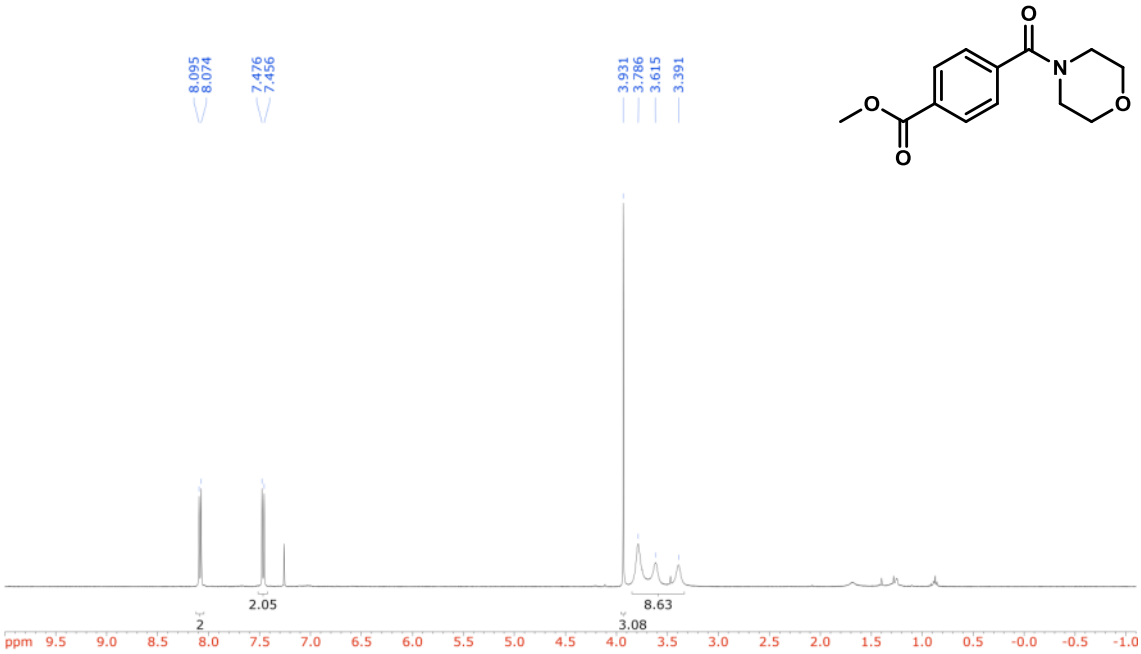

^{13}C-NMR ($CDCl_3$, 100 MHz)

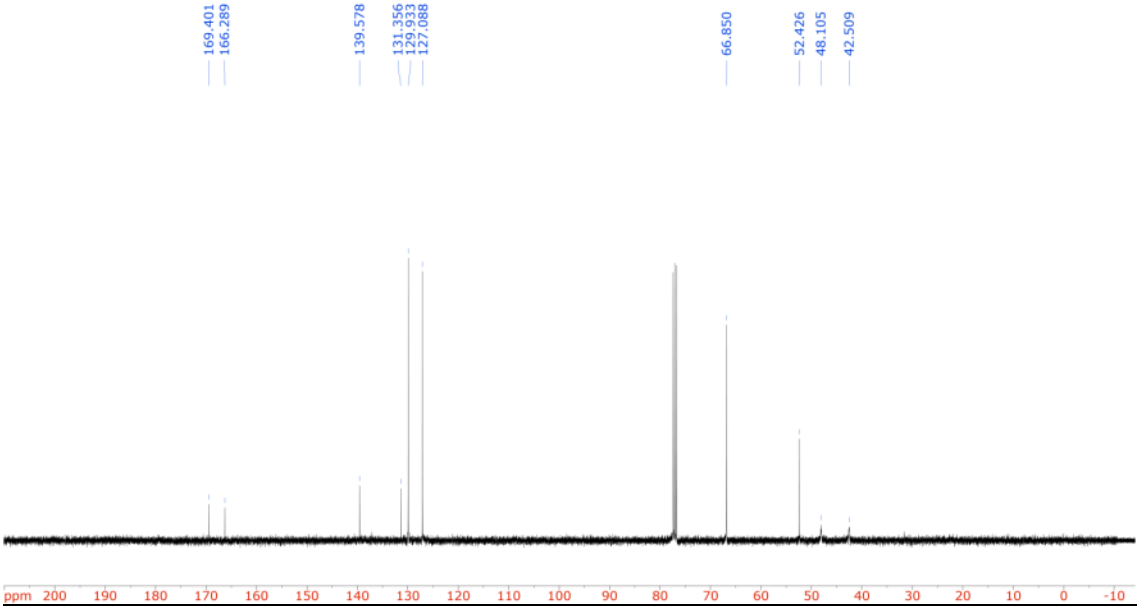

methyl 3-(morpholine-4-carbonyl)benzoate (230bb)

^{1}H-NMR ($CDCl_3$, 400 MHz)

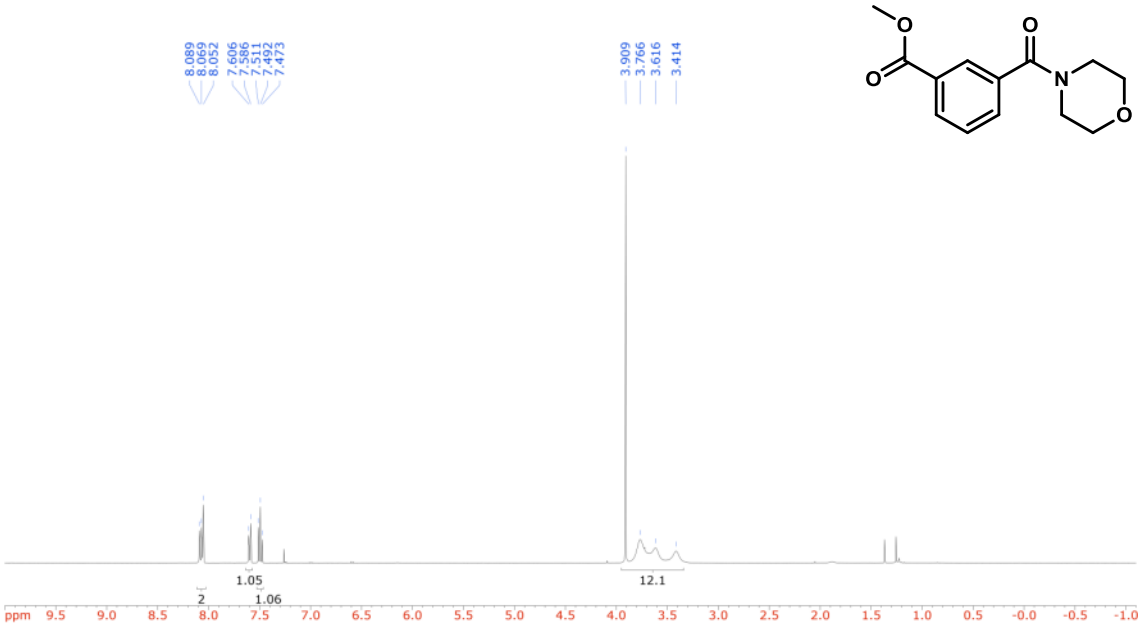

^{13}C-NMR ($CDCl_3$, 100 MHz)

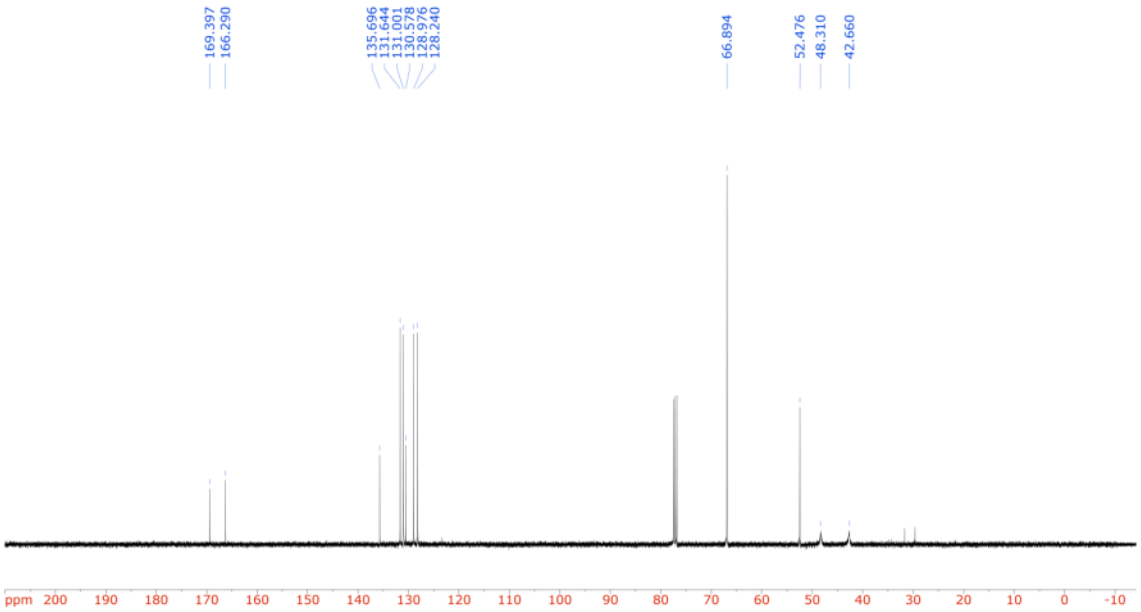

1-(4-(morpholine-4-carbonyl)phenyl)ethan-1-one (230ca)

^{1}H-NMR ($CDCl_3$, 400 MHz)

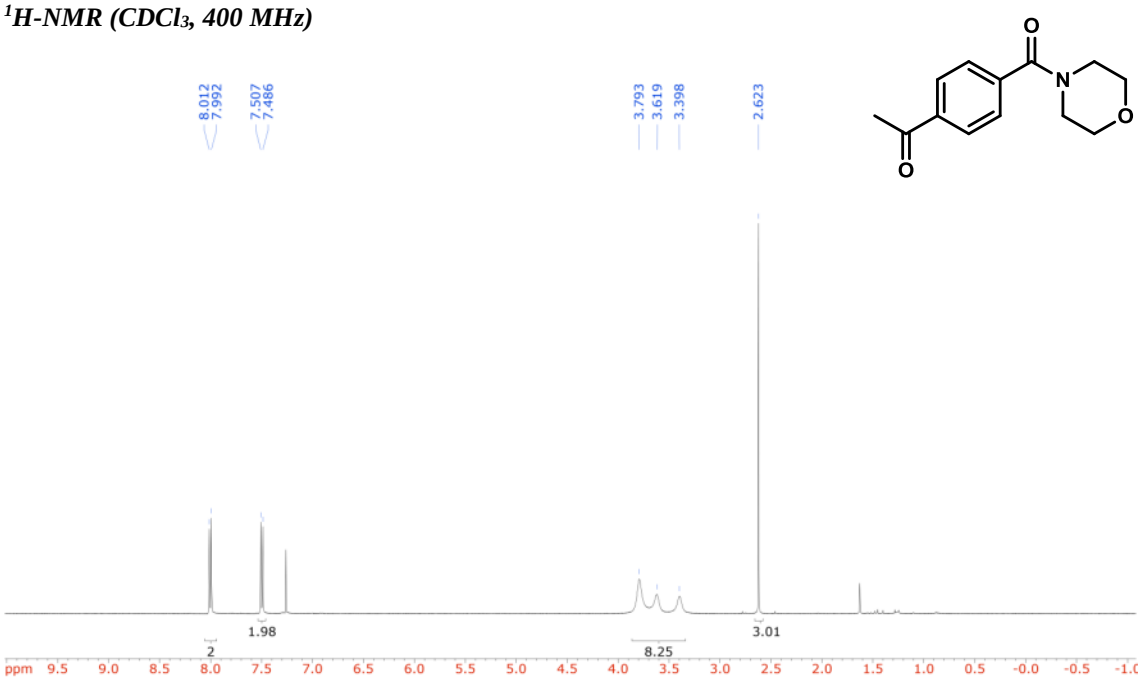

^{13}C-NMR ($CDCl_3$, 100 MHz)

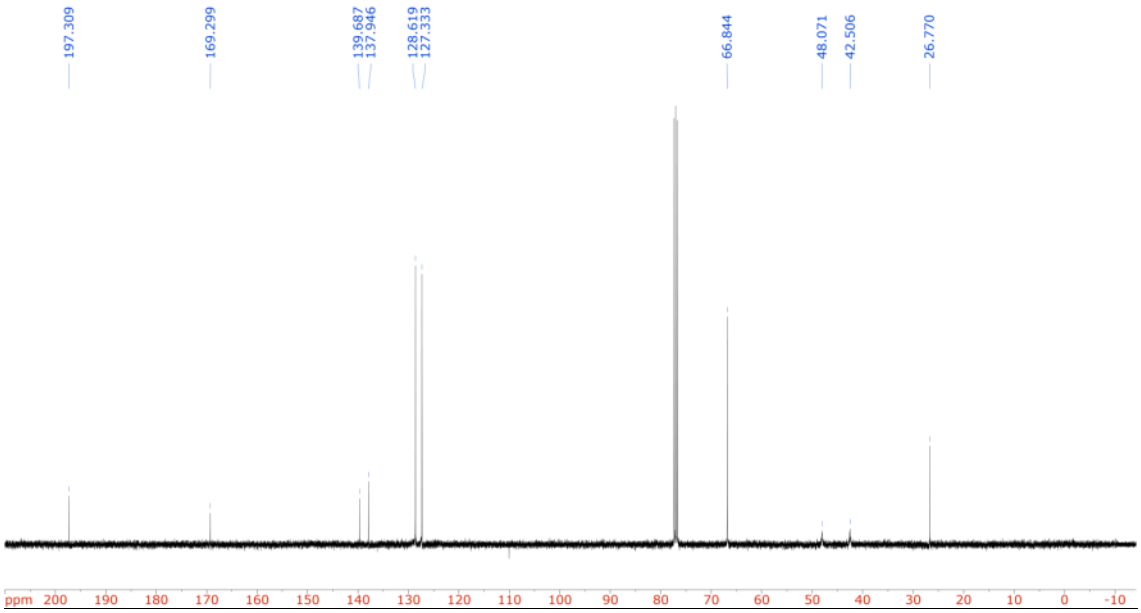

morpholino(4-(trifluoromethyl)phenyl)methanone (230da)

^{1}H-NMR ($CDCl_3$, 400 MHz)

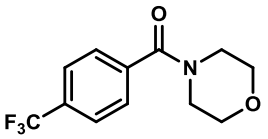

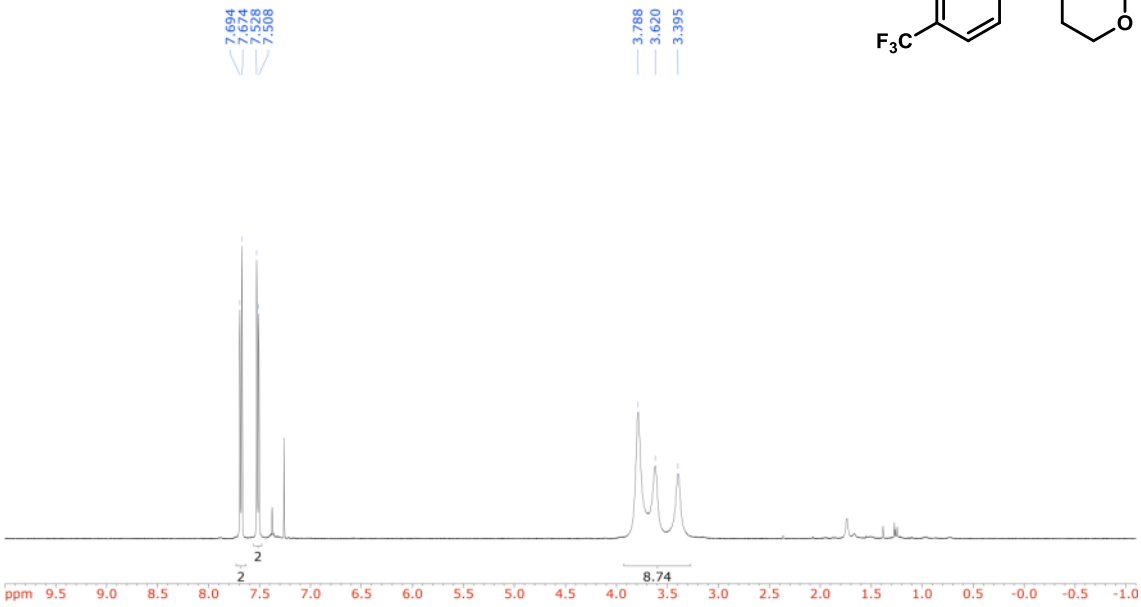

^{13}C-NMR ($CDCl_3$, 100 MHz)

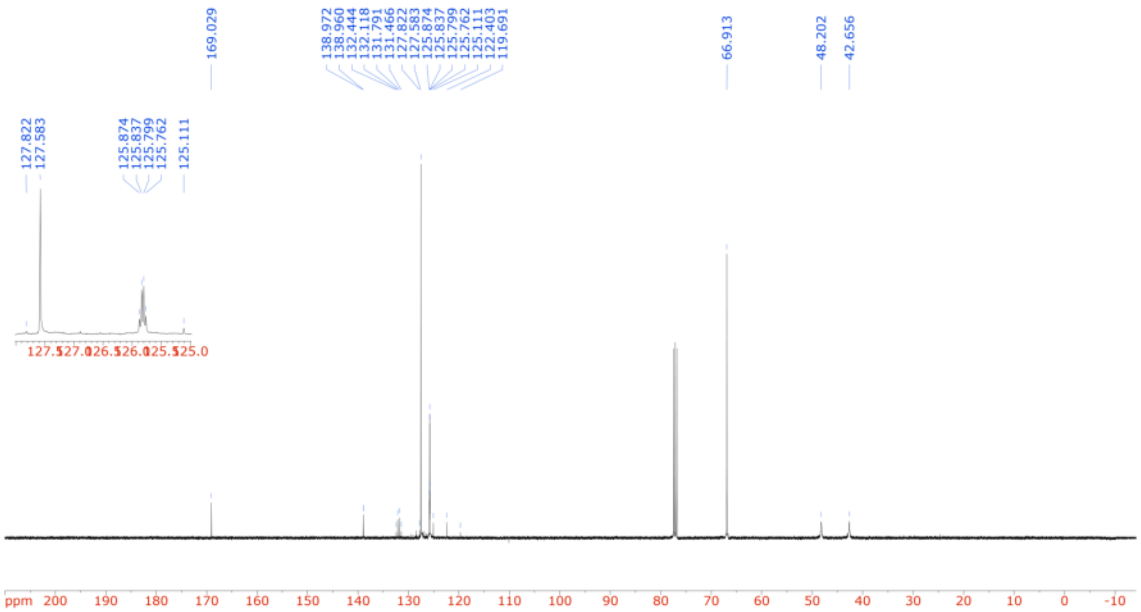

^{19}F-NMR ($CDCl_3$, 376 MHz)

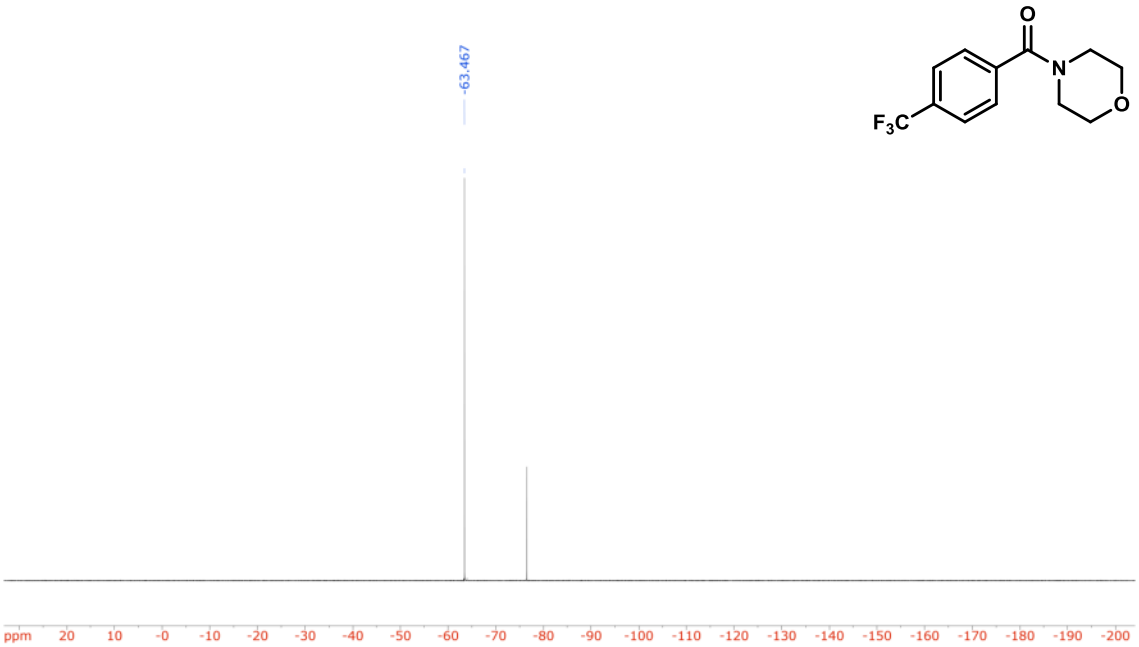

morpholino(4-(trifluoromethyl)phenyl)methanone (230db)

^{1}H-NMR ($CDCl_3$, 400 MHz)

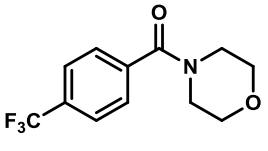

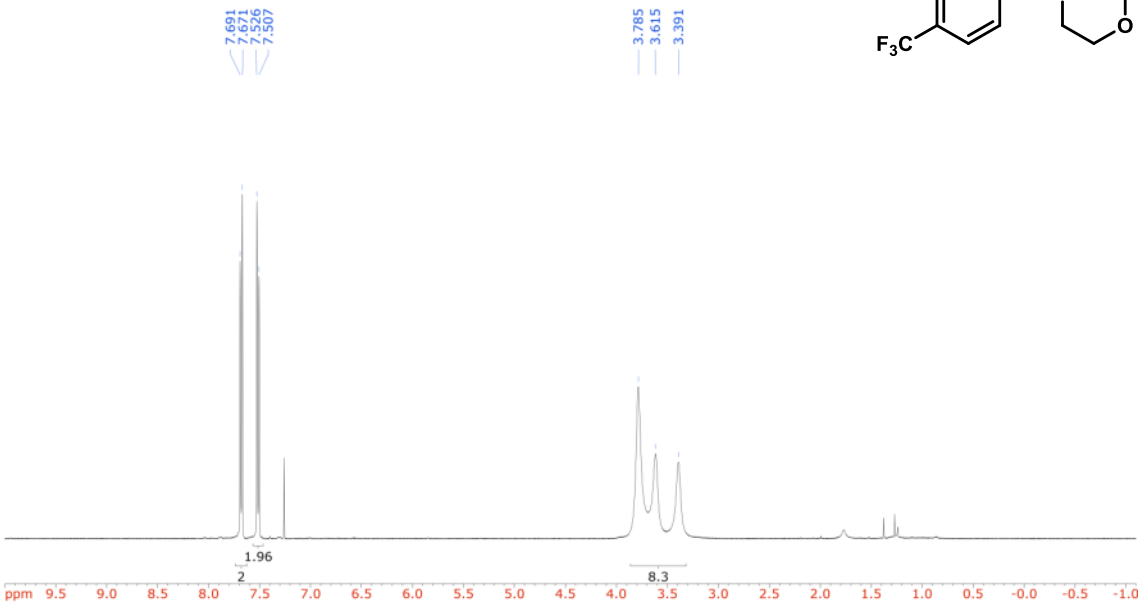

^{13}C-NMR ($CDCl_3$, 100 MHz)

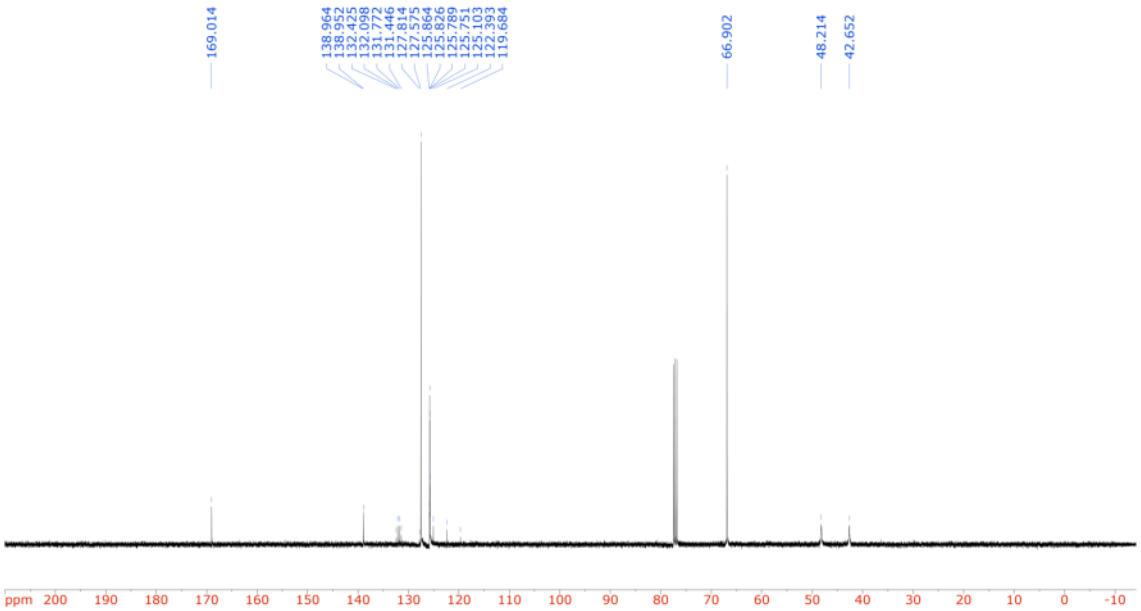

^{19}F-NMR ($CDCl_3$, 376 MHz)

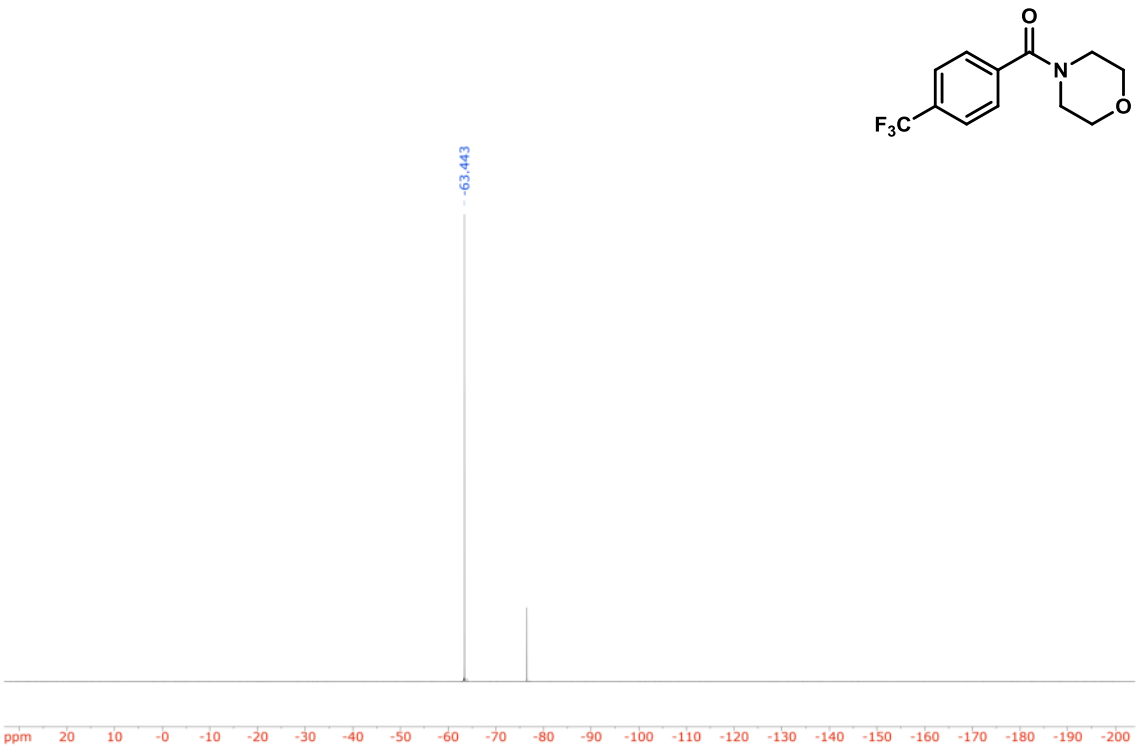

4-(morpholine-4-carbonyl)benzonitrile (230ea)

^{1}H-NMR ($CDCl_3$, 400 MHz)

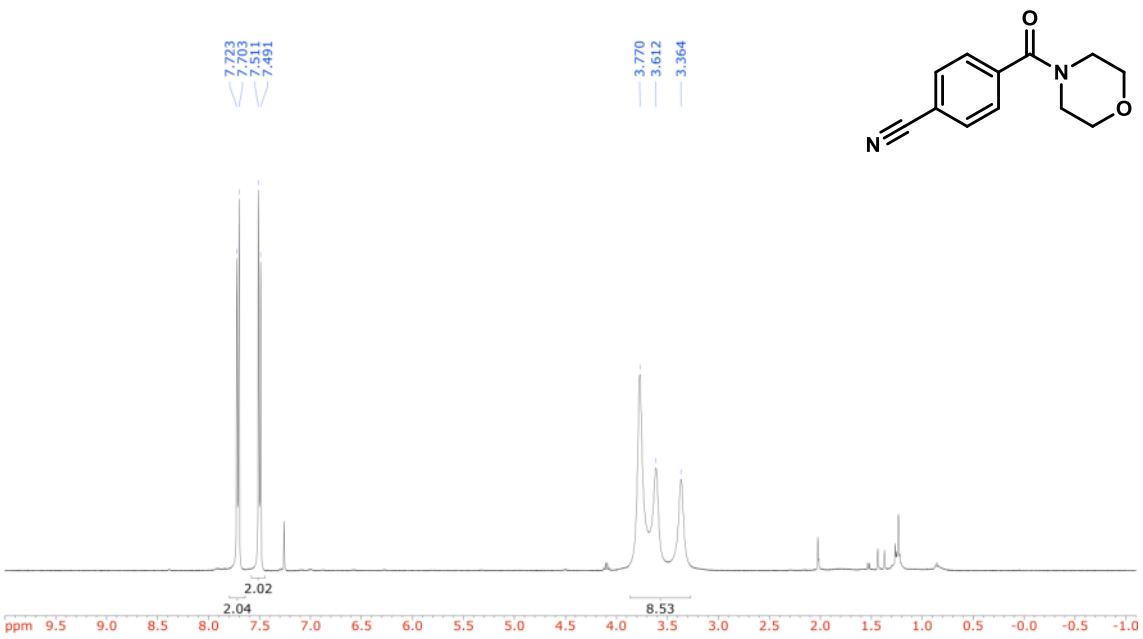

^{13}C-NMR ($CDCl_3$, 100 MHz)

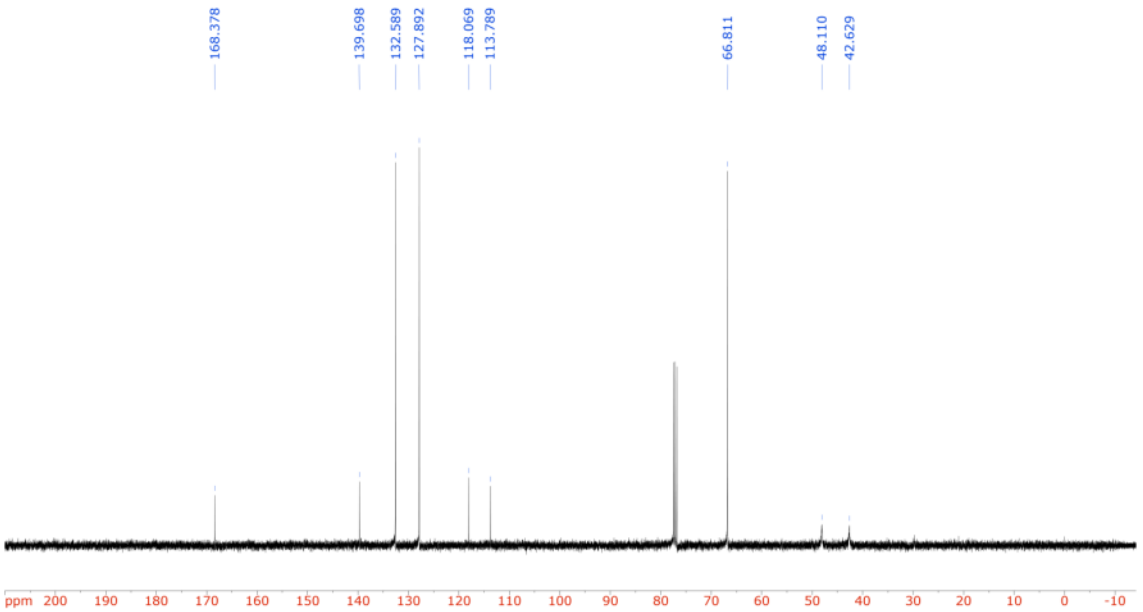

4-(morpholine-4-carbonyl)benzonitrile (230eb)

^{1}H-NMR ($CDCl_3$, 400 MHz)

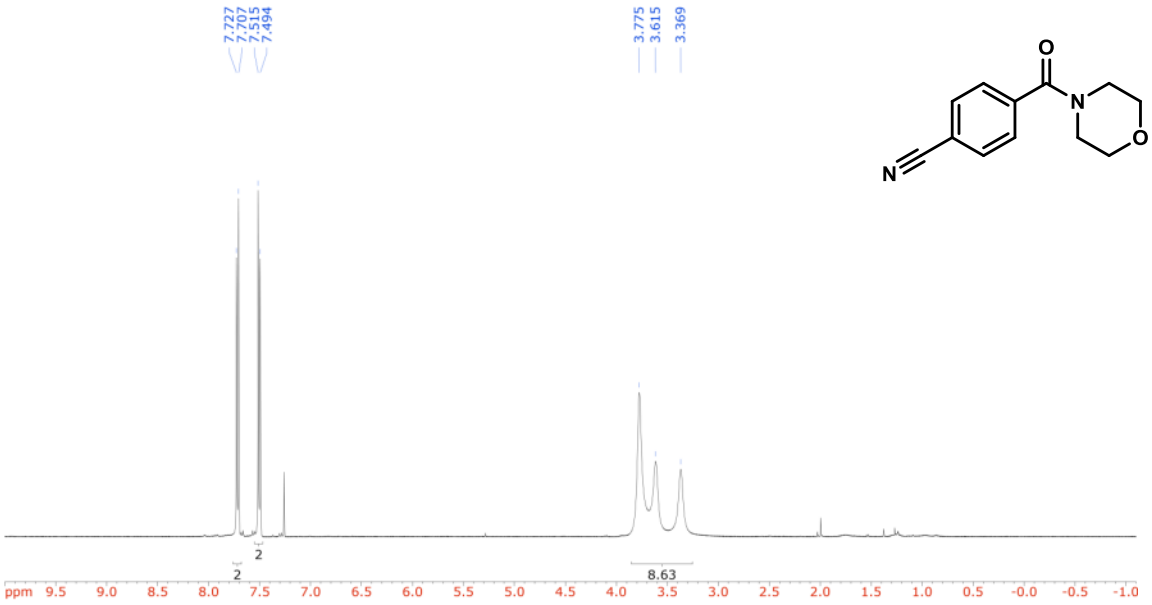

^{13}C-NMR ($CDCl_3$, 100 MHz)

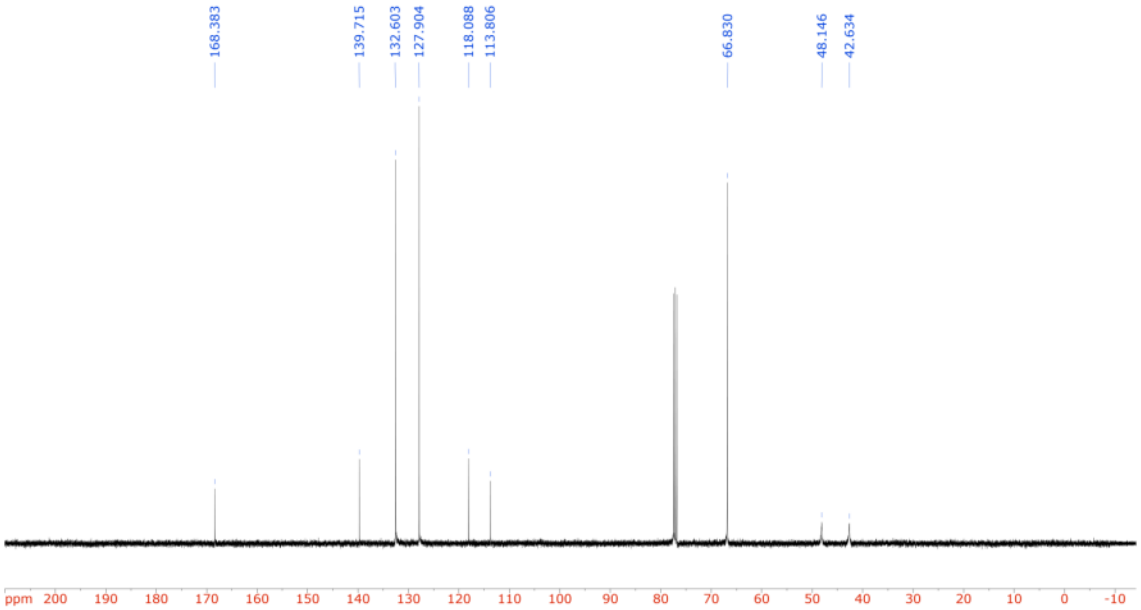

(4-chlorophenyl)(morpholino)methanone (230fa)

^{1}H-NMR ($CDCl_3$, 400 MHz)

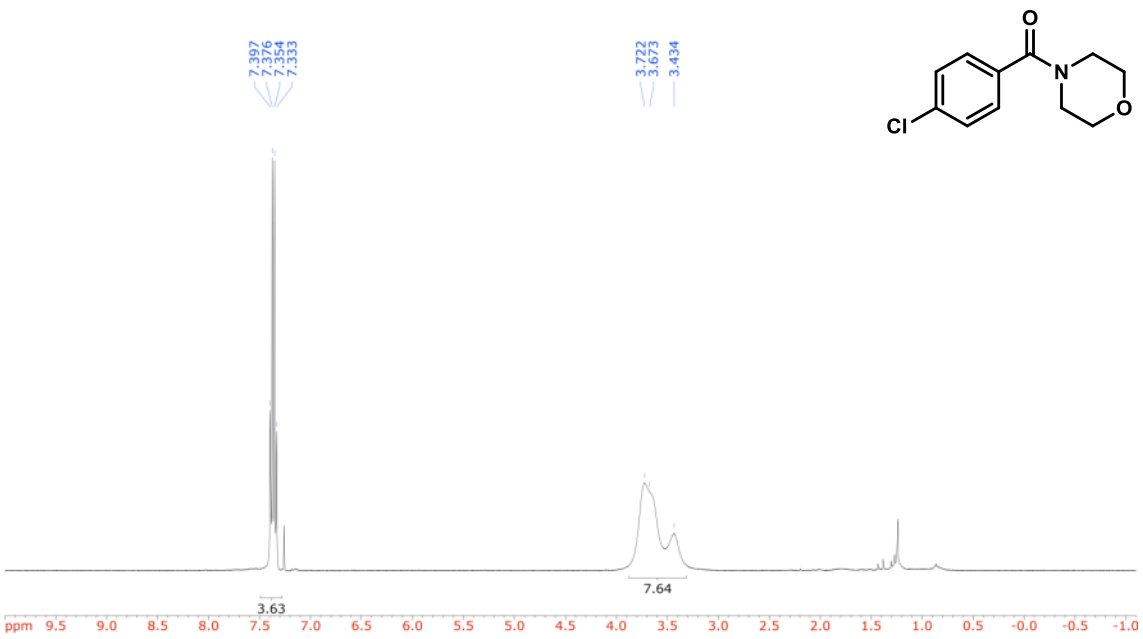

^{13}C-NMR ($CDCl_3$, 100 MHz)

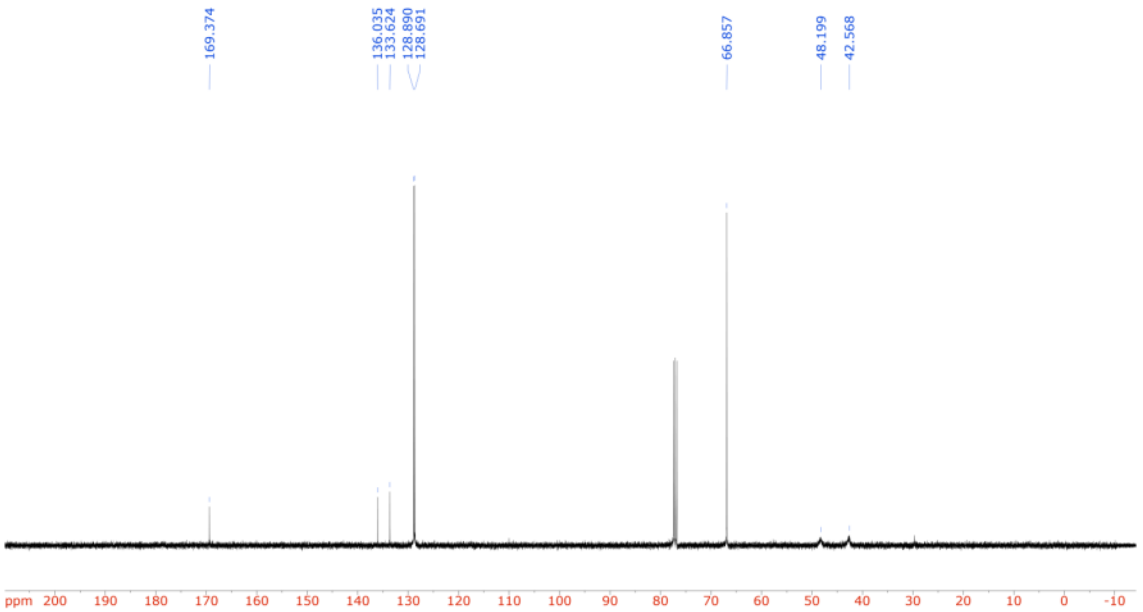

(4-chlorophenyl)(morpholino)methanone (230fb)

^{1}H-NMR ($CDCl_3$, 400 MHz)

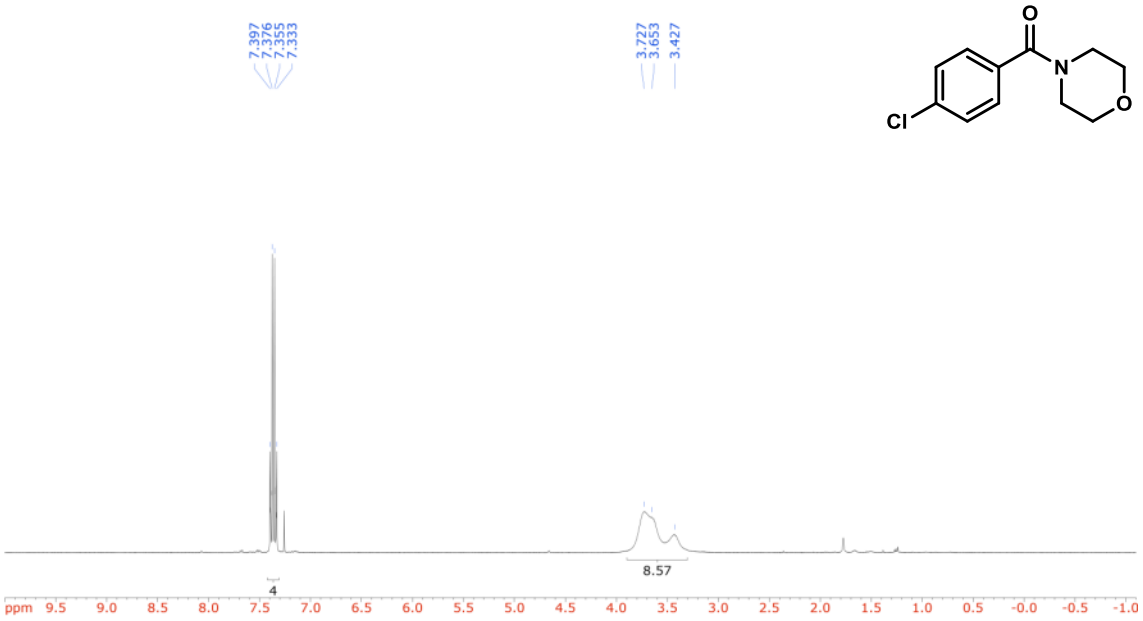

^{13}C-NMR ($CDCl_3$, 100 MHz)

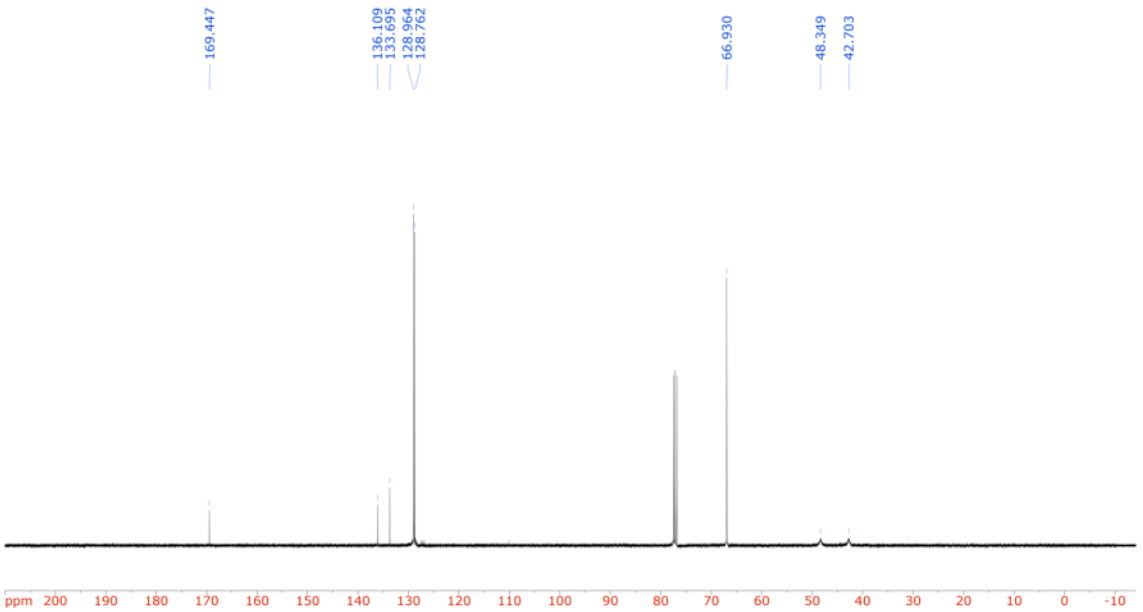

(4-fluorophenyl)(morpholino)methanone (230gb)

^{1}H-NMR ($CDCl_3$, 400 MHz)

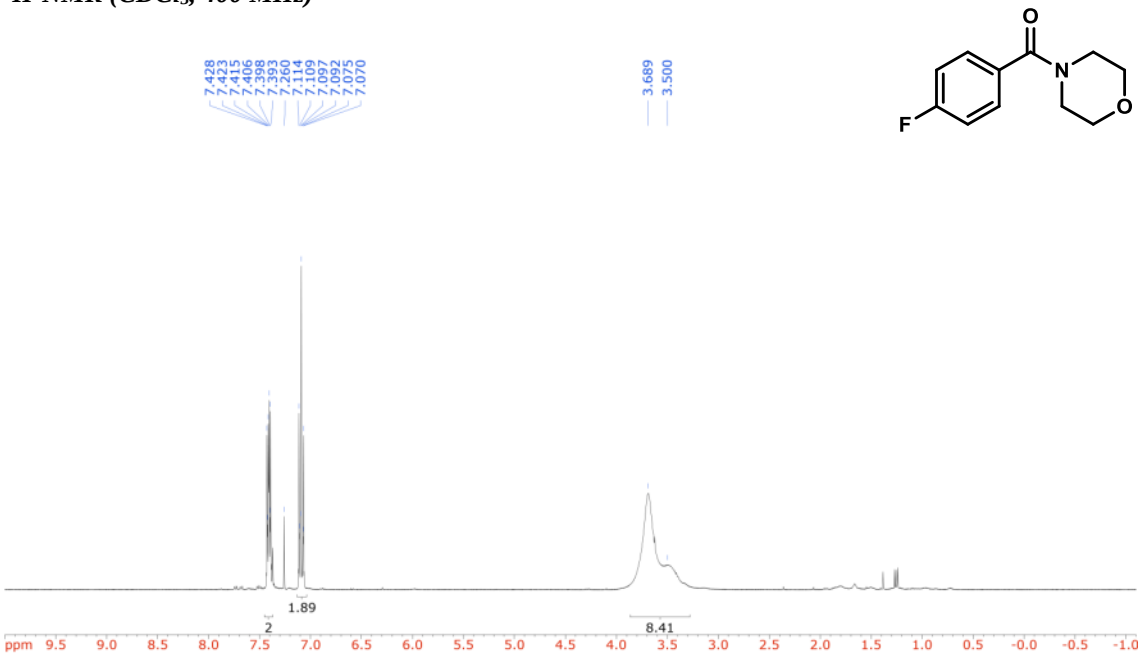

^{13}C-NMR ($CDCl_3$, 100 MHz)

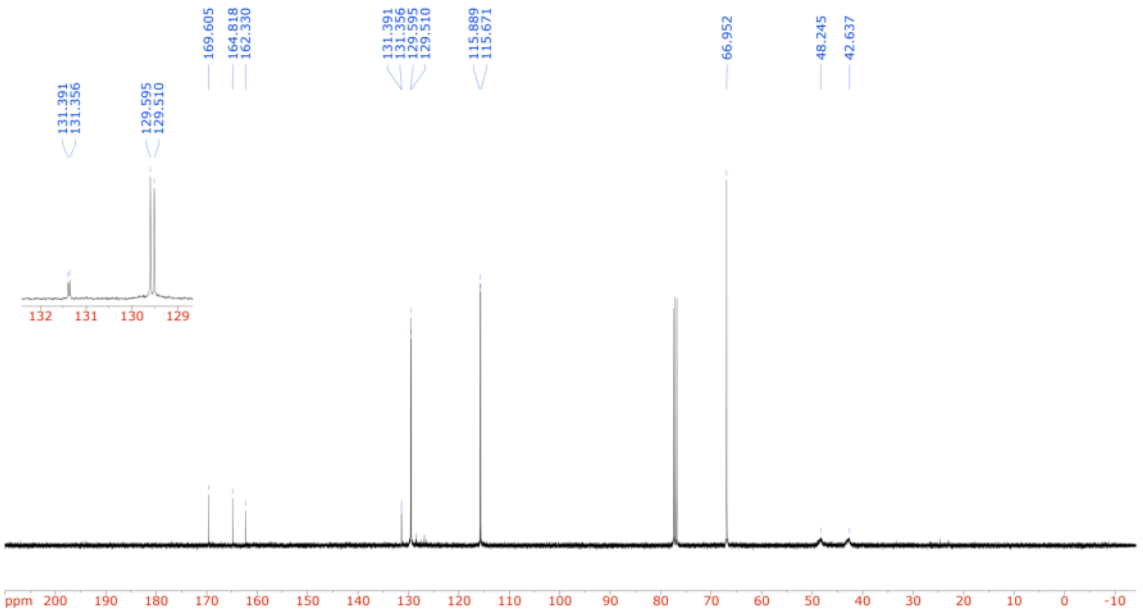

^{19}F-NMR ($CDCl_3$, 376 MHz)

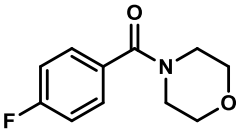

2-fluoro-5-(morpholine-4-carbonyl)benzonitrile (230hb)

^{1}H-NMR ($CDCl_3$, 400 MHz)

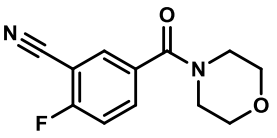

^{13}C-NMR ($CDCl_3$, 100 MHz)

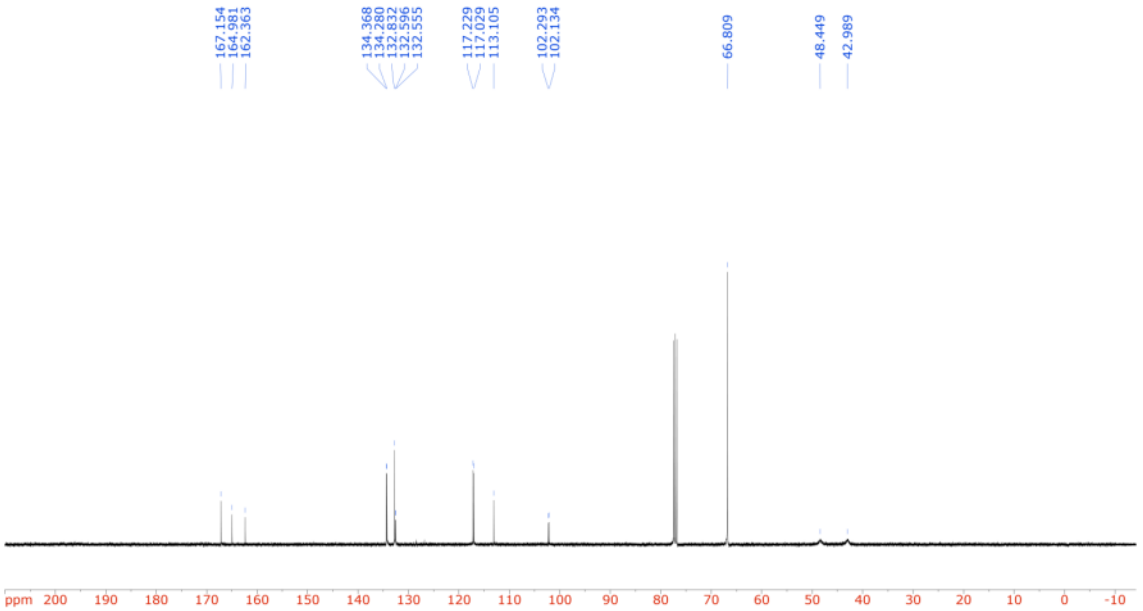

^{19}F-NMR ($CDCl_3$, 376 MHz)

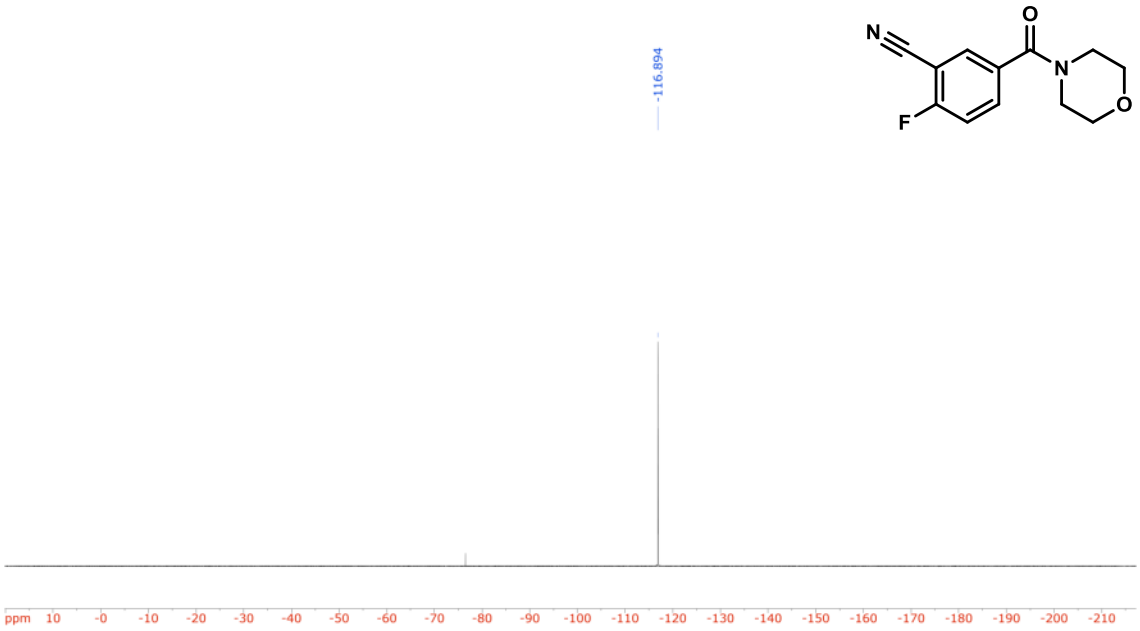

morpholino(4-(4,4,5,5-tetramethyl-1,3,2-dioxaborolan-2-yl)phenyl)methanone (230lb)

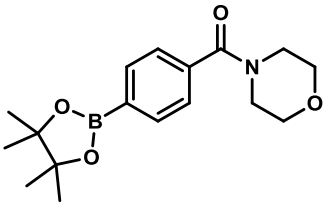

^{1}H-NMR ($CDCl_3$, 400 MHz)

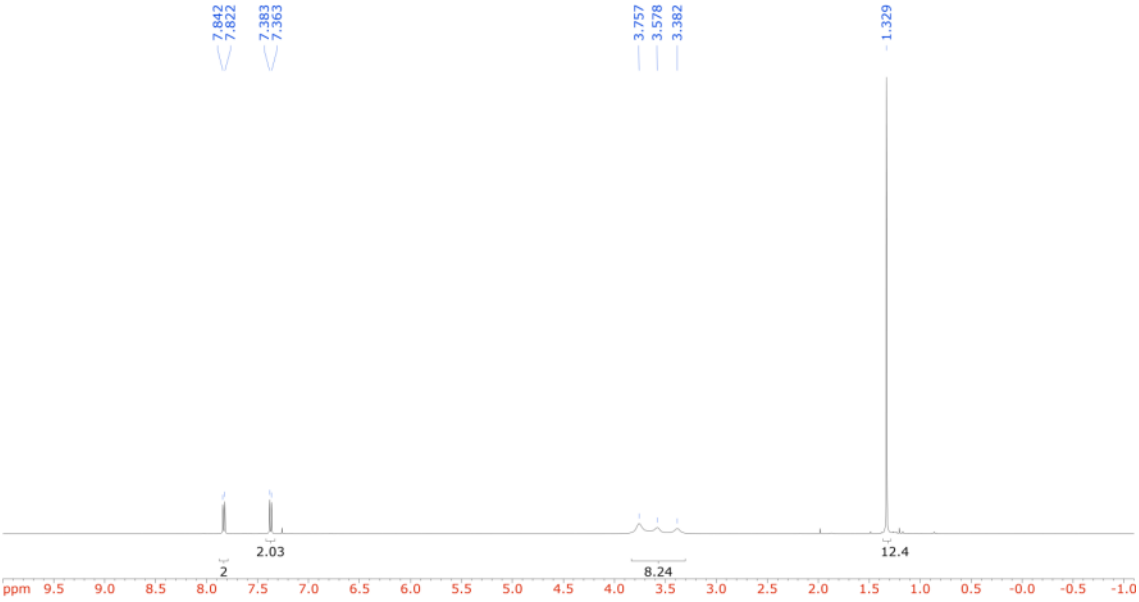

^{13}C-NMR ($CDCl_3$, 100 MHz)

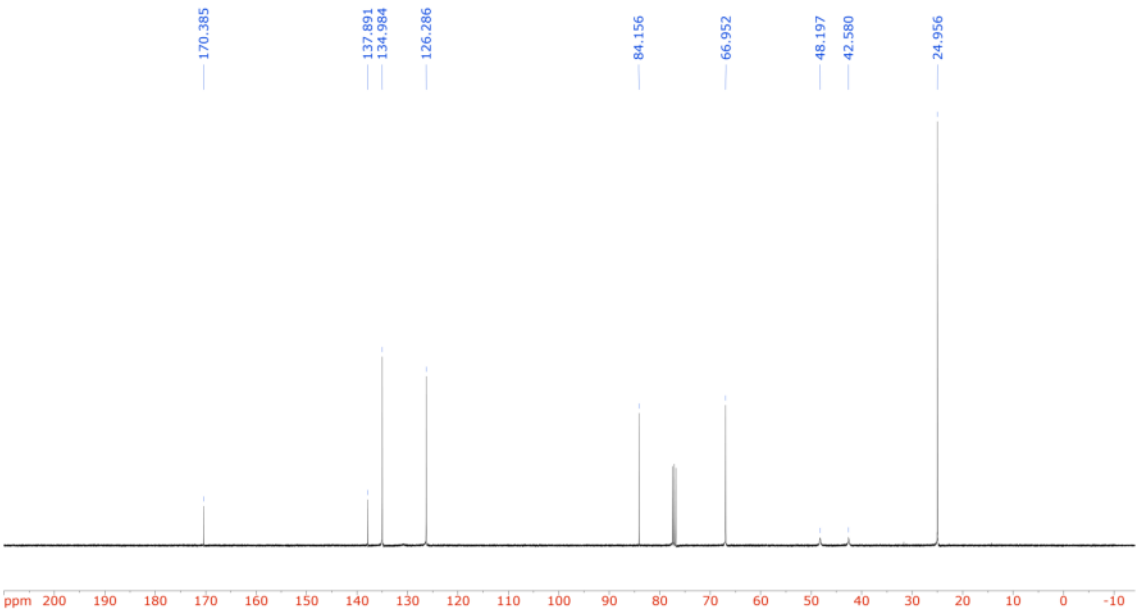

morpholino(phenyl)methanone (230ja)

^{1}H-NMR ($CDCl_3$, 400 MHz)

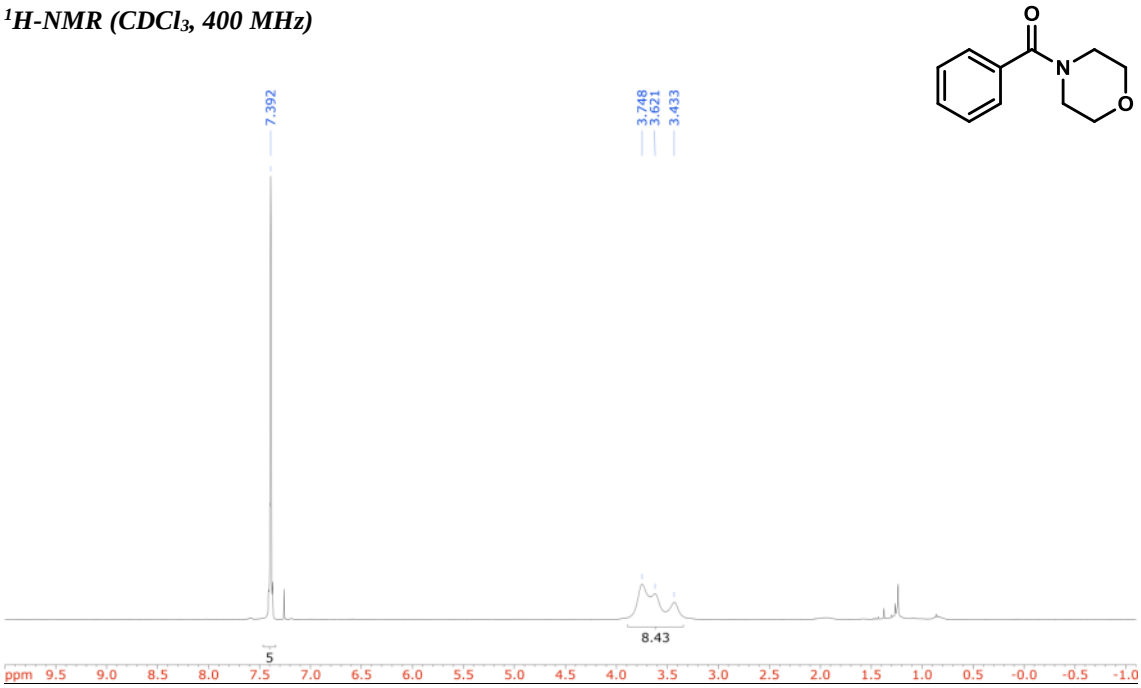

^{13}C-NMR ($CDCl_3$, 100 MHz)

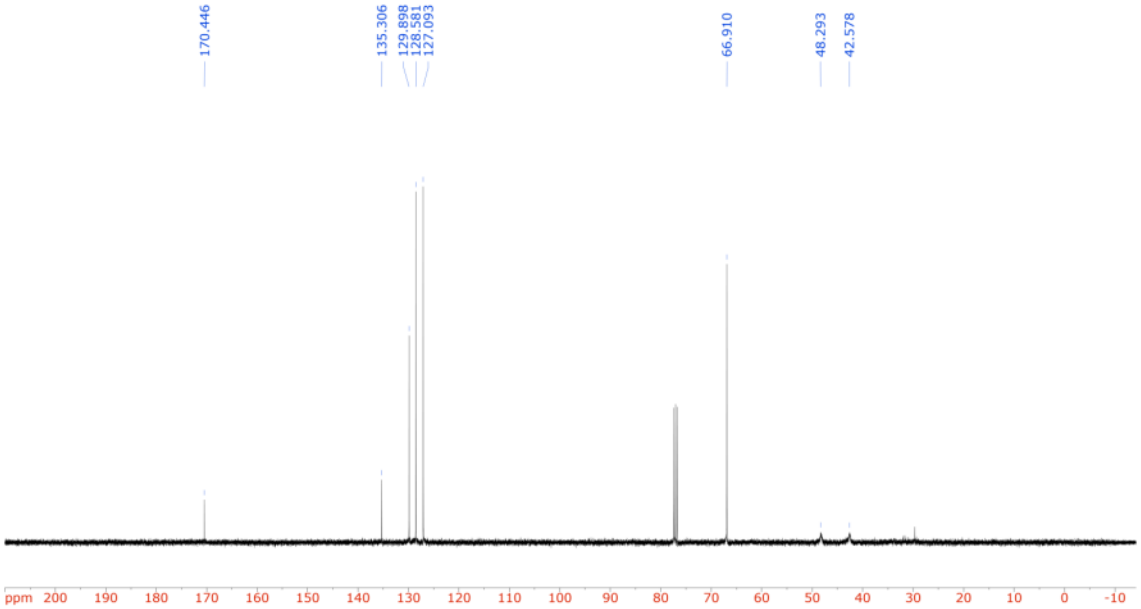

morpholino(phenyl)methanone (230jb)

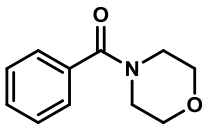

^{1}H-NMR ($CDCl_3$, 400 MHz)

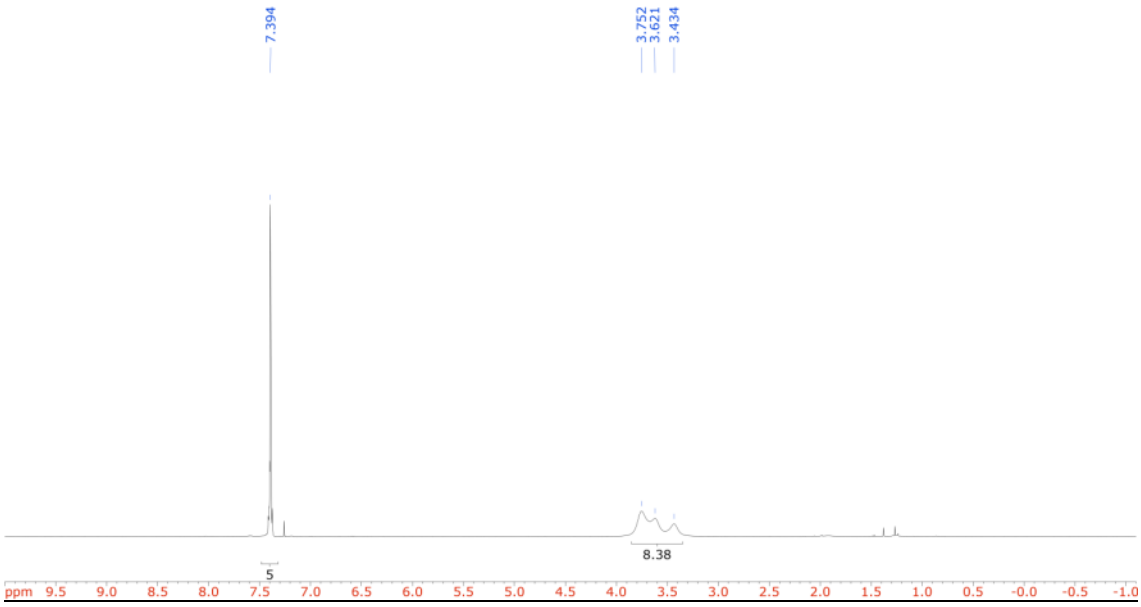

^{13}C-NMR ($CDCl_3$, 100 MHz)

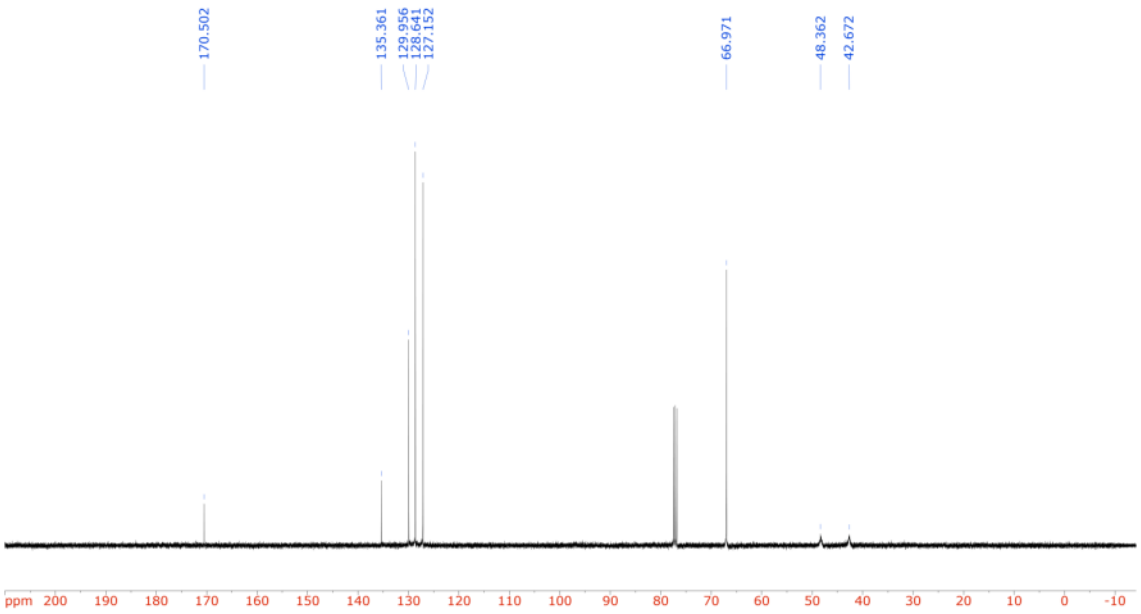

morpholino(*p*-tolyl)methanone (230ka)

^{1}H-NMR ($CDCl_3$, 400 MHz)

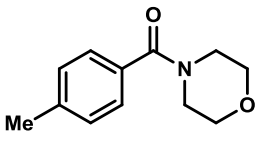

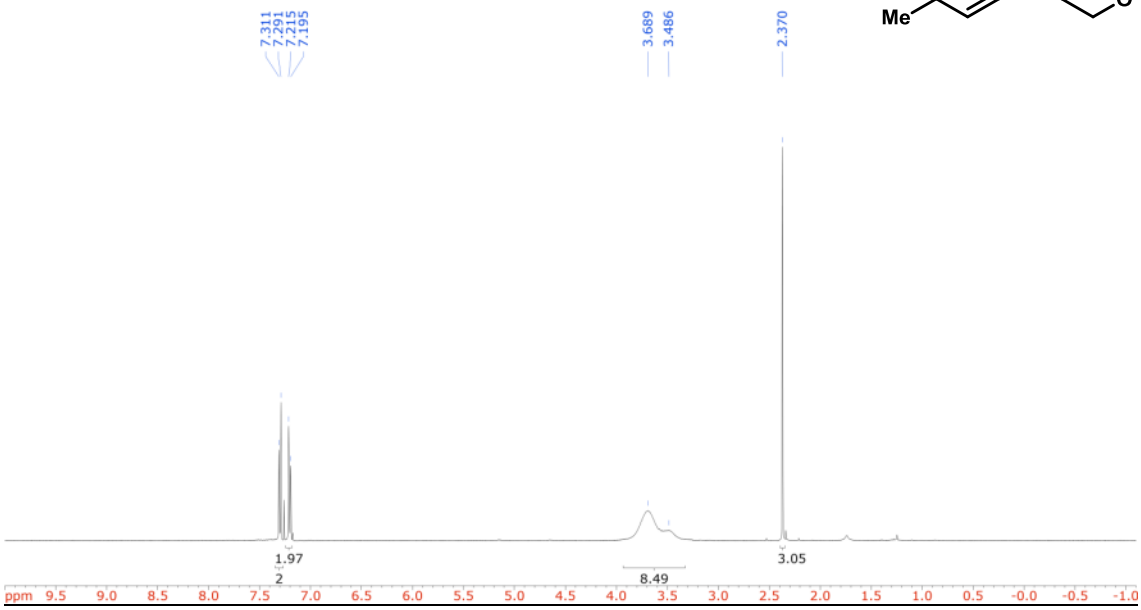

^{13}C-NMR ($CDCl_3$, 100 MHz)

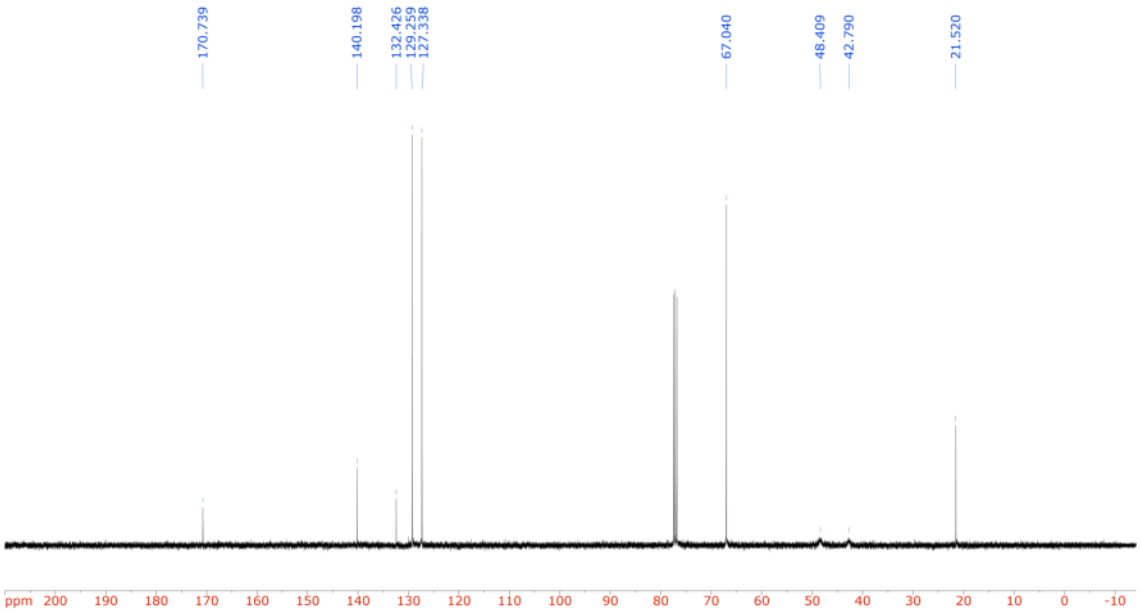

morpholino(*p*-tolyl)methanone (230kb)

^{1}H-NMR ($CDCl_3$, 400 MHz)

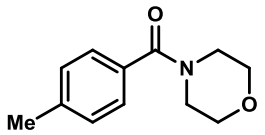

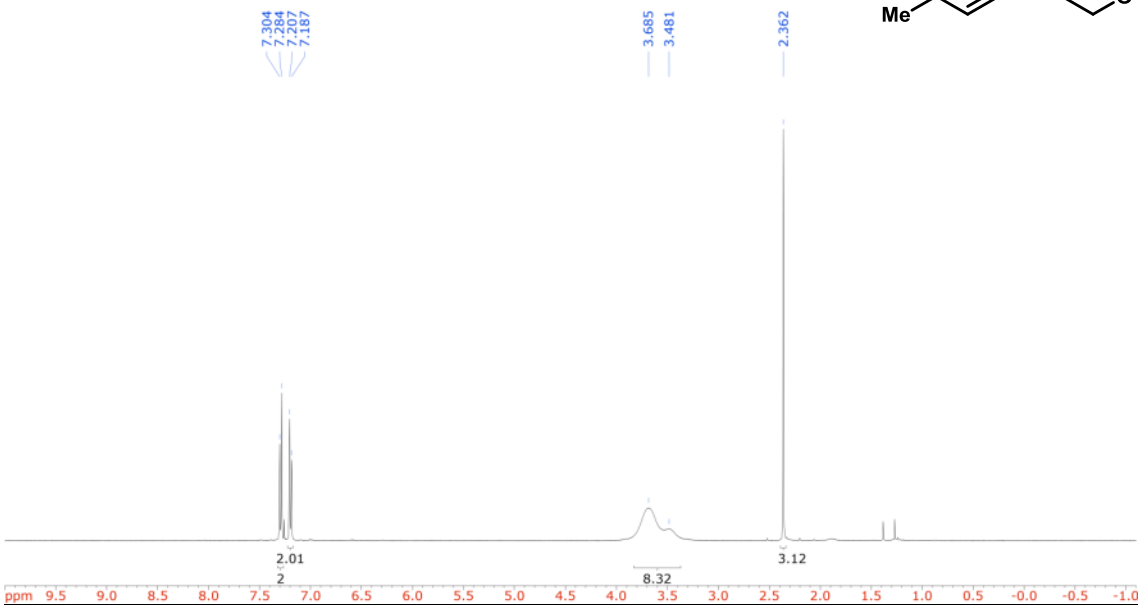

^{13}C-NMR ($CDCl_3$, 100 MHz)

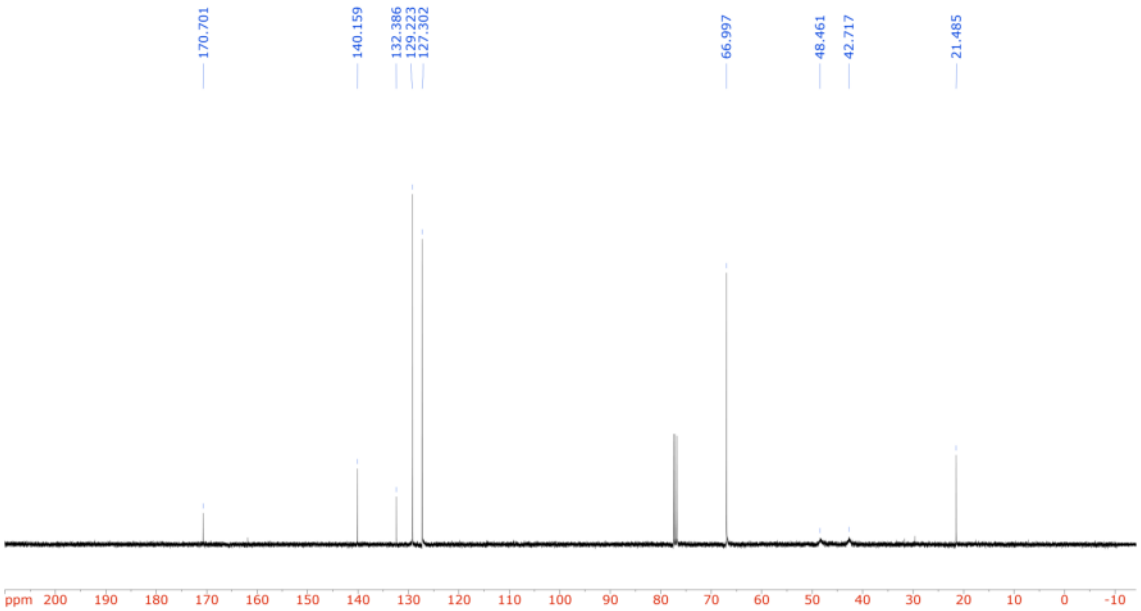

morpholino(*o*-tolyl)methanone (230la)

^{1}H-NMR ($CDCl_3$, 400 MHz)

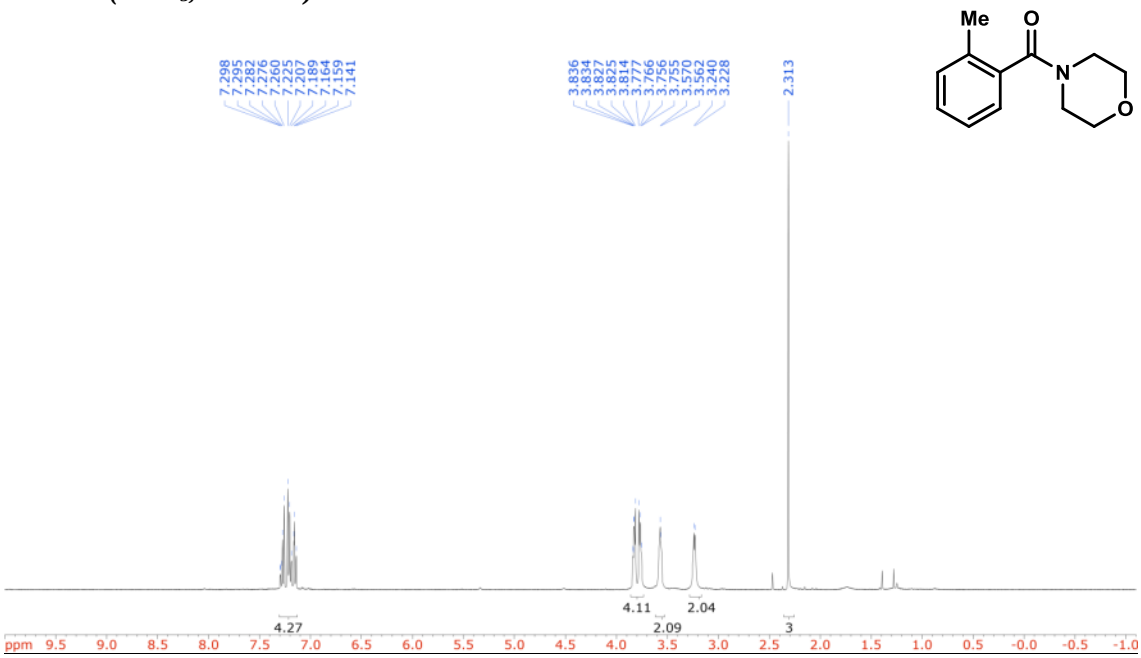

^{13}C-NMR ($CDCl_3$, 100 MHz)

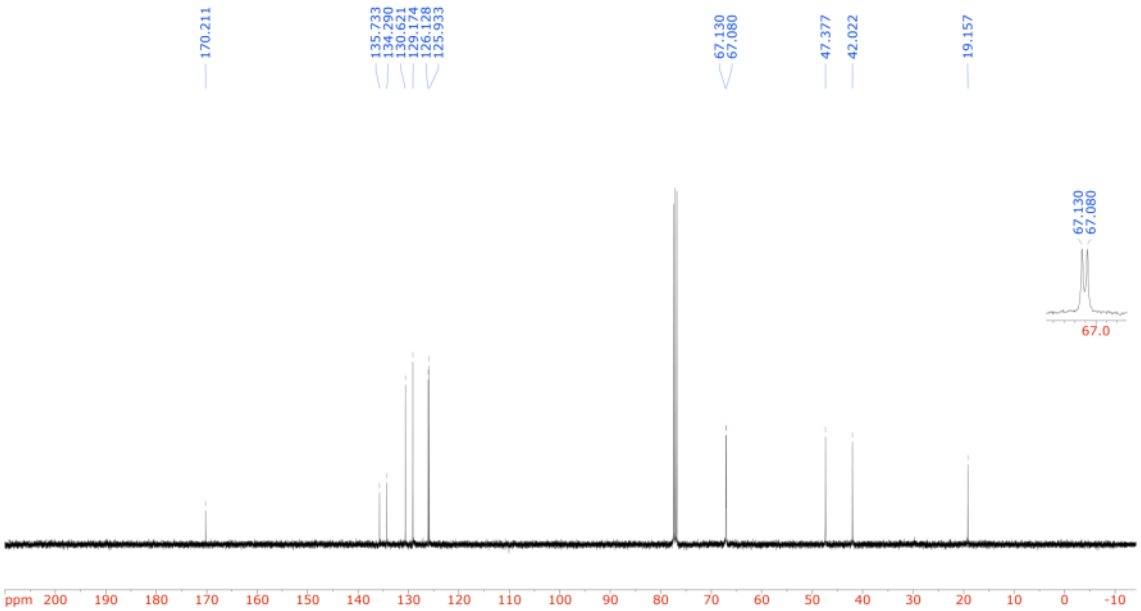

morpholino(*m*-tolyl)methanone (230lb)

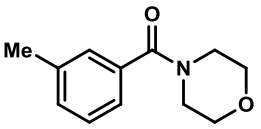

^{1}H-NMR ($CDCl_3$, 400 MHz)

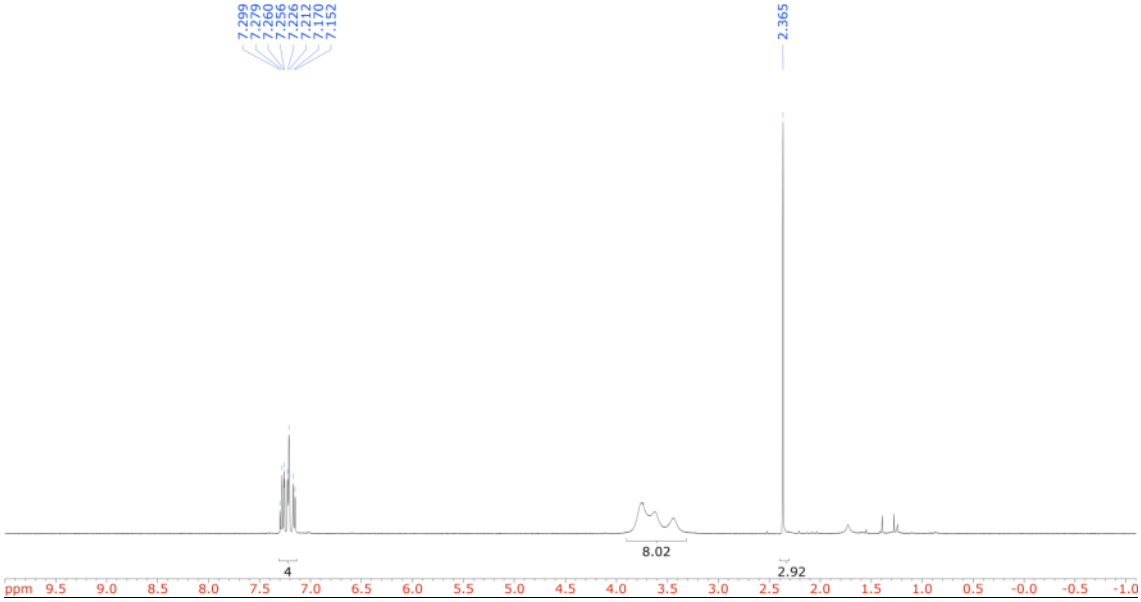

^{13}C-NMR ($CDCl_3$, 100 MHz)

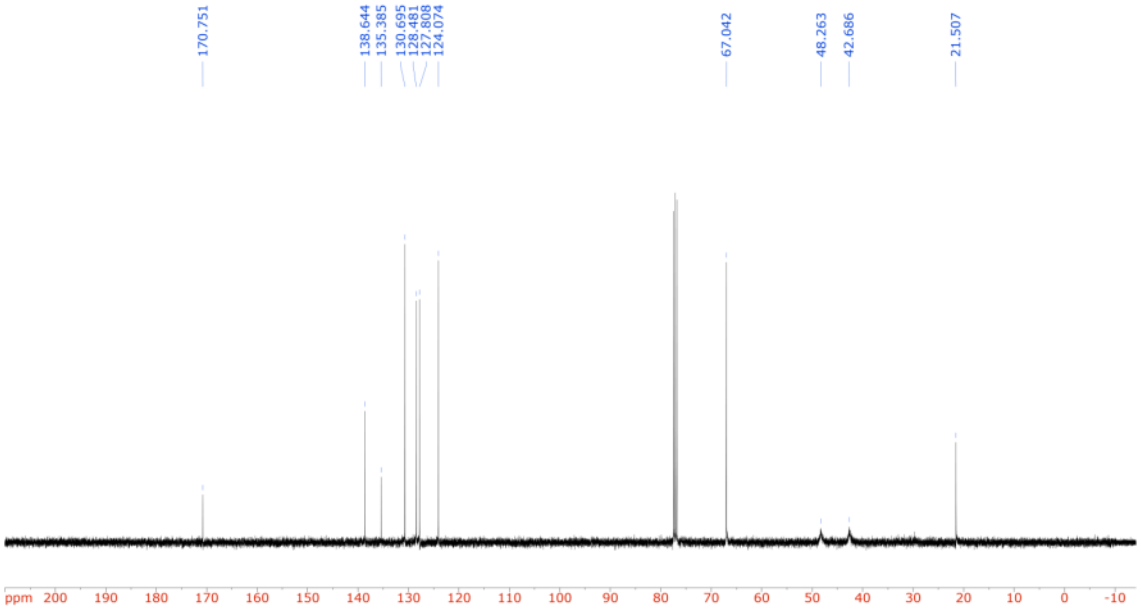

(4-(*tert*-butyl)phenyl)(morpholino)methanone (230mb)

^{1}H-NMR ($CDCl_3$, 400 MHz)

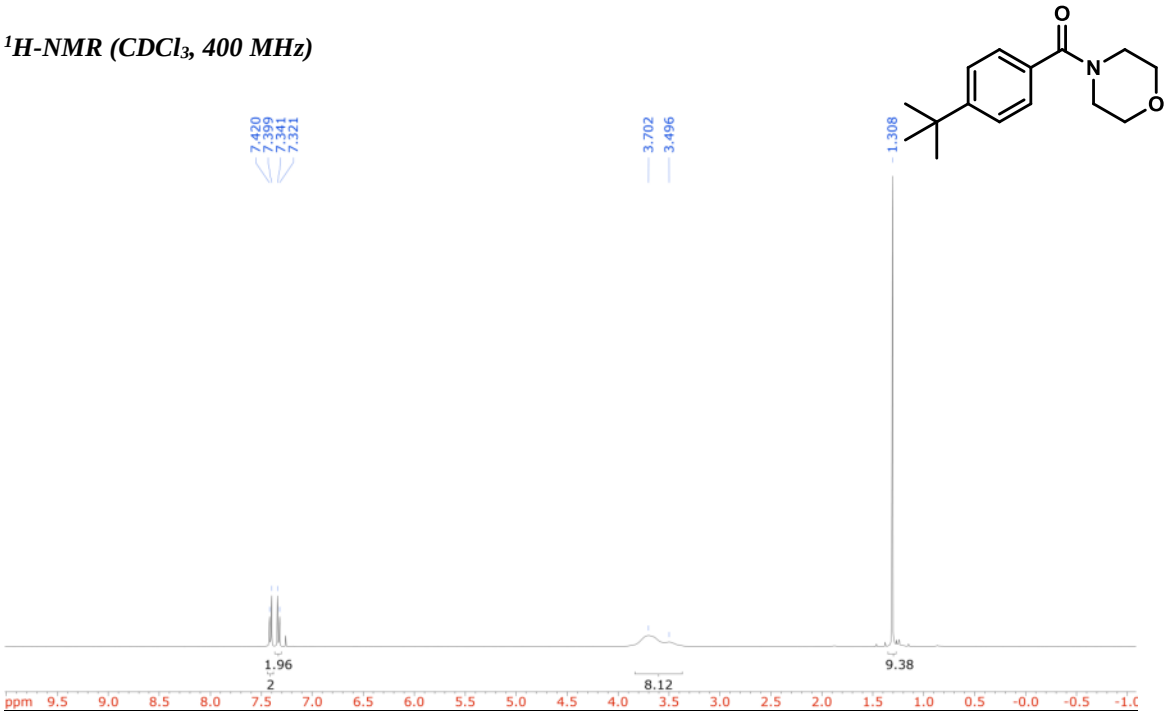

^{13}C-NMR ($CDCl_3$, 100 MHz)

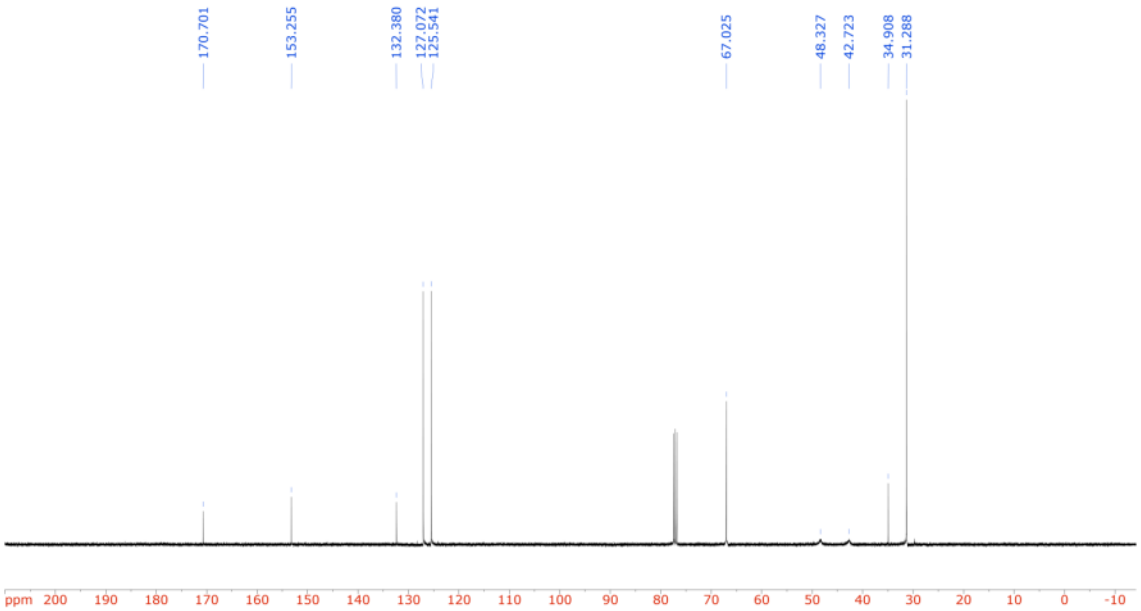

[1,1'-biphenyl]-4-yl(morpholino)methanone (230nb)

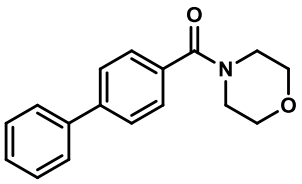

^{1}H-NMR ($CDCl_3$, 400 MHz)

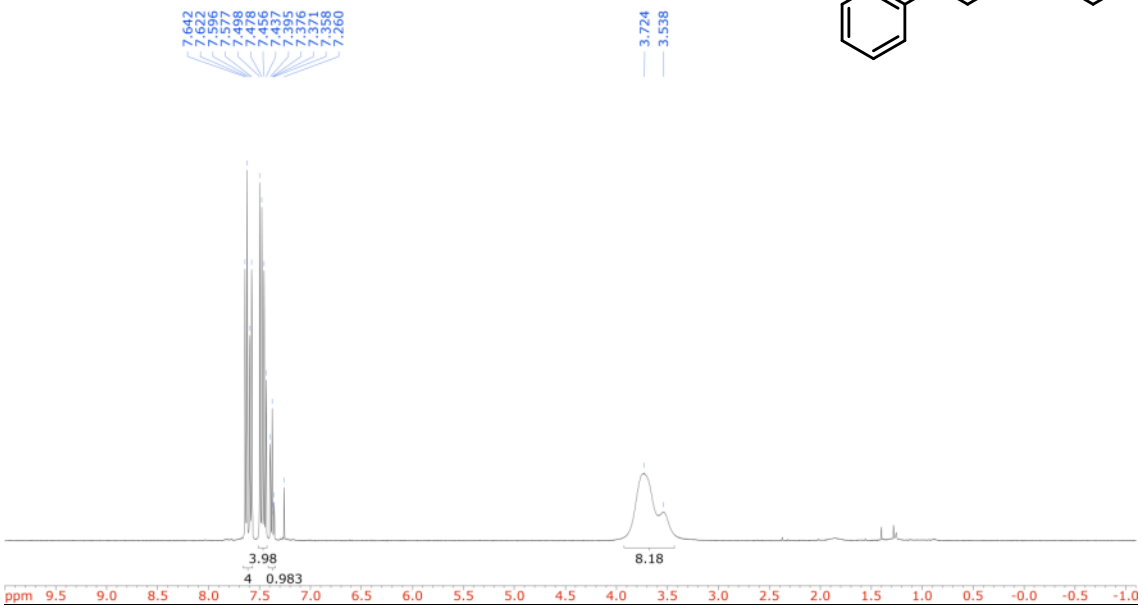

^{13}C-NMR ($CDCl_3$, 100 MHz)

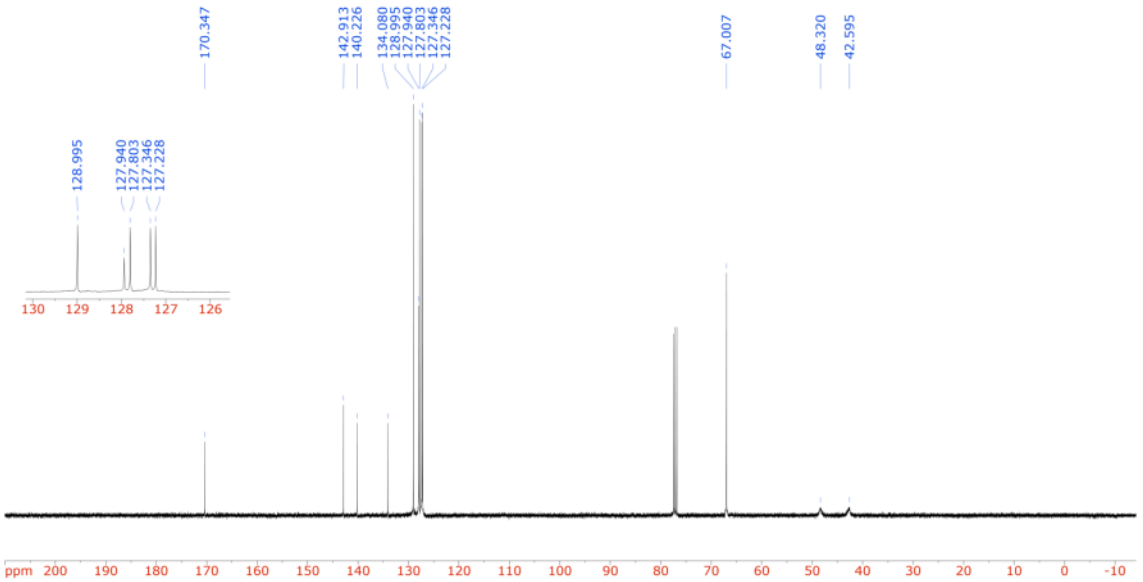

N-(4-(morpholine-4-carbonyl)phenyl)acetamide (230oa)

^{1}H-NMR ($CDCl_3$, 400 MHz)

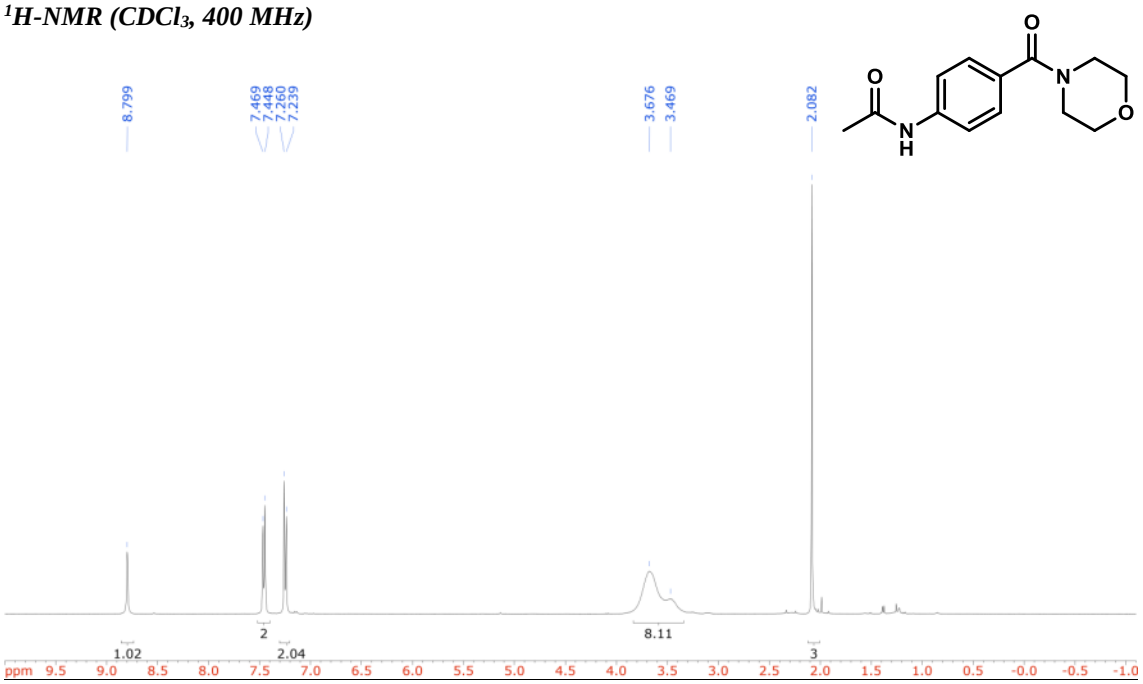

^{13}C-NMR ($CDCl_3$, 100 MHz)

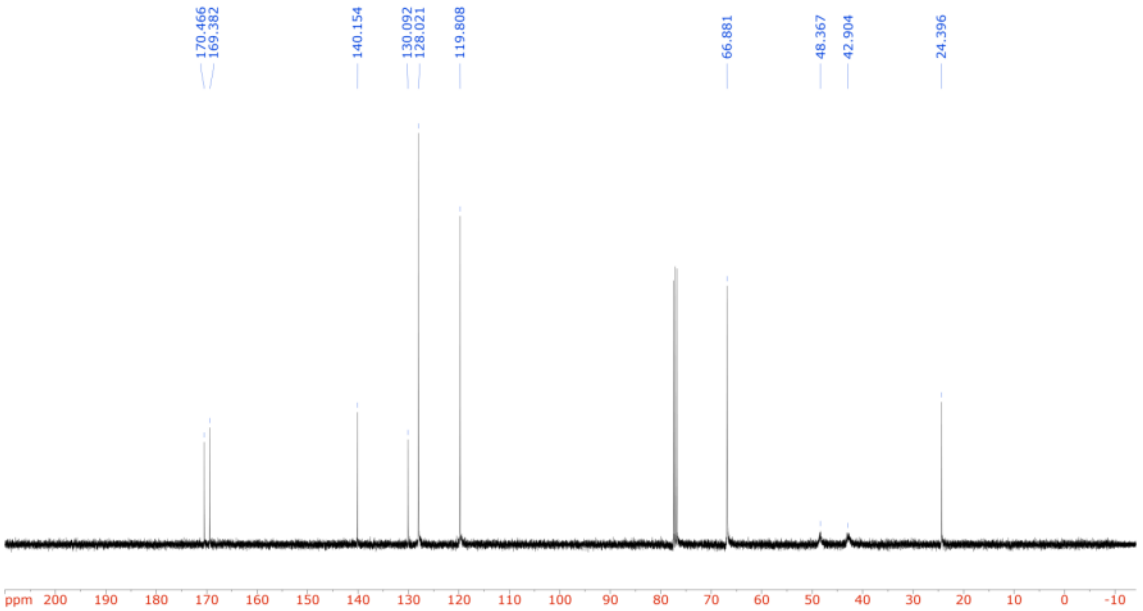

N-(4-(morpholine-4-carbonyl)phenyl)acetamide (230ob)

^{1}H-NMR ($CDCl_3$, 400 MHz)

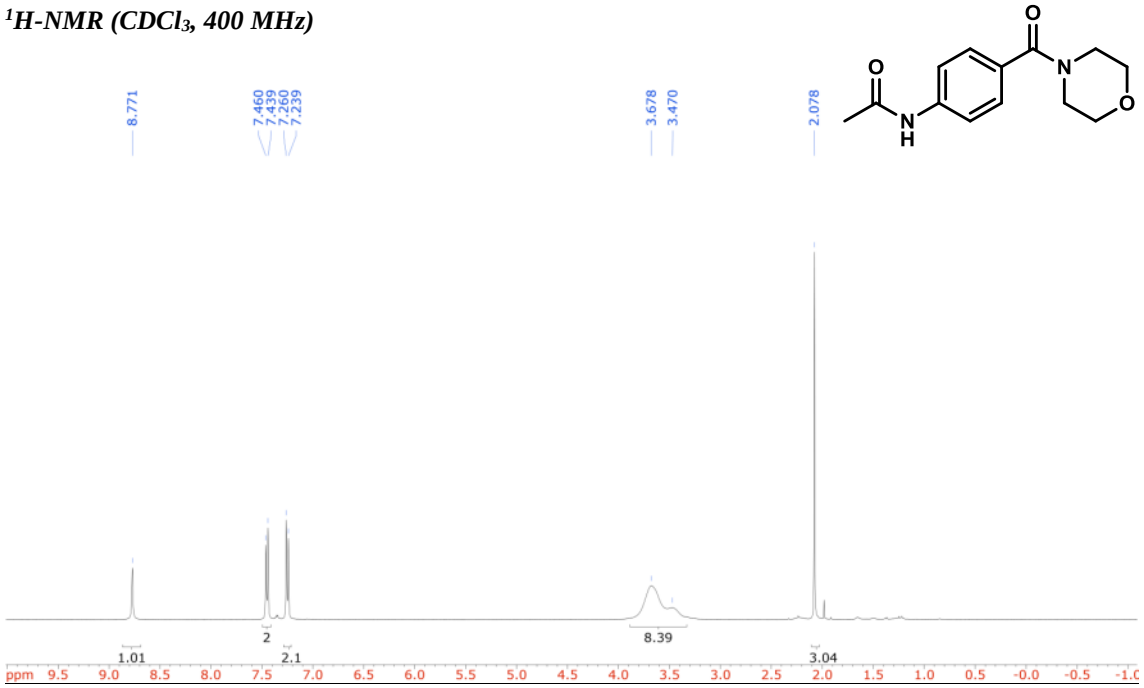

^{13}C-NMR ($CDCl_3$, 100 MHz)

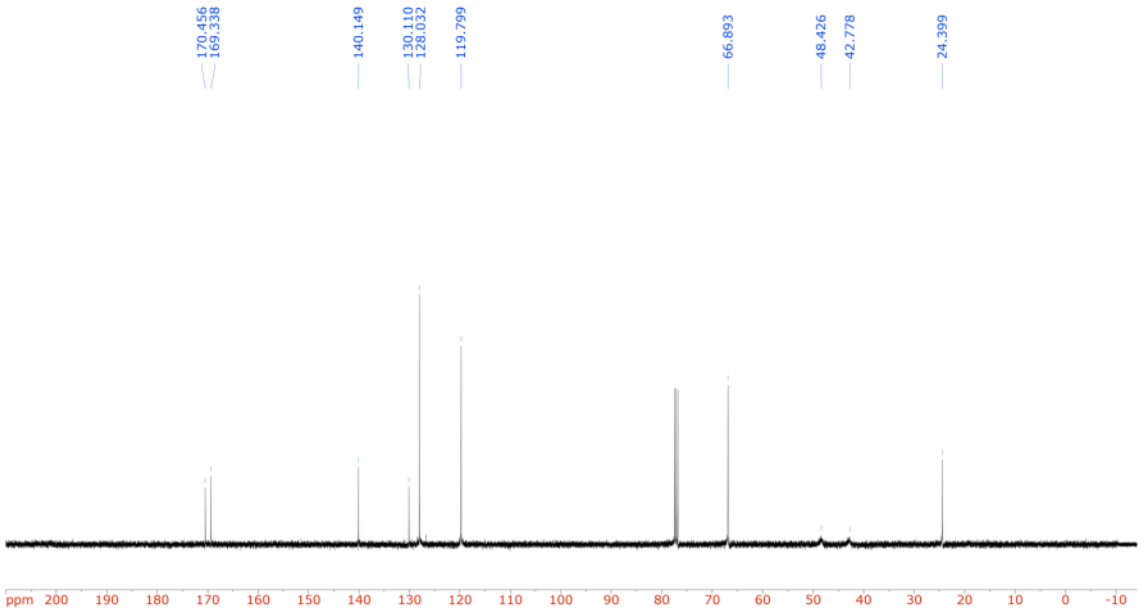

(4-methoxyphenyl)(morpholino)methanone (230pa)

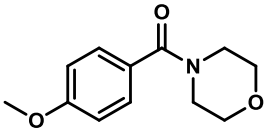

^{1}H-NMR ($CDCl_3$, 400 MHz)

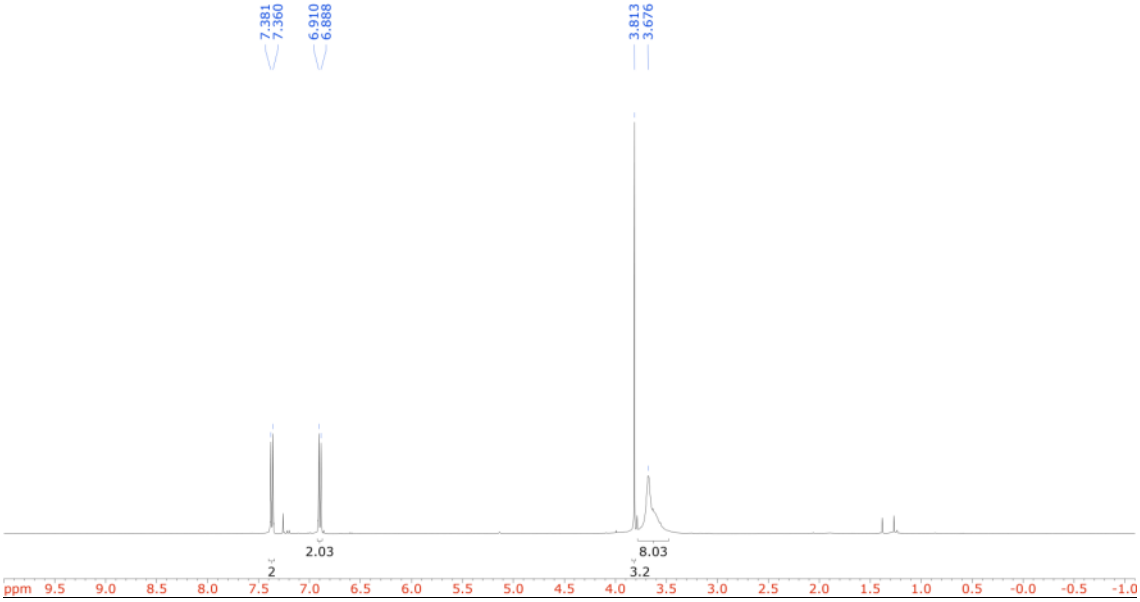

^{13}C-NMR ($CDCl_3$, 100 MHz)

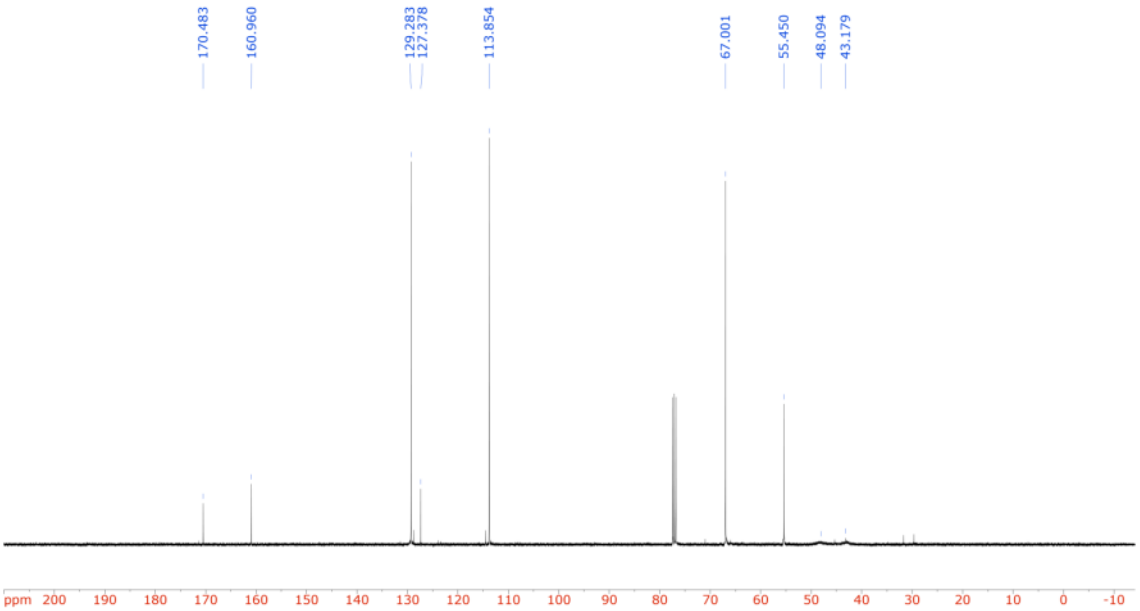

(4-methoxyphenyl)(morpholino)methanone (230pb)

^{1}H-NMR ($CDCl_3$, 400 MHz)

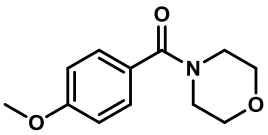

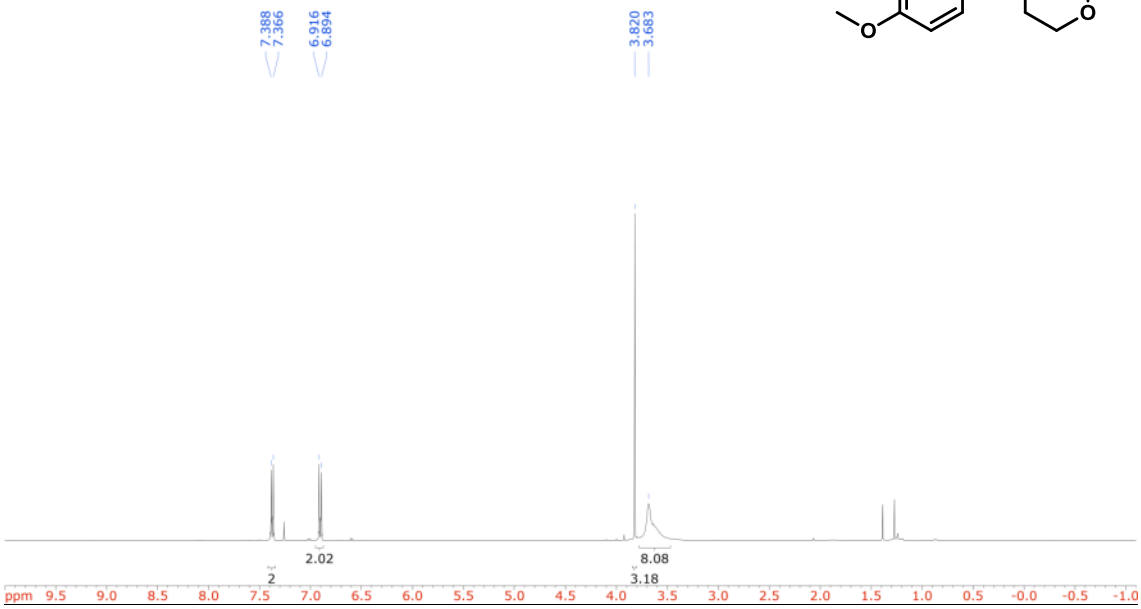

^{13}C-NMR ($CDCl_3$, 100 MHz)

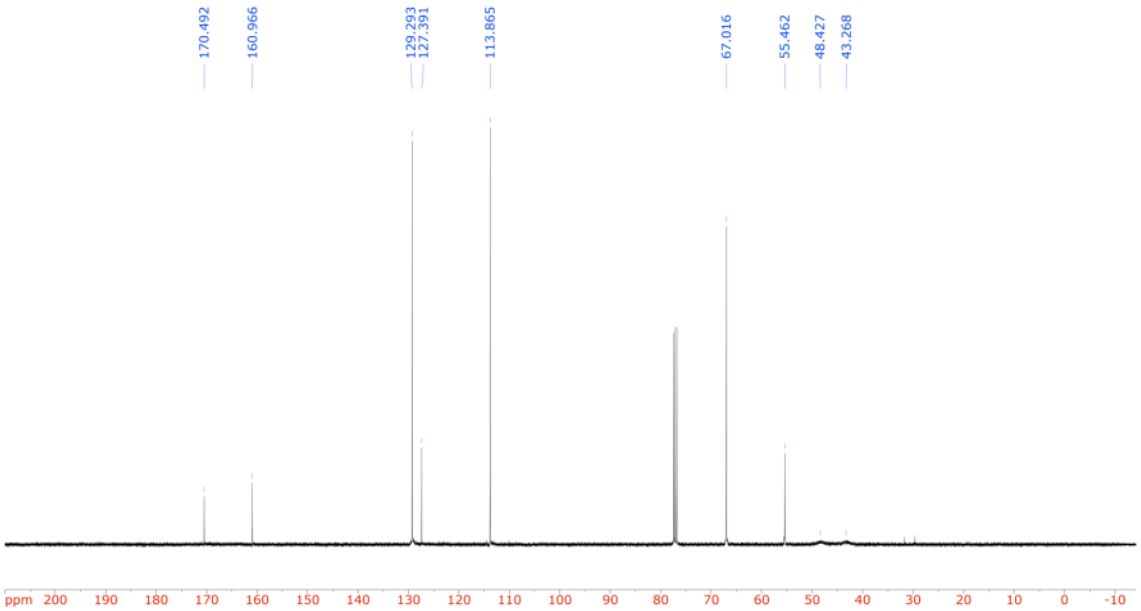

(4-hydroxyphenyl)(morpholino)methanone (230qa)

^{1}H-NMR ($CDCl_3$, 400 MHz)

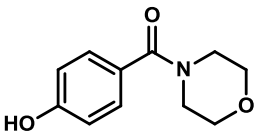

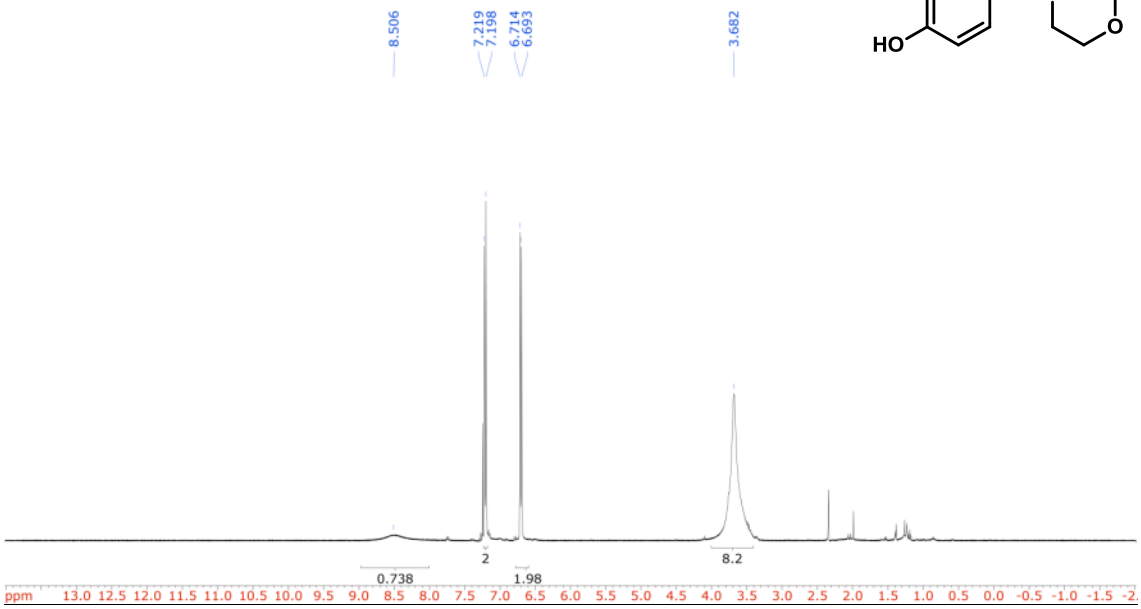

^{13}C-NMR ($CDCl_3$, 100 MHz)

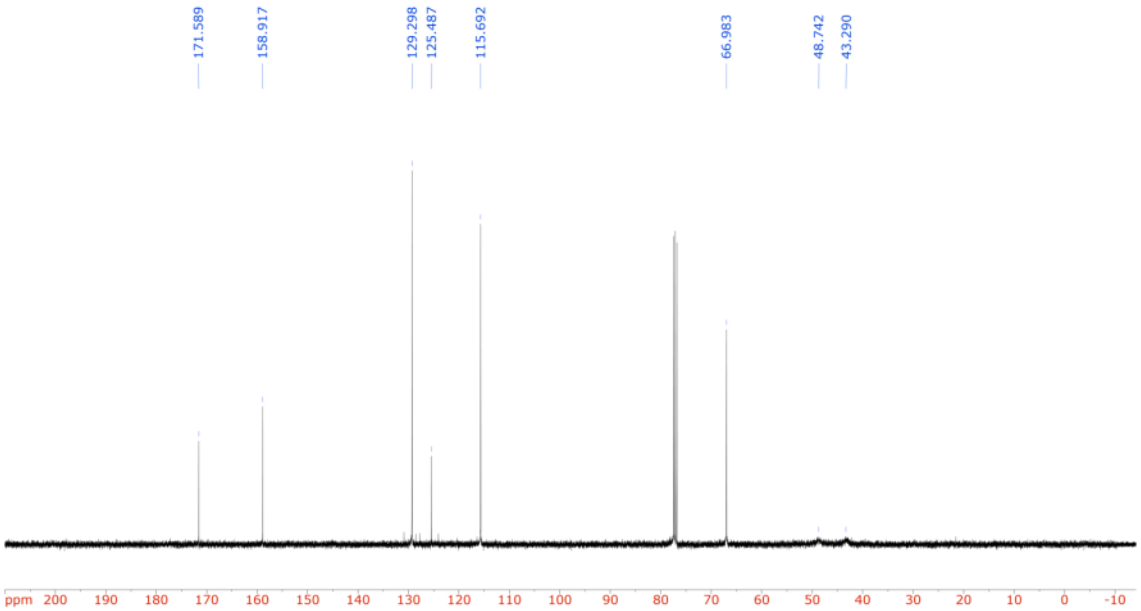

(4-hydroxyphenyl)(morpholino)methanone (230qb)

^{1}H-NMR ($CDCl_3$, 400 MHz)

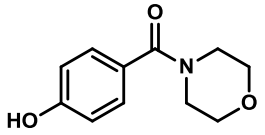

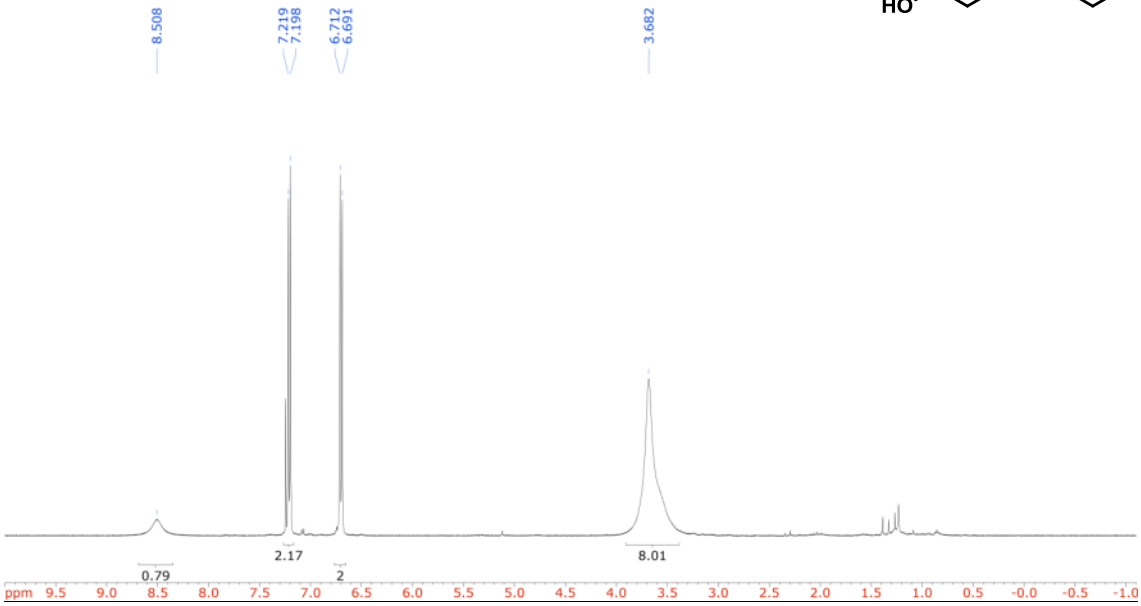

^{13}C-NMR ($CDCl_3$, 100 MHz)

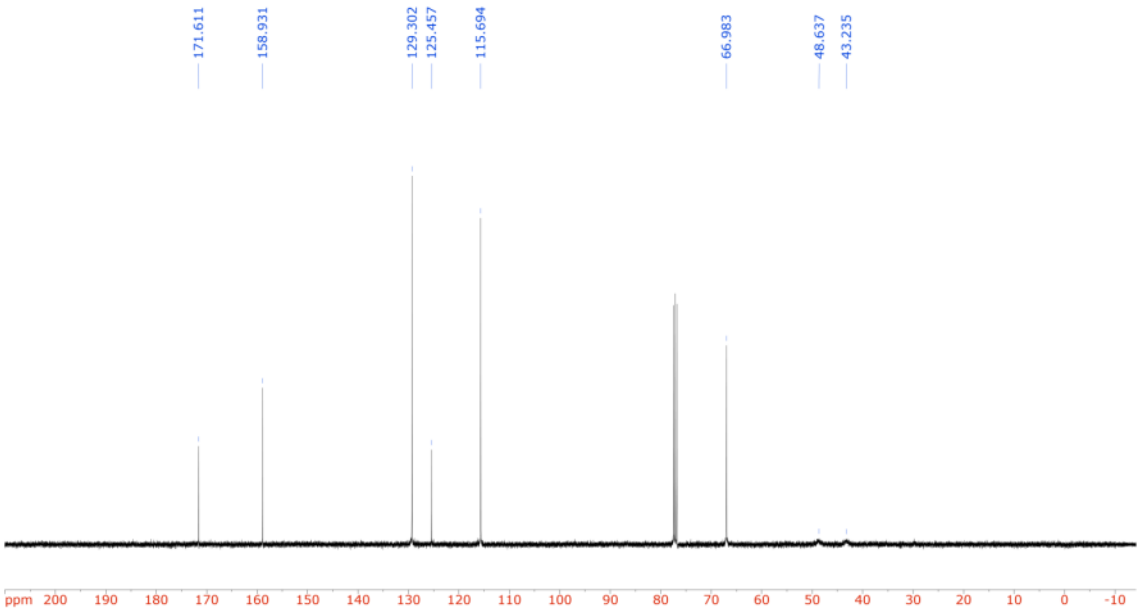

(4-(methylthio)phenyl)(morpholino)methanone (230rb)

^{1}H-NMR ($CDCl_3$, 400 MHz)

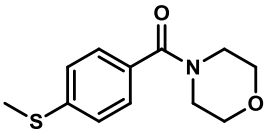

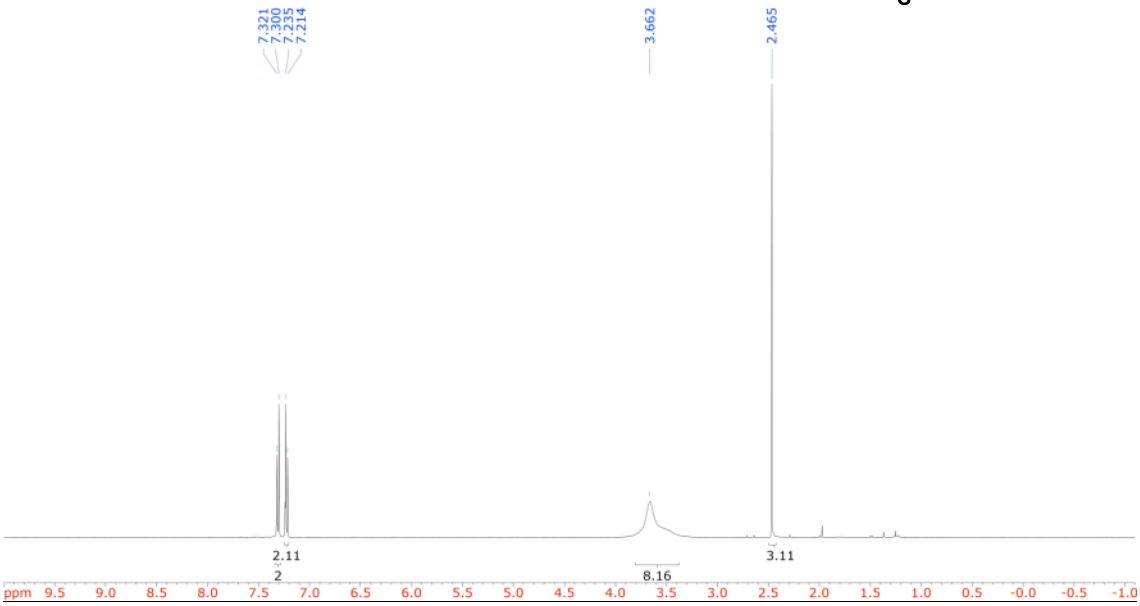

^{13}C-NMR ($CDCl_3$, 100 MHz)

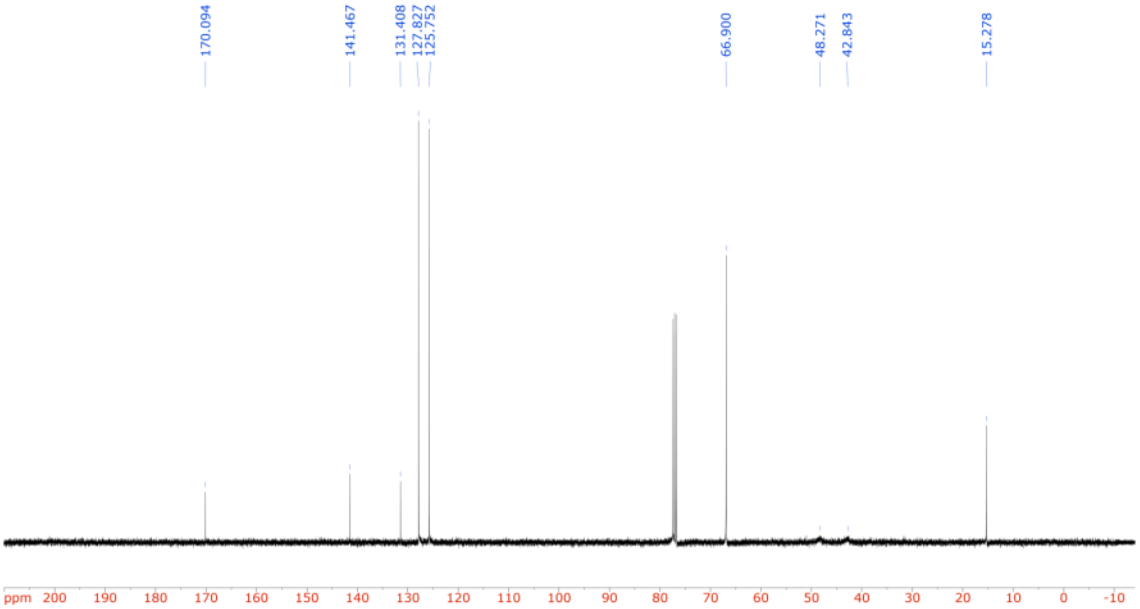

morpholino(pyridin-2-yl)methanone (230sa)

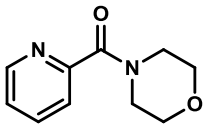

^{1}H-NMR ($CDCl_3$, 400 MHz)

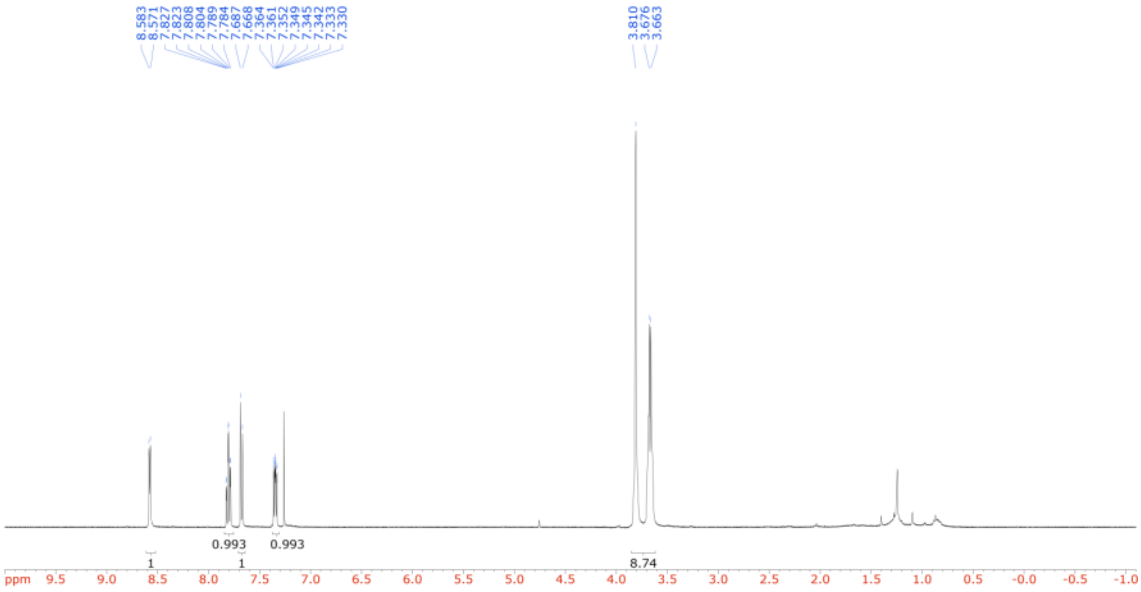

^{13}C-NMR ($CDCl_3$, 100 MHz)

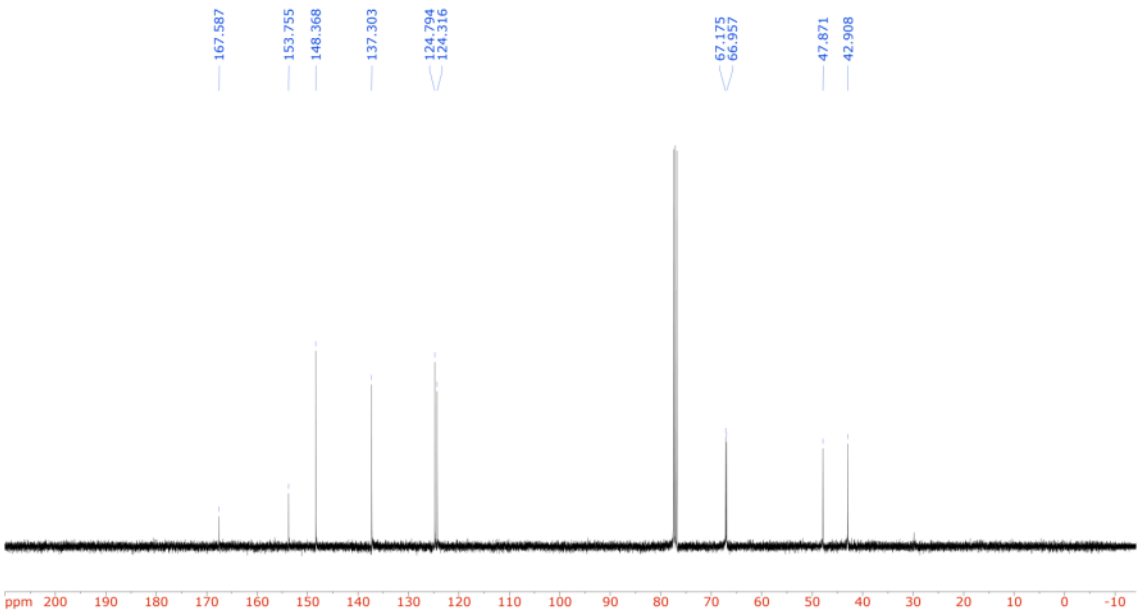

morpholino(pyridin-2-yl)methanone (230sb)

^{1}H-NMR ($CDCl_3$, 400 MHz)

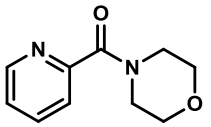

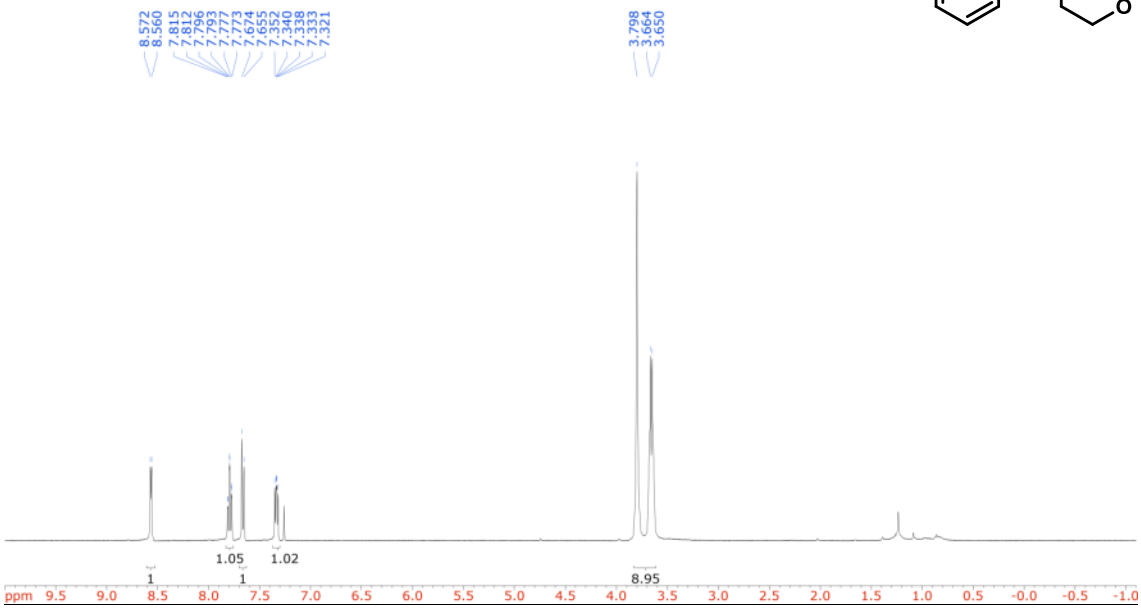

^{13}C-NMR ($CDCl_3$, 100 MHz)

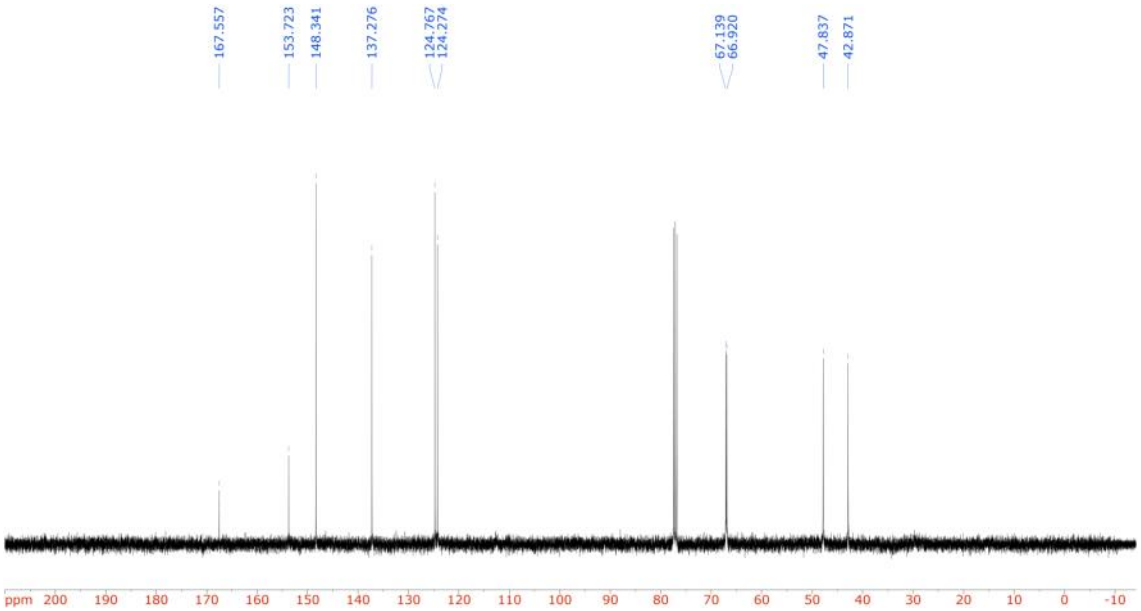

(1H-indol-7-yl)(morpholino)methanone (230ta)

^{1}H-NMR ($CDCl_3$, 400 MHz)

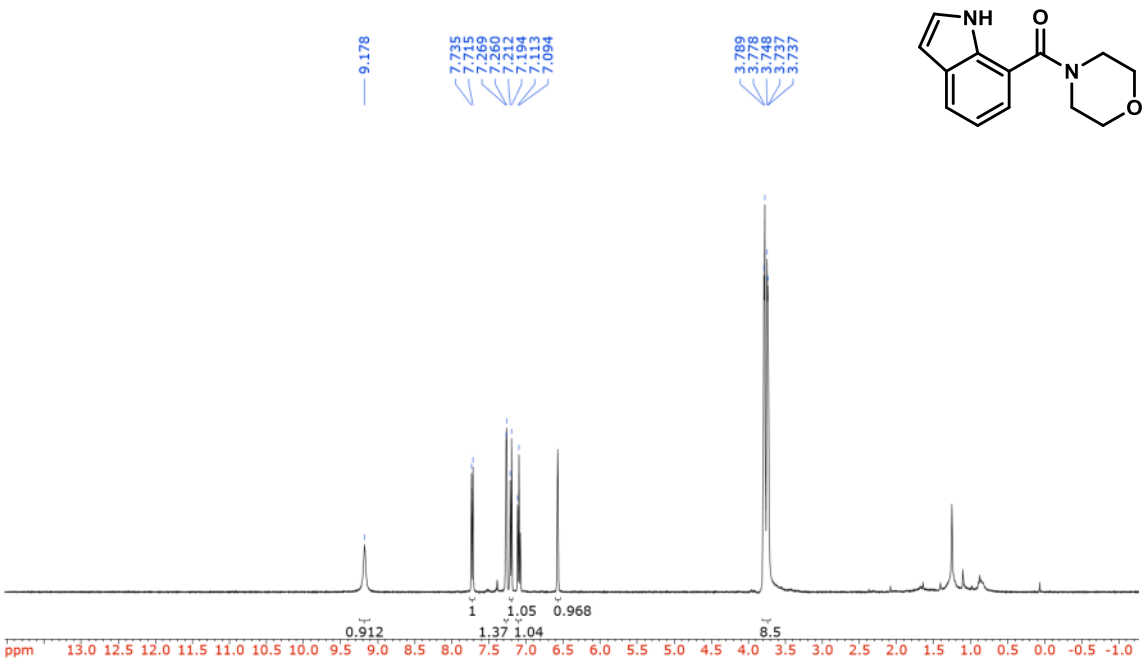

^{13}C-NMR ($CDCl_3$, 100 MHz)

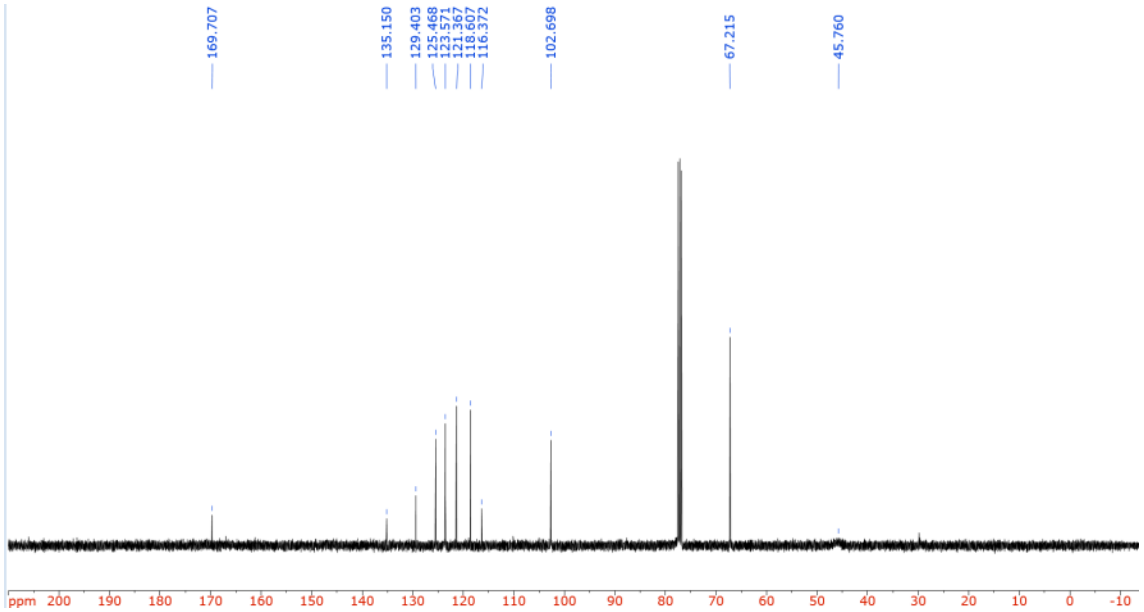

phenyl(pyrrolidin-1-yl)methanone (232a)

^{1}H-NMR ($CDCl_3$, 400 MHz)

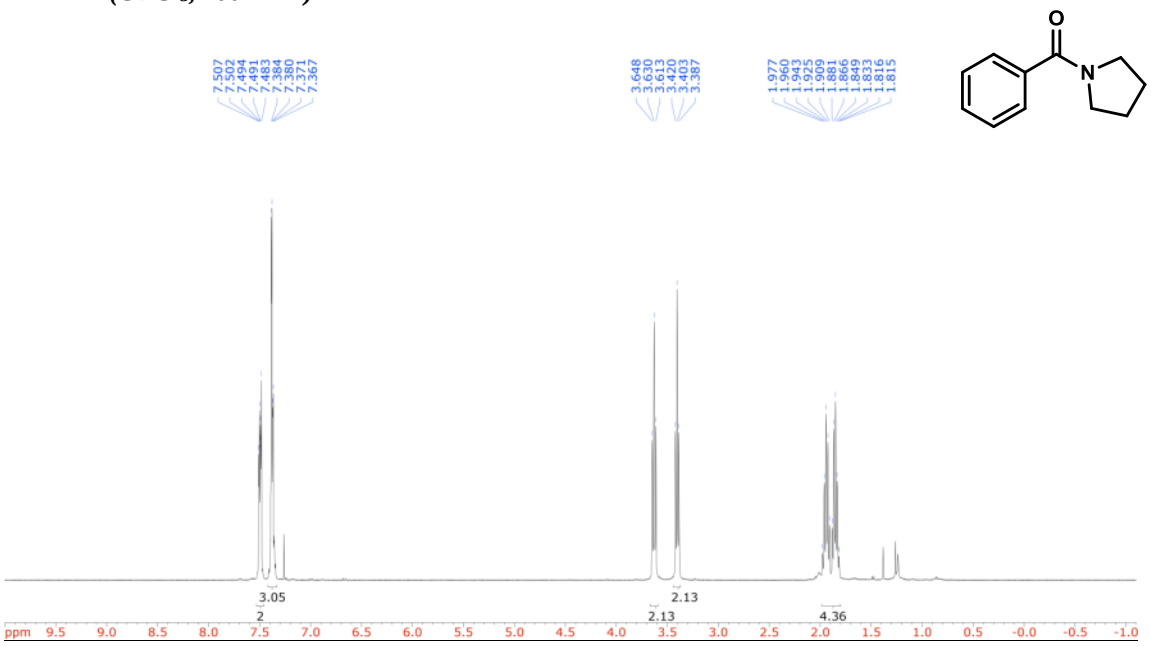

^{13}C-NMR ($CDCl_3$, 100 MHz)

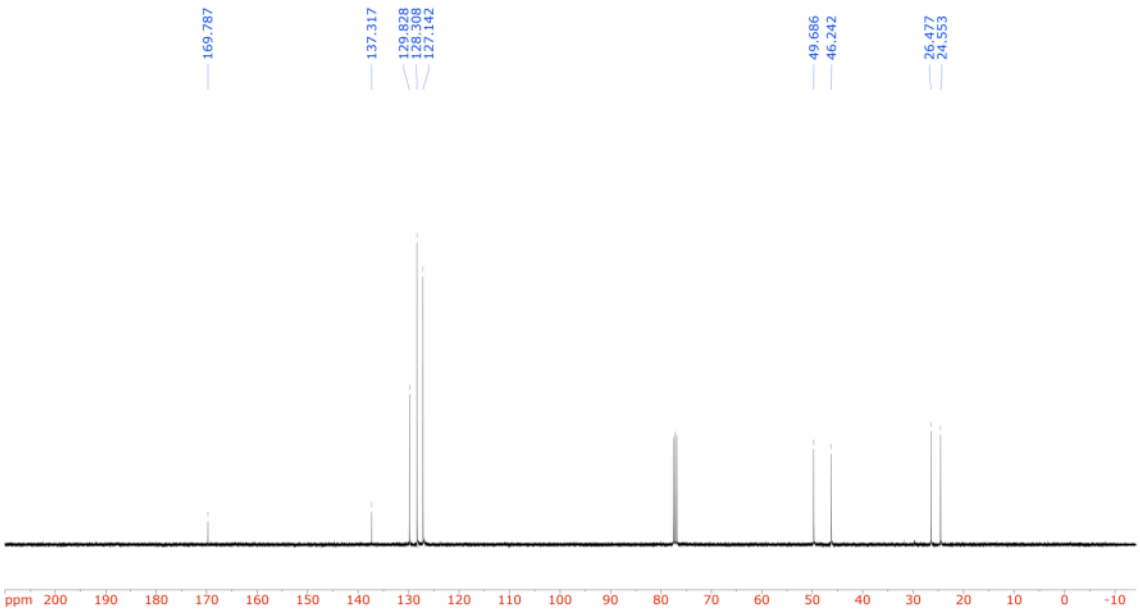

phenyl(piperidin-1-yl)methanone (232b)

^{1}H-NMR ($CDCl_3$, 400 MHz)

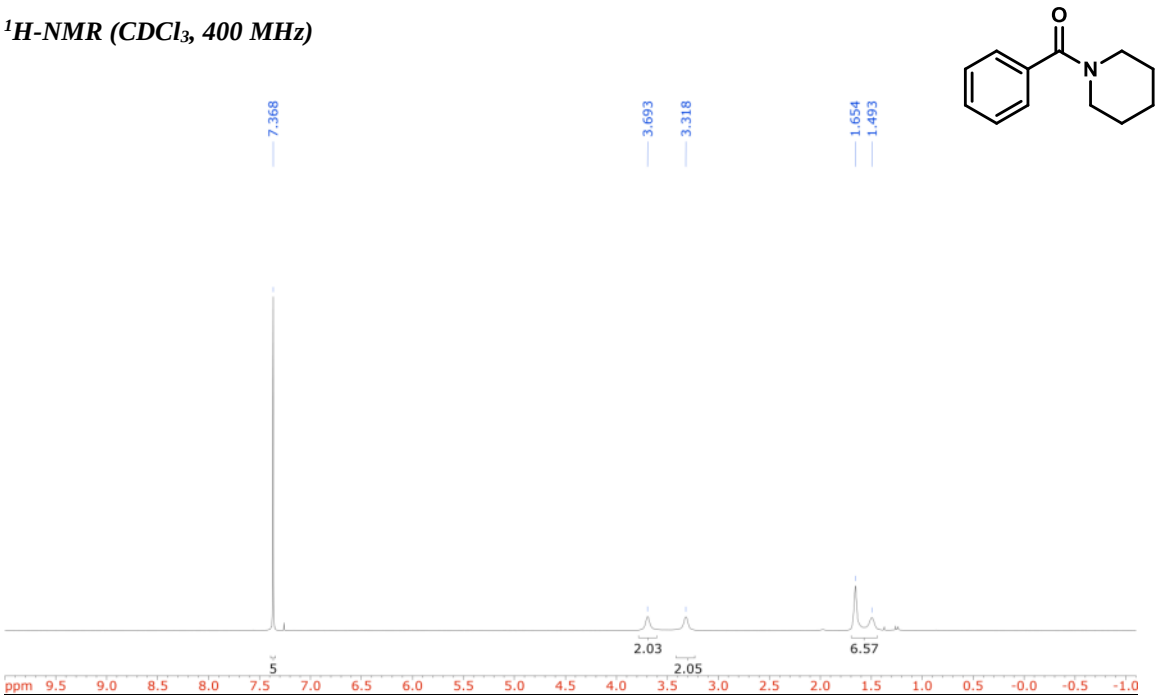

^{13}C-NMR ($CDCl_3$, 100 MHz)

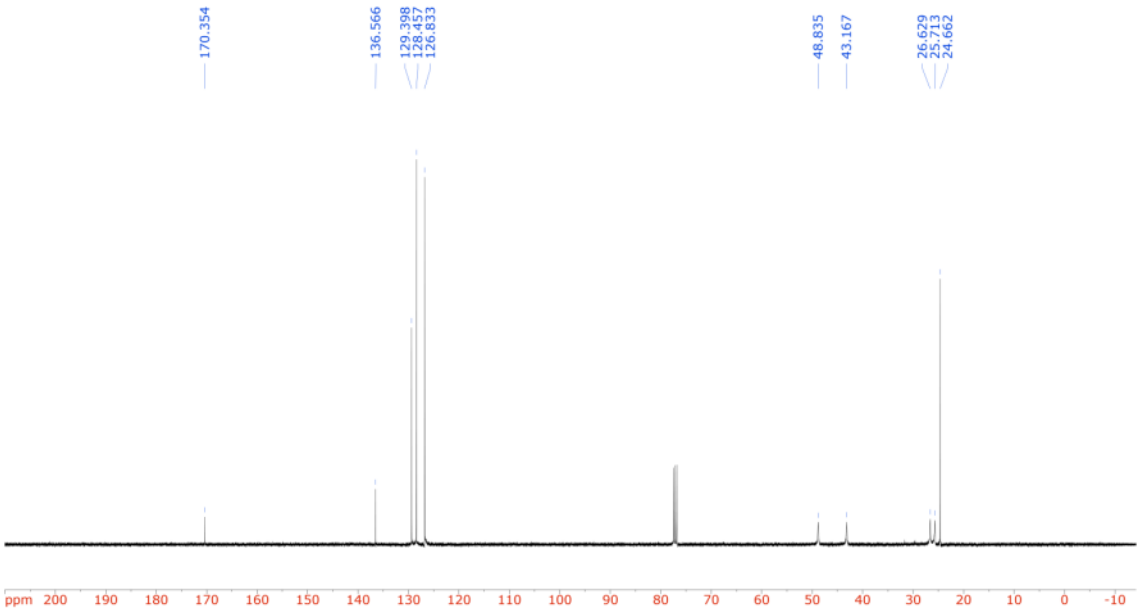

N,N-dipropylbenzamide (232c)

^{1}H-NMR ($CDCl_3$, 400 MHz)

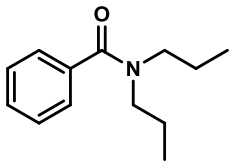

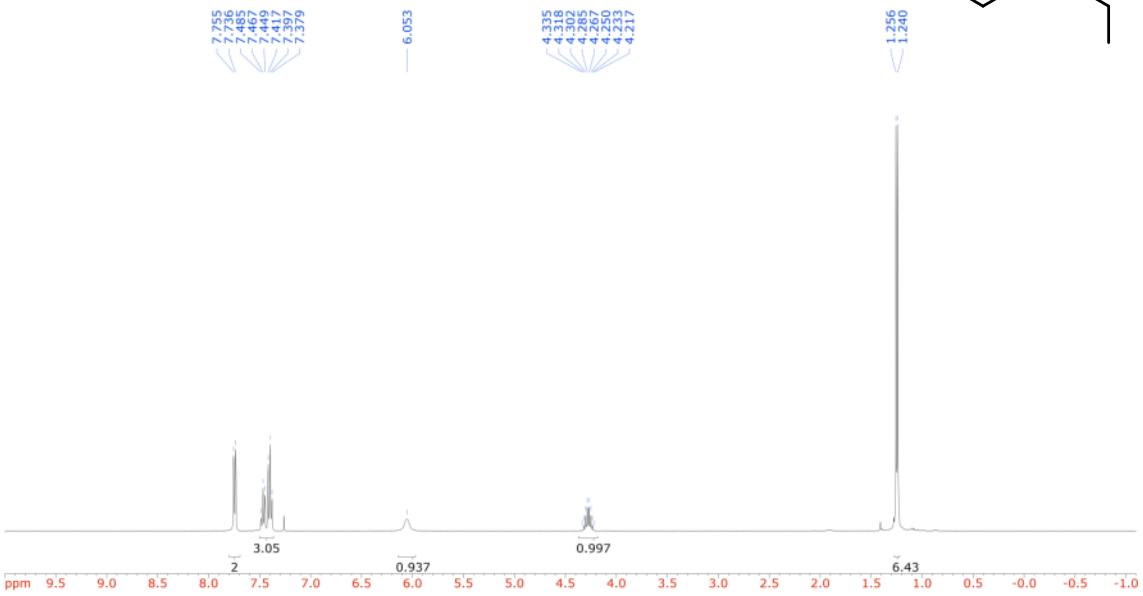

^{13}C-NMR ($CDCl_3$, 100 MHz)

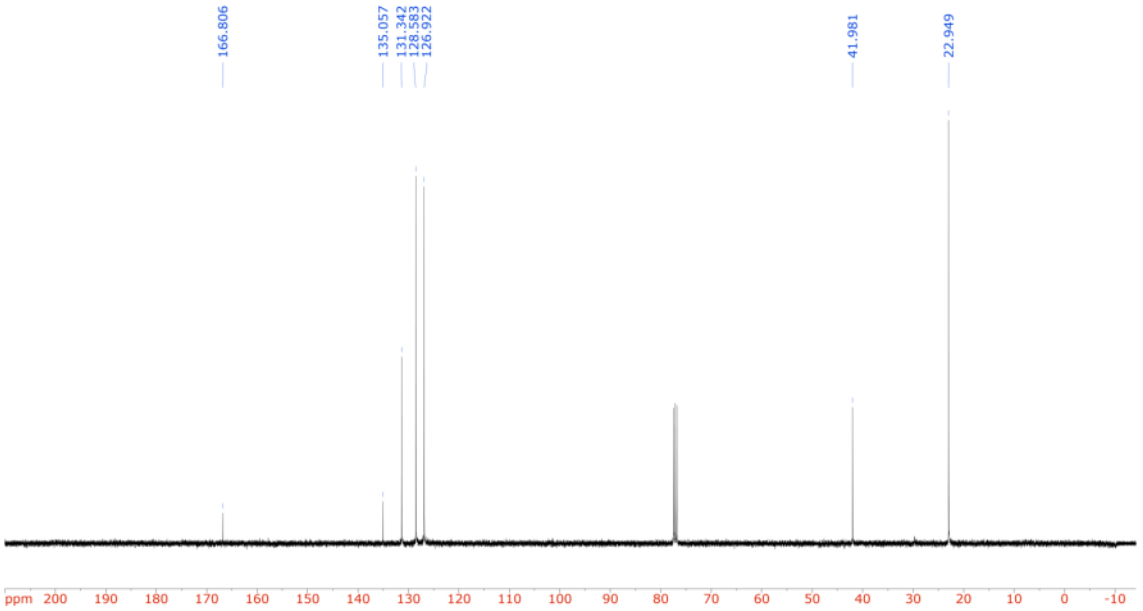

N-(2-hydroxyethyl)benzamide (232d)

^{1}H-NMR ($CDCl_3$, 400 MHz)

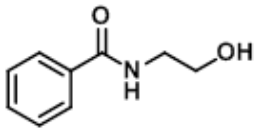

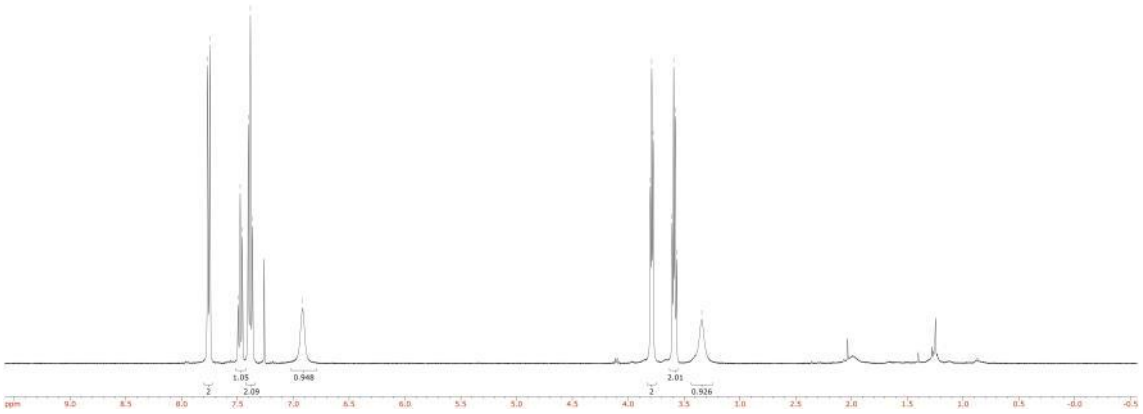

N-hexylbenzamide (232e)

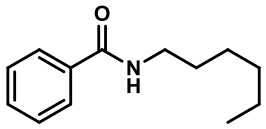

^{1}H-NMR ($CDCl_3$, 400 MHz)

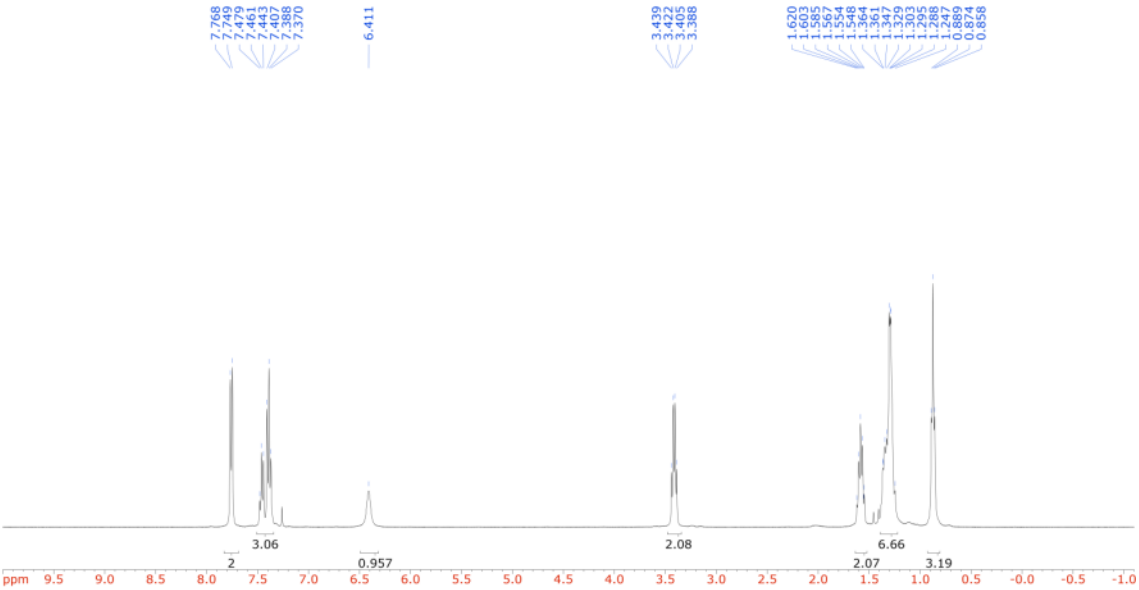

^{13}C-NMR ($CDCl_3$, 100 MHz)

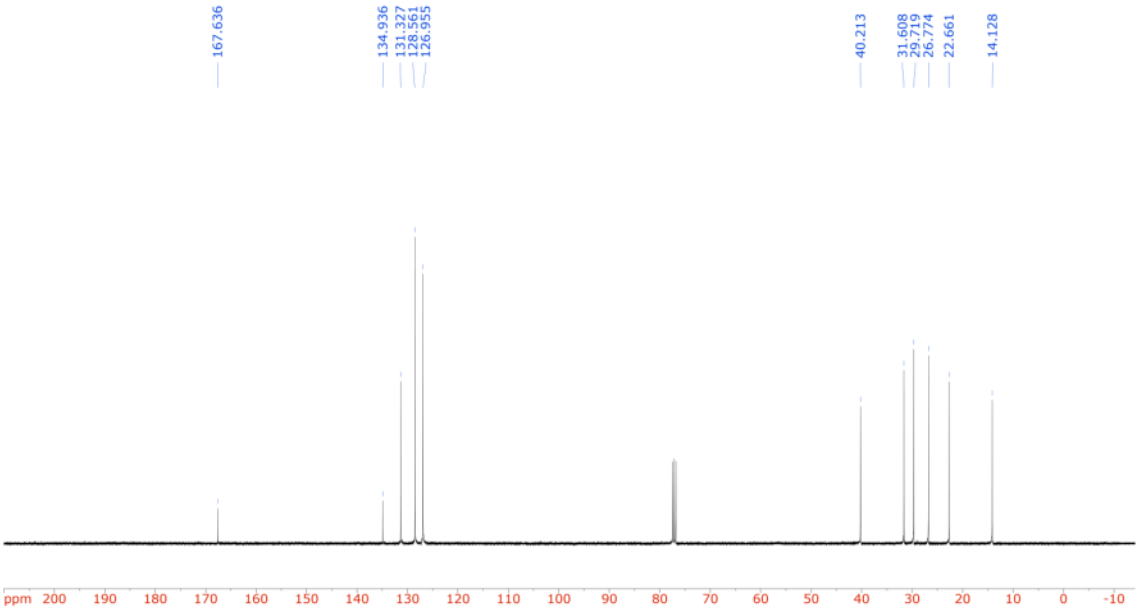

N-isopropylbenzamide (232f)

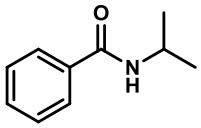

^{1}H-NMR ($CDCl_3$, 400 MHz)

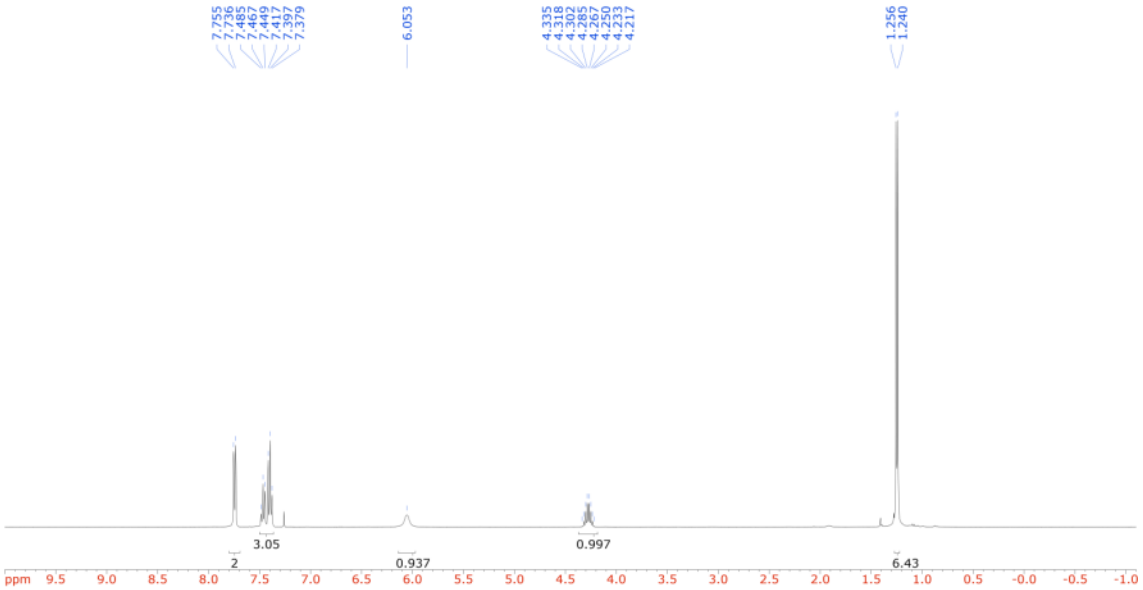

^{13}C-NMR ($CDCl_3$, 100 MHz)

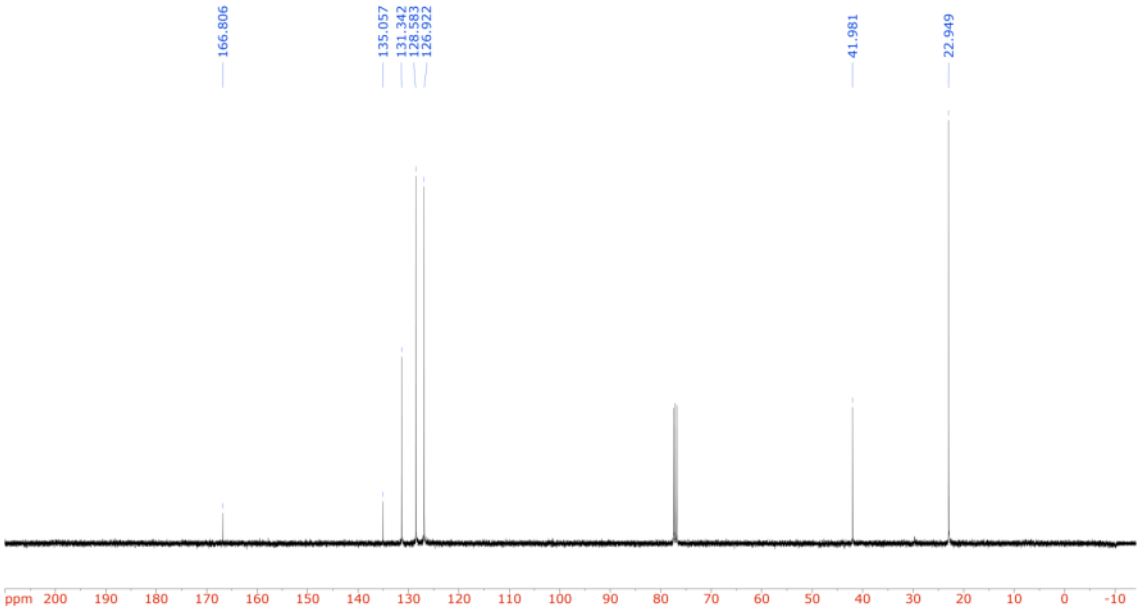

N-(*tert*-butyl)benzamide (232g)

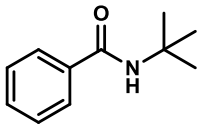

^{1}H-NMR ($CDCl_3$, 400 MHz)

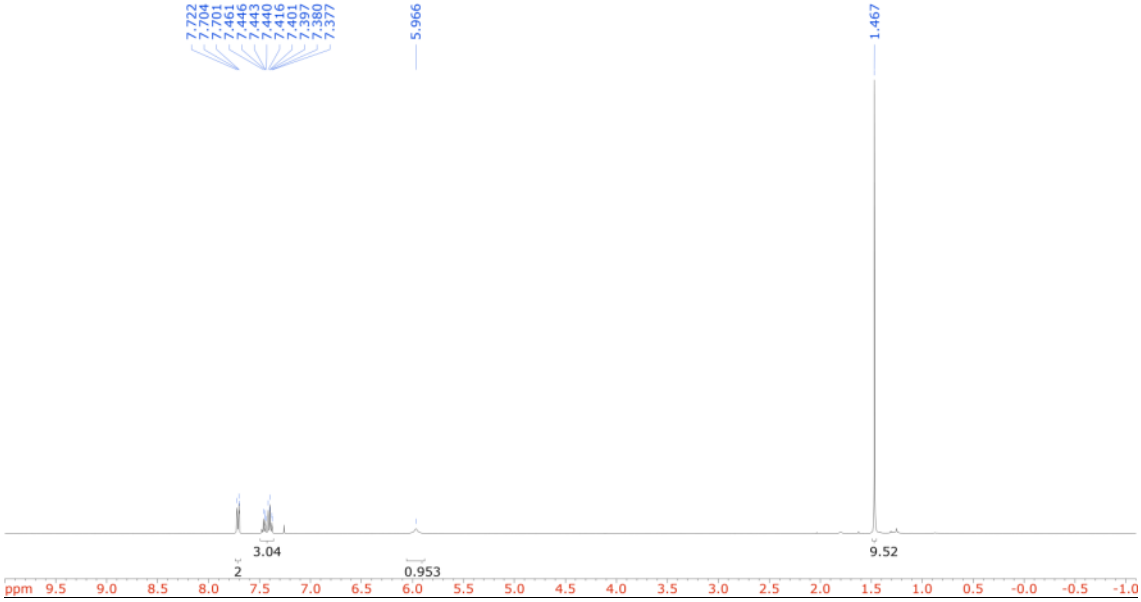

^{13}C-NMR ($CDCl_3$, 100 MHz)

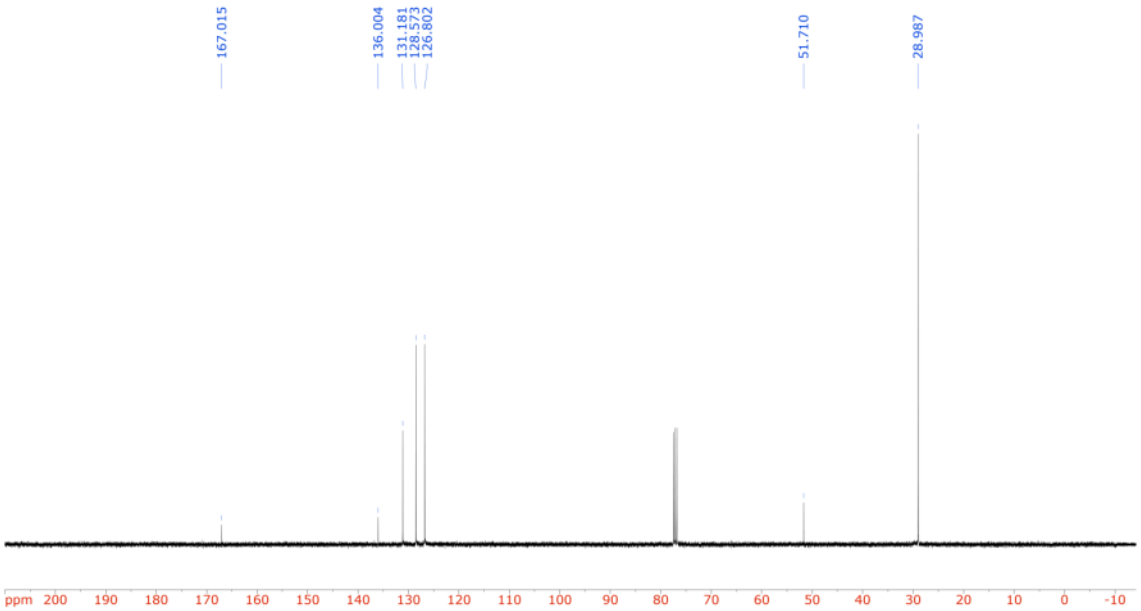

N-benzylbenzamide (232h)

^{1}H-NMR ($CDCl_3$, 400 MHz)

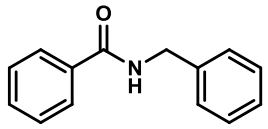

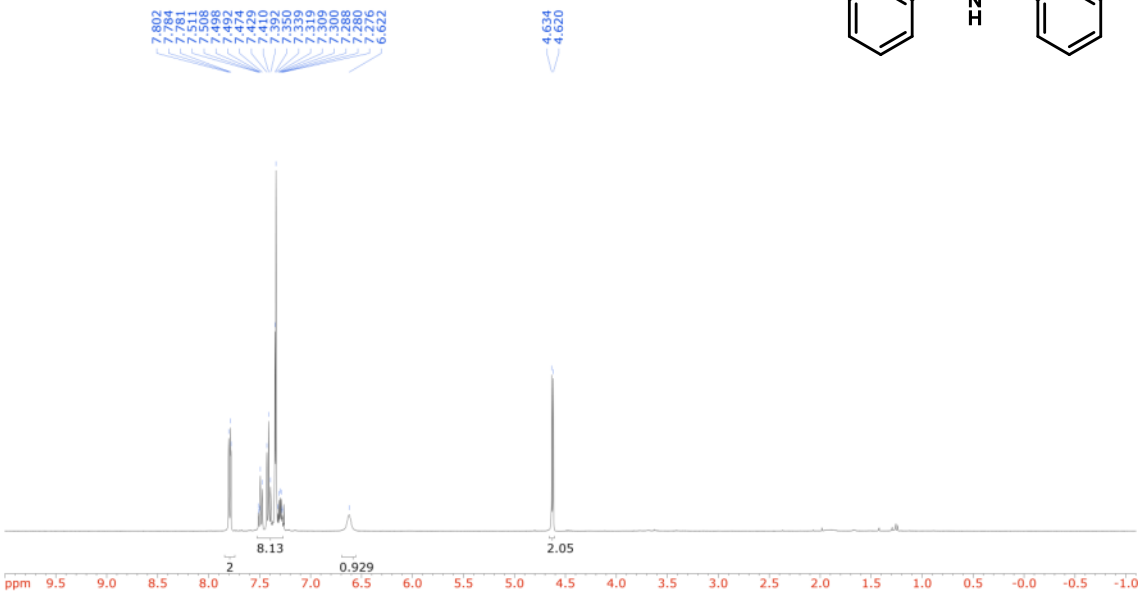

^{13}C-NMR ($CDCl_3$, 100 MHz)

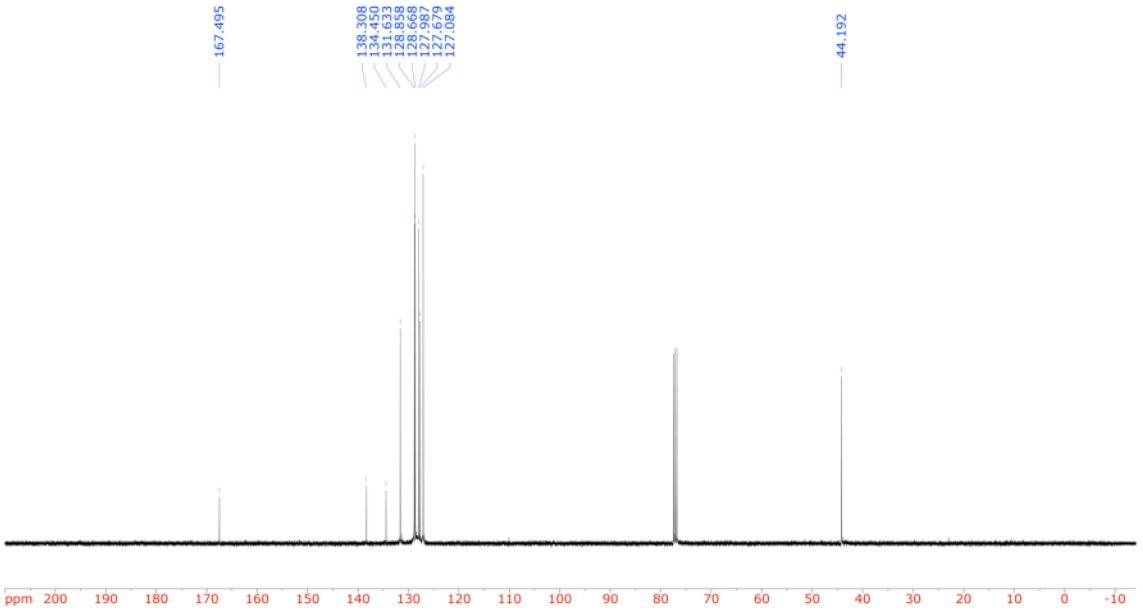

N-allylbenzamide (232i)

^{1}H-NMR ($CDCl_3$, 400 MHz)

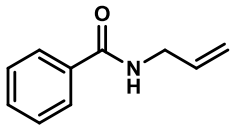

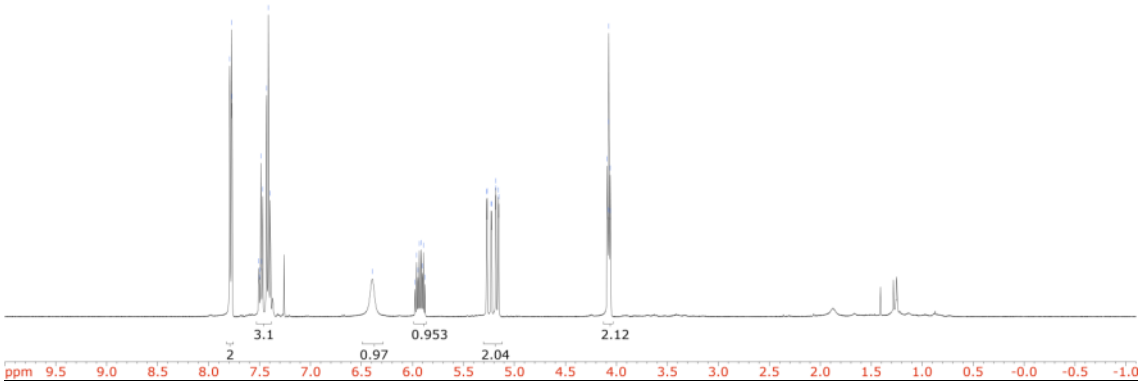

^{13}C-NMR ($CDCl_3$, 100 MHz)

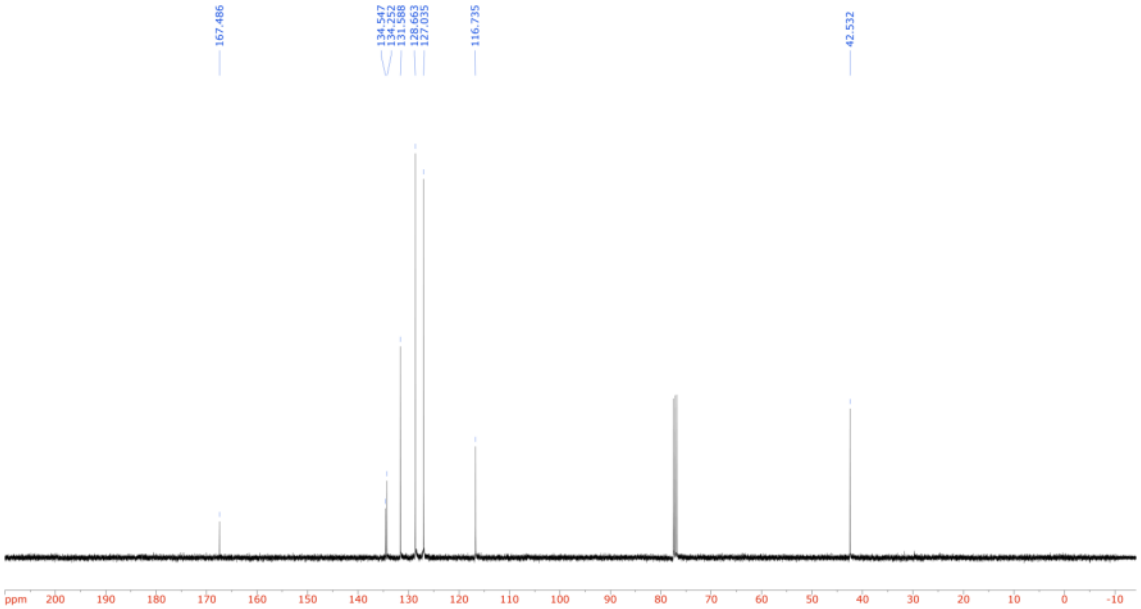

3-(2,3-dihydrobenzofuran-3-yl)-1-(piperidin-1-yl)propane-1,2-dione (234)

^{1}H-NMR ($CDCl_3$, 400 MHz)

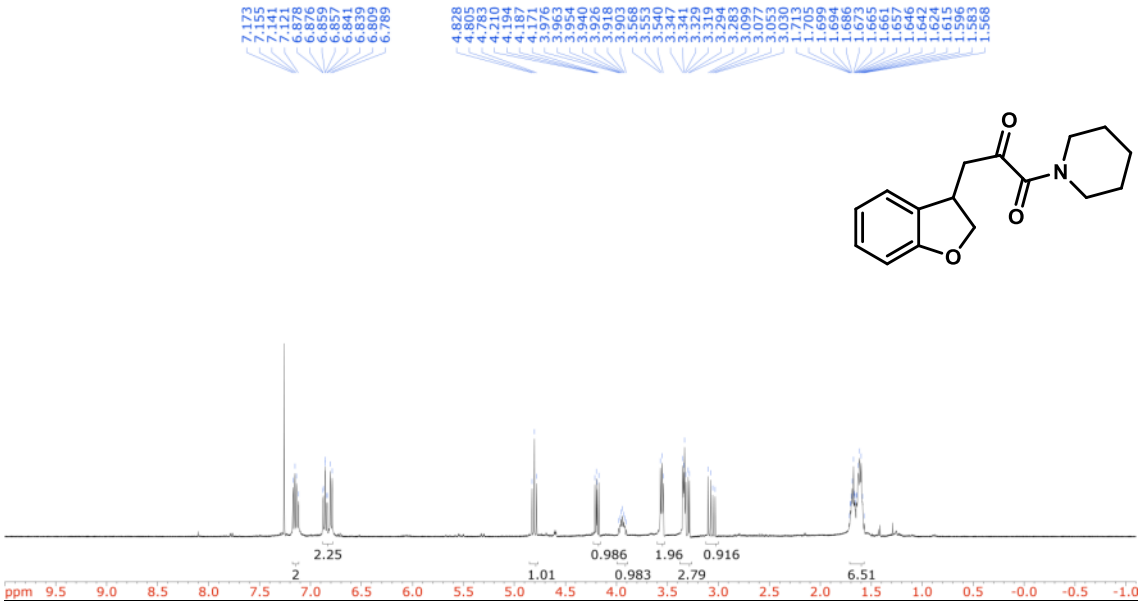

^{13}C-NMR ($CDCl_3$, 100 MHz)

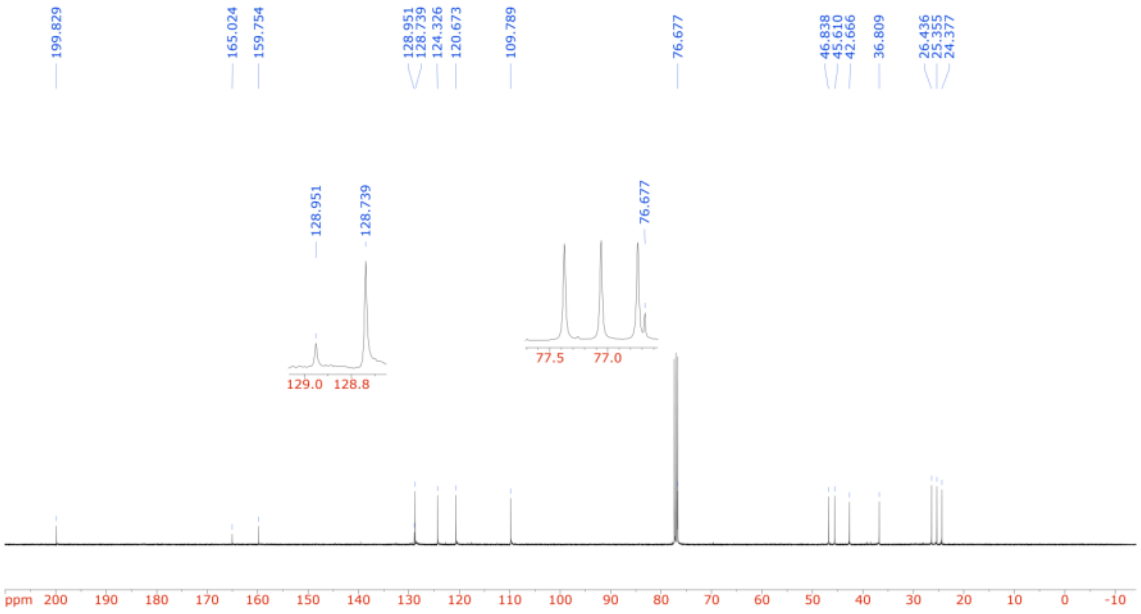

A.5. Cartesian Coordinates and Energies for DFT Calculated Structures

Optimised structures in acetonitrile using B3LYP/6-311+G(g,p)

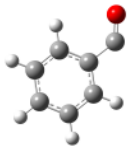
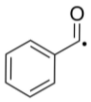

Sum of electronic and zero-point Energies= -344.924531
Sum of electronic and thermal Energies= -344.918177
Sum of electronic and thermal Enthalpies= -344.917233
Sum of electronic and thermal Free Energies= -344.955834

C	-1.704445	-1.058804	-0.000001
C	-0.333956	-1.302343	0.000005
C	0.564071	-0.227615	0.000002
C	0.087581	1.095482	0.000005
C	-1.281141	1.330389	0.000002
C	-2.175173	0.254640	-0.000006
H	-2.402854	-1.886963	-0.000005
H	0.050389	-2.315584	0.000003
H	0.792082	1.918693	0.000006
H	-1.656416	2.347068	0.000000
H	-3.242525	0.443858	-0.000009
C	2.009133	-0.504903	0.000003
O	2.932862	0.246481	-0.000007

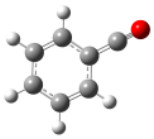
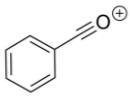

Sum of electronic and zero-point Energies= -344.759147
Sum of electronic and thermal Energies= -344.753011
Sum of electronic and thermal Enthalpies= -344.752067
Sum of electronic and thermal Free Energies= -344.789598

C	-1.510399	-1.221053	0.000005
C	-0.129529	-1.243382	-0.000015
C	0.553749	-0.000113	-0.000011
C	-0.129370	1.243293	-0.000014
C	-1.510143	1.221264	0.000004
C	-2.193826	0.000125	0.000012
H	-2.059784	-2.153209	0.000014
H	0.420580	-2.174570	-0.000019
H	0.421201	2.174212	-0.000018
H	-2.059279	2.153556	0.000012
H	-3.277104	0.000054	0.000022
C	1.932647	-0.000297	-0.000010
O	3.059451	0.000116	0.000021

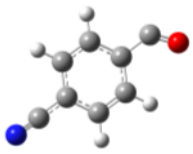
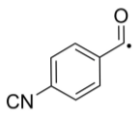

Sum of electronic and zero-point Energies= -437.193085
Sum of electronic and thermal Energies= -437.184875
Sum of electronic and thermal Enthalpies= -437.183931
Sum of electronic and thermal Free Energies= -437.227349

C	-0.827247	1.259341	0.000001
C	0.556964	1.370908	0.000003
C	1.350763	0.219538	0.000050
C	0.761370	-1.055014	0.000048
C	-0.619083	-1.174127	0.000018
C	-1.413309	-0.014442	0.000006
H	-1.450859	2.143588	-0.000022
H	1.027974	2.346039	-0.000013
H	1.387403	-1.938533	0.000064
H	-1.086783	-2.150348	0.000016
C	2.822714	0.366892	0.000056
O	3.663539	-0.471929	-0.000098
C	-2.840051	-0.136003	-0.000019
N	-3.991253	-0.235409	-0.000035

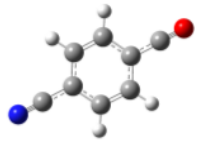
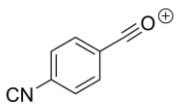

Sum of electronic and zero-point Energies= -437.018401
Sum of electronic and thermal Energies= -437.010505
Sum of electronic and thermal Enthalpies= -437.009561
Sum of electronic and thermal Free Energies= -437.051562

C	-0.734565	1.226872	-0.000011
C	0.645704	1.240940	-0.000060
C	1.325423	-0.000121	-0.000045
C	0.645880	-1.241222	-0.000051
C	-0.734328	-1.227642	-0.000019
C	-1.419378	-0.000441	0.000044
H	-1.282925	2.158830	-0.000009
H	1.191145	2.174568	-0.000080
H	1.191689	-2.174635	-0.000074
H	-1.282461	-2.159719	-0.000018
C	2.711968	0.000305	0.000018
O	3.836045	0.000490	0.000071
C	-2.851663	-0.000191	0.000021
N	-4.005721	0.000862	0.000033

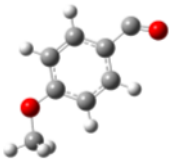
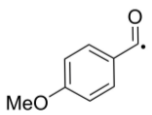

Sum of electronic and zero-point Energies= -459.454085
Sum of electronic and thermal Energies= -459.445178
Sum of electronic and thermal Enthalpies= -459.444234
Sum of electronic and thermal Free Energies= -459.488821

C	0.536293	1.469061	-0.000178
C	-0.844598	1.427160	-0.000107
C	-1.520877	0.194267	0.000064
C	-0.775417	-0.997569	0.000182
C	0.610650	-0.966296	0.000124
C	1.274736	0.272831	-0.000064
H	1.070016	2.411392	-0.000321
H	-1.417933	2.346883	-0.000192
H	-1.291730	-1.950373	0.000323
H	1.164942	-1.894638	0.000231
C	-2.979588	0.172160	0.000136

O -3.743582 -0.745776 0.000238
O 2.617386 0.412243 -0.000129
C 3.445000 -0.760017 -0.000199
H 4.468607 -0.393235 -0.000400
H 3.269395 -1.360614 0.895390
H 3.269082 -1.360728 -0.895650

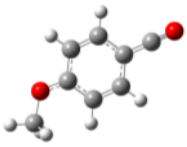
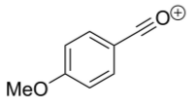

Sum of electronic and zero-point Energies= -459.296423
Sum of electronic and thermal Energies= -459.287655
Sum of electronic and thermal Enthalpies= -459.286711
Sum of electronic and thermal Free Energies= -459.330459

C 0.439519 1.420383 0.000220
C -0.919778 1.290127 0.000239
C -1.484449 -0.021231 0.000246
C -0.654833 -1.177305 0.000274
C 0.708504 -1.025731 0.000292
C 1.272175 0.272494 0.000015
H 0.904523 2.397303 0.000400
H -1.562001 2.160058 0.000363
H -1.096575 -2.164819 0.000373
H 1.336659 -1.904274 0.000547
C -2.841697 -0.168542 -0.000036
O -3.967875 -0.288735 -0.000513
O 2.570663 0.516504 -0.000498
C 3.526862 -0.569061 -0.000151
H 4.499425 -0.086116 0.000122
H 3.408680 -1.175508 0.898320
H 3.409156 -1.175599 -0.898628

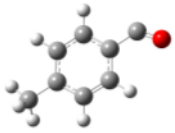
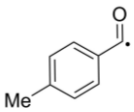

Sum of electronic and zero-point Energies= -384.226717
Sum of electronic and thermal Energies= -384.218478
Sum of electronic and thermal Enthalpies= -384.217533
Sum of electronic and thermal Free Energies= -384.261380

C -1.127857 1.206154 -0.006443
C 0.254750 1.355306 -0.001545
C 1.081667 0.225910 0.000581
C 0.505661 -1.058409 -0.003111
C -0.873028 -1.193993 -0.007966
C -1.713248 -0.066127 -0.007422
H -1.761497 2.085913 -0.010807
H 0.702670 2.342308 -0.001482
H 1.146126 -1.932609 -0.004393
H -1.313188 -2.185577 -0.013753
C 2.537524 0.401100 0.004238
O 3.411091 -0.410252 0.004936
C -3.209907 -0.232954 0.009185
H -3.528424 -1.004181 -0.696456
H -3.548814 -0.544819 1.002767
H -3.718966 0.699064 -0.240470

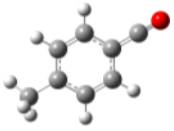
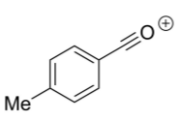

Sum of electronic and zero-point Energies= -384.064969
Sum of electronic and thermal Energies= -384.056990
Sum of electronic and thermal Enthalpies= -384.056045
Sum of electronic and thermal Free Energies= -384.098328

C -1.009581 1.216424 -0.009841
C 0.366808 1.239858 -0.002842
C 1.059217 -0.000021 0.000641
C 0.366344 -1.239785 -0.002847
C -1.009868 -1.215789 -0.009861
C -1.721084 0.000518 -0.011322
H -1.552629 2.153307 -0.016473
H 0.912024 2.174044 -0.002760
H 0.911279 -2.174128 -0.002771
H -1.553354 -2.152435 -0.016497
C 2.432549 -0.000158 0.004198
O 3.561572 -0.000327 0.007123
C -3.217541 -0.000095 0.010329
H -3.622844 -0.882797 -0.485851
H -3.563888 -0.020051 1.050490
H -3.624226 0.898958 -0.453846

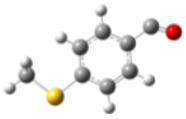
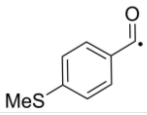

Sum of electronic and zero-point Energies= -782.437743
Sum of electronic and thermal Energies= -782.428109
Sum of electronic and thermal Enthalpies= -782.427165
Sum of electronic and thermal Free Energies= -782.474031

C 0.414776 1.072530 0.000054
C -0.952299 1.320055 0.000076
C -1.870606 0.263411 0.000037
C -1.395415 -1.064255 -0.000028
C -0.037369 -1.315071 -0.000051
C 0.886230 -0.248276 -0.000009
H 1.100931 1.907841 0.000086
H -1.317082 2.340743 0.000126
H -2.101027 -1.886609 -0.000060
H 0.321881 -2.338236 -0.000105
C -3.302749 0.555006 0.000062
O -4.241979 -0.181455 0.000032
S 2.598161 -0.693056 -0.000043
C 3.477581 0.902979 -0.000051
H 3.252130 1.478451 0.897192
H 4.535491 0.641584 -0.000109
H 3.252039 1.478481 -0.897253

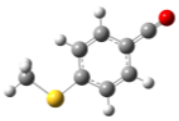
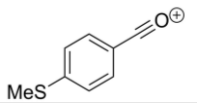

Sum of electronic and zero-point Energies= -782.279125
Sum of electronic and thermal Energies= -782.269688
Sum of electronic and thermal Enthalpies= -782.268744
Sum of electronic and thermal Free Energies= -782.314509

C 0.063746 1.410681 -0.000362
C -1.297104 1.274357 -0.000249
C -1.856377 -0.038117 -0.000249
C -1.019550 -1.189561 -0.000586
C 0.342408 -1.025184 -0.000719
C 0.911002 0.270983 -0.000375
H 0.498377 2.402390 -0.000337
H -1.941953 2.142389 -0.000123
H -1.454320 -2.180159 -0.000756
H 0.970435 -1.903817 -0.001160
C -3.213259 -0.192130 0.000281
O -4.339269 -0.318688 0.000811
S 2.616184 0.588348 0.000253
C 3.404965 -1.054310 0.000570
H 3.147754 -1.610099 -0.899711
H 4.473929 -0.844730 0.001499
H 3.146002 -1.610349 0.900189


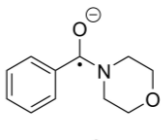

Sum of electronic and zero-point Energies= -632.233417
Sum of electronic and thermal Energies= -632.221554
Sum of electronic and thermal Enthalpies= -632.220610
Sum of electronic and thermal Free Energies= -632.272392

C	2.754135	-1.632195	0.508610
C	1.520733	-1.006836	0.451858
C	1.391590	0.364233	0.035441
C	2.617898	1.038924	-0.297652
C	3.840289	0.394970	-0.240118
C	3.940960	-0.954987	0.158272
H	2.805918	-2.665811	0.840848
H	0.635901	-1.551433	0.759494
H	2.563923	2.076762	-0.605139
H	4.740392	0.942364	-0.508000
H	4.901999	-1.454447	0.201945
C	0.149982	1.071329	-0.032026
O	0.062482	2.333061	-0.191428
C	-2.248158	1.076583	0.482855
C	-1.375449	-0.620784	-0.976457
C	-3.385193	0.131814	0.853848
H	-2.574532	1.728839	-0.342840
H	-2.016864	1.719423	1.334696
C	-2.534598	-1.529273	-0.587052
H	-0.501709	-1.230854	-1.209383
H	-1.647989	-0.059699	-1.887922
H	-4.301722	0.691029	1.051996
H	-3.119533	-0.442419	1.752950
H	-2.834837	-2.156828	-1.428303
H	-2.235917	-2.176978	0.249697
N	-1.061655	0.299362	0.125989
O	-3.689555	-0.772830	-0.213250

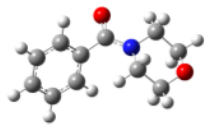
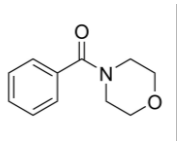

Sum of electronic and zero-point Energies= -632.156681
Sum of electronic and thermal Energies= -632.144898
Sum of electronic and thermal Enthalpies= -632.143953
Sum of electronic and thermal Free Energies= -632.195830

C	2.867598	-1.350193	0.855217
C	1.611486	-0.745553	0.884773
C	1.354259	0.380301	0.094799
C	2.368069	0.896232	-0.719676
C	3.616070	0.278289	-0.762567
C	3.869143	-0.844364	0.026741
H	3.062232	-2.215238	1.478818
H	0.837396	-1.142185	1.532137
H	2.176287	1.778074	-1.320070
H	4.391740	0.676360	-1.406760
H	4.842929	-1.319812	-0.000905
C	0.046326	1.121994	0.183578
O	0.042688	2.298547	0.561488
C	-2.393418	1.136622	-0.006147
C	-1.175005	-0.799162	-0.888753
C	-3.434055	0.164579	0.541089
H	-2.706485	1.505641	-0.990644
H	-2.279897	1.989039	0.660414
C	-2.262425	-1.695723	-0.304461
H	-0.216239	-1.311023	-0.870390
H	-1.419320	-0.565414	-1.932525
H	-4.422954	0.623982	0.524977
H	-3.185566	-0.105726	1.576509
H	-2.403402	-2.573810	-0.935598
H	-1.979644	-2.024521	0.704868
N	-1.099108	0.456108	-0.129284
O	-3.519138	-1.019329	-0.254413

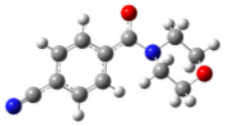
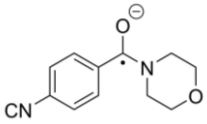

Sum of electronic and zero-point Energies= -724.527879
Sum of electronic and thermal Energies= -724.514286
Sum of electronic and thermal Enthalpies= -724.513341
Sum of electronic and thermal Free Energies= -724.569519

C	2.305461	-1.111685	0.486397
C	1.010911	-0.655592	0.458050
C	0.683625	0.669327	0.017266
C	1.783989	1.507026	-0.361654
C	3.079779	1.057979	-0.350488
C	3.391643	-0.277933	0.066381
H	2.515923	-2.112940	0.846678
H	0.223930	-1.305383	0.821278
H	1.571761	2.522734	-0.674292
H	3.884399	1.716641	-0.659454
C	-0.653787	1.214948	0.012141
O	-0.882539	2.450034	0.005764
C	-3.055597	0.898955	0.355590
C	-1.854896	-0.744779	-0.940803
C	-4.024462	-0.197308	0.782949
H	-3.456088	1.417050	-0.529341
H	-2.957790	1.636339	1.152689
C	-2.855818	-1.801272	-0.490261
H	-0.886036	-1.209012	-1.115263
H	-2.196627	-0.310239	-1.894447
H	-5.028419	0.209350	0.916122
H	-3.692504	-0.640457	1.732430
H	-3.016334	-2.538325	-1.278854
H	-2.479851	-2.315277	0.405583
N	-1.744469	0.309247	0.079358
O	-4.132760	-1.223536	-0.208372
C	4.712050	-0.744976	0.080654
N	5.816275	-1.133618	0.092128

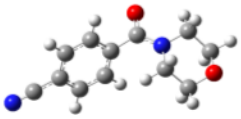
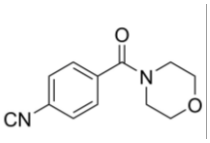

Sum of electronic and zero-point Energies= -724.428425
Sum of electronic and thermal Energies= -724.414758
Sum of electronic and thermal Enthalpies= -724.413813
Sum of electronic and thermal Free Energies= -724.470879

C	2.412397	-0.768102	0.957337
C	1.091714	-0.337211	0.984134
C	0.655064	0.658191	0.103733
C	1.555210	1.226440	-0.803502
C	2.873442	0.792742	-0.849873
C	3.306478	-0.207098	0.034192
H	2.751082	-1.534124	1.643256
H	0.403376	-0.773943	1.697862
H	1.223764	2.007412	-1.477011
H	3.566471	1.224623	-1.560631
C	-0.744433	1.217303	0.195566
O	-0.894854	2.366583	0.620241
C	-3.158813	0.912111	-0.066573
C	-1.665287	-0.855598	-0.887998
C	-4.046166	-0.182676	0.518204
H	-3.517997	1.193232	-1.063481
H	-3.169348	1.796103	0.567732
C	-2.612609	-1.879915	-0.269052

H	-0.641605	-1.221016	-0.852086
H	-1.935574	-0.694746	-1.938290
H	-5.091815	0.125381	0.490302
H	-3.761276	-0.378529	1.560843
H	-2.623668	-2.790535	-0.868793
H	-2.285656	-2.128230	0.749776
N	-1.778933	0.422057	-0.172379
O	-3.953711	-1.391304	-0.238513
C	4.664439	-0.654265	-0.005087
N	5.762097	-1.016255	-0.037592

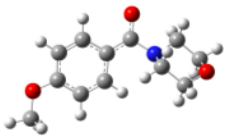

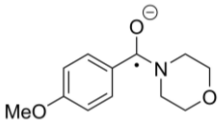

Sum of electronic and zero-point Energies= -746.754569
Sum of electronic and thermal Energies= -746.739789
Sum of electronic and thermal Enthalpies= -746.738845
Sum of electronic and thermal Free Energies= -746.798201

C	-2.273672	-0.931975	-0.300744
C	-0.935443	-0.549911	-0.299671
C	-0.525836	0.792971	-0.000512
C	-1.591966	1.714848	0.285526
C	-2.916271	1.327337	0.284490
C	-3.282319	-0.003507	-0.003310
H	-2.521071	-1.958458	-0.544335
H	-0.187837	-1.287552	-0.563699
H	-1.334832	2.743774	0.507325
H	-3.699699	2.045931	0.506500
C	0.828437	1.247217	0.008371
O	1.166367	2.478149	0.107176
C	3.149785	0.748211	-0.610085
C	2.062900	-0.626169	1.031046
C	4.067565	-0.421896	-0.942684
H	3.640471	1.389921	0.139409
H	2.994217	1.353407	-1.506025
C	3.008648	-1.767727	0.679452
H	1.104829	-1.038653	1.352469
H	2.485714	-0.055554	1.877292
H	5.059451	-0.066425	-1.229136
H	3.647120	-1.006166	-1.773645
H	3.236276	-2.369259	1.561665
H	2.546487	-2.413796	-0.080786
N	1.861875	0.242136	-0.137594
O	4.260501	-1.278980	0.188484
C	-5.050805	-1.611267	-0.272325
H	-6.137300	-1.621064	-0.191948
H	-4.762336	-1.900387	-1.289467
H	-4.630826	-2.334133	0.436481
O	-4.641860	-0.284835	0.029805

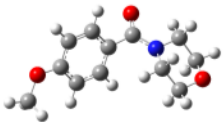

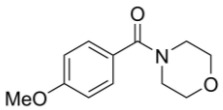

Sum of electronic and zero-point Energies= -746.683607
Sum of electronic and thermal Energies= -746.669232
Sum of electronic and thermal Enthalpies= -746.668288
Sum of electronic and thermal Free Energies= -746.725974

C	-2.296780	-0.782725	-0.601922
C	-0.955409	-0.403970	-0.664914
C	-0.504432	0.768123	-0.055257
C	-1.434208	1.571848	0.621552
C	-2.764743	1.196888	0.711926
C	-3.207386	0.015742	0.097625
H	-2.613533	-1.689210	-1.098986
H	-0.263908	-1.028609	-1.218789
H	-1.105240	2.495221	1.083544
H	-3.480837	1.808385	1.247987
C	0.905661	1.258492	-0.203442
O	1.114072	2.408557	-0.606963
C	3.312532	0.830385	-0.154117
C	1.836235	-0.772906	0.957923
C	4.143501	-0.352800	-0.640715
H	3.734918	1.228157	0.777445
H	3.313761	1.625996	-0.896507
C	2.719883	-1.896691	0.427208
H	0.805589	-1.108096	1.037491
H	2.180692	-0.486165	1.959966
H	5.195521	-0.072838	-0.705813
H	3.798093	-0.667245	-1.635140
H	2.744054	-2.723304	1.138186
H	2.330935	-2.264287	-0.532286
N	1.929519	0.398347	0.075240
O	4.069230	-1.458448	0.261711
C	-5.048390	-1.455529	-0.369461
H	-6.109412	-1.470399	-0.129669
H	-4.919588	-1.436053	-1.455182
H	-4.567430	-2.345938	0.044772
O	-4.531931	-0.264507	0.232486

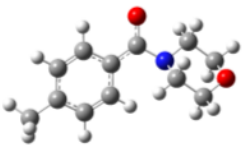

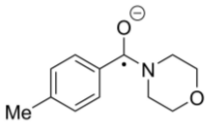

Sum of electronic and zero-point Energies= -671.243913
Sum of electronic and thermal Energies= -671.230477
Sum of electronic and thermal Enthalpies= -671.229533
Sum of electronic and thermal Free Energies= -671.284947

C	2.478729	-1.258125	0.459944
C	1.192842	-0.754930	0.430732
C	0.930419	0.598737	0.033261
C	2.081436	1.387905	-0.296716
C	3.355295	0.855257	-0.262924
C	3.600772	-0.481924	0.105936
H	2.632531	-2.286729	0.778686
H	0.366670	-1.383400	0.744589
H	1.931867	2.423878	-0.578370
H	4.198959	1.489212	-0.527027
C	-0.371338	1.174705	-0.017822
O	-0.597156	2.410471	-0.188148
C	-2.739837	0.926329	0.496957
C	-1.693192	-0.646554	-0.960118
C	-3.774652	-0.130563	0.846687
H	-3.113879	1.537895	-0.338276
H	-2.586172	1.588117	1.351097
C	-2.753644	-1.669075	-0.589898
H	-0.761187	-1.159985	-1.200769
H	-2.022135	-0.093223	-1.856161
H	-4.742970	0.329374	1.048549
H	-3.450569	-0.688176	1.736145
H	-2.975600	-2.322264	-1.434715
H	-2.396788	-2.279619	0.251692
N	-1.481921	0.272453	0.160661
O	-3.973266	-1.036831	-0.230178
C	4.989215	-1.065988	0.087514
H	5.217580	-1.558897	-0.865316
H	5.745509	-0.291313	0.237449
H	5.116749	-1.815812	0.873080

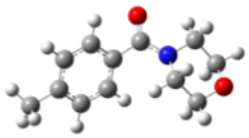

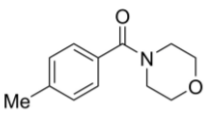

Sum of electronic and zero-point Energies= -671.170480
Sum of electronic and thermal Energies= -671.157050
Sum of electronic and thermal Enthalpies= -671.156105
Sum of electronic and thermal Free Energies= -671.212006

C	2.483922	-1.102080	0.725411
C	1.190386	-0.595617	0.726162
C	0.905405	0.601898	0.069188
C	1.933271	1.288269	-0.574464
C	3.220917	0.765094	-0.589140
C	3.516331	-0.436662	0.058497
H	2.697658	-2.025315	1.253408
H	0.402045	-1.122871	1.253921
H	1.719325	2.232080	-1.062917
H	4.011479	1.301440	-1.103438
C	-0.455340	1.230142	0.132672
O	-0.569688	2.410432	0.449623
C	-2.877208	0.984686	0.048925
C	-1.516459	-0.779714	-0.929897
C	-3.787453	-0.101977	0.602305
H	-3.255029	1.335171	-0.919209
H	-2.832787	1.829383	0.733145
C	-2.473133	-1.797527	-0.329077
H	-0.511387	-1.187553	-0.993923
H	-1.853206	-0.526605	-1.942725
H	-4.817149	0.252193	0.642949
H	-3.460846	-0.373404	1.614888
H	-2.542512	-2.675363	-0.971038
H	-2.117343	-2.104625	0.663751
N	-1.532575	0.438118	-0.117656
O	-3.779447	-1.256380	-0.222744
C	4.907314	-1.012236	0.026608
H	5.006095	-1.724993	-0.796805
H	5.653741	-0.230490	-0.118580
H	5.133302	-1.543955	0.951999

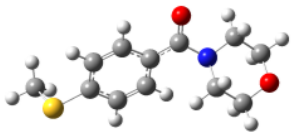

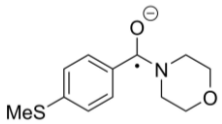

Sum of electronic and zero-point Energies= -1069.749215
Sum of electronic and thermal Energies= -1069.733769
Sum of electronic and thermal Enthalpies= -1069.732825
Sum of electronic and thermal Free Energies= -1069.793925

C	1.854651	-1.040927	0.135063
C	0.541958	-0.622201	0.213247
C	0.159582	0.728121	-0.097998
C	1.228862	1.612731	-0.473414
C	2.535828	1.182421	-0.556406
C	2.892796	-0.159441	-0.261361
H	2.102156	-2.066384	0.392621
H	-0.210874	-1.323528	0.552530
H	0.986562	2.643789	-0.703496
H	3.311240	1.881509	-0.855480
C	-1.180654	1.228534	-0.016046
O	-1.467700	2.463647	-0.035052
C	-3.516825	0.818895	0.601988
C	-2.459054	-0.662133	-0.970407
C	-4.446669	-0.319930	1.003105
H	-4.001935	1.425123	-0.179241
H	-3.344472	1.469075	1.461330
C	-3.416618	-1.768628	-0.546579
H	-1.512187	-1.103117	-1.282083
H	-2.885126	-0.130702	-1.838919
H	-5.431189	0.065135	1.275289
H	-4.028223	-0.861672	1.863205
H	-3.657779	-2.415501	-1.392052
H	-2.957072	-2.376449	0.245857
N	-2.239728	0.269214	0.146270
O	-4.657805	-1.235083	-0.077320
S	4.575486	-0.718545	-0.397083
C	5.275650	-0.397201	1.282012
H	6.317182	-0.724329	1.258118
H	5.235396	0.667147	1.514943
H	4.733639	-0.967820	2.036575

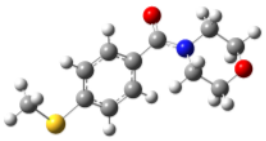

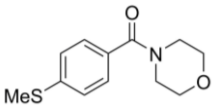

Sum of electronic and zero-point Energies= -1069.668020
Sum of electronic and thermal Energies= -1069.652849
Sum of electronic and thermal Enthalpies= -1069.651905
Sum of electronic and thermal Free Energies= -1069.712236

C	-1.804585	-0.950813	-0.892194
C	-0.490577	-0.502712	-0.869844
C	-0.142781	0.659648	-0.168735
C	-1.146849	1.362266	0.501149
C	-2.463436	0.907372	0.503823
C	-2.806137	-0.255111	-0.196776
H	-2.054849	-1.844188	-1.453664
H	0.263888	-1.053602	-1.419832
H	-0.898763	2.273666	1.032683
H	-3.209714	1.469695	1.048489
C	1.244588	1.234106	-0.212192
O	1.409061	2.403540	-0.577113
C	3.663188	0.939202	0.004575
C	2.202101	-0.789131	0.939618
C	4.588329	-0.176015	-0.472721
H	3.998991	1.313727	0.979757
H	3.670497	1.767687	-0.700865
C	3.180092	-1.839054	0.422887
H	1.188248	-1.180521	0.929192
H	2.459366	-0.534032	1.975573
H	5.625571	0.160102	-0.450294
H	4.330094	-0.460786	-1.501847
H	3.200343	-2.697209	1.095533
H	2.877786	-2.178322	-0.577350
N	2.293111	0.426611	0.119109
O	4.511497	-1.324687	0.373873
S	-4.452377	-0.928772	-0.279966
C	-5.455325	0.226745	0.710022
H	-5.445942	1.228450	0.281003
H	-6.469766	-0.169507	0.667137
H	-5.125588	0.249073	1.748422

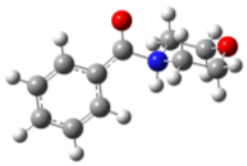

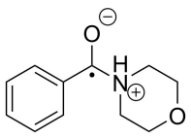

Sum of electronic and zero-point Energies= -632.684290
Sum of electronic and thermal Energies= -632.672165
Sum of electronic and thermal Enthalpies= -632.671221
Sum of electronic and thermal Free Energies= -632.724117

C	2.992406	-1.675740	0.000062
C	1.710840	-1.148914	0.000153
C	1.488929	0.265852	0.000074
C	2.660366	1.094266	0.000003
C	3.930183	0.546851	-0.000083

C	4.122861	-0.844770	-0.000084
H	3.115666	-2.753884	0.000119
H	0.887556	-1.856350	0.000362
H	2.528992	2.169155	0.000002
H	4.790722	1.208689	-0.000147
H	5.120261	-1.267583	-0.000166
C	0.226668	0.916105	0.000030
O	-0.041376	2.140305	-0.000023
C	-1.856268	0.217894	1.239240
C	-1.856149	0.217775	-1.239247
C	-3.139432	-0.599364	1.172959
H	-2.063320	1.285872	1.277806
H	-1.249846	-0.066157	2.099355
C	-3.139329	-0.599453	-1.173028
H	-1.249660	-0.066356	-2.099291
H	-2.063193	1.285750	-1.277951
H	-3.767193	-0.351362	2.028905
H	-2.918159	-1.674962	1.207544
H	-3.767011	-0.351474	-2.029040
H	-2.918098	-1.675061	-1.207533
N	-1.020558	-0.000528	0.000033
O	-3.888585	-0.296999	-0.000073
H	-0.709577	-0.972042	0.000098

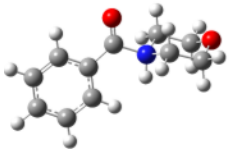

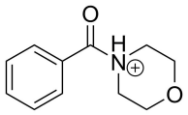

Sum of electronic and zero-point Energies= -632.556576
Sum of electronic and thermal Energies= -632.544697
Sum of electronic and thermal Enthalpies= -632.543753
Sum of electronic and thermal Free Energies= -632.596360

C	3.001643	-1.675171	-0.000185
C	1.715347	-1.149268	-0.000155
C	1.525912	0.243303	0.000003
C	2.647829	1.095503	0.000122
C	3.927014	0.562606	0.000102
C	4.105576	-0.823230	-0.000052
H	3.140476	-2.748785	-0.000310
H	0.889277	-1.849424	-0.000262
H	2.496443	2.166899	0.000232
H	4.785914	1.222104	0.000205
H	5.106119	-1.239049	-0.000076
C	0.217814	0.901800	0.000023
O	-0.007595	2.076350	0.000104
C	-1.865167	0.233124	1.249378
C	-1.865312	0.233549	-1.249274
C	-3.143717	-0.590596	1.172896
H	-2.077078	1.300191	1.273014
H	-1.260962	-0.046146	2.111905
C	-3.143869	-0.590196	-1.172945
H	-1.261243	-0.045390	-2.112004
H	-2.077273	1.300616	-1.272544
H	-3.769581	-0.340466	2.029068
H	-2.919156	-1.664545	1.211242
H	-3.769829	-0.339756	-2.028955
H	-2.919333	-1.664137	-1.211683
N	-1.029398	-0.006666	-0.000072
O	-3.887009	-0.284941	0.000075
H	-0.739576	-0.985265	-0.000243

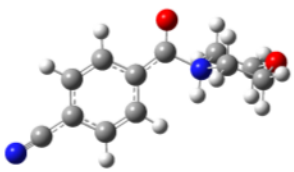

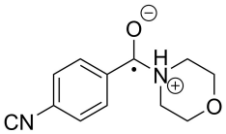

Sum of electronic and zero-point Energies= -724.967649
Sum of electronic and thermal Energies= -724.953889
Sum of electronic and thermal Enthalpies= -724.952944

Sum of electronic and thermal Free Energies= -725.009711

C	2.498781	-1.246304	-0.000419
C	1.179188	-0.860630	-0.000374
C	0.804138	0.522575	0.000015
C	1.873915	1.480934	0.000335
C	3.189649	1.093549	0.000281
C	3.541086	-0.283485	-0.000092
H	2.747051	-2.300922	-0.000676
H	0.441458	-1.655203	-0.000615
H	1.620832	2.533154	0.000640
H	3.972646	1.842881	0.000541
C	-0.518409	1.032279	0.000192
O	-0.908799	2.208375	0.000621
C	-2.519441	0.123432	1.239733
C	-2.520119	0.125066	-1.239496
C	-3.704234	-0.830317	1.173634
H	-2.843448	1.162072	1.271296
H	-1.887357	-0.087745	2.102072
C	-3.704766	-0.828891	-1.173986
H	-1.888509	-0.084847	-2.102487
H	-2.844290	1.163704	-1.269458
H	-4.354794	-0.649967	2.029211
H	-3.366014	-1.874703	1.211162
H	-4.355744	-0.647644	-2.029052
H	-3.366420	-1.873190	-1.212870
N	-1.664868	-0.012620	-0.000217
O	-4.481635	-0.613409	0.000136
H	-1.258922	-0.948702	-0.000951
C	4.894883	-0.685301	-0.000151
N	6.010431	-1.015389	-0.000196

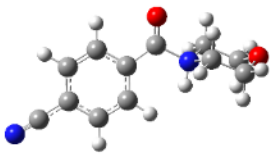

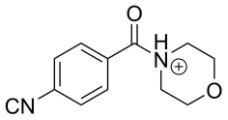

Sum of electronic and zero-point Energies= -724.821625
Sum of electronic and thermal Energies= -724.808062
Sum of electronic and thermal Enthalpies= -724.807118
Sum of electronic and thermal Free Energies= -724.863222

C	2.518775	-1.248849	-0.048882
C	1.187116	-0.864058	-0.105935
C	0.845969	0.497188	-0.086903
C	1.858852	1.469698	-0.014697
C	3.188035	1.091476	0.050511
C	3.519740	-0.272355	0.034155
H	2.780663	-2.298072	-0.069993
H	0.448735	-1.651139	-0.190328
H	1.590825	2.517580	-0.003423
H	3.966415	1.840085	0.113449
C	-0.534103	1.008316	-0.158304
O	-0.869942	2.142127	-0.319524
C	-2.540563	0.359200	1.208820
C	-2.521614	-0.090477	-1.252287
C	-3.718307	-0.602223	1.296434
H	-2.870160	1.382448	1.041091
H	-1.914840	0.308657	2.099259
C	-3.702063	-1.022726	-1.011346
H	-1.885405	-0.451041	-2.060151
H	-2.849814	0.926027	-1.461071
H	-4.373913	-0.272451	2.101921
H	-3.377947	-1.621356	1.523596
H	-4.345491	-1.000190	-1.890386
H	-3.359880	-2.054971	-0.859339
N	-1.672344	-0.010155	0.011020
O	-4.482053	-0.594455	0.097202
H	-1.274267	-0.933274	0.190991
C	4.893711	-0.670191	0.101104
N	6.002024	-0.990371	0.155687

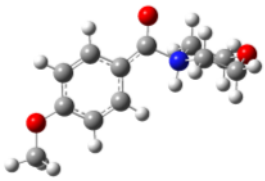
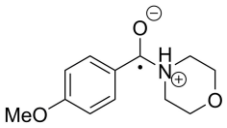

Sum of electronic and zero-point Energies= -747.207144
Sum of electronic and thermal Energies= -747.192324
Sum of electronic and thermal Enthalpies= -747.191380
Sum of electronic and thermal Free Energies= -747.250298

C	2.445223	-1.007854	0.069992
C	1.090927	-0.687720	0.072113
C	0.632723	0.663191	0.005717
C	1.656593	1.666839	-0.061527
C	2.995701	1.341124	-0.062917
C	3.414930	-0.000761	0.001663
H	2.729112	-2.051001	0.120875
H	0.402041	-1.524605	0.124926
H	1.355426	2.705495	-0.113484
H	3.748962	2.120127	-0.115572
C	-0.718008	1.102073	-0.003942
O	-1.180776	2.269617	-0.077253
C	-2.733709	0.197642	1.212561
C	-2.581018	-0.053852	-1.245780
C	-3.860529	-0.825705	1.180764
H	-3.112386	1.214071	1.123450
H	-2.144578	0.109088	2.125446
C	-3.720504	-1.059870	-1.150916
H	-1.885434	-0.318732	-2.042018
H	-2.953212	0.956134	-1.409793
H	-4.570985	-0.602272	1.976684
H	-3.469920	-1.839911	1.341654
H	-4.327513	-1.000920	-2.054455
H	-3.331110	-2.083611	-1.063870
N	-1.798506	-0.002861	0.045091
O	-4.577940	-0.773521	-0.049454
H	-1.333816	-0.902678	0.168534
O	4.774511	-0.213444	-0.008485
C	5.244533	-1.557573	0.048399
H	6.331315	-1.497140	0.025338
H	4.928558	-2.051780	0.972878
H	4.895538	-2.138654	-0.811464

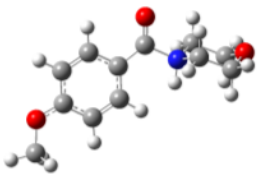
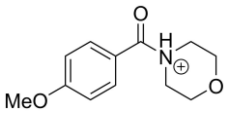

Sum of electronic and zero-point Energies= -747.088062
Sum of electronic and thermal Energies= -747.073715
Sum of electronic and thermal Enthalpies= -747.072770
Sum of electronic and thermal Free Energies= -747.129756

C	-2.440587	-1.019691	-0.084073
C	-1.094544	-0.692525	-0.089799
C	-0.671024	0.646492	-0.012190
C	-1.655784	1.661042	0.066514
C	-2.993211	1.346374	0.072130
C	-3.403283	-0.000641	-0.000509
H	-2.730241	-2.058769	-0.143708
H	-0.397111	-1.518797	-0.155887
H	-1.341783	2.694980	0.125647
H	-3.749510	2.118608	0.134341
C	0.711530	1.086375	0.001962
O	1.129955	2.209887	0.057972
C	2.739046	0.210548	-1.218766
C	2.585962	-0.031087	1.257961
C	3.863800	-0.814610	-1.175402
H	3.118549	1.225205	-1.118088
H	2.153035	0.122404	-2.133153
C	3.722319	-1.039999	1.157556
H	1.895148	-0.287246	2.060549
H	2.962104	0.980258	1.400514
H	4.572899	-0.588289	-1.971046
H	3.474277	-1.828074	-1.337688
H	4.327304	-0.973954	2.061371
H	3.330855	-2.062674	1.077973
N	1.801549	-0.011551	-0.044107
O	4.574741	-0.752862	0.055525
H	1.359017	-0.923828	-0.162219
O	-4.727206	-0.207984	0.016986
C	-5.238874	-1.551178	-0.042827
H	-6.320310	-1.448900	-0.007549
H	-4.943099	-2.035576	-0.975571
H	-4.893986	-2.133433	0.814056

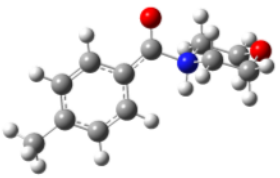
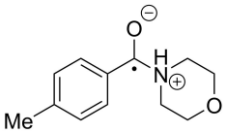

Sum of electronic and zero-point Energies= -671.983614
Sum of electronic and thermal Energies= -671.969590
Sum of electronic and thermal Enthalpies= -671.968646
Sum of electronic and thermal Free Energies= -672.026425

C	2.690424	-1.361076	0.020015
C	1.371699	-0.933044	0.014203
C	1.040992	0.458879	0.001174
C	2.151762	1.365246	-0.001486
C	3.456884	0.910674	0.004689
C	3.771723	-0.462995	0.013463
H	2.888901	-2.428986	0.032244
H	0.607256	-1.703933	0.024288
H	1.947062	2.428662	-0.004595
H	4.264310	1.638124	0.005037
C	-0.264954	1.015913	-0.004924
O	-0.623270	2.218939	-0.014369
C	-2.295648	0.173982	1.234113
C	-2.286605	0.148760	-1.240941
C	-3.504517	-0.749511	1.175183
H	-2.591704	1.221297	1.257059
H	-1.671619	-0.045553	2.100413
C	-3.496204	-0.773313	-1.172342
H	-1.656245	-0.088074	-2.098062
H	-2.582630	1.195321	-1.287202
H	-4.154461	-0.545036	2.026016
H	-3.192364	-1.801770	1.224420
H	-4.139881	-0.585721	-2.031788
H	-3.184286	-1.826517	-1.198310
N	-1.439236	0.008838	0.001268
O	-4.273160	-0.527239	-0.003707
H	-1.052609	-0.935388	0.012279
C	5.200923	-0.944148	-0.016713
H	5.284229	-1.966911	0.359785
H	5.609923	-0.939484	-1.035026
H	5.851340	-0.307685	0.590578

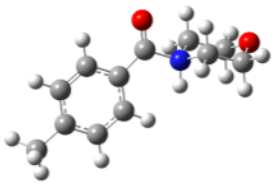
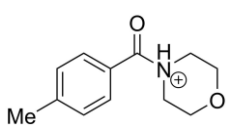

Sum of electronic and zero-point Energies= -671.859729
Sum of electronic and thermal Energies= -671.846075
Sum of electronic and thermal Enthalpies= -671.845130
Sum of electronic and thermal Free Energies= -671.901517

C	2.696267	-1.369809	0.014298

C	1.376506	-0.941562	0.008241
C	1.079532	0.432643	0.000366
C	2.143868	1.357777	-0.000415
C	3.453907	0.917769	0.005907
C	3.756874	-0.454545	0.010821
H	2.906203	-2.432718	0.023399
H	0.608449	-1.705421	0.011985
H	1.921585	2.416946	-0.003619
H	4.259595	1.642978	0.008739
C	-0.266498	0.996147	-0.005453
O	-0.578833	2.152307	-0.015064
C	-2.301672	0.190237	1.243922
C	-2.296314	0.167969	-1.249374
C	-3.508922	-0.734746	1.176986
H	-2.598574	1.237187	1.251449
H	-1.679727	-0.025392	2.111922
C	-3.504013	-0.755802	-1.171279
H	-1.670796	-0.062664	-2.110944
H	-2.593476	1.214497	-1.276623
H	-4.155401	-0.525121	2.028640
H	-3.197919	-1.786305	1.229856
H	-4.146771	-0.561295	-2.029308
H	-3.193086	-1.808245	-1.204141
N	-1.446203	-0.000206	0.000669
O	-4.272601	-0.505610	-0.000918
H	-1.083464	-0.954492	0.010051
C	5.184787	-0.923552	-0.008923
H	5.269392	-1.963497	0.308774
H	5.590754	-0.849285	-1.023622
H	5.812201	-0.304471	0.636034

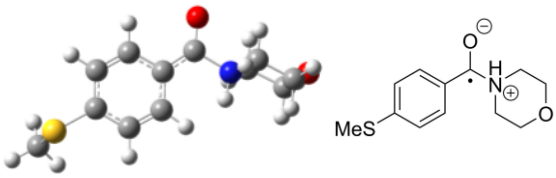

Sum of electronic and zero-point Energies= -1070.196697
Sum of electronic and thermal Energies= -1070.181062
Sum of electronic and thermal Enthalpies= -1070.180118
Sum of electronic and thermal Free Energies= -1070.241921

C	2.031269	-1.014300	-0.462302
C	0.692035	-0.697035	-0.332659
C	0.265785	0.641484	-0.054215
C	1.302637	1.625704	0.066998
C	2.634706	1.291996	-0.063874
C	3.035426	-0.035494	-0.324627
H	2.312646	-2.039056	-0.678247
H	-0.016660	-1.508373	-0.463954
H	1.018050	2.650703	0.268695
H	3.389723	2.064601	0.035786
C	-1.073410	1.079844	0.105470
O	-1.514529	2.228060	0.321878
C	-2.964173	-0.087875	1.293712
C	-3.093457	0.242056	-1.158049
C	-4.111432	-1.080362	1.155767
H	-3.327972	0.920084	1.484233
H	-2.278880	-0.383214	2.088194
C	-4.230318	-0.770152	-1.168383
H	-2.498129	0.178723	-2.068877
H	-3.463986	1.258375	-1.035350
H	-4.725477	-1.044173	2.055613
H	-3.730857	-2.104443	1.039419
H	-4.931640	-0.513055	-1.962144
H	-3.847228	-1.781731	-1.360316
N	-2.170506	-0.010116	0.011258
O	-4.956196	-0.750177	0.057124
H	-1.717976	-0.913478	-0.131191
S	4.760750	-0.454393	-0.525252
C	5.258013	-0.907425	1.188169
H	6.316534	-1.169131	1.145441
H	5.120588	-0.061739	1.861724
H	4.686133	-1.766701	1.538140

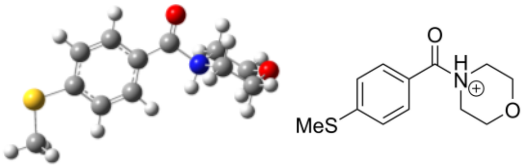

Sum of electronic and zero-point Energies= -1070.071458
Sum of electronic and thermal Energies= -1070.056313
Sum of electronic and thermal Enthalpies= -1070.055369
Sum of electronic and thermal Free Energies= -1070.114852

C	-2.120350	-0.884257	-0.083359
C	-0.762928	-0.608034	-0.088450
C	-0.294554	0.716166	-0.014265
C	-1.243035	1.762472	0.058969
C	-2.592375	1.491977	0.063668
C	-3.055935	0.160124	-0.004186
H	-2.440838	-1.914555	-0.140499
H	-0.094088	-1.458082	-0.150374
H	-0.895605	2.785860	0.114930
H	-3.302791	2.308037	0.123339
C	1.103762	1.109168	0.001372
O	1.557618	2.218536	0.057901
C	3.100101	0.170304	-1.218552
C	2.937245	-0.068923	1.258962
C	4.198148	-0.883695	-1.173936
H	3.506654	1.174460	-1.118771
H	2.512466	0.096989	-2.133191
C	4.046466	-1.107445	1.158353
H	2.238152	-0.308379	2.059481
H	3.340376	0.931489	1.404705
H	4.914163	-0.674350	-1.968036
H	3.784238	-1.887000	-1.338164
H	4.651362	-1.058819	2.063366
H	3.628742	-2.119390	1.076465
N	2.155702	-0.023936	-0.044432
O	4.908164	-0.840854	0.058338
H	1.682862	-0.920975	-0.163362
S	-4.798494	-0.066011	0.018169
C	-5.025433	-1.872873	-0.050574
H	-4.578897	-2.357892	0.816574
H	-6.104856	-2.019888	-0.026576
H	-4.628879	-2.285147	-0.977499

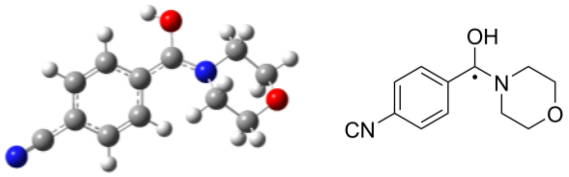

Sum of electronic and zero-point Energies= -724.971862
Sum of electronic and thermal Energies= -724.957896
Sum of electronic and thermal Enthalpies= -724.956952
Sum of electronic and thermal Free Energies= -725.013765

C	-2.299042	-1.144522	-0.450707
C	-1.001372	-0.695764	-0.412520
C	-0.686381	0.639393	0.000769
C	-1.784132	1.485198	0.365292
C	-3.081197	1.030738	0.330498
C	-3.372169	-0.295852	-0.074863
H	-2.509515	-2.152687	-0.787166

H	-0.208272	-1.351240	-0.747427
H	-1.601070	2.494188	0.716096
H	-3.889701	1.687969	0.627214
C	0.640540	1.118955	0.017387
O	0.911443	2.453659	0.007790
C	3.054084	0.884071	-0.375148
C	1.896330	-0.755579	1.026031
C	3.949697	-0.250355	-0.863540
H	3.535300	1.401916	0.464815
H	2.901069	1.604265	-1.177654
C	2.838229	-1.825485	0.489551
H	0.923436	-1.188700	1.249221
H	2.306644	-0.338903	1.956360
H	4.949392	0.129190	-1.078274
H	3.531794	-0.689405	-1.779585
H	3.033991	-2.573373	1.258555
H	2.391970	-2.321296	-0.383250
N	1.756523	0.330075	0.037557
O	4.101758	-1.265903	0.128948
H	0.172736	2.945120	-0.374288
C	-4.706943	-0.762895	-0.109196
N	-5.803559	-1.146719	-0.137535

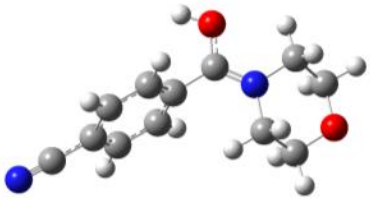

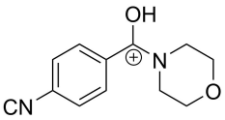

Sum of electronic and zero-point Energies= -724.833777
Sum of electronic and thermal Energies= -724.820018
Sum of electronic and thermal Enthalpies= -724.819074
Sum of electronic and thermal Free Energies= -724.875704

C	-2.431270	-0.776087	-0.964352
C	-1.104837	-0.367467	-0.991531
C	-0.663508	0.607220	-0.089880
C	-1.543871	1.180079	0.834973
C	-2.868002	0.763921	0.870456
C	-3.312124	-0.213381	-0.030470
H	-2.782592	-1.525321	-1.661355
H	-0.425297	-0.796734	-1.716554
H	-1.198783	1.933155	1.532295
H	-3.552408	1.192593	1.590452
C	0.737663	1.097751	-0.148846
O	0.964823	2.309507	-0.612574
C	3.159525	0.907750	0.126152
C	1.674376	-0.914530	0.910775
C	4.020616	-0.172397	-0.528373
H	3.511903	1.122828	1.137220
H	3.170250	1.821627	-0.460131
C	2.615359	-1.899382	0.219209
H	0.648744	-1.271870	0.890093
H	1.978974	-0.765636	1.949108
H	5.062215	0.146934	-0.515654
H	3.707738	-0.323073	-1.569234
H	2.633979	-2.830391	0.784824
H	2.266889	-2.109423	-0.799625
N	1.766354	0.407728	0.245917
O	3.947526	-1.399560	0.188142
H	0.153402	2.717109	-0.952581
C	-4.678886	-0.639814	0.002347
N	-5.781219	-0.983919	0.028918

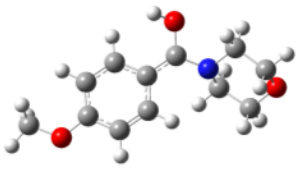

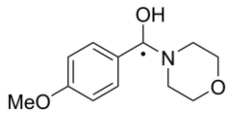

Sum of electronic and zero-point Energies= -747.216187
Sum of electronic and thermal Energies= -747.201108
Sum of electronic and thermal Enthalpies= -747.200163
Sum of electronic and thermal Free Energies= -747.259428

C	2.103466	-1.272374	-0.513833
C	0.818672	-0.775458	-0.461691
C	0.554194	0.563530	-0.037682
C	1.683838	1.347860	0.329786
C	2.978869	0.842441	0.270805
C	3.203284	-0.472994	-0.149507
H	2.286750	-2.287490	-0.848334
H	-0.007170	-1.402347	-0.773539
H	1.550207	2.359670	0.695636
H	3.801395	1.480242	0.566316
C	-0.764150	1.078329	-0.004534
O	-1.007214	2.425640	0.160226
C	-2.161905	-0.622592	1.082437
C	-3.138140	0.887172	-0.563505
C	-3.186110	-1.673278	0.674127
H	-2.541116	-0.054212	1.945670
H	-1.232906	-1.110865	1.378656
C	-4.125882	-0.217228	-0.922413
H	-2.909577	1.476596	-1.452953
H	-3.594321	1.556347	0.179951
H	-3.464777	-2.287968	1.531141
H	-2.767006	-2.322117	-0.107427
H	-5.084124	0.212660	-1.218097
H	-3.733422	-0.816956	-1.755180
N	-1.901149	0.284715	-0.052157
O	-4.389453	-1.068057	0.195941
O	4.434417	-1.067636	-0.240070
C	5.584933	-0.300501	0.113452
H	6.439257	-0.958198	-0.035384
H	5.687357	0.579772	-0.528573
H	5.546067	0.013455	1.161075
H	-0.276976	2.939383	-0.207296

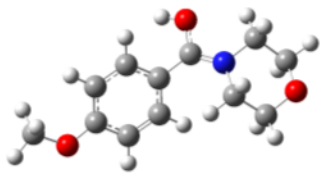

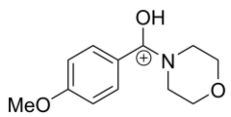

Sum of electronic and zero-point Energies= -747.096316
Sum of electronic and thermal Energies= -747.081855
Sum of electronic and thermal Enthalpies= -747.080911
Sum of electronic and thermal Free Energies= -747.138302

C	2.117095	-1.162540	0.748005
C	0.816174	-0.704053	0.711080
C	0.514935	0.527481	0.097556
C	1.555851	1.281975	-0.464267
C	2.863110	0.815557	-0.448680

C	3.152717	-0.413271	0.161457
H	2.360512	-2.098249	1.235258
H	0.040208	-1.284693	1.193870
H	1.345352	2.226765	-0.952030
H	3.639227	1.408383	-0.910938
C	-0.841359	1.080820	0.095318
O	-1.015320	2.343504	0.454389
C	-3.283074	1.004633	-0.085533
C	-1.937900	-0.864979	-0.965123
C	-4.180586	-0.042793	0.573690
H	-3.659219	1.266048	-1.077531
H	-3.229600	1.902088	0.523250
C	-2.898312	-1.824946	-0.267816
H	-0.934749	-1.275446	-1.020295
H	-2.290355	-0.661575	-1.979733
H	-5.203824	0.330631	0.604591
H	-3.841308	-0.233422	1.599853
H	-2.989749	-2.735338	-0.859514
H	-2.524795	-2.086994	0.730237
N	-1.924792	0.434802	-0.255490
O	-4.201098	-1.258025	-0.167744
O	4.383946	-0.953279	0.240506
C	5.499368	-0.246530	-0.324471
H	6.366248	-0.874578	-0.134948
H	5.369705	-0.112823	-1.400896
H	5.632554	0.722085	0.162825
H	-0.215000	2.697767	0.869939

-

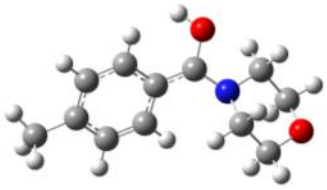

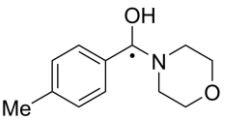

Sum of electronic and zero-point Energies= -671.991639
Sum of electronic and thermal Energies= -671.977364
Sum of electronic and thermal Enthalpies= -671.976419
Sum of electronic and thermal Free Energies= -672.034469

C	-2.499057	-1.287568	-0.474802
C	-1.210372	-0.789065	-0.433741
C	-0.949560	0.551198	-0.014845
C	-2.082358	1.335364	0.354336
C	-3.366279	0.811470	0.301249
C	-3.613910	-0.507516	-0.108166
H	-2.655447	-2.308297	-0.811968
H	-0.384246	-1.411095	-0.755372
H	-1.950944	2.350772	0.712355
H	-4.200848	1.440994	0.595161
C	0.364367	1.075582	0.009712
O	0.598405	2.425468	0.138495
C	2.747071	0.914075	-0.532210
C	1.763795	-0.648226	1.061217
C	3.734808	-0.179954	-0.922741
H	3.200524	1.558704	0.234100
H	2.521802	1.531559	-1.402790
C	2.788108	-1.686162	0.622018
H	0.833947	-1.143963	1.340409
H	2.141953	-0.107057	1.941925
H	4.694306	0.258658	-1.200860
H	3.344643	-0.751304	-1.776240
H	3.063062	-2.328295	1.459812
H	2.370975	-2.309082	-0.181296
N	1.508494	0.296650	-0.042849
O	3.993466	-1.066808	0.168004
H	-0.151206	2.924241	-0.210285
C	-5.008760	-1.080047	-0.138934
H	-5.162333	-1.805738	0.668338
H	-5.761480	-0.296935	-0.024540
H	-5.206253	-1.603899	-1.079368

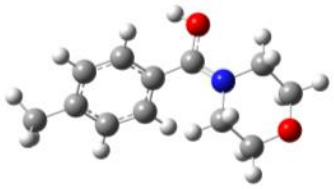

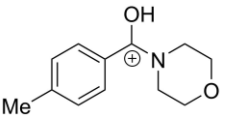

Sum of electronic and zero-point Energies= -671.869441
Sum of electronic and thermal Energies= -671.855643
Sum of electronic and thermal Enthalpies= -671.854698
Sum of electronic and thermal Free Energies= -671.911323

C	-2.543666	-1.133374	-0.711987
C	-1.231204	-0.679449	-0.715337
C	-0.906686	0.515859	-0.058548
C	-1.915299	1.247231	0.588079
C	-3.218558	0.768735	0.597614
C	-3.556930	-0.426904	-0.050373
H	-2.785908	-2.048386	-1.240232
H	-0.475482	-1.235063	-1.256907
H	-1.679253	2.171238	1.103331
H	-3.985157	1.335097	1.114044
C	0.455084	1.072532	-0.101854
O	0.615419	2.321284	-0.505112
C	2.896596	1.008820	0.062802
C	1.561421	-0.866161	0.954018
C	3.789556	-0.036541	-0.605962
H	3.280833	1.268885	1.051882
H	2.834686	1.907029	-0.544018
C	2.518763	-1.821290	0.245549
H	0.559003	-1.278519	1.011163
H	1.918928	-0.664967	1.967005
H	4.811485	0.339394	-0.646296
H	3.440999	-0.227390	-1.628916
H	2.616910	-2.733012	0.834075
H	2.136292	-2.080993	-0.749596
N	1.540942	0.435852	0.247518
O	3.819186	-1.251403	0.135307
H	-0.206055	2.670736	-0.882283
C	-4.969849	-0.945995	-0.020746
H	-5.140046	-1.531151	0.889310
H	-5.692867	-0.127997	-0.022706
H	-5.173174	-1.595697	-0.873569

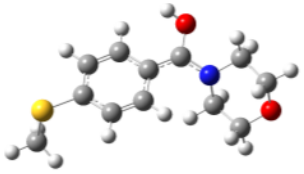

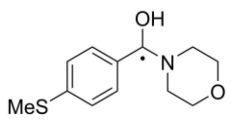

Sum of electronic and zero-point Energies= -1070.203180
Sum of electronic and thermal Energies= -1070.187279
Sum of electronic and thermal Enthalpies= -1070.186335
Sum of electronic and thermal Free Energies= -1070.248634

C	1.893434	-0.776623	-0.731506
C	0.560448	-0.447062	-0.586973
C	0.163716	0.801918	-0.014947

C	1.210172	1.682748	0.399427
C	2.541410	1.333928	0.253888
C	2.912775	0.099545	-0.307459
H	2.160698	-1.720922	-1.193001
H	-0.197818	-1.126800	-0.954827
H	0.973498	2.630405	0.870659
H	3.311238	2.019723	0.589264
C	-1.197464	1.159894	0.107926
O	-1.579216	2.455781	0.339383
C	-2.309984	-0.859102	0.972739
C	-3.579739	0.775138	-0.324253
C	-3.214086	-1.950249	0.415799
H	-2.706912	-0.508565	1.936974
H	-1.310112	-1.257049	1.141959
C	-4.435737	-0.376142	-0.840794
H	-3.485766	1.537780	-1.097608
H	-4.066376	1.232337	0.548465
H	-3.353959	-2.740253	1.154630
H	-2.767675	-2.384862	-0.489180
H	-5.458285	-0.037341	-1.013147
H	-4.023002	-0.756059	-1.785455
N	-2.245845	0.267614	0.022508
O	-4.513328	-1.440421	0.109621
C	4.951101	-1.429030	0.902741
H	5.994373	-1.739865	0.830424
H	4.794452	-0.896376	1.840455
H	4.308279	-2.307492	0.853641
H	-0.904110	3.064184	0.012677
S	4.638530	-0.318426	-0.529690

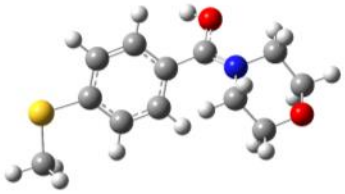

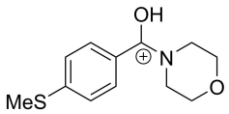

Sum of electronic and zero-point Energies= -1070.079656
Sum of electronic and thermal Energies= -1070.064504
Sum of electronic and thermal Enthalpies= -1070.063560
Sum of electronic and thermal Free Energies= -1070.122940

C	1.966243	-0.735224	0.470375
C	0.611477	-0.440628	0.521349
C	0.129947	0.783861	0.037852
C	1.040322	1.717734	-0.491686
C	2.387729	1.415643	-0.561011
C	2.871515	0.184842	-0.079536
H	2.306164	-1.680423	0.869256
H	-0.063205	-1.155451	0.975218
H	0.691315	2.667655	-0.879794
H	3.072714	2.136552	-0.991410
C	-1.285290	1.150153	0.149918
O	-1.598152	2.337971	0.643232
C	-3.701630	0.759777	0.079137
C	-2.181210	-0.821001	-1.045469
C	-4.404361	-0.455065	0.686395
H	-4.173637	1.048627	-0.862803
H	-3.728383	1.601492	0.764579
C	-2.953058	-1.962593	-0.389045
H	-1.138409	-1.080239	-1.197413
H	-2.628200	-0.580128	-2.013521
H	-5.464338	-0.232699	0.806425
H	-3.975419	-0.681167	1.670862
H	-2.962316	-2.822663	-1.057891
H	-2.478074	-2.254136	0.556437
N	-2.293557	0.400030	-0.215243
O	-4.310084	-1.594857	-0.161682
C	4.861788	-1.741420	0.516494
H	5.934411	-1.919698	0.445567
H	4.565505	-1.760179	1.564725
H	4.334403	-2.506769	-0.051770
H	-0.826060	2.759047	1.049572
S	4.612092	-0.088839	-0.210148

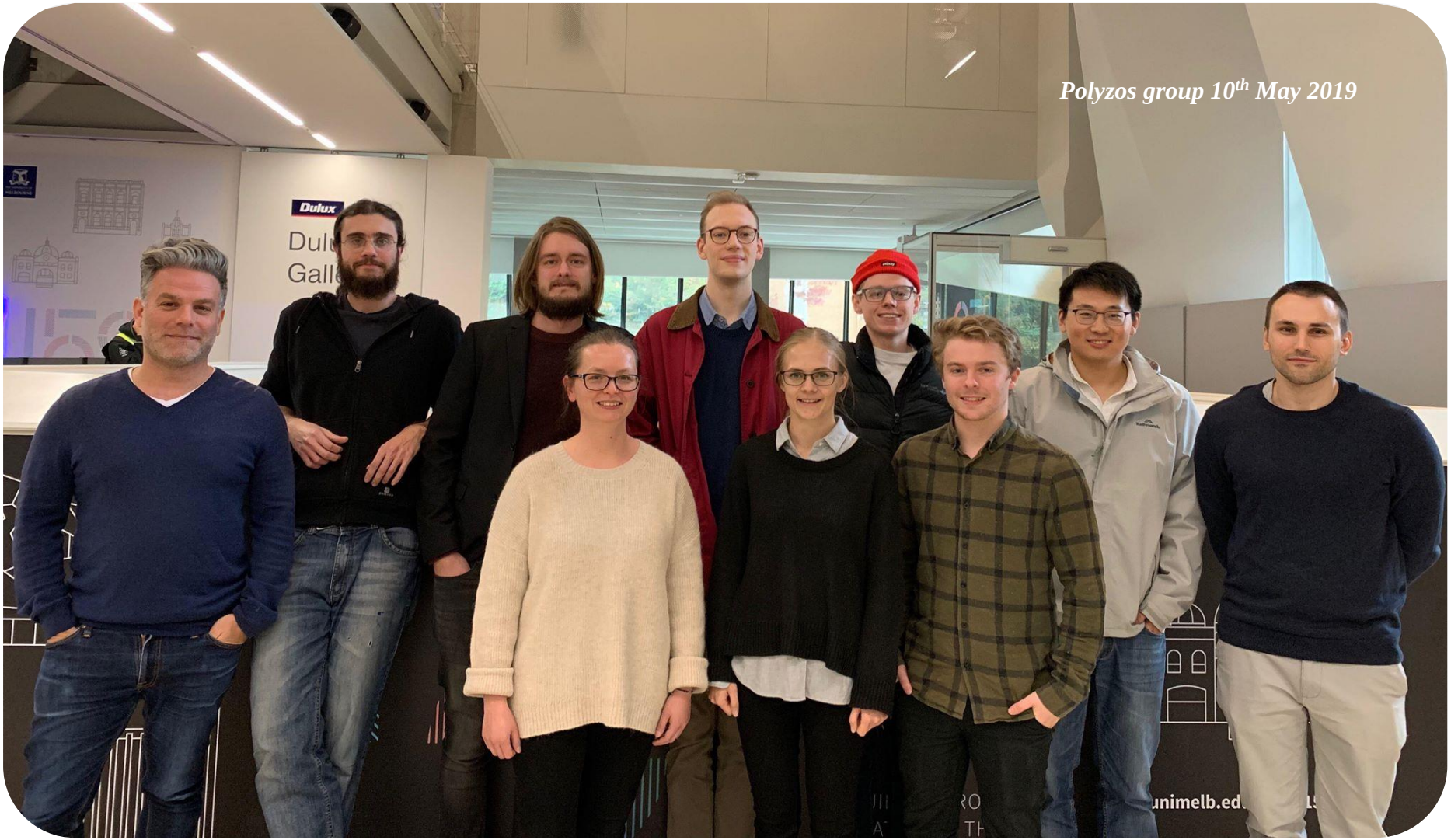

From left to right: Anastasios Polyzos, Jose Forni, Dean Van As, Milena Czyz, Mitchell Taylor, Tyra Horngren, Nikolai Rossouw, Rowen Pilkington, Xiaocong Guan, Nenad Micic